Sheffield Hallam University

A Sheffield Hallam University thesis

ProQuest Number: 10694459

ProQuest 10694459

Long Period Fibre Grating as Gas Sensor for Environmental Pollution Monitoring

Kenneth Paul Dowker

A thesis submitted in partial fulfilment of the requirements of Sheffield Hallam University for the degree of Doctor of Philosophy

December 2003
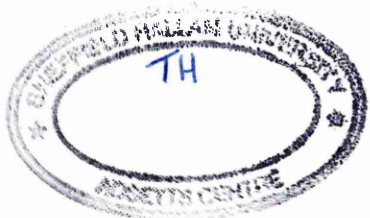
Abstract

The principle objective of the work presented in this thesis is to investigate and demonstrate the possibility of utilising the inherent properties of long-period gratings (LPGs) to detect the existence and concentration of a given gas in the region immediately surrounding the fibre cladding. The principle and the viability of using LPGs for sensor applications is supported by the preliminary results reported here. However, the sensitivity of the sensor requires further improvement before it can in any way challenge the existing sensors in this field.

The operational characteristics and limitations of existing optical sensors are reviewed and the advantages of a LPG based optical sensor highlighted. Thorough explanations of the theory and principles of light propagation, mode formation, and mode coupling in optical fibres are presented.

Computer simulations predicting the optical effects due to changes in ambient indices from theoretical conditions are successfully derived, confirming the results obtained by experimental investigation.

Various established coating methods are investigated and utilised in the application of optically sensitive compounds adsorbed onto the cladding with different levels of success, the poly-electrolyte self assembly (PESA) and evaporation methods proving most suitable. A novel method of monitoring the build up of PESA layers in-situ using surface plasmon resonance (SPR) methods is introduced.

The coating chemicals used in this investigation showed some optical sensitivity at the optimum wavelengths used in optical fibres to the various gases being monitored, in most cases causing a detectable change in the optical characteristics of the modes in the LPG.

This study has shown the possibility of using a suitably prepared LPG as a gas sensor. The LPG is coated with a chemical whose refractive index is changed by absorption of a given gas and thus the change in the coupling wavelengths being caused by the existence of the gas. Maximum shifts in coupling wavelength of ± 1.5 nm for relatively high gas concentrations are observed.

The possibility of using a coating material which absorbs water, or surrounding the LPG with a suitable liquid is also demonstrated, the refractive index of the coating or liquid and thus the coupling wavelength shift being affected by the reaction of the gas.

The possibility of using a single temperature immune LPG for ambient index sensing by observing different coupling wavelengths in the same grating is also reported.

Acknowledgements

Declaration

No portion of the work referred to in this thesis has been submitted in support of an application for another degree or qualification to this, or any other university, other institute of learning, or industrial organisation.

Kenneth Paul Dowker

January 2004

Glossary of Abbreviations

CCD	Charged coupled device
Chromo 1	Cyclo-tetrachromotropylene
$CuPc^- (C(CH_3))_4$	CopperIIphthalocyanine-tetra-tert-butyl
$CuPc^- (SO_3^- Na^+)_4$	CopperIIphthalocyanine-tetra-sulphuric-sodium salt
EELED	Edge emitting light emitting diode
EMI	Electro-magnetic interference
FBG	Fibre Bragg grating
LB	Langmuir-Blodgett
LED	Light emitting diode
LP	Linearly polarised
LPG	Long period grating
N_2	Nitrogen
NO_2	Nitrogen Dioxide
OSA	Optical spectrum analyser
PESA	Polyelectrolyte self-assembly
PAA	Poly-alylamine hydrochloride
PPI	Planar polarized interferometer
PPS	Poly-phenylsulphide
SPR	Surface plasmon resonance
TE	Transverse electric
TIR	Total internal reflection
TM	Transverse magnetic
UV	Ultra-violet

Glossary of Symbols

B	Magnetic induction
D	Electric displacement
d_P	Penetration depth of evanescent field
E	Electric field
f	Frequency
I_m	m^{th} order modified Bessel function of the second kind
J_m	m^{th} order Bessel function of the first kind
J'_m	First derivative (wrt radius) of the mth order Bessel function of the first kind
k	Wave number
K_m	m^{th} order modified Bessel function of the first kind
K'_m	First derivative (wrt radius) of the mth order modified Bessel function of the first kind
l	Radial mode number
L_g	Grating length
m	Azimuthal mode number
n	Refractive index
n_{eff}	Effective refractive index
N_m	m^{th} order Bessel function of the second kind
R	Reflectance
$R_z(r)$	Radial field function
r	Radius
T	Transmittance

t	Time
u	Normalised transverse phase constant (normalised propagation constant) in the guiding medium
w	Normalised transverse attenuation constant (normalised propagation constant) in the surrounding medium
β	Propagation constant
β_t	Transverse propagation constant
δn_{core}	Difference in refractive indices of core and grating
ε_0	Free space permittivity
ϕ	Phase shift
κ	Coupling coefficient
Λ	Grating period
λ	Wavelength
λ_{BRAGG}	Coupling wavelength in FBG
λ_{cup}	LPG coupling wavelength
μ_0	Free space permeability
θ	Incident angle at the refractive index boundary of the guiding medium
θ_c	Critical angle
ρ	Reflection coefficient
ρ_c	Current density
τ	Transmission coefficient
ω	Angular frequency
Ψ	Total electric field of a 2 wave guide coupler
ψ	Wave displacement of electric field vector

List of Figures

List of Tables

List of Contents

Chapter 1

Introduction

1.1 Importance and Relevance of Gas Sensors

There are many industrial and commercial situations where it is important to be aware of the presence and concentration of various gases. These situations may include emissions of waste gases into the atmosphere, human exposure to ambient gases or fumes in industrial, commercial or public environments, or the build up of gases in potentially volatile environments. Detection of the types and concentrations of these various gases will allow the control of emission rate and safe working conditions or exposure limits to be determined and implemented. Gas sensing is currently performed using electrical and/or optical techniques, which offer limited accuracy and reliability.

1.2 Limitations of Electronics Based Gas Sensors

Existing electrical sensors are sensitive to electro-magnetic interference from electrical or magnetic equipment in the vicinity of the sensor or the cables carrying the information to the processing mechanism. This interference may swamp the low level signal detected by the sensor-receiver. The electrical connections may also be close to the sensing head, which would be undesirable in a potentially volatile environment.

1.3 Limitations of Existing Optical Based Gas Sensors

Optical Sensors are inherently immune to electro-magnetic interference and can therefore be used more effectively in such environments. Optical sensors which rely on variations in the intensity of the input signal can be affected by fluctuations in the light source due to internal or external conditions. For accurate intensity detection it is therefore imperative to employ a high stability light source with compensating equipment for ambient variations. The most effective optical methods of gas detection include interferometric devices or optical fibres, as in fibre Bragg gratings (FBGs). These optical methods do not rely on intensity of the signal from the detector, but use a more reliable and accurate measurement of wavelength shift. While

the optical signal can be transported far away from any volatile environment before any electrical connections are made, the interferometric devices require intricate positioning of the optical components, whilst the optical fibre devices may require accurate modifications to the cladding, which reduce the strength and integrity of the fibre.

1.4 Advantages of using Long Period Gratings as Gas Sensors

The spectral response of a long period grating (LPG) is dependant among other considerations on the medium surrounding the cladding and thus overcomes the problems associated with the previously mentioned types of sensors, requiring no electrical connections anywhere near the sensing environment or any intricate positioning or modifications to the cladding. To use an LPG as a gas sensor therefore requires only that the refractive index of the medium around the cladding change adequately in the presence of a given gas. This refractive index change may be caused by coating the cladding with a chemical whose refractive index will change on contact with that gas. Research into the possibilities of the LPG as such a sensor is the subject of this thesis.

1.5 Research Objectives

The fundamental objective of the work presented in this thesis is to investigate the suitability of utilising a suitably adapted long period grating for use as a gas sensor, which can overcome the inherent problems of existing gas sensors whilst providing equal or improved levels of reliability, accuracy and sensitivity. In order to achieve this, the following objectives have been identified:

- Review existing extrinsic and intrinsic fibre sensors, the production of fibre gratings, and the operational characteristics of fibre Bragg gratings and long period gratings.

- Review the equations and computer programs used to simulate light propagation, the formation of modes, and mode coupling in optical fibres.

- Review the existing optical detection techniques and the suitability of each for processing the optical signals received from the sensor.

- To gain a thorough understanding of the characteristics of light propagation within an optical wave guide, mode formation , classification and coupling in optical fibres, including derivation and applications of the relevant equations and theories.

- To create computer simulation programs to predict the light propagation, mode formation and mode coupling in optical fibres and long period gratings, with which to compare the experimental findings.

- To investigate existing methods of thin film coating procedures and optically sensitive compounds and the suitability of each for coating the fibre cladding.

- To gain experience, confidence and proficiency in handling, cleaving, coating, illuminating, and working with optical fibres.

- To experimentally confirm and reproduce existing theory and reported results in long period grating applications.

- To experimentally investigate the viability of using a suitably coated long period grating as a gas sensor and the possibility of inherent temperature compensation.

1.6 Order of Thesis Presentation

This thesis is divided into eight chapters beginning with an introduction in Chapter 1.

Chapter 2 is a literature review which details the history and development of optical fibre technology, from uses as merely a light guiding medium to the concepts of stand alone sensors such as interferometry, fibre Bragg gratings (FBGs), and long period gratings (LPGs). This chapter also discusses existing techniques available to process the optical signals into electronic information for storage or visual display, and the progress of computer simulation in this field.

Chapter 3 explains the theoretical aspects of optical fibre technology, from the conditions required for simple light guidance, through the derivation of equations describing the properties of the various guided modes, to the operational characteristics of the LPGs.

Chapter 4 describes the computer programs written as part of this investigation to simulate and compare to the results obtained by experiment, utilising the formulae derived in the previous chapter.

Chapter 5 explains various chemical coating procedures and the methods used to investigate the feasibility of these procedures for the coating of the fibre cladding.

Chapter 6 describes the experimental section of the investigation, drawing conclusions as to the practical possibility of using a suitably coated LPG as a gas or temperature sensor, and as a multi parameter sensor with its own integral immunity or compensation to the effects of the unwanted measurand.

Chapter 7 outlines the major contributions of this thesis and the conclusions reached.

Chapter 8 discusses the direction in which further investigation may be taken, to possibly allow the long period grating to be ultimately used as a gas sensor.

1.7 Original Contributions

During the course of this work the author has:

1. Gained a thorough understanding of the principles of optical fibres, with special focus on long period gratings, allowing the application of these principles towards the investigation into the suitability of using such gratings in the monitoring of gaseous environments.

2. Derived and modified existing equations describing and predicting the propagation of light, mode formation and mode coupling in long period gratings, and the effects of external influences on each.

3. Designed computer simulations to predict, verify, and compare with, the results obtained experimentally.

4. Determined suitable methods of coating the fibre cladding, including a novel method of monitoring the build up of in-situ polyelectrolyte self assembly coatings using surface plasmon resonance techniques.

5. Demonstrated for the first time the principle and the viability of utilising a suitably prepared LPG for gas sensing applications, the temperature dependence of the directional shift in coupling wavelength on the grating period, and thus the possibility of the inherent temperature immunity of this and other types of LPG sensors.

Chapter 2

Literature Review

2.1 Introduction

The use of light in communication and sensing mechanisms is growing rapidly due to the comparatively limitless speed of information transfer and the immunity to most types of interference. Optical fibres are proving to be a most efficient medium in the field of optical systems development.

An optical fibre consists of a central cylindrical glass core and a surrounding cylindrical glass cladding as shown in Figure 2.1, the core being of slightly higher refractive index than the cladding [1-3].
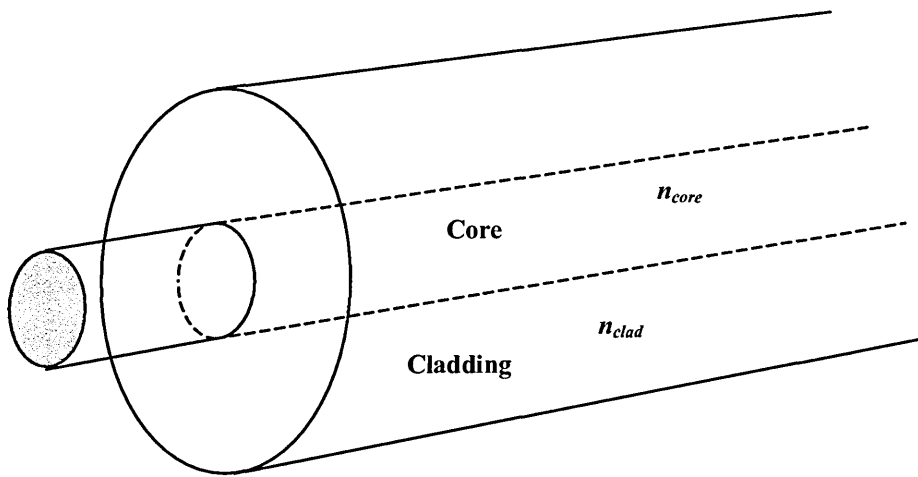
Figure 2.1: Optical fibre structure

The history of integrated optics began in December 1969 with a paper published in the *Bell Technical Journal* [4], discussing the idea of integrated circuits using photons instead of electrons [5-9]. The designs of today's optical fibre technology have differed very little from these original proposals [10]. Since then optical fibre technology has not only taken over a major share of the communication market, due mainly to its much greater bandwidth availability, but has also branched out into other fields such as signal processing [11-16], amplification [17-19], and sensors [20-33] to name but a few.

Optical fibre is a physical medium and as such is affected by various external influences such as heat [34-39], stress, [40-45] etc., each of which, to some degree, will affect the propagation of the light within the fibre. These are undesirable consequences in communication systems, but can be effectively utilized in sensor applications [46,47]. Advantages of optical fibre sensors over most conventional sensors include greater sensitivity, electrical passiveness, wide dynamic range,

10

multiplexing capabilities, small physical size and weight, robust, corrosion resistance, fast response times and less susceptibility to electro-magnetic interference (EMI) [48-50]. Both point and distributed configurations and simultaneous sensing of more than one parameter are possible [51-63].

This chapter is a review of the existing types of sensors which utilise the light guiding capability and the intrinsic and extrinsic qualities of optical fibres. The inherent advantages and disadvantages of each type of sensor are highlighted. Section 2.2 is an overview of the different types of sensors explaining the characteristics of the fibre which are utilised and the disadvantages for use as a gas sensor inherent to their design. Section 2.3 describes the history and concept of fibre gratings and production methods. Section 2.4 briefly explains the theory of fibre Bragg gratings and their uses and limitations as sensors. Section 2.5 introduces the concept of the long period grating and its greater suitability over previous types of optical fibre based sensors for use as a gas/chemical sensor. Section 2.6 discusses suitable methods for capturing and processing the output signal from a long period grating sensor. Section 2.7 covers the background and the origins of the equations used in the computer programs written as part of this research to simulate the actual results obtained experimentally.

2.2 Review of Optical Fibre Sensors

Existing optical fibre and integrated optics are classified as:

(i) extrinsic sensors where an unmodified fibre is used as the sensing medium or to transport light to and from an external sensing mechanism [64-66],

(ii) intrinsic sensors where the sensing mechanism is an integral part of the modified fibre [67,68].

2.2.1 Typical Examples of Extrinsic Optical Fibre Sensors

(i)   Current Sensors [69-71]
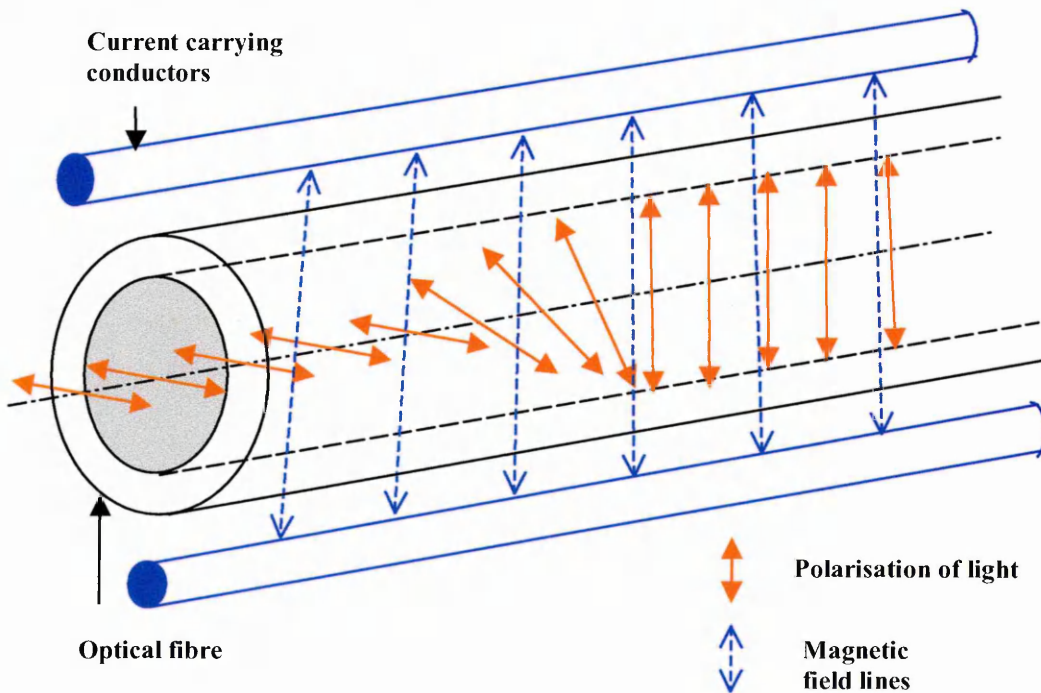
Figure 2.2:   Effect of electric/magnetic field on light polarization

Linearly polarised light is transmitted through a fibre which is in close proximity to a current carrying medium. The magnetic field associated with this current will affect the polarisation of the light in the fibre as shown in Figure 2.2. Thus the comparative change in polarisation of the light at the detector will be an indication of the existence and strength of the current in the medium under test. This effect obviously cannot be utilized for gas sensing of any kind.

(ii)   Interferometric Sensors
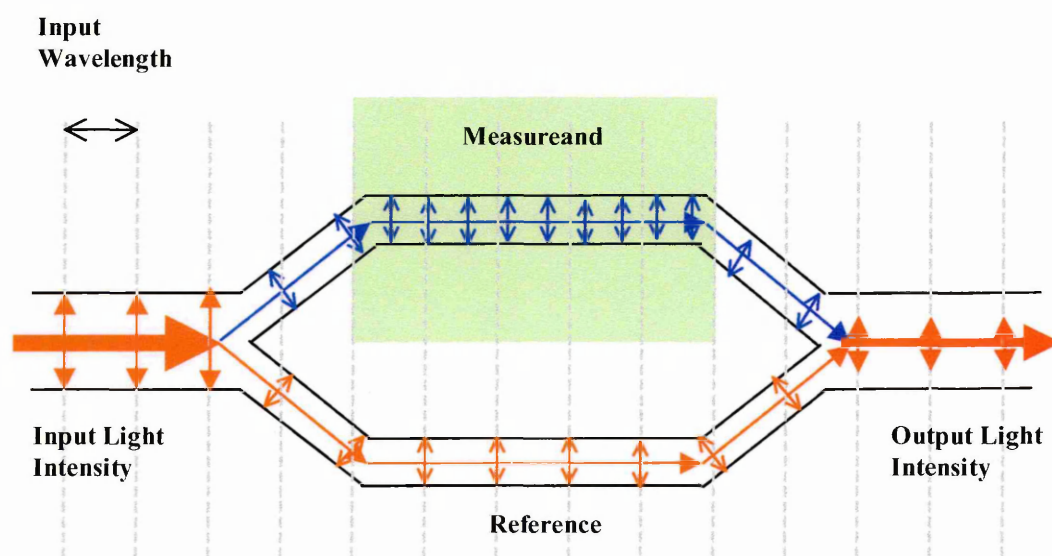
Figure 2.3:   Operation of interferomic sensor

Interferometric methods [72-87] involve the sensing of changes to the refractive index or dimensions of the fibre as in strain or temperature sensing. Interferometry utilises two identical fibres connected in parallel to the same light source and detector as shown in Figure 2.3. Only one of the fibres is exposed to a measurand, while the other is used as a reference. As a result the optical properties of only the exposed fibre change, resulting in an optical phase or polarisation shift between the two fibres

at their output ends and thus an intensity change in the interfering rays in the detected signal. The degree of phase shift indicates the stress or temperature change being measured. This process can also be used to detect ambient index changes (due to a gaseous or chemical environment) by removal of the cladding allowing the ambient conditions into direct contact with the core and thus to directly affect the mode structure of the core [88,89]. The limitations of this method are the reduction in the strength and integrity of the fibres due to the removal of the cladding, the intricate positioning of the sensor and the fact that the interference is cyclic. This means that a phase shift of 2π would have the same interference effect on the output signal as phase shifts of 4π, 6π, or any whole number of 2π. Allowing for this cyclic effect would involve complicated modifications to the detected signal [90].

(iii)   Selective absorption sensors [91,92]

Absorbing Medium

Optical Fibre

Collimating Lens   Focussing Lens
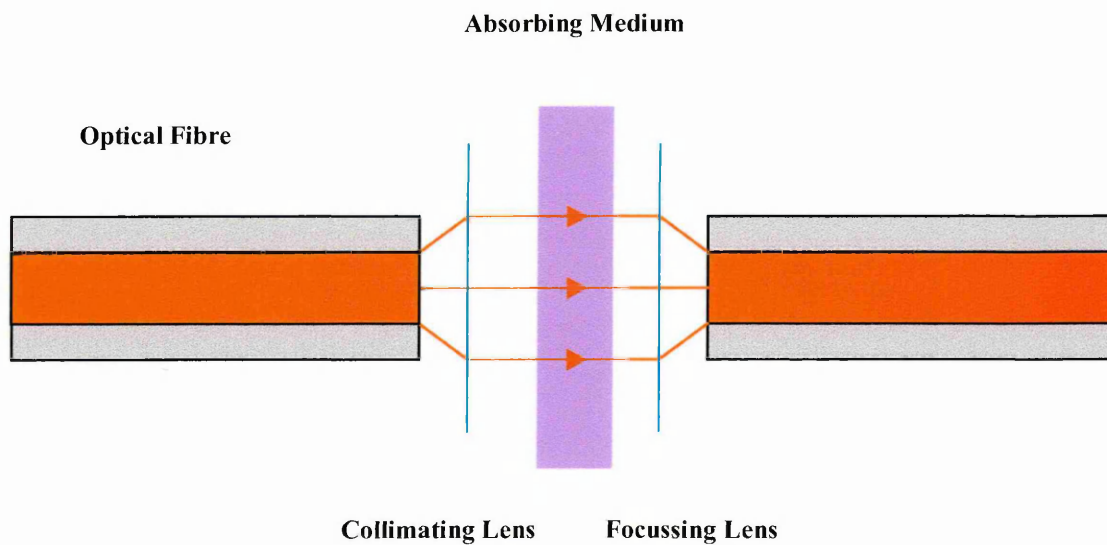
Figure 2.4:   Operation of selective absorption gas sensor

The fibre is used merely as a light guide as shown in Figure 2.4 to route the light to the sensing position, perhaps emitting the light through a gaseous environment where

14

selective absorption will take place, and returning the resulting light back to a detector where the absorption spectrum will be processed. The fact that the light is not confined in the fibre core, the need for intricate positioning and the inflexibility of the associated optical components, and the possibility of contamination of the absorption spectrum by unwanted scattering prevents the use of this type of sensor in many applications.

2.2.2 Typical Examples of Intrinsic Optical Fibre Sensors

(i)   Ambient Index (Evanescent Field) Sensors [93-111]
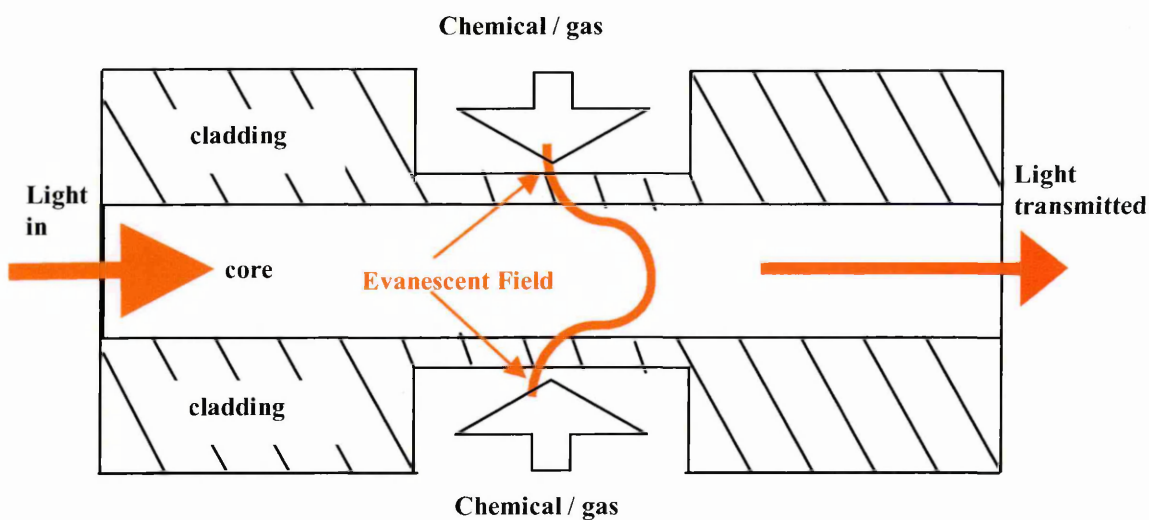
Figure 2.5:   Operation of ambient index (evanescent field) sensor

If the fibre cladding is removed to a thickness where the evanescent field will penetrate into the surrounding atmosphere as shown in Figure 2.5, selective absorption of the energy in the evanescent field and thus the light in the core will take place. The absorbed radiation will show a reduction in intensity when observed in the transmission spectrum, the wavelength of which will be dependent on the gas or

chemical surrounding the reduced cladding. Different gases/chemicals may absorb different wavelengths but again, the reduction of the cladding is intricate, time consuming and severely reduces the strength and integrity of the fibre.

(ii)   Fibre Bragg Grating Based Sensors [112-122]
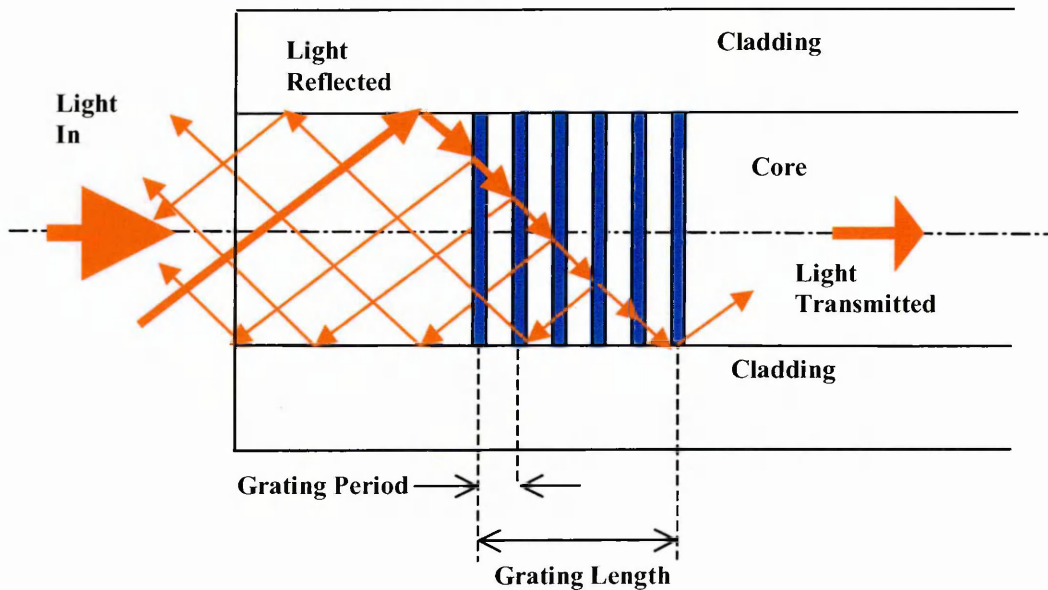
Figure 2.6:   Operation of fibre Bragg grating sensor

Fibre Bragg gratings (FBGs), which are refractive index perturbations produced in the core by lithographic methods, reflect the wavelengths of incident radiation which are half the length of the grating period, whilst transmitting all other wavelengths as shown in Figure 2.6. FBG based sensors therefore only can be used to sense such effects as strain or temperature changes, as only a change in the period of the grating or the refractive index of the core in the region of the grating will result in a shift in the Bragg wavelength absent at the output of the fibre. They cannot be used to sense any measureand which does not directly affect these parameters and thus cannot

easily be adapted to detect changes in gas/chemical concentrations in the region surrounding the cladding

(iii)   Integrated Interferometric Methods [123-125]

These methods involve wave guide interferometers which are permanently integrated onto a chip, the operational characteristics and limitations being as in extrinsic interferometric methods.

2.3 Fibre Gratings

The concept of the fibre grating was demonstrated in 1978 by Hill et-al at the Canadian Communications Research Centre [126,127]. Launching intense blue light with a wavelength of 488 nm from an Argon ion laser into a germanium doped fibre core, it was observed that the fraction of the light intensity reflected increased with time, until virtually all of the light was being reflected. Further investigation led to the conclusion that the standing wave produced by the fraction of the light reflected from the end of the fibre had interfered with the forward travelling wave causing refractive index perturbations at the points of constructive interference in the core [128].   These refractive index perturbations themselves also effect fractional reflections creating further standing waves in phase with the original standing waves and compounding the effect on the refractive index perturbations, hence the gradual increase in the reflected fraction of the light towards saturation.   These first

experiments resulted in the formation of gratings of approximately 90% reflectivity, but they could only operate at the writing wavelength. The increase in the refractive index with exposure time led to the discovery of a new non-linear effect in the fibres now known as photosensitivity [129].

The limitations of the Hill gratings to operational wavelengths at or close to the writing wavelength were overcome about 10 years later by Meltz et-al [130]. They demonstrated a method of writing a grating into a fibre core using ultraviolet radiation at 244 nm, whereby the radiation was made to form a holographic interference pattern through the cladding, which is essentially transparent to ultra violet radiation, on to the side of the core which is highly absorbing in the ultra violet. This meant that the gratings could be written into a core without the need for the removal of the cladding, and that the period could be controlled by the separation of the interference pattern maxima. The reflected wavelength was no longer limited to the writing wavelength but could be made to reflect almost any wavelength, including the longer wavelengths used in communications and sensors applications at which the transmission windows are situated [131-140].

Further improvements to the writing method have led to the phase mask technique in which a length of silica glass, periodically etched using photolithographic techniques is placed between the UV source and the side of the fibre [141-144]. The resulting diffraction pattern on the side of the fibre determines the grating period, which can therefore be controlled by the period and position of the mask and the writing wavelength. A typical phase mask writing technique is shown in figure 2.7. [145].

244 nm UV Light Source

Mirror Translating along Fibre at Pre-dertmines Rate

Diffracted UV Light Alters Refractive Index of Fibre Core at Selected Positions to Create Grating

Phase Mask

Optical Fibre

Piezzo Electric Stage Translating Fibre at Pre-determined Rate
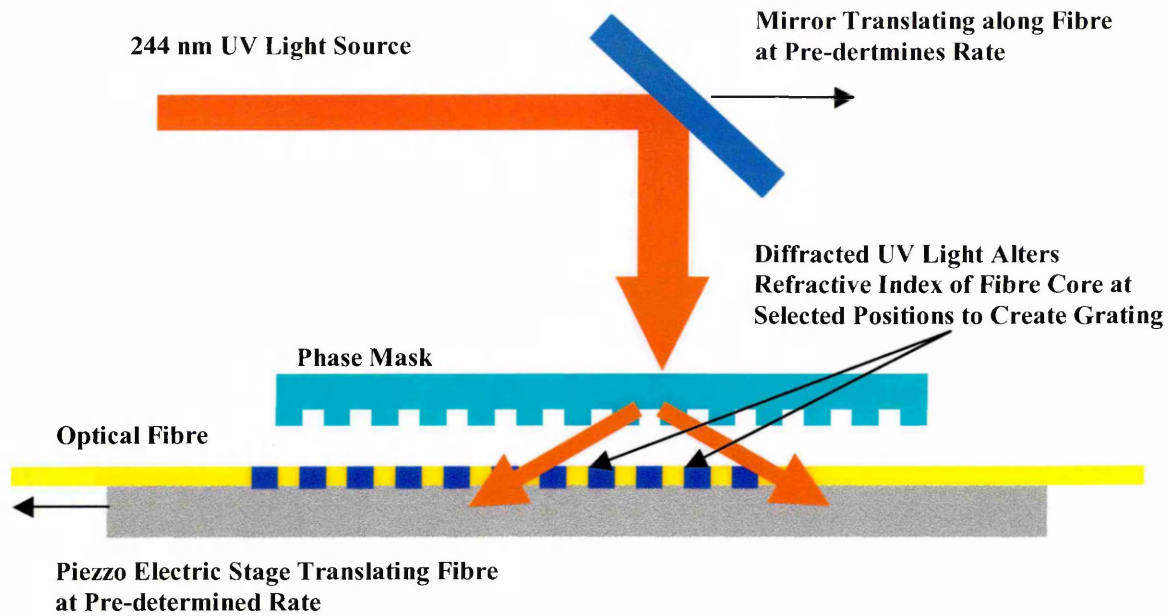
Figure 2.7:   Phase mask writing technique for fibre grating

2.4 Fibre Bragg Gratings

Fibre Bragg gratings (FBGs) are usually written into the core of a single mode fibre using the phase mask method [78,146]. A typical fibre Bragg grating is shown in figure 2.8.
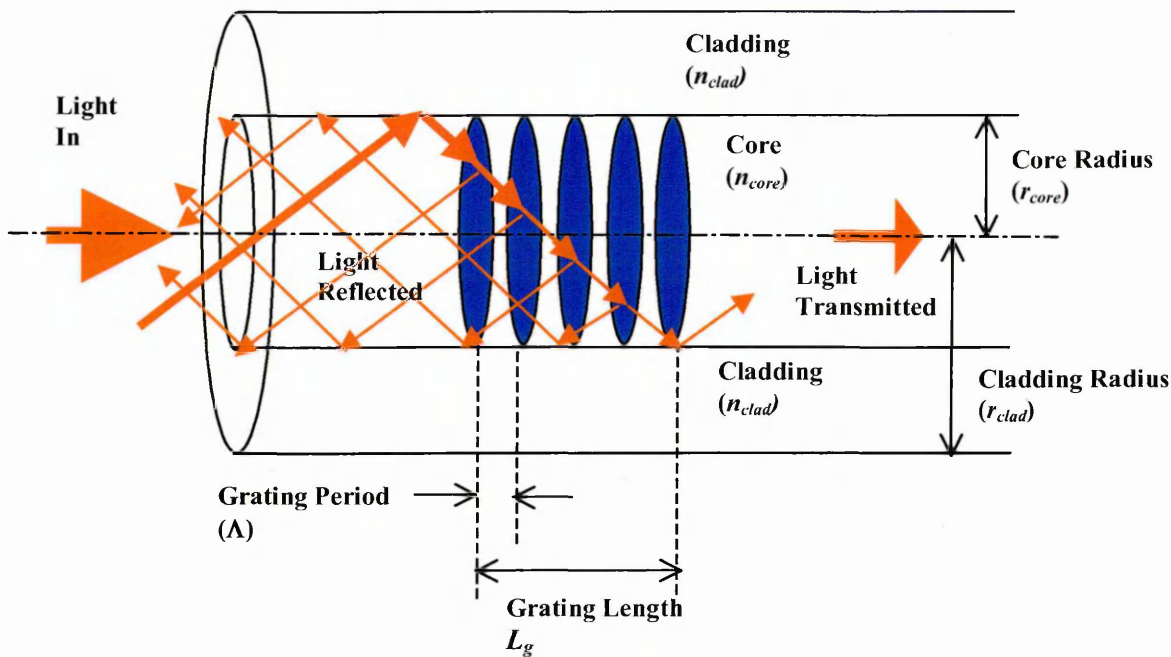
Figure 2.8:   Design and principle of operation of fibre Bragg grating

Typical specifications of a fibre Bragg grating [147-149] are shown in Table 2.1.

Parameter	Typical Value
core radius(r_{core})	2-5 μm
cladding radius (r_{clad})	50-75μm
grating period (Λ)	200-1000 nm
overall grating length (L_g)	1 - 5 cm
index modulation of grating (δn_{core}) (difference in refractive index between grating and core)	10^{-4}
core refractive index (n_{core})	1.480
cladding refactive index (n_{clad})	1.458

Table 2.1:   Typical specifications of fibre Bragg grating

The period of the grating is designed to reflect a required wavelength when the fibre is unperturbed [125,150,151]. This is achieved by selecting an appropriately spaced phase mask and finely adjusting the position and thus the separation of the diffraction maxima, whilst monitoring the output or reflected spectrum of the fibre. The

conditions which must be met for a given wavelength (λ_{BRAGG}) to experience maximum reflection are given by (2.1) [152-154]:

$$\lambda_{BRAGG} = 2\, n_{eff}\, \Lambda \qquad (2.1)$$

where n_{eff} is the refractive index of the core allowing for the angle of propagation of the radiation. This equation shows that only wavelengths which have an effective axial optical path length equal to twice the grating period will experience maximum reflection. This is because successive reflections will only be in phase if the extra optical path length travelled between periods is a multiple of whole wavelengths [155]. As the extra distance travelled will be twice the grating period, then a wavelength which is equal to twice the period will interfere totally constructively on reflection and destructively on transmission, effectively disappearing from the transmission spectrum as the phase imbalance compounds over successive reflections along the grating length [156]. So far only the reflection properties from successive periods have been considered. By treating the grating as a diffraction grating rather than a series of partially reflecting mirrors, the FBG condition can also be explained by diffraction theory. Thus the effect can be understood and the resulting formula proved using both theories as will be explained in the theory section. In both cases the forward propagating mode at which a given wavelength matches the aforementioned condition is said to couple into a reverse propagating mode at that wavelength. The fibre Bragg grating can be used in the reflection mode where only the coupling wavelength is present in the observed spectrum, or in the transmission mode where the coupling wavelength is absent from the observed spectrum, or both [151,152,157-159]. If an external measureand, for example temperature or strain, causes a change in either the grating period, the dimensions of the core, or the refractive index of the core or cladding, then the coupling wavelength will change

proportionally thus allowing the FBG to be used as a sensor [160-162]. As shown in figure 2.8, since both reflected/diffracted and transmitted light rays are confined to the core then the characteristics of the resulting transmission or reflected spectra will not be affected by the medium surrounding the cladding [163,164]. To use a fibre Bragg grating as a gas/chemical sensor it is essential that all of the cladding is etched away at the sensor position allowing the effect of the gas/chemical on the ambient refractive index to interact with the light propagation and thus the modal structure in the core [88,163] (see figure 2.9).
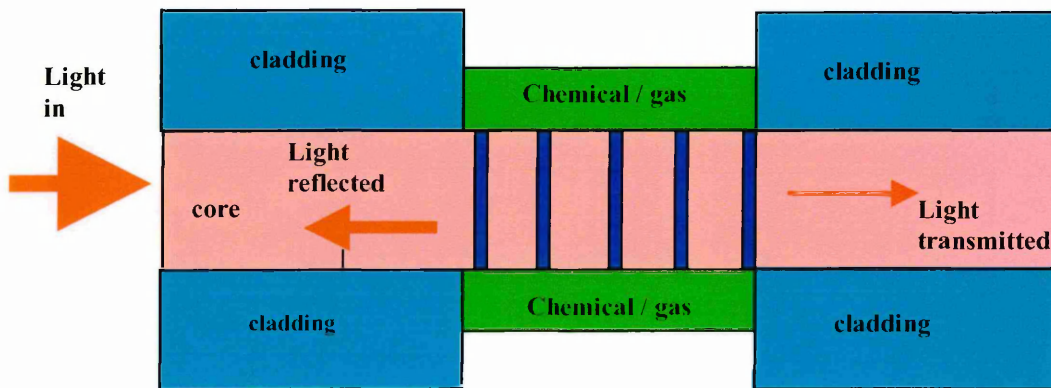
Figure 2.9:   Design and operation of the FBG as ambient index sensor

The wavelength of interaction depends on the refractive index and thus the concentration or constitution of the surrounding medium. Fabrication of such sensors are rather complex and costly, and at the position where the cladding has been removed the mechanical strength and flexibility of the fibre is considerably reduced [165]. To overcome this difficulty there exists an alternative fibre grating design known as the long period grating (LPG).

2.5 Long Period Gratings

Long period gratings (LPGs) can be written into the core of a single mode fibre by the same method as for an FBG [166-173]. A typical long period grating is shown in Figure 2.10.
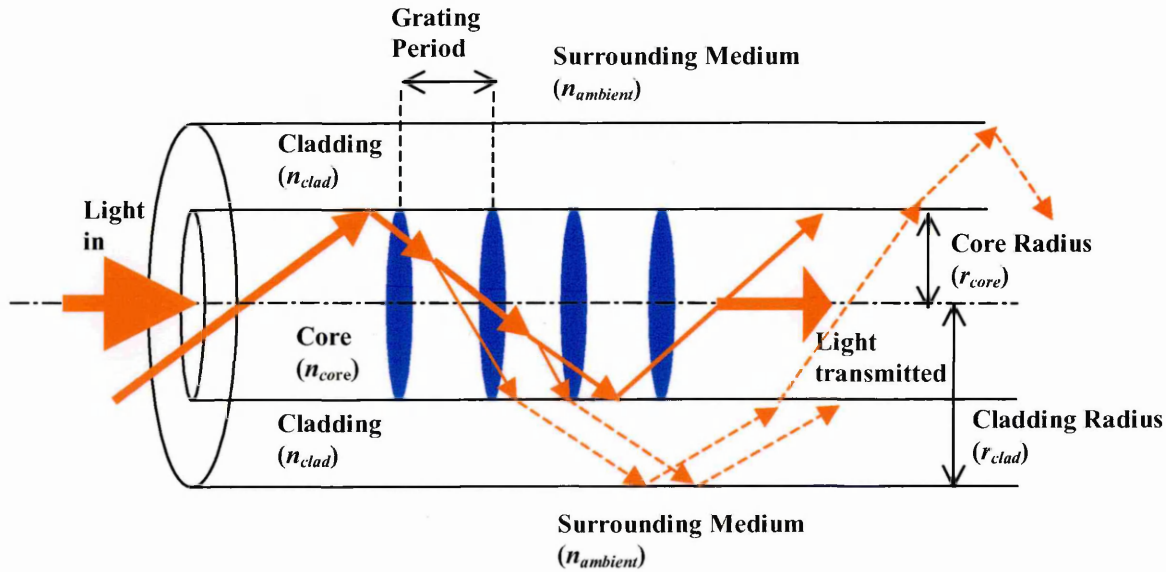
Figure 2.10: Design and principle of operation of long period grating

Typical specifications of a long period grating are shown in table 2.2 [174,175].

Parameter	Typical Value
core radius(r_{core})	2-5 μm
cladding radius (r_{clad})	50-75 μm
grating period (Λ)	5-500 μm
overall grating length (L_g)	1 - 5 cm
index modulation of grating (δn_{core}) (difference in refractive index between grating and core)	10^{-4}
core refractive index (n_{core})	1.480
cladding refactive index (n_{clad})	1.458

Table 2.2:   Typical specifications of long period grating

As shown in figure 2.10, specific wavelengths of the light propagating within the single mode core are coupled (diffracted) into one or more of the forward propagating cladding modes according to the LPG coupling formula, (2.2) [166,174-176]:

$$\lambda^{(i)} = \left(n^{\lambda^i}_{eff.core} - n^{\lambda^i}_{eff.clad} \right) \Lambda \qquad (2.2)$$

where the effective refractive indices are quoted as functions of the mode cladding number i and coupling wavelength λ. On entering the cladding these wavelengths are attenuated due to further multiple partial reflections at the refractive index boundaries and imperfections at the cladding / air boundary, resulting in a detectable intensity loss of the affected wavelengths in the transmission spectrum at the output of the fibre. The wavelength and intensity of this coupling is determined by the refractive index of the medium surrounding the cladding [166,174-177]. The refractive index of the surrounding medium $n_{ambient}$ will only affect the effective refractive index of the cladding, whilst the core mode for each transmitted wavelength will remain unaffected. However, in order to escape from the core the wavelengths in the core mode must couple to a suitable cladding mode [177-179], thus any change in the cladding modes will cause a different core wavelength to match the coupling conditions in (2.2) and hence will determine the wavelengths at which core to cladding coupling will take place [180-183].
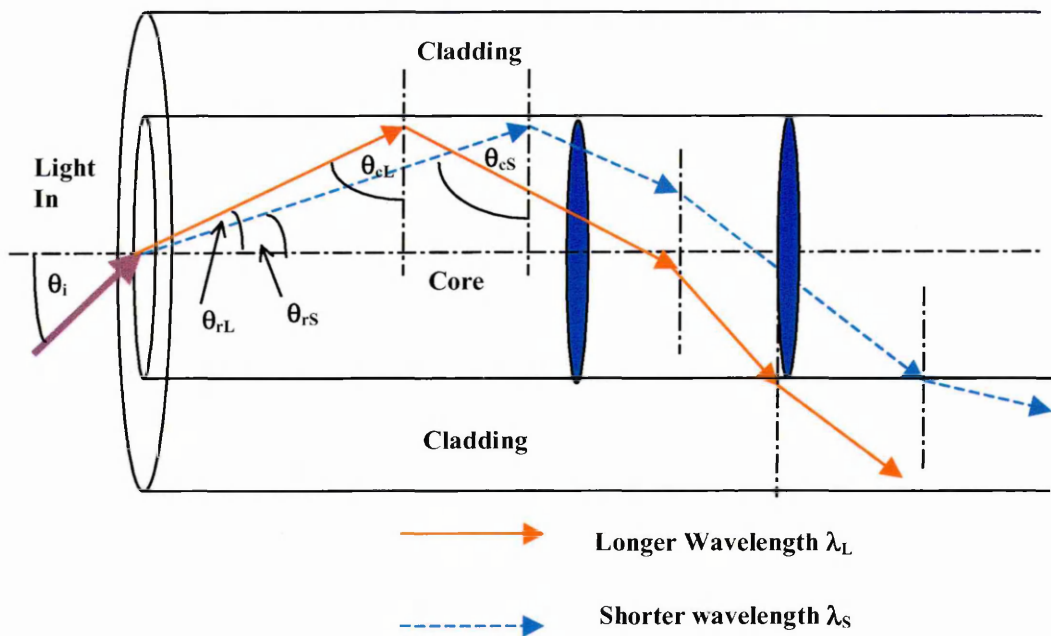
Figure 2.11:   Wavelength dependency of ray paths and critical angles of light propagating through a fibre core.

As shown in Figure 2.11, the longer wavelengths in the core traverse at steeper reflection angles than the shorter wavelengths, since they are refracted less than the shorter wavelengths on entering the fibre core and have smaller critical angles θ_c (allowing steeper incidence angles for total internal reflection) [184].   Longer wavelengths are also diffracted through greater angles than shorter wavelengths and thus they will be incident on the core/cladding interface at steeper angles [185], causing them to couple to the higher order cladding modes, which themselves have steeper directions of propagation in the cladding [186-189]. As the reflectivity of the core/cladding interface reduces with the angle of incidence [190], these steeper rays will be attenuated more than the shorter wave lengths as a greater percentage of the energy will be transmitted out of the core into the more dispersive cladding. This condition and the fact that the propagation constants of the higher order cladding

25

modes are affected to a greater degree by ambient index change [191], generally leads to utilization of the higher order mode coupling in long period sensors [192].

It has been shown that the coupling wavelengths display greater shifts in the higher order cladding modes as the ambient index approaches the cladding index, than when the ambient index is much less than the cladding index [165,193]. When the ambient index reaches that of the cladding the attenuation of the longer core wavelengths which couple to the higher order cladding modes is greatly reduced to almost negligible proportions, (as in this situation there are then no existing cladding modes into which the wavelengths in the core mode can couple) not increased as would be expected for a now almost infinite cladding. However, as the ambient index increases above that of the cladding, the coupling wavelengths again begin to be attenuated, but can be seen to have shifted back to values similar to the coupling wavelengths in air. As the ambient refractive index increases further a slight red shift is evident, but the greatest detectable effect is the gradual increase in the attenuation of these coupling wavelengths.

Another aspect of the LPG has been reported where the LPG is utilized in the reflective mode, using higher order harmonics of the broadband source [194]. This allows more tolerance in the source wavelength range and more selectivity of the wavelength(s) to be monitored, rather than the more accurate matching of wavelength and grating as in normal fibre Bragg grating reflective strain or temperature sensing. But as the light is confined to the core, the ambient refractive index should not affect these propagation conditions, a consideration which may prevent the use of this in the development of a gas sensor.

2.6 Signal Processing

The vast majority of the published data are based on laboratory experiments where the wavelength shifts using an optical spectrum analyzer have been detected. No references as to how the signal would be processed for an actual operational sensor are provided. Methods proposed for capturing and processing the output signal include the use of:

i)   optical filters [195] in which a wavelength band of the transmitted radiation will be selected via an optical filter placed at the exit of the fibre and directed onto an optical detector. Thus any shift in the transmitted wavelength will result in a change in the flux density of the radiation incident on the detector and a corresponding change in detector current. The problem with this method is that there may be uncertainty in the direction of shift, and if the shift is too great the signal may disappear entirely.

ii)   wavelength selective optical detectors [196,197]which would show a change in detector current as the transmitted wavelength shifts.

iii)   charged coupled device (CCD) arrays [198-200] in which each CCD detector would be positioned such that it would detect the intensity of a given wavelength after the transmitted light has been split into its spectrum via a diffraction grating or prism.

iv)   co-ordinated wavelength sweeping lasers with broad sensitivity optical detectors [201], in which the laser wavelength would be swept over a given range whilst the detector current output is coordinated with the wavelength of the transmitted radiation.

2.7 Computer Simulations

Several papers [202,203] show comparisons between computer simulated results and the actual experimental results, but give very little information on what methods were used in the simulation calculations. Analytical techniques used to model the modes in the core and cladding, which may be used in computer simulations seem to be split into two schools of thought. The first [204,205] treats the cladding as a multimode fibre core when calculating the properties of the cladding modes, whilst the other [206] takes the refractive indices of both the core and the cladding into account. The former method uses a much simpler expression than the latter, accepting and allowing for the errors introduced by the fact that the effect of the core index on the cladding modes is ignored. The latter, however, is a more accurate but far more complicated expression. Attempts have been made to reproduce the results from one of the few papers found which actually shows the calculations used to determine the mode coupling wavelengths and attenuation. However, errors were uncovered in the quoted expression [207], and corrected by inspection of another publication [205] referenced by the author.

2.8 Summary

This chapter has reviewed the existing types of sensors highlighting the advantages and disadvantages of each, explaining the characteristics of the fibre which are utilised and the disadvantages for use as a gas sensor inherent to their design. The theory of fibre Bragg gratings, the long period grating, and suitable methods of signal processing have been briefly discussed. Finally the equations used in the computer programs designed as part of this investigation were introduced.

Chapter 3

Theory

3.1 Introduction

The following chapter explains the theory of light propagation in optical fibres and the effects any inconsistencies in the optical or physical parameters may have on the propagation characteristics.

Section 3.2 gives the requirements which need to be met for light to undergo total internal reflection (TIR) and therefore be guided along the fibre length. Section 3.3 explains how modes are formed in the fibre, the classification of these modes being discussed in Section 3.4. In Section 3.5 the equations predicting the characteristics of

light propagation are derived from Maxwell's Equations. These equations are then applied to the light rays in optical fibres in Section 3.6, and the mathematical derivation progresses to mode classification in Section 3.7. Section 3.8 explains the concept of the evanescent field which is an important consideration in light propagation in optical fibres. Section 3.9 briefly introduces coupled mode theory, which is the concept used to explain energy transfer between modes in fibre gratings. Fibre Bragg grating theory is discussed in Section 3.10, one major aspect of which, the effective refractive index, being covered thoroughly in Section 3.11. Finally, Section 3.12 introduces the theory behind long period gratings, with the effect of changes in ambient index on the mode coupling and the intensity of this coupling being explained in Sections 3.13 and 3.14 respectively.

3.2 Light Propagation Within an Optical Wave Guide

An optical wave guide consists of a central glass core and a surrounding glass cladding, the core being of slightly higher refractive index than the cladding [175,208] as shown in Figure 3.1.
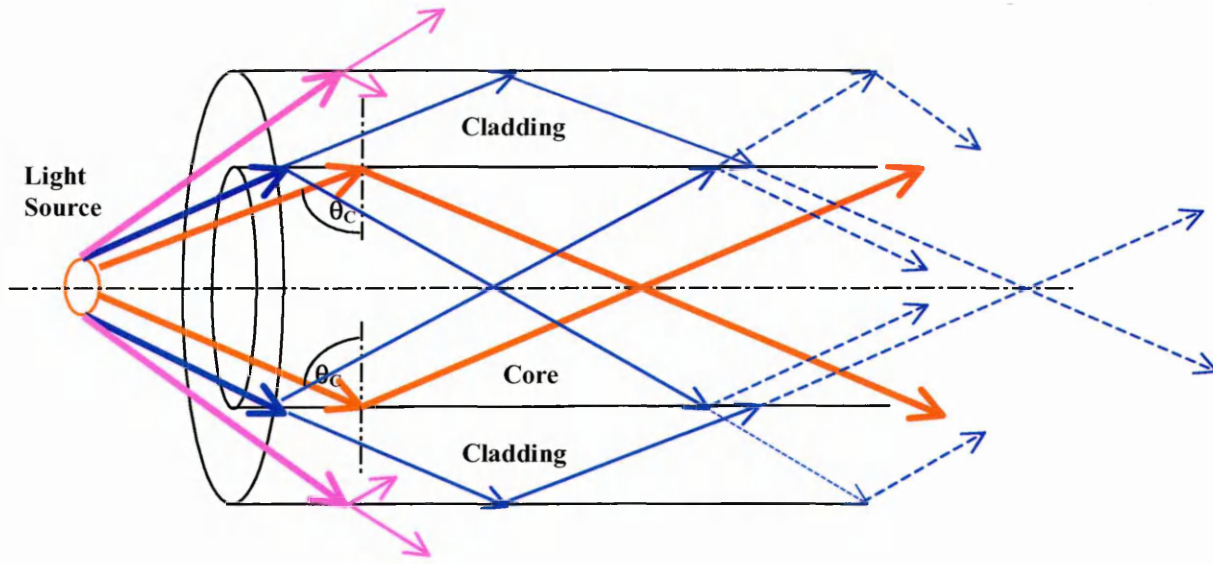
Figure 3.1:   Incident angle dependency of ray paths in optical fibre

As light is launched into the core it will enter the core at a continuum of incident angles limited only by the solid angle between the source and the fibre aperture [209-214].   Light entering the core which is incident on the core/cladding interface at angles less than the critical angle will be partially reflected back into the core and partially transmitted into the cladding [215], whilst light incident on the core cladding interface at angles greater than the critical angle will undergo total internal reflection (TIR) and remain within the core [216]. The partially reflected light remaining in the core will undergo the same partial effects each time it meets the core cladding interface as it travels along the fibre until, after only a short distance, the reflected fraction of the light is negligible within the core. The partially transmitted light in the cladding will undergo a similar process as the light within the core. Depending on the critical angle at this interface, it will undergo TIR or be partially reflected back into the cladding and partially transmitted into the air. The light leaving the cladding is immediately lost from the fibre, whilst the partially reflected light will again undergo the same effect each time it meets the cladding/air interface until the reflected fraction is again negligible.   The light in the cladding which experiences TIR at the

cladding/air boundary, however, will travel along the wave guide being partially transmitted and partially reflected to and from the core and the cladding each time it is incident on the core/cladding interface. The cladding is more dispersive than the core [177] and as such each time the light re-enters the cladding more and more will be attenuated until its effect is negligible in the wave guide [217]. Thus, after only a very short distance, the only guided rays travelling along the wave guide are those which enter the core at angles greater than the critical angle of the core/cladding interface.

3.3 Formation of Modes

The guided radiation propagating along the fibre core reflects back and forth from the core/cladding interfaces thus experiencing interference as shown in Figure 3.2.
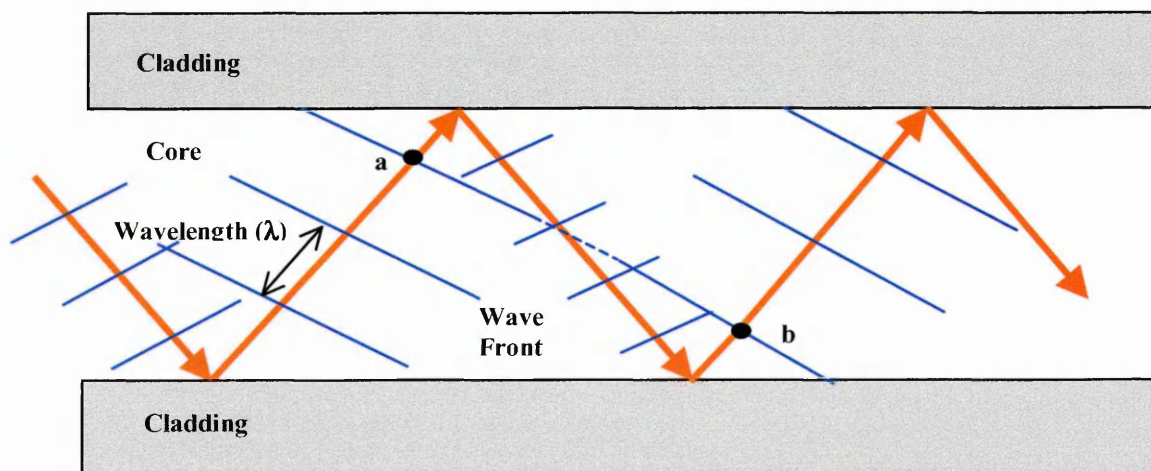
Figure 3.2:   Mode formation in optical wave guides

If the optical path length (a to b) after reflections from 2 successive boundaries is a whole number of wavelengths, then the interference will be totally constructive and the light will travel through the fibre at this angle of propagation [218]. However, if the distance is not a whole number of wavelengths then the interference will be destructive. The light intensity attenuates at each reflection until after a short distance no light will be evident at any angle of propagation other than the angles at which constructive interference occurs. Depending on the diameter and optical properties of the core and cladding, the core may allow the possibility of one or many directions in which this condition may be satisfied. These directions are known as modes [46] and are given numerical values from 0 for the first mode to one less than the maximum number existing in the core. As the numerical value increases the angle of incidence at the core cladding boundary decreases [219] (the ray follows a steeper path within the core). Thus the light forms travelling waves reflecting back and forth in modes along the length of the wave guide [220]. As the light propagates, however, interference will not only occur between the rays reflected from successive interfaces to form the modes, but also between those incident and reflected from the same interface in each modal direction [220]. This will form a standing wave across the core as shown in Figures 3.3 and 3.4 and its electric field intensity pattern will depend on the mode number. The mode number is determined by the number of times the transverse standing wave pattern contains zero amplitude across the fibre [218,221-224].
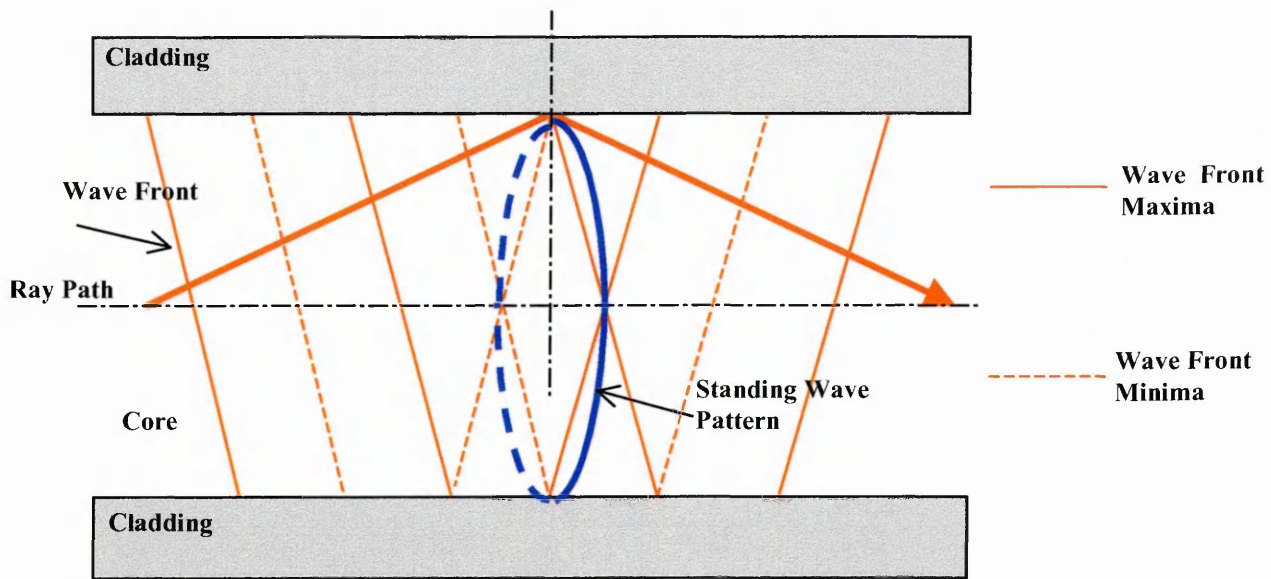
Figure 3.3: Transverse electric field pattern of the first mode m=0
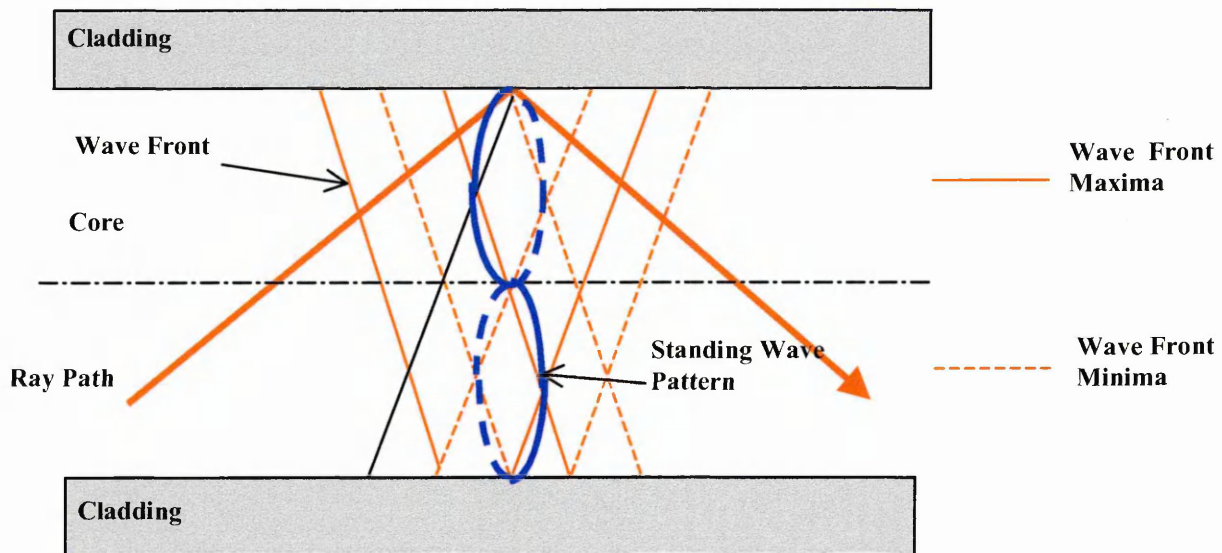
Figure 3.4: Transverse electric field pattern of the second mode m=1

35

3.4 Mode Classification in Optical Fibres

Since the fibres utilised in long period gratings are single mode, understanding of the modal structure is an important part of this report.

Light travels through a medium as an electromagnetic disturbance that has both electric (E) and a magnetic (H) fields which are orthogonal to each other and to the direction of propagation [225-229], as shown in Figure 3.5.
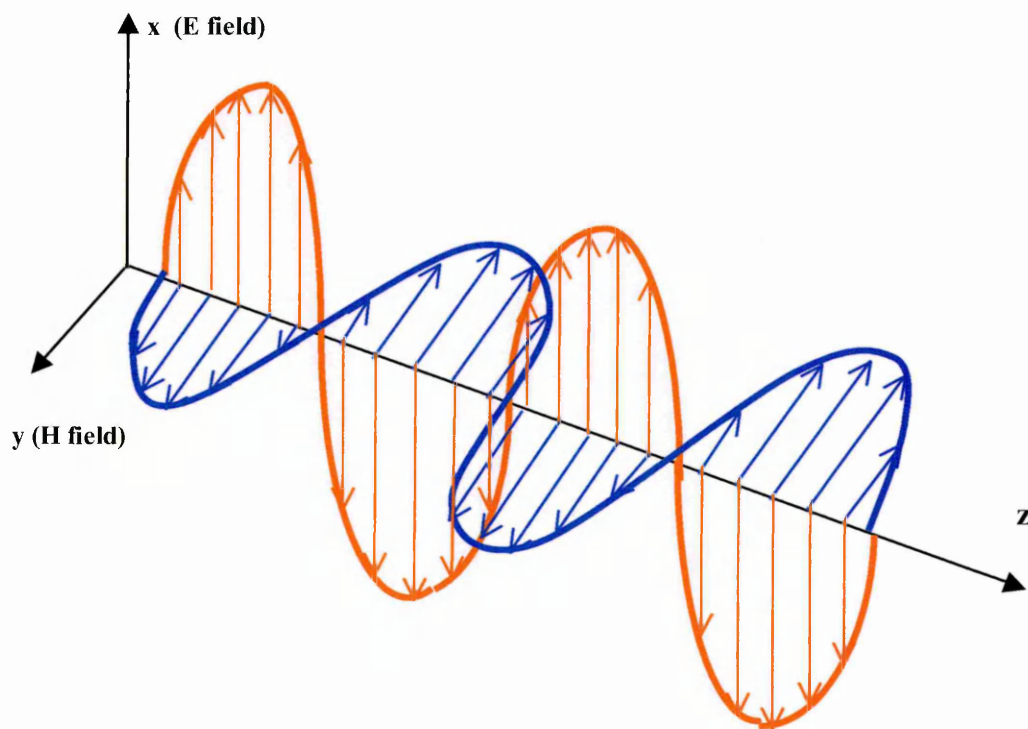
Figure 3.5:   Electro-magnetic wave propagation

As light enters the fibre core in the form of a conical beam it will propagate over a range of 360° about the core axis [209-214]. The magnetic and electric field vectors will therefore be in various orientations perpendicular to the actual direction of travel. As the light is reflected back and forth along the core, the overall direction of the ray

36

is along the core axis, thus the electric and magnetic vectors may not necessarily be perpendicular to this direction of propagation. These field directions (with respect to the general direction of propagation) determine the classification of the mode [230].

i)   Transverse electric (TE) modes:

Modes in which the electric vector has no component along the fibre axis as shown in Figure 3.6.
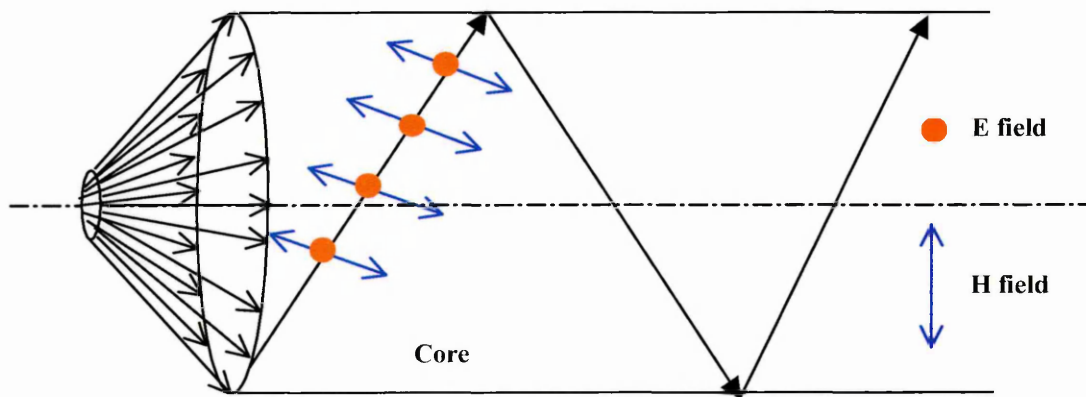
Figure 3.6:   Transverse electric (TE) mode field orientation

ii)   Transverse magnetic (TM) modes:

Modes in which the magnetic vector has no component along the fibre axis as shown in Figure 3.7.
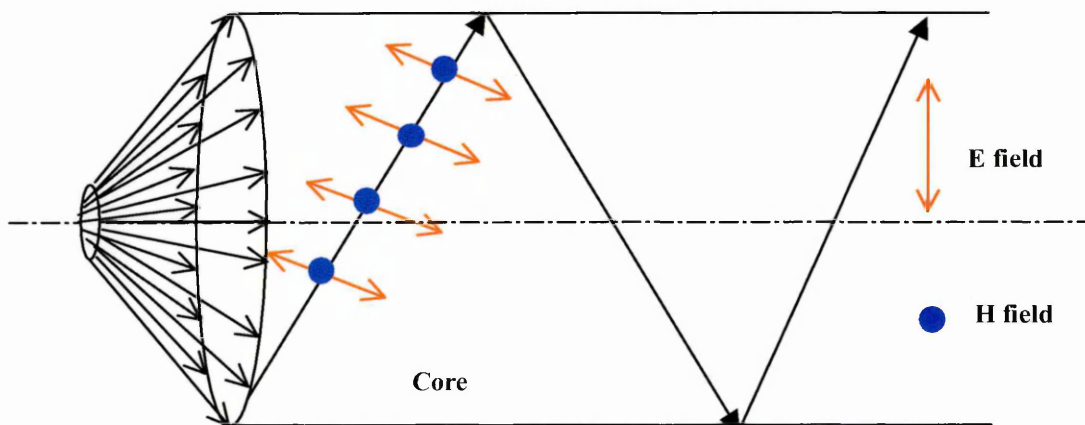
Figure 3.7:   Transverse magnetic (TM) mode field orientation

The probability of a mode having its electric or magnetic vector exactly transverse to the fibre axis as shown in Figures 3.6 and 3.7 is extremely slight (unless polarised light is used). Effectively the modes split into TE and TM components, length of each component determining the intensity of each. The path of the two different modes will differ due to the fact TE and TM modes experience different phase changes on reflection at the core/cladding boundary [231].

iii)   Skew modes:

TE and TM modes intersect the core axis as they reflect back and forth along the core. But there are other paths within the guided modes of the core which never cut the axis and which will be much more prevalent than the TE or TM modes [232] due to the greater range of possible propagation angles available. Obviously these modes will never have either field totally orthogonal to the core axis (as the electric and magnetic vectors must always be orthogonal to the direction of propagation). They will always have components in both the transverse and longitudinal directions in the core. These are known as skew modes or hybrid modes and are designated as HE (if the magnetic field has a greater value in the direction orthogonal to the core axis) and EH (if the electric field has a greater value in the direction orthogonal to the core axis) modes [188,233,234].

iv)   Linearly Polarised (LP) modes:

If the refractive index difference between the core and the cladding is very small ($\Delta n \ll 1$) the radiation in the core is said to be weakly guided and the 'weakly guiding approximation' can be used to describe the modes [235-237]. In this approximation the differences between the phase changes on reflection at the optical boundary of

certain types of modes are so small that they may effectively be neglected, and modes for which the components of the electric field in the transverse direction are of the same distribution are grouped together as a family of linearly polarised modes [238]. For the weakly guiding condition each family of LP modes have the same intensity distribution of the electric field across the core and hence the same intensity pattern.

v)   Mode indexing (mode designation):

Modes in slab wave guides are effectively infinite in one of the transverse directions (x or y) and therefore will have no mode component in that direction [239,240]. These have only one subscript number to signify the mode number, such as TE_m and TM_m. The lowest mode which travels at the shallowest grazing angle is labelled as m = 0. Figures 3.3 and 3.4 show the standing waves perpendicular to the fibre core formed by the first two TE_m modes, TE_0 and TE_1.

In optical fibres, having cylindrical geometry, light propagates in all directions of 360° through the core, therefore it is necessary to use two subscript values to identify the modes such as: LP_{Ml}, TE_{ml}, TM_{ml}, HE_{ml}, and EH_{ml}. When using the LP notation, the M subscript signifies half the number of field maxima in a 360° rotation about the core axis, while the l subscript signifies the number of field maxima along a radius [241].

M Half No of Maxima In 360°	l No of Maxima along Radius	LP mode Ml	Actual Mode ml	E Field Pattern
0	1	LP_{01}	HE_{11}	
1	1		TE_{01}	
1	1	LP_{11}	TM_{01}	
1	1		HE_{21}	
2	1		EH_{11}	
2	1	LP_{21}	HE_{31}	

Figure 3.8:   Mode patterns and designations for different types of modes

Figure 3.8 shows the mode patterns of the first six modes in a fibre and the notation used to describe them [242]. The subscripts on the traditional mode notation can be converted to the LP notation by the following [241,243]:

For HE_{ml} modes $\qquad$ M = m-1 $\qquad$ so $\quad HE_{ml}$ $\quad \rightarrow \quad$ $LP_{Ml} = LP_{m-1\ 1}$

For EH_{ml} modes $\qquad$ M = m+1 $\qquad$ so $\quad EH_{ml}$ $\quad \rightarrow \quad$ $LP_{Ml} = LP_{m+1\ 1}$

For TE_{nm} & TM_{ml} modes $\quad$ M = m+ 1 $\qquad$ so $\quad TE_{ml}$ $\quad \rightarrow \quad$ $LP_{Ml} = LP_{m+1\ 1}$

$$TM_{ml} \quad \rightarrow \quad LP_{Ml} = LP_{m+1\ 1}$$

40

In TE and TM modes m and M can only have a value of 0 and 1 respectively [244]. The number of modes available within a fibre and their respective directions of propagation is predicted by (3.1) [245-247] and can be derived from first principles using Maxwell's equations given as shown in section 3.7:

$$\left(\frac{J'm(u)}{uJm(u)}+\frac{K'm(w)}{wKm(w)}\right)\left(n_1^2\frac{J'm(u)}{uJm(u)}+n_2^2\frac{K'm(w)}{wKm(w)}\right)=\frac{\beta^2m^2}{k^2}\left(\frac{1}{u^2}+\frac{1}{w^2}\right)^2 \qquad (3.1)$$

where :

Jm is the mth order Bessel function of the first kind

$J'm$ is the first derivative (wrt radius) of the mth order Bessel function of the first kind

Km is the mth order modified Bessel function of the first kind

$K'm$ is the first derivative (wrt radius) of the mth order modified Bessel function of the first kind

n_1 is the refractive index of the guiding medium

n_2 is the refractive index of the surrounding medium

u is the normalised transverse phase constant (normalised propagation constant) in the guiding medium ($=r\sqrt{kn_1-\beta}$)

w is the normalised transverse attenuation constant (normalised propagation constant) in the surrounding medium ($=r\sqrt{\beta-kn_2}$)

β is the propagation constant in the guiding medium ($=kn_1\sin\theta$)

k is the wave number ($=2\pi/\lambda$)

θ is the incident angle at the refractive index boundary of the guiding medium

r is the radius of the guiding medium

m is the mode number

The formulae describing each family of modes in the core and cladding can be derived by manipulation of (3.1) as outlined in Section 3.5. As previously stated, the diameter and characteristics of the core and the wavelength of the light determine how many modes can exist in the core. Fibres which can support more than one mode at a given wavelength are known as multimode fibres, and those that can support only one mode are known as single mode or monomode at a given wavelength.

The HE_{11} mode (m=1 $\rightarrow$ J_{m-1} $\rightarrow$ J_0) is the only mode which will generate the J_0 Bessel function, as the TE, TM, and EH modes all involve the J_{m+1} Bessel function, the subscipt of which can never be 0 as m cannot be a negative value. This J_0 Bessel function has no cut off value and will therefore always exist within a fibre regardless of core size, and therefore this mode must be the only mode in existence in a single mode fibre [242,248,249]. Also as the difference between the core and cladding indices is very small the weakly guiding approximation can be used when calculating this core mode, (3.1) can be manipulated to generate equation (3.2).

$$\left(\frac{J'm(u)}{uJm(u)}+\frac{K'm(w)}{wKm(w)}\right)\left(\frac{n_1^2}{n_2^2}\frac{J'm(u)}{uJm(u)}+\frac{K'm(w)}{wKm(w)}\right)=\frac{n_{eff}^2 m^2}{n_2^2}\left(\frac{1}{u^2}+\frac{1}{w^2}\right)^2 \qquad (3.2)$$

The equation in this form allows the following weakly guiding approximation (3.3) to be introduced into the standard equation describing the propagation of modes in a fibre [250,251]:

$$as \quad \frac{n_1^2}{n_2^2} \approx \frac{n_{eff}^2}{n_2^2} \approx 1 \qquad (3.3)$$

This allows (3.2) to be reduced to the much simpler (3.4) for weakly guided core modes, where the right hand side can have positive or negative values [252-254].

$$\left(\frac{J'm(u)}{uJm(u)} + \frac{K'm(w)}{wKm(w)}\right) = \pm m \left(\frac{1}{u^2} + \frac{1}{w^2}\right) \tag{3.4}$$

The formulae describing each family of modes in the core can be derived by manipulation of this weakly guiding equation as shown in Section 3.5.

A fibre normally stated to be single mode at a given wavelength (λ_0) will also be single mode at wavelengths longer than that wavelength, but at a certain shorter wavelength (cut off wavelength) it will become possible for more than one mode to exist [255-260]. The number of possible modes increases as the wavelength decreases below the cut off wavelength. Since the refractive index and the allowed angles of propagation of the light in a fibre core (modes) are wavelength dependent, then the fibre can be single mode for all wavelengths greater than the cut-off wavelength and the allowed angles of propagation (modes) will be different for each wavelength. Since no light source can be truly monochromatic [261] the light launched into a fibre will consist of a range of wavelengths, each of which will have different mode angles of propagation, even though the fibre is still operating in single mode. Thus the single mode fibre can be thought to transmit one mode of light, effectively separated into submodes for each wavelength for which the fibre operates as single mode. Core modes may be considered as the allowed angles at which light within a core will propagate [262], suggesting that the modes only exist in a fibre when the light is actually travelling in those modes. However, it may be more convenient to think of modes as allowed paths which light of a given wavelength would follow if that wavelength were present in the core. Thus in a core of given characteristics there are quantized directions which are always available for a given wavelength whether that wavelength is contained in the spectrum of the light in the

core or not. Even though the light which enters the fibre cladding will be quickly attenuated as previously explained, it follows from the previous paragraph that the cladding will also have allowed paths which light of a given wavelength may take if it were present in the cladding. As the cladding is of much greater diameter than the core, it will always be multimode even for wavelengths at which the core is single mode.

In an ideal fibre the individual modes should travel indefinitely along the length of the fibre without affecting each other. However, in a real fibre, bends, or dimensional or material inconsistencies can cause the light to couple between the various modes [263]. In a monomode core the light has no further forward propagating core modes into which it can couple, but a change in the core or cladding parameters will cause the direction in which constructive interference at each wavelength occurs and thus the angle of propagation of the modes. It is possible therefore to modify the core or cladding in order to promote mode coupling. One method is to create a periodic refractive index perturbation in the core, of such spacing that it will diffract the incident radiation through a given angle. If the period of the grating is around half of a wavelength in the transmission spectrum, it will diffract that wavelength into its reverse propagating core mode. As the period is increased the angle of diffraction will decrease causing the core mode to couple into reverse propagating cladding modes, radiation modes, and finally forward propagating cladding modes [264]. The first and last conditions in the above order of mode coupling are used in the fibre Bragg grating and the long period grating respectively. It is logical therefore to conclude that any coupling between core and cladding modes will be dependent on the modal structure in the cladding, as well as that of the core. The refractive index of

the medium surrounding the cladding will not only determine the critical angle at that interface [265], but more importantly the phase change on reflection [266] which will affect the optical path lengths of each wavelength and the directions in which constructive interference will take place, and therefore control the mode structure. This will in turn determine the wavelengths at which core to cladding mode coupling will occur. The ambient index dependency of the mode coupling in this long period diffraction grating is the underlying aspect of this thesis.

3.5 Derivation of Light Propagation Equations from Maxwell's Equations

The derivations in this section and sections 3.6 and 3.7 follow that of Okushi [204], with more in depth explanations of the relevant aspects. Maxwell's Equations for isotropic, linear, non-conducting, and non-magnetic medium are given in the following four definitions [267-271]:

Maxwell's first equation (Gauss's Law for Electricity):

$$\nabla.E = \nabla.D = \frac{\rho_c}{\varepsilon} = 0 \text{ for non-conducting medium} \qquad (3.5)$$

Maxwell's second equation (Gauss's Law for magnetism)

$$\nabla.B = 0 \text{ or } \nabla.H = 0 \qquad (3.6)$$

Maxwell's third equation (Faradays Law of Induction)

$$\nabla \times E = -\frac{\partial B}{\partial t} = -\mu_0 \frac{\partial H}{\partial t} \qquad (3.7)$$

Maxwell's fourth equation (Amperes Law)

$$\nabla \times H = \frac{\partial D}{\partial t} = \varepsilon_0 n^2 \frac{\partial E}{\partial t} \quad \text{or} \quad \nabla \times B = \mu_0 \frac{\partial D}{\partial t} = \mu_0 \varepsilon_0 n^2 \frac{\partial E}{\partial t} \qquad (3.8)$$

where

E = electric field = $D/\varepsilon_0 n^2$ $\qquad\qquad$ D = electric displacement = $E\varepsilon_0 n^2$

B = magnetic induction = $\mu_0 H$ $\qquad\qquad$ μ_0 = free space permeability

H = magnetic intensity = B/μ_0 = free space magnetic permeability $\quad Ns^2C^{-2}$

ε_0 = free space permittivity $\qquad\qquad$ $\varepsilon_0 n^2$ = dielectric permittivity of medium

ρ_c = current density

The equations describing the electric and magnetic fields of light take the form [272-277]:

$$E_\alpha = E_{\alpha 0} EXP\left[i(k.r - \omega t)\right] \text{ and } H_\alpha = H_{\alpha 0} EXP\left[i(k.r - \omega t)\right]$$

where $\alpha = (x,y,z)$, $k = (k_x, k_y, k_z)$, $r = (x,y,z)$ and $k.r = (k_x x + k_y y + k_z z)$.
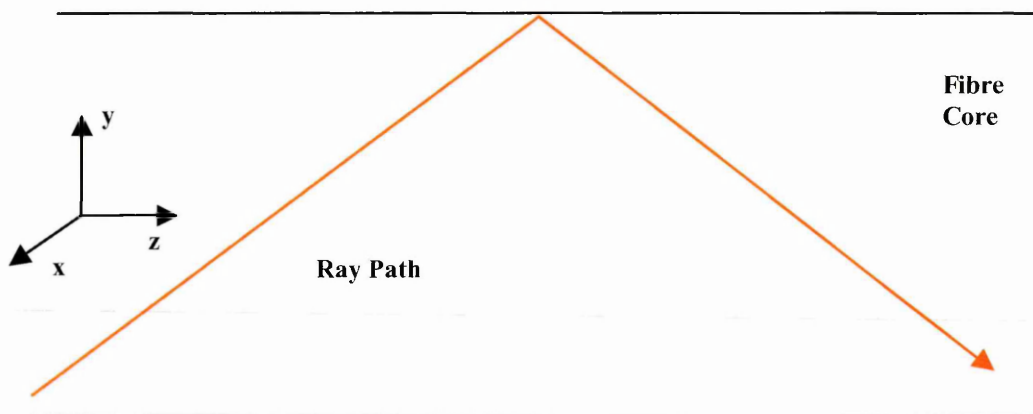
Figure 3.9: **Cartesian coordinates of light in optical fibre**

The cartesian components of the electric (E_x, E_y, E_z) and magnetic (H_x, H_y, H_z) vectors as shown in Figure 3.9 can be obtained by examination of Maxwell's third and fourth equations, equations (3.7) and (3.8).

Maxwell's 3rd Equation (3.7) expands to give:

$$\left(\frac{\partial}{\partial x}, \frac{\partial}{\partial y}, \frac{\partial}{\partial z}\right) \times E_{(x,y,z)} = -\mu_0 \frac{\partial}{\partial t} H_{(x,y,z)}$$

$$\left(\frac{\partial E_z}{\partial y} - \frac{\partial E_y}{\partial z}, \frac{\partial E_x}{\partial z} - \frac{\partial E_z}{\partial x}, \frac{\partial E_y}{\partial x} - \frac{\partial E_x}{\partial y}\right) = -\mu\left(\frac{\partial H_x}{\partial t}, \frac{\partial H_y}{\partial t}, \frac{\partial H_z}{\partial t}\right)$$

where $\quad E_x = E_{x0}\exp[i(k.r-\omega t)] \qquad\qquad H_x = H_{x0}\exp[i(k.r-\omega t)]$

$\qquad\qquad\quad E_y = E_{y0}\exp[i(k.r-\omega t)] \qquad\qquad H_y = H_{y0}\exp[i(k.r-\omega t)]$

$\qquad\qquad\quad E_z = E_{z0}\exp[i(k.r-\omega t)] \qquad\qquad H_z = H_{z0}\exp[i(k.r-\omega t)]$

Most applications of Maxwell's Equations assume that the ray is travelling axially in the z direction. If this were the case there would be no variation in the electric field in any direction (x or y) perpendicular to the axis (z), and the differentials with respect to x and y would be zero

$$\frac{\partial E_y}{\partial x} = \frac{\partial E_x}{\partial y} = 0$$

Also there would be no component of the electric or magnetic fields along the axis in the z direction and the z components of the electric field would also be zero

$$\frac{\partial E_z}{\partial y} = \frac{\partial E_z}{\partial x} = \frac{\partial H_z}{\partial x} = 0$$

This would reduce the previous equation to:

$$\left(-\frac{\partial E_y}{\partial z}, \frac{\partial E_x}{\partial z}, 0\right) = -\mu\left(\frac{\partial H_x}{\partial t}, \frac{\partial H_y}{\partial t}, 0\right)$$

In optical fibres the ray is not travelling directly along the fibre axis in the z direction, Thus the change in the electric field in the transverse x and y directions will not be zero as they would for axial rays and all components must be accounted for in this special case.

Equating components in each of the brackets gives

$$\frac{\partial E_z}{\partial y} - \frac{\partial E_y}{\partial z} = -\mu_0 \frac{\partial H_x}{\partial t} \qquad (3.9)$$

$$\frac{\partial E_x}{\partial z} - \frac{\partial E_z}{\partial x} = -\mu_0 \frac{\partial H_y}{\partial t} \qquad (3.10)$$

$$\frac{\partial E_y}{\partial x} - \frac{\partial E_x}{\partial y} = -\mu_0 \frac{\partial H_z}{\partial t} \qquad (3.11)$$

Differentiating E_y wrt z and H_x wrt t in equation (3.9) yields:

$$\frac{\partial E_z}{\partial y} + i\beta E_y = -i\omega\mu_0 H_x \qquad (3.12)$$

where $\beta = k_z$

Differentiating E_x wrt z and H_y wrt t in equation (3.10) results in:

$$\frac{\partial E_z}{\partial x} + i\beta E_x = -i\omega\mu_0 H_y \qquad (3.13)$$

Differentiating H_z wrt t in equation (3.11) gives:

$$\frac{\partial E_y}{\partial x} - \frac{\partial E_x}{\partial y} = -i\omega\mu_0 H_z \qquad (3.14)$$

Similarly Maxwell's 4th equation (3.8) expands to give:

$$\left(\frac{\partial}{\partial x}, \frac{\partial}{\partial y}, \frac{\partial}{\partial z}\right) \times H_{(x,y,z)} = \varepsilon_0 n^2 \frac{\partial}{\partial t} E_{(x,y,z)}$$

$$\left(\frac{\partial H_z}{\partial y} - \frac{\partial H_y}{\partial z}, \frac{\partial H_x}{\partial z} - \frac{\partial H_z}{\partial x}, \frac{\partial H_y}{\partial x} - \frac{\partial H_x}{\partial y}\right) = -\varepsilon_0 n^2 \left(\frac{\partial E_x}{\partial t}, \frac{\partial E_y}{\partial t}, \frac{\partial E_z}{\partial t}\right)$$

Equating components in each of the brackets gives

$$\frac{\partial H_z}{\partial y} - \frac{\partial H_y}{\partial z} = \varepsilon_0 n^2 \frac{\partial E_x}{\partial t} \qquad (3.15)$$

$$\frac{\partial H_x}{\partial z} - \frac{\partial H_z}{\partial x} = \varepsilon_0 n^2 \frac{\partial E_y}{\partial t} \qquad (3.16)$$

$$\frac{\partial H_y}{\partial x} - \frac{\partial H_x}{\partial y} = \varepsilon_0 n^2 \frac{\partial E_z}{\partial t} \qquad (3.17)$$

Differentiating H_y wrt z and E_x wrt t in equation (3.15) gives:

$$\frac{\partial H_z}{\partial y} + i\beta E_y = i\omega\varepsilon_0 n^2 E_x \qquad (3.18)$$

Differentiating H_x wrt z and E_y wrt t in equation (3.16) gives:

$$-\frac{\partial H_z}{\partial x} - i\beta H_x = -i\omega\varepsilon_0 E_y \qquad (3.19)$$

Differentiating E_z wrt t in equation (3.17) gives

$$\frac{\partial H_y}{\partial x} - \frac{\partial H_x}{\partial y} = -i\omega\varepsilon_0 E_z \qquad (3.20)$$

The x and y components of both the electric and magnetic fields may now be expressed in terms of their respective z components by combinations of the equations (3.12), (3.13), (3.14), and (3.18), (3.19), (3.20).

To find E_x in terms of E_z and H_z, manipulating (3.13) to make H_y the subject and substituting into (3.18) gives the following result:

$$E_x = -\frac{i}{\beta_t^2}\left(\beta\frac{\partial E_z}{\partial x} + \omega\mu_0\frac{\partial H_z}{\partial y}\right) \qquad (3.21)$$

where $\beta_t = \sqrt{k^2 n^2 - \beta^2}$ is the transverse propagation constant (the component of the wave vector kn in the radial direction) [278], as shown in Figure 3.10.
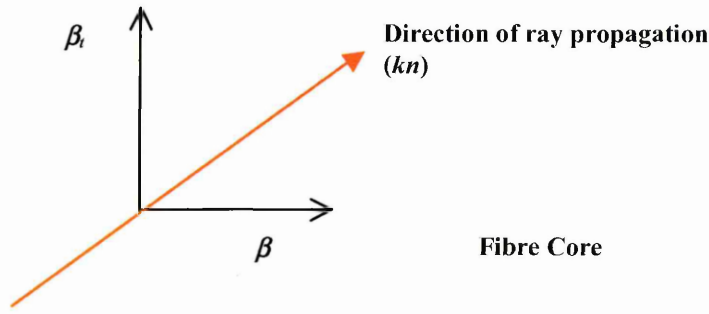
Figure 3.10:   Transverse propagation constant of light in fibre core

To find E_y in terms of E_z and H_z, manipulating (3.12) to make H_x the subject and substituting into (3.19) gives the following result:

$$E_y = -\frac{i}{\beta_t^2}\left(\beta\frac{\partial E_z}{\partial y} - \omega\mu_0\frac{\partial H_z}{\partial x}\right) \qquad (3.22)$$

To find H_x in terms of E_z and H_z, manipulating (3.19) to make E_y the subject and substituting into (3.12) gives the following result:

$$H_x = -\frac{i}{\beta_t^2}\left(\beta\frac{\partial H_z}{\partial x} + \omega\varepsilon_0\frac{\partial E_z}{\partial y}\right) \qquad (3.23)$$

To find H_y in terms of E_z and H_z, manipulating (3.19) to make E_y the subject and substituting into (3.13) gives the following result:

$$H_y = -\frac{i}{\beta_t^2}\left(\beta\frac{\partial H_z}{\partial y} - \omega\varepsilon_0\frac{\partial E_z}{\partial x}\right) \qquad (3.24)$$

All components describing the electric and magnetic fields are now expressed in terms of the axial direction of propagation z.

Solutions of E_z and H_z are obtained by solutions to the differential equations previously derived as follows:

Substituting (3.23) and (3.24) into (3.20) and differentiating gives

$$\frac{\partial^2 E_z}{\partial x^2} + \frac{\partial^2 E_z}{\partial y^2} + \beta_t^2 E_z = 0 \qquad (3.25)$$

Substituting (3.23) and (3.24) into (3.14) and differentiating gives

$$\frac{\partial^2 H_z}{\partial x^2} + \frac{\partial^2 H_z}{\partial y^2} + \beta_t^2 H_z = 0 \qquad (3.26)$$

The equations (3.21) to (3.26) describe the three dimensional wave propagation in cartesian coordinates. As the fibre is of cylindrical geometry these equations can be expressed in cylindrical coordinates [279-282], as shown below:

$$E_r = -\frac{i}{\beta_t^2}\left(\beta\frac{\partial E_z}{\partial r} + \omega\mu_0\frac{1}{r}\frac{\partial H_z}{\partial \theta}\right) \qquad (3.27)$$

$$E_\theta = -\frac{i}{\beta_t^2}\left(\beta\frac{1}{r}\frac{\partial E_z}{\partial \theta} - \omega\mu_0\frac{\partial H_z}{\partial r}\right) \qquad (3.28)$$

$$H_r = -\frac{i}{\beta_t^2}\left(\beta\frac{\partial H_z}{\partial r} + \frac{1}{r}\omega\varepsilon_0\frac{\partial E_z}{\partial \theta}\right) \qquad (3.29)$$

$$H_\theta = -\frac{i}{\beta_t^2}\left(\beta\frac{1}{r}\frac{\partial H_z}{\partial \theta} - \omega\varepsilon_0\frac{\partial E_z}{\partial r}\right) \qquad (3.30)$$

$$\frac{\partial^2 E_z}{\partial r^2} + \frac{1}{r}\frac{\partial E_z}{\partial r} + \frac{1}{r^2}\frac{\partial^2 E_z}{\partial \theta^2} + \beta_t^2 E_z = 0 \qquad (3.31)$$

$$\frac{\partial^2 H_z}{\partial r^2} + \frac{1}{r}\frac{\partial H_z}{\partial r} + \frac{1}{r^2}\frac{\partial^2 H_z}{\partial \theta^2} + \beta_t^2 H_z = 0 \qquad (3.32)$$

Solving equations (3.31) and (3.32) by separation of variables of the form $E_z = R_z(r)\Theta_z(\theta)$ results in:

$$\frac{d^2 R}{dr^2} + \frac{1}{r}\frac{dR}{dr} + R\left(\beta_t^2 - \frac{m^2}{r^2}\right) = 0 \qquad \Theta_z(\theta) = \cos m\theta \text{ or } \sin m\theta \quad (3.33)$$

This is known as a Bessel differential equation which has the solutions given as:

$$R_z(r) = AJ_m(\beta_t r) + A'N_m(\beta_t r) \text{ for real } \beta_t \qquad (3.33a)$$

$$R_z(r) = CK_m(|\beta_t|r) + C'I_m(|\beta_t|r) \text{ for imaginary } \beta_t \qquad (3.33b)$$

where $R_z(r)$ = the radial field function

m = the azimuthal mode number

A,A',C,C' = arbitrary constants

J_m, = mth order Bessel function of the first kind

N_m = mth order Bessel function of the second kind

K_m = mth order modified Bessel function of the first kind

I_m = mth order modified Bessel function of the second kind

Bessel functions of the first kind are oscillatory (with gradual damping) with respect to the radius, whereas the modified Bessel functions of the first kind decay exponentially with respect to the radius. Bessel functions of the second kind are not significant in the theory of uniform fibres [204].

3.6 Application of Propagation Equations to Optical Fibres

The light propagation equations can be applied to the determination of the modal structure of an optical fibre providing the boundary conditions of the optical fibre are observed.
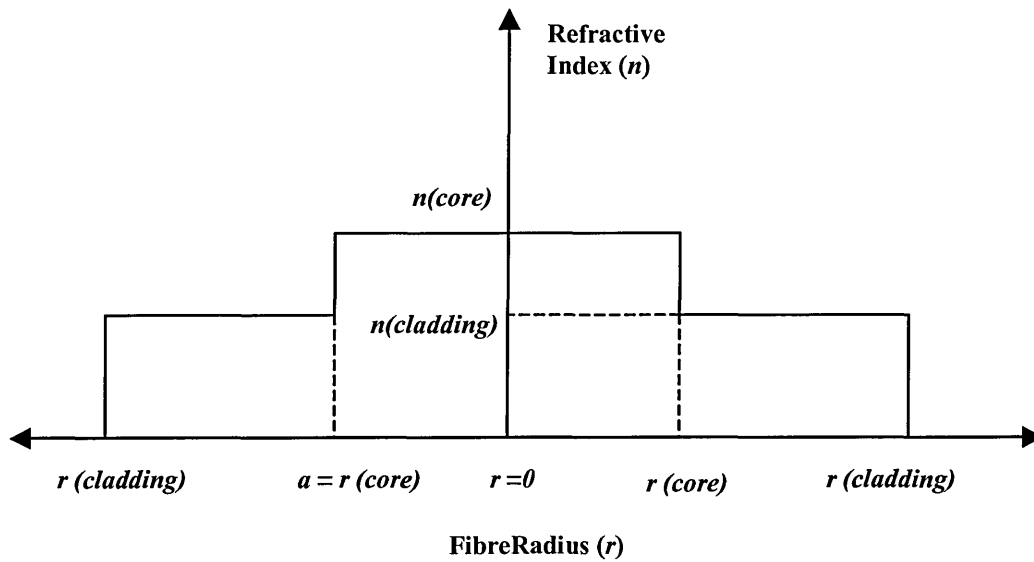
Figure 3.11: Refractive index profile of an optical fibre core and cladding

Figure 3.11 shows a graphical representation of the refractive index profile of an optical fibre. The boundary conditions at the core/cladding interface apply to all optical fibres and are as follows:

- Axial electric and magnetic field components in the core and cladding must be of equal magnitude at the core/cladding boundary:

$$E_z^{core} = E_z^{clad}, \qquad H_z^{core} = H_z^{clad}$$

- Electric and magnetic field components in the propagation direction in the core and cladding must be of equal magnitude at the core/cladding boundary:

$$E_\theta^{core} = E_\theta^{clad}, \qquad H_\theta^{core} = H_\theta^{clad}$$

- Electric and magnetic field components in the radial direction in the core and cladding are dependent on the permittivity and permeability of the media and must be of equal magnitude at the core/cladding boundary:

$$\varepsilon_1 E_r^{core} = \varepsilon_2 E_r^{clad}, \qquad \mu_1 H_r^{core} = \mu_2 H_r^{clad}$$

53

In Cladding

For light energy to propagate axially (in z direction) in a uniform cylindrical waveguide core, being confined radially, the radial field function $R_z(r)$ must exponentially decay outside the core and in the cladding must therefore be of the form:

$$R_z(r) = CK_m\left(|\beta_t|r\right) + C'I_m\left(|\beta_t|r\right)$$

Since C' diverges as r tends to infinity it can then be discarded leaving

$$R_z(r) = CK_m\left(|\beta_t|r\right) \tag{3.34}$$

In Core

In the core region, solutions proportional to N_m or K_m cannot be present as they both diverge on the axis. Also as the boundary conditions require the core and cladding fields to be continuous, any I_m dependency in the core would prevent this condition. Thus the radial field function $R_z(r)$ in the core must therefore be of the form:

$$R_z(r) = AJ_m(\beta_t r) \tag{3.35}$$

The dependency of the radial field function can be seen to be:

$$R_z(r) \propto J_m \text{ in core}$$

$$R_z(r) \propto K_m \text{ in cladding}$$

As $\beta_t = \sqrt{k^2n^2 - \beta^2}$

For guided radiation in the core $kn_{core} \geq \beta \geq kn_{clad}$

Thus,

- $\beta_{t(core)} = \sqrt{k^2n_{core}^2 - \beta^2}$ will always be real as β will always be less than kn_{core}

    and

- $\beta_{t(clad)} = \sqrt{k^2 n_{clad}^2 - \beta^2}$ will always be imaginary as β will always be greater than kn_{clad}

To give the core and cladding transverse propagation constants radial dependency let

$u = a\beta_{t(core)}$ and $w = a|\beta_{t(clad)}|$,

thus $\qquad\qquad\qquad\qquad \beta_{t(core)} = u/a$ and $|\beta_{t(clad)}| = w/a$

so $\qquad\qquad\qquad\qquad u = a\sqrt{k^2 n_{core}^2 - \beta^2}$ and $w = a\sqrt{\beta^2 - k^2 n_{clad}^2}$

where u and w are the normalized transverse propagation constant and the normalized transverse attenuation constant in the core and cladding regions respectively and a is the radius.

3.7 Mode Classification
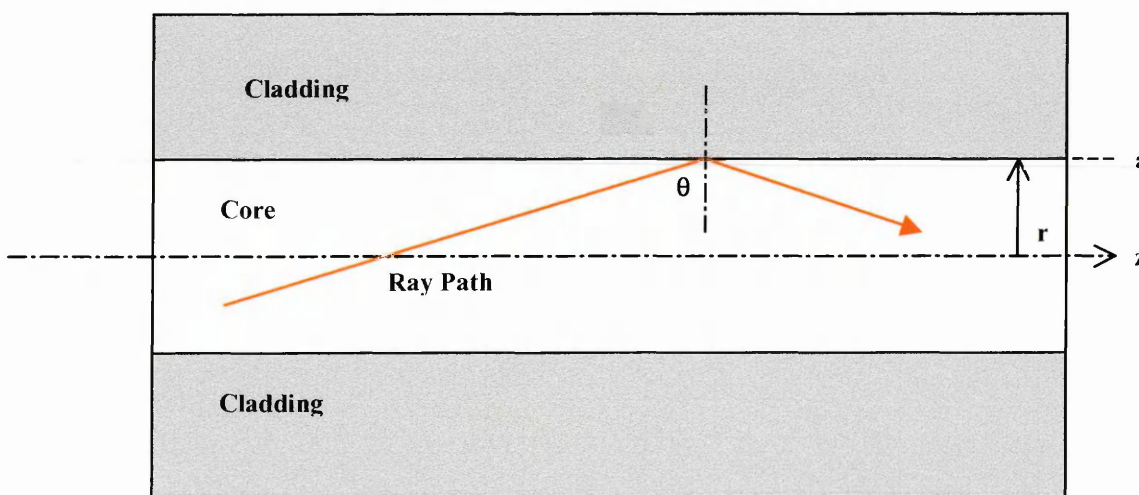
Figure 3.6.1:   Ray path of guided mode in optical fibre core

For Transverse Magnetic (TM) modes the electric and magnetic fields in the core and cladding can be described as follows:

$$E_{z(core)} = AJ_m \frac{ur}{a} \sin m\theta \qquad r \leq a \qquad (3.36a)$$

$$E_{z(clad)} = CK_m \frac{wr}{a} \sin m\theta \qquad r \geq a \qquad (3.36b)$$

$$H_{z(core)} = 0 \qquad\qquad\qquad (3.36c)$$

$$H_{z(clad)} = 0 \qquad\qquad\qquad (3.36d)$$

For Transverse Electric (TE) modes the electric and magnetic fields in the core and cladding can be described as follows::

$$E_{z(core)} = 0 \qquad\qquad\qquad (3.37a)$$

$$E_{z(clad)} = 0 \qquad\qquad\qquad (3.37b)$$

$$H_{z(core)} = BJ_m \frac{ur}{a} \cos m\theta \qquad r \leq a \qquad (3.37c)$$

$$H_{z(clad)} = DK_m \frac{wr}{a} \sin m\theta \qquad r \geq a \qquad (3.37d)$$

The sin term in the TM equations and the cos term in the TE equations allows for the connection of the fields at the core and cladding interface for hybrid modes.

In optical fibres TE and TM modes can only exist when $m = 0$, otherwise the boundary conditions at the core cladding interface can only be satisfied when one linear combination of TE and TM modes exists in the core and a different linear combination of TE and TM modes exists in the cladding. These linear combinations of modes are known as hybrid modes.

Combinations of (3.36a) to (3.37d) with (3.27) to (3.30) allow the determination of expressions for the general field components incorporating all the TE, TM and hybrid (HE, EH) modes.

3.7.1 Cylindrical Components of Electric and Magnetic Fields In the Core

The E_z and H_z dependencies are given in (3.36a) and (3.37c). The E_r and H_r dependencies are obtained by substituting (3.36a) and (3.37c) into (3.27) and (3.29) respectively and differentiating to obtain:

$$E_{r(core)} = \left[-A\frac{i\beta}{\frac{u}{a}}J'_m\left(\frac{ur}{a}\right) + B\frac{i\omega\mu_0}{\left(\frac{u}{a}\right)^2}\frac{m}{r}J_m\left(\frac{ur}{a}\right) \right]\sin m\theta \qquad (3.38)$$

$$H_{r(core)} = \left[A\frac{i\omega\varepsilon_{core}}{\left(\frac{u}{a}\right)^2}\frac{m}{r}J_m\left(\frac{ur}{a}\right) - B\frac{i\beta}{\frac{u}{a}}J'_m\left(\frac{ur}{a}\right) \right]\cos m\theta \qquad (3.39)$$

where the prime symbol (') is the differentiated form of the function with respect to r

The E_θ and H_θ dependencies are obtained by substituting both (3.36a) and (3.37c) into (3.27) and (3.30) respectively and differentiating to get

$$E_{\theta(core)} = \left[-A\frac{i\beta}{\left(\frac{u}{a}\right)^2}\frac{m}{r}J_m\left(\frac{ur}{a}\right) + B\frac{i\omega\mu_0}{\frac{u}{a}}J'_m\left(\frac{ur}{a}\right) \right]\cos m\theta \qquad (3.40)$$

$$H_{\theta(core)} = \left[-A \frac{i\omega\varepsilon_{core}}{\dfrac{u}{a}} J'_m\left(\frac{ur}{a}\right) + B \frac{i\beta}{\left(\dfrac{u}{a}\right)^2} \frac{m}{r} J_m\left(\frac{ur}{a}\right) \right] \sin m\theta \qquad (3.41)$$

3.7.2 Cylindrical Components of Electric and Magnetic Fields In the Cladding

The E_z and H_z dependencies are given in (3.36b) and (3.37d). The E_r and H_r dependencies are obtained by substituting these equations into equations (3.26) and (3.29) respectively and differentiating to obtain

$$E_{r(clad)} = \left[C \frac{i\beta}{\dfrac{w}{a}} K'_m\left(\frac{wr}{a}\right) - D \frac{i\omega\mu_0}{\left(\dfrac{w}{a}\right)^2} \frac{m}{r} K_m\left(\frac{wr}{a}\right) \right] \sin m\theta \qquad (3.42)$$

$$H_{r(clad)} = \left[-C \frac{i\omega\varepsilon_{clad}}{\left(\dfrac{w}{a}\right)^2} \frac{m}{r} K_m\left(\frac{wr}{a}\right) + D \frac{i\beta}{\dfrac{w}{a}} K'_m\left(\frac{wr}{a}\right) \right] \cos m\theta \qquad (3.43)$$

The E_θ and H_θ dependencies are obtained by substituting both (3.36a) and (3.37c) into (3.27) and (3.30) respectively and differentiating to get

$$E_{\theta(clad)} = \left[C \frac{i\beta}{\left(\dfrac{w}{a}\right)^2} \frac{m}{r} K_m\left(\frac{wr}{a}\right) - D \frac{i\omega\mu_0}{\dfrac{w}{a}} K'_m\left(\frac{wr}{a}\right) \right] \cos m\theta \qquad (3.44)$$

$$H_{\theta(clad)} = \left[C \frac{i\omega\varepsilon_{clad}}{\frac{w}{a}} K'_m\left(\frac{wr}{a}\right) - D\frac{i\beta}{\left(\frac{w}{a}\right)^2}\frac{m}{r} K_m\left(\frac{wr}{a}\right) \right] \sin m\theta \qquad (3.45)$$

3.7.3 Mode Propagation Constants

Propagation constants are determined by the boundary conditions, which are the conditions for continuity of the fields at the core/cladding boundary ($r = a$).

Thus at $r = a$:

$$E_{z(core)} = E_{z(clad)} \qquad\qquad H_{z(core)} = H_{z(clad)}$$

$$E_{\theta(core)} = E_{\theta(clad)} \qquad\qquad H_{\theta(core)} = H_{\theta(clad)}$$

$$\varepsilon_{(core)}E_{r(core)} = \varepsilon_{(clad)}E_{r(core)} \qquad\qquad \mu_0 H_{r(core)} = \mu_0 H_{r(clad)} \; *$$

$*as \; \mu_{core} = \mu_{clad} = \mu_0$ for non magnetic media.

Substituting (3.36a) to (3.45) into the above boundary conditions gives:

$E_{z(core)} = E_{z(clad)}$ gives

$$AJ_m(u) - CK_m(w) = 0 \qquad (3.46)$$

$H_{z(core)} = H_{z(clad)}$ gives

$$BJ_m(u) - DK_m(w) = 0 \qquad (3.47)$$

$E_{\theta(core)} = E_{\theta(clad)}$ gives

$$A\frac{i\beta}{\left(\frac{u}{a}\right)^2}\frac{m}{a}J_m(u) - B\frac{i\omega\mu_0}{\frac{u}{a}}J'_m(u) + C\frac{i\beta}{\left(\frac{w}{a}\right)^2}\frac{m}{a}K_m(w) - D\frac{i\omega\mu_0}{\frac{w}{a}}K'_m(w) = 0 \quad (3.48)$$

$H_{\theta(core)} = H_{\theta(clad)}$ gives

$$A\frac{i\omega\varepsilon_{core}}{u}J'_m(u) - B\frac{i\beta}{\left(\frac{u}{a}\right)^2}\frac{m}{a}J_m(u) + C\frac{i\omega\varepsilon_{clad}}{w}K'_m(w) - D\frac{i\beta}{\left(\frac{w}{a}\right)^2}\frac{m}{a}K_m(w) = 0$$

(3.49)

$\varepsilon_{(core)}E_{r(core)} = \varepsilon_{(clad)}E_{r(core)}$ gives

$$\varepsilon_{core}A\frac{i\beta}{u}J'_m(u) - \varepsilon_{core}B\frac{i\omega\mu_0}{\left(\frac{u}{a}\right)^2}\frac{m}{a}J_m(u) + \varepsilon_{clad}C\frac{i\beta}{w}K'_m(w) - \varepsilon_{clad}D\frac{i\omega\mu_0}{\left(\frac{w}{a}\right)^2}\frac{m}{a}K_m(w) = 0$$

(3.50)

$\mu_0 H_{r(core)} = \mu_0 H_{r(clad)}$ gives

$$\mu_0 A\frac{i\omega\varepsilon_{core}}{\left(\frac{u}{a}\right)^2}\frac{m}{a}J_m(u) - \mu_0 B\frac{i\beta}{u}J'_m(u) + \mu_0 C\frac{i\omega\varepsilon_{clad}}{\left(\frac{w}{a}\right)^2}\frac{m}{a}K_m(w) - \mu_0 D\frac{i\beta}{w}K'_m(w) = 0$$

(3.51)

To arrive at a general equation describing all modes it is necessary to unify four of these equations in matrix form [283]:

$$[M]\begin{bmatrix}A\\B\\C\\D\end{bmatrix} = 0$$

For the solution to be nontrivial the determinant of the matrix M must be zero.

Okushi [204] uses (3.46), (3.47), 3.48) and (3.51) to form the matrix, while Yariv [205] uses (3.46), (3.47), 3.48) and (3.49).

Following the Okushi method the general equation for all types of mode becomes as:

$$\left(\frac{J'_m(u)}{uJ_m(u)} + \frac{K'_m(w)}{wK_m(w)}\right)\left(\frac{\varepsilon_{core}}{\varepsilon_{clad}}\frac{J'_m(u)}{uJ_m(u)} + \frac{K'_m(w)}{wK_m(w)}\right) = m^2\left(\frac{1}{u^2} + \frac{1}{w^2}\right)\left(\frac{\varepsilon_{core}}{\varepsilon_{clad}}\frac{1}{u^2} + \frac{1}{w^2}\right) \quad (3.52)$$

As *m* >0 for HE and EH modes (3.52) describes both the HE$_{ml}$ and EH$_{ml}$ modes. At this point this derivation can't be separated to give different values for each of the two families.

For TE$_{ml}$ and TM$_{ml}$ modes m can only be zero thus (3.52) becomes:

$$\left(\frac{J'_m(u)}{uJ_m(u)}+\frac{K'_m(w)}{wK_m(w)}\right)\left(\frac{\varepsilon_{core}}{\varepsilon_{clad}}\frac{J'_m(u)}{uJ_m(u)}+\frac{K'_m(w)}{wK_m(w)}\right)=0 \qquad (3.53)$$

The subscript *m* denotes the azimuthal (angular) variation of E_z within a 360° rotation around the core axis, and the number of roots of the propagation constant β which will satisfy the condition is the number of radial variations of E_z and is denoted as subscript *l*

TM$_{ml}$ modes are described by the second term on the left hand side only, and are given by:

$$\left(\frac{\varepsilon_{core}}{\varepsilon_{clad}}\frac{J'_m(u)}{uJ_m(u)}+\frac{K'_m(w)}{wK_m(w)}\right)=0 \qquad (3.54)$$

TE$_{ml}$ modes are described by the first term on the left hand side only, and are given by:

$$\left(\frac{J'_m(u)}{uJ_m(u)}+\frac{K'_m(w)}{wK_m(w)}\right)=0 \qquad (3.55)$$

Since the difference between the core and cladding refractive index is very small (*Δn*<<1) one can use the weakly guiding approximation ($\varepsilon_{core}=\varepsilon_{clad}$), the equation describing the HE$_{ml}$ and EH$_{ml}$ modes can be given as:

$$\frac{J'_m(u)}{uJ_m(u)}+\frac{K'_m(w)}{wK_m(w)}=\pm m\left(\frac{1}{u^2}+\frac{1}{w^2}\right) \qquad (3.56)$$

Given the fact that HE$_{ml}$ modes use the negative term on the RHS of (3.56) this becomes

$$\frac{J'_m(u)}{uJ_m(u)} + \frac{K'_m(w)}{wK_m(w)} = -m\left(\frac{1}{u^2} + \frac{1}{w^2}\right)$$ (3.57)

and that EH$_{ml}$ modes use the positive term on the RHS of (3.56) this becomes

$$\frac{J'_m(u)}{uJ_m(u)} + \frac{K'_m(w)}{wK_m(w)} = m\left(\frac{1}{u^2} + \frac{1}{w^2}\right)$$ (3.58)

In the weakly guiding approximation the propagation constants of each of the TE and TM modes degenerate to become effectively equal, reducing (3.54) and (3.55) to a single equation which describes both modes,

$$\frac{J'_m(u)}{uJ_m(u)} + \frac{K'_m(w)}{wK_m(w)} = 0$$ (3.59)

Unfortunately in this derivation the expression for the HE$_{ml}$ cladding modes (3.52) is the same as that of the EH$_{ml}$ cladding modes and the two cannot be distinguished until the weakly guiding approximation is assumed. As the radiation in the cladding cannot be assumed to be weakly guided, due to the large difference between the cladding and ambient refractive indices, this equation is deemed unsatisfactory to predict the HE$_{ml}$ cladding modes, and the following Yariv derivation was utilised in all further calculations.

Following the Yariv method the general equation becomes

$$\left(\frac{J'_m(u)}{uJ_m(u)} + \frac{K'_m(w)}{wK_m(w)}\right)\left(n^2_{core}\frac{J'_m(u)}{uJ_m(u)} + n^2_{clad}\frac{K'_m(w)}{wK_m(w)}\right) = \frac{\beta^2}{k^2}m^2\left(\frac{1}{u^2} + \frac{1}{w^2}\right)^2$$ (3.60)

Equation (3.60) can be seen to be a quadratic in $\dfrac{J'_m(u)}{uJ_m(u)}$, solving for this gives

$$\frac{J'_m(u)}{uJ_m(u)} = -\left(\frac{n_{core}^2 + n_{clad}^2}{2n_{core}^2}\right)\frac{K'_m(w)}{wK_m(w)} \pm \left[\left(\frac{n_{core}^2 - n_{clad}^2}{2n_{core}^2}\right)^2\left(\frac{K'_m(w)}{wK_m(w)}\right)^2 + \left(\frac{\beta m}{kn_{core}}\right)^2\left(\frac{1}{w^2} + \frac{1}{u^2}\right)^2\right]^{\frac{1}{2}}$$

$$(3.61)$$

Again the HE$_{ml}$ modes are described by the negative term on the RHS of (3.61)

$$\frac{J'_m(u)}{uJ_m(u)} = -\left(\frac{n_{core}^2 + n_{clad}^2}{2n_{core}^2}\right)\frac{K'_m(w)}{wK_m(w)} - \left[\left(\frac{n_{core}^2 - n_{clad}^2}{2n_{core}^2}\right)^2\left(\frac{K'_m(w)}{wK_m(w)}\right)^2 + \left(\frac{\beta m}{kn_{core}}\right)^2\left(\frac{1}{w^2} + \frac{1}{u^2}\right)^2\right]^{\frac{1}{2}}$$

$$(3.62)$$

and the EH$_{ml}$ modes are described by the positive term on the RHS of (3.61)

$$\frac{J'_m(u)}{uJ_m(u)} = -\left(\frac{n_{core}^2 + n_{clad}^2}{2n_{core}^2}\right)\frac{K'_m(w)}{wK_m(w)} + \left[\left(\frac{n_{core}^2 - n_{clad}^2}{2n_{core}^2}\right)^2\left(\frac{K'_m(w)}{wK_m(w)}\right)^2 + \left(\frac{\beta m}{kn_{core}}\right)^2\left(\frac{1}{w^2} + \frac{1}{u^2}\right)^2\right]^{\frac{1}{2}}$$

$$(3.63)$$

For TE$_{ml}$ and TM$_{ml}$ modes, as $m = 0$ (3.61) reduces to

$$\frac{J'_m(u)}{uJ_m(u)} = -\left(\frac{n_{core}^2 + n_{clad}^2}{2n_{core}^2}\right)\frac{K'_m(w)}{wK_m(w)} \pm \left[\left(\frac{n_{core}^2 - n_{clad}^2}{2n_{core}^2}\right)^2\left(\frac{K'_m(w)}{wK_m(w)}\right)^2\right]^{\frac{1}{2}} \quad (3.64)$$

where TE$_{ml}$ modes are described using the positive sign on the right of (3.64)

$$\frac{J'_m(u)}{uJ_m(u)} = -\left(\frac{n_{core}^2 + n_{clad}^2}{2n_{core}^2}\right)\frac{K'_m(w)}{wK_m(w)} + \left[\left(\frac{n_{core}^2 - n_{clad}^2}{2n_{core}^2}\right)^2\left(\frac{K'_m(w)}{wK_m(w)}\right)^2\right]^{\frac{1}{2}} \quad (3.65)$$

and TM$_{ml}$ modes are described using the negative sign on the right of (3.64)

$$\frac{J'_m(u)}{uJ_m(u)} = -\left(\frac{n_{core}^2 + n_{clad}^2}{2n_{core}^2}\right)\frac{K'_m(w)}{wK_m(w)} - \left[\left(\frac{n_{core}^2 - n_{clad}^2}{2n_{core}^2}\right)^2\left(\frac{K'_m(w)}{wK_m(w)}\right)^2\right]^{\frac{1}{2}} \quad (3.66)$$

Again, in the core the weakly guiding approximation assumptions that

$n_{core} \approx n_{clad}$ and $\beta \approx k$ in (3.60), can be made leading to the same equation as in the

Okushi derivation:

$$\frac{J'_m(u)}{uJ_m(u)} + \frac{K'_m(w)}{wK_m(w)} = \pm m\left(\frac{1}{u^2} + \frac{1}{w^2}\right) \qquad (3.56)$$

and hence the same equations to predict the HE_{ml}, EH_{ml}, TE_{ml}, and TM_{ml}, core modes.

Thus it can be seen that the two routes lead to the same equations to describe the modes families in the weakly guiding core, but different equations to describe the modes families in the cladding. This derivation gives an equation which uniquely describes the HE_{ml} cladding modes and is one of the two used in the programming codes in Chapter 4.

3.8 Evanescent Field

When radiation is incident on a refractive index boundary under the condition of total internal reflection, the associated EM fields do not cease at that boundary but will enter the adjacent medium, where they will decay exponentially [283]. This creates an evanescent field around the guiding core in a fibre which carries no power in the direction perpendicular to the core axis, as shown in Figure 3.13
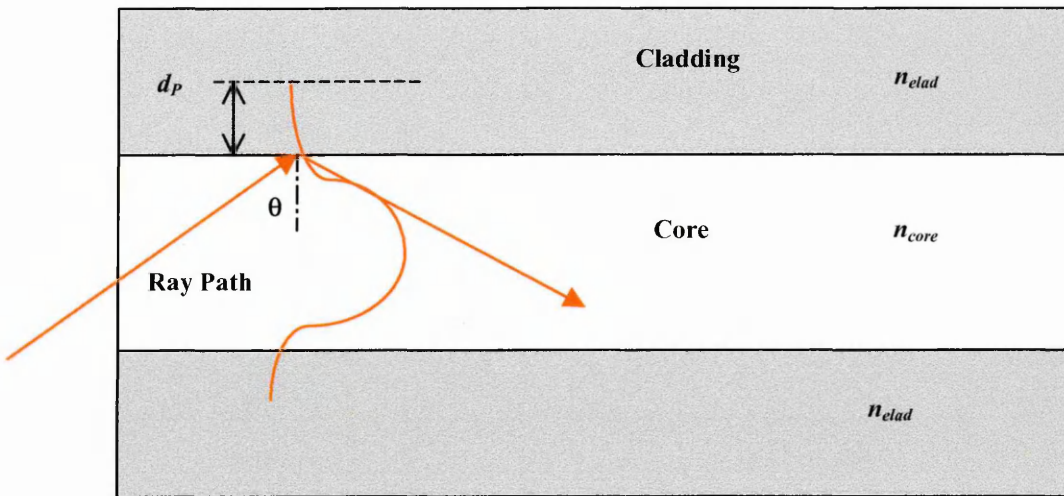
Figure 3.13: Evanescent field in optical fibre

The depth of penetration d_P of the evanescent field is described as the distance at which the amplitude of the field has reduced to e^{-1} of its value at the boundary [284], and is given by the Goos-Haenchen shift [285]:

$$d_P = \frac{\lambda}{2\pi\sqrt{n_{core}^2 \sin^2 \theta - n_{clad}^2}} \tag{3.67}$$

where λ is the wavelength of radiation, and θ is greater than the critical angle

Figure 3.14 shows the evanescent field penetration depth over the range of incident angles up to the critical angle, θ_c for an interface with the following values, n_{core} : 2, n_{clad} : 1.46, λ : 630nm. The dependence of the penetration depth of the evanescent field can be seen to decrease rapidly with the angle of incidence.
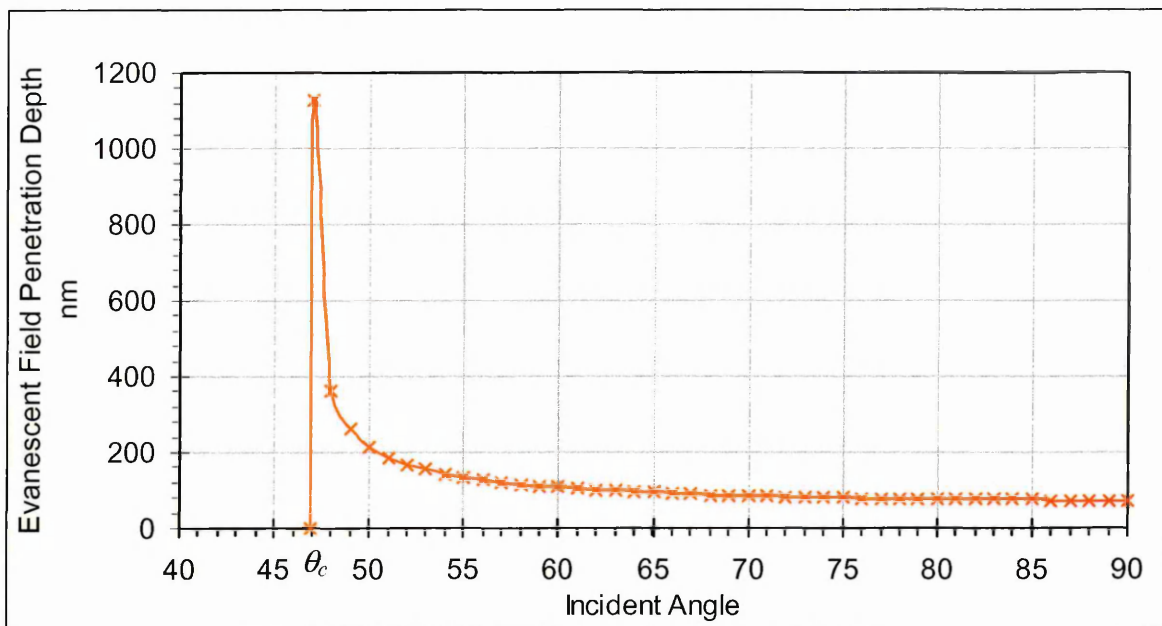
**Figure 3.14:   Dependence of penetration depth of evanescent field
on incident angle**

If the medium into which the field extends is absorbing at the transmitted wavelength some of the energy in the evanescent field will be absorbed according to the absorptivity of the medium, and the intensity of the guided radiation will be reduced accordingly. Thus the intensity of a higher order mode will be reduced by a greater margin than that of a lower order mode due to the difference in the penetration depth of the respective evanescent fields into the absorbing medium.   If the medium is not absorbing then the energy in the evanescent field will remain constant and the intensity of the guided radiation will ideally not be affected.

3.9 Coupled Mode Theory

Coupled mode theory describes the coupling of energy between modes due to the influence of one mode on another and is popularly used to describe mode coupling in fibre gratings [152,286,287]. Section 3.9.1 follows the derivation of coupled mode theory from Maxwell's Equations as described by Ghatak [288], expanding various aspects where necessary for a more complete and comprehensible result. The basic theory is then adapted to include explanations of mode coupling in fibre gratings in section 3.9.2.

3.9.1 Derivation of Coupled Mode Equations from Maxwell's Equations

From Maxwell's equations for isotropic, linear, non-conducting, non-magnetic medium, given in section 3.5 the third equation (Faraday's Law of induction) is used in this derivation.

$$\nabla \times E = -\frac{\partial B}{\partial t} = -\mu_0 \frac{\partial H}{\partial t} \tag{3.68}$$

Taking the curl of (3.68) in order to remove the magnetic vector dependency, leaving only the electric vectors components

$$\nabla \times (\nabla \times E) = \nabla \times \left(-\mu_0 \frac{\partial H}{\partial t} \right) = -\mu_0 \frac{\partial}{\partial t} (\nabla \times H) \tag{3.69}$$

and using the following identities

$$\nabla \times (\nabla \times E) = \nabla(\nabla .E) - \nabla^2 E \quad \text{and} \nabla .E = \frac{\rho}{\varepsilon} = 0 \quad \text{and} \nabla \times H = \varepsilon_0 n^2 \frac{\partial E}{\partial t}$$

as $\mu_0 \varepsilon_0 = \frac{1}{c^2}$ and ψ is the wave displacement of the electric field vector E of the

wave travelling in the z direction, (3.69) can be re-written as the 3D wave equation

$$\nabla^2 \psi = \frac{n^2}{c^2} \frac{\partial^2 \psi}{\partial t^2} \tag{3.70}$$

which has solutions of the form

$$\psi = \psi_0 e^{i(k.r - \omega t)} \tag{3.71}$$

Substituting (3.71) into (3.70) and differentiating with respect to t yields the result for

the 3D wave equation with x,y,z, dependence.

$$\nabla^2 \psi = \frac{n^2}{c^2} \frac{\partial^2}{\partial t^2} \psi_0 e^{i(k.r - \omega t)}$$

$$\nabla^2 \psi = -\frac{n^2 \omega^2}{c^2} \psi$$

$$\nabla^2 \psi = -k^2 n^2 \psi \qquad \text{as} \frac{\omega}{c} = k \tag{3.72}$$

As consideration only involves the transverse field vectors, the z dependency can be

removed, giving

$$\nabla_t^2 \psi = \nabla^2 \psi - \frac{\partial^2 \psi}{\partial z^2} = -k^2 n^2 \psi - \frac{\partial^2 \psi}{\partial z^2} \tag{3.73}$$

$$\nabla_t^2 \psi = -k^2 n^2 \psi - \frac{\partial^2}{\partial z^2} \psi_0 e^{i(k.r - \omega t)}$$

$$\nabla_t^2 \psi = -\psi(k^2 n^2 - \beta^2) \tag{3.74}$$

where β is the z component of the wave vector k_z

So for 2 separate wave guides A & B with no interaction the transverse mode patterns of each may be written as:

$$\nabla_t^2 \psi_A = -\psi_A \left(k^2 n_A^2 - \beta_A^2\right) = \psi_A \left(\beta_A^2 - k^2 n_A^2\right) \qquad (3.75)$$

$$\nabla_t^2 \psi_B = -\psi_B \left(k^2 n_B^2 - \beta_B^2\right) = \psi_B \left(\beta_B^2 - k^2 n_B^2\right) \qquad (3.76)$$

The total field of a 2 wave guide coupler which will be dependent on the progression of the 2 fields along the z axis defined as $\Psi_{(x,y,z)}$, can be represented by the same type of equation as (3.70).

$$\nabla^2 \Psi = \frac{n^2}{c^2} \frac{\partial^2 \Psi}{\partial t^2} \qquad (3.77)$$

which has solutions of the form

$$\Psi = \Psi_0 e^{i(k.r - \omega t)} \qquad (3.78)$$

substituting (3.78) into (3.77) and differentiating wrt t as before gives

$$\nabla^2 \Psi + k^2 n^2 \Psi = 0 \qquad (3.79)$$

or
$$\nabla^2 \Psi_0 e^{i(k.r - \omega t)} + k^2 n^2 \Psi_0 e^{i(k.r - \omega t)} = 0 \qquad (3.80)$$

Ψ_0 can be approximated by a superposition of the fields in the 2 wave guides with amplitudes $A(z)$ and $B(z)$ such that

$$\Psi_0(x,y,z) = A(z)\psi_A(x,y)e^{-i\beta_A z} + B(z)\psi_B(x,y)e^{-i\beta_B z} \qquad (3.81)$$

Substituting (3.81) into (3.80) gives

$$\nabla^2 \left[A(z)\psi_A(x,y)e^{-i\beta_A z} + B(z)\psi_B(x,y)e^{-i\beta_B z} \right]$$
$$+ k^2 n^2(x,y)\left[A(z)\psi_A(x,y)e^{-i\beta_A z} + B(z)\psi_B(x,y)e^{-i\beta_B z} \right] = 0$$

and differentiating gives

$$Ae^{-i\beta_A z}\left(\nabla_t^2 \psi_A - \beta_A^2 \psi_A + k^2 n^2 \psi_A\right) + Be^{-i\beta_B z}\left(\nabla_t^2 \psi_B - \beta_B^2 \psi_B + k^2 n^2 \psi_A\right) -$$
$$2i\beta_A \psi_A e^{-i\beta_A z}\frac{\partial A}{\partial z} - 2i\beta_B \psi_B e^{-i\beta_B z}\frac{\partial B}{\partial z} + \psi_A e^{-i\beta_A z}\frac{\partial^2 A}{\partial z^2} + \psi_B e^{-i\beta_B z}\frac{\partial^2 B}{\partial z^2} = 0$$

69

The second differential of A and B with respect to z are slowly varying functions and as such can be ignored in the context of this derivation leaving

$$Ae^{-i\beta_A z}\left(\nabla_t^2\psi_A - \beta_A^2\psi_A + k^2n^2\psi_A\right) + Be^{-i\beta_B z}\left(\nabla_t^2\psi_B - \beta_B^2\psi_B + k^2n^2\psi_A\right) -$$
$$2i\beta_A\psi_A e^{-i\beta_A z}\frac{\partial A}{\partial z} - 2i\beta_B\psi_B e^{-i\beta_B z}\frac{\partial B}{\partial z} = 0 \tag{3.82}$$

Substituting for $\nabla_t^2\psi$ from (3.75) and (3.76) into (3.82) gives

$$Ak^2\Delta n_A^2\psi_A + Bk^2\Delta n_B^2\psi_B e^{i\Delta\beta z} - 2i\beta_A\frac{\partial A}{\partial z}\psi_A - 2i\beta_B\frac{\partial B}{\partial z}\psi_B e^{i\Delta\beta z} = 0 \tag{3.83}$$

where $\quad \Delta n_A^2 = n^2 - n_A^2; \Delta n_B^2 = n^2 - n_B^2; \Delta\beta = \beta_A - \beta_B.$

Multiplying by the complex conjugate ψ_A^* and ψ_B^* in turn and integrating both in x and y produces

$$\frac{\partial A}{\partial z} = \frac{Ak^2\int\limits_{-\infty}^{\infty}\int\Delta n_A^2\psi_A\psi_A^* dxdy}{2i\beta_A\int\limits_{-\infty}^{\infty}\int\psi_A\psi_A^* dxdy} + \frac{Be^{i\Delta\beta z}k^2\int\limits_{-\infty}^{\infty}\int\Delta n_B^2\psi_B\psi_A^* dxdy}{2i\beta_A\int\limits_{-\infty}^{\infty}\int\psi_A\psi_A^* dxdy} - \frac{\partial B}{\partial z}\frac{\beta_B}{\beta_A}e^{i\Delta\beta z}\frac{\int\limits_{-\infty}^{\infty}\int\psi_B\psi_A^* dxdy}{\int\limits_{-\infty}^{\infty}\int\psi_A\psi_A^* dxdy}$$

$$(3.84)$$

$$\frac{\partial B}{\partial z} = \frac{Ak^2\int\limits_{-\infty}^{\infty}\int\Delta n_A^2\psi_A\psi_B^* dxdy}{2i\beta_B e^{i\Delta\beta z}\int\limits_{-\infty}^{\infty}\int\psi_B\psi_B^* dxdy} + \frac{Bk^2\int\limits_{-\infty}^{\infty}\int\Delta n_B^2\psi_B\psi_B^* dxdy}{2i\beta_B\int\limits_{-\infty}^{\infty}\int\psi_B\psi_B^* dxdy} - \frac{\partial A}{\partial z}\frac{\beta_A}{\beta_B e^{i\Delta\beta z}}\frac{\int\limits_{-\infty}^{\infty}\int\psi_A\psi_B^* dxdy}{\int\limits_{-\infty}^{\infty}\int\psi_B\psi_B^* dxdy}$$

$$(3.85)$$

As $\int\limits_{-\infty}^{\infty}\int\psi_B\psi_A^* dxdy \ll \int\limits_{-\infty}^{\infty}\int\psi_A\psi_A^* dxdy$, and $\int\limits_{-\infty}^{\infty}\int\psi_A\psi_B^* dxdy \ll \int\limits_{-\infty}^{\infty}\int\psi_B\psi_B^* dxdy$, the last

term in each differential equation known as the overlap integrals can be neglected in weakly coupling conditions. Letting coupling coefficients κ be represented as

$$\kappa_{AA} = \frac{k^2\int\limits_{-\infty}^{\infty}\int\Delta n_A^2\psi_A\psi_A^* dxdy}{2\beta_A\int\limits_{-\infty}^{\infty}\int\psi_A\psi_A^* dxdy}, \text{ and } \kappa_{AB} = \frac{k^2\int\limits_{-\infty}^{\infty}\int\Delta n_B^2\psi_B\psi_A^* dxdy}{2\beta_A\int\limits_{-\infty}^{\infty}\int\psi_A\psi_A^* dxdy}$$

70

and $\quad \kappa_{BA} = \dfrac{k^2 \int \int\limits_{-\infty}^{\infty} \Delta n_A^2 \psi_A \psi_B^* \, dx dy}{2\beta_B \int \int\limits_{-\infty}^{\infty} \psi_B \psi_B^* \, dx dy}$, and $\kappa_{BB} \dfrac{k^2 \int \int\limits_{-\infty}^{\infty} \Delta n_B^2 \psi_B \psi_B^* \, dx dy}{2i\beta_B \int \int\limits_{-\infty}^{\infty} \psi_B \psi_B^* \, dx dy}$

then the coupled mode equations are given by:

$$\frac{\partial A}{\partial z} = -i\kappa_{AA}A - \kappa_{AB}Be^{i\Delta\beta z} \tag{3.86}$$

$$\frac{\partial B}{\partial z} = -i\kappa_{BB}B - i\kappa_{BA}Ae^{-i\Delta\beta z} \tag{3.87}$$

3.9.2 Using Coupled Mode Equations to Describe Mode Coupling in an Optical Fibre

Letting $\quad a(z,t) = A(z,t)e^{i(\omega t - \beta_A z)}$ $\quad$ and $\quad b(z,t) = B(z,t)e^{i(\omega t - \beta_B z)}$ represent 2 modes travelling along the fibre core and cladding respectively, and differentiating wrt z to predict the interaction along the fibre:

$$\frac{\partial a}{\partial z} = A\frac{\partial}{\partial z}e^{i(\omega t - \beta_A z)} + e^{i(\omega t - \beta_A z)}\frac{\partial A}{\partial z} = -i(\beta_A + \kappa_{AA})a - i\kappa_{AB}b$$

$$\frac{\partial b}{\partial z} = B\frac{\partial}{\partial z}e^{i(\omega t - \beta_{BA} z)} + e^{i(\omega t - \beta_{BA} z)}\frac{\partial B}{\partial z} = -i(\beta_B + \kappa_{BB})b - i\kappa_{BA}a$$

The constants κ_{AA} and κ_{BB} are modifications to the modes in one wave guide due to the locality of the other, and are negligible compared to the cross coupling constants κ_{AB} and κ_{BA}, so the coupled mode equations predicting the effect of one mode on the other as they propagate in the z direction may be written as

$$\frac{\partial a}{\partial z} = -i\beta_A a - i\kappa_{AB}b \tag{3.88}$$

$$\frac{\partial b}{\partial z} = -i\beta_B b - i\kappa_{BA} a \qquad (3.89)$$

where the cross coupling constants κ_{AB} and κ_{BA} determine the amount of coupling between the 2 modes and are dependent on the wave guide parameters, and the operating wavelength. If the differential propagation constant $\Delta\beta$ in (3.86) and (3.87) matches the condition

$$\Delta\beta = \beta_A - \beta_B = \frac{2\pi}{\Lambda}$$

maximum energy will be transferred between modes.

3.10 Fibre Bragg Grating Theory

A Fibre Bragg grating (FBG) is a periodic array of refractive index perturbations (grating elements) along a very short length of the single mode fibre core [128,152]. The principle behind the operation of the FBG can be explained by either of the two following theories.

i)   Considering the Grating as a Diffraction Grating
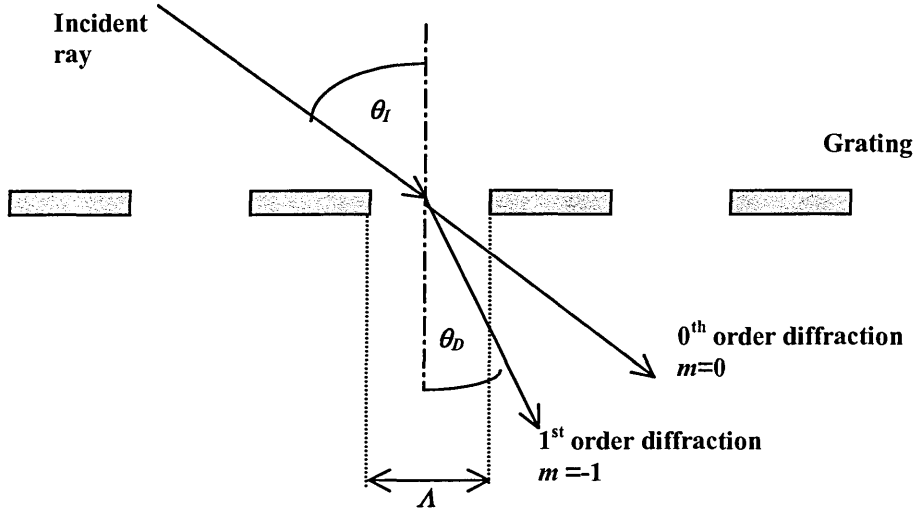
Figure 3.15:   **Zeroth and first order diffraction of radiation incident on a diffraction grating**

As shown in Figure 3.15, from diffraction theory the angle of diffraction θ_d, of a ray of angle of incidence $\theta_i = 0°$, is given by the formula [289]:

$$\sin \theta_d = \frac{m\lambda}{\Lambda} \qquad (3.90)$$

where m is the order of diffraction and Λ is the grating period.

For a ray of incident angle $\theta_i \neq 0°$ then the refracted angle will be offset by the value of the incident angle [290], thus:

$$\sin \theta_d = \sin \theta_i + \frac{m\lambda}{\Lambda} \qquad (3.91)$$

If the medium through which the light is propagating is not air (or a vacuum) then the refractive index of the medium (the fibre core) must be accounted for as [290]:

$$n_{core} \sin \theta_{core} = n_{core} \sin \theta_{core} + \frac{m\lambda}{\Lambda} \qquad (3.92)$$

which can be used to derive the FBG coupling equation as outlined below.
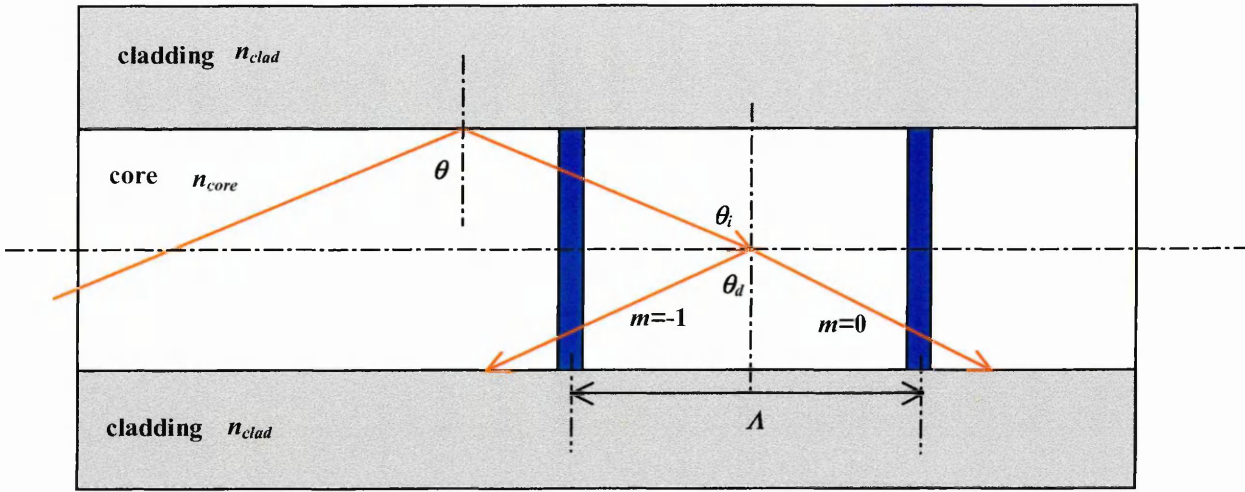
Figure 3.16:   FBG as a diffraction grating

From Figure 3.16 equation (3.92) can be written as:

$$n_{core} \sin \theta_d = n_{core} \sin \theta_i + \frac{m\lambda}{\Lambda} \qquad (3.93)$$

As the $m = -1$ order is the most prominent order of diffraction at the grating [290], then (3.93) becomes:

$$n_{core} \sin \theta_d = n_{core} \sin \theta_i - \frac{\lambda}{\Lambda} \qquad (3.94)$$

Recognizing that θ_d is in the opposite direction to θ_i, and θ_d will therefore be negative, the wavelength at which forward propagating modes will be coupled into reverse propagating modes can be written as:

$$\lambda = \left(n_{core} \sin \theta_i + n_{core} \sin \theta_d \right) \Lambda \qquad (3.95)$$

Since the absolute value of θ_d is equal to that of θ_i, and θ_i is the same as the incident angle at the core/cladding boundary θ, then the FBG coupling wavelength (λ_B)is given as [152]:

$$\lambda_B = 2n_{core} \Lambda \sin \theta \qquad (3.96)$$

74

For example, in order to satisfy the FBG coupling equation, an FBG with a period Λ of 1000nm, in a core of n_{core} = 1.5, a cladding of n_{clad} = 1.49 and at a incident angle θ of 84° (just greater than the critical angel (for TIR), where $\theta_C = \sin^{-1} n_{clad}/n_{core}$ = 83.38°)

$$\lambda_B = 2\times1.5\times\sin84\times1000*10^{-9}$$

$$\lambda_B = 2983.6\text{nm}$$

thus an FBG with the above parameters will couple light from a forward propagating core mode to a backward propagating core mode at a wavelength of 2983.6 nm.

To show that this wavelength at the above parameters will cause the diffracted ray angle to be the same (but negative) as the incident angle the diffraction grating formula is utilized:

$$n_{core} \sin\theta_d = n_{core} \sin\theta_i + \frac{m\lambda}{\Lambda}$$

$$\theta_d = \sin^{-1}\left(\frac{n_{core}\sin\theta_i + \dfrac{m\lambda}{\Lambda}}{n_{core}} \right)$$

$$\theta_d = \sin^{-1}\left(\frac{1.5\sin84 - \dfrac{2983.6\times10^{-9}}{1000}}{1.5} \right)$$

$$\theta_d = -84°$$

So, it can be seen that wavelengths which are diffracted through a fibre grating to give the first negative maxima at an angle equal to that of the angle of incidence will be diffracted back along the core at successive grating elements, and will interfere constructively as it does so.

ii)   Considering the Grating as a Series of Resonant Cavities [291,292]

(3.92) can be used to derive the FBG coupling equation as outlined below.
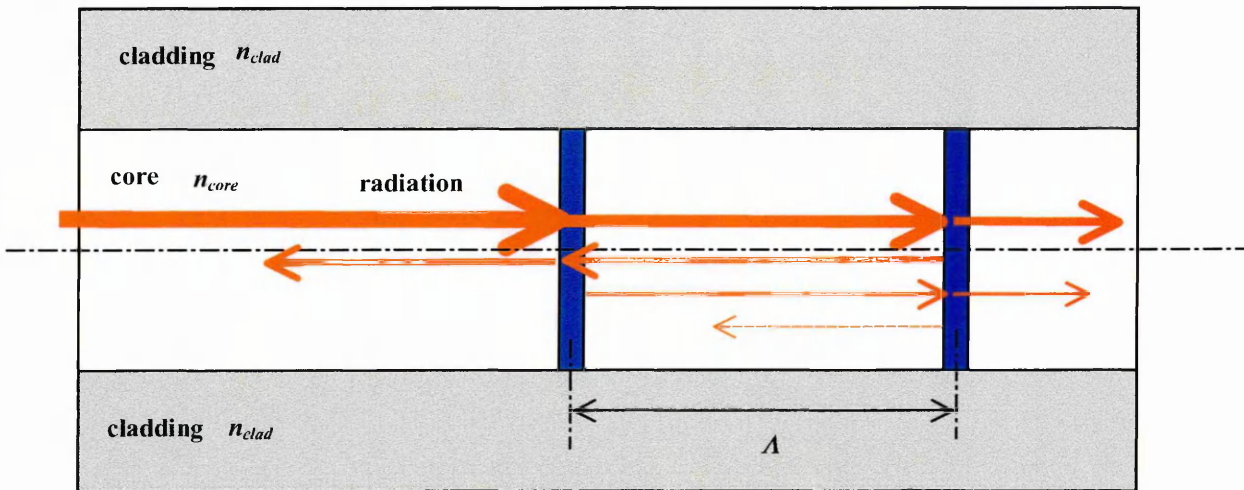
Figure 3.17:   FBG as a resonant cavity for axial direction of propagation

When light travelling through the fibre is incident on the grating elements it will be partially reflected and partially transmitted at each successive element as shown in Figure 3.17, due to the refractive index difference between the core and the element. Any wavelengths in the incident radiation for which the optical path length of grating period is equal to a whole number of half wavelengths will interfere constructively on reflection, and destructively on transmission from successive elements. All other wavelengths which do not match this criteria will interfere constructively on transmission and destructively on reflection from successive elements. Thus the constructively reflected wavelengths will be absent from the transmission profile detected at the end of the fibre, and will be the only wavelengths evident in the reflection profile detected at the input of the fibre [157]. The reflectivity of an element will be almost the same for every wavelength (except for slight variations due to the wavelength dependency of the refractive index difference between the element and the core). It is therefore preferable to have many elements of low reflectivity,

rather than few elements of high reflectivity, as the reflected fraction from the first period will be lost for all transmitted wavelengths, reducing the detected intensity by that amount.

FBGs are mainly used as strain [86,100,293-295] or temperature [38,118,296] sensors, where the measurand affects the grating period and/or the refractive index of the core, either of which will alter the optical path length of the reflected rays from successive grating elements, and thus the wavelength which matches this new path length will also change. The degree to which this reflected wavelength changes will determine the degree of change in the measurand. As rays never travel parallel to the core axis, their angle of propagation must be taken into account as they are reflected from successive grating elements. If a ray did travel along the axis then the condition for constructive interference on reflection would simply be:

$$\frac{m\lambda}{2} = n_{core}\Lambda \qquad (3.97)$$

where λ is the wavelength of constructive interference on reflection.

This shows that the wavelengths for which the partial reflections from successive grating elements are in phase, will have a difference in optical path length of a whole number of wavelengths. However, if the ray is travelling through the core at an angle θ as shown in Figure 3.18, the optical path length between the first and second reflections that the ray must travel in order to be in phase will no longer be the same as double the grating period.
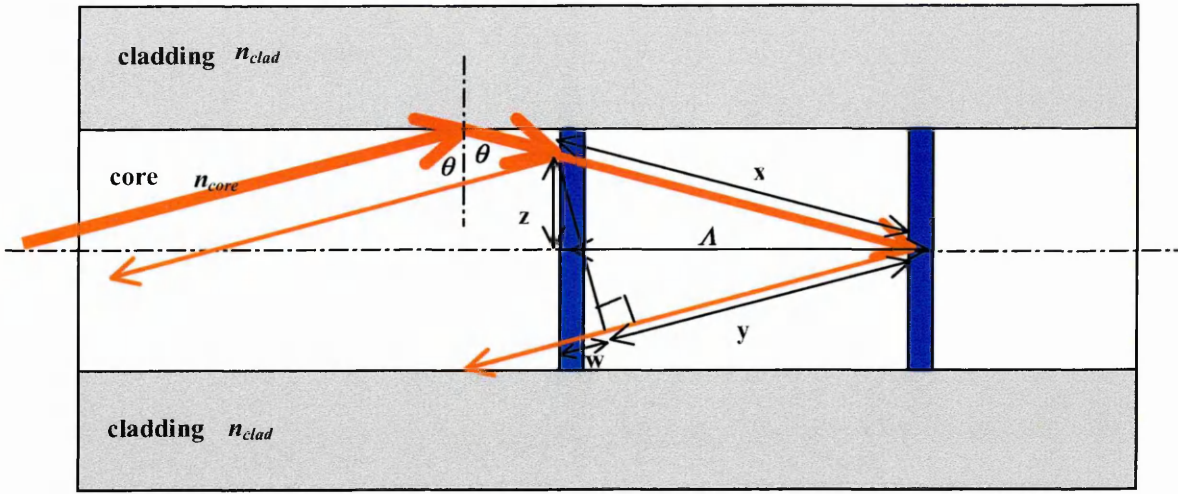
Figure 3.18: **FBG as a resonant cavity for non-axial direction of propagation**

Considering a ray undergoing TIR at an angle of incidence at the core/cladding boundary of θ, then for constructive interference of the two partially reflected rays, the extra distance travelled by the part of the ray reflected from the second grating must be equal to a whole number of wavelengths (see Figure 3.9.3).

i.e.
$$m\lambda_{core} = x + y$$

Note
$$\lambda_{air} n_{air} = \lambda_{core} n_{core} \rightarrow \lambda_{core} = \frac{\lambda_{air}}{n_{core}}$$

Thus
$$\frac{m\lambda_{air}}{n_{core}} = x + y$$

As $\quad x = \dfrac{\Lambda}{\sin\theta} \quad$ and $\quad y = x - w$, $\qquad$ where $\quad w = 2z\cos\theta \quad$ and $\quad z = \dfrac{\Lambda}{\tan\theta}$

So for $m = 1$, from (3.97) it can be shown that the reflected wavelength is given as:

$$\lambda_{air} = 2n_{core}\Lambda\sin\theta$$

This can be seen to be the same as the formula for the diffracted wavelength for a fibre Bragg grating (3.96), however this manipulation has shown that the $\sin\theta$ component in the formula is used to convert the optical path length of a non axial ray into terms of the axial period of the grating.

3.11 Effective Refractive Index

Even in optical fibres with no grating the $\sin\theta$ factor is used to convert the rays travelling at an angle θ into the component of these rays travelling axially [297-300], to allow comparisons between the core and cladding propagation constants β in the axial plane of the fibre. $n\sin\theta$ is known as the effective refractive index (n_{eff}) [301], thus the Bragg wavelength can be written as [152-154]:

$$\lambda_B = 2n_{eff_{core}}\Lambda \qquad (3.98)$$

The term effective refractive index is somewhat misleading, as the refractive index is a scalar quantity in a step index fibre and as such is not affected by the direction of the ray travel within what is assumed at this stage of the calculation to be an isotropic medium (other factors involving non-linearities in the refractive index profile etc. may be allowed for in separate calculations if necessary). It would therefore seem more appropriate to mentally connect the $\sin\theta$ factor of the Bragg wavelength to the effective period of the grating as seen by the rays of incident angle θ, and thus the propagation constant β than with the term effective refractive index.

The concept of the effective refractive index is often utilised to explain the confinement limitations of radiation within the core and cladding, as explained below. As stated previously the 'effective refractive index' of the core is given as

$$n_{eff_{core}} = n_{core}\sin\theta \quad \text{where} \quad \theta_c \leq \theta \leq 90° \qquad (3.99)$$

It can be seen that the maximum value of $n_{eff_{core}}$ will occur when the ray is travelling parallel to the fibre axis, thus the incident angle θ is 90° (i.e. $\sin\theta = 1$) and will be equal to n_{core}. The minimum value of $n_{eff_{core}}$ will occur when the ray is incident on the core cladding boundary at the critical angle θ_c.

From Snell's law of refraction, $n_{core}\sin\theta_{core} = n_{clad}\sin\theta_{clad}$ at the critical angle θ_{core} is θ_c, and the ray is refracted parallel to the core/cladding interface into the cladding, so θ_{clad} is 90°, thus as $\sin\theta_c = \dfrac{n_{clad}}{n_{core}}$, it follows that $n_{eff_{core}} = n_{clad}$. Therefore when the ray is incident on the core/cladding boundary at an angle equal to the critical angle θ_c the effective refractive index is equal to the refractive index of the cladding. This is as would be expected since the ray will no longer undergo total internal reflection within the core and will enter the cladding. As the incident angle gets smaller the rays will be refracted at the core/cladding boundary through angles of 0° to 90°. The cladding also has an effective refractive index given as:

$$n_{eff_{clad}} = n_{clad}\sin\theta \qquad\qquad \text{where } \theta_c \leq \theta \leq 90° \qquad (3.100)$$

It follows therefore that the maximum value of $n_{eff_{clad}}$ will occur when the ray is travelling parallel to the fibre axis, thus the incident angle θ is 90° (i.e. $\sin\theta = 1$) and will be equal to n_{clad}. Also the minimum value of $n_{eff_{core}}$ will occur when the ray is incident on the core cladding boundary at the critical angle θ_c. Thus when the ray is incident on the core/cladding boundary at an angle equal to the critical angle θ_c the effective refractive index is equal to the refractive index of the surrounding air. This is again as expected as the ray will no longer undergo total internal reflection within the cladding and will escape into the air.

If the previous explanation is undertaken using the propagation constant, however, the confusion of the refractive index being direction dependent is removed as shown in Figure 3.19.
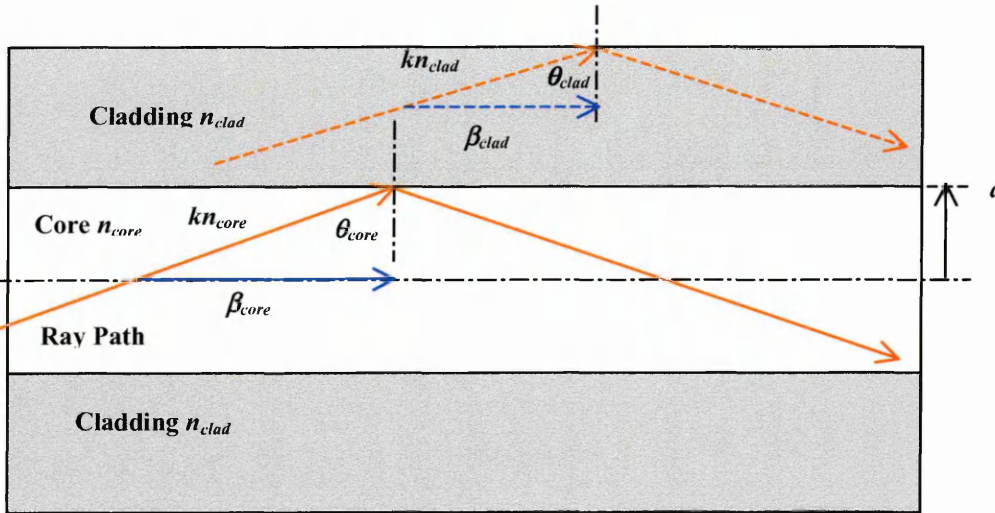
Figure 3.19:   Propagation constants (β) in optical fibre

β_{core} is the propagation constant of the radiation of a given wavelength within the core, and is the component of the wave vector $k = \dfrac{2\pi}{\lambda}$ (which is in the actual direction of propagation of the ray) in the axial plane of the core, and from Figure 3.19 can be seen to be defined as $\beta = kn\ sin\theta$. It can be seen that shorter wavelengths (λ) will have larger wave vectors (k), and thus larger propagation constants (β).   The maximum value of β_{core} must occur when the wave vector k is parallel to the core axis and θ is 90°, thus, $\beta_{core} = kn_{core}$. The minimum value of β_{core} must occur when the wave vector k is propagating at the critical angle θ_c to the core/cladding boundary, thus, $\beta_{core} = kn_{core}\ sin\theta_c$

since $sin\theta_c = n_{clad} / n_{core}$ [302]

$$\beta_{core} = kn_{clad}$$

From Figure 3.19 the propagation constant in the cladding β_{clad} is given as:

$$\beta_{clad} = kn_{clad} \sin\theta$$

If the ray is propagating within the cladding parallel to the core axis (as is the ray incident at the critical angle on the core /cladding interface) then θ will be 90°, thus

$$\beta_{clad} = kn_{clad}$$

Again when the ray is incident on the core/cladding boundary at the critical angle the propagation constant in the core is equal to the propagation constant in the cladding, which would be expected as the ray is no longer confined to the core, and is escaping into the cladding. The possible range of values of the propagation constant in the core, β_{core} is therefore,

$$kn_{clad} \leq \beta_{core} \leq kn_{core}$$

The magnitude of β_{core} reduces as the angle of incidence at the core/cladding interface decreases (gets steeper), until the angle reaches the critical angle, beyond which the magnitude of β_{core} is smaller than the minimum value allowed in the core, thus becoming within the range of the cladding propagation constant as the ray escapes the core into the cladding.

The alterative FBG coupling equation given in terms of the propagation constants in the core and the cladding is shown as [303]:

$$\lambda_{BRAGG} = 2\beta_{core} \frac{\Lambda}{k} \qquad\qquad (3.101)$$

This formula can be easily derived from (3.98)

3.12 Long Period Grating Theory

The long period grating sensor (LPG) is a variation on the fibre Bragg grating (FBG) sensor, and as its name suggests differs in construction from the FBG by the length of the grating period. FBG grating periods are typically less than 1μm whereas LPG grating periods are typically in the range of hundreds of μm [304]. The greater period spacings in the LPG result in much smaller diffraction angles, eliminating the possibility of the ray being diffracted in the opposite direction to the incident ray. The FBG utilises the reflections from (or diffraction by) successive grating elements in the sensing mechanism, with all of the radiation remaining in forward or reverse propagation modes within the core. The LPG, however, can only be explained using the diffraction properties of the grating, with the guided radiation undergoing diffraction on contact with the grating. The angle of this diffraction results in a modification of the propagation constant β_{core}, of the core mode of each wavelength, which in turn affects the coupling conditions of those wavelengths. Thus unlike the FBG there is no reflected (reverse diffracted) radiation due to this effect (but there may be some reflected radiation of higher harmonics from the FBG effect of the grating) [194], and only transmission profiles may be observed.

The ith coupling wavelength for LPG's is given as [32,47,166,175,305-309]:

$$\lambda_i = \left(\beta_{(\lambda_i)core} - \beta_{(\lambda_i)clad}\right)\frac{\Lambda}{k} \tag{3.102}$$

or

$$\lambda_i = \left(n_{eff(\lambda_i)core} - n_{eff(\lambda_i)clad}\right)\Lambda \tag{3.103}$$
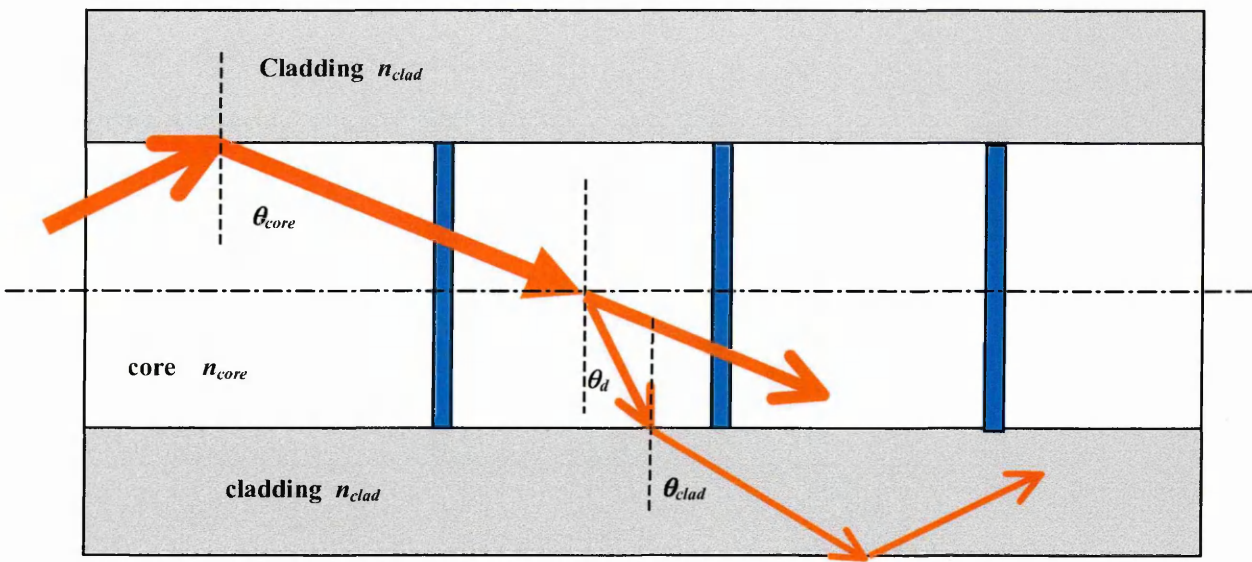
Figure 3.20:   Operation of LPG as diffraction grating

Referring to Figure 3.20, when the mode in the core is incident on the grating at an angle θ_{core} it is diffracted through an angle θ_d. The angle θ_d is determined by [107]:

$$n_{core} \sin \theta_d = n_{core} \sin \theta_{core} + \frac{m\lambda}{\Lambda}$$

where m is the order of diffraction

transposing
$$n_{core} \sin \theta_{core} = n_{core} \sin \theta_d - \frac{m\lambda}{\Lambda}$$

for the 1st order diffraction, $m = -1$, so:

$$n_{core} \sin \theta_{core} = n_{core} \sin \theta_d + \frac{\lambda}{\Lambda} \qquad (3.104)$$

To explain the operation of the LPG coupling equation the angle of the diffracted ray can be related to the angle of the refracted ray from the core/cladding boundary, using (3.103) for the core to cladding coupling where $n_{eff} = n \sin \theta$

$$n_{core} \sin \theta_{core} - n_{clad} \sin \theta_{clad} = \frac{\lambda}{\Lambda} \qquad (3.105)$$

substituting (3.104) into (3.105) results in:

$$n_{core} \sin \theta_d = n_{clad} \sin \theta_{clad} \qquad (3.106)$$

84

Thus the LPG coupling equations (3.102) and (3.103) are merely Snell's law using the original propagation angle of the core mode before the point of diffraction at the grating. So the propagation constant of the core mode after diffraction must be equal to that of a cladding mode for core to cladding coupling to occur.

Since $n \sin \theta = \dfrac{\beta}{k} = n_{eff}$, (3.106) can be re-written as:

$$\beta_{(\lambda_i)core(d)} = \beta_{(\lambda_i)clad}$$

or
$$n_{eff(\lambda_i)core(d)} = n_{eff(\lambda_i)clad}$$

As the angle of diffraction is wavelength dependent, each wavelength of radiation in the core will have a different incident angle on the core / cladding interface, and thus a different propagation constant β_{core}. The cladding will in effect be a multimode fibre and thus will have a range of allowed propagation angles (and therefore a range of propagation constants β_{clad}) available for each wavelength within the core.

Only if the angle of the propagation constant of a given wavelength within the core is modified by the angle of diffraction at the grating such that its propagation constant (β_{core}) is equal to that of a propagation constant for that wavelength in the cladding (β_{clad}) will that wavelength transfer (couple) from the core into the cladding and be quickly attenuated. As the allowed angles (directions) of propagation (modes) in the cladding are dependent on the refractive index of both the cladding and the medium immediately surrounding the cladding, any change in this surrounding refractive index will result in changes in the allowed propagation directions (modes) within the cladding. While a change in the refractive index of the surrounding medium will not alter the optical properties of the cladding, it will cause a change in the critical angle

thereby possibly changing the number of modes within the cladding. More importantly it will also alter the phase change of the rays at reflections from this interface [207], resulting in a change in the ray directions at which constructive interference will occur and thus the allowed possible propagation directions (modes) within the cladding. The allowed angles (directions) of propagation (modes) in the core will not be affected by the change in refractive index of the medium immediately surrounding the cladding, but the wavelengths at which coupling from core to cladding occurs will change as different wavelengths of the radiation within the core will match the coupling conditions given in (3.102) or (3.103) and couple into the modified allowed propagation directions within the cladding. This phenomena allows the long period fibre grating to be used as an ambient refractive index sensor, and thus a gas or chemical sensor as different types or concentrations of the gas/chemical surrounding the cladding will change this ambient refractive index and therefore change the wavelength at which core to cladding coupling occurs.

Examination of the derivation of the LPG coupling equation highlights an anomaly that has never been covered in any literature on the subject, and therefore requires explanation. Referring to (3.102) (3.103) and Figure 3.20, as $n_{eff\,core}$ is determined by the angle of travel of the mode in the core and given as $n_{core}\,sin\theta_{core}$, the range of angles over which a core mode may be 'guided' through the core are from 90° for modes which travel parallel to the axis to those which travel at the critical angle (θ_c). Thus the range of $n_{eff\,core}$ values for a 'guided' core mode is given by:

$$n_{core} > n_{eff\,core} > n_{clad} \qquad\qquad (3.107)$$

By the same reasoning the range of $n_{eff\,clad}$ values for a 'guided' cladding mode is given by:

$$n_{clad} > n_{eff\,clad} > n_{ambient} \qquad (3.108)$$

In (3.103) $n_{eff\,core}$ refers to the angle of travel of the mode before being diffracted by the grating and is guided in the core. It can be written in terms of the diffracted ray as:

$$n_{eff\,(d)} = n_{eff\,clad} \qquad (3.109)$$

As the effective indices of the cladding modes are unaffected by the grating, the effective index of the core mode must be changed by the grating (as expected due to the now steeper angle of the modal path after diffraction at the grating). Thus $n_{eff\,core}$ has reduced to such a value that it is now equal to a value in the range of the cladding effective indices as shown in (3.109).

Given the allowed ranges of effective refractive indices for 'guided' core and 'guided' cladding modes predicted in (3.107) and (3.108), there is no possibility of a guided core mode having the same effective index of any of the cladding modes. Thus if the effective index of the core mode after diffraction by the grating is now within the range of the cladding effective indices, the core mode can no longer be guided and must therefore be incident on the core cladding interface at an angle less than the critical angle of the core. As the minimum limit of $n_{core}\,sin\theta_{core}$ ($= n_{eff}$) for guided core modes is n_{clad} , θ_d must be less than or equal to θ_c and the coupling core mode can therefore no longer be guided.

The fibre core is single mode but as the light source consists of a range of wavelengths, e.g. $\Delta\lambda \sim$ 30nm for typical LED, each wavelength will have its own propagation constant, β. When a propagation constant of one of these wavelengths in the core and the propagation constant of that wavelength in one the many cladding

modes matches the condition set by (3.102), this wavelength will be coupled into that forward propagating mode in the cladding. As any core propagation constant β_{core} only has a range of kn_{core} to kn_{clad} (β_{clad} max) and the cladding propagation constants only have a range of kn_{clad} to $kn_{ambient}$ (greater β_{clad} values will become radiation modes), the only value at which $\beta_{core(d)}$ can be the same as β_{clad} is when the radiation in the core is incident on the core cladding boundary at an angle equal to or less than the critical angle of the core. If this is the case then it would be expected that once a wavelength on the shorter side of the transmitted spectrum has overcome its critical angle all longer wavelengths should also have overcome their critical angles as depicted in Figure 3.21, so by Snells law it would be expected that they also should escape the core.
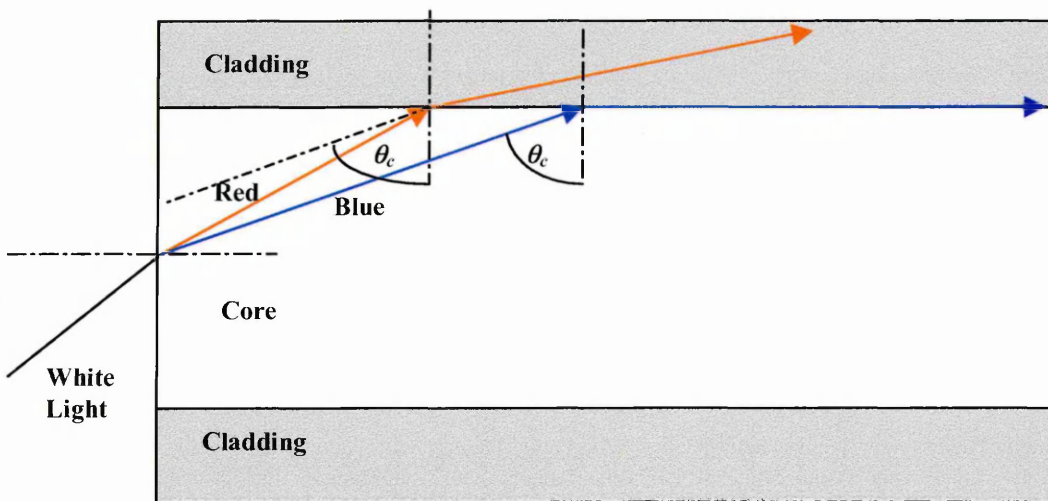
Figure 3.21: **Critical angles of shorter wavelength (blue) and longer wavelength (red) of radiation in fibre core**

This would create a continuum of radiation absent in the transmission spectrum of all wavelengths greater than the minimum coupled wavelength. As this is not the case, and only selected wavelengths where the core and cladding propagation constants are comparable escape into the cladding, coupled mode theory must be considered to

account for the selective escape of radiation into the cladding as explained in Section 3.9.

Coupled mode theory works on the evanescent field principle, and states that when the propagation constants, β, of two wave guides in close proximity are equal then the radiation from one guide will pass totally into the other [310]. If the propagation constants are almost equal then a proportional fraction of the radiation will pass into the other wave guide. This would account for the wavelength selective nature of the LPG and also the width of the coupling wavelength dip, as the propagation constants of the wavelengths each side of the actual coupling wavelength approach and then exceed those of the cladding propagation constants for those wavelengths. In the case of the optical fibre the core can be classed as one wave guide whilst the cladding classed as the other in close proximity and core to cladding coupling will therefore take place as previously described.

It can be seen from (3.102) and (3.103) that the wavelength at which coupling will occur depends on the propagation constants of that wavelength matching these formulae. As previously stated, the propagation constant of the core mode depends only on the core and cladding properties (refractive index, diameter), the modes of each wavelength in the core will not alter due to changes in refractive index of the ambient medium immediately surrounding the cladding, so these will be constant. However, as the propagation constants of each wavelength in the multimode cladding depend on the properties of the cladding (refractive index, diameter) and coating (ambient refractive index), any change in the ambient refractive index will cause a corresponding change in the propagation constants of all of the modes for each

wavelength in the multimode cladding. This will result in a different wavelength in the core matching the above conditions and thus coupling from the core into the cladding.

On inspection of (3.102) and (3.103) it may appear to be a simple conclusion to state that as β_{core}, Λ, and k are constant for a given wavelength, the change in coupling wavelength must be due to a change in β_{clad} at that wavelength (i.e. subtracting a greater or lesser value of β_{clad} from the existing β_{core} will give a lesser or greater value of λ). This conclusion would be in error as a change in coupling wavelength will mean that the β_{core} and β_{clad} values would both need to be changed in (3.102), as would the value of k ($=2\pi/\lambda$). To remove all wavelength dependent variables except the β values (3.102) can be transformed to become:

$$\left(\beta_{(\lambda_i)core} - \beta_{(\lambda_i)clad} \right) = \frac{2\pi}{\Lambda}$$

Thus if the coupling wavelength decreases as the ambient refractive index increases (as experimental and simulated results show it does), and as $\beta = \left(\frac{2\pi}{\lambda} \right) n_{eff}$, then β_{core} and β_{clad} must both be of a higher value. (β_{core} is a higher value than for the original coupling wavelength corresponding to the new shorter coupling wavelength, it has not changed in value itself, as it was always that value for this new wavelength, but β_{clad} has changed to a higher value itself due to the new allowed propagation directions (modal changes) at all wavelength as well as being a higher value than for the original coupling wavelength corresponding to the new shorter coupling wavelength). Thus both β_{core} and β_{clad} will increase in value, but as the difference between them is always $2\pi/\Lambda$, they must each increase by the same amount.

Returning to the original LPG equation (3.102), as the value $(\beta_{(\lambda i)core} - \beta_{(\lambda i)clad})$ is always constant $(=2\pi/\Lambda)$ when coupling occurs, then the change in the resulting coupling wavelength must be totally dependent on k, which will be different for each wavelength.

3.13 Effect of Change in Ambient RI on Coupling

As the ambient index increases from $n_{ambient}$ to $n_{ambient}'$ the following effects will occur in the cladding:

i) The critical angle, $\theta_c = \sin^{-1}\left(\dfrac{n_{ambient}}{n_{clad}}\right)$ [301], increases proportionally from θ_c to θ_c'
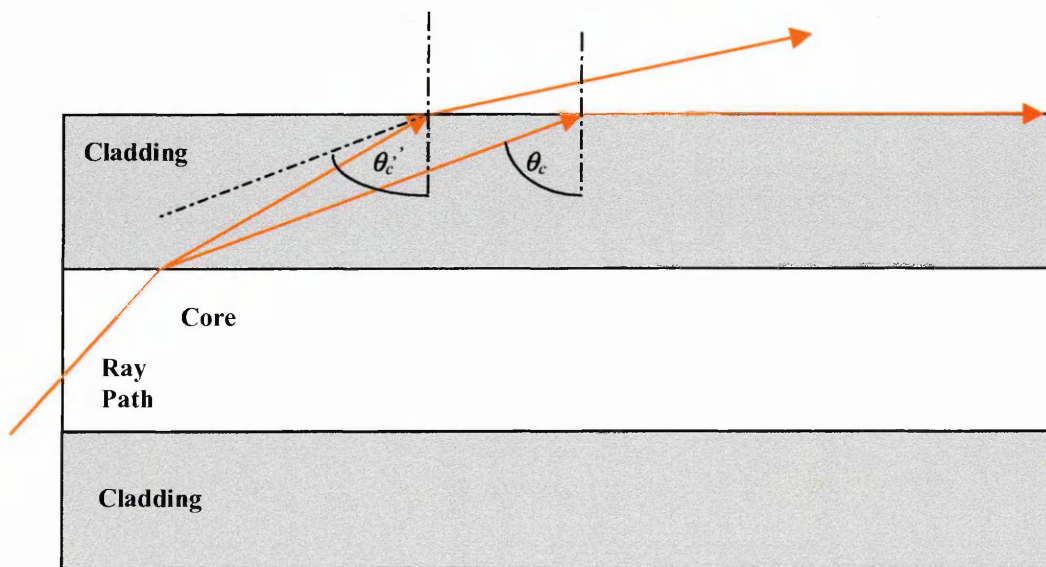
Figure 3.22:   **Increase in critical angle due to increase in ambient index**

It can be seen in Figure 3.22 that this will reduce the amount of light that will be guided by the cladding. As the critical angle is slightly different for each wavelength (due to wavelength dependence of the refractive index), the amount of light guided and therefore the number of modes at each wavelength will be reduced. It will have no effect however on the direction and therefore the β values of the TIR rays in the cladding as the angle of reflection will equal the angle of incidence whatever the ambient index is.

As the cladding can (and does) contain hundreds of modes and as core to cladding coupling is normally designed to utilize only the first ten or so cladding modes [302] the loss of these higher order modes will have no appreciable effect on the observed output spectrum of the fibre core.

ii) The phase change on reflection at the cladding/ambient boundary is dependent on the angle of incidence (which will not change with ambient RI) and the RI difference at that boundary [265]. As the modes only exist under TIR conditions, the phase shift at angles greater than the critical angle need only be determined, which will be different for TE and TM modes [231]. The phase shift ϕ is given by [311-314]:

For TE modes
$$\phi_{TE} = 2\tan^{-1}\left(\frac{\sqrt{\sin^2\theta - N^2}}{\cos\theta}\right)$$

For TM modes
$$\phi_{TM} = 2\tan^{-1}\left(\frac{\sqrt{\sin^2\theta - N^2}}{N^2\cos\theta}\right)$$

Where $N = \dfrac{n_{ambient}}{n_{clad}}$, i.e. $N < 1$

The phase changes versus the incident angle for both TE and TM rays are shown in Figures 3.23 to 3.26 for various values of n_{clad} and $n_{ambient}$.
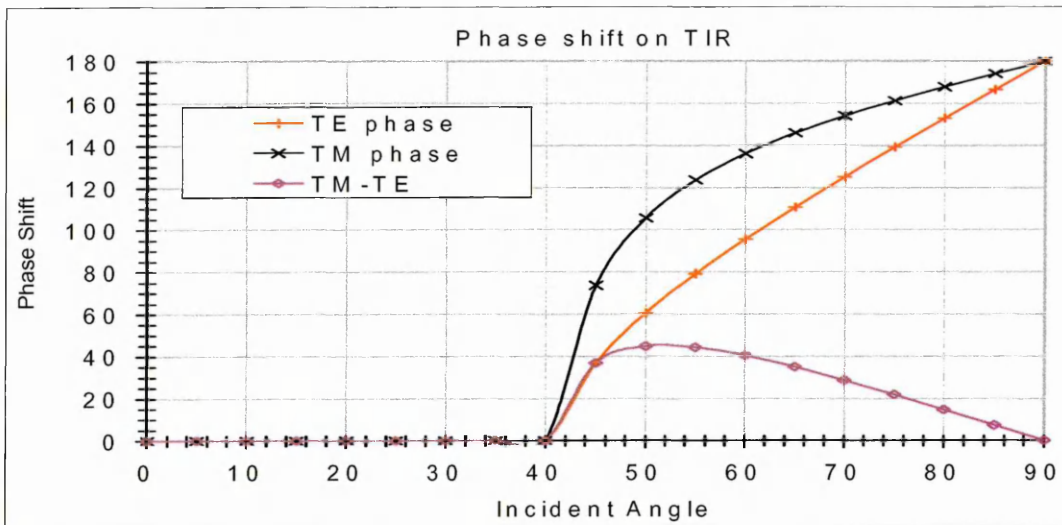
Figure 3.23: Phase changes versus the incident angle for both TE and TM rays with $n_{clad} = 1.5$, $n_{ambient} = 1.0$
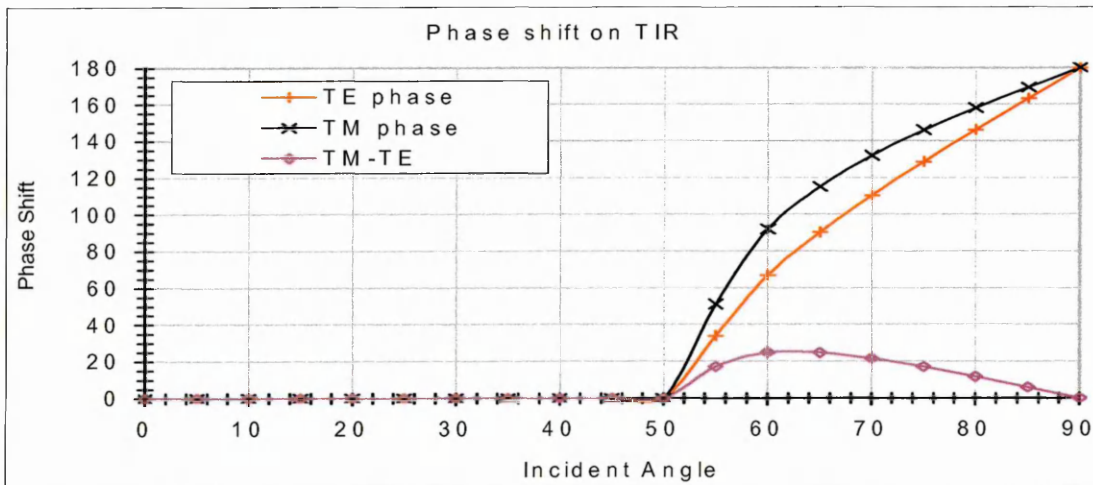
Figure 3.24: Phase changes versus the incident angle for both TE and TM rays with $n_{clad} = 1.5$, $n_{ambient} = 1.2$
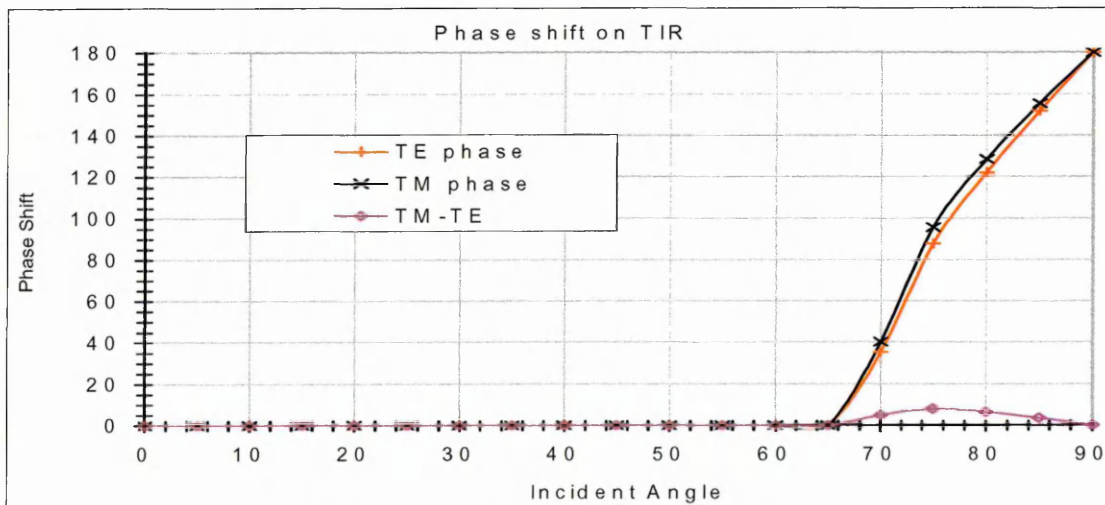
Figure 3.25: Phase changes versus the incident angle for both TE and TM rays with $n_{clad} = 1.5$, $n_{ambient} = 1.4$

93
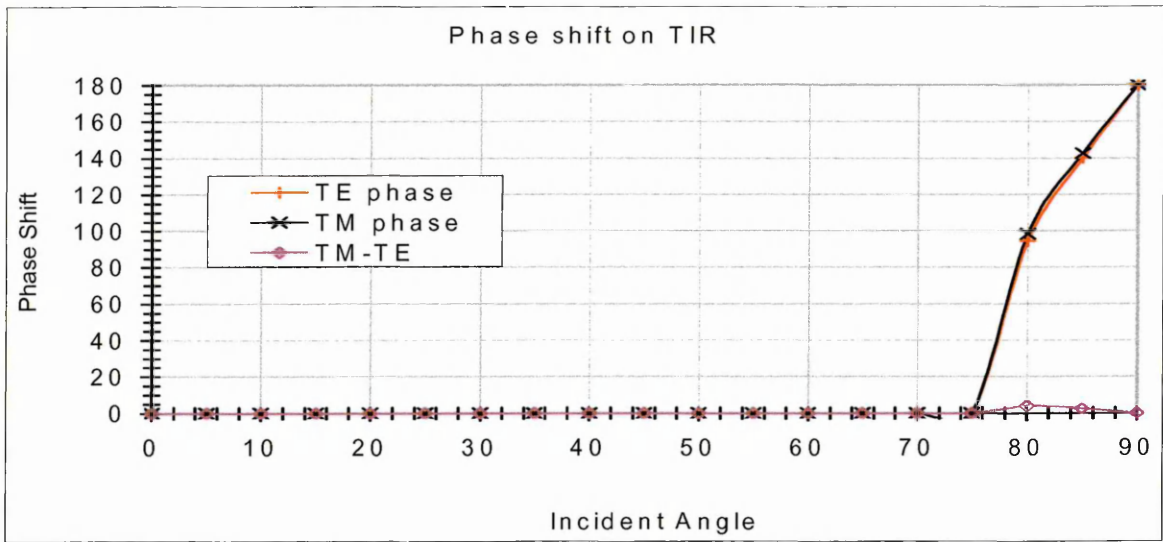
Figure 3.26: **Phase changes versus the incident angle for both TE and TM rays with n_{clad} = 1.5, $n_{ambient}$ = 1.45**

Incident Angle	Phase Shift ϕ at given ambient index n_3							
	$n_3 = 1$		$n_3 = 1.2$		$n_3 = 1.4$		$n_3 = 1.45$	
	TE	TM	TE	TM	TE	TM	TE	TM
80°	153.1	167.8	146.3	158.1	122.1	128.6	94.6	98.5
81°	155.8	169.1	149.8	160.4	128.3	134.3	104.7	108.4
82°	158.5	170.3	153.2	162.6	134.4	139.8	114.1	117.6
83°	161.2	171.6	156.6	164.9	140.3	145.1	123.2	126.3
84°	163.9	172.8	160.9	167.1	146.1	150.3	131.8	134.6
85°	166.6	174.0	163.3	169.3	151.9	155.4	140.2	142.6
86°	169.3	175.2	166.6	171.4	157.6	160.4	148.4	150.4
87°	171.9	176.4	170.0	173.6	163.2	165.4	156.4	157.9
88°	174.6	177.6	173.3	175.7	168.8	170.3	164.3	165.3
89°	177.3	178.8	176.7	177.9	174.4	175.1	172.2	172.7
90°	180	180	180	180	180	180	180	180

Table 3.1: **Summary of phase changes versus the incident angles between 80° and 90° for both TE and TM rays at a range of ambient indices**

As can be seen from Figures 3.23 to 3.26 and Table 3.1, as the ambient index is increased the critical angle increases as stated in (i), and the phase change of any given wavelength which remains within the critical angle decreases as stated in (ii). As the ambient index approaches that of the cladding, the difference between the TE

94

and TM phase changes decreases. This fact is utilised in the weakly guiding approximation discussed in Section 3.4 of this thesis.

Thus as the ambient index increases towards that of the cladding the phase change on reflection at each cladding to ambient interface decreases, altering the optical path length of each wavelength, and thereby altering the angles at which constructive interference will occur at that wavelength (and therefore the β values of the modes). This will result in the wavelengths coupling from the core to the cladding given in (3.102) changing also.

3.14 Intensity Profile of Coupled Radiation

The intensity of the radiation coupled between core and cladding modes is dependent on the coupling coefficient as explained in section 3.9. This section uses ray theory to give a more intuitive description of the concepts.

As shown in Figure 3.27, when radiation enters the fibre aperture the longer wavelengths will be refracted less than the shorter wavelengths, and will therefore be incident on the core/cladding boundary at a smaller (steeper) angle than the shorter wavelengths.
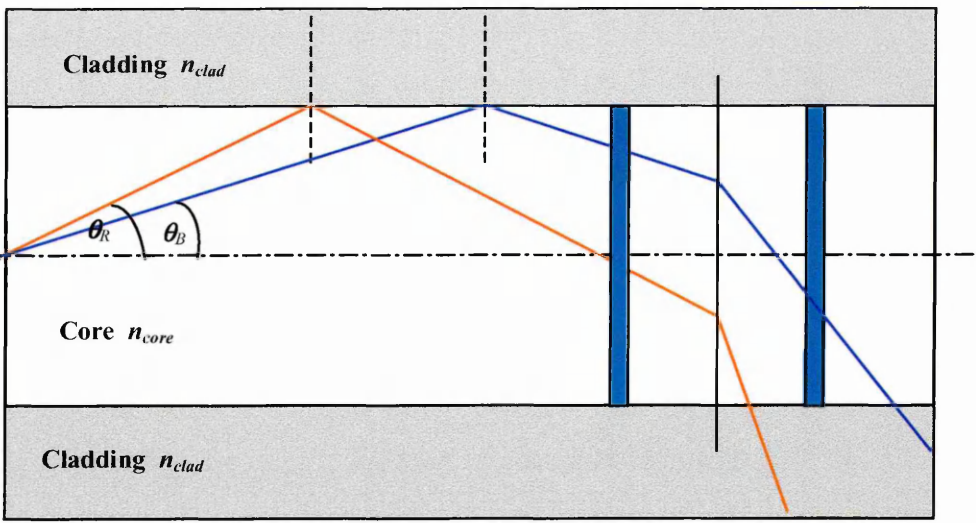
Figure 3.27: Refraction and diffraction of different wavelengths of light at refractive index boundaries

When the rays encounter the grating the longer wavelengths will be diffracted through a greater angle than the shorter wavelengths. Both these effects ensure that the longer wavelengths in the spectrum within the fibre core will be incident on the core/cladding boundary at steeper angles than the shorter wavelengths after diffraction by the grating. As previously stated the core/cladding incident angle of the coupling wavelength paths after diffraction by the grating is less than the critical angle at that wavelength. As such the radiation will be partially reflected back into the core and partially diffracted into the cladding at core/cladding interface. The fraction of the radiation which will be reflected or transmitted will depend on the angle of incidence. The reflection coefficient ρ determines the fraction of the electric field reflected at a boundary, for normal incidence ($\theta = 0°$) [315]:

$$\rho = \frac{n_1 - n_2}{n_1 + n_2}$$

If n_2 is greater than n_1, (external reflection, no TIR possible) ρ will be negative, indicating that there is a 180° phase shift on reflection between the incident and reflected electric fields.

96

Reflectance R is the fraction of the incident beam intensity which is reflected at a boundary, and is equal to ρ^2, for normal incidence ($\theta = 0°$) [316]

$$R = \frac{(n_1 - n_2)^2}{(n_1 + n_2)^2}$$

If the angle of incidence is not normal to the surface then the polarisation of the radiation will affect the reflection coefficient ρ as predicted in (3.110) and (3.111) (see Appendix 1 for derivation) [317-319]:

For parallel polarisation (TE)

$$\rho_{TE} = \frac{\cos\theta_I - \sqrt{N^2 - \sin^2\theta_I}}{\cos\theta_I + \sqrt{N^2 - \sin^2\theta_I}} \qquad (3.110)$$

For perpendicular polarisation (TM)

$$\rho_{TM} = \frac{N^2\cos\theta_I - \sqrt{N^2 - \sin^2\theta_I}}{N^2\cos\theta_I + \sqrt{N^2 - \sin^2\theta_I}} \qquad (3.111)$$

By the same theory the transmission coefficients for TE and TM polarisations are predicted in (3.112) and (3.113) (see Appendix 1 for derivation) [319,320]:

For parallel polarisation (TE)

$$\tau_{TE} = \frac{2\cos\theta_I}{\cos\theta_I + \sqrt{N^2 - \sin^2\theta_I}} \qquad (3.112)$$

For perpendicular polarisation (TM)

$$\tau_{TM} = \frac{2N\cos\theta_I}{N^2\cos\theta_I + \sqrt{N^2 - \sin^2\theta_I}} \qquad (3.113)$$

where $N = \dfrac{n_{core}}{n_{clad}}$

It is logical also to state that $\tau = 1 - \rho$ [321]

Reflectance (R) is the fraction of power in the incident wave which is reflected from the surface [322]:

$$R_{TE} = \rho_{TE}{}^2$$

$$R_{TM} = \rho_{TM}{}^2$$

Transmittance (T) is not equal to the square of the transmission coefficient but can be shown to be [323]:

$$T_{TE} = 1 - R_{TE}$$

$$T_{TM} = 1 - R_{TM}$$

The Reflectance, R, and Transmittance, T, are shown in Figure 3.28 for a fibre/air interface of n_{core} = 1.5, $n_{ambient}$ = 1.0, resulting in a critical angle (θ_c) of 41.81° and a Brewster angle (θ_b) of 33.69°.
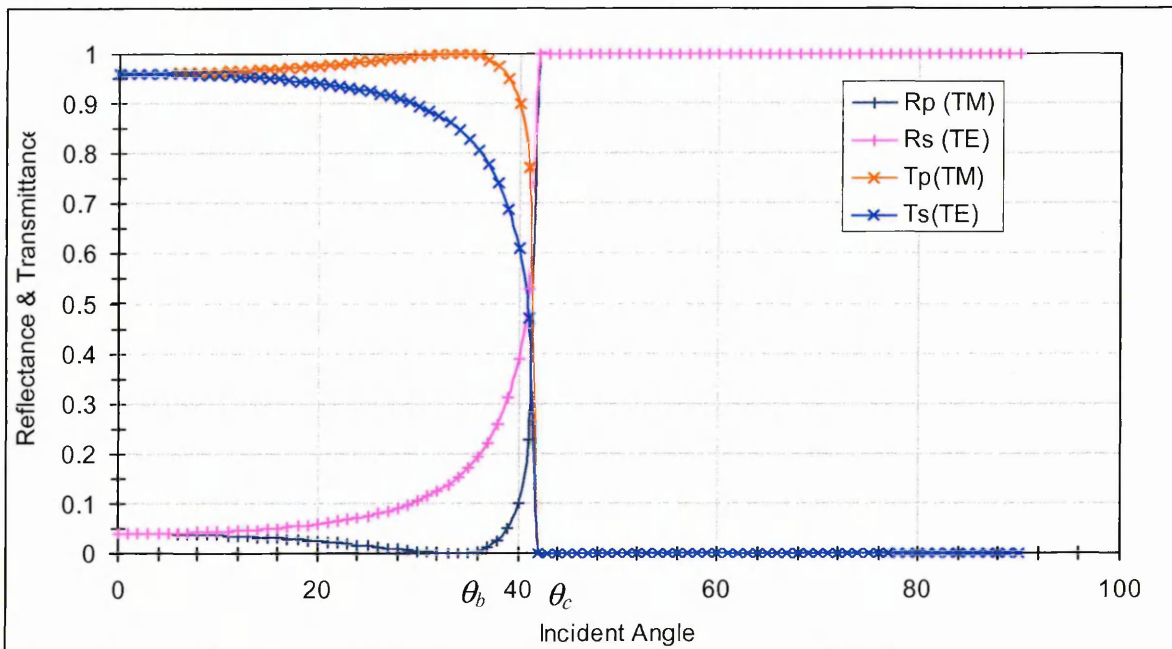
Figure 3.28:   Reflectance & transmittance for $n_{core} > n_{clad}$

It can be seen that for the TE rays as the incident angle increases from zero the reflectance increases and the transmission decreases, until TIR is achieved at the

critical angle. For TM rays however, it can be seen that as the incident angle initially increases from zero the reflectance decreases and the transmission increases until the Brewster angle is reached at which all of the light is transmitted across the interface and none reflected (due to the polarising effect at the Brewster angle, see Appendix 2). For incident angles greater than the Brewster angle it can again be seen that the reflectance increases and the transmission decreases, until TIR is achieved at the critical angle. Thus as the longer coupling wavelengths in the core which are incident on the core cladding interface at the steepest (smallest) angles (the incident angles being just less than the critical angle after diffraction by the grating) will experience a greater fraction of transmitted radiation than the shorter wavelengths which will be incident at shallower angles. This will result in a greater dip in the transmission spectrum for longer coupling wavelengths than the shorter ones as confirmed by theory [142,324-326].

It can be seen that the reflectance increases as the incidence angle increases (rays incident at shallower angles), until the critical angle is reached, thus more transmission occurs across the core/cladding interface at longer wavelengths. The LPG spectra show this as the shorter wavelengths couple to the lower order cladding modes with the intensity of the coupling reducing as the core wavelength and cladding mode order decreases.

For incident angles greater than the critical angle, $\theta_i > \theta_c$ in the reflection coefficient equations, where $n_1 > n_2$, $n_1^2\sin^2\theta_i > n_2^2$ (guided waves) causing the rooted term to become negative and thus imaginary, resulting in the reflection coefficients being given by equations of the form [327]:

$$|\rho| = \frac{|A - jB|}{|A + jB|}$$

As the magnitudes of $|A - jB|$ and $|A + jB|$ are both $(A^2 + B^2)^{1/2}$, the magnitude of ρ will be unity (1), with the associated angle giving the phase shift of the reflected wave relative to the incident wave. The Reflectance ($R = \rho^2$) will therefore also be total (unity) for all incident angles greater than the critical angle.

3.15 Summary

This chapter has introduced the concepts of light guidance, mode formation and mode classification in optical fibres. The equations predicting the characteristics of light propagation are derived from Maxwell's Equations and subsequently applied to the light propagation in optical fibres and mode classification. The concept of the evanescent field, coupled mode theory, fibre Bragg gratings, effective refractive index, long period gratings, and the relevant effects of changes in ambient index have been discussed.

Chapter 4

Computer Simulations

4.1 Introduction

A major part of this research was to develop a mathematical model to predict the core

and cladding mode propagation constants in fibres of given optical and physical

parameters, to allow comparison with the results obtained experimentally. Computer

programs were developed to determine HE_{11} core modes and HE_{ml} cladding modes

from expression (3.4) developed in section 3.5 to 3.7, and by Erdogan [278]. The

program is also used to predict various outcomes which could not be verified

experimentally due to lack of resources etc.

Section 4.2 introduces the equations used to predict the modes in the core and cladding. Section 4.3 shows the program constructed to predict the number of modes and their optical constants in an ideal fibre core and cladding. The code is expanded in section 4.4 to predict a grating period which would couple the core mode to a specific cladding mode, and thus predict further coupling of all shorter wavelengths in the core into the lower order cladding modes. Section 4.5 shows how this program code can be used to design an optical fibre grating period to couple a selected wavelength from the core into a specific cladding mode. The simulation in section 4.6 predicts the coupling wavelength shifts with a range of ambient indices up to that of the cladding using the actual parameters of the fibres involved in the experimental investigations, and the simulation in section 4.7 adapts the previous code to determine the coupling wavelength shifts for ambient indices greater than that of the cladding.

4.2 Equations Used to Predict Core and Cladding modes

In the simulation using the derived expression (3. 4) [205] the cladding is treated as a multimode fibre core and takes no account of the effect which the refractive index of the actual core would have on the mode formation in the cladding. Simulations based on the expression developed by Erdogan [328] did include the core when predicting the cladding mode formation and was therefore expected to give more accurate

representations of the actual effects observed. In both cases the HE$_{11}$ core mode is described in equation (3.57)

The simulations are carried out using matlab, but matlab cannot operate on the differential form of the Bessel functions (denoted by the prime sign). Therefore (3.57) is converted into non differential values to predict the propagation constants of the core modes and becomes equation (4.1) [329-331]:

$$\frac{J_{m-1}(u)}{uJ_m(u)} = \frac{K_{m-1}(w)}{wK_m(w)}$$

(4.1)

which was used to predict the propagation constants of the core modes in both sets of programs.

Similarly, converting equation (3.65) describing the HE$_{ml}$ cladding modes derived in section 3.7 into non-differential form gives [332]:

$$\frac{J_{m-1}(u)}{uJ_m(u)} = -\left(\frac{n^2_{core}+n^2_{clad}}{2n^2_{core}}\right)\left(-\frac{K_{m-1}(w)-K_{m+1}(w)}{2wK_m(w)}\right)+\frac{m}{u^2}-$$

$$\left[\left(\frac{n^2_{core}-n^2_{clad}}{2n^2_{core}}\right)^2\left(-\frac{K_{m-1}(w)-K_{m+1}(w)}{2wK_m(w)}\right)^2+\left(\frac{\beta m}{kn_{core}}\right)^2\left(\frac{1}{w^2}+\frac{1}{u^2}\right)^2\right]^{\frac{1}{2}}$$

(4.2)

Here the cladding is treated as a multimode core, thus the cladding specifications are represented by the core subscript and the ambient specifications are represented by the cladding subscript.

The alternative program utilises the equation describing the HE$_{ml}$, cladding modes taken from Erdogan [328]:

$$\zeta_0 = \zeta_0'$$

(4.3)

where

$$\zeta_0 = \frac{1}{\sigma_2} \frac{u_2\left(JK + \dfrac{\sigma_1\sigma_2 u_{21}u_{32}}{n_2^2 r_1 r_2}\right)p_m(r_2) - Kq_m(r_2) + Jr_m(r_2) - \dfrac{1}{u_2}s_m(r_2)}{-u_2\left(\dfrac{u_{32}}{n_2^2 r_2}J - \dfrac{u_{21}}{n_1^2 r_1}K\right)p_m(r_2) + \dfrac{u_{32}}{n_1^2 r_2}q_m(r_2) + \dfrac{u_{21}}{n_1^2 r_1}r_m(r_2)}$$

$$\zeta_0' = \sigma_1 \frac{u_2\left(\dfrac{u_{32}}{r_2}J - \dfrac{n_3^2 u_{21}}{n_2^2 r_1}K\right)p_m(r_2) - \dfrac{u_{32}}{r_2}q_m(r_2) - \dfrac{u_{21}}{r_1}r_m(r_2)}{u_2\left(\dfrac{n_3^2}{n_2^2}JK + \dfrac{\sigma_1\sigma_2 u_{21}u_{32}}{n_1^2 r_1 r_2}\right)p_m(r_2) - \dfrac{n_3^2}{n_1^2}Kq_m(r_2) + Jr_m(r_2) - \dfrac{n_2^2}{n_1^2 u_2}s_m(r_2)}$$

where

$$\sigma_1 = \frac{imn_{eff}}{z_0}$$

$$\sigma_2 = imn_{eff}z_0 \qquad\qquad u_j = \sqrt{k^2 n_j^2 - \beta^2}$$

$$z_0 = \sqrt{\frac{\mu_0}{\varepsilon_0}} = 377\Omega \qquad\qquad w_j = \sqrt{\beta^2 - k^2 n_{ambient}^2}$$

$$u_{21} = \frac{1}{u_1^2} - \frac{1}{u_2^2} \qquad\qquad J = \frac{J_{m-1}(u_1 r_1) - J_{m+1}(u_1 r_1)}{2u_1 J_m(u_1 r_1)}$$

$$u_{32} = \frac{1}{w_2^2} - \frac{1}{u_2^2} \qquad\qquad K = \frac{-K_{m-1}(w_2 r_2) - K_{m+1}(w_2 r_2)}{2w_2 K_m(w_2 r_2)}$$

$$p_m(r) = J_m(u_2 r)N_m(u_2 r_1) - J_m(u_2 r_1)N_m(u_2 r)$$

$$q_m(r) = J_m(u_2 r)\left(\frac{N_{m-1}(u_2 r_1) - N_{m+1}(u_2 r_1)}{2}\right) - \left(\frac{J_{m-1}(u_2 r_1) - J_{m+1}(u_2 r_1)}{2}\right)N_m(u_2 r)$$

$$r_m(r) = \left(\frac{J_{m-1}(u_2 r) - J_{m+1}(u_2 r)}{2}\right)N_m(u_2 r_1) - J_m(u_2 r_1)\left(\frac{N_{m-1}(u_2 r) - N_{m+1}(u_2 r)}{2}\right)$$

$$s_m(r) = \left(\frac{J_{m-1}(u_2 r) - J_{m+1}(u_2 r)}{2}\right)\left(\frac{N_{m-1}(u_2 r_1) - N_{m+1}(u_2 r_1)}{2}\right) -$$

$$\left(\frac{J_{m-1}(u_2 r_1) - J_{m+1}(u_2 r_1)}{2}\right)\left(\frac{N_{m-1}(u_2 r) - N_{m+1}(u_2 r)}{2}\right)$$

subscripts 1, 2, 3, represent core, cladding and ambient values respectively.

104

The simulation is designed to perform the following tasks over the range of wavelengths specified:

- Ensure the core will only support one mode

- Determine the value of the propagation constant of that core mode

- Determine the number of cladding modes

- Determine the propagation constants of each cladding mode

- Find at which wavelengths coupling between core and any cladding mode will occur.

As the propagation constants of the determined core and cladding modes are required to be used in the coupling equation, and all of the above equations are functions of the propagation constants of the selected wavelengths in the core and cladding, rather than attempt to perform very involved mathematics to make β the subject, the program was designed to perform the calculations over a range of β values and select the ones which matched the conditions and hence represented the modes. In all cases the right hand side of the equations were subtracted from the left, and the solutions to the equations therefore occurred at β values at which zero values were obtained.

4.3 Simulation 1: Determination and Comparison of Optical Constants of Fibre Core and Cladding using Equations 4.2 & 4.3

The first programs (Appendix 3 and Appendix 4) were designed to test equations 4.2 and 4.3, and consequently to determine the propagation constants (β), and propagation angles (θ), for the core and cladding modes of a fibre using the parameters shown in table 4.1.

Parameter	Value
Core refractive index (n_{core})	1.458
Cladding refractive index (n_{clad})	1.455
Ambient refractive index $(n_{ambient})$	1.000
Core radius (r_{core})	2.625μm
Cladding radius (r_{clad})	62.5μm
Operational wavelength (λ)	1550nm

Table 4.1:   **Optical and Physical parameters used in simulation 1**

Figures 4.1 to 4.4 show the shape of the graphs of the solutions to the HE_{ml} equations as functions of propagation constant in the core and the cladding. Figures 4.1 and 4.2 show that the line crosses zero only once, thus there is only 1 solution to (4.1) and the fibre core is operating in single mode.

106
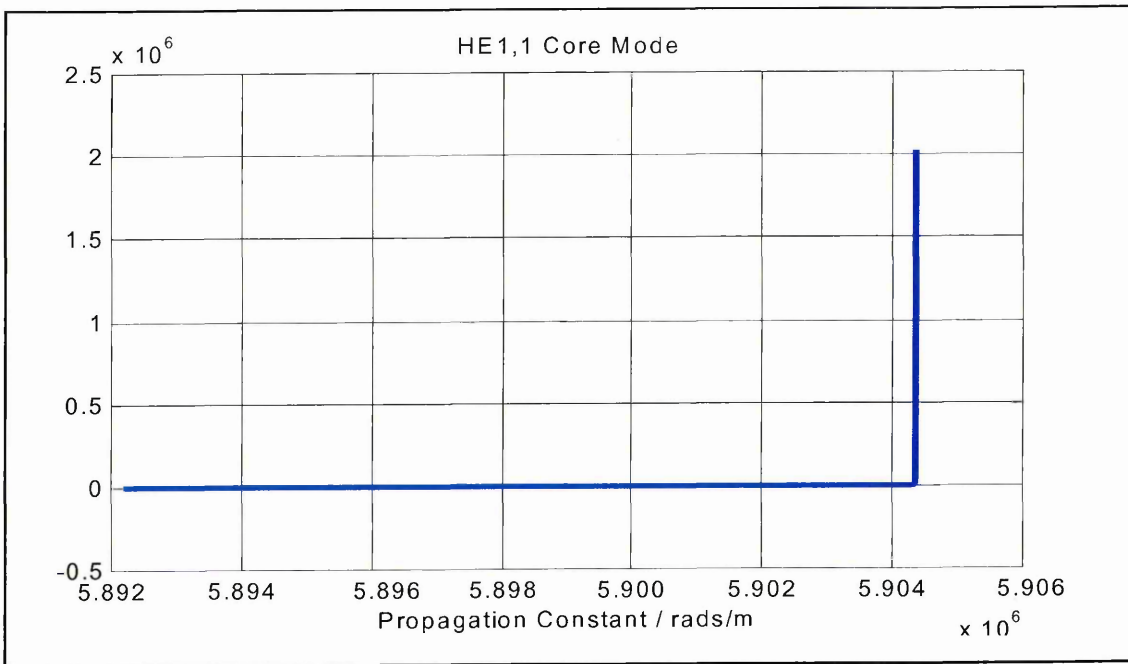
Figure 4.1:   Graph of solution to core mode equation 4.1
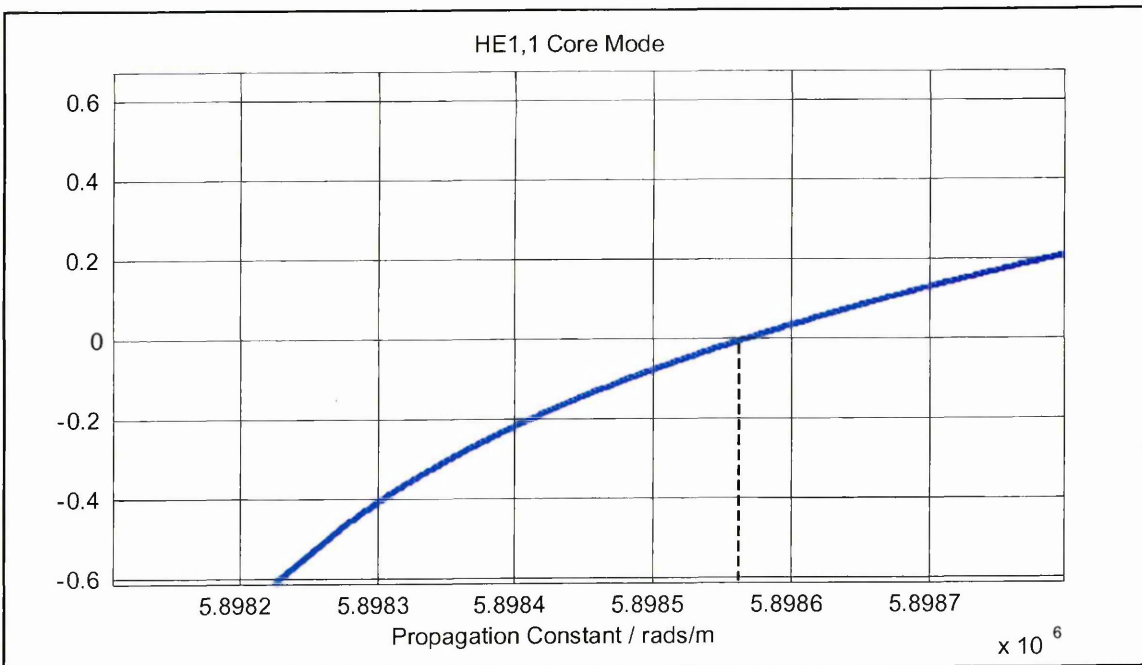
Figure 4.2:   Magnified graph of solution to core mode equation 4.1

Figures 4.3 and 4.4 show that the line crosses zero many times, thus there are many

solutions to (4.2) and the fibre cladding is operating in multimode.
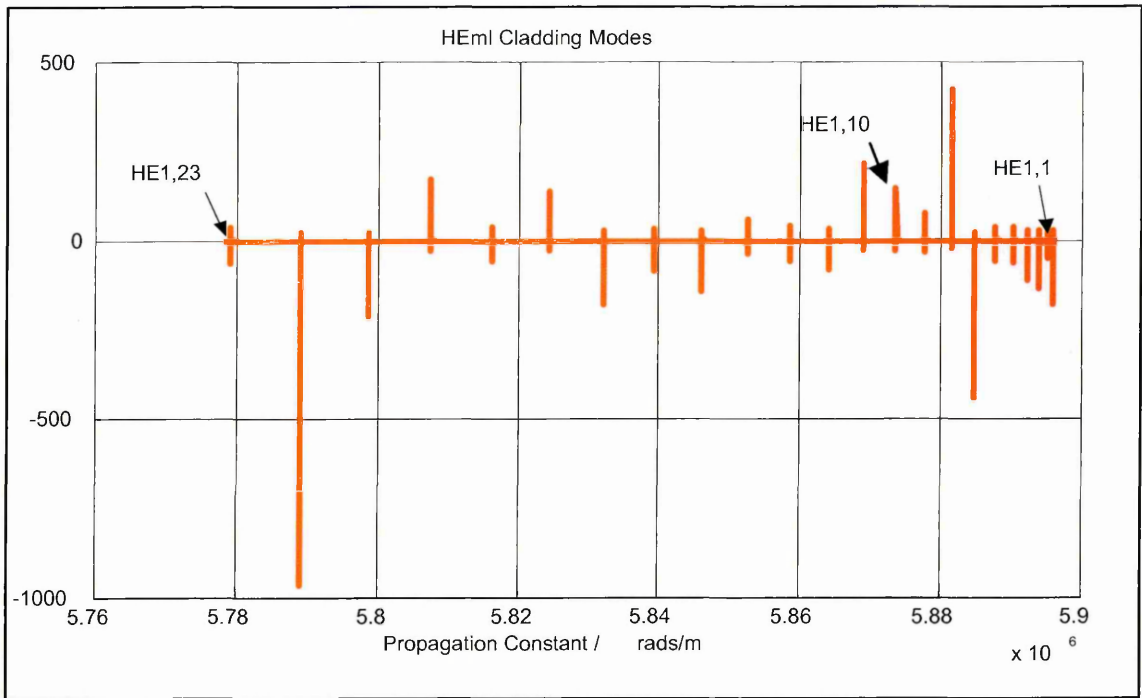
Figure 4.3: Graph of solution to cladding mode equation 4.2 showing first 23 cladding modes
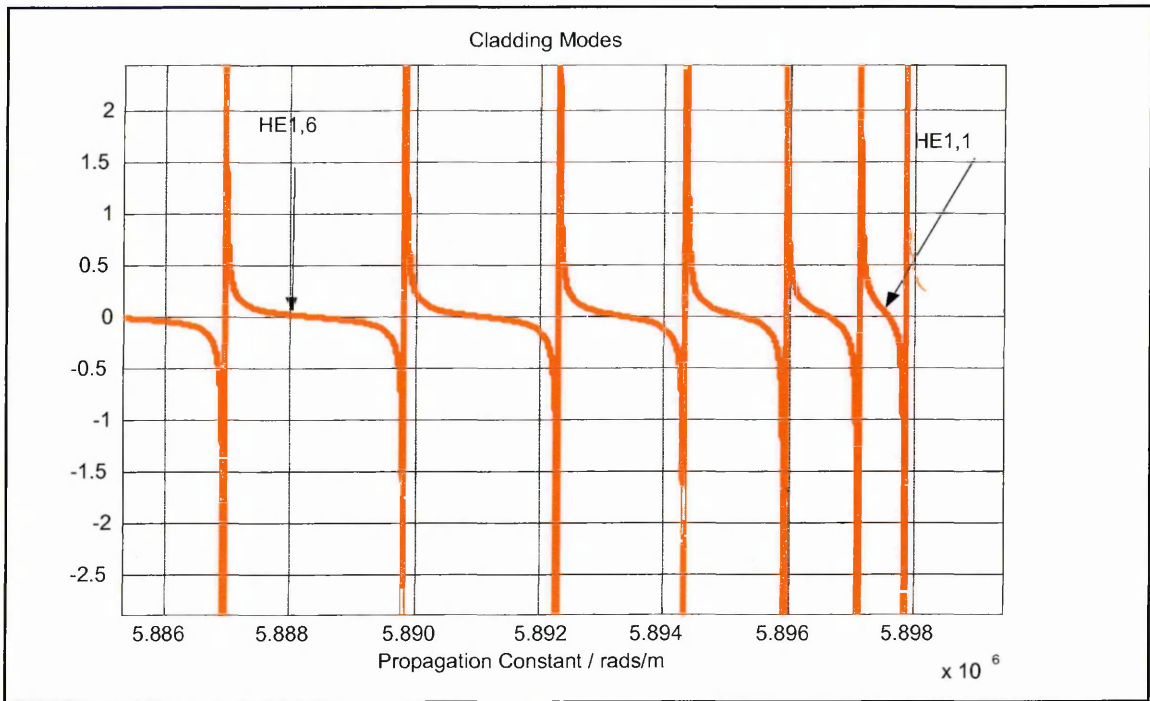
Figure 4.4: Magnified graph of solution to cladding mode equation 4.2 showing first 6 cladding modes

108

Table 4.2 and Figures 4.5 and 4.6 show the simulated results for radiation of wavelength 1550 nm for the core mode and the first 10 cladding modes using (4.2) and (4.3).

Mode	β value rads m^{-1}		Propagation Angle θ°	
	Equ 4.2	Equ 4.3	Equ 4.2	Equ 4.3
$HE_{1,1}$ (core)	5898568.726564	5898568.726564	86.397437	86.397437
$HE_{1,1}$ (clad)	5897510.471958	5897765.001768	89.198985	89.401435
$HE_{1,2}$ (clad)	5896540.307610	5897517.849634	88.687882	89.204129
$HE_{1,3}$ (clad)	5895140.393655	5896899.969298	88.188867	88.850541
$HE_{1,4}$ (clad)	5893308.885675	5896556.907380	87.693609	88.694943
$HE_{1,5}$ (clad)	5891045.783669	5895577.520938	87.200087	88.328615
$HE_{1,6}$ (clad)	5888351.087638	5895171.748777	86.707492	88.198530
$HE_{1,7}$ (clad)	5885224.797580	5893814.256457	86.215433	87.819007
$HE_{1,8}$ (clad)	5881665.069079	5893360.529405	85.723455	87.706109
$HE_{1,9}$ (clad)	5877673.746552	5891610.175856	85.231718	87.314668
$HE_{1,10}$(clad)	5873247.141161	5891121.404845	84.739732	87.215166

Table 4.2: β and θ values for core and first 10 cladding modes
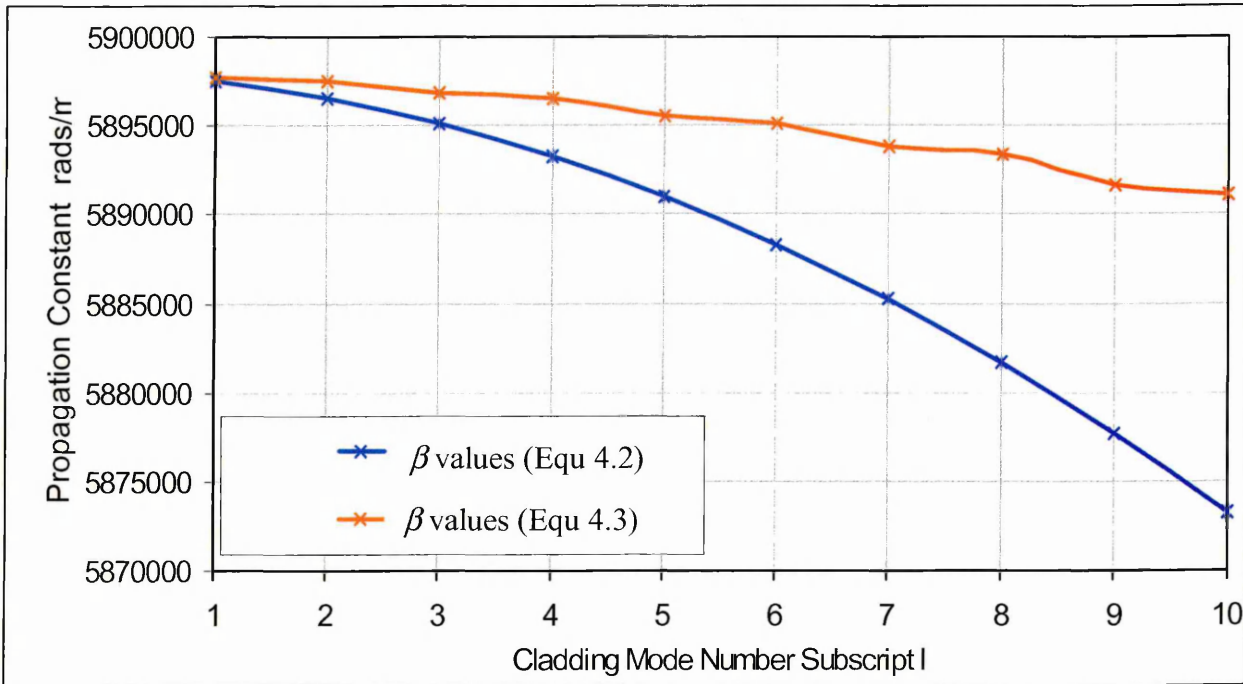
Figure 4.5:   Propagation constants of first 10 cladding modes using equations
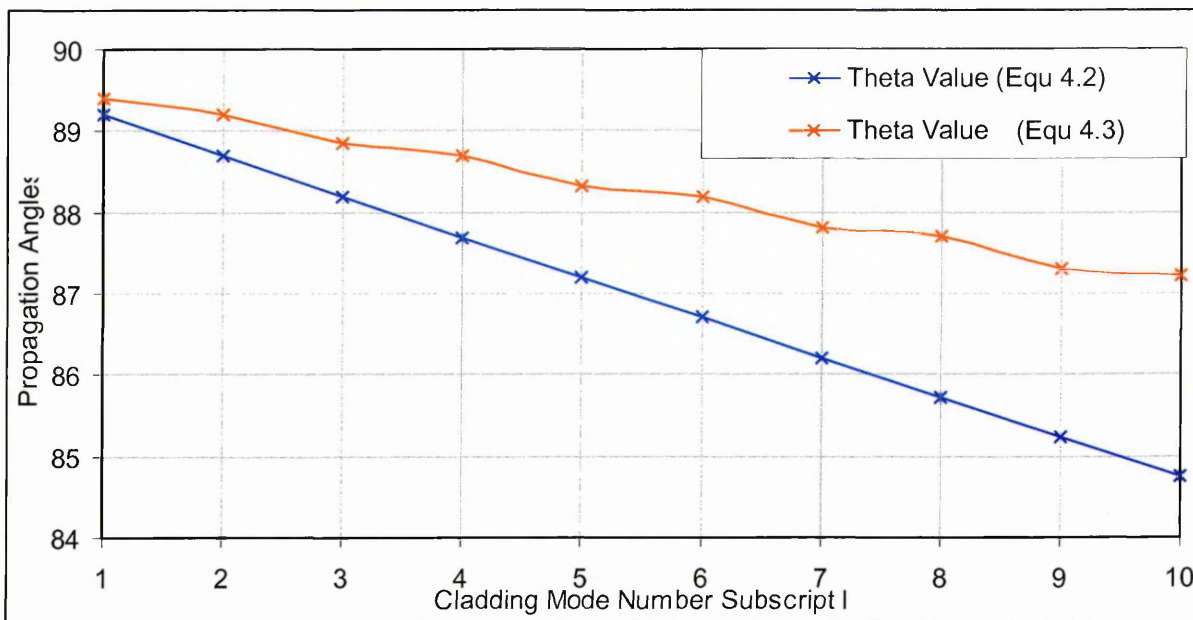
4.2 & 4.3

Figure 4.6: **Propagation angles of first 10 cladding modes using equations 4.2 & 4.3**

The programs were designed to locate the values of β at which the lines of the equation crossed zero. In order to perform this computation, the solutions to the relevant mode equations were sampled to find the positions at which one value was positive and the following value negative. The β value of the mode was taken as the average of these two β values. Ideally these values should be of equal magnitude, but this was not always the case and errors are therefore introduced into the solutions at this point. In an attempt to minimise these errors the sampling rate was increased to a point where the computation time did not become a burden. Using one million samples of propagation constant values each simulation took about a day to complete.

The β values and the propagation angles shown in table 4.2 can be seen to decrease as the mode number increases as expected from theory. It can also be seen from figure 4.3 that the modes become more widely separated as the mode number increases.

Table 4.2 and figures 4.5 and 4.6 show the mismatch between the 2 formulae. As (4.3) is a more accurate representation of the core and cladding geometry it is adopted in further analysis.

4.4 Simulation 2: Operation of Simulation Code Using Ideal Parameters

This part of the program code was written to ensure the completed part of the code would operate properly and to allow debugging and accurate results on ideal parameters which were calculated to match coupling conditions. The programs were then modified to allow for the fibre specifications used in the experiments.

In order to ensure selection of the correct wavelengths, the program was modified to use values calculated and matched by itself.

The first part of the program was designed to determine the propagation constants of the core and first ten cladding modes at a given wavelength (1550 nm). The grating periods required to couple the core mode to each of the cladding modes were then calculated using the manipulated LPG coupling equation given as:

$$\Lambda = \frac{\lambda_{cup}^{(i)} k}{\left(\beta_{core}^{\lambda^{(i)}} - \beta_{clad}^{\lambda^{(i)}}\right)} \qquad (4.4)$$

The second part of the program was designed to determine the propagation constants of the core and first six cladding modes over a range of wavelengths and compare them with the LPG coupling equation using the previously selected (6th) grating period. The fact that the 1550 nm wavelength was predicted to couple to the 6th cladding mode suggested that the programs were operating properly. Other wavelengths in the selected range at which the coupling equation was satisfied were stored along with their β values and the HE_{ml} cladding mode number to which they would couple. The program is given in Appendix 5.

Using the same parameters given in Table 4.1, β values of the core and cladding coupling modes for a range of cladding mode numbers and coupling wavelengths are tabulated in table 4.3. It can be seen that the simulation predicts the core mode at 1550 nm will couple to the 6th cladding mode (HE_{16}) and that the wavelengths which will couple to the previous five cladding modes are also predicted. This suggests that the program is operating properly.

Cladding Mode No	Coupling Wavelength/ nm	β_{core} rads/m	β_{clad} rads/m
HE_{11}	1425	6405229.246017	6393223.172390
HE_{12}	1439	6342687.849250	6330685.685971
HE_{13}	1453	6281354.041903	6269351.380686
HE_{14}	1480	6166350.885864	6154357.189382
HE_{15}	1508	6061447.316717	6039455.320071
HE_{16}	1550	5886893.070433	5874893.487724

Table 4.3: **Coupling wavelengths and propagation constants for the first 6 cladding modes**

4.5 Simulation 3: Prediction of Grating Periods Required to Couple Selected Wavelengths into a Given Cladding Mode

It is possible, using the above program, to predict the grating periods required to couple a selected wavelength to a given cladding mode in a fibre with arbitrary optical and physical properties. This is a very useful set of results, as shown in figure 4.7, to allow gratings to be designed to operate at a required wavelength.

For example, at a wavelength of 1550 nm the grating period required to couple the core mode to the $HE_{1,1}$ or the $HE_{1,10}$ cladding modes can be seen to be 675μm and 390μm respectively.
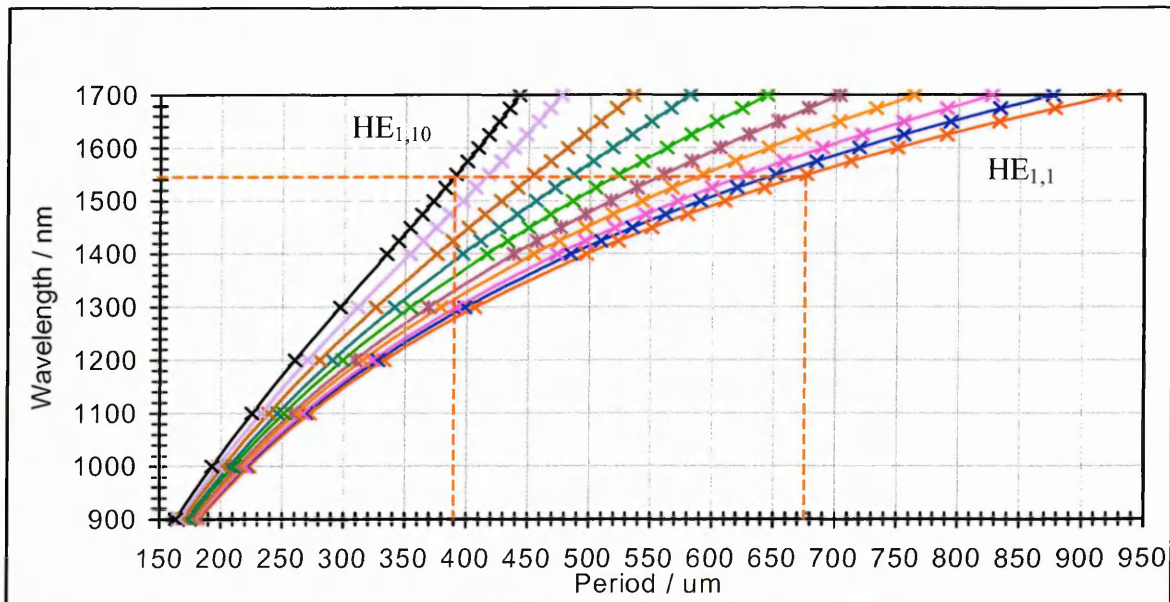
Figure 4.7: Determination of period designed to couple a selected wavelength into a given cladding mode

4.6 Simulation 4: Prediction of Shifts in Coupling Wavelengths Using the Actual Parameters of the Fibres and Gratings Used in Experimental Investigations for Ambient Indices up to that of the Cladding.

As most of the experiments involving coating of the fibre and thus changing of the ambient refractive index were performed using the fibre C1, the optical and physical parameters of this fibre shown in table 4.4 were used in this program to predict the coupling wavelengths in air and compare them to the experimental values.

Parameter	Value
Core refractive index (n_{core})	1.4535
Cladding refractive index (n_{clad})	1.4483
Ambient refractive index ($n_{ambient}$)	1
Core radius (r_{core})	4.1 μm
Cladding radius (r_{clad})	62.5 μm
Operational wavelength (λ)	1550 nm
Grating period (Λ)	280 μm
Wavelength range ($\Delta\lambda$)	900-1600 nm

Table 4.4:   Optical and Physical parameters used in simulation 4

For a range of coupling modes, the predicted and measured coupling wavelengths are shown in table 4.5. The range for the wavelengths is simply limited by the non-availability of a broadband light source. The code was modified, removing the section which predicted the period of the LPG, the period of the C1 LPG being used from the outset and can be seen in Appendix 6.

Simulated results		Experimental results	
Coupling mode	Coupling wavelength / nm	Coupling mode	Coupling wavelength / nm
$HE_{1,1}$	995.0	Unknown	1281.0
$HE_{1,2}$	1001.5	Unknown	1297.5
$HE_{1,3}$	1007.0	Unknown	1317.0
$HE_{1,4}$	1019.0	Unknown	1407.0
$HE_{1,5}$	1029.0	Unknown	1426.5
$HE_{1,6}$	1046.5	Unknown	1447.0
$HE_{1,7}$	1064.0	Unknown	1468.5
$HE_{1,8}$	1087.0	Unknown	1493.0
$HE_{1,9}$	1117.0	Unknown	1525.5
$HE_{1,10}$	1148.0	Unknown	1590.0
$HE_{1,11}$	1203.0		
$HE_{1,12}$	1246.0		
$HE_{1,13}$	1372.0		
$HE_{1,14}$	1452.0		

Table 4.5:   Simulated and experimental coupling wavelengths for fibre C1

Table 4.5 shows that the predicted and measured coupling wavelengths are very different with none of the values matching. The program predicts no coupling at wavelengths between 1452nm and 1600nm, where as the experimental findings show four coupling wavelengths in that range. The cladding modes into which the wavelengths were found to couple in the actual fibre are unknown and cannot be determined by practical methods available in this investigation, as a broadband source covering a lower wavelength range was not available. This is not a totally unexpected outcome as the actual refractive index profile along the grating is not linear, as the program code assumes it to be. As stated in the experimental section, the refractive index profile of the grating section approximates a Gaussian profile, the separation of the maxima of which are known, but the width of the profile, depends on many factors and properties of the fibre. Some of these properties can only be estimated and can never be accurately modelled without empirical adjustment of the parameters until the model fits the measured results as close as possible. This adjustment would have to be

performed as fibres of different properties were used, making the actual accuracy of any predicted values suspect. The simulation was repeated for a range of ambient refractive indices (air to cladding) to determine the change in coupling wavelengths. The results are shown in Table 4.6 and Figure 4.8.

Cladding coupling mode	Coupling wavelength at ambient index / nm					
	1	1.3	1.35	1.4	1.44	1.445
$HE_{1,1}$	995	995	995	995	995	995
$HE_{1,2}$	1001.5	1001.5	1001.5	1001.5	1001.5	1001.5
$HE_{1,3}$	1007	1007	1007	1007	1007	1006.5
$HE_{1,4}$	1019	1019	1019	1018.5	1018.5	1017.5
$HE_{1,5}$	1029	1029	1028.5	1028.5	1028.5	1027.5
$HE_{1,6}$	1046.5	1046.5	1046.5	1045.5	1045.5	1043.5
$HE_{1,7}$	1064	1063.5	1063.5	1062.5	1062.5	1059.5
$HE_{1,8}$	1087	1086.5	1086.5	1086	1085.5	1081.5
$HE_{1,9}$	1117	1116.5	1116	1115.5	1114.5	1108.5
$HE_{1,10}$	1148	1147	1146.5	1145.5	1144.5	1136.5
$HE_{1,11}$	1203	1202	1201	1199	1197.5	1183.5
$HE_{1,12}$	1246	1244	1243.5	1241	1239	1221
$HE_{1,13}$	1372	1367	1364.5	1359.5	1355.5	1313
$HE_{1,14}$	1452	1444.5	1440.5	1433.5	1426.5	1368

Table 4.6: Coupling wavelength for a range of ambient refractive indices

For a given ambient index, the longer wavelengths can be seen to couple to higher order cladding modes. Increasing the ambient index has no effect on the coupling wavelengths to the first three cladding modes. However, an increase in the ambient index shows a general decrease in coupling wavelength to all higher cladding modes. These results confirm the trend of the results obtained experimentally.
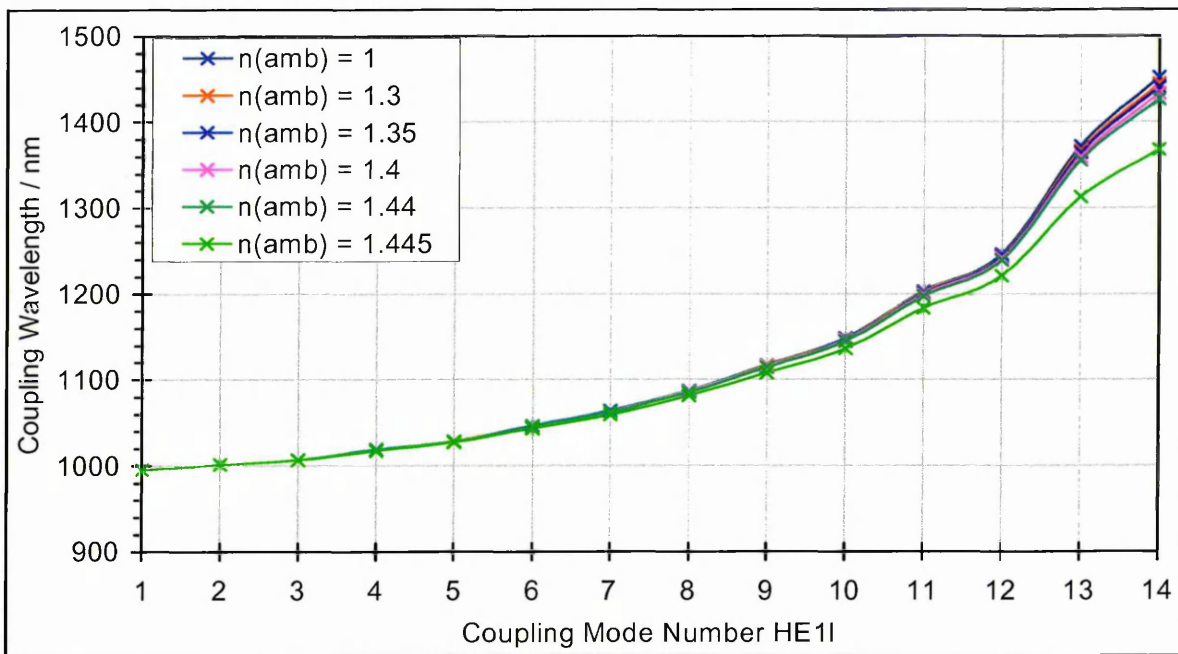
Figure 4.8: **Coupling wavelength versus the coupling mode for a range of ambient refractive indices**

Further simulations carried out confirmed the following features of LPGs

1. As the radius of the cladding increases the total number of cladding modes increases linearly (shown in figure 4.9), as predicted by theory due to the greater volume of the cladding.
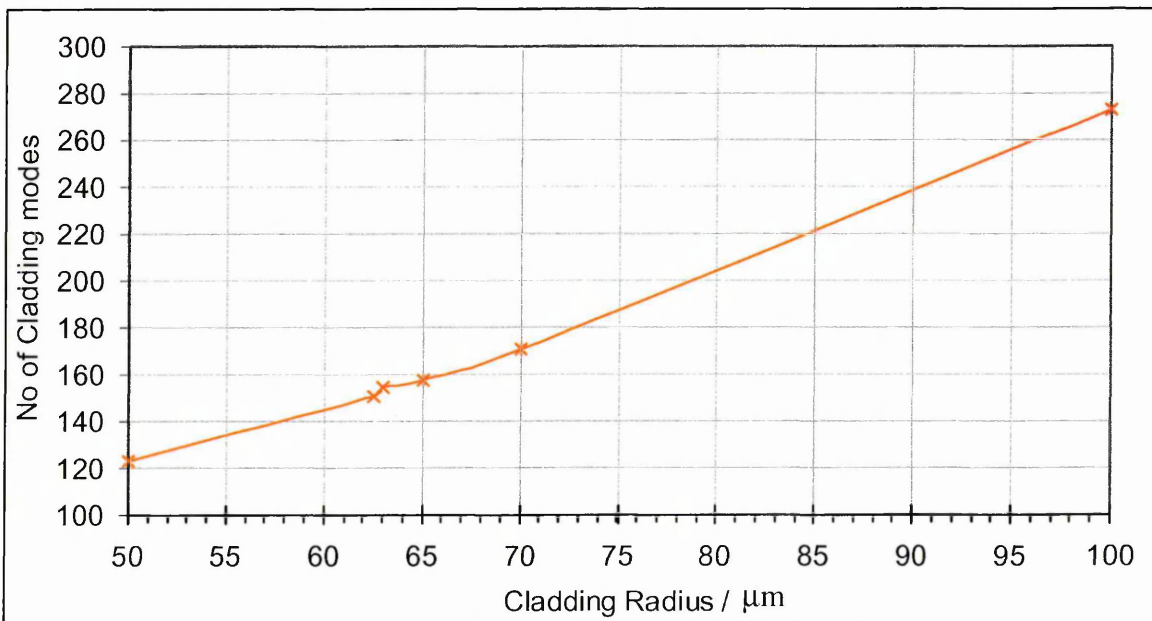
Figure 4.9: **Number of cladding modes as a function of cladding radius**

2. As the ambient index increases from that of air (1) to around 1.4 the total number of cladding modes decreases linearly. As the ambient index increases beyond 1.4 to that of the cladding (1.4483) there is a sharp fall in the number of cladding modes (see figure 4.10) due to the increase in the critical angle as a function of ambient index change.
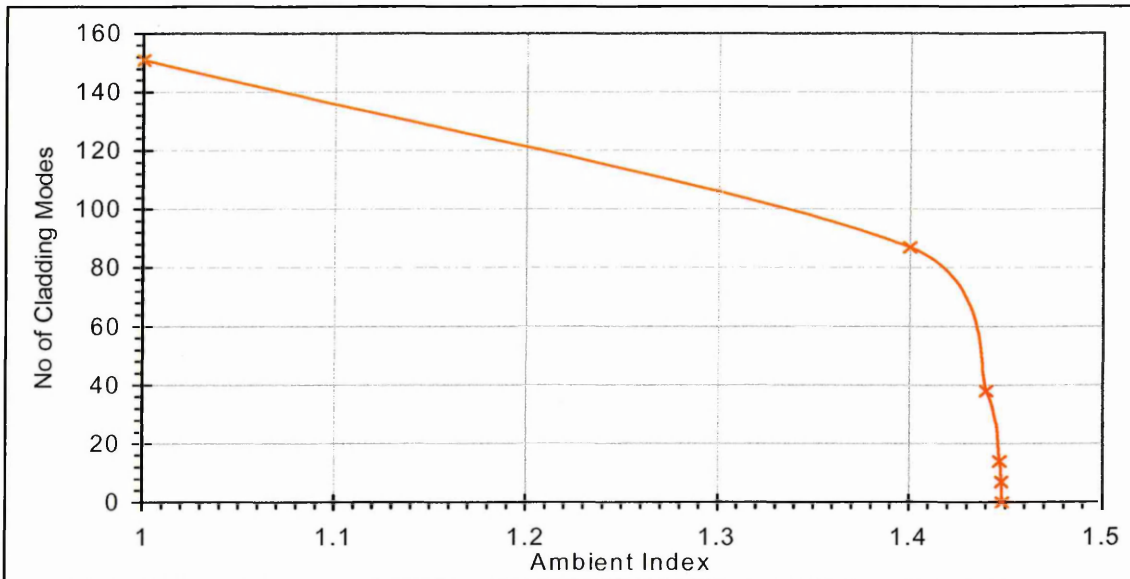
Figure 4.10: Number of cladding modes as a function of ambient index

4.7 Simulation 5: Prediction of Shifts in Coupling Wavelengths Using the Actual Parameters of the Fibres and Gratings Used in Experimental Investigations for Ambient Indices Beyond that of the Cladding

Experimental results and literature [193] showed that the coupling wavelengths decrease as the ambient index increases up to that of the cladding at which point no

coupling is evident as the dips on the output spectrum disappear. Above the index of the core, however, coupling is again evident, but this time returning immediately to the coupling wavelength in air, and increasing as the ambient index increases. This effect could not be modelled using (4.7) since it is only valid for ambient indices lower than the cladding index. However, (4.6) can be used to predict coupling wavelengths at indices higher than the cladding index. Using (4.6), the coupling wavelength versus ambient index for different cladding modes are shown in figure 4.11 (see Appendix 7 for code).
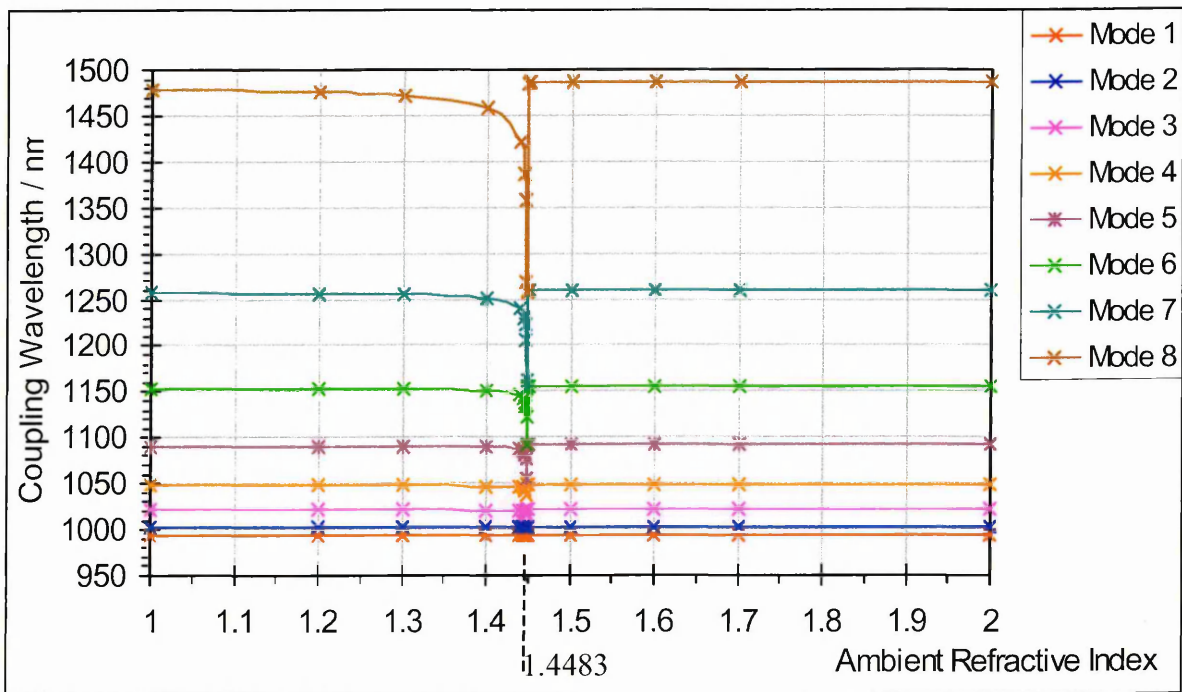
Figure 4.11: Coupling wavelength versus ambient refractive index for the first eight cladding modes

The graph confirms the effects observed in the experimental procedures with respect to the ambient index profiles of LPGs. It can be seen that the coupling wavelengths decrease steeply as the ambient index approaches that of the cladding (1.4483), the effect being more prevalent as the cladding mode order to which each wavelength will couple increases. When the ambient index reaches that of the cladding no mode

coupling occurs due to the absence of mode formation in the now effectively infinite cladding. The coupling wavelengths can be seen to jump back to the same values as were predicted in air for all modes as soon as the ambient index is greater than that of the cladding, increasing only slightly from that value as the ambient index increases to 2.

4.8 Summary

This chapter has explained the basis of the equations used to predict the modes in the core and cladding. These equations have been used in the programs written to predict the number of modes and their optical constants in an ideal fibre core and cladding, and to predict a grating period which would couple the core mode to a specific cladding mode. This program code was used to design an optical fibre grating period to couple a selected wavelength from the core into a specific cladding mode, and modified to predict the coupling wavelength shifts with a range of ambient indices up to that of the cladding using the actual parameters of the fibres involved in the experimental investigations. The code was then adapted further to determine the coupling wavelength shifts for ambient indices greater than that of the cladding.

Chapter 5

Fibre Coating Procedures

5.1 Introduction

In order to use an LPG as a gas/chemical sensor it was necessary that the ambient index outside the cladding should change when the measureand is present. As the gas/chemical under investigation is unlikely to noticeably affect the ambient index on contact with the cladding, a coating, whose refractive index would change with a given measureand was investigated.

Section 5.2 describes the compounds used in the coating experiments, their functions and the gases to which they are optically sensitive. Section 5.3 introduces the

Polyelectrolyte Self-Assembly (PESA) coating method, while Section 5.4 explains how automated method of PESA was utilized to coat the glass slides and the planar polarized interferometers (PPIs) used in the determination of the absorption spectrum and the sensitivity to NO_2 of CuPc as described in sections 6.5.3 and 6.5.4 respectively. Section 5.5 describes the method used to investigate the adaptability of PESA to in-situ coating using surface plasmon resonance (SPR) to monitor the build up of the layers, with Section 5.6 progressing to the coating of the LPGs in-situ. Section 5.7 explains the final coating method used in these investigations, by immersion in solutions of chemicals.

5.2 Compounds Used in the Coating Procedures

The following compounds shown in Figures 5.1 to 5.10 [333-340] were involved in this investigation. Their functions are listed in Table 5.1.
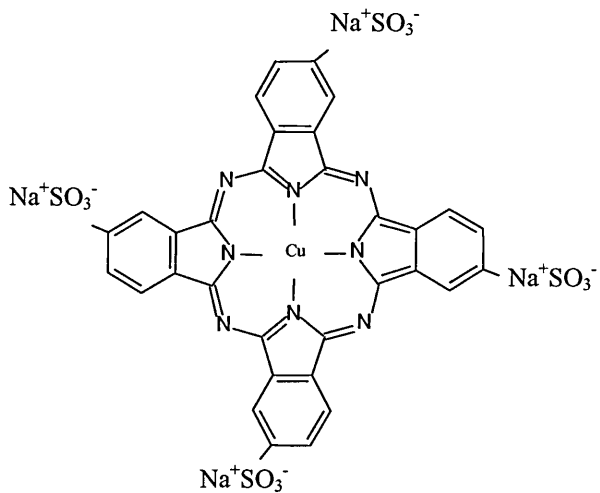
Figure 5.1: CuPc⁻ (SO₃⁻Na⁺)₄
CopperIIphthalocyanine-
tetra-sulphuric-sodium salt
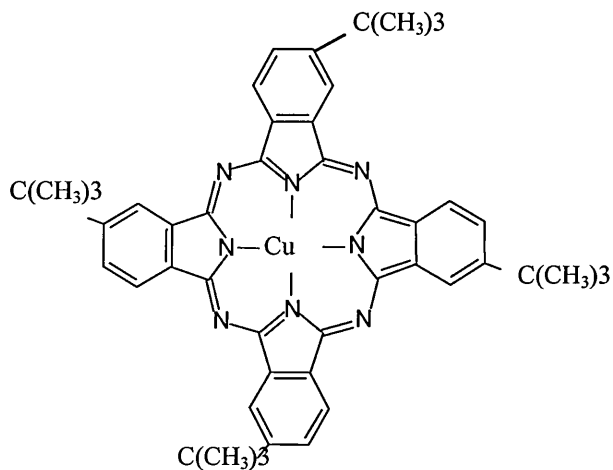
Figure 5.2: CuPc⁻ (C(CH₃))₄
CopperIIphthalocyanine-
tetra-tert-butyl
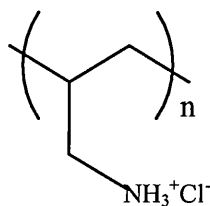
Figure 5.3: PAA
Poly-alylamine hydrochloride
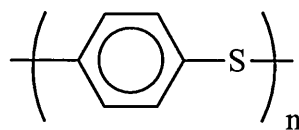
Figure 5.4: PPS
Poly-phenylsulphide
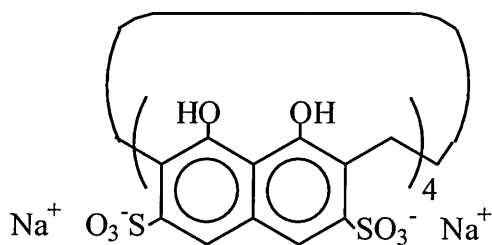
Figure 5.5: Chromo 1
Cyclo-tetrachromotropylene
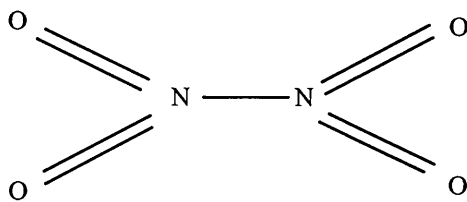
Figure 5.6: NO₂   Nitrogen Dioxide
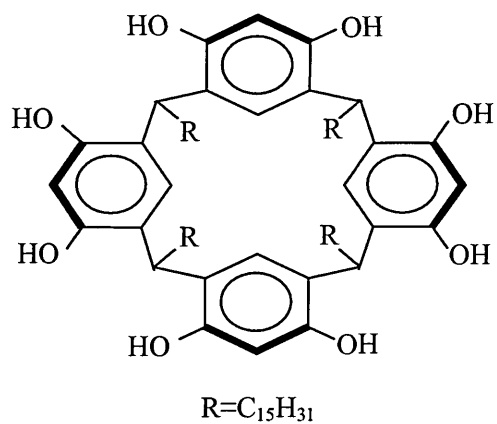
Figure 5.7: **Calixarene C[4]RA**
Calix[4]resorcinearene

R=$C_{15}H_{31}$
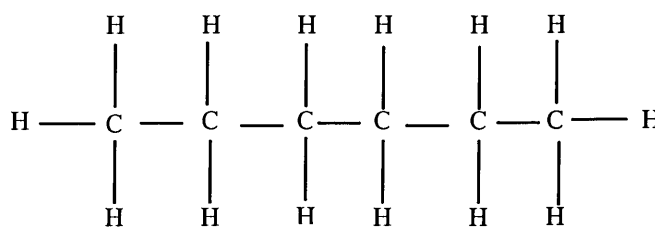
Figure 5.8: **Hexane** **$CH_3(CH_2)_4CH_3$**
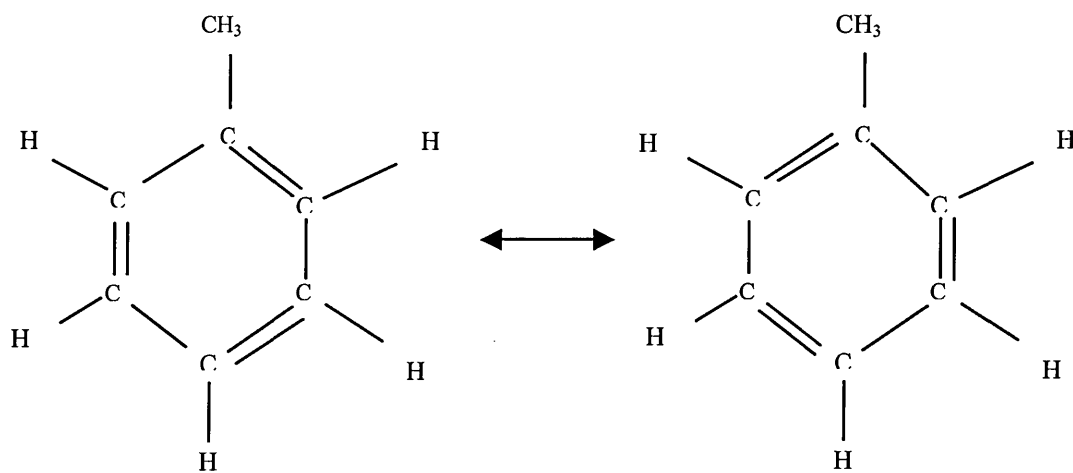
Figure 5.9: **Toluene** **C_6H_5-CH_3**
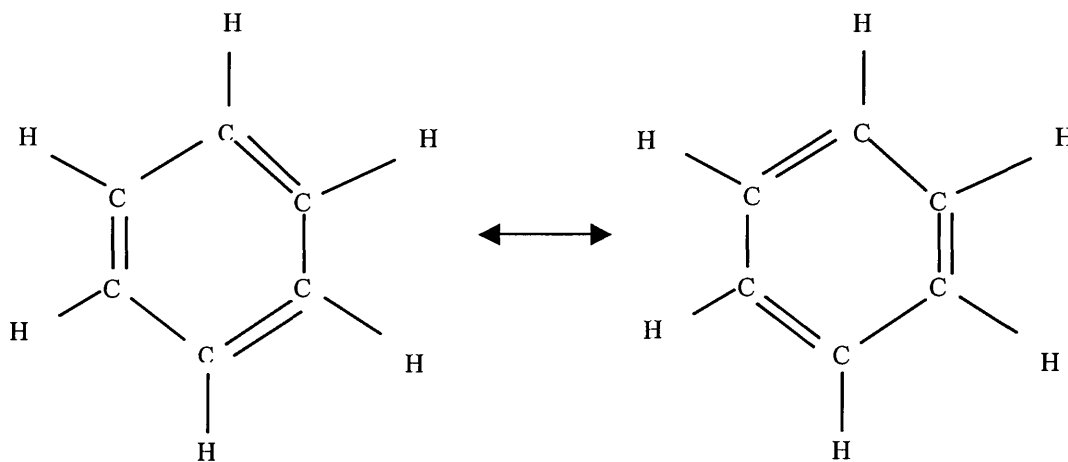
Figure 5.10: **Benzene** **C_6H_6**

124

Compound	Function
CuPc⁻ (SO₃⁻Na⁺)₄	Sensitive to NO_2
CuPc⁻ (C(CH₃))₄	Sensitive to NO_2
Chromo 1	Sensitive to Ammonia
Calixarene	Sensitive to Hexane, Toluene, Benzene
PAA	Electrostatic Bonding
PPS	Electrostatic Bonding

Table 5.1:   Compounds used in the coating process and the gases to which they are optically sensitive

5.3 Polyelectrolyte Self-Assembly (PESA) Coating Method

The technique of depositing multilayer coatings by the adsorption of consecutively alternating layers of anionic and cationic bipolar amphiles and/or polyelectrolytes was developed as a method of thin film coating by Lvov et al in 1993 [341]. It has proved to be a simple and efficient method of applying thin films onto various substrates. A glass slide will have a negative charge at its surface due to the discontinuity of the structure at that point. If the slide is immersed in a solution of positive (cationic) polyelectrolyte a layer of this polycation will be adsorbed onto the glass surface, leaving the surface of this new layer with a positive charge. If, after thorough rinsing with water to remove all of the unbonded polycations, the slide is then immersed in a solution of negative (anionic) polyelectrolyte a layer of this polyanion will be adsorbed onto the surface of the polycation layer. Cyclic repetition of these 2 steps will allow the build up of multilayers of the 2 polyelectrolytes to the required coating thickness [342-347].

For the first series of experiments, poly(alylamine hydrochloride) (PAA) was used as the positive (cationic) polyelectrolyte (polycation) and copper phthalocyanine-tetra sulphonic sodium salt $(CuPc^-(SO_3^-Na^+)_4)$ was used as the negative (anionic) polyelectrolyte (polyanion). Both compounds are water soluble allowing solutions of 2 mg/ml of PAA in water and 0.5 mg/ml of $CuPc^-(SO_3^-Na^+)_4$ in water to be produced and used as the polyelectrolytes in the PESA coating method.

Figure 5.11 shows an experimental set up adopted to investigate the absorption and coating thickness dependency of PAA/ $CuPc^-(SO_3^-Na^+)_4$. It was possible to coat the slides and planar polarisation interferometer (PPI) chips using the fully automatic, computer controlled set up which had previously been designed and produced in house.
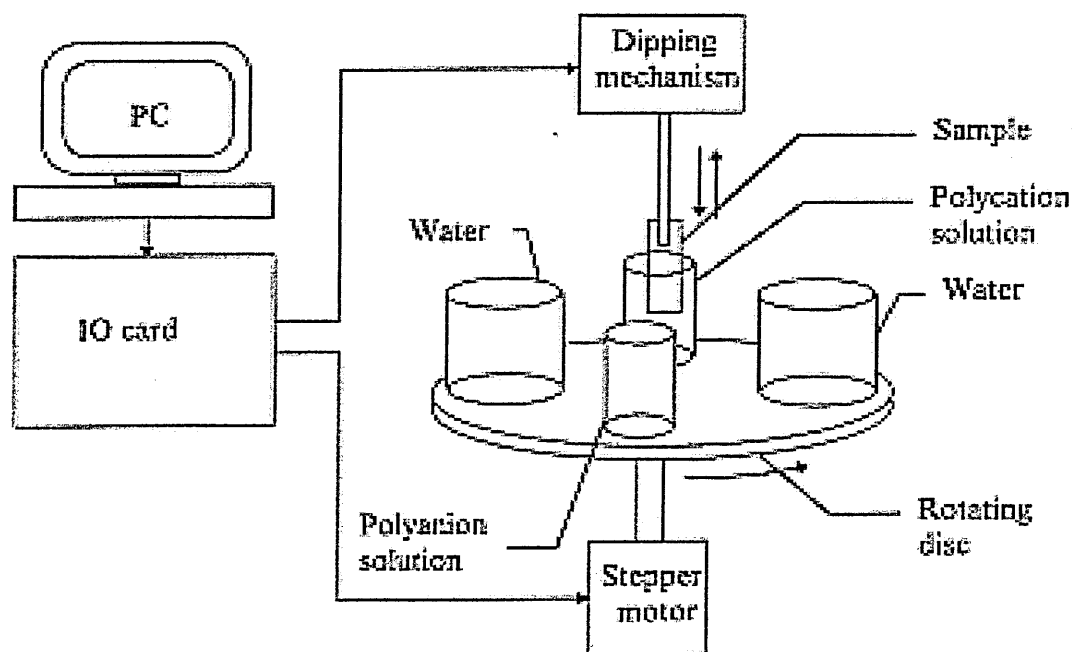
Figure 5.11:   PESA coating set up

Two beakers, one containing the polycation solution and the other containing the polyanion solution are positioned alternately with two beakers of millipore de-ionised water on a rotating disc. The sample to be coated is mounted in a clamp, the vertical movement of which is controlled in time and distance by the computer program as is the rotational position of the beakers. The program allows accurate setting of the immersion time into each polyelectrolyte, the number of immersions into the rinsing water for removal of excess unbonded ions, coordination of the immersion and rotation of the disc, and the number of cycles (bi-layers) required.

5.4 Coating of Glass Slides and Planar Polarisation Interferometers Using Automatic PESA Set Up

A glass slide, previously coated with 100 nm thick layer of aluminium by thermal evaporation (PVD), was mounted in the above set up. The number of cycles (bi-layers), immersion duration, and wash duration were entered into the computer, and the system was activated. Starting with the PAA cation polyelectrolyte solution the slide was sequentially immersed in PAA and $CuPc^-(SO_3^-Na^+)_4$ solutions for 20 minute durations, the excess unbonded ions of the previous solution being rinsed off in millipore water before immersion in the proceeding solution, until the required number of bi-layers were attained. Figure 5.12 shows a schematic diagram of the build up of the alternate layers of PAA and $CuPc^-(SO_3^-Na^+)_4$ on the glass slide [348].
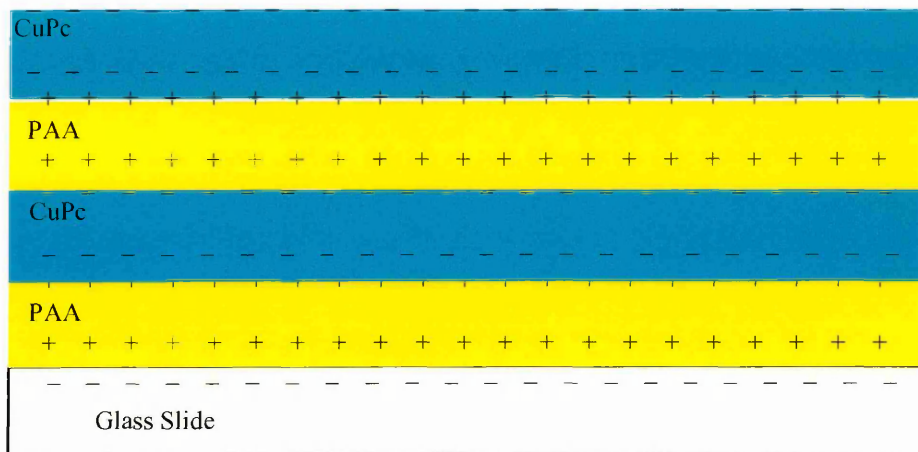
Figure 5.12: Build up of consecutive layers of PAA/ $CuPc^-(SO_3^-Na^+)_4$ on glass slide using PESA method

The same procedure was performed on the PPI chips, with the difference being that the surface of the silicon nitride (Si_3N_4) window on which the coating was to be applied has an overall positive charge, resulting in the immersion cycle beginning with the negative $CuPc^-(SO_3^-Na^+)_4$ anion polyelectrolyte. The coating of the fibre cladding in the LPG region of the core could not be performed using the automatic computer controlled set up for reasons that are explained in the experimental section (Chapter 6). This led to an investigation into the possibility of coating the fibre cladding in the surroundings in which the sensing experiments would be performed, to allow continuous monitoring of the coating and gas exposure procedures at all stages of the experiment.

5.5 Investigation into Adaptability of PESA Method to In-Situ Coating of Fibre Using Surface Plasmon Resonance (SPR)

This experiment was performed to determine if the PESA method would be effective when a body was maintained in a cavity, which would be filled with the various polyelectrolytes in sequence, with intermediate flushing with water to remove the unbonded ions, and to monitor the build up of the coating due to the resulting shift in coupling wavelength observed on the OSA as it occurred. In order to carry out this investigation surface plasmon resonance (SPR) [349-351] was utilised to monitor the in situ PESA coating of a gold coated slide. Surface plasmon resonance is a well known and widely used technique to investigate the properties of thin films [352,353]. Plasmons at the surface of gold will have a resonant frequency at which they will vibrate. If a thin layer of gold is deposited onto the surface of a glass slide and a narrow beam of light is made incident on the under-side of the gold film, wavelengths for which the component of the wave vector k in the direction of the plasmon vibration are equal to the resonant frequency will be significantly absorbed by the gold film, whilst other wavelengths will be reflected. A coating on the surface of the film will affect the resonant frequency of the surface plasmons and therefore the wavelength of incident light which will be absorbed. It follows, therefore, that the underside of the gold film can be interrogated by a single wavelength (known to be close to the resonant frequency of the plasmons) made incident over a range of angles, or by a range of wavelengths made incident at a given angle, both of which methods will modify the component of the incident wave vector in the direction of the plasmon

vibration. The build up of coating layers can therefore be monitored by this procedure as they are applied. The experimental set up is shown in Figure 5.13. The prism and the slide thickness combine to form a homogenous semicircle of glass. The point of incidence of the ray on the gold surface is at the centre of the semi-circle ensuring the ray is not refracted on entering or leaving the medium.
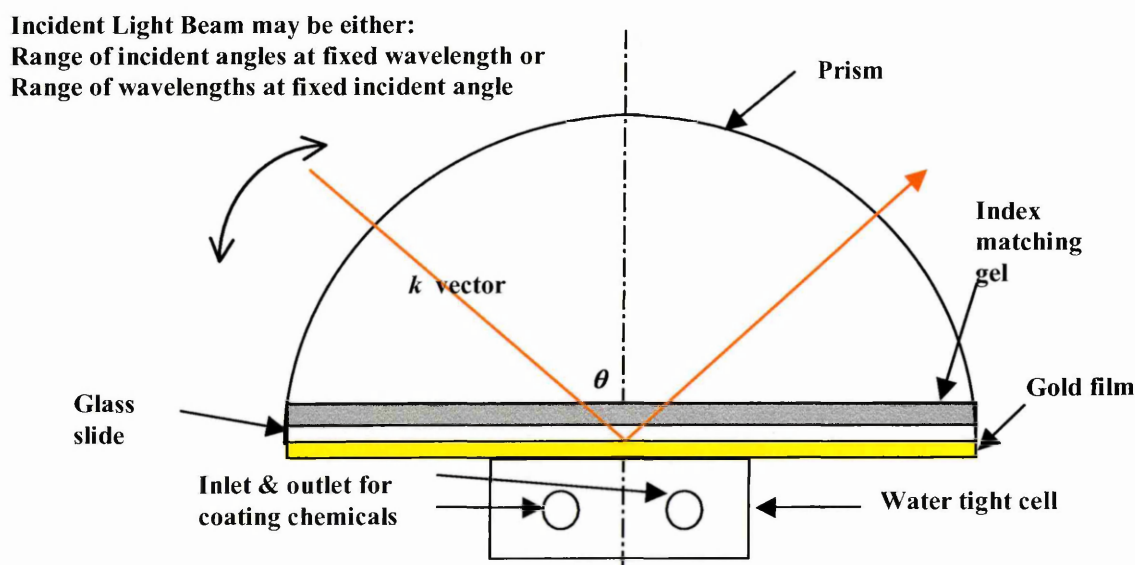
Figure 5.13: Optical set up for SPR investigation of in-situ PESA coatings

Light from a 633 nm helium-neon laser source was initially made incident on the under-side of the gold coating over a range of angles from 0° to 90°, and the reflected intensity monitored in increments of 0.1°, to determine the angle of greatest absorption. The procedure was then focussed around the observed intensity dip over a range of 65° to 80° in increments of 0.05°. The intensity of the SPR reflection spectrum at each angular iteration was detected using a silicon photodiode and recorded in Lab View. The cavity was filled with PAA solution of the previously stated constituency and left for twenty minutes to allow bonding of the PAA cations to the surface of the gold. The cavity was then flushed thoroughly with de-ionised

millipore water and the underside of the gold coating scanned over the previously stated range of angles. The cavity was then filled with $CuPc^-(SO_3^-Na^+)_4$ and the same procedure carried out. This was repeated until three bi-layers of $PAA/CuPc^-(SO_3^-Na^+)_4$ had been applied, the reflection intensity observed and recorded as each part of the procedure was completed. The resulting intensity traces can be seen in Figure 5.14, and the changes in resonance matching angle are shown in Figure 5.15.
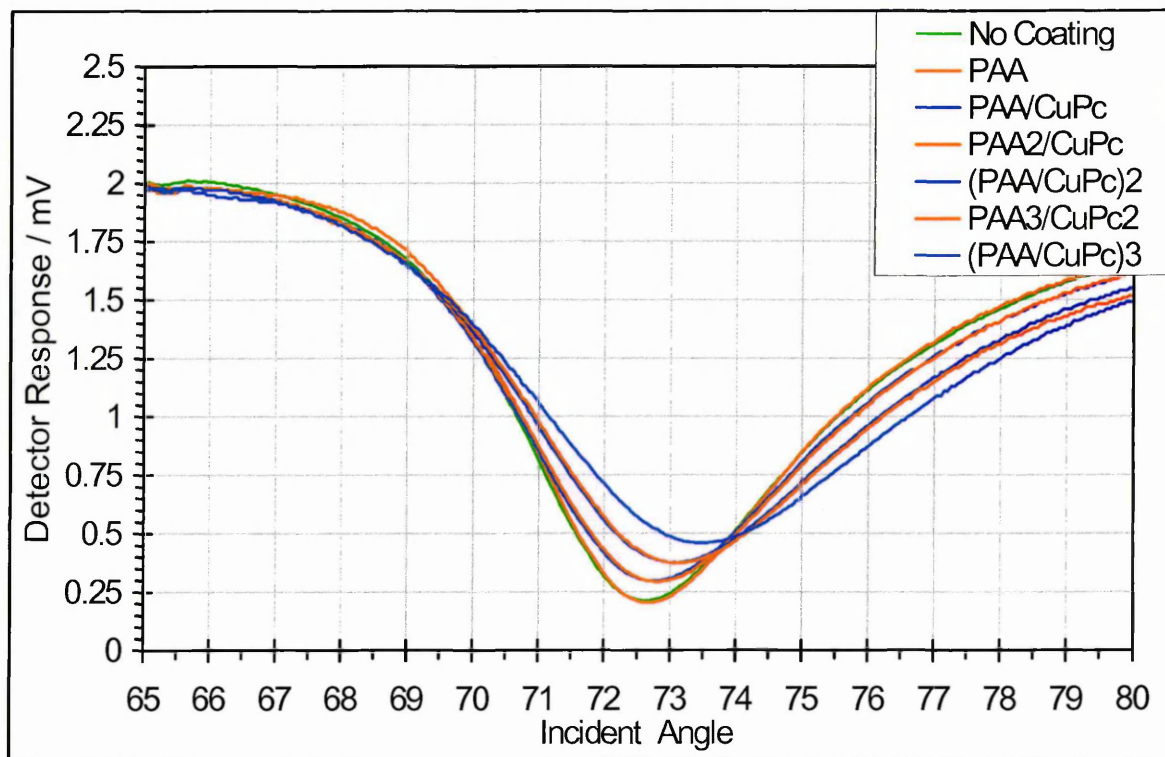
Figure 5.14: Set of SPR curves showing in-situ growth of successive layers of PAA and CuPc⁻(SO₃⁻Na⁺)₄ onto gold coated slide
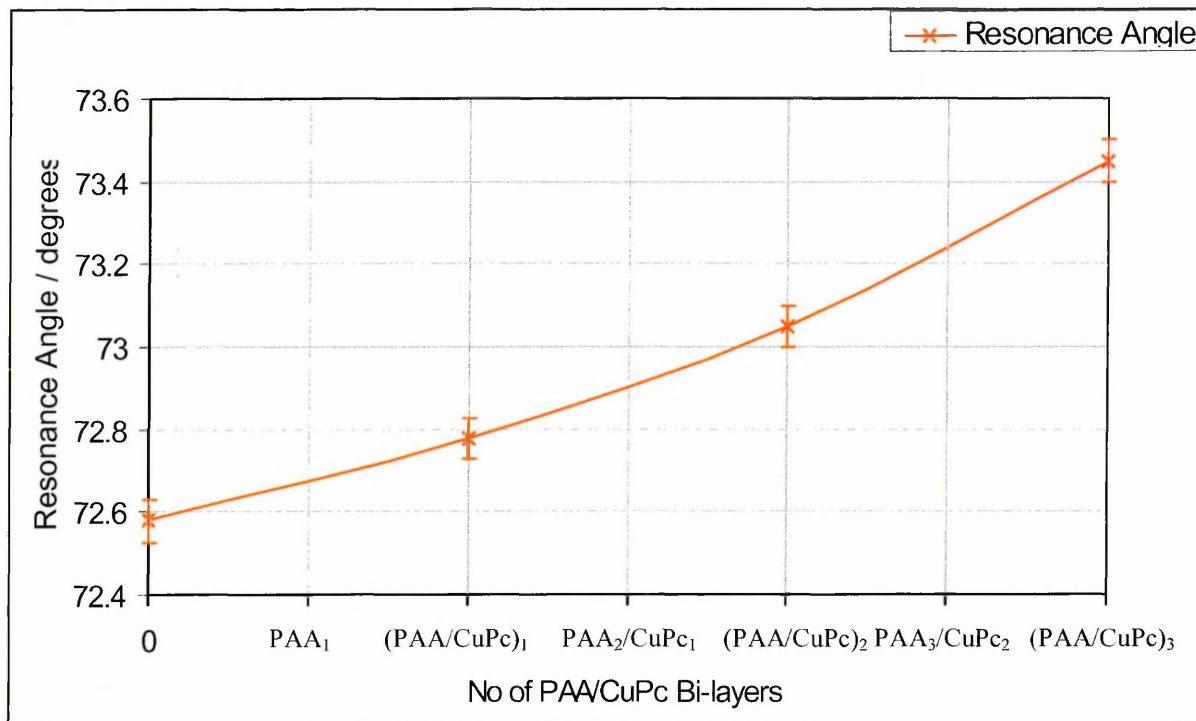
Figure 5.15: Shift in resonant angle of incident radiation with number of bi-layers growth

The change in the resonance wavelength due to the change in the resonant frequency of the surface plasmons, suggests the $PAA/CuPc^-(SO_3^-Na^+)_4$ coating is bonding successfully as successive solutions are inserted into the cavity. This seems to confirm the adaptability of the PESA method to in-situ coating and will be adopted as the method used to coat the fibre cladding in the same cavity as will be used for the gas exposures. This will also allow the continuous monitoring of both the coating and exposure procedures in a consistent set up.

5.6 Coating of the Fibre Cladding Using In-Situ PESA Method

The LPG section of the fibre was clamped under slight tension in a purpose built coating/gas cell as shown in Figure 5.16.
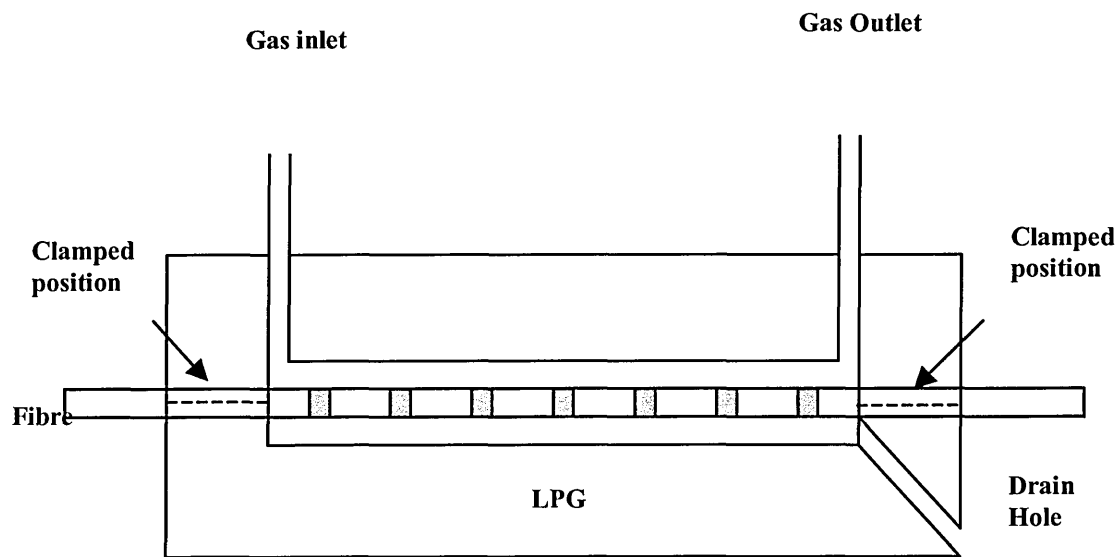
Figure 5.16: **Purpose built cell made in house for in-situ PESA coating and gas Exposure**

The top and bottom sections of the cell were made from separate pieces of perspex as shown in Figure 5.17, to allow the fibre to be easily positioned, reducing the risk of breaking, which would be evident if the fibre had to be threaded through a small water-tight hole at each end of the cell. Rubber gaskets were positioned between the mating surfaces of the top and bottom halves of the cell, with the fibre sandwiched in

133

between, before ten screws were sequentially tightened to form a water/gas tight seal between the two sections and around the fibre entry and exit points.
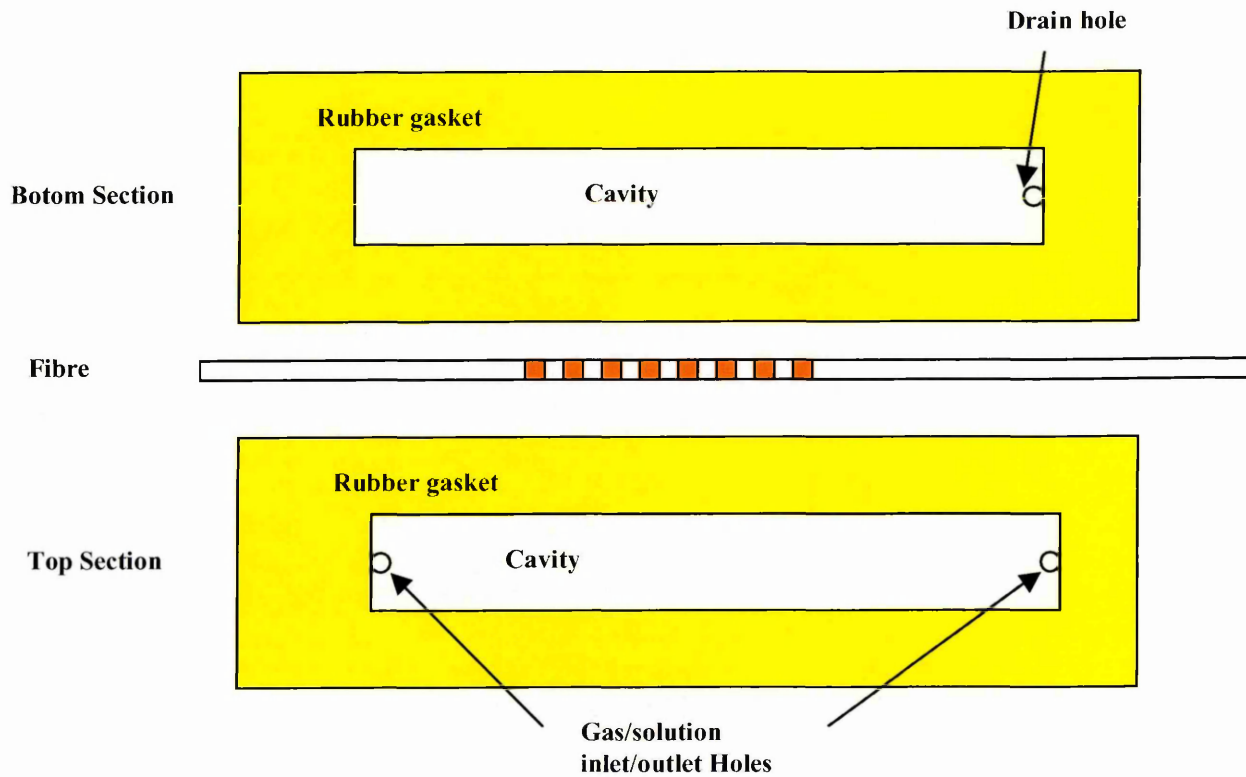
Figure 5.17:   Plan view of the LPG and the separate halves of coating cell

The fibre was connected to a light source and the OSA throughout the procedure to allow any shift in coupling wavelength due to the applied coatings to be observed.

The drain hole was blocked and the cavity was filled with PAA solution and left for 20 minutes to allow the PAA cations to bond to the surface of the cladding, after which time the cell was flushed with de-ionised millipore water to remove the unbonded ions.   The cell was then filled with $CuPc^-(SO_3^-Na^+)_4$ solution, left as previously for the bonding to take place and again flushed with de-ionised water.

134

This procedure was repeated until the desired number of bi-layers was achieved, at which point the drain hole was opened and the cavity was flushed with N_2 to remove as much moisture as possible. A visible shift in coupling wavelengths observed on the OSA suggested that the fibre was successfully coated. The fibre remained in-situ for the gas exposure part of the experiment as reported in Chapter 6.

This method was repeated in Experiment 2 but with a solution of 2 mg/ml of Chromo 1 in water instead of the $CuPc^-(SO_3^-Na^+)_4$ solution.

5.7 Coating of the Fibre Cladding by Immersion in Solutions of Chemicals

A further method of coating was utilsed to allow the LPG to be coated with a gas sensitive compound, calixarene, whose refractive index is known to change on contact with hexane, toluene, and benzene vapours [354], which was not suitable for use in the PESA method.

The fibre was again connected to a light source and the OSA throughout the procedure to allow any shift in coupling wavelength due to the applied coatings to be observed.

The LPG section of the fibre was held under slight tension above a glass slide placed on a moveable platform immediately beneath. The slide was raised until it was almost, but not quite in contact with the LPG, at which point a solution of 10 mg/ml of calixarine in chloroform was 'pooled' onto the slide to totally immerse the LPG section of the cladding as shown in Figure 5.18. Removing the fibre from the solution before total evaporation of the chloroform allowed maximum bonding of the calixarene to the cladding without allowing the fibre to adhere to the slide.
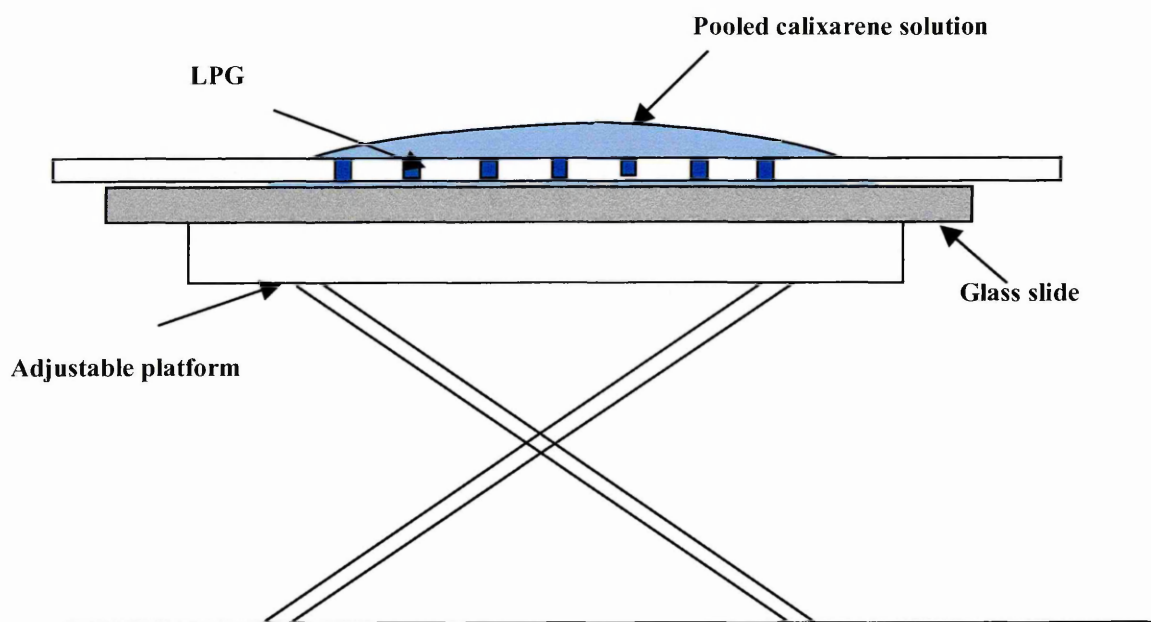
Figure 5.18:   Coating LPG by immersion in calixarene solution

5.8 Summary

This chapter has introduced the compounds used in the coating experiments and the gases to which they are optically sensitive. Automated polyelectrolyte self-assembly

(PESA) coating used to coat glass slides and planar polarized interferometers (PPIs) were discussed and investigations into the adaptability of PESA to in-situ coating using surface plasmon resonance (SPR) were reported.   Finally the application of the various coating method to LPGs are explained.

Chapter 6

Experimental Investigations

6.1 Introduction

This chapter describes the experimental investigations performed in order to verify existing principles and to expand these principles in order to investigate the possibility of using an LPG as a stand alone gas sensor. As a result of preliminary experiments performed to gain familiarity with optical fibres, experiments were also carried out to investigate the possibility of multi-parameter sensing using different mode coupling wavelengths in the same grating to simultaneously observe temperature and ambient refractive index changes.

Section 6.2 lists the optical and physical specifications of all LPGs and the optical spectrum analyser (OSA) and light source used in these experiments. Section 6.3 describes the preliminary experiments performed to gain familiarity with usage of LPGs, which led to further experiments into the temperature sensitvity of LPGs. Section 6.4 covers the experimental investigation into the difference between the ambient index and temperature profiles of LPGs of various periods. Section 6.5 details the investigations performed in the determination of the methods and compounds to be used to coat the cladding most effectively. Sections 6.6 and 6.7 cover the experimental investigations into using an LPG as a gas sensor after coating the cladding with a suitable compound by the poly-electrolyte self assembly (PESA) method and the solvent evaporation method respectively.

6.2 Specifications of Long Period Gratings Used in Experimental Investigations

Table 6.1 lists the optical and physical specifications of the LPGs used in the experimental investigations described in this chapter.

LPG No	S1	S2	S3	S4
Core radius / μm	3.9	3.9	3.9	3.9
Cladding radius / μm	62.5	62.5	62.5	62.5
Core refractive index *	1.4499	1.4499	1.4499	1.4499
Cladding refractive index *	1.4441	1.4441	1.4441	1.4441
Grating period / μm	700	700	700	700
Approx Grating length/cm	3	3	3	3

LPG No	S5	S6	S7	S8	C1
Core radius / µm	3.9	3.9	3.9	3.9	4.1
Cladding radius / µm	62.5	62.5	62.5	62.5	62.5
Core refractive index *	1.4499	1.4499	1.4499	1.4499	1.4535
Cladding refractive index *	1.4441	1.4441	1.4441	1.4441	1.4483
Grating period / µm	700	700	450	450	280
Approx Grating length/ cm	3	3	3	3	4.5
LPG No	A400	A403	A407	A410	A416
Core radius / µm	4.5	4.5	4.5	4.5	4.5
Cladding radius / µm	62.5	62.5	62.5	62.5	62.5
Core refractive index *	1.4487	1.4487	1.4487	1.4487	1.4487
Cladding refractive index *	1.4440	1.4440	1.4440	1.4440	1.4440
Grating period / µm	400	403	407	410	416
Approx Grating length/ cm	3	3	3	3	3

*before writing of grating

Table 6.1:   Optical and physical specifications of LPGs used in experimental investigations

The LPGs listed in the Table 6.1 were obtained from production facilities in Singapore, Canada, and Aston University, and are identified by the initials S, C and A respectively. LPGs S1 to S8 are written into a boron doped silica single mode core with a cladding of pure silica, LPG C1 is written into a Corning SMF 28 fibre core and LPGs A400 to A416 are written into standard low germanium doped (approx. 3%) silica core.

Initial transmission profiles of all of these fibres except S1 and S2 were taken in air at room temperature and can be seen in Appendix 8. To allow a more in depth study over a broader wavelength range both the 1300nm and 1550nm integral light sources of the OSA were utilised. The OSA used to observe the transmission spectra in each experiment was a HP86142A and the light source was the integral 1550nm edge emitting light emitting diode (EELED) of the OSA.

6.3 Preliminary Experiments, Results and Conclusions

Initial experiments were performed using LPGs S1 and S2 mainly to gain familiarity in handling and connecting the fibres between the light source and the OSA, and to observe the sensitivity of the spectrum to connection losses, bending, tension, temperature, and ambient index variations. The relevant results are tabulated and displayed in graphical form. The grating section of these fibres had been supplied fixed into a v-groove to protect the section which may be weakened due to the removal of the plastic fibre coating when the grating was written. This v-groove also keeps the grating section straight removing the possibility of any bending effect on the coupling wavelengths.

The fibres were connected in turn between the light source and the OSA using bare fibre connectors and the transmission spectrum of each was observed at room temperature.

The first thing to be noticed was that, even though the fibres have the same specifications, the wavelengths at which coupling occurs are not the same, where S1 shows a coupling wavelength of 1548nm and S2 shows a coupling wavelength of 1551.5nm. This is the first indication that writing of two identical gratings may involve more accurate control of the writing parameters than first expected.

141

The second noticeable result was the difference in the intensity between the two transmission spectra, the shorter fibre, S2 showing around twice the intensity of the longer fibre, S1. It is well known that transmission intensity reduces as length of fibre increases, but the amount of signal reduction in this case is far too great to be accounted for by this reasoning. Re-cleaving and adjustment of the fibre end faces in the bare fibre adapter showed significant changes in the transmitted intensity of both spectra, suggesting that inconsistencies in positioning, and the condition of the cleaved face of the fibre are more likely to be the cause of this intensity mismatch. Intensity changes observed in further experiments must allow for this potential problem, which must always be evident when bare fibre connectors are used.

It was also noticed that slight deformation of the grating section caused shifts in the coupling wavelength of each of the fibres as predicted by theory, but deformation of fibre itself had no noticeable effect on the transmission spectrum. It was therefore deemed necessary that the grating must be kept straight, under constant tension for all further experiments to eliminate the spurious bend/strain induced coupling shifts.

6.3.1 Initial Investigation into Temperature and Ambient Refractive Index Effects on LPG S2

Preliminary investigations into the temperature and ambient index characteristics of LPGs were undertaken using LPG S2, after noticing a blue shift in the coupling wavelength when the palm of the hand was in contact with the grating section of the fibre. In this initial investigation water was used due to the simplicity of temperature range and regulation, and of its function as the surrounding heat transfer medium.

The grating was clamped under slight tension in a purposely designed bath as shown in Figure 6.1 and the transmission profile of the LPG was taken in air at room temperature.
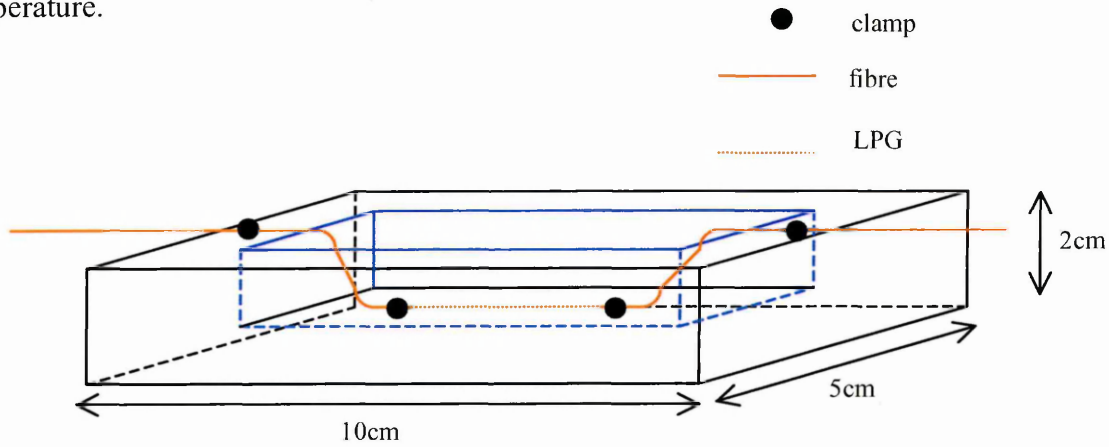
Figure 6.1:   Temperature controlling water bath used to investigate coupling wavelength over a range of temperatures in air

The bath was filled with water at a temperature of 8°C and the coupling wavelength shift was noted at various intervals as the water temperature was increased slowly to 40°C, the wavelength shifts being shown in figure 6.2.
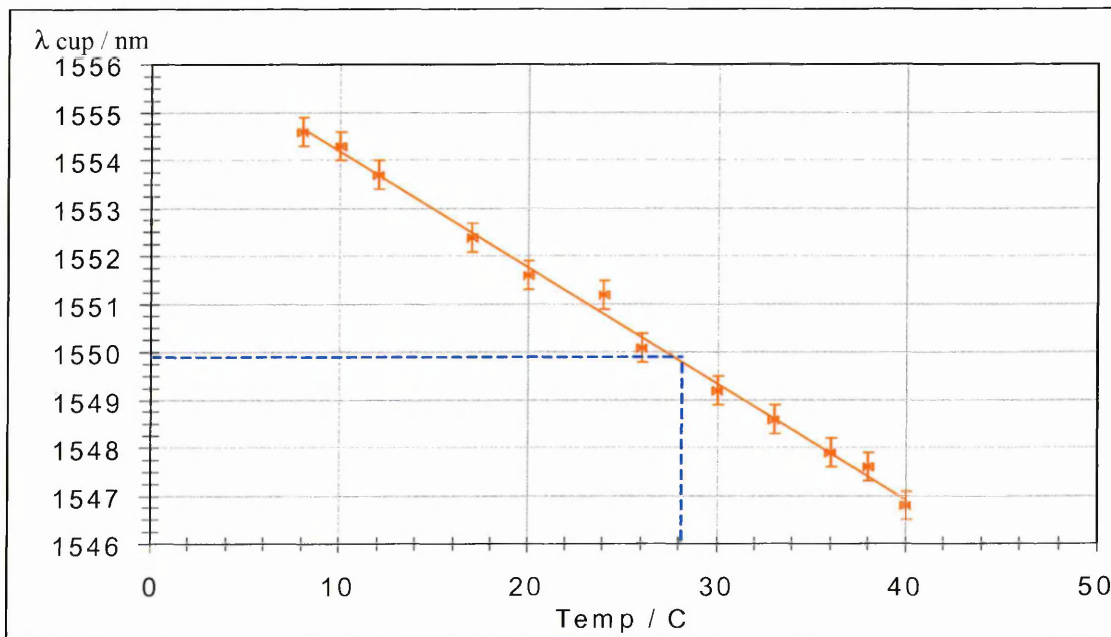
Figure 6.2:   Shift in coupling wavelength with increase in temperature of water around LPG

The coupling wavelength in water at room temperature of 28°C can be read from the graph in Figure 6.2 or calculated from the equation of the trend line:

$$\lambda_{cup} = -0.2419T + 1556.6$$

to be 1549.8 nm, which is less than the coupling wavelength at room temperature in air of 1551.5 nm. This is to be expected from theory as the higher refractive index of the water will result in a shift to shorter coupling wavelengths than in air. It is understood from theory and can be seen by inspection of the LPG coupling equation (3.102) that there are two parameters which are affected by the ambient temperature, the effective refractive indices of the core and cladding which are dependent on the radial dimensions and the (density related) refractive indices of each, and also the period of the grating. Further investigation and analysis of this effect will be documented later in this chapter. At this point it suffices to deduce that there is a linear negative temperature profile of this LPG with a change in coupling wavelength of approximately -0.25 nm for every 1°C rise in temperature, or a temperature increase of 4°C is required to reduce the coupling wavelength by 1 nm.

To determine whether the ambient index of the heat transfer medium was an integral function of the coupling wavelength shift (causing an increase in the rate of change of wavelength with temperature) or merely an offset value, the previous experiment was repeated in air. A second purpose built heat chamber was produced and can be seen in Figure 6.3:
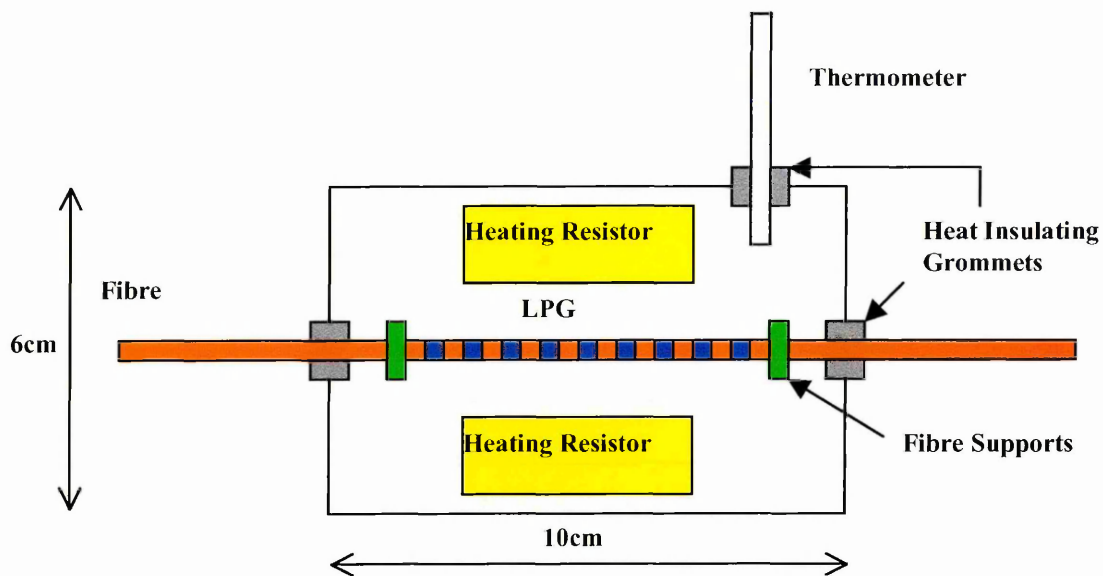
Figure 6.3: Heat chamber produced to investigate coupling wavelength over a range of temperatures in air

The coupling wavelengths were recorded at various temperature intervals between the room temperature of 24°C and the temperature at the maximum voltage of the resistors of 74°C, and are displayed in Figure 6.4. It was not possible at this point to reduce the air temperature below the room temperature.
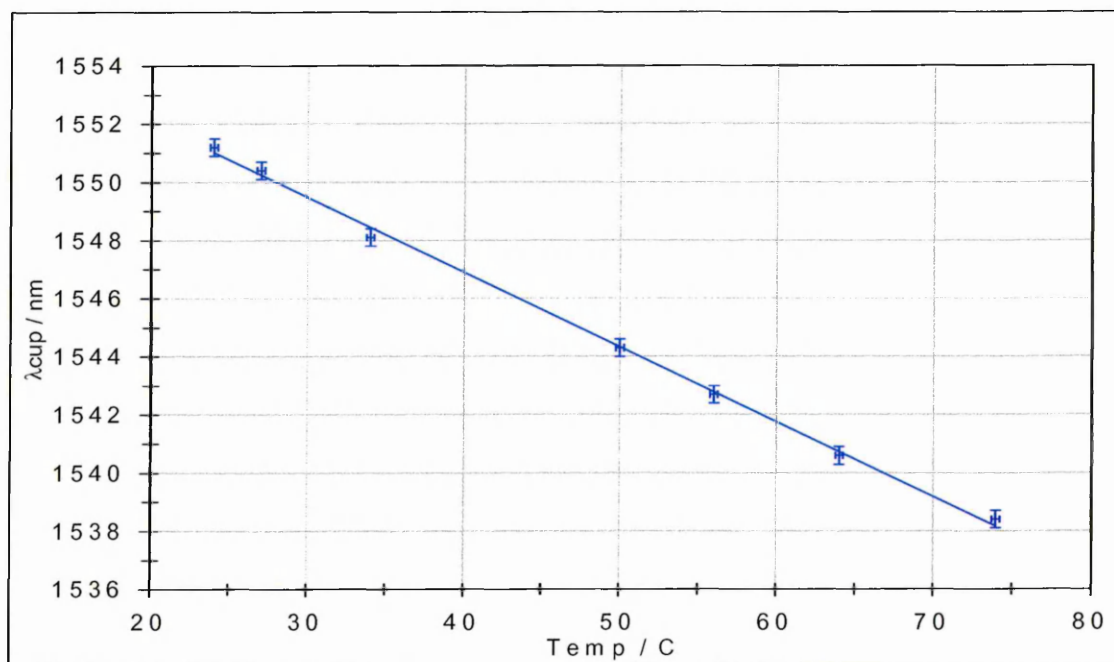
Figure 6.4: Shift in coupling wavelength with increase in air temperature around LPG

Again an expected negative temperature profile is evident with a very similar gradient

to the profile in ambient water, the equation of the trend line being

$$\lambda_{cup} = -0.2569T + 1557.2$$

A combination of the two graphs extrapolated over the same temperature range can be

seen in Figure 6.5
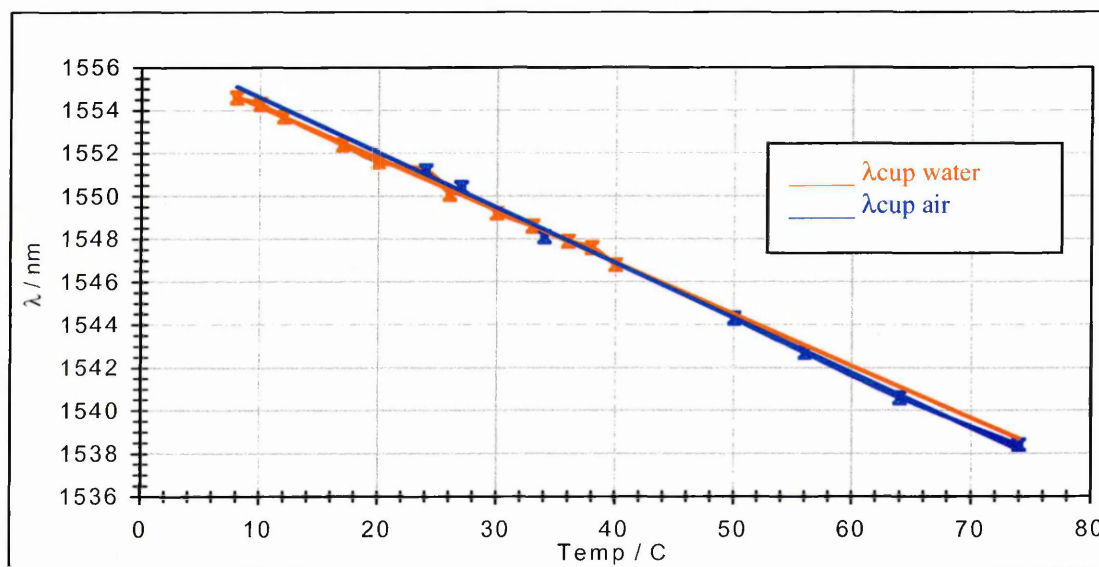
Figure 6.5: **Comparison between the shift in coupling wavelengths with increase in temperature of water and air around LPG**

It can be seen that each line is within the error bars of the other over the range

investigated. The effect on the coupling wavelength of the greater refractive index of

the water seems negligible for the LPG used is this experiment. This negligible effect

of quite a large change in ambient index lead to the following investigation into the

refractive index profile of the LPG.

6.3.2 Preliminary Experiment to Determine Ambient Refractive Index Profile of LPG S2

As no index matching gels were available at this stage of the research program, saline solutions of various salt concentrations ranging from 0 to 25% weight were produced and the refractive indices determined using an Atago refractometer with a range from 1.333 to 1.360 and a resolution of 0.0005. The 25% saline solution was found to be out of the range of the refractometer, so a graph of the refractive indices as a function of salt concentration was produced and extrapolated using an empirically fitted trend line as shown in figure 6.6 to estimate this refractive index. The value was also calculated using the equation of the trend line:

$$RI = 0.0015c + 1.3368$$
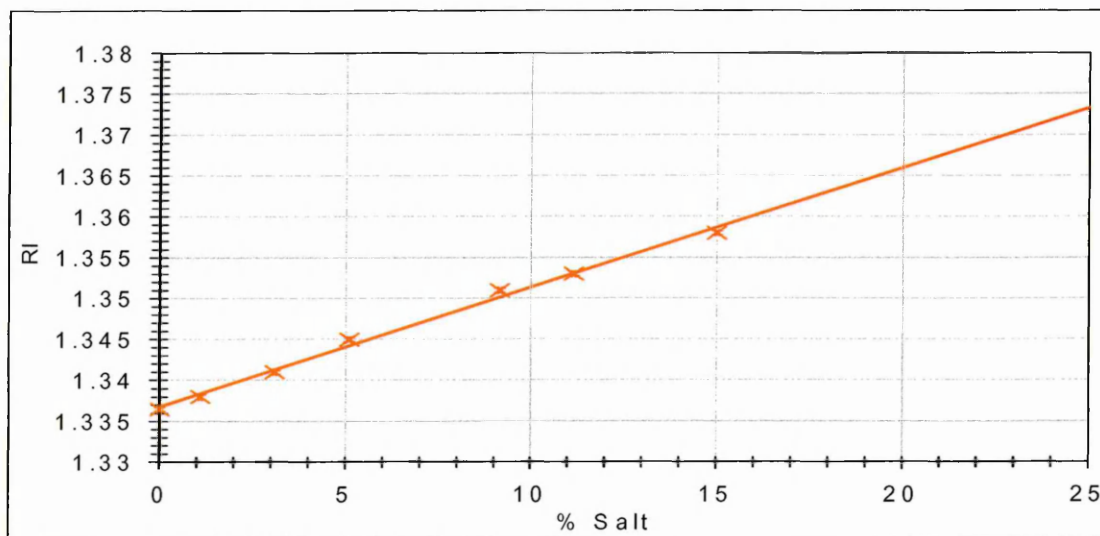
Figure 6.6: Graph to determine relationship of salt concentration to refractive index of saline solution at room temperature

LPG S2 was clamped under slight tension in the purpose built bath and the coupling wavelength in air recorded. The LPG was then immersed in each solution

concentration maintained at a constant temperature, and the coupling wavelengths recorded as shown in Table 6.2

% Salt in Solution ± 0.1%	RI of Solution ± 0.0025	Coupling Wavelength / ± 0.3 nm
Air	1.0000	1551.9
0	1.3365	1551.3
1.1	1.3380	1551.3
3.1	1.3410	1551.3
5.1	1.3450	1551.3
9.15	1.3510	1551.3
11.15	1.3530	1551.3
15.0	1.3580	1551.3
25.0	1.3743*	1550.7

*value read from extrapolated graph in Figure 6.6 and calculated from equation of line.

Table 6.2:   Coupling wavelengths when LPG immersed in selected concentrations of saline solution

The difference in the coupling wavelengths in air and in water between this and the previous experiment may be due to differences in room temperature and clamping tension of the fibre in each case.

The results show a blue shift of 0.6nm as the ambient refractive index is increased from 1 (air) to 1.3365 (water), no discernible shift from 1.3365 (water) to 1.3580 (15% salt) and a further blue shift of 0.6nm as the ambient index is raised to 1.3743 (25% salt). Literature [164, 165, 172] has demonstrated blue shifts of between 5 and 30nm when changing the ambient index from that of air (1) to that of water (1.33). The much smaller shift in this experiment may be due to 2 factors:

1.   A red shift due to the difference in temperature between the air and the water could reduce the blue shift caused by the ambient index increase by 0.25nm per degree C drop in temperature. However, to make up for the reduction from -5nm to –

0.6nm, a temperature change of -18°C would be required, which certainly did not occur. A more realistic figure would be a maximum of -2 °C which would allow a possible blue shift of 1.1nm.

2.   The grating period of this LPG was almost twice as long as those in which the greater shifts were observed. From theory this would mean that each wavelength would experience a smaller angle of diffraction by the grating, resulting in all of the coupling modes moving to longer wavelengths. Thus the 1550nm radiation is coupling to lower order cladding modes in this longer period LPG than in the shorter period LPGs reported in literature [172]. As the lower order cladding modes are much less affected by change (less sensitive) in the ambient index this would better explain the discrepancies in the results.

The conclusions drawn from these preliminary experiments are that LPGs S1 and S2 display very poor sensitivity to ambient index changes over the range of indices used in this preliminary investigation, due to the periodicity of the grating. Investigations into ambient indices greater than 1.3743 were carried out later in the program as index matching gels from 1.4 to 1.456 became available.

6.3.3 Preliminary Experiment to Determine the Viability of Long Period Gratings for Use as Gas Sensors

Observation of the spectral profiles of each of the Singapore gratings (Appendix 8) showed that the repeatability of process of writing the gratings seems to have its

limitations as it can be seen that even though fibres originally had the same optical and physical parameters, and each of the grating lengths was written using the same respective phase masks, exposure time, light source and intensity, the wavelengths at which core to cladding mode coupling occurs differs in each grating of the same period. The differences in coupling wavelengths in LPGs S3, S4, S5, and S6 with the same period and optical and physical parameters are shown in Figure 6.7 and in LPGs S7 and S8 in Figure 6.8, the dips in the spectra showing the wavelengths at which coupling occurs.
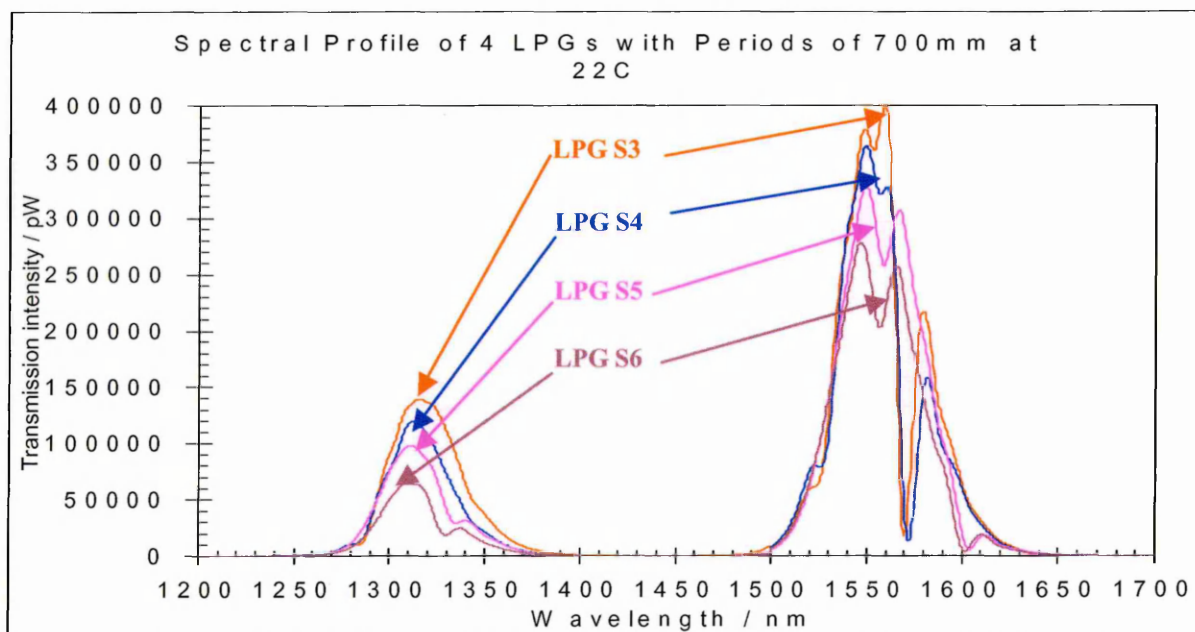
Figure 6.7: **Spectral profiles of LPGs S3, S3, S5, and S6 with identical optical and physical parameters and grating periods of 700 μm**

LPG S3 can be seen to have coupling wavelengths at 1552.8 nm and 1570.0 nm. LPG S4 can be seen to have coupling wavelengths at 1258.5 nm, 1525.5 nm, 1556.5 nm and 1572.5 nm. LPG S5 can be seen to have coupling wavelengths at 1335.0 nm, 1558.5 nm, and 1604.0 nm. LPG S6 can be seen to have coupling wavelengths at 1329.5 nm, 1556.0 nm and 1601.5 nm.

150
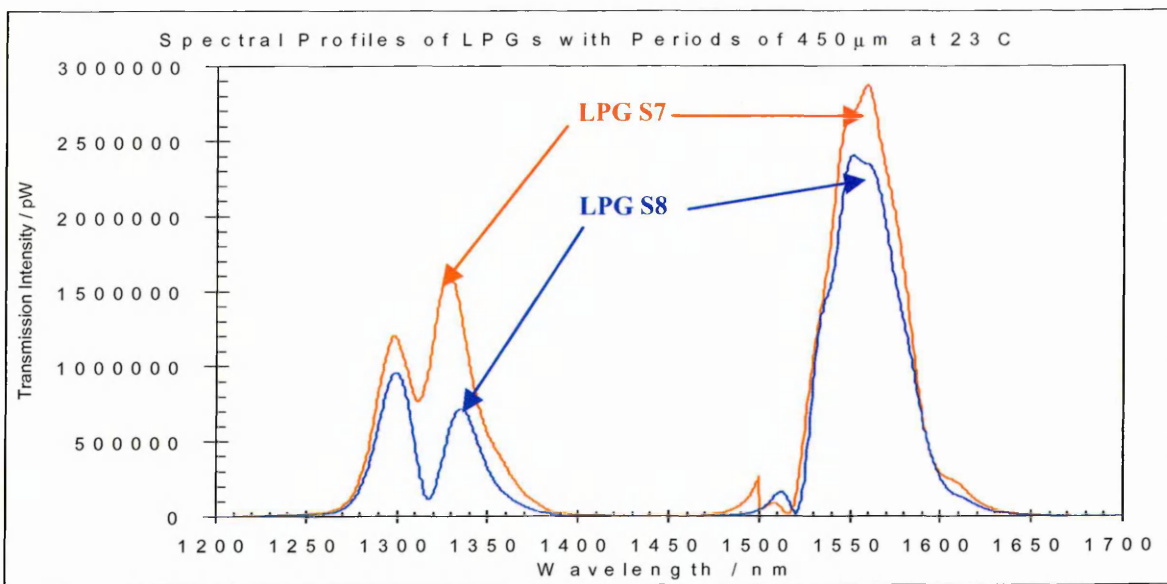
Figure 6.8: **Spectral profiles of LPGs S7 and S8 with identical optical and physical parameters and grating periods of 450 μm**

LPG S7 can be seen to have coupling wavelengths at 1311.5 nm, 1516.0 nm and 1550.0nm. LPG S8 can be seen to have coupling wavelengths at 1317.5 nm, 1520.0 nm, and 1558.0 nm.

The peak intensity differences must not be considered as these may be caused by the inconsistency of the condition of the ends of the fibres and the positioning of the fibre ends in the bare fibre adapters which connect into the light source and the OSA. The resonant wavelengths at which core to cladding mode coupling occurs appear as the dips in the transmission spectrum. The position of these dips is not affected by the connection limitations affecting the intensity, but is determined by the optical and physical characteristics of the fibre, and by the temperature and the ambient refractive index around the cladding. Care was taken that the temperature, ambient conditions and the tension of the fibre in the grating region were the same for each set of initial profiles. The differences must therefore be due to inconsistencies in the writing procedure. As stated in the theory, as the grating is written the diffraction pattern formed on the side of the core is not a step profile along the core but tends to be more

of a raised sine or Gaussian profile [355], as can be expected from the intensity profile of any diffraction pattern as shown in Figure 6.9.
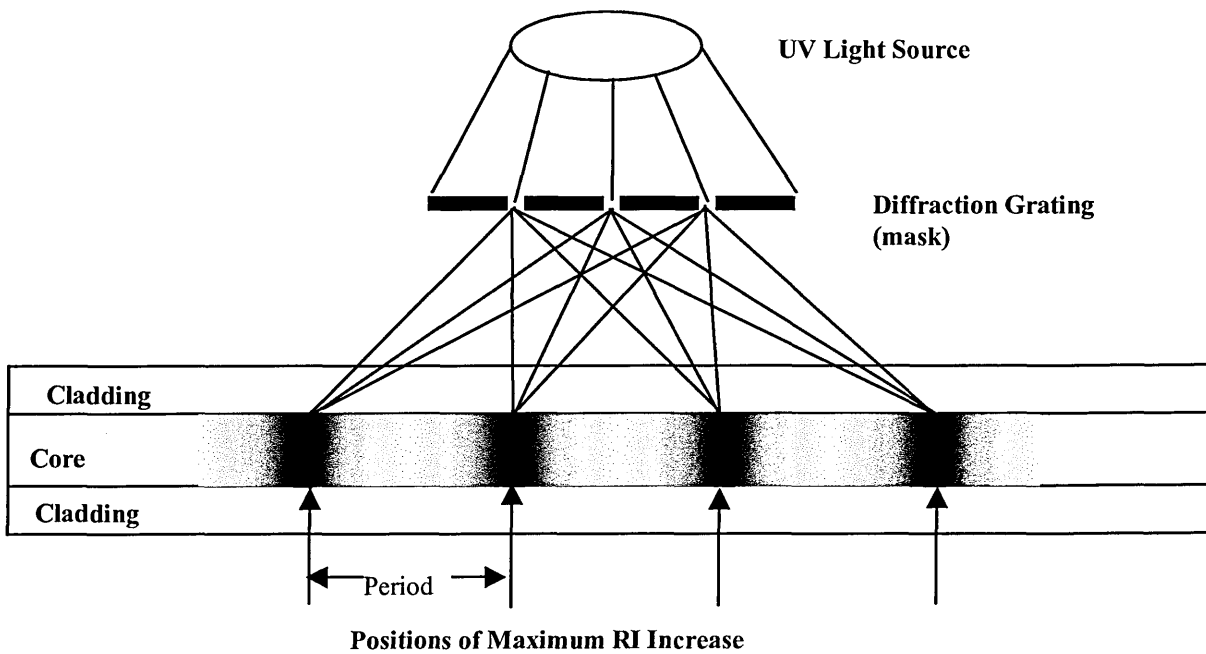
Figure 6.9: Refractive index profile of an LPG in the writing process

This results in a peak refractive index change in the core at the points of maximum constructive interference, with a gradual reduction to the minimum refractive index change at the centre of successive peaks. The position of these maxima form the grating and their separation is the period of the grating. The intensity and exposure time of the writing optical source determines the degree by which the refractive index of the grating lines exceed that of the core, but this will only affect the intensity of the affected wavelength, not its position in the spectrum. However, the path length and diffraction properties of the grating determine the modified core modal structure required for core to cladding mode coupling to occur. This gradually changing refractive index profile along the core between the peak values will therefore strongly affect the wavelengths at which this coupling will occur [169,170, 173,356,357].

Any slight discrepancy in exposure time, light intensity, scanning rate, fibre to mask separation, ambient temperature, fibre strain etc. could therefore cause different refractive index profiles between the peaks and thus affect the coupling wavelengths in the fibre gratings. The refractive indices used to calculate the coupling wavelength from the LPG coupling equation will not be the same as the original refractive indices of the core and cladding and must therefore be modified to allow for the above effect. Ideally some function should be determined which takes into account the gradual change in refractive index along the grating. The change in refractive index along the core can only be assumed, and a trial and error procedure performed until the mathematical model is as close as possible to the experimental findings.

The availability of fibres with the same optical and physical specifications, but with two different grating periods allowed investigation into the period dependency of the temperature and ambient index profiles of LPGs. Previous reports have shown the effects of different types of fibres with LPGs of different periodicities on the ambient index and temperature profiles [193,325,358]. These reports, however, were usually concerned with fibres of different consistencies, and with period changes of around 1 to 5% of the initial value not 64% as in this case, or comparisons made between the LPG and FBG sensitivity [324]. As the ambient temperature of the environment in which a sensor may be situated may affect the coupling wavelength shift due to ambient index variations, the period dependency of the temperature profile of the LPG may be of considerable importance, and will be investigated as an integral part of this research.

The two main experimental routes of this research will therefore be:

153

1.   To investigate the temperature dependence of LPGs of different period and to predict a suitable method of compensation for this effect.

2.   To investigate the possibility of utilising the ambient index sensitivity of an LPG as a gas sensor, by coating the fibre cladding in the vicinity of the LPG with a chemical whose refractive index is known to be affected by a given gas.

6.4 Investigation into the Ambient Refractive Index and Temperature Dependence of LPGs of Different Periods

6.4.1 Experimental Procedure
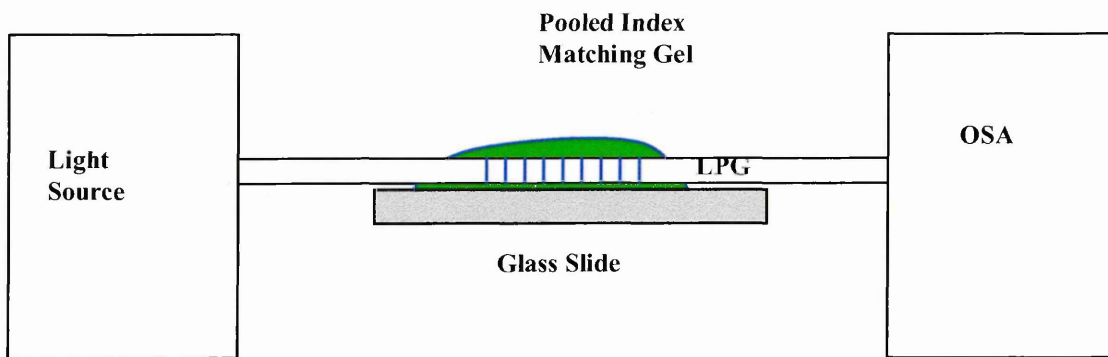
Figure 6.10:   Experimental set-up for the determination of the ambient refractive index profiles of the LPGs

Refractive index profiles and temperature profiles of the LPGs used in this part of the

investigation were taken prior to starting any experiments and can be seen in Appendices 9 and 10. LPGs S3, S4, S5, S6, S7 and S8 were in turn clamped under slight tension above a moveable platform. The ends of each fibre were connected into the light source and detector inputs of the OSA using bare fibre connectors and the spectral profile in air was recorded. A glass slide was placed on the platform and the platform raised until it was almost touching the grating. A range of index matching gels were then 'pooled' over the fibre as shown in Figure 6.10 until it was completely immersed and the spectral profile recorded. Previous traces of gel were removed using acetone, ensuring that the profile returned to that in air, before the next gel was applied. The ambient temperature of the room was monitored and controlled to minimise the possibility of spurious results due to temperature changes.
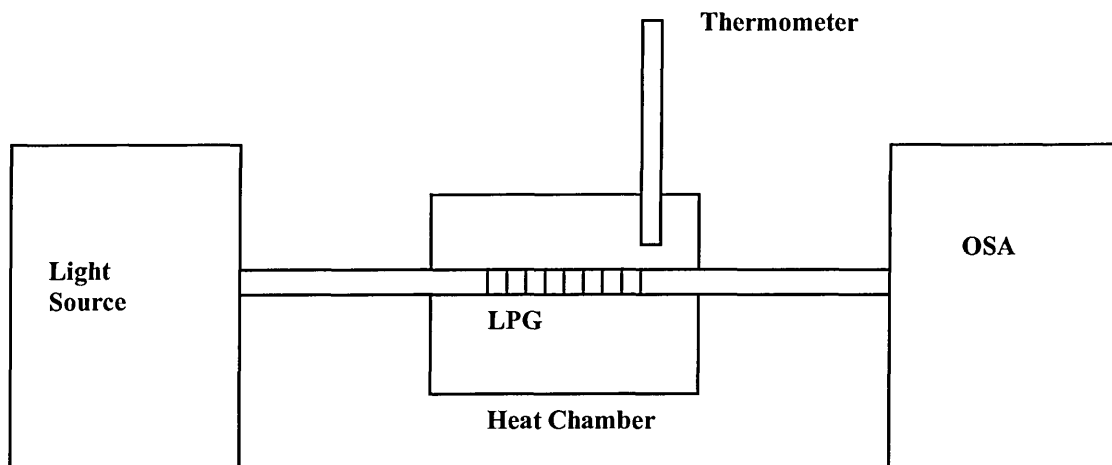
Figure 6.11: **Experimental set-up for the determination of temperature profiles of the LPGs**

To obtain the temperature profiles of the gratings each grating in turn was again clamped under slight tension above the moveable platform as shown in Figure 6.11. The ends of each fibre were connected into the light source and detector inputs of the

OSA using bare fibre connectors as previously described. The purposely designed heat chamber as described earlier in this chapter was fitted around the grating section of the fibre and clamped securely to the platform. The spectral profile was recorded at room temperature, then at selected temperatures up to a maximum of around 80°C as the heating chamber was activated. Care was taken that a steady temperature had been evident for at least 15 minutes before each spectral profile was taken to ensure constant temperature along the grating section of the fibre.

Further temperature profiles of the fibres A400-A416 and C1 were taken. Although these LPGs were not of the same optical and physical parameters as the previous LPGs, they did have periods comparable to LPGs S7 and S8. This would allow the comparison of LPGs of different parameters but of similar periodicities, and the effect of these parameters on the temperature profiles.

6.4.2 Results and Discussion

The ambient refractive index spectral profiles of all six fibres (Appendix 9) showed shifts to shorter wavelengths of each modal coupling as the ambient refractive index was increased. All six spectral ambient index profiles showed the degree of shift in coupling wavelength to increase as the ambient refractive index approached that of the cladding as summarized in Figures 6.12 to 6.17, agreeing with findings in previously referenced literature [164, 165, 172].

156
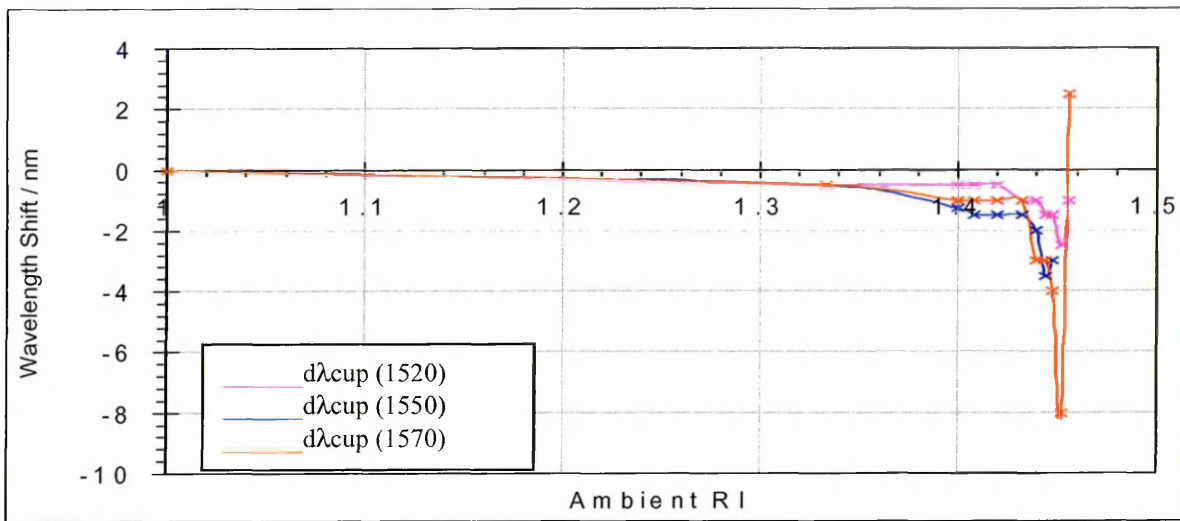
Figure 6.12: Relative change in coupling wavelength with ambient refractive index for LPG S3
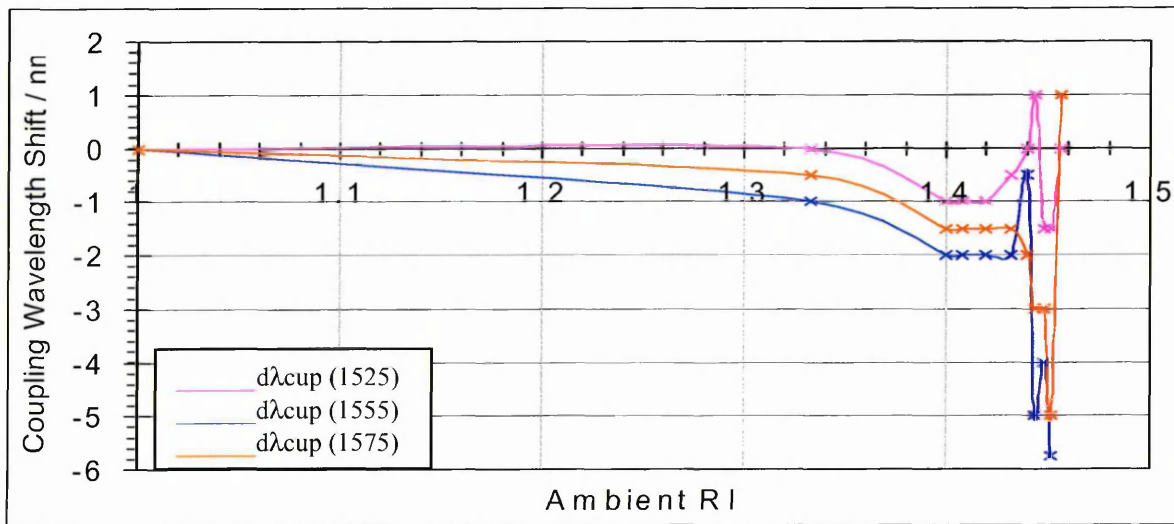
Figure 6.13: Relative change in coupling wavelength with ambient refractive index for LPG S4
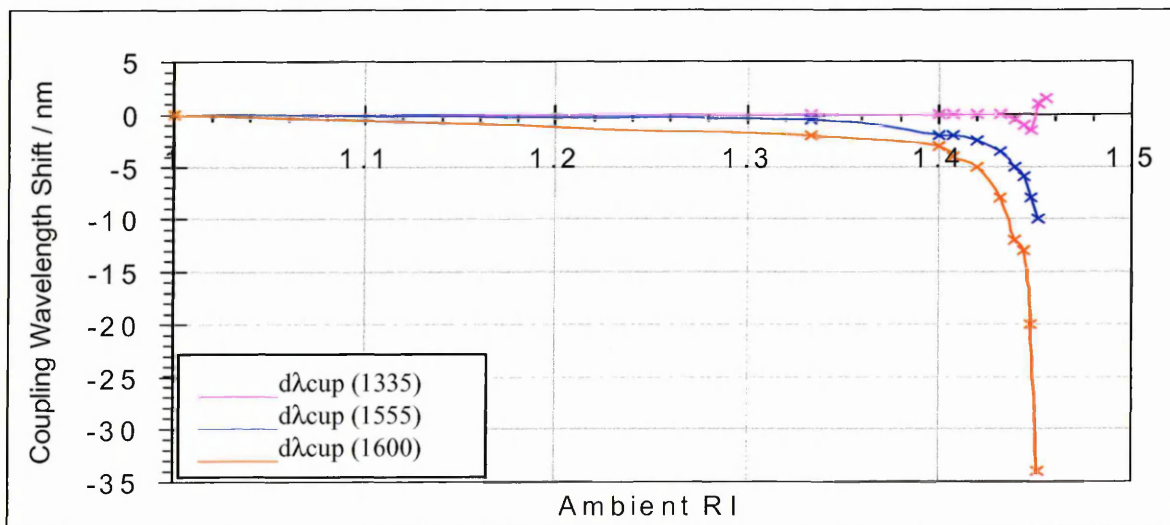
Figure 6.14: Relative change in coupling wavelength with ambient refractive index for LPG S5

157
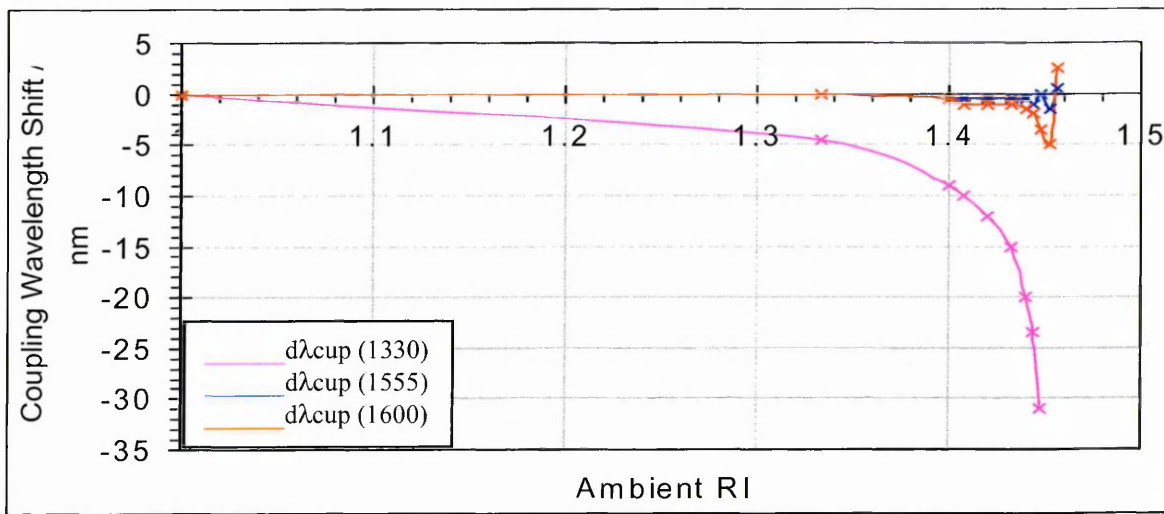
Figure 6.15: Relative change in coupling wavelength with ambient refractive index for LPG S6
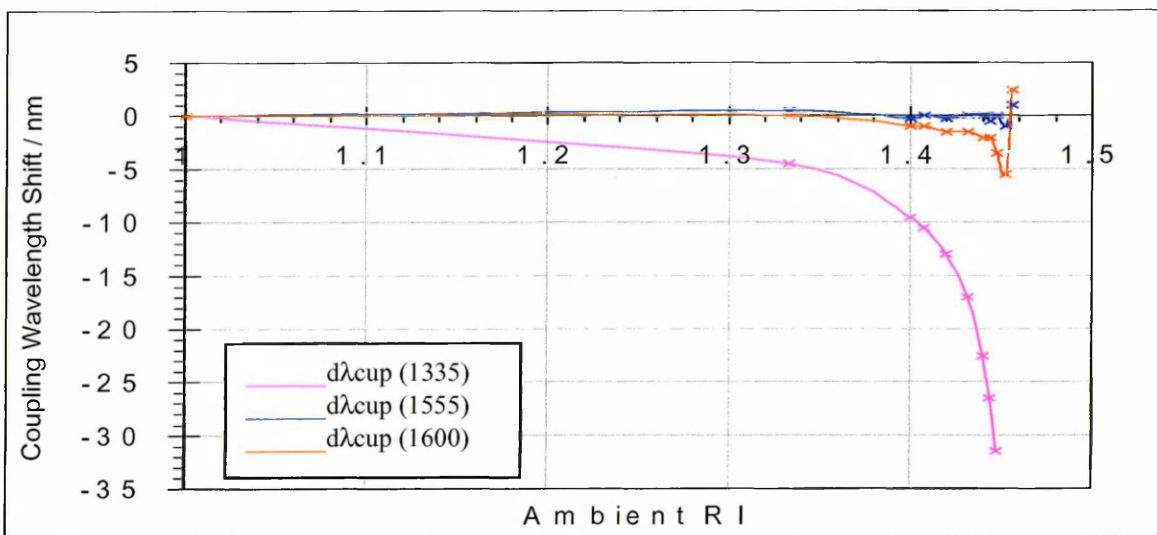
Figure 6.16: Relative change in coupling wavelength with ambient refractive index for LPG S7
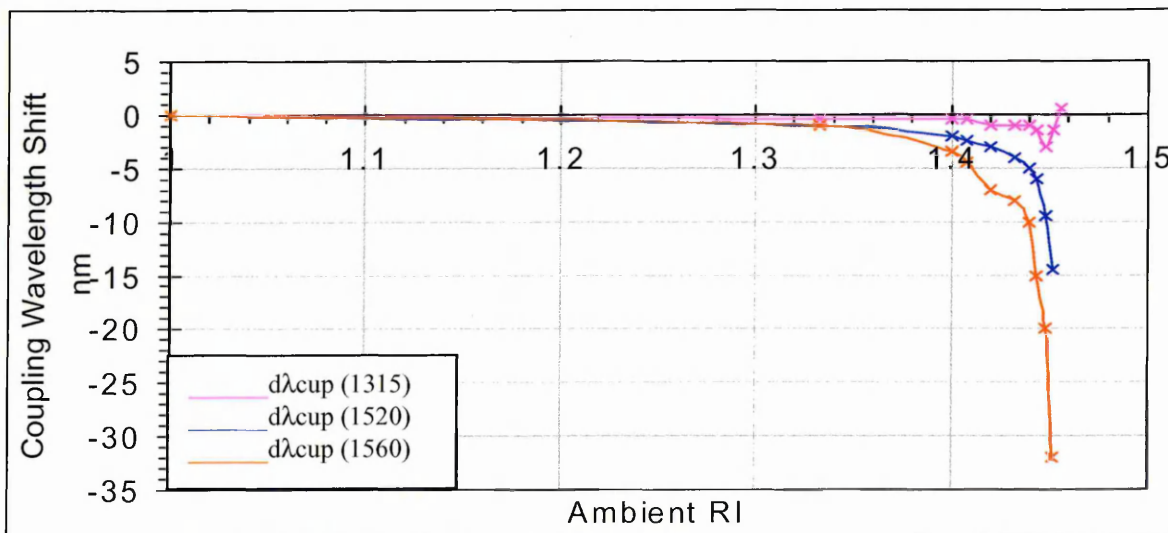
Figure 6.17: Relative change in coupling wavelength with ambient refractive index for LPG S8

158

Previous reports [193] have shown that when the ambient refractive index reaches that of the cladding, the cladding effectively becomes infinite and as such will have no mode structure and therefore no core to cladding mode coupling can occur. As the ambient refractive index exceeds that of the cladding leaky cladding modes are formed due to the partial internal reflection at the cladding/ambient interface and coupling will again take place but will occur at wavelengths greater than coupling wavelengths in air. Due to the limitations of the light source range available at this stage of the research, some of the coupling wavelengths moved out of range as the higher ambient indices were applied, but where visible, the coupling wavelengths showed a positive shift to values greater than in air as an ambient refractive index of 1.452 was exceeded. The range of index matching gels used in this investigation did not include a gel of the same refractive index as the core as the coupling wavelengths were not seen to disappear, but as the coupling wavelengths shifted immediately to higher values when an ambient index of 1.456 was applied this suggests that the refractive index of the cladding is between 1.452 and 1.456. The refractive indices of the cladding (n_{clad}) and the core (n_{core}) before the grating was written was stated to be 1.4441 and 1.4499 respectively. If this was still the case then the jump in the coupling wavelength to values greater than in air should have occurred at the next higher ambient index in the range of 1.448. It seems then that the process of writing the grating in the core does not only increase the core refractive index in and around the grating but also the refractive index of the cladding around the grating. If this is the case the minimum possible value of the cladding index is 1.452 and has increased by 0.0079. The core index which was originally 0.0058 greater than the cladding index must also have increased to a value greater than 1.452 for guided modes to exist in the core. This change in the respective refractive index values will have a

considerable effect on the mode coupling shifts and again must be taken into account in any computer simulations.

The fibres containing the gratings of around 450 μm period, which are in the period range used in most previously reported experiments [197,325,326,359-362], seem to react as predicted. The longer wavelengths which couple to the higher order cladding modes are more sensitive to ambient refractive index changes than the shorter wavelengths which couple to the lower order cladding modes. The fibres containing the longer period of 700 μm however, do not all seem to follow this trend on first inspection of the results. While LPG S3 and LPG S4 responded as expected with the longer wavelengths generally showing greater sensitivity to the ambient index changes, LPG S5 and LPG S6 showed the shortest visible coupling wavelength to be around six times more sensitive than the longer coupling wavelengths. When the guided radiation transmitted along the core is incident on the grating the longer wavelengths will undergo a greater angle of diffraction than the shorter wavelengths. A minimum wavelength will exist therefore at which the core mode will couple to the first cladding mode. The cladding modes into which subsequent core wavelengths couple will increment as the modified mode paths of certain wavelengths in the core meet the coupling condition in (3.102). An increase in the grating period would result in a smaller angle of diffraction of all wavelengths in the transmitted spectrum. This would result in an increase in the wavelength which would couple to the first cladding mode, and therefore subsequent core to cladding mode coupling would also be at longer wavelengths. In the gratings with the 450 μm period the cladding modes into which the respective wavelengths are coupling will be a higher order than for the gratings with the 700 μm period. This would explain the greater sensitivity of the

shorter period gratings to the ambient refractive index, as sensitivity is known to increase as the coupling mode increases [193]. This does not explain the high sensitivity of the 1310 nm coupling wavelength in LPGs S5 and S6 however, as this wavelength range should be of a low order mode coupling and thus less sensitive than the coupling wavelengths in the 1500 to 1600 nm region in the same fibre. The high sensitivity of this wavelength suggests that this may be a higher harmonic of the grating period as reported by [170,171] and this higher order of diffraction is actually coupling to a much higher cladding mode than the wavelengths in the 1500 to 1600 nm region.

The ambient temperature spectral profiles of all six LPGs are shown in Appendix 10. The coupling wavelength shifts are summarized in Figures 6.18 to 6.23.
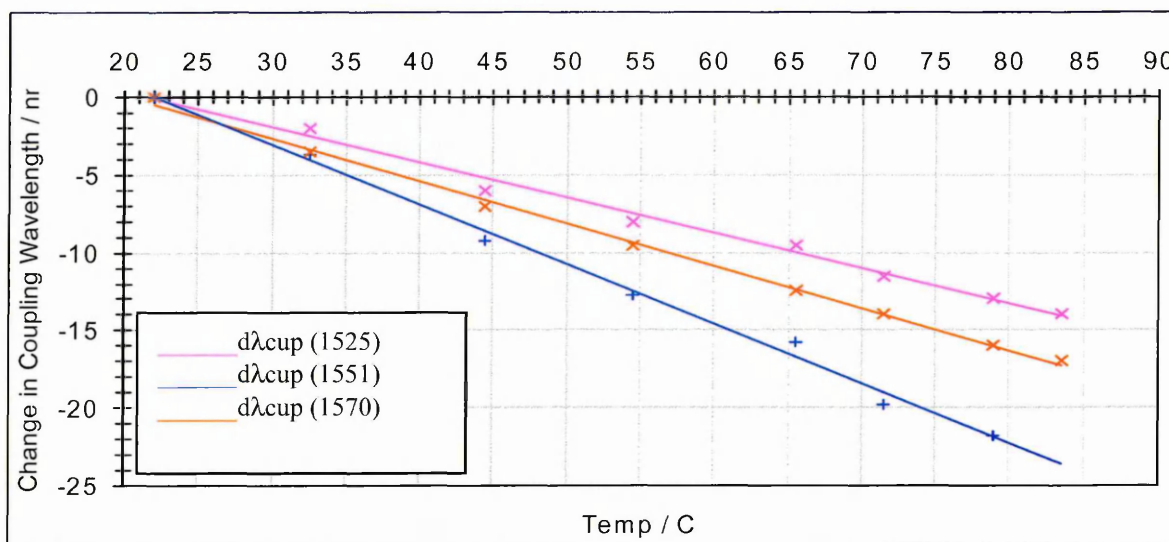
Figure 6.18: **Relative change in coupling wavelength with temperature for LPG S3**

The equations of the trend lines for LPG S3 are:

$$d\lambda_{cup(1525)} = -0.227T + 4.856$$

$$d\lambda_{cup(1551)} = -0.3837T + 8.3979$$

$$d\lambda_{cup(1570)} = -0.2734T + 5.5415$$

161
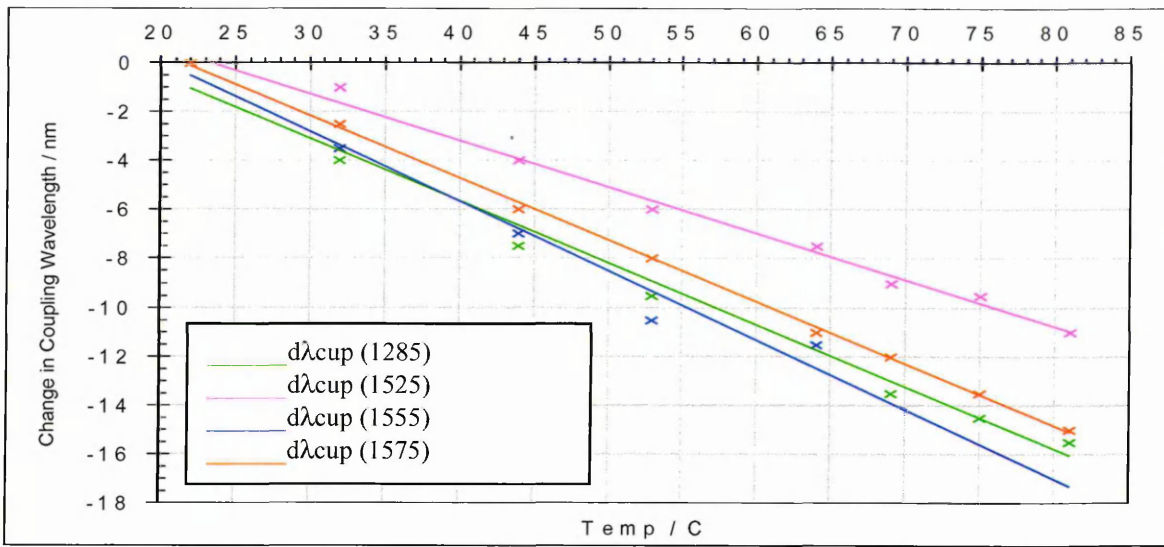
Figure 6.19: Relative change in coupling wavelength with temperature for LPG S4

The equations of the trend lines for LPG S4 are:

$$d\lambda_{cup(1285)} = -0.2544T + 4.5523$$

$$d\lambda_{cup(1525)} = -0.1907T + 4.4901$$

$$d\lambda_{cup(1555)} = -0.2853T + 5.769$$

$$d\lambda_{cup(1575)} = -0.2544T + 5.4898$$
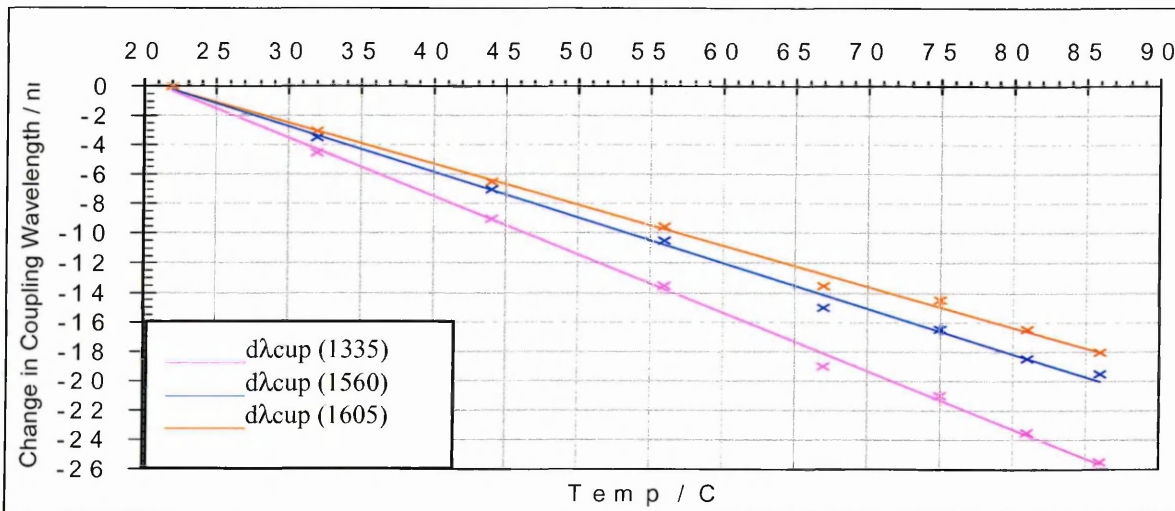
Figure 6.20: Relative change in coupling wavelength with temperature for LPG S5

The equations of the trend lines for LPG S5 are:

$$d\lambda_{cup(1335)} = -0.3961T + 8.4255$$

162

$$d\lambda_{cup(1560)} = -0.3083T + 6.5282$$

$$d\lambda_{cup(1605)} = -0.2573T + 5.7251$$
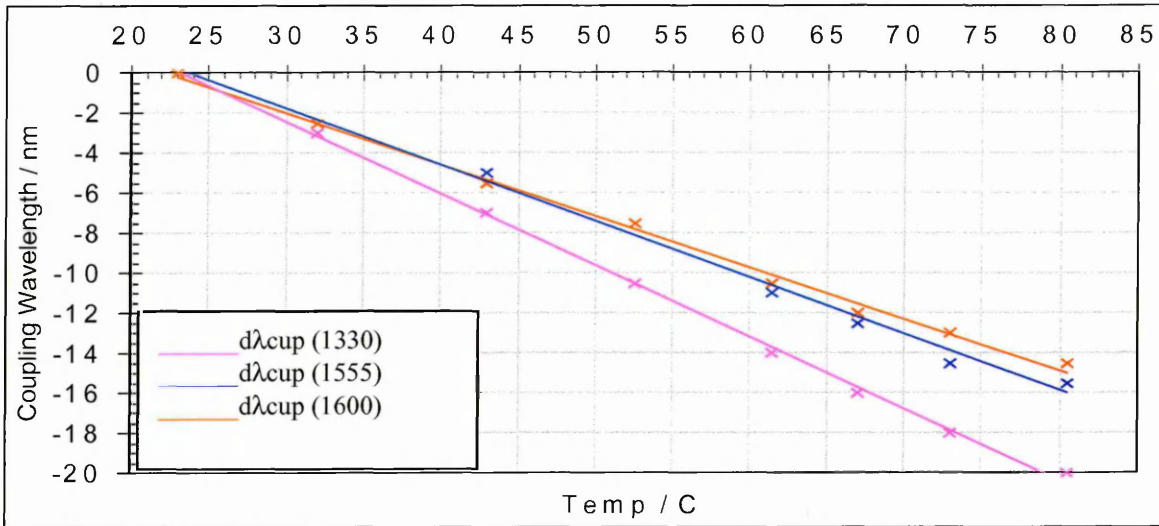
Figure 6.21:   Relative change in coupling wavelength with temperature for LPG S6

The equations of the trend lines for LPG S6 are:

$$d\lambda_{cup(1330)} = -0.3573T + 8.2543$$

$$d\lambda_{cup(1555)} = -0.282T + 6.6855$$

$$d\lambda_{cup(1600)} = -0.2785T + 5.9323$$
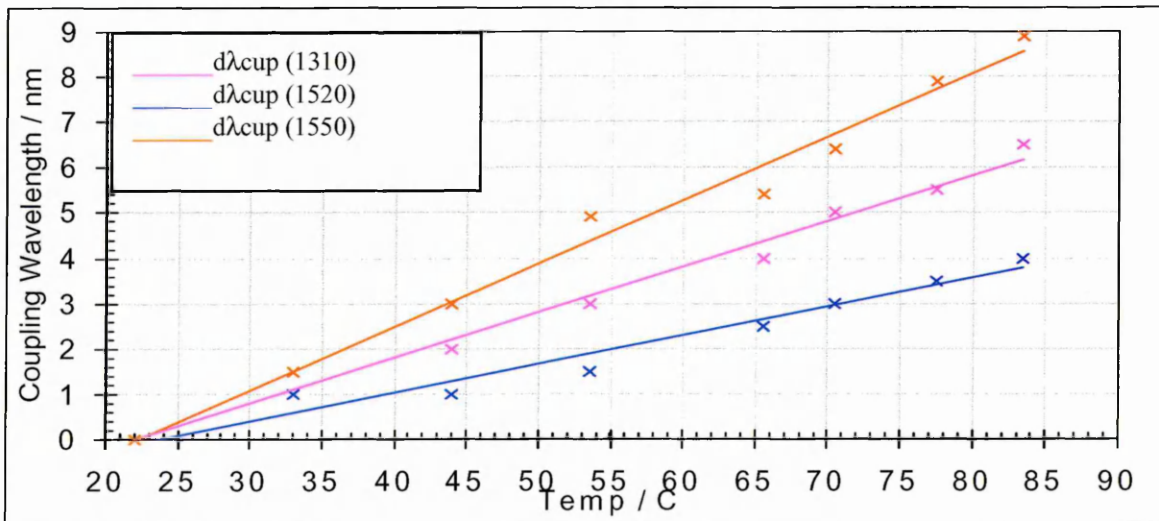
Figure 6.22:   Relative change in coupling wavelength with temperature for LPG S7

The equations of the trend lines for LPG S7 are:

$$d\lambda_{cup(1310)} = 0.1003T - 2.1971$$

$$d\lambda_{cup(1520)} = 0.0628T - 1.4665$$

$$d\lambda_{cup(1550)} = 0.1398T - 3.104$$
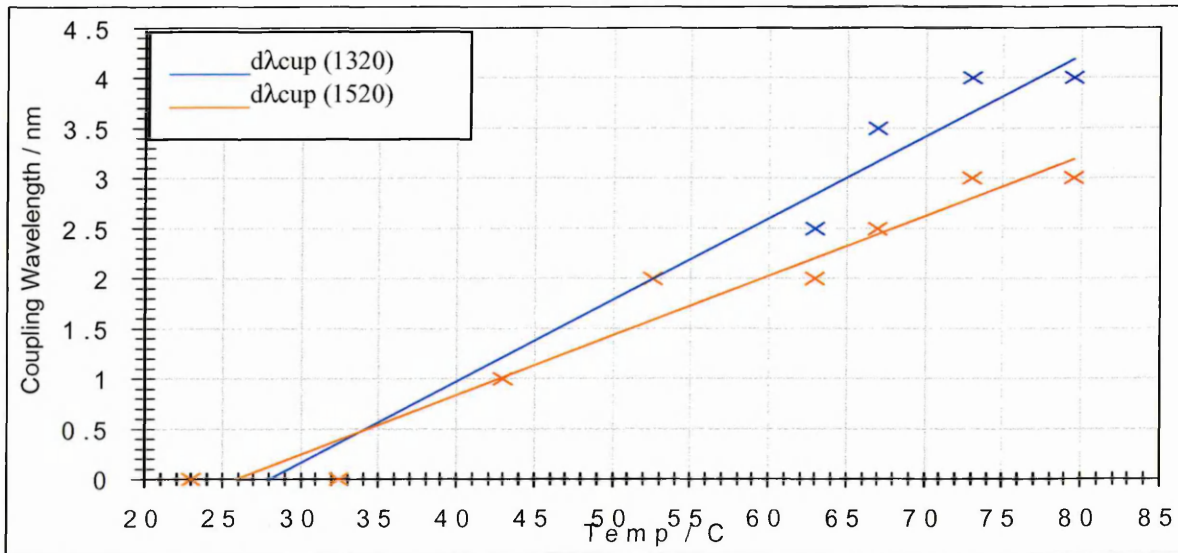
Figure 6.23: **Relative change in coupling wavelength with temperature for LPG S8**

The equations of the trend lines for LPG S8 are:

$$d\lambda_{cup(1320)} = 0.0815T - 2.2914$$

$$d\lambda_{cup(1520)} = 0.0597T - 1.5448$$

The main feature of this investigation is the fact that all of the LPGs with 700μm periods have a negative temperature profile whilst all of the LPGs with 450 μm periods have a positive temperature profile. The LPG coupling equations (3.102) and (3.103) consist of 2 parameters, the period of the grating (Λ) and the refractive indices of the core (n_{core}) and cladding ($n_{cladding}$), both of which are temperature dependent.

164

The effect on the coupling wavelength with temperature can be shown if these equations are differentiated with respect to temperature resulting in [363]:

$$\frac{d\lambda}{dT} = \frac{d\lambda}{d(\delta n_{eff})}\left(\frac{dn_{eff\,core}}{dT} - \frac{dn_{eff\,clad}}{dT}\right) + \Lambda\frac{d\lambda}{d\Lambda}\frac{1}{L}\frac{dL}{dT} \qquad (6.1)$$

or

$$\frac{d\lambda}{dT} = \frac{1}{k}\left[\frac{d\lambda}{d(\delta\beta)}\left(\frac{d\beta_{core}}{dT} - \frac{d\beta_{clad}}{dT}\right) + \Lambda\frac{d\lambda}{d\Lambda}\frac{1}{L}\frac{dL}{dT}\right] \qquad (6.2)$$

where L is the length of the grating, δn_{eff} is the difference between the core and cladding effective indices, $\delta\beta$ is the difference between the core and cladding propagation constants, and Λ is the grating period. The first term on the right hand side of these equations represents the temperature effect on the refractive indices or propagation constants of the core and cladding, while the second term represents the temperature effect on the grating periodicity.

The increase in temperature will cause expansion of the fibre and hence an increase in the grating length. This increase will cause different wavelengths to satisfy the coupling equations (3.102) and (3.103) and, as is evident from the previous reasoning will cause the coupling wavelengths to shift to longer wavelengths.

The shift to higher or lower values of the coupling wavelength due to the change in refractive indices of the core and the cladding caused by the temperature change is not as obvious to deduce. As there is a shift to shorter wavelengths in the LPGs with 700 μm periods this suggests that the effect of temperature change on the refractive index causes a shift to shorter wavelengths, but the exact change of the refractive indices cannot be easily explained. Firstly, as previously stated, the increase in grating period due to the temperature increase would result in coupling to longer wavelengths. As these new wavelengths have their own individual modal paths in both the core and the

165

cladding, and the effective refractive indices are dependent on the modal path (unlike actual refractive index which ideally has no directional dependence), this factor will itself cause different effective refractive indices in both media to be considered. Thus a change in only the period of the grating has caused every value in the formula to change.

The LPG coupling formula (3.102) can be manipulated to give

$$\beta_{core}^{\lambda i} - \beta_{clad}^{\lambda i} = \frac{2\pi}{\Lambda} \qquad (6.3)$$

where β is the propagation constant (= $kn\sin\theta$). Shorter wavelengths have higher wave numbers ($k = 2\pi / \lambda$) than the longer wavelengths and the mode paths travel in the core at shallower angles. Thus the propagation constants of the shorter wavelengths will be greater than those of the longer wavelengths in any given fibre. As the right hand side of this equation involves only constants this manipulation shows that the difference between the propagation constants in the core and cladding of any given wavelength must be equal to this constant value for coupling to occur. It is not obvious therefore whether the propagation constants would increase or decrease as the refractive indices change and this factor may depend on the optical and physical parameters of any given fibre [364].

The increase in temperature expands the fibre resulting in a decrease in refractive index as the medium becomes less dense. This in turn reduces the optical path length and modifies the phase change on reflection at the refractive index boundaries of each wavelength in the core and cladding. The ray paths in which constructive interference will occur and therefore the modal paths will also change. As the propagation constants (β) are the components of the modal wave vector in the axial plane of the

fibre these will change proportionally also, resulting in the difference between core and cladding propagation constants of a different set of given wavelengths matching the coupling condition $2\pi/\lambda$.

The coupling wavelengths were seen to decrease with increasing temperature and thus decreasing refractive indices in the 700 μm LPGs, but were seen to increase with increasing temperature and thus decreasing refractive indices in the 450 μm LPGs. As the refractive indices of the core and cladding are ideally the same for all of the fibres the effect of the temperature should also be constant in all the fibres and will have the same shift to shorter wavelengths for both 450 μm and 700 μm LPGs. The expansion coefficient should also ideally be constant in all the fibres and the LPGs should therefore expand by the same degree. However, a given expansion length per °C will increase the period of the 450 μm LPG by a much larger fraction than the 700 μm LPG, causing a much greater shift to longer wavelengths in the former case.

The shift to shorter wavelengths effected by the refractive index change will counteract this positive shift due to the period increase. The negative shift due to the refractive index decrease is great enough to overcome the smaller positive shift in the 700 μm LPGs, but not the larger positive shift in the 450 μm LPGs. This introduces the possibility of the existence of an intermediary period at which the 2 opposite effects would cancel each other and the LPG would be insensitive to temperature changes at one or more of the coupling wavelengths. The results show a much greater negative coupling wavelength shift in the 700 μm LPGs than the positive shift in the 450 μm LPGs. This suggests that the period required for the 2 shifts to match will be closer to the 450 μm value than the 700 μm value. The ambient index experiment

shows the sensitivity to increase with mode order and the rate of change of each mode order to increase with increasing ambient refractive index (for values of ambient refractive index less than that of the cladding). The temperature profiles of all the LPGs show a linear change in coupling wavelength within the temperature range utilised, and there is no correlation between mode order and sensitivity in either of the sets of LPGs. In some cases the lower order modes showed greater sensitivity and in others the middle or higher order modes showed greater sensitivity.

Comparison of the temperature profiles of the A400, A403, A407, A410, A416 andC1 LPGs (Appendix 5) show that they too have all a positive profile. As they are of different optical and physical specifications to the Singapore LPGs this suggests that the period length has the greater effect on the sense of the temperature profile than the properties of the fibre, unlike the assumptions made in a previous report [363]. It may be possible therefore to select a coupling wavelength and design a period at which the temperature effect on the period and the refractive indices are matched. This would allow the monitoring of ambient index changes and remove the problems of spurious results due to temperature effects. It may also be possible to monitor any temperature changes by focussing on a different coupling wavelength in the same grating if the ambient index profile has previously been determined for that wavelength.

6.4.3 Conclusions

The direction of the temperature gradient of an LPG has been shown to depend on the period of the grating, for fibres with identical optical and physical properties. If the

period can be designed to be of a length where the fractional increase in length counteracts the effects on the refractive index changes the LPG may become immune to limited changes in temperature. It may be possible therefore to use a single LPG of optimum period to allow temperature immunity and reasonable sensitivity to ambient index changes at selected wavelengths, or to simultaneously sense changes in both ambient index and temperature by observation of different selected wavelengths.

6.5 Experimental Investigations into the Method of Coating and the Types of Chemicals to be Used

6.5.1 Coating Methods Investigated

Various chemicals and methods of coating the fibre cladding were investigated as the research progressed.

6.5.1.1 Langmuir-Blodgett (LB) Coating

Langmuir-Blodgett (LB) coating [252,253,365-367] was the first method to be attempted. This method would have allowed monitoring of the number of mono-layers and accurate repeatability of the coating thickness in order to determine an optimum thickness for the greatest reaction to the gas. Unfortunately, the dimensions

of the trough into which the grating was to be immersed as part of the coating procedure meant that the fibre had to be severely deformed in order to fit. Also to ensure consistency of the coating along the length of the grating the grating had to be as straight as possible as it entered the trough. Initial attempts with ordinary single mode fibres resulted in a number of breakages due to this deformation as the fibre was being mounted in the LB equipment. For fibres which were successfully mounted it was discovered that the surface tension of the fluid in the trough was such that the fibre did not always manage to attain full immersion on every cycle. This would make any accurate determination of the number of layers impossible, and as the fibres were easily broken whilst mounting them in the equipment, this method of coating was abandoned.

6.5.1.2   Poly-Electrolyte-Self-Assembley (PESA) Coating

The next method to be investigated was poly-electrolyte-self-assembley (PESA) [341-347]. As in the LB method this would allow accurate monitoring of the thickness and repeatability, but this again involve deformation of the fibre to allow the grating to be straight when immersed in the coating solution, a problem which again could not be overcome with the equipment available.

For the first time tests were performed on the viability of applying PESA methods in situ to allow the LPG to be coated in the same environment as would be used for the gas detection experiment itself. These proved successful and are covered in Chapter 5 of this thesis.

6.5.2 Gas Sensitive Coating Chemicals Investigated

It is well known that the optical properties of CuPc compounds are affected by absorption of NO_2 [368-370], the optical properties of Chromo 1 are affected by absorption of ammonia [335] and that the optical properties of calixarene are affected by absorption of hexane, toluene and benzene [354,371].

As CuPc and Chromo 1 are suitable for use in PESA coating methods, and immersion of a body in a solution of calixarene in chloroform will leave a coating of calixarene on the body as the chloroform evaporates, these chemicals were used in the following investigations.

6.5.3 Background Experiment 1: To Determine the Absorption Spectrum of $CuPc^-(SO_3^-Na^+)_4$

6.5.3.1   Experimental Procedure

The spectrum analyser used in this experiment was the Ocean Optics S 2000 Spectrometer which has a range of $200 - 1100$ nm and the light source used was the integral tungsten halogen $360 - 2000$ nm broadband source. This experiment was carried out as part of a totally separate investigation into the properties of CuPc compounds, but the results are appropriate to this thesis.

A special cell was designed and produced in house which allowed accurate positioning of the apparatus involved in the experiment, and prevented ambient light from entering the system, producing a good level of repeatability of the procedures.

A glass slide was scribed into 14 mm square sections to enable accurate insertion into the mounting position in the cavity. One side of the slide was coated with aluminium to a thickness of 100 nm using PVD, to form a highly reflective surface on the glass. 20 bi-layers of $CuPc^-(SO_3^-Na^+)_4$/PAA were then deposited on the aluminium surface using the PESA method as described in Chapter 5 before the slide was finally cut into the previously scribed dimensions. One of the 14 mm square sections of the slide was placed in the cell as shown in Figure 6.24.
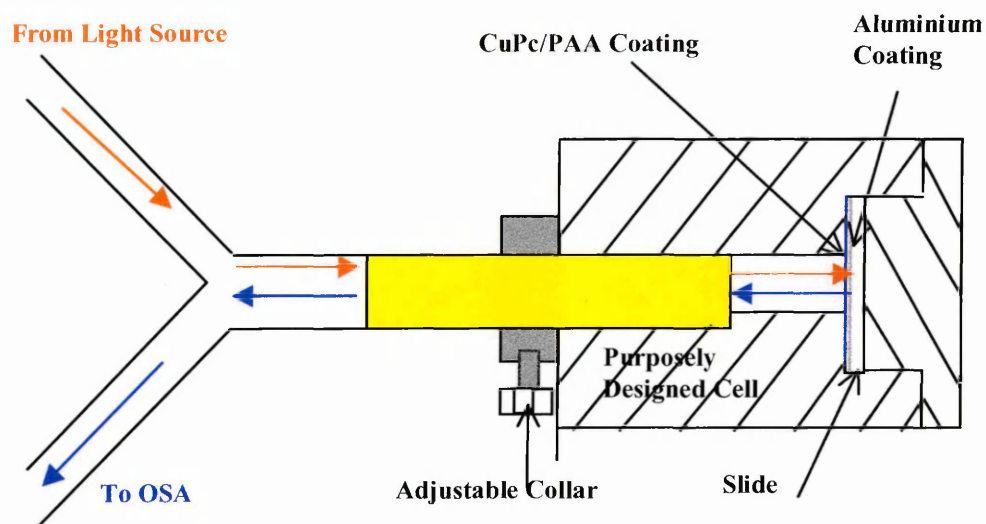
Figure 6.24: **Experimental set up for absorption of light by $CuPc^-(SO_3^-Na^+)_4$ Coating**

This set up allowed the incident radiation to pass through the $CuPc^-(SO_3^-Na^+)_4$ layer twice giving double the absorption, allowed accurate re-positioning of the apparatus as other slides were tested, and removed the inherent effects of absorption, scattering, surface reflections etc. evident if the radiation was made to travel through the glass.

The surface of the coated slide was illuminated with the integral broadband source of the Ocean Optics S 2000 spectrometer and the reflection spectrum recorded using the corresponding software. Attempts to investigate absorbance as a function of coating thickness were aborted when inspection of the slides showed inconsistencies in the aluminium coating due to the application of the $CuPc^-(SO_3^-Na^+)_4/PAA$ bi-layers, which would itself affect the reflected fraction of the incident radiation.

6.5.3.2   Results & Discussion
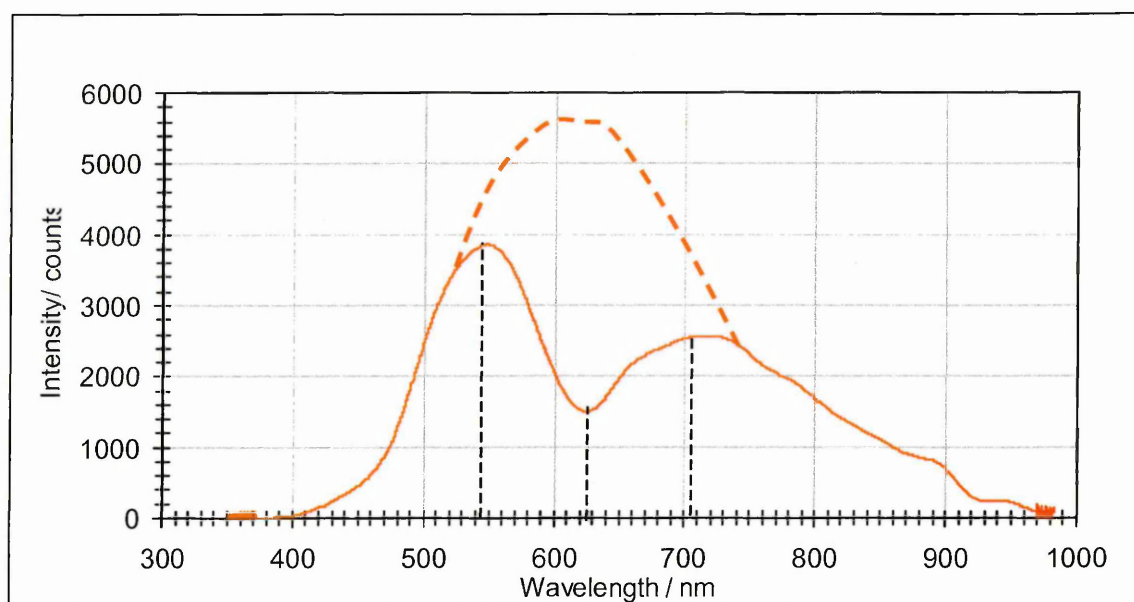
Figure 6.25:   Absorption spectrum of $CuPc^-(SO_3^-Na^+)_4$

Figure 6.25 shows spectrum of the broadband light source and the $CuPc^-(SO_3^-Na^+)_4$ absorbance spectrum centring at 625 nm with a spread of ± 80 nm.

6.5.4 Background Experiment 2: To Determine the Sensitivity of CuPc⁻(SO₃⁻ Na⁺)₄ to NO₂

These experiments were performed on planar polarisation interferometer (PPI) wave guides [372,373] firstly to investigate the effect of the number of layers of $CuPc^-(SO_3^-Na^+)_4$ on the transmission spectrum and then to observe the effect on the transmission spectrum of exposure of the coated planar guide to NO_2. The guided radiation will undergo TIR at each reflection from the core/cladding boundary. The evanescent field associated with the guided mode [283-285] will penetrate a short distance into the medium surrounding the core, which in the position of the window will be coated with $CuPc^-(SO_3^-Na^+)_4$. As $CuPc^-(SO_3^-Na^+)_4$ absorbs radiation at a wavelength of 625nm some of the radiation on the evanescent field will be absorbed, reducing the intensity of the transmitted signal. The optical properties of $CuPc^-(SO_3^-Na^+)_4$ are sensitive to NO_2, changing its refractive index, reducing the absorption and therefore increasing the intensity of the transmitted radiation.

6.5.4.1   Experimental Procedure

Planar polarised interferometer (PPI) wave guides were used in these experiments and were of the following specifications as shown in Figure 6.26.
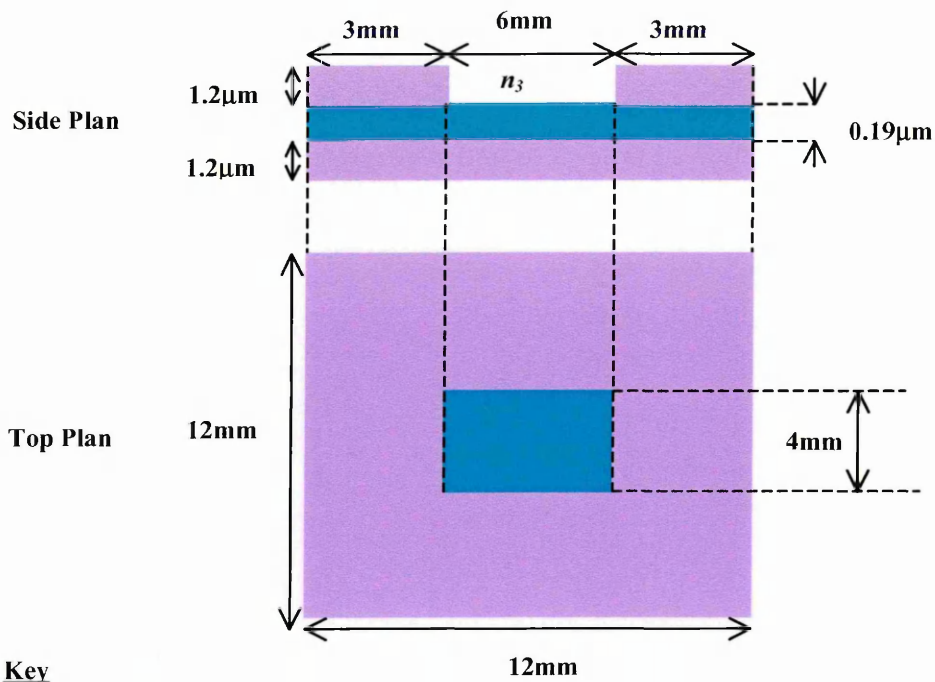
Figure 6.26: Planar polarised interferometer (PPI) wave guide

To confirm that the wave guide was operating in single mode at the operating wavelength the following formula was used (see Appendix 11 for derivation):

$$m = \frac{n_1}{\lambda}\left(2t\cos\theta + 2\phi\right) \tag{6.4}$$

where m = no of modes

   λ = wavelength of radiation: 625nm

   t = thickness of core: 0.19μm

   θ = angle of incidence at core / cladding boundary

   ϕ = phase change on reflection at core / cladding boundary given by [311-314]

175

$$\phi = \frac{\lambda}{360} \left(2 \tan^{-1} \left[\frac{\sqrt{\sin^2 \theta - \left(\frac{n_1}{n_2} \right)^2}}{\left(\frac{n_1}{n_2} \right)^2 \cos \theta} \right] \right)$$

where n_1 = core refractive index: 2

n_2 = cladding refractive index: 1.46

To make θ the subject of the formula would make the final equation too complicated to compute, so incremental values of θ starting at the critical angle were entered into a spreadsheet until the calculated value of m was seen to be 1, 2 , 3 etc. The resulting graphs can be seen in Figures 6.27 and 6.28.
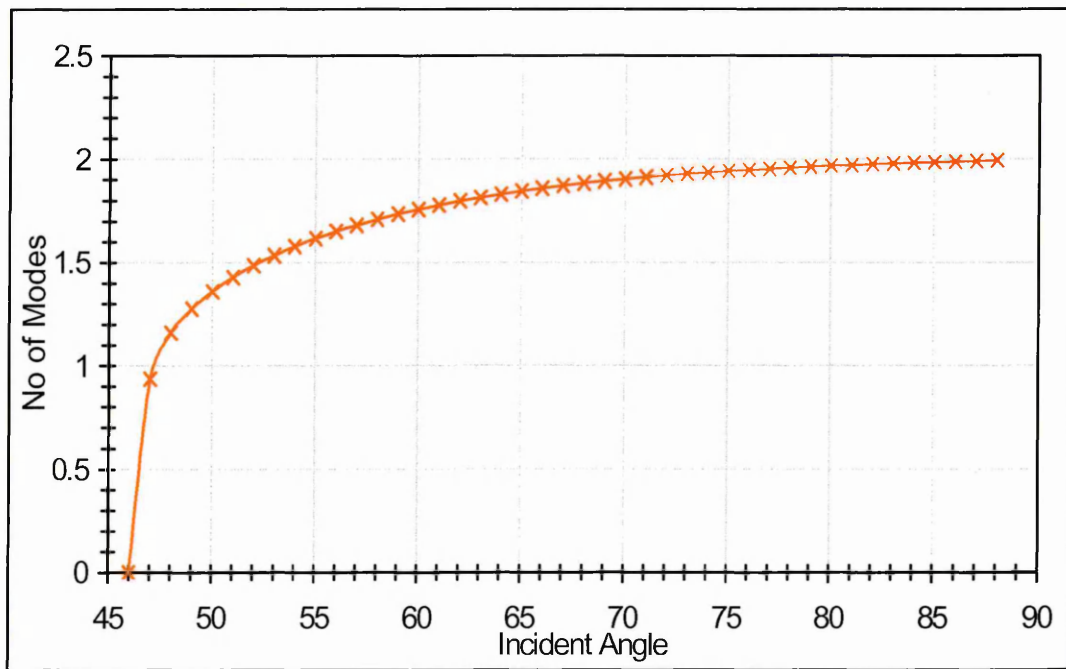
Figure 6.27:   Graph to show mode characteristics in wave guide
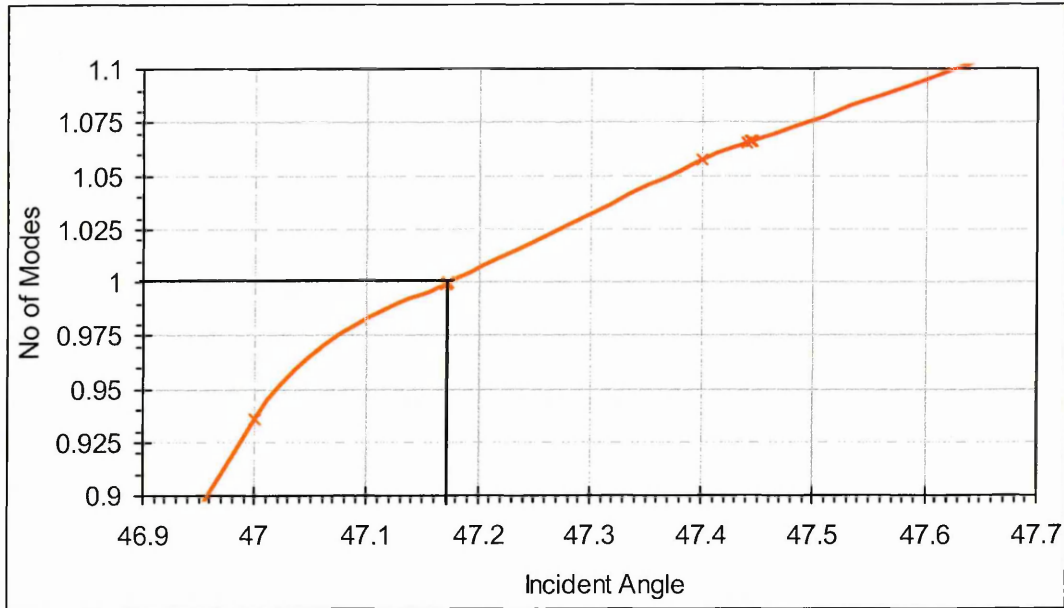
Figure 6.28: Graph magnified to show incident angle required to excite the single mode in wave guide

The critical angle for the guiding layer of the chip is 46.89° and the specifications of this waveguide means that it should be operating in single mode at 630nm, with a mode angle of 47.17°. However it can be seen that, using Snell's Law, the range over which the radiation can travel through the waveguide is limited by the refractive index difference at the entrance to the waveguide as shown in Figure 6.29.
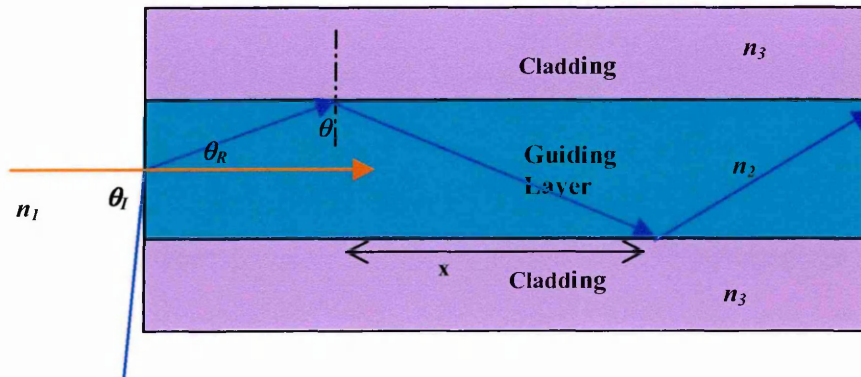
Figure 6.29: Range of angles possible for radiation to be incident on the guiding layer/cladding boundary

$$\theta = 90 - \sin^{-1}\left(\frac{n_1 \sin \theta_I}{n_2}\right)$$

$$\theta_{max} = 90 - \sin^{-1}\left(\frac{1 \sin 0}{2}\right) = 90°$$

$$\theta_{min} = 90 - \sin^{-1}\left(\frac{1 \sin 90}{2}\right) = 60°$$

Thus the range of angles over which any ray entering the guiding layer can be incident on the core cladding boundary is 60° to 90°. It is therefore not possible, due to the high refractive index of the core for the mode path to be excited by any angle of incidence on the entrance plane of the waveguide. However, as the experiments progress it can be seen that light is travelling through the waveguide, which can only be due to the light scattering due to imperfections at that boundary. Microscopic inspection of the edges of the PPI show the edges to be very uneven. The only way in which the PPIs could be modified to allow the modes to be excited properly would be to shamfer the entry and exit faces to a predetermined angle, which was not possible in house. Initial attempts to accurately investigate the effect of the number of layers on the transmission spectrum of a PPI wave guide were aborted when the transmission spectra of 12 uncoated PPIs were seen to vary randomly, the intensity of the lowest transmission being around 20% of the highest transmission. Also it was discovered that the positioning of the PPI in the optical set up was very critical and not repeatable to an accuracy required to enable fine intensity comparisons before and after the PPI was removed from the set up in order to be coated.

The experimental set up is shown in Figure 6.30
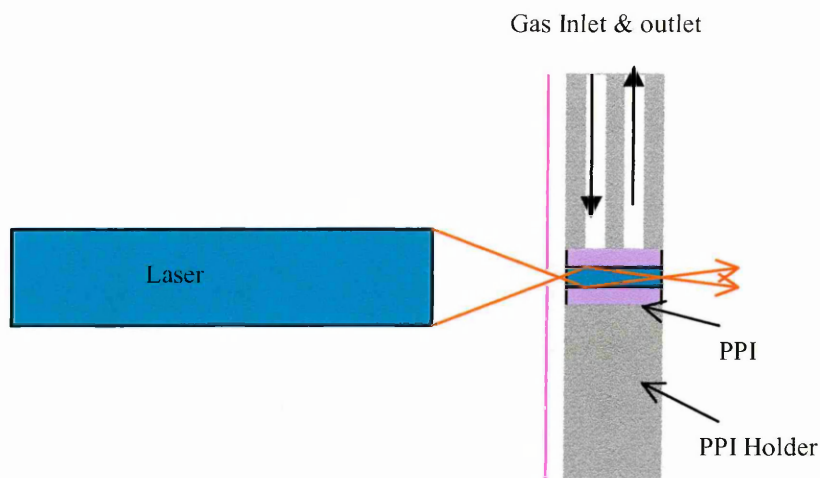
Figure 6.30: **Experimental set up to observe transmission intensities and absorption of $CuPc^-(SO_3^-Na^+)_4$ coatings of different thickness on PPIs when exposed to gas**

The transmission intensities of the 12 uncoated PPIs were observed and recorded. They were then separated into four sets of three and each set coated with 1,2,3 and 4 layers of $CuPc^-(SO_3^-Na^+)_4$/PAA using the PESA method in the clean room facility. After coating the transmission intensities of all the PPIs were seen to reduce to between 1% and 6% of the uncoated values. However, due to the previously mentioned limitations no correlation between coating thickness and intensity reduction could be ascertained. A PPI coated with 1 bi-layer was placed in the set up as shown in Figure 6.30, the PPI holder being a purposely designed gas cell which allowed the window of the PPI to be in contact with a through flow of gas. The intensity of the transmitted signal was recorded and NO_2 was then made to flow over the surface of the coated window at 400ppm concentration, the change in intensity being noted over time. After a predetermined time the NO_2 supply was terminated and the cell flushed with N_2 until the intensity change seemed to level out. This procedure was carried out on all of the PPIs and the change in intensity values observed and recorded.

6.5.4.2 Results and Discussion

Graphs of transmission intensity of PPI with increasing thickness of $CuPc^-(SO_3^-Na^+)_4$/PAA coatings after exposure to NO_2 and flushing with N_2 are shown in Figures 6.31 and 6.32.
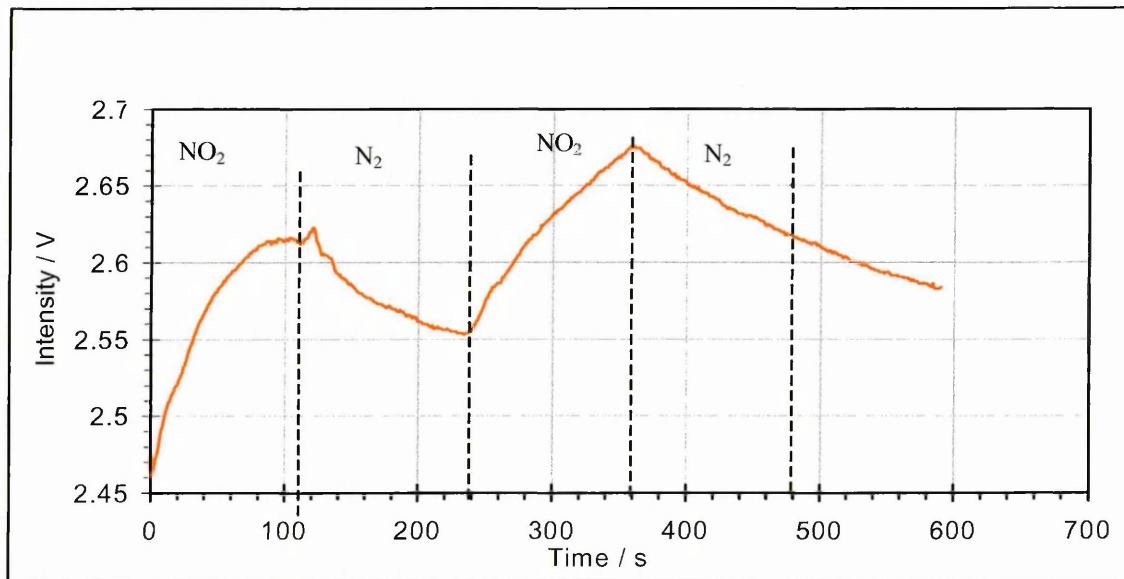
Figure 6.31: Typical transmission intensity with time of PPI with 1 bi-layer of $CuPc^-(SO_3^-Na^+)_4$/PAA during exposure to NO_2 and flushing with N_2
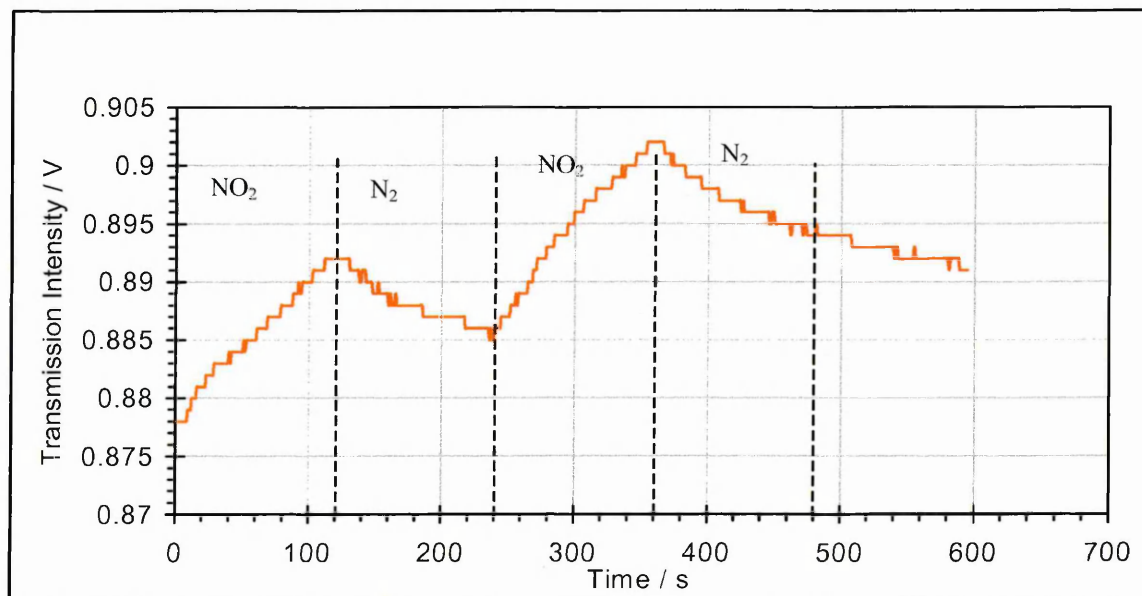
Figure 6.32: Typical transmission intensity with time of PPI with 2 bi-layers of $CuPc^-(SO_3^-Na^+)_4$/PAA during exposure to NO_2 and flushing with N_2

It can be seen from Figures 6.31 and 6.32 that transmission intensity of the PPI before gas exposure (t=0) seems to have some dependency on the number of bi-layers of $CuPc^-(SO_3^-Na^+)_4$/PAA in this case. The change in transmitted intensity can be seen to decrease as the number of bi-layers increases, and the radiation was totally absorbed when more than 2 bi-layers were applied.

Due to the dimensions of the PPIs as shown in Figure 6.26 and the mode angle at which the radiation must travel through the wave guide the number of reflections m, at the core/cladding boundaries can be determined by dividing the window length by the distance between successive reflections. For a ray propagating at the previuosly determined angle of 47.17°.

$$m = \frac{6 \times 10^{-3}}{2x0.19 \times 10^{-6} \times \tan 47.17} \approx 14637 \text{ reflections}$$

Thus the severity of the incident angle means that the mode undergoes approximately 14637 reflections from the absorptive surface which accounts for the severe reduction in transmitted intensity with increase in layer thickness.

Figures 6.31 and 6.32 show a gradual increase in intensity with the time of exposure to NO_2 for 1 and 2 bi-layers respectively confirming the sensitivity of the $CuPc^-(SO_3^- Na^+)_4$ to the gas. At the end of each procedure the apparatus was left untouched for 24 hours to allow the coating to recover as much as possible. The intensity of the transmitted signal was seen to level out at about 50% of the peak value in both waveguides, thus recovery is not total, suggesting that the chemical change of the coating is partially permanent.

As the radiation is still guided the increase in the transmitted intensity must be due to the reduction in absorbance of the evanescent field of the guided mode. The gas, which is absorbed due to electron transfer, changes the absorbtivity of the coating to radiation at 630nm. This may not affect the absorption at 1550nm, but it may alter the physical structure of the $CuPc^-(SO_3^-Na^+)_4$ coating which, it is assumed for the purposes of this investigation, will alter the refractive index of the coating to some degree. This refractive index change due to gas absorption will affect radiation at 1550nm also and it is therefore feasible to use $CuPc^-(SO_3^-Na^+)_4$ to coat the cladding of an LPG. If the change in refractive index due to the NO_2 is sufficient it may be possible to detect the subsequent change in the coupling wavelength. Experiments on the LPGs will therefore be carried out, coating the cladding with up to 4 layers of $CuPc^-(SO_3^-Na^+)_4$, exposing to NO_2 and observing the resulting shift in coupling wavelength.

6.6 Investigations into Utilising a Suitably Coated Long Period Grating as a Gas Sensor Using an In Situ PESA Method of Coating

LPG C1 was used in this investigation as it contained the shortest period of the LPGs available. This LPG should therefore be operating at higher order coupling modes than the others, and should be the most sensitive to changes in ambient index, as

shown if the changes in coupling wavelength are compared in the ambient index profiles of all LPGs (Appendix 9). The transmission spectra of LPG C1 were observed and recorded using a HP 86142A Optical Spectrum Analyser, the light source used being the integral 1330nm and 1550nm EELED sources of the OSA. Ambient refractive index and ambient temperature profiles of LPG C1 under investigation were produced before the experimental procedure began in order to allow interpretation of any coupling wavelength shifts observed during the experiment and can be seen in Appendices 9 and 10.

6.6.1 Experiment into Applying $CuPc^-(SO_3^-Na^+)_4$ by In-Situ PESA Coating Method and NO_2 as the Gas to be Detected

6.6.1.1 Experimental Procedure

The fibre was connected to the light source and optical input of the OSA using bare fibre connectors and the optical transmission spectrum observed through all stages of the procedure. The grating section of the fibre was clamped under slight tension in a second purpose built cavity, as shown in Figure 6.33, which was air-tight except at designed entry and exit points to allow the injection and extraction of the coating chemicals and the flow of the gas.
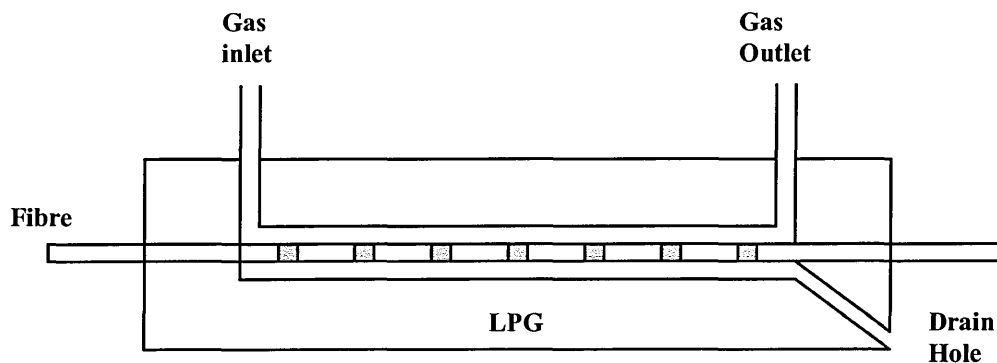
Figure 6.33: Purpose-built cavity in which coating and exposure of the LPG could be performed

The cladding of the LPG was coated in situ by the PESA method as explained in chapter 5 with one bi-layer of PAA/ CuPc⁻(SO₃⁻Na⁺)₄. The water was removed from the cavity, the cavity was flushed with N_2 to dry the fibre between each coating layer, and the transmission spectrum recorded. A steady flow of 400 ppm of NO_2 was introduced into the cavity for two minutes, and then flushed using N_2 to ensure that all NO_2 was removed and to observe any recovery made in the coating. The apparatus was then left untouched for four days to observe any recovery which may occur over time. The shift in coupling wavelength was observed and noted at each stage. The fibre was disconnected from the OSA and removed from the gas cell. The CuPc⁻(SO₃⁻Na⁺)₄ coating was removed by immersion of the grating section in sulfo-chromic acid, and the fibre reconnected to the OSA ensuring that the spectrum had returned to its original pre-coated position This procedure was then repeated using 2, 3, and 4 bi-layers of PAA/ CuPc⁻(SO₃⁻Na⁺)₄.

6.6.1.2 Results and Discussion

From experimentally measured SPR curve fitting the refractive index of PAA/ CuPc⁻ (SO₃⁻Na⁺)₄ bi-layer coatings was found to be 1.3 ± 0.05. This value is very different

to previous reported findings of around 1.8 for phthalocyanine compounds in general [374]. The coupling wavelength shifts observed as the coatings were applied should help to confirm or deny this result.

The shift in coupling wavelength as each bi-layer was applied to the required thickness, exposed to NO_2 and then flushed with N_2 are shown in Figures 6.34 to 6.41.
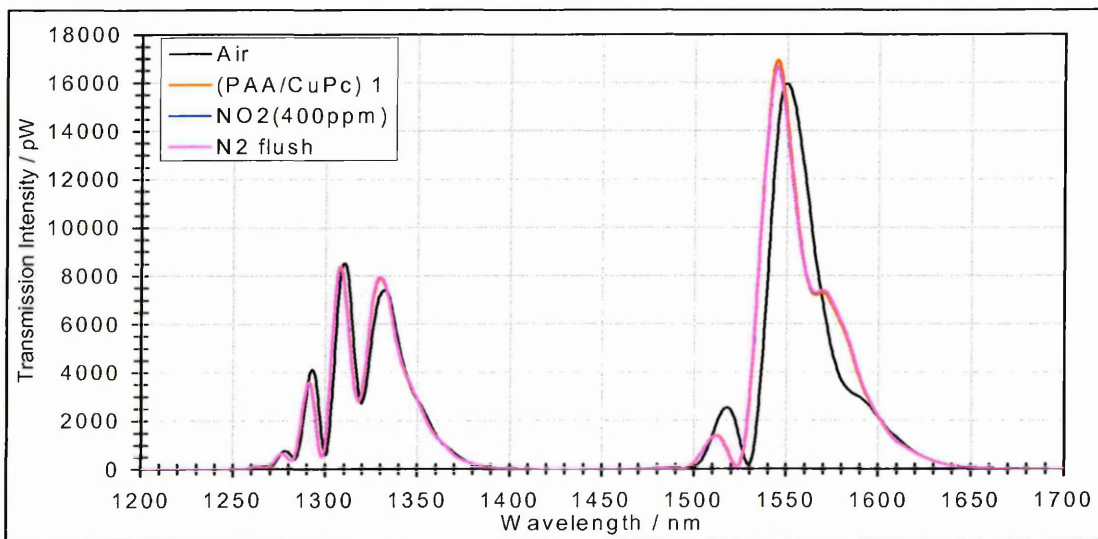
Figure 6.34: **Spectrum of C1 as 1 coating of PAA/CuPc$^-$(SO$_3^-$Na$^+$)$_4$ applied and exposure to NO_2**
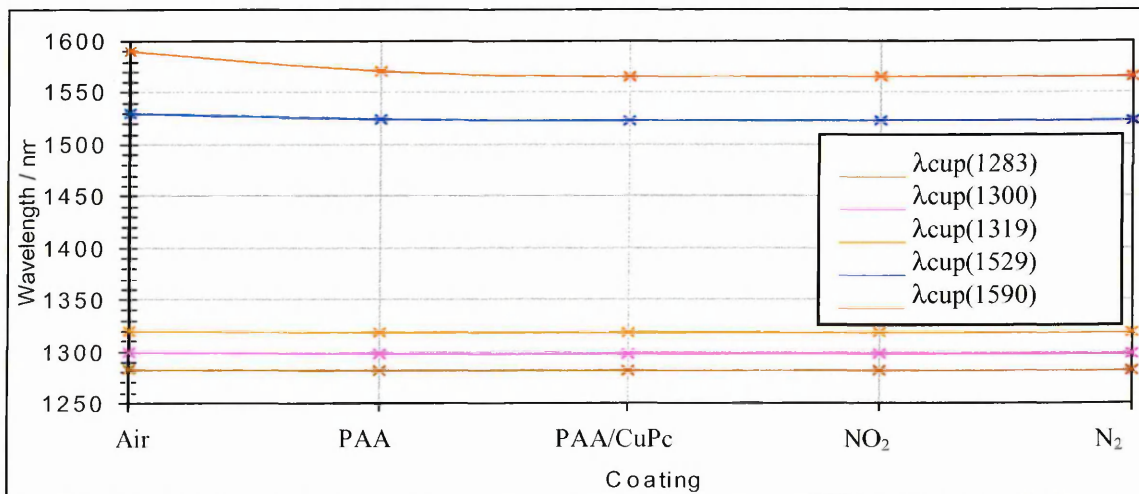
Figure 6.35: **Coupling wavelength shift of LPG C1 as 1 coating of PAA/CuPc$^-$ (SO$_3^-$Na$^+$)$_4$ applied and exposure to NO_2**
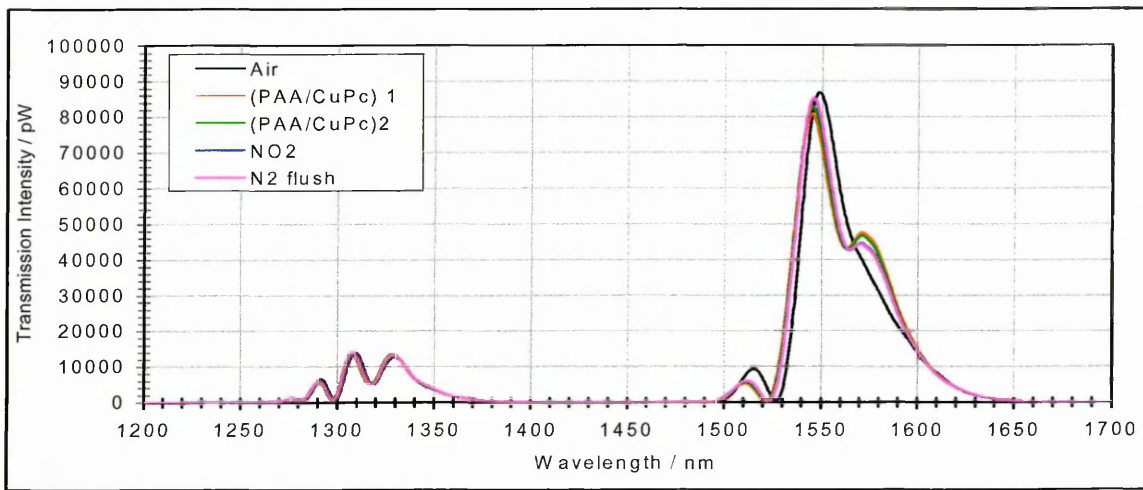
Figure 6.36: Spectrum of C1 as 2 coatings of PAA/CuPc⁻(SO₃⁻Na⁺)₄ applied and exposure to NO₂
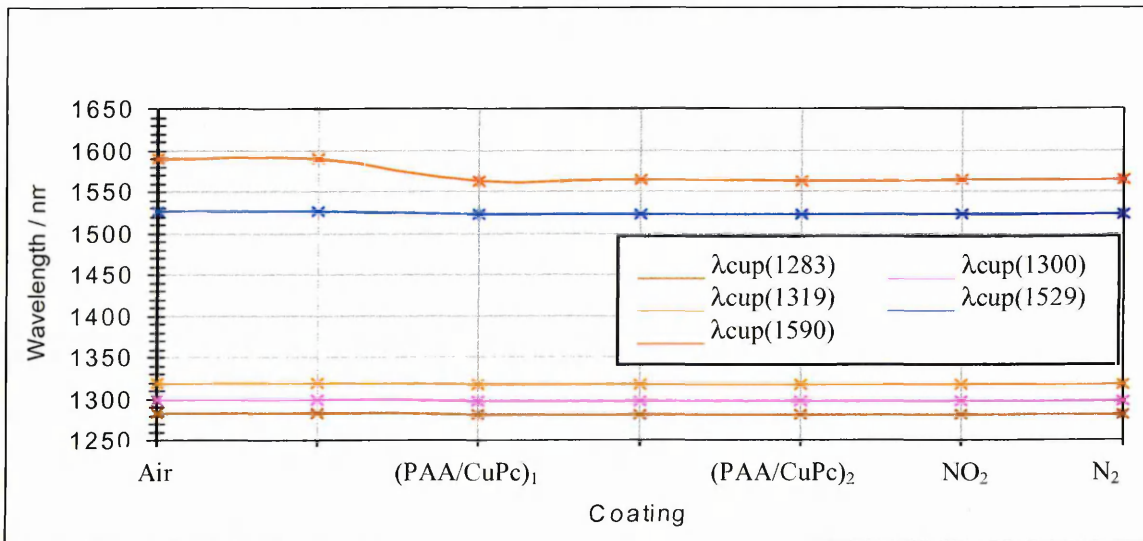
Figure 6.37: Coupling wavelength shift of LPG C1 as 2 coatings of PAA/CuPc⁻ (SO₃⁻Na⁺)₄ applied and exposure to NO₂
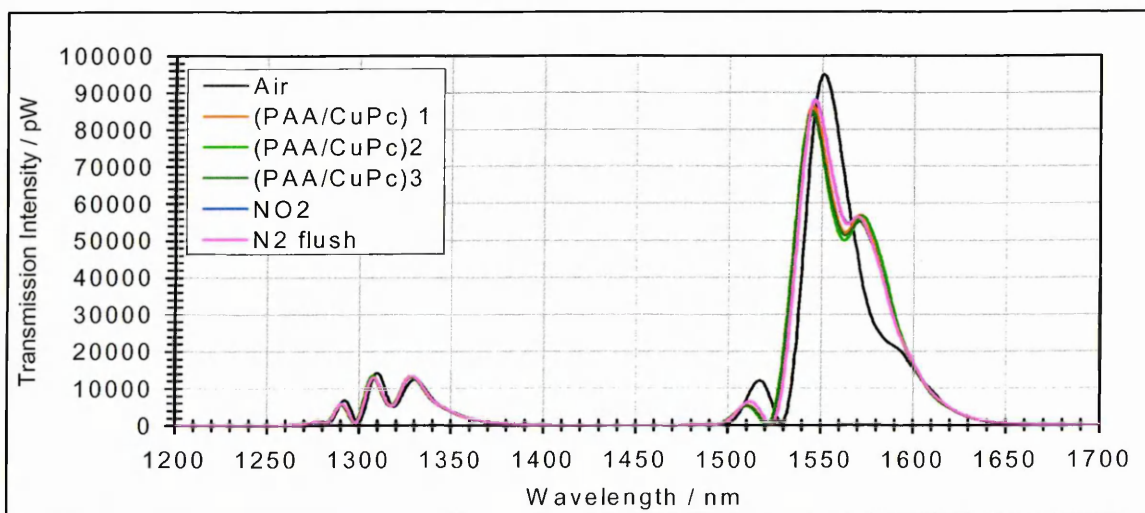
Figure 6.38: Spectrum of C1 as 3 coatings of PAA/CuPc⁻(SO₃⁻Na⁺)₄ applied and exposure to NO₂
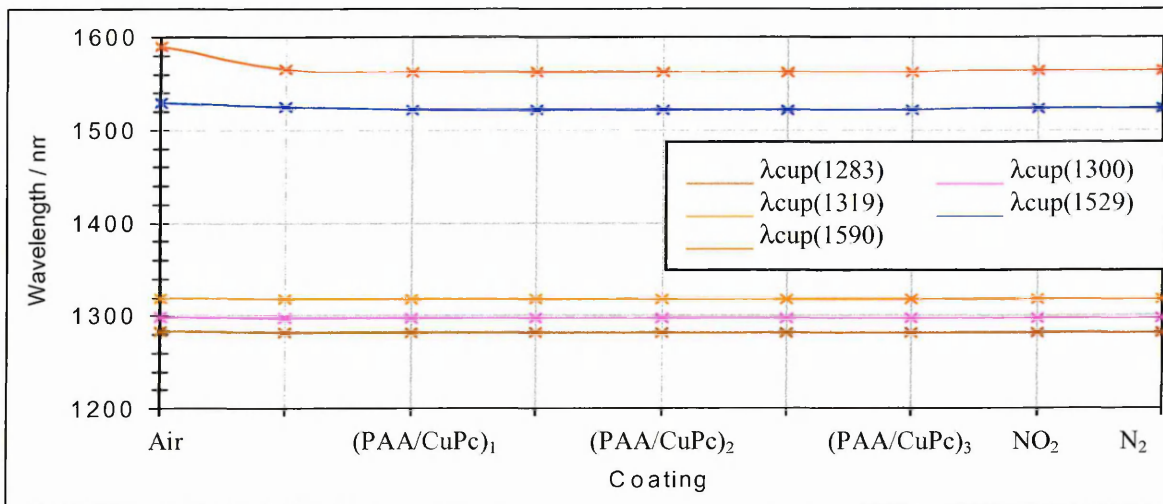
Figure 6.39: Coupling wavelength shift of LPG C1 as 3 coatings of PAA/CuPc⁻ $(SO_3^-Na^+)_4$ applied and exposure to NO_2
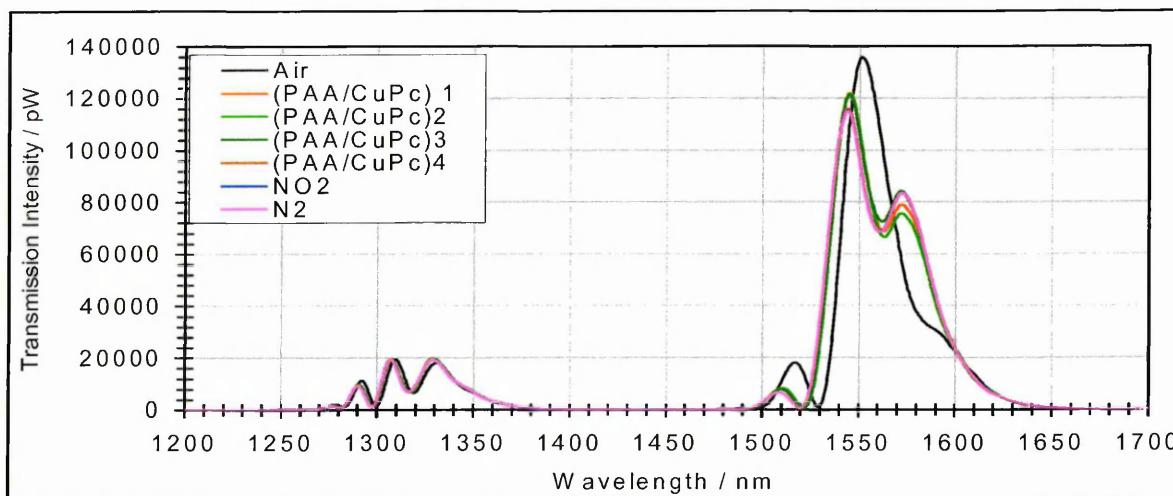
Figure 6.40: Spectrum of C1 as 4 coatings of PAA/CuPc⁻$(SO_3^-Na^+)_4$ applied and exposure to NO_2
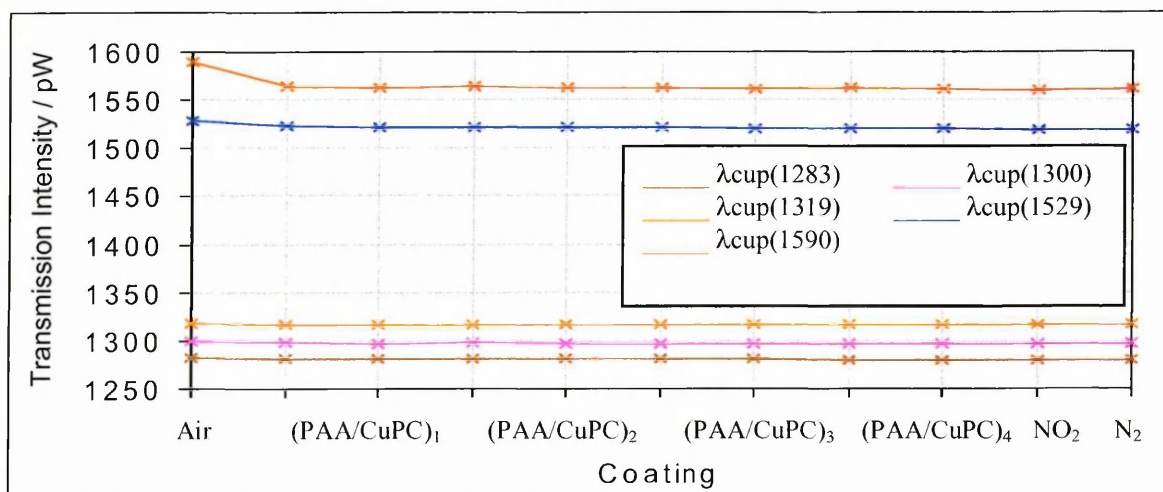
Figure 6.41: Coupling wavelength shift of LPG C1 as 4 coatings of PAA/CuPc⁻ $(SO_3^-Na^+)_4$ Applied and Exposure to NO_2

It can be seen from Figures 6.34 to 6.41 that the coupling wavelengths returned to the value in air at the beginning of each part of the experiment, suggesting that the previous coating had been completely removed at the end of each stage prior to the beginning of the subsequent stage. There are very similar shifts in coupling wavelength in all cases as the first coating of PAA/ $CuPc^-(SO_3^-Na^+)_4$ is applied, the shift being greater as the order of coupling mode increases, as expected. The coupling wavelengths show very little shift as further bi-layers are applied which may be expected as refractive index is independent of thickness. The coupling wavelength shifts due to exposure to NO_2 seem to increase with number of bi-layers and mode order up to a maximum of 3 bi-layers at which point the gas seems to have no effect on the coupling wavelengths. This suggests that as the thickness of the coating increases the gas may not be penetrating deep enough to affect the refractive index of the coating closer to the cladding.

The results suggest that 3 bi-layers of PAA/ $CuPc^-(SO_3^-Na^+)_4$ is the optimum coating thickness for best reaction to the gas exposure. As the most sensitive condition was observed at the highest order visible coupling mode of 1590nm when the LPG was coated with 3 bi-layers of PAA/ $CuPc^-(SO_3^-Na^+)_4$, the following results are focussed on observation of the modal shift at this wavelength and coating thickness.
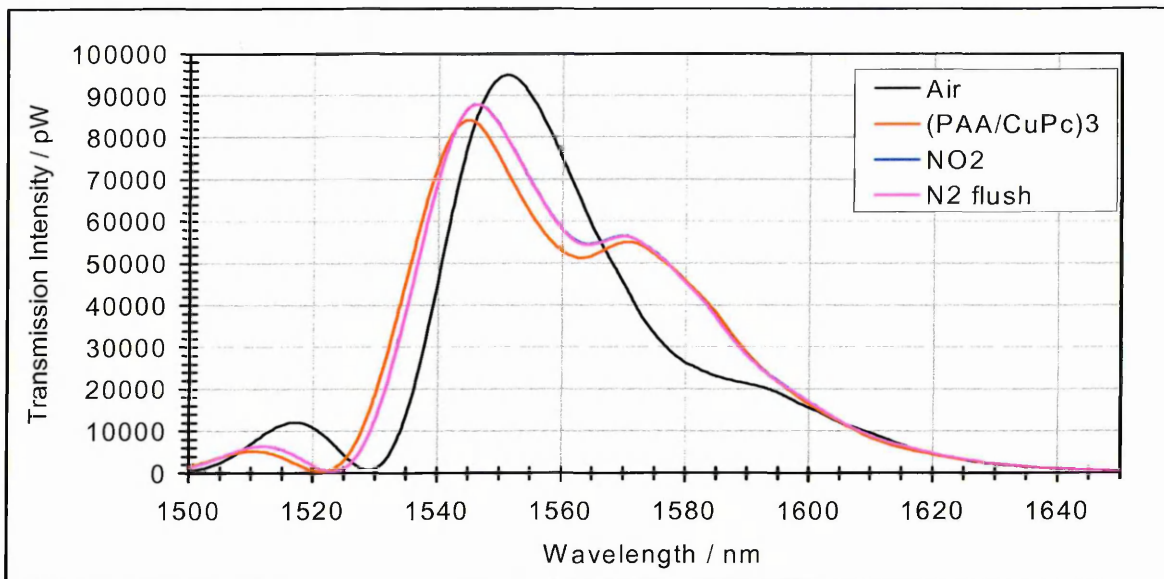
Figure 6.42: Spectrum of C1 around 1590 nm as 3 coatings of PAA/ CuPc⁻ $(SO_3^- Na^+)_4$ applied and exposure to NO_2
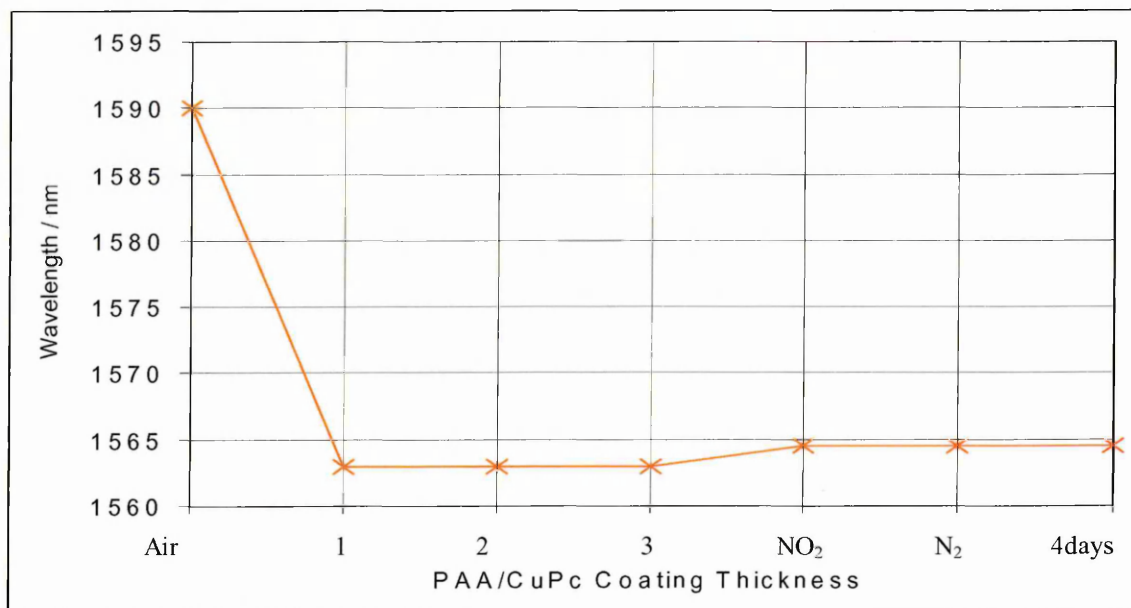
Figure 6.43: Coupling wavelength shift of LPG C1 around 1590 nm as 3 coatings of PAA/ CuPc⁻$(SO_3^-Na^+)_4$ applied and exposure to NO_2

As can be seen in Figures 6.42 and 6.43, when the cavity contained only air the coupling wavelength was 1590 ± 0.5 nm. As the first bi-layer was applied to the cladding in the cavity the coupling wavelength was seen to move by -27 ± 0.5 nm to 1563 ± 0.5 nm, remaining at this value as successive bi-layers were applied. As the

refractive index of the coating is greater than air but less than the cladding the coupling wavelength can be seen to shift to shorter values as expected freom theory. As refractive index is independent of thickness, it can be expected to remain virtually constant as the number of bi-layers increases.

From the previously determined ambient index profile (Appendix 9), a shift from 1590 ± 0.5 nm in air to 1563 ± 0.5 nm when coated shows the refractive index of the coating to be 1.3015 ± 0.005 as shown in Figure 6.44.
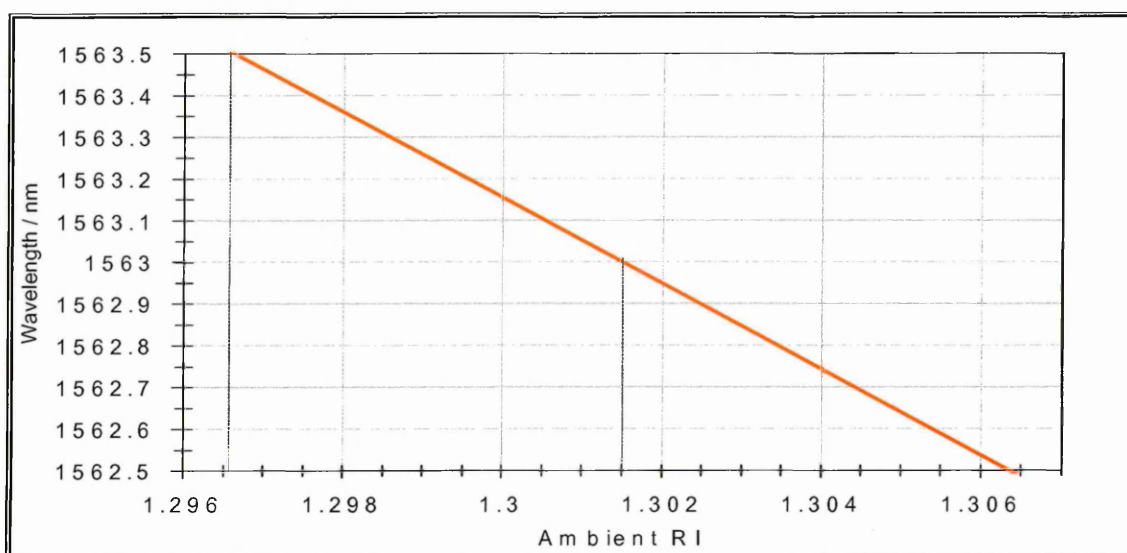
Figure 6.44: **Section of ambient refractive index profile of LPG corresponding to 1563 ± 0.5 nm coupling wavelength of PAA/ $CuPc^-(SO_3^-Na^+)$ coating**

When the cavity was filled with NO_2 the coupling wavelength was seen to shift by $+1.5$ nm to 1564.5 ± 0.5 nm and remain at that value even after flushing with N_2. This positive shift in coupling wavelength suggests that the refractive index of the coating has decreased due to the exposure to NO_2, and that this is a permanent effect with no recovery observed of the $CuPc^-(SO_3^-Na^+)_4$ coating after flushing with N_2 or with time. Information taken from the previously determined ambient refractive

index profile of the grating leads to the conclusion that a shift in coupling wavelength of +1.5 nm from 1563 nm to 1564.5 nm would be caused by a change in coating refractive index of -0.0147 from 1.3015 to 1.2868 as shown in Figure 6.45.
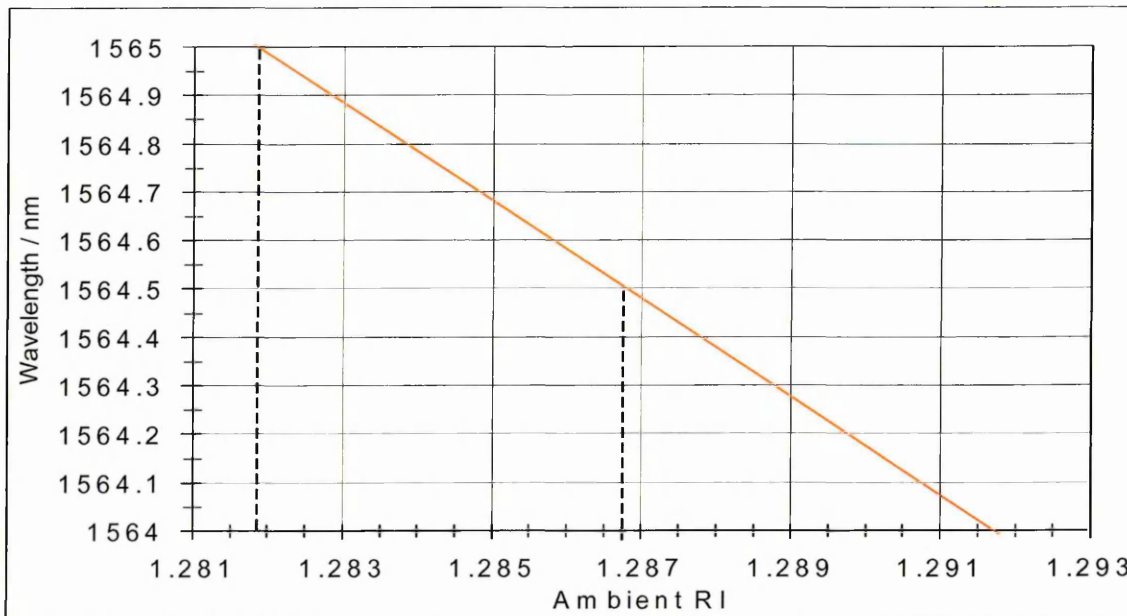
Figure 6.45: Section of ambient refractive index profile of LPG corresponding to 1564.5 ± 0.5 nm coupling wavelength of PAA/ $CuPc^-(SO_3^-Na^+)_4$ coating after exposure to NO_2

It can be seen from the ambient index profile (Appendix 9) that the sensitivity to changes in ambient refractive index of LPGs increases more as the ambient index approaches that of the cladding. The fact that the refractive index of the PAA/ $CuPc^-$ $(SO_3^-Na^+)_4$ coatings of around 1.3 is considerably lower than that of the cladding and is situated on the more linear section of the profile may explain why the coupling wavelength shift is so small. To increase the sensitivity of the LPG either a coating with refractive index approaching that of the cladding, or a chemical with a higher sensitivity to a given gas must be used. If a suitable coating could be found with a refractive index around 1.44 then a change of –0.0147 to 1.4253 would result in a much greater coupling wavelength shift of 12.5 nm as shown in Figure 6.46.
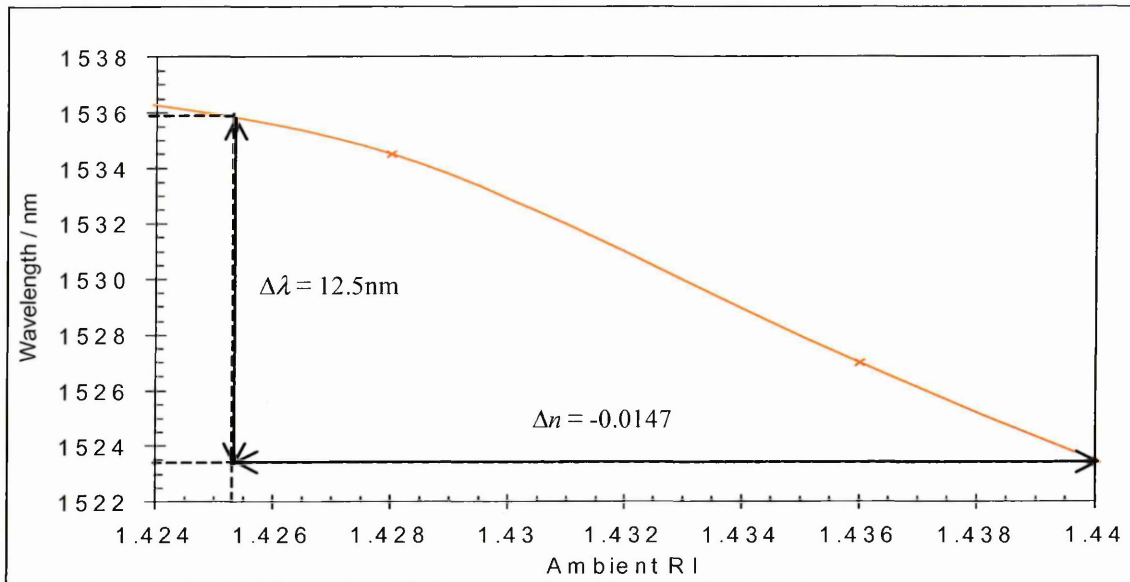
Figure 6.46: **Change in coupling wavelength with ambient refractive index for LPG magnified in 1.44 region**

As stated earlier in this report, all traces of the previous coating layers were removed by immersion of the grating section in sulfo-chromic acid after removing the fibre from the OSA. It was decided to monitor the removal of the final coating of 4 bi-layers by leaving the fibre connected to the OSA and observe the shift as it occurred. However, when the LPG was removed from the cavity whilst the transmission spectrum was still being monitored the spectrum and the coupling wavelengths were seen to shift back to the original positions in air before removal of the coating. This suggested that the observations made during the experiment were not due to the effects originally assumed, though it is quite certain that the sulfo-chromic acid had removed the previous coating between stages. Examination of the cavity showed a small amount of water in the bottom, but it is doubtful if there was enough to be in contact with the LPG. The diameter of the cavity and the inlet and outlet holes must not be big enough to allow the water inside to evaporate even after flushing with N_2

and standing for four days. Previous experiments carried out as part of this research have shown that water vapour condensing on the LPG will cause a shift to shorter wavelengths comparable to the shift due to water emersion. The determined refractive index of the PAA/ CuPc$^-$(SO$_3^-$Na$^+$)$_4$ coatings from the ambient index profile of 1.3015 shows that it cannot be only the effect of the water around the cladding which is being observed as the refractive index of water as determined by the 'Atago' refractometer is 1.3365. The refractive indices of the PAA and CuPc$^-$(SO$_3^-$Na$^+$)$_4$ solutions were investigated using the refractometer and were found to be the same as water, suggesting that remnants of the coating solution was not the ambient medium being observed either. This introduces the possibility that the PAA/ CuPc$^-$(SO$_3^-$Na$^+$)$_4$ bi-layers are retaining the water molecules or that the atmosphere in the small cavity is such that the water droplets in the bottom are cyclically evaporating and condensing on the LPG cladding. When the NO$_2$ is introduced into the cell it is reacting with the water droplets around or within the coating and changing the refractive index of the coating.

The experiment was repeated, coating the LPG with 3 bi-layers of PAA/ CuPc$^-$(SO$_3^-$Na$^+$)$_4$, but this time removing the grating from the gas cell to ensure it was completely dry before replacing it in the dry cell, exposing to NO$_2$ and flushing with N$_2$. The transmission spectrum showed no appreciable change in coupling wavelength at any stage in the proceedings.

The fact that the coating with a refractive index previously determined as 1.3 by SPR curve fitting, does not cause a coupling wavelength shift may be explained by either or all of the following:

- the thickness of the 3 bi-layers alone is not enough to be 'seen' by the incident radiation as a refractive index boundary

- the coating procedure is not as effective in this situation as it was in the SPR set up

- the refractive index of the coatings determined by SPR is in error and the refractive index is greater than that of the cladding agreeing closer to recorded previous work of around 1.8 [374], which suggests that the SPR determined index may also be affected by the water surrounding or absorbed by the coating on the slide.

As the results from this part of the investigation show that the $CuPc^-(SO_3^-Na^+)_4$ coating will not be suitable to commercial use due to its lack of sensitivity, it was not deemed worthwhile to perform further experiments to try to determine the optimum thickness of $CuPc^-(SO_3^-Na^+)_4$ at which the refractive index of the coating will cause a shift in the coupling wavelength whilst not being too thick for the gas to penetrate far enough to cause significant change in refractive index.

6.6.2 Experiment Applying Chromo 1 by In Situ PESA Coating Method and Ammonia as the Gas to be Detected

6.6.2.1 Experimental Procedure

The fibre was connected to the light source output and optical input of the OSA using bare fibre connectors and the optical transmission spectrum observed through all

stages of the procedure. The grating section of the fibre was clamped under slight tension in a second purpose built cavity, as in the previous experiment.

The cladding of the LPG was coated in situ by the PESA method as explained in chapter 5 with 20 bi-layer of PAA/Chromo1, care being taken that the coating was completely dry, and the transmission spectrum recorded as each dry bi layer was produced. The grating was removed from the gas cell after 20 layers to allow total drying of the coating. It was then replaced in the cell, exposed to a steady flow of ammonia for twenty minutes, and flushed using N_2 to ensure that all ammonia was removed and to observe any recovery made in the coating.

6.6.2.2 Results and Discussion
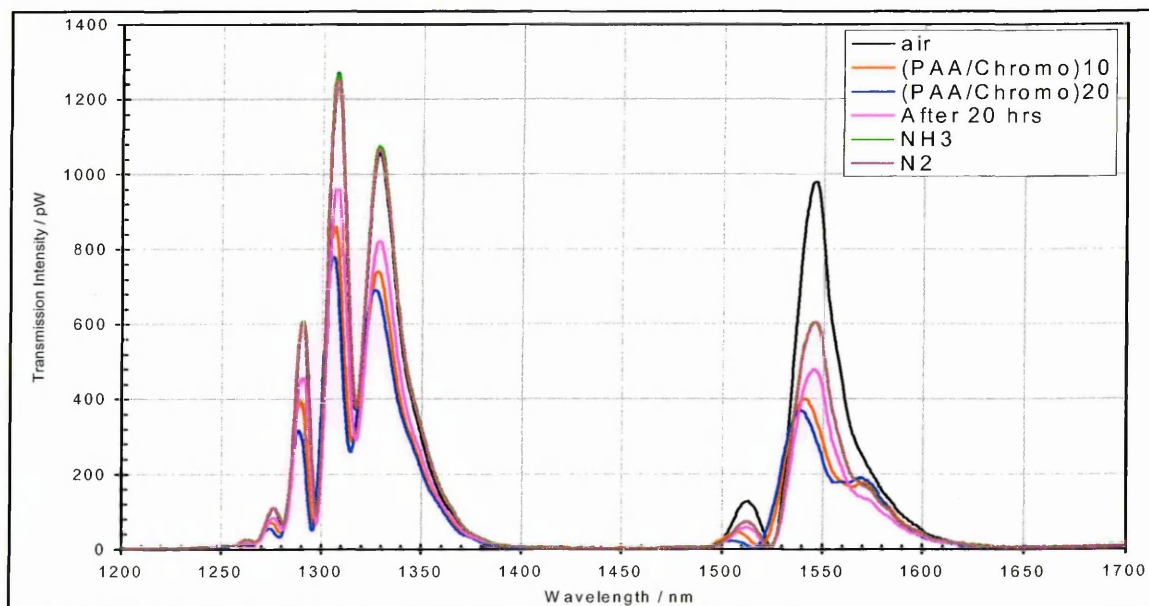
Figure 6.47: **Refractive index profile of LPG C1 as coatings of (PAA/Chromo1)$_n$ are applied and exposure to ammonia**
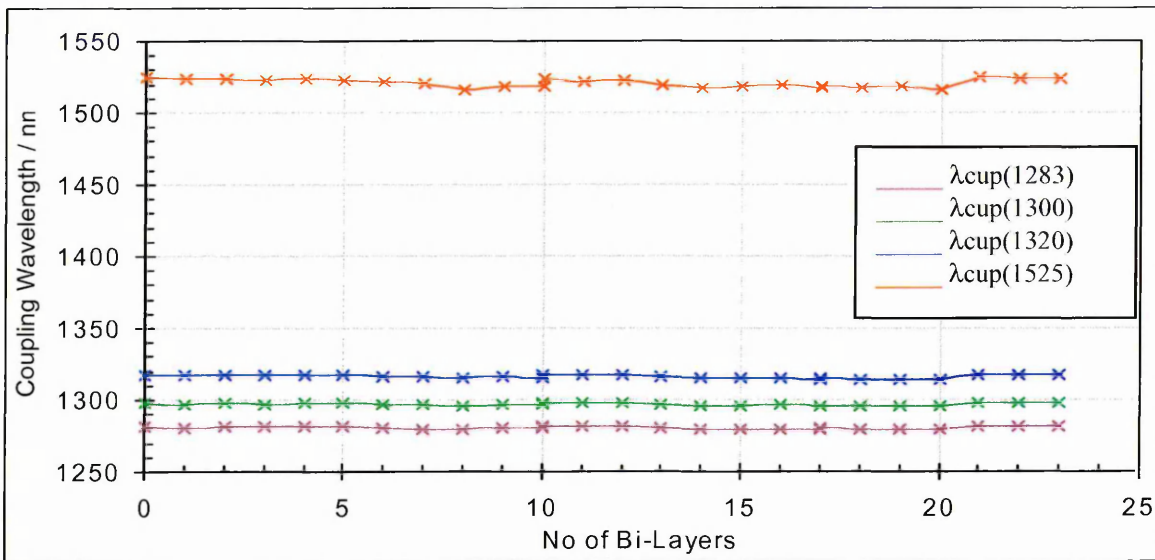
Figure 6.48: **Coupling wavelength shift of LPG C1 coatings of(PAA/Chromo1)$_n$ applied and exposure to ammonia**

Positions 21, 22, 23 are after removal from cavity and allowed to dry in air, after 20 minutes exposure to ammonia and after flushing with N_2 respectively.

Figures 6.47 and 6.48 show the changes in coupling wavelengths as the coating was built up, after drying in air, after exposure to ammonia and after flushing with N_2. The transmission spectrum corresponding to NH_3 exposure is almost identical to that of the N_2 exposure and can be seen just above the N_2 peaks in the region between 1300 nm and 1350 nm.

It can bee seen from the results that the shift at any point in the proceedings is negligible. Even the application of 20 bi-layers of PAA/Chromo 1 has no significant effect on the transmission spectra. This may be due to the coating having a higher refractive index than the cladding, the coating not being of sufficient thickness to be 'seen' by the transmitted radiation, or that the coating is not bonding properly to the surface of the cladding.

It was decided to abort this method in favour of a less accurate coating method in which the number of layers of the coating material cannot be monitored, but is a proven method of chemical deposition. Attempts were made to coat the cladding by mixing 1 part CuPc⁻ $(C(CH_3))_4$ to 4 parts PPS in solution with chloroform at 5mg per ml. The mixture was pooled around the grating until the chloroform evaporated, leaving the PPS/ CuPc⁻ $(C(CH_3))_4$ coated to the fibre in alternate layers as they bond to the each other due to opposing polarity of charges. This again proved unsuccessful and the coating did not cause any significant shift in the coupling wavelengths. The shift was therefore investigated concentrating the OSA around the 1550nm band, but the noise level on the signal resulted in more than one minimum value at the coupling wavelength dip, preventing accurate determination of the actual wavelength shift.

6.6.3 Conclusions to Experiments in Sections 6.6.1 and 6.6.2 Utilising the In-Situ PESA Coating Methods

Coating of the cladding using the in situ PESA method proved unsuccessful in both previous experiments. These results also suggest that the CuPC and Chromo 1 coatings have refractive indices greater than that of the cladding. This would result in very slight shifts to longer coupling wavelengths as predicted by simulation (Chapter 4), which may be too small to be detected at the resolution used in this experiment. Again, as the shifts were never going to be great enough to allow this method to be utilised as a practical sensor, this experiment was taken no further and other coating chemicals were investigated.

6.7 Investigations into Utilising a Suitably Coated Long Period Grating as a Gas Sensor Using Evaporation Method of Coating

In this experiment calixarene was used as the gas sensitive coating and hexane, toluene, and benzene as the gases to be detected.

6.7.1 Experimental Procedure

Again the fibre was connected to the OSA using bare fibre connectors at the start of proceedings to allow observation of the effects of each stage of the experiment on the transmission spectrum. During the time between this experiment and the previous experiment a broadband light source became available, allowing observation of the coupling shifts at intermediate wavelengths.

The grating section of the fibre was coated by evaporation methods as described in Chapter 5, clamped under slight tension in the purpose built cavity and saturated vapour of hexane was injected into the cavity using a syringe. The cavity was then flushed with N_2 to ensure that all hexane vapour was removed and to observe any recovery made in the coating. The shift in coupling wavelength was observed and noted at each stage. The coating was removed using chloroform until the spectrum

returned to that of air and the coating and exposure procedure repeated using toluene and benzene saturated vapours.

6.7.2 Results and Discussion

The shift in coupling wavelength as the calixarene coating was applied, exposed to the relevant vapours and then flushed with N_2 are shown in Figures 6.49 to 6.54.
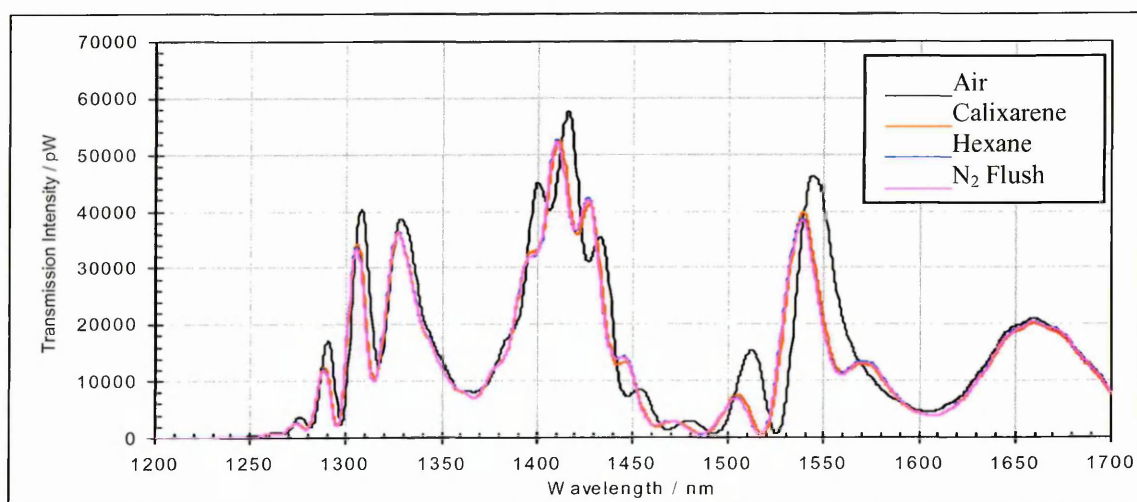
Figure 6.49: **Transmission spectra of LPG C1 after coating of calixarene, exposure to saturated hexane vapour and flushing with N_2**
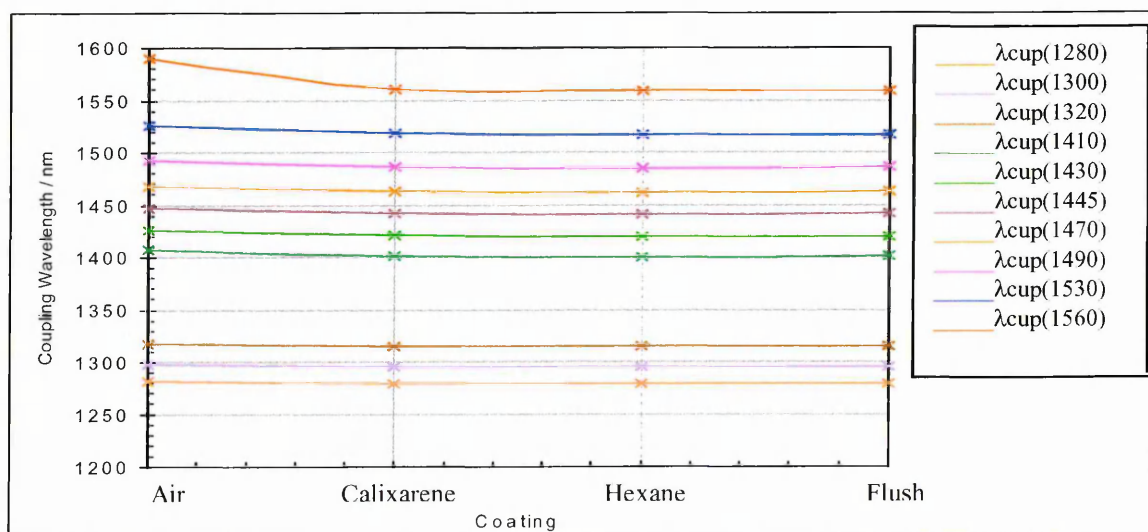
Figure 6.50: **Shift in coupling wavelength with calixarene coating, exposure to saturated hexane vapour and flushing with N_2 for LPG C1**
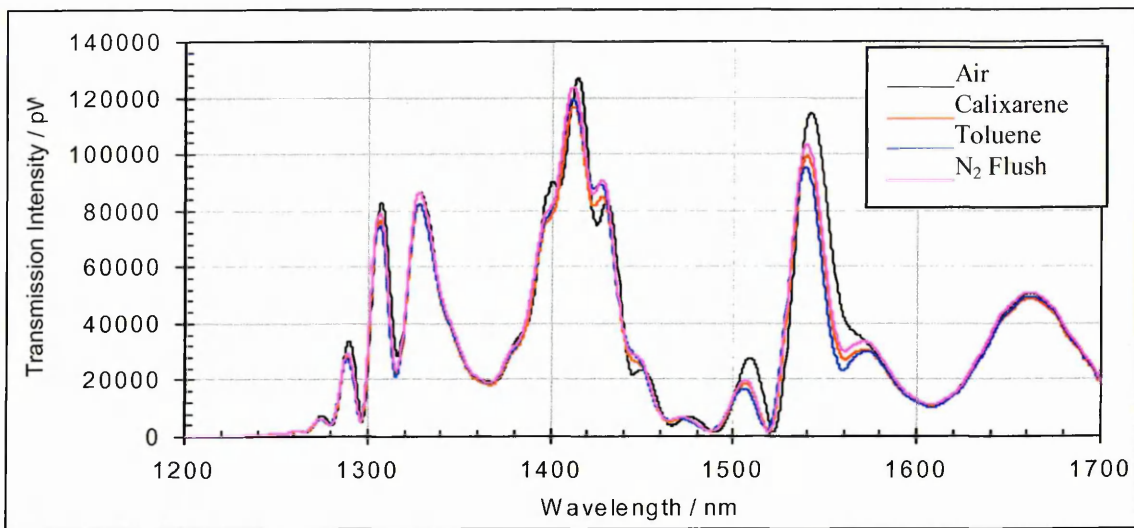
Figure 6.51:   Transmission spectra of LPG C1 after coating of calixarene,
exposure to saturated toluene vapour and flushing with N_2
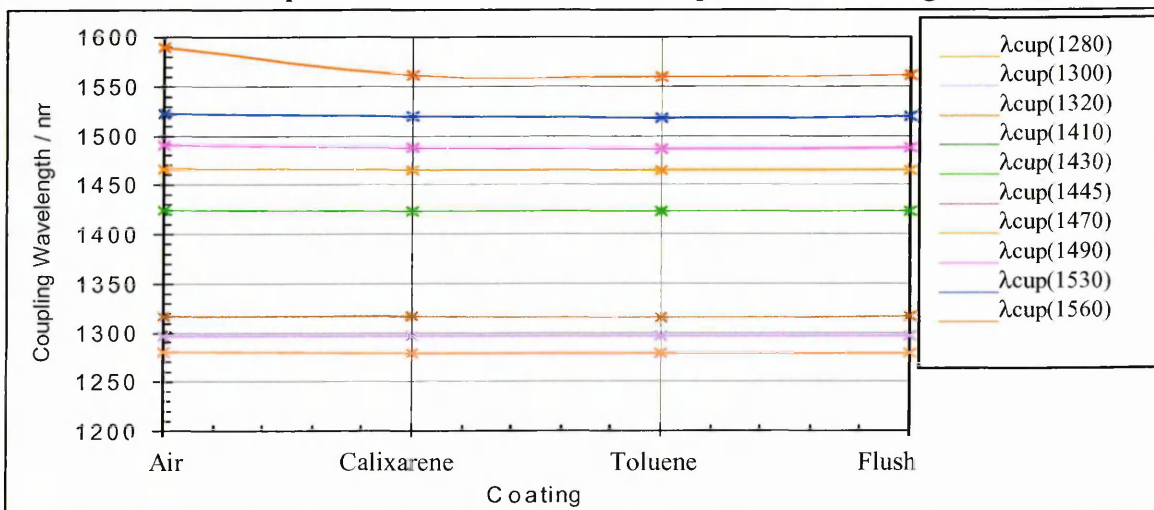
Figure 6.52:   Shift in coupling wavelength with calixarene coating, exposure to
saturated toluene vapour and flushing with N_2 for LPG C1
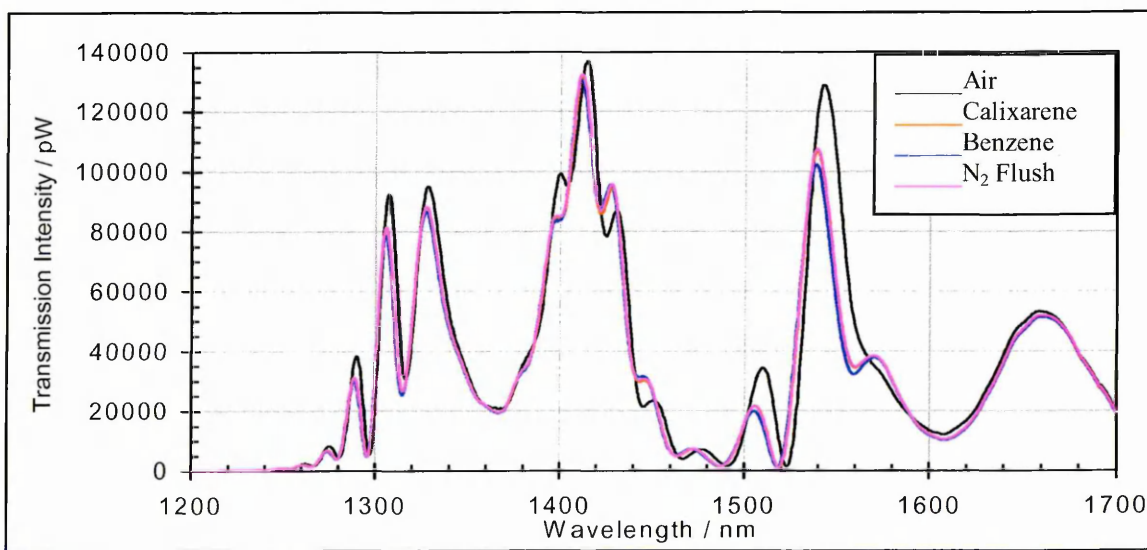
Figure 6.53:   Transmission spectra of LPG C1 after coating of calixarene,
exposure to saturated benzene vapour and flushing with N_2

200
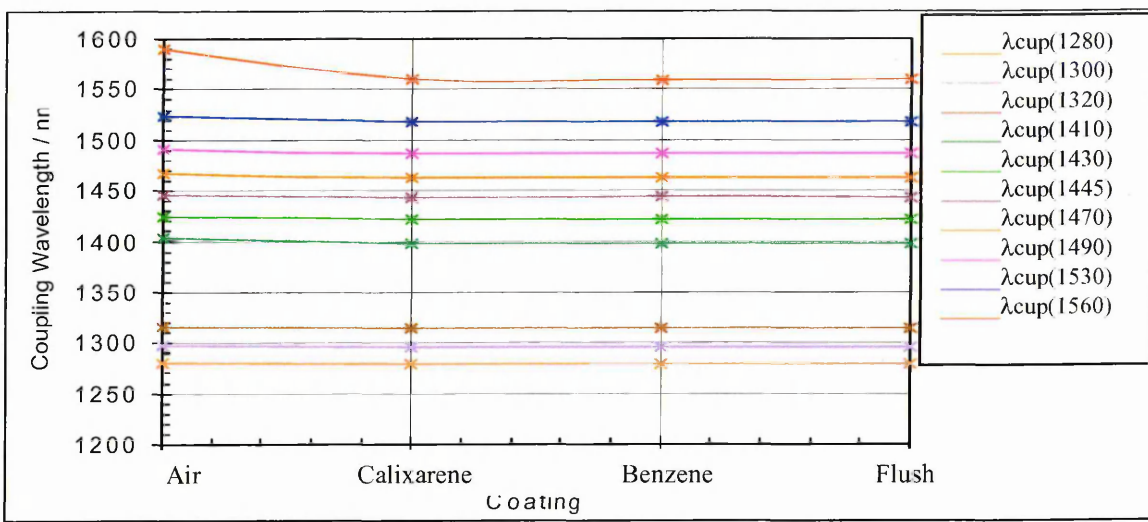
Figure 6.54: **Shift in coupling wavelength with calixarene coating, exposure to saturated benzene vapour and flushing with N_2 for LPG C1**

The fact that the coupling wavelength values in air are the same at the beginning of each coating (within uncertainty limits) show that the previous possibly contaminated coatings were successfully removed at the end of each stage. The change in coupling wavelength when the calixarene is applied is again virtually constant, suggesting regular consistency of each coating in each section of the experiment. All coupling wavelengths can be seen to remain stationary (at the shorter wavelengths) or to decrease (at the longer wavelengths) as the coatings are exposed to the various saturated vapours. As expected the most sensitive coupling occurs in the 1590 nm band, which couples to the highest order cladding mode available for the range of the light source. Figure 6.55 shows the shift in coupling wavelength due to the calixarene coating in the highest visible wavelength range, from 1590±0.5 nm to 1560.5±0.5 nm, a shift of –29.5±0.5 nm.
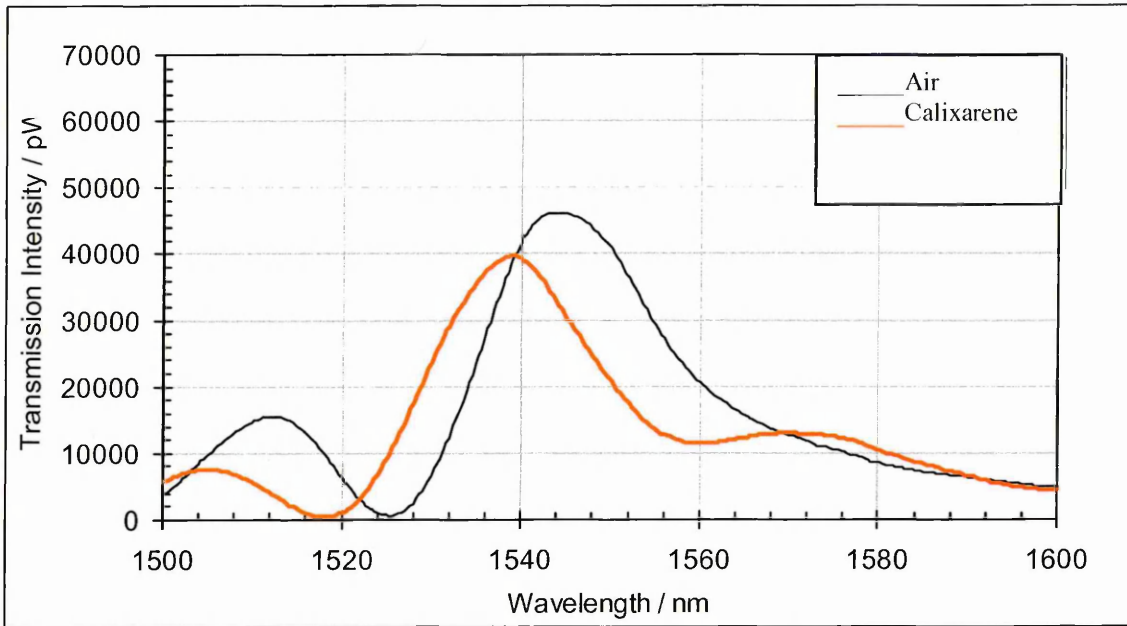
Figure 6.55: Shift in coupling wavelength when calixerine coating applied to cladding of LPG C1

The 1560 nm-1561 nm section of the ambient refractive index profile of LPG C1 from Appendix 9 shown in Figure 6.56 shows the refractive index of the calixerine coating to be 1.3254 ± 0.005 nm.
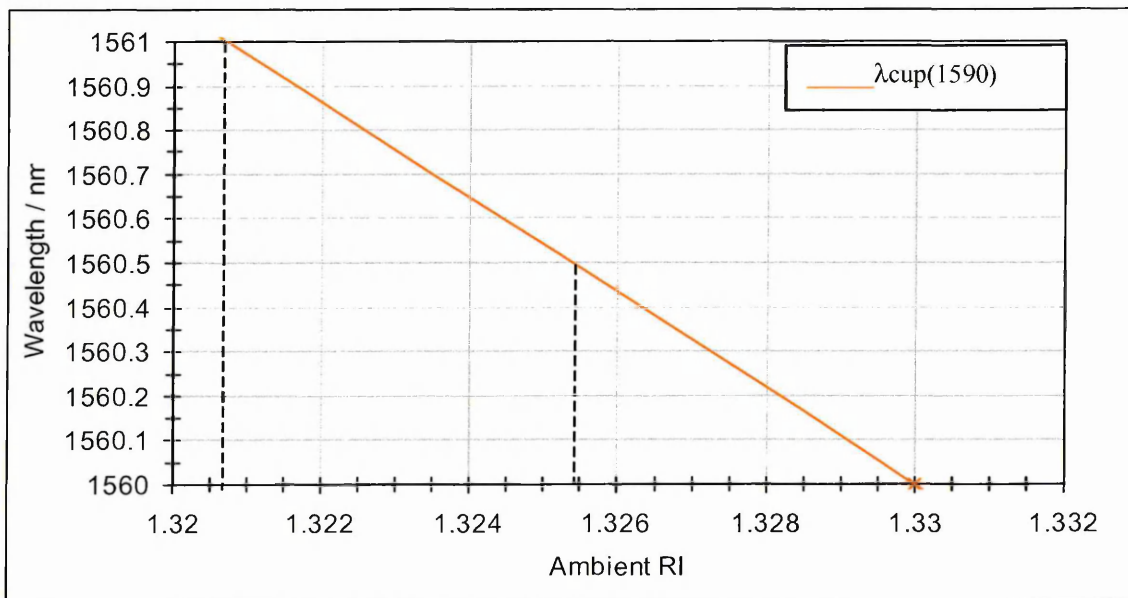
Figure 6.56: 1560 nm-1561 nm section of the ambient refractive index profile of LPG C1

Figures 6.57 to 6.59 focus on the coupling wavelength shifts in the 1590 nm band at each step of the procedure for each saturated vapour exposure.
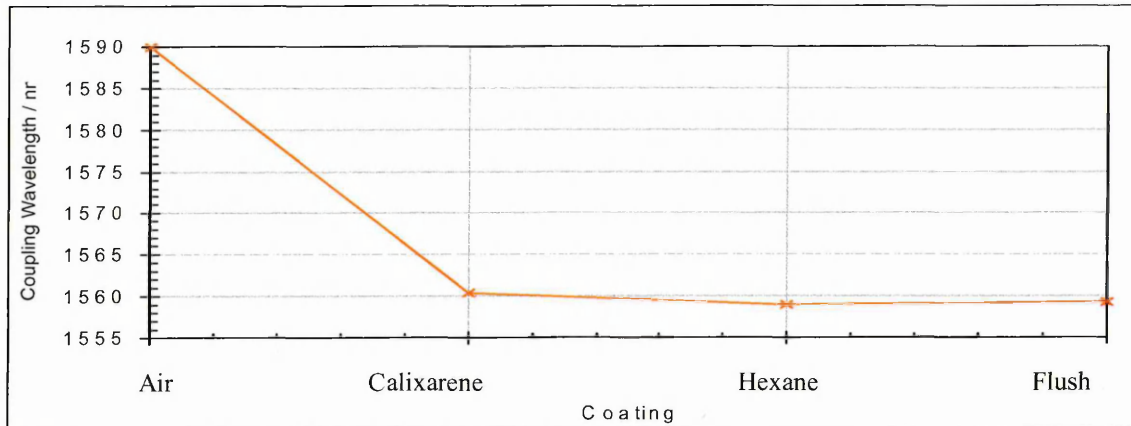
Figure 6.57: **Coupling wavelength shifts in 1590 nm band as LPG C1 is coated with calixarene, exposed to hexane saturated vapour and flushed with N$_2$**
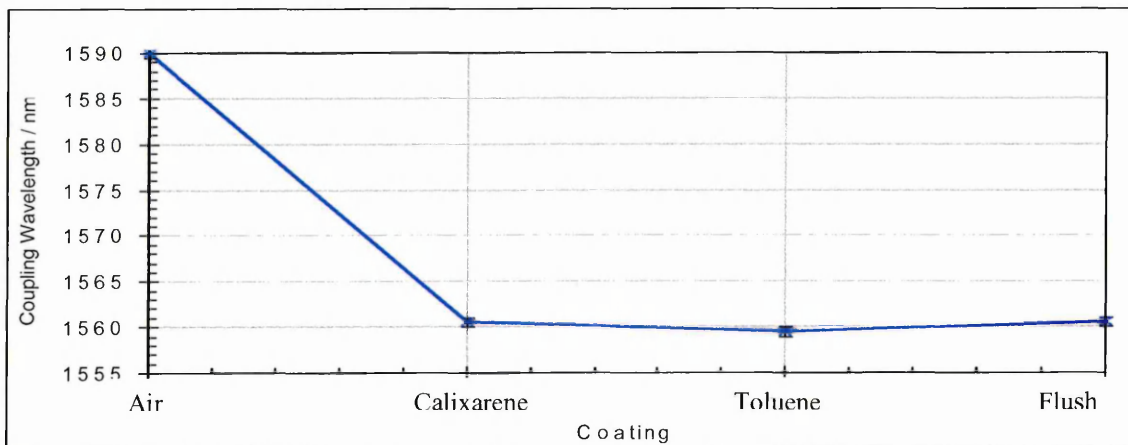
Figure 6.58: **Coupling wavelength shifts in 1590 nm band as LPG C1 is coated with calixarene, exposed to toluene saturated vapour and flushed with N$_2$**
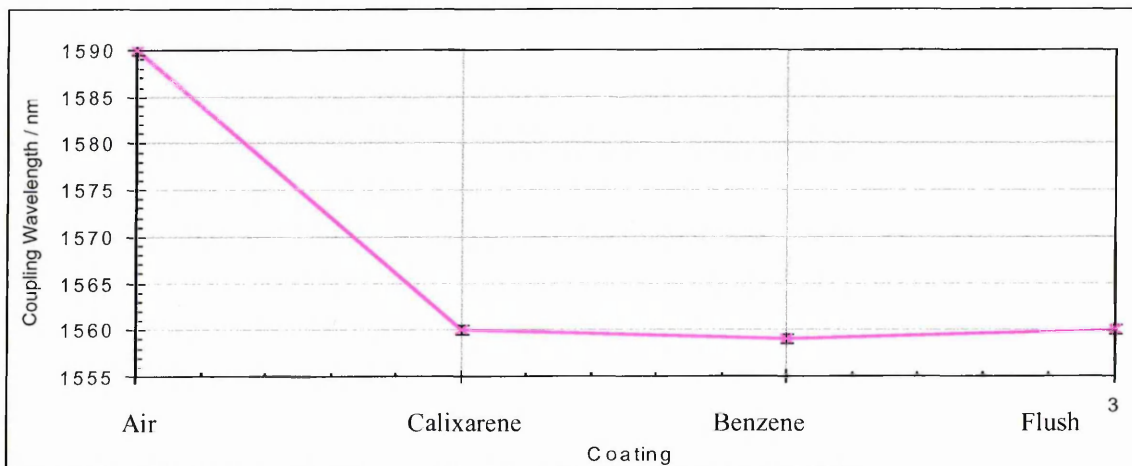
Figure 6.59: Coupling wavelength shifts in 1590 nm band as LPG C1 is coated with calixarene, exposed to benzene saturated vapour and flushed with N$_2$

Table 6.3 shows shifts in coupling wavelengths with exposure to the three 3 types of saturated vapours.

Gas	Coupling λ of calixarene coating $\pm$ 0.005nm	Coupling λ after gas exposure $\pm$ 0.005nm	Coupling λ shift $\pm$ 0.005nm
Hexane	1560.5	1559	-1.5
Toluene	1560.5	1559.5	-1
Benzine	1560.5	1559.5	-1

Table 6.3: **Shifts in coupling wavelength with exposure to each vapour**

Figures 6.60 to 6.62 show the sections of the ambient index profiles corresponding to the coupling wavelengths after each vapour exposure.
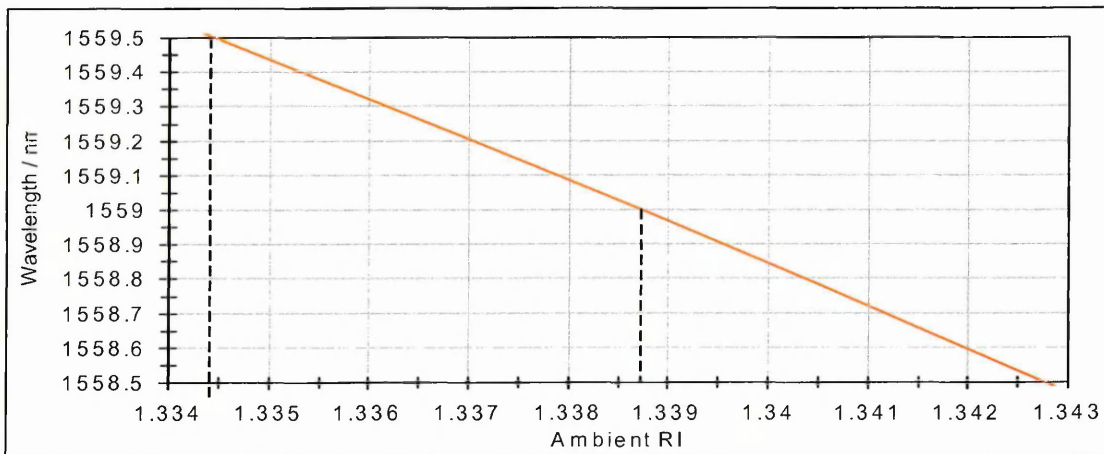
Figure 6.60: **Section of LPG C1 ambient index profiles corresponding to the coupling wavelength of 1559 nm after exposure to hexane saturated vapour.**
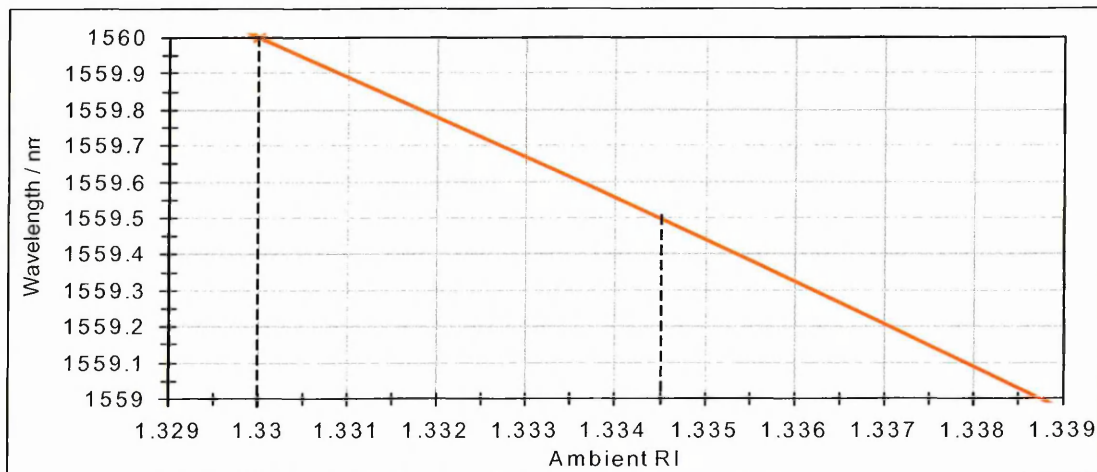
Figure 6.61: **Section of LPG C1 ambient index profiles corresponding to the coupling wavelength of 1559.5 nm after exposure to toluene saturated vapour.**
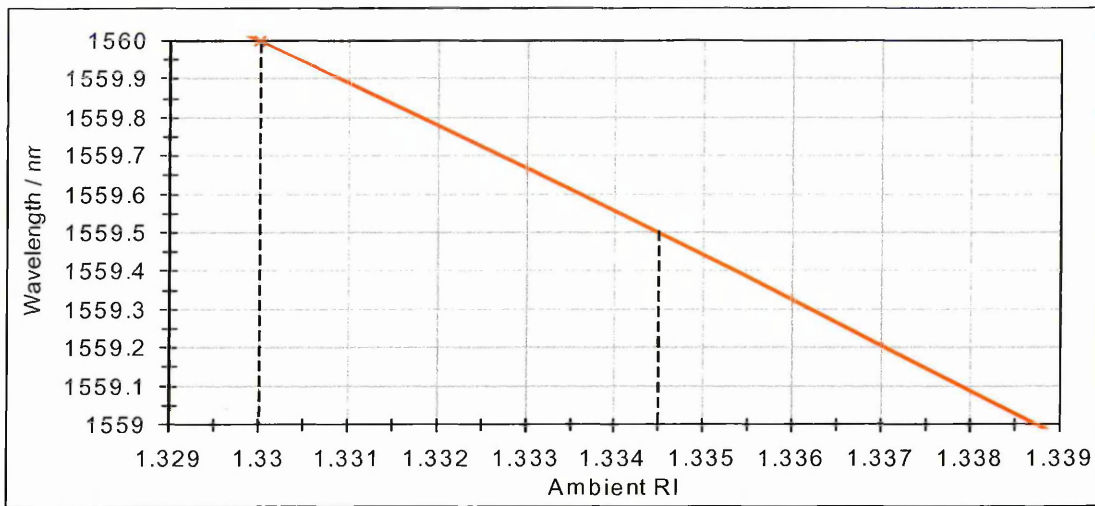
Figure 6.62: Section of LPG C1 ambient index profiles corresponding to the coupling wavelength of 1559.5 nm after exposure to benzene saturated vapour.

The corresponding refractive index changes of the calixarene coating due to the various vapour exposures are summarised in Table 6.4.

Gas	Coupling λ after gas exposure $\pm$ 0.005 nm	Modified RI of calixarene coating $\pm$ 0.005	Change in RI of calixarene coating $\pm$ 0.005
Hexane	1559	1.339	+0.014
Toulene	1559.5	1.335	+0.009
Benzine	1559.5	1.335	+0.009

Table 6.4: Refractive index changes of the calixarene coating due to the various vapour exposures

6.7.3 Conclusions to Experiments Utilising the Evaporation Method of Coating

As in the first experiments the shift is small even though the gas concentration is high, and therefore detection of small traces of gas would not be possible using these coating chemicals. The previously determined temperature profile of the LPG (Appendix 10) shows the temperature sensitivity of this coupling mode to be linear

between 20°C and 80°, with a sensitivity of 0.07 nm/°C (the temperature must change by 14°C to cause a shift of 1 nm). This rules out any relevant effects of temperature on the results as the room temperature was constant to $\pm$ 1°C throughout all experiments. Also strain inconsistencies can be ignored as the fibre was maintained in the same position throughout each experiment. The effect of the coatings and gas exposures was also observed at the lower coupling modes, which as expected were not as sensitive as the higher mode related in these experiments. Even though the shifts were smaller, in some cases less than the resolution setting (0.5 nm) of the OSA they were still seen to move in the same direction as the highest observable mode. This constant trend suggests that the shifts were not due to random effects but were due to the effect being investigated. In all three cases a degree of recovery was observed after flushing the cavity with N_2. The hexane exposure showed only slight recovery of 0.25 nm, but the toluene and benzene exposures showed full recovery of the calixarene coating, which suggests if the sensitivity aspect can be dealt with then it may be possible to re-use the gas sensor for multiple exposures.

6.8 Summary

This chapter has described the experimental investigations into using an LPG as a gas sensor and a multi-parameter sensor. Experiments into the difference between the ambient index and temperature profiles of LPGs of various periods have been described. Coating methods and compounds to be used to coat the cladding have been

investigated and experimental investigations into using suitably coated LPG as a gas sensor have been explained.

Chapter 7

Conclusions

The principle objective presented in this thesis was to investigate the possibility of utilising a suitably adapted LPG as a gas sensor.

In order to perform the investigations successfully it was necessary to investigate the operational characteristics and limitations of existing optical sensors and the advantages which an LPG based optical sensor would incorporate, which the literature review reported in chapter 2 confirms.

A thorough understanding of the theory and principles of light propagation, mode formation, and mode coupling in optical fibres discussed in chapter 3 allowed their effective application to the computer simulations described in chapter 4, and the development and limited success of the LPG as a gas sensor as reported in chapter 6.

The coating procedures undertaken in this investigation described in chapter 5 were shown to be reasonably successful, a novel method of monitoring the build up of layers in-situ using SPR methods being introduced.

The coating chemicals used in this investigation showed some optical sensitivity at the optimum wavelengths used in optical fibres to the various gases being monitored, in most cases causing a detectable change in the optical characteristics of the modes in the LPG as described in chapter 6.

This study has shown that it may be possible to use a suitably prepared LPG as a gas sensor. The LPG can be coated with a chemical whose refractive index can be changed by absorption of a given gas. It may also be possible to utilise a coating material which absorbs water, the refractive index of the coating being affected by the reaction of the gas with the water in the coating.

The possibility has been suggested also to surround the LPG with a suitable liquid in a gaseous atmosphere, the change in the refractive index of the liquid due to absorption of the gas giving the required shift in coupling wavelength.

The possibility of using a single temperature immune LPG for ambient index sensing by observing different coupling wavelengths in the same grating has also been demonstrated.

The maximum shift in coupling wavelength in both investigations of ±1.5 nm for such high gas concentrations suggests that the sensitivity of the sensor requires further

improvement before it can in any way challenge the existing sensors in this field. The principle and the viability of using LPGs for sensor applications however, has been supported by the preliminary results reported here.

Chapter 8

Further Work

As stated in the previous chapter, the maximum shift in coupling wavelength of ±1.5 nm for such high gas concentrations suggests that the sensitivity of the sensor requires further improvement to become a viable gas sensor.

Investigations should continue into other chemicals with greater optical sensitivity to a given gas, or with an initial refractive index closer to that of the cladding, which will show much greater shifts for the same level of optical sensitivity.

Other coating methods may also have to be investigated by which these chemicals may be applied to the fibre cladding, perhaps by modifying the existing LB or PESA coating procedures to allow for the physical constraints of immersing the grating section in the solution.

LPGs manufactured with grating periods designed to couple higher orders of diffraction or higher harmonics of the same order of diffraction into the core may also be a route to follow in an attempt to improve the sensitivity of the sensor

Further work is suggested to investigate an optimum period length at which temperature will have negligible effect on the optical profile of one or more of the coupling modes, but is still of a period length which is sensitive enough to detect small changes in ambient indices.

Further investigations into coating materials which absorb water may also be undertaken, the refractive index of the coating and thus the shift in coupling wavelength being affected by the reaction of the gas with the absorbed water.

The final aspect of further investigation adapted from this study is to surround the LPG with a suitable liquid in a gaseous atmosphere, the change in the refractive index of the liquid due to absorption of the gas giving the required shift in coupling wavelength.

References

1. Rogers, A.: "Distributed Optical Fibre Sensing", Meas. Sci. Technol. Vol 10, IOP Publishing Ltd., pp. R77, 1999.

2. Senior, J.M.: "Optical Fiber Communications: Principles and Practice", 2nd Edition, Chapter 2, Prentice Hall, pp. 13, 1992, ISBN 0-13635-426-2.

3. Keiser, G.: "Optical Fiber Communications", 3rd Edition, Chapter 2, McGraw-Hill, pp. 39, 2000, ISBN 0-07-232101-6.

4. "Optical Sensor Technologies", Chapter 6, pp.14, 1999, http://itri.loyola.edu/opto/c6_s3.htm.

5. "How Persistence Paid Off for the Pioneers of Fibre Optics", Physics World, pp. 14-16, July 1996.

6. Doran, N. and Bennion, I.: "Optical Networks to Span the Globe", Physics World, pp. 35-39, November 1996.

7. "Optical Fiber" pp. 1, 1998, visited Sept 2001, http://www.geocities.com/Athens/Aegean/6641/fibers.html.

8. Stange, S.T.: "Fiber White Paper", pp.1,5, 1999, visited Sept 2001, http://www.transition.com/products/fiber_wp.html.

9. Bhatti, S.: "Optical Fibre Waveguide" pp. 1, 1995, visited Sept 2001, http://www.cs.ucl.ac.uk/staff/S.Bhatti/D51-notes/node21.html.

10. Dakin, J. and Culshaw, B.: "Optical Fiber Sensors", Vol. 1, Chapter 9, Norwood, pp.277, 1988, ISBN 0-89006-317-6.

11. Giles, C.R.: "Lightwave Applications of Fibre Bragg Gratings", JOLT, Vol. 15, No. 8, pp.1393-1397, 1997.

12. Geiger, H., Set, S.Y., Laming, R.I., Cole, M.J. and Reekie, L.: "Comparison of DSF and SOA Based Phase Conjugators by Incorporating Noise-Suppression Fibre Gratings", ORC Research Review, 1996, http://www.orc.soton.ac.uk/orchelp/pubs.

13. Koch, F., Chernikov, S.V. and Taylor, J.R.: "Dispersion Measurement in Optical Fibres over the Entire Spectral Range From 1.1 μm to 1.7μm", Optics Communications, Vol. 175, pp.209-213, 2000.

14. Geiger, H., Fu, A., Petropoulos, P., Ibsen, M., Richardson, D.J. and Laming, R.I.: "Demonstration of a Simple CDMA Transmitter and Receiver using Sampled Fibre Fratings", ORC Research Review, http://www.orc.soton.ac.uk/orchelp/pubs.

15. Dakin, J. and Culshaw, B.: "Optical Fiber Sensors", Vol. 1, Chapter 2, Norwood, pp.20, 1988, ISBN 0-89006-317-6.

16. Hecht, J.: "Understanding Fiber Optics", Third Edition, Chapter 7, Prentice-Hall, pp.125-128, 1999, ISBN 0-13-956145-5.

17. Lee, Y.W., Nilsson, J., Hwang, S.T. and Kim, S.J.: "Experimental Characterisation of a Dynamically Gain-Flattened Erbium-Doped Fiber Amplifier", ORC Research Review, http://www.orc.soton.ac.uk/orchelp/pubs.

18. Laming, R.I. and Loh, W.H.: "Fibre Bragg Gratings; Application to Lasers and Amplifiers", ORC Research Review, 1997, http://www.orc.soton.ac.uk/orchelp/pubs.

19. Poulson, C.V., Graydon, O.C., Laming, R.I., Zervas, M.N. and Dong, L.: "Self Regulating Spectral Characteristics of a 4 Channel WDM Link Utilizing Twincore Erbium Doped Fibre Amplifiers", ORC Research Review, 1996, http://www.orc.soton.ac.uk/orchelp/pubs.

20. Khandaker, I.I., Glavas, E. and Jones, G.R.: "A Fibre-optic Condition Monitor Based on Chromatic Modulation", Meas. Sci. Technol. Vol. 4, IOP Publishing Ltd., pp.608-613, 1993.

21. Guerrero, H., Escudero, J. L. and Bernabeu, E.: "Magneto-optical Tachometer using Plastic Optical Fibre", Meas. Sci. Technol. Vol. 4, IOP Publishing Ltd., pp.133-135, 1993.

22. Murukeshan, V.M., Chan, P.Y., Seng, O.L. and Asundi, A.: "On-Line Health Monitoring of Smart Composite Structures Using Fiber Polarimetric Sensor", Smart Mater. Struct. Vol. 8., pp.544-548, 1999.

23. Hotate, K.: "Fiber Sensor Technology Today", Optical Fibre Technology, Vol. 3, pp.356-358, 1997.

24. Hill, K.O. and Meltz, G.: "Fiber Bragg Grating Technology Fundamentals and Overview", JOLT, Vol. 15, No. 8, pp.1273, 1997.

25. Volanthen, M.V., Geiger, H., Trundle, K.J. and Dakin, J.P.: "Fibre Bragg Grating Sensors", ORC Research Review, http://www.orc.soton.ac.uk/orchelp/pubs.

26. Kersey, A.D., Davis, M.A., Patrick, H.J., LeBlanc, M., Koo, K.P., Askins, C.G., Putnam, M.A. and Friebele, E.J.: "Fibre Grating Sensors", JOLT, Vol. 15, No. 8, pp.1442-1460, 1997.

27. Kersey, A.D.:"A Review of Recent Developments in Fiber Optic Sensor Technology", Optical Fiber Technology, Vol. 2, pp.291-317, 1996.

28. Egan, D.A., James, S.W. and Tatam, R.P.: "A Polarization-Based Optical Fibre Vibrometer", Meas. Sci. Technol. Vol. 8, pp.343-347, 1997.

29. Ronot, C., Archenault, M., Gagnaire, M., Goure, J.P., Jaffrezic-Renault, N. and Pichery, T.: "Detection of Chemical Vapours with a Specifically Coated Optical-Fibre Sensor", Sensors and Actuators, B11, pp. 375-381, 1993.

30. Archenault, M., Gagnair, H., Goure, J.P. and Jaffrezic-Renault, N.: "A Simple Intrinsic Optical Fibre Refractometer", Sensors and Actuators, B5, pp. 173-179, 1991.

31. Butler, M.A.: "Micromirror Optical-Fiber Hydrogen Sensor", Sensors and Actuators, B22, pp. 155-163, 1994.

32. Otsuki, S., Adachi, K. and Taguchi, T.: "A Novel Fiber-Optic Gas-Sensing Configuration using Extremely Curved Optical Fibers and an Attempt for Optical Humidity Detection", Sensors and Actuators, B53, pp. 91-96, 1998.

33. "Fibre Optic Sensors", Systems and Sensors, pp. 2-5, http//floti.bell.ac.uk/MathsPhysics/optsens.htm.

34. Belotserkovsky, E., Bar-Or, O., and Katzir, A.: "Infrared Fibreoptic Temperature Monitoring During Machining Procedures", Meas. Sci. Technol. Vol. 5, IOP Publishing Ltd., pp.451-453, 1994.

35. Naci, M., Barton, J.S. and Jones, J.D.C.: "A Fibre-Optic Thermometric Sensor Based on the Thermo-Optic Effect of Titanium Dioxide Coatings", Optics and Laser Technology, Vol. 29, No. 3, pp.121-124, 1997.

36. Bertrand, S., Jalocha. A., Tribillon, G., Bouazaoui, M. and Rouhet, J.: "Optical Fibre Temperature Sensor in the Cryogenic Range", Optics and Laser Technology, Vol. 28, No. 5, pp.363-366, 1996.

37. Chen, S., Meggit, B.T., Palmer, A.W., Thomas, K., Grattan, V. and Pinnock, R.A.: "An Intrinsic Optical-Fiber Position Sensor with Schemes for Temperature Compensation and Resolution Enhancment", JOLT, Vol. 15, No. 2, pp.261-265, 1997.

38. Rao,Y., Webb, D.J., Jackson, D.A., Zhang, L. and Bennion, I.: "In Fiber Grating Temperature Sensor System for Medical Applications", JOLT, Vol. 15, No. 5, pp.779-784, 1997.

39. Pinnock, R.A.: "Optical Pressure and Temperature Sensors for Aerospace Applications", Sensor Review, Vol. 18, No. 1, pp. 32-38, 1998.

40. Sharma, A. and Posey, R.: "Transverse Stress Induced LP_{02}-LP_{21} Modal Interference of Stimulated Raman Scattered Light in a Few-Mode Optical Fiber", Optics Communications, Vol. 124, pp. 111-117, 1996.

41. Pomarico, J.A., Sicre, E.E., Patrignani, D. and De Pasquale, L.: "Optical Fiber Strain Guage Based on Speckle Correlation", Science Direct, Optics and Laser Technology, http://www.sciencedirect.com/science.

42. Valera, J.D.R., Sinha, P.G., Yoshino, T. and Lokberg, O.J.: "Large Amplitude Point-Vibration Measurement with Optical-Fiber Moire-Based Technique", Science Direct, Optics and Laser Technology, http://www.sciencedirect.com/science.

43. "Fibre Optic Sensors", Systems and Sensors, pp. 1-2, http://floti.bell.ac.uk/MathsPhysics/optsens.htm.

44. Storgaard-Larsen, T., Bouwstra, S. and Leistiko, O.: "Opto-Mechanical Accelerometer Based on Strain Sensing by a Bragg Grating in a Planar Waveguide", Sensors and Actuators, A52, pp. 25-32, 1996.

45. Tao, X., Tang, L. Du. W. and Choy, C.: "Internal Strain Measurement by Fiber Bragg Grating Sensors in Textile Composites", Composites Science and Technology, Vol. 60, pp.657-669, 2000.

46. Selvarajan,A.: "Fiber Optic Sensors and Their Applications", pp.1, 1999, http://www.ntu.edu.sg/mpe/resear...sensors/sensors/fos/fosselva.html.

47. Patrick, H.J., Kersey,A.D. and Bucholtz,F.: "Analysis of the Response of Long Period Fiber Gratings to External Index of Refraction", Journal of Lightwave Technology, Vol.16, No. 9, pp.1606, 1998.

48. Keck, D.B.: "Optical Sensor Technologies", JTEC Panel on Optoelectronics in Japan and the United States, Maryland, http://itri.loyola.edu/opto/c6_s3.htm, pp.1, 1996.

49. Udd, E.: "Fiber Optic Sensors An Introduction for Engineers and Scientists", Chapter 1, Wiley, pp. 5, 1991, ISBN 0-471-83007-0.

50. Hecht, J.: "Understanding Fiber Optics", Third Edition, Chapter 4, Prentice-Hall, pp.56, 1999, ISBN 0-13-956145-5.

51. Selvarajan,A.: "Fiber Optic Sensors and Their Applications", pp.12-13, 1999, http://www.ntu.edu.sg/mpe/resear...sensors/sensors/fos/fosselva.html.

52. "Optical Sensor Technologies", Chapter 6, pp.6, 1999, http://itri.loyola.edu/opto/c6_s3.htm

53. Zhang, J., Handerek, V.A., Cokgor, I., Pantelic, V. and Rogers, A.J.: " Distributed Sensing of Polarisation Coupling in High Birefringence Optical Fibers Using Intense Arbitrarily Polarized Light", JOLT, Vol. 15, No. 5, pp.794-801, 1997.

54. Singh, H. and Sirkis, J.S.: "Simultaneously Measuring Temperature and Strain Using Optical Fiber Microcavities", JOLT, Vol. 15, No. 4, pp.647-653, 1997.

55. Hotate, K.: "Fiber Sensor Technology Today", Optical Fibre Technology, Vol. 3, pp.376-394, 1997.

56. Volanthen, M.V., Geiger, H., Trundle, K.J. and Dakin, J.P.: "Fibre Bragg Grating Sensors", ORC Research Review, pp.2-4, http://www.orc.soton.ac.uk/orchelp/pubs.

57. Kersey, A.D., Davis, M.A., Patrick, H.J., LeBlanc, M., Koo, K.P., Askins, C.G., Putnam, M.A. and Friebele, E.J.: "Fibre Grating Sensors", JOLT, Vol. 15, No. 8, pp.1449-1450, 1997.

58. Kersey, A.D.: "A Review of Recent Developments in Fiber Optic Sensor Technology", Optical Fiber Technology, Vol. 2, pp.299-304, 1996.

59. Rogers, A.: "Distributed Optical Fibre Sensing", Meas. Sci. Technol. Vol 10, IOP Publishing Ltd., 1999.

60. Volanthen, M.V., Geiger, H. and Dakin, J.P.: "Distributed Fibre Grating Sensor for Smart Structures Applications", ORC Research Review, http://www.orc.soton.ac.uk/orchelp/pubs.

61. Kersey, A.D.: "Distributed and Multiplexed Fiber Optic Sensors", Fiber Optic Sensors: An Introduction for Engineers and Scientists, John Wiley & Sons Inc., pp.325-368, 1991, ISBN 0-471-83007-0.

62. De la Chapelle, M., Vertatschitsch, E.J., Abbas, G.L. and Porter, C.R.: "Multiplexed Ladar Fiber-Optic System", SPIE, Vol. 1586, pp.146-154, 1991.

63. Handerek, V.A., "Optical Fibre Bragg Gratings: a New Sensor Multiplexing Tool", Sensor Review, Vol. 18 No. 1, pp. 39-43, 1998.

64. Shiping, C., Meggit, B.T., Palmer, A.W., Grattan, K.T.V. and Pinnock, R.A.: "An Intrinsic Optical-Fiber Position Sensor with Schemes for Temperature Compensation and Resolution Enhancement", JOLT, Vol. 15, No. 2, pp.261-265, 1997.

65. Dakin, J. and Culshaw, B., A.M.: "Optical Fiber Sensors", Vol. 1, Chapter 9, Norwood, pp.189-205, 1988, ISBN 0-89006-317-6.

66. Rogers, A.J.: "Intrinsic Optical Fibre Current Sensors", Sensor Review, Vol. 18, No. 1, pp.17-22, 1998.

67. "Science of Fibre Optic Sensors", Background on Fibre Optic Sensors, http:www.fft.com.au/backgrnd.html, pp.2, 1999.

68. Hassan,A., Molina,M.V., Ray,A.K., Nabok,A., Ghassemlooy,Z., Yates,R., Saatchi,R.: "Chemical Sensors for the Detection of Organic Pollutants", Proceedings of SPIE's 6th Ann. Intern. Symp. on Smart Structures and Materials, pp.3673-40, 1999.

69. "Optical Sensor Technologies", Chapter 6, pp.8-9, 1999, http://itri.loyola.edu/opto/c6_s3.htm.

70. Wang, Z., Liao, Y., Lai, S., Zhao, H. and Chen, X.: "A Novel Method for Simultaneous Measurement of Current and Voltage Using One Low-Bierefringence Fiber" Science Direct, Optics and Laser Technology, Vol 30. Issue 5, pp.257-262, 1998, http://www.sciencedirect.com/science.

71. Rose, A.H., Etzel, S.M. and Rochford, K.B.: "Optical Fiber Cirrent Sensors in High Electric Field Environments", JOLT, Vol. 17, No. 6, pp.1042-1047, 1999.

72. Selvarajan,A.: "Fiber Optic Sensors and Their Applications", pp.8-10, 1999, http://www.ntu.edu.sg/mpe/resear...sensors/sensors/fos/fosselva.html.

73. "Optical Sensor Technologies", Chapter 6, pp.5, 1999, http://itri.loyola.edu/opto/c6_s3.htm.

74. Kidd, S.R., Barton, J.S., Inci, M.N. and Jones, J.D.C.: "Unsteady Gas Temperature Measurement Using an Ulra-Short Optical Fibre Fabry-Perot Interferometer", Meas. Sci. Technol. Vol. 55, pp.816-822, 1994.

75. Bhatia, V., Murphy, K.A., Claus, R.O., Jones, M.E., Grace, J.L., Tran, T.A. and Greene, J.A.: "Optical Fibre Based Absolute Extrinsic Fabry-Perot Interferometric Sensing System", Meas. Sci. Technol. Vol. 7, pp.58-61, 1996.

76. Yuan, L.: "Optical Path Automatic Compensation Low-Coherence Interferometric Fibre-Optic Temperature Sensor", Optics and Laser Technology, Vol. 30, pp.33-38, 1998.

77. Kim, H.S., Haaksman, P.H., Newson, T.P. and Richardson, D.J.: "Noise Properties of Dual Mach-Zender Interferometers Employing Narrowband Fiber ASE Sources", ORC Research Review, http://www.orc.soton.ac.uk/orchelp/pubs.

78. De Souza, K., Lees, G.P., Wait, P.C. and Newson, T.P.: "A Diode Pumped Landau-Placzek Based Distributed Temperature Sensor Utilising an All-Fibre Mach-Zender Interferometer", ORC Research Review, 1996, http://www.orc.soton.ac.uk/orchelp/pubs.

79. Szafraniec, B., Sanders, G.G.: "Theory of Polarization Evolution in Interferometric Fiber-Optic Depolarized Gyros", JOLT, Vol. 17, No. 4, pp. 359-389, 1999.

80. Hotate, K.: "Fiber Sensor Technology Today", Optical Fibre Technology, Vol. 3, pp.360-370, 1997.

81. Kersey, A.D.:"A Review of Recent Developments in Fiber Optic Sensor Technology", Optical Fiber Technology, Vol. 2, pp. 292-299, 1996.

82. Rogers, A.: "Distributed Optical Fibre Sensing", Meas. Sci. Technol. Vol 10, IOP Publishing Ltd., pp. R81-R83, 1999.

83. Kersey, A.D., Davis, M.A., Patrick, H.J., LeBlanc, M., Koo, K.P., Askins, C.G., Putnam, M.A. and Friebele, E.J.: "Fibre Grating Sensors", JOLT, Vol. 15, No. 8, pp.1447-1449, 1997.

84. Ezbiri, A. and Tatam, R.P.: "Interrogation of Low Finesse Optical Fibre Extrinsic Fabry-Perot Interferometers Using a Four Wavelength Technique", Meas. Sci. Technol. Vol 7, IOP Publishing Ltd., pp. 117-120, 1996.

85. Lees, G.P., Wait, P.C., Hartog, A.H. and Newson, T.P.: "Recent Advances in distributed Optical Fibre Temperature Sensing Using the Landau-Placzek Ratio", ORC Research Review, http://www.orc.soton.ac.uk/orchelp/pubs.

86. Fernando, G.F., Liu, T., Crosby, P., Doyle, C., Martin, A., Brroks, D., Ralph, B. and Badcock, R.: "A Multi-Purpose Optical Fibre Sensor Design for Fibre Reinforced Composite Materials", Meas. Sci. Technol. Vol8, IOP Publishing Ltd., pp. 1065-1079, 1997.

87. Singh, M., Tuck, C.J. and Fernando, G.F.: "Multiplexed Optical Fibre Fabry-Perot Sensors for Strain Metrology", Smart Mater. Struct.,ol. 8, pp. 549-553, 1999.

88. Meltz, G., Hewlett, S.J. and Love, J.D.: "Fibre Grating Evanescent-Wave Sensors", SPIE, Vol. 2836, pp.343, 1996.

89. Crosby, P.A., Powell, G.R., Fernando, G.F., France, C.M., Spooncer, R.C. and Waters, D.N.: "In Situ Cure Monitoring of Epoxy Resins Using Optical Fibre Sensors", Smart Mater. Struct. Vol. 5, pp. 422, 1996.

90. Yuan, L.: "A Simple Way for Improving the Identification of the Central Fringe in a Fibre-Optic White Light Interferometer", Optics and Laser Technology, Vol. 29, No. 7, pp. 365-369, 1997.

91. "Optical Sensor Technologies", Chapter 6, pp.4, 1999, http://itri.loyola.edu/opto/c6_s3.htm.

92. Dakin, J. and Culshaw, B.: "Optical Fiber Sensors", Vol. 1, Chapter 6, Norwood, pp.190-200, 1988, ISBN 0-89006-317-6.

93. Egami, C., Takeda, K., Isai, M. and Ogita, M.: "Evanescent-Wave Spectroscopic Fibre Optic PH Sensor", Optics Communications, Vol. 122 pp. 122-126, 1996.

94. Dakin, J. and Culshaw, B.: "Optical Fiber Sensors", Vol. 1, Chapter 9, Norwood, pp.305-307, 1988, ISBN 0-89006-317-6.

95. "Optical Sensor Technologies", Chapter 6, pp.12, 1999, http://itri.loyola.edu/opto/c6_s3.htm.

96. "Fibre Optic System", Systems and Sensors, pp. 2-4, http://floti.bell.ac.uk/MathsPhysics/optsens.htm.

97. Dakin, J. and Culshaw, B.: "Optical Fiber Sensors", Vol. 1, Chapter 6, Norwood, pp.200-203, 1988, ISBN 0-89006-317-6.

98. Khijwania, S.K. and Gupta, B.D.: "Maximum Achievable Sensitivity of the Fiber Optic Evanescent Field Absorption Sensor Based on the U-Shaped Probe", Optics Communications, Vol. 175 pp. 125-137, 2000.

99. Rogers, A.: "Distributed Optical Fibre Sensing", Meas. Sci. Technol. Vol 10, IOP Publishing Ltd., pp. R81-R83, 1999.

100. Du, W., Tao, X.M., Tam, H.Y. and Choy, C.L.: "Fundamentals and Applications of Optical Fiber Bragg Grating Sensors to Textile Structural Composites", Composite Structures, Vol. 42, pp. 217-229, 1998.

101. Crosby, P.A., Powell, G.R., Fernando, G.F., France, C.M., Spooncer, R.C. and Waters, D.N.: "In Situ Cure Monitoring of Epoxy Resins Using Optical Fibre Sensors", Smart Mater. Struct. Vol. 5, pp. 415-428, 1996.

102. Tobiska, P., Chomat, M., Matejec, V. Berkova, D. and Huttel, I.: "Investigation of Fiber-Optic Evanescent-Wave Sensors for Detection of Liquid Hydrocarbons", Sensors and Actuators, B51, pp. 152-158, 1998.

103. Schwotzer, G., Latka, I., Lehmann, H. and Willsch, R.: "Optical Sensing of Hydrocarbons in Air or in Water Using UV Absorption in the Evanescent Field of Fibers", Sensors and Actuators, B38-39, pp. 150-153, 1997.

104. Tabib-Azar, M., Sutapun, B., Petrick, R. and Kazemi, A.: "Highly Sensitive Hydrogen Sensors Using Palladium Coated Fiber Optics with Exposed Cores and Evanescent Field Interactions", Sensors and Actuators, B, Vol 56, pp. 158-163, 1999.

105. Zaatar, Y., Zaouk, D., Bechara, J., Khoury, A., Llinaress, C. and Charles, J.P.: "Fabrication and Characterisation of an Evanescent Wave Fiber Optic Sensor for Air Pollution Control", Materials for Science and Engineering, B74, pp. 296-298, 2000.

106. Stewart, G., Jin, W. and Culshaw, B.: "Prospects for Fibre-optic Evanescent-Field Gas Sensors Using Absorption in the Near Infrared", Sensors and Actuators, B38-39, pp. 42-47, 1997.

107. Khijwania, S.K. and Gupta, B.D.: "Fiber Optic Evanescent Field Absorption Sensor with High Sensitivity and Linear Dynamic Range", Optics Communications, Vol. 152 pp. 259-262, 1998.

108. Sekimoto, S., Nakagawa, H., Okazaki, S., Fukuda, K., Asakura, S., Shigemori, T. and Takahashi, S.: "A fiber-Optic Evanescent-Wave Hydrogen Gas Sensor Using Palladium-Supported Tungsten Oxide", Sensors and Actuators, B66, pp. 142-145, 2000.

109.	Tabib-Azar, M., Sutapun, B., Srikhirin, T., Lando, J. and Adamovsky, G.: Fiber Optic Electric Field Sensors Using Polymer-Dispersed Liquid Crystal Coatings and Evanescent Field Interactions", Sensors and Actuators, B84, pp. 134-139, 2000.

110.	Hale, Z.M. and Payne, F.P.: "Demonstration of an Optimised Evanescent Field Optical Fibre Sensor", Analytica Chemica Acta 293, pp. 49-54, 1994.

111.	Udd, E.: "Fiber Optic Sensors An Introduction for Engineers and Scientists", Chapter 2, Wiley, pp. 32, 1991, ISBN 0-471-83007-0.

112.	Degrieck, J. and De Waele, W.: "Embedded Optical Fibre Sensors for the Permanent Monitoring of Filament Wound Pressure Vessels", NDT.net, Vol. 4, No. 3, 2000, http://www.ndt.net/article/v04n03/5/5.htm.

113.	Takahashi, N.: "Development of an Optical Fibre Hydrophone with Fibre Bragg Grating", Ultrasonics, Vol. 38, pp. 581-585, 2000.

114.	Kersey, A.D.: "A Review of Recent Developments in Fiber Optic Sensor Technology", Optical Fiber Technology, Vol. 2, pp.304-311, 1996.

115.	Giles, C.C.: "Lightwave Applications of Fiber Bragg Gratings", JOLT, Vol. 15, No. 8, pp.1391-1403, 1997.

116.	Meltz, G., Hewlett, S.J. and Love, J.D.: "Fibre Grating Evanescent-Wave Sensors", SPIE, Vol. 2836, pp.342-350, 1996.

117.	Meltz, G., Morey, W.W. and Dunphy, J.R..: "Fibre Bragg Grating Chemical Sensor", SPIE, Vol. 1587, pp.350-361, 1991.

118.	Hathaway, M.W., Fisher, N.E., Webb, D.J., Pannell, C.N., Jackson, D.A., Gavrilov, L.R., Hand, J.W., Zhang, L. and Bennion, I.: "Combined Ultrasound and Temperature Sensing Using a Fibre Bragg Grating", Optical Communications, Vol. 171 pp. 225-231, 1999.

119.	Rogers, A.: "Distributed Optical Fibre Sensing", Meas. Sci. Technol. Vol 10, IOP Publishing Ltd., pp. R84-R85, 1999.

120.	Sutapun, B., Tabib-Azar, M. and Kazemi, A.: "Pd-Coated Elastooptic Fibre Optic Bragg Grating Sensors for Multiplexed Hydrogen sensing", Sensors and Actuators, B60, pp. 27-34, 1999.

121.	Shi, W.J., Ning, Y.N., Grattan, K.T.V. and Palmer, A.W.: "The Wavelength Measurement Error Induced by Using Interferomic Detection Schemes for Fibre-Grating Sensors", Meas. Sci. Technol. Vol 8, IOP Publishing Ltd., pp. 217-220, 1997.

122.	Guemes, J.A., Diaz-Carrillo, S., Menendez, J.M., Pardo de Vera, C., Vionis, P., Scherer, R., Bercebal, D. and Cuerva, A.: "Strain and Damage Monitoring of Wind Turbine Blades by Piezoelectrics and Fiber Optic Sensors", 1999, http://www.dmpa.upm.es/smart/napoles.htm.

123.   Dakin, J. and Culshaw, B.: "Optical Fiber Sensors", Vol. 1, Chapter 9, Norwood, pp.288-302, 1988, ISBN 0-89006-317-6.

124.   Dakin, J. and Culshaw, B.: "Optical Fiber Sensors", Vol. 1, Chapter 9, Norwood, pp.307-309, 1988, ISBN 0-89006-317-6.

125.   Selvarajan, A.: "Fiber Optic Sensors and Their Applications", pp.13-17, 1999, http://www.ntu.edu.sg/mpe/resear...sensors/sensors/fos/fosselva.html.

126.   Hill, K.O., Fujii, Y., Johnson, D.C. and Kawasaki, B.S.: "Photo-Sensitivity in Optical Fiber Wavguides: Application to Reflection Filter Fabrication", Appl. Phys Lett., Vol. 32, pp. 647-649, 1978.

127.   Kawasiki, B.S., Hill, K.O., Johnson, D.C. and Fujii, Y.: "Narrow-Band Bragg Reflectors in Optical Fibers", Optics Letters, Vol. 3, pp. 66-68, 1978.

128.   Hill, K.O. and Meltz, G.:"Fiber Bragg Grating Technology Fundamentals and Overview", JOLT, Vol 15, No. 8, pp.1263, 1997.

129.   Hill, K.O. and Meltz, G.:"Fiber Bragg Grating Technology Fundamentals and Overview", JOLT, Vol 15, No. 8, pp.1263-1265, 1997.

130.   Meltz, G., Morey, W.W. and Glenn, W.H.: "Formation of Bragg Gratings in Optical Fibers by a Transverse Holographic Method", Opt. Lett., Vol. 14, pp. 823-825, 1989.

131.   Goff, D.R.: "Fiber Optic Reference Guide", Chapter 3, Butterworth-Heinemann, pp. 24, 1996, ISBN 0-240-80263-2.

132.   Wolfbeis, O.S.: "Fiber Optic Chemical Sensors and Biosensors", Vol. 1, Chapter 4, CRC Press Inc., pp. 116, 1991, ISBN 0-8493-5508-7.

133.   Grattan, K.T.V. and Meggitt, B.T.: "Optical Fiber Sensor Technology", Chapter 2, Chapman and Hall, pp. 29, 1995, ISBN 0-412-59210-X.

134.   Wilson, J. and Hawkes, J.F.B.: "Optoelectronics: An Introduction", Chapter 8, Prentice-Hall, pp. 363, 1983, ISBN 0-13-63895-5.

135.   Kao, K.: "Optical Fiber Systems", Chapter 1, McGraw-Hill, pp. 12, 1986, ISBN 0-07-Y66433-1.

136.   Senior, J.M.: "Optical Fiber Communications: Principles and Practice", 2nd Edition, Chapter 3, Prentice Hall, pp. 89,91, 1992, ISBN 0-13635-426-2.

137.   Keiser, G.: "Optical Fiber Communications", 3rd Edition, Chapter 1, McGraw-Hill, pp. 7, 12, 2000, ISBN 0-07-232101-6.

138.   Keiser, G.: "Optical Fiber Communications", 3rd Edition, Chapter 3, McGraw-Hill, pp. 93, 2000, ISBN 0-07-232101-6.

139.   Ungar, S.: "Fibre Optics: Theory and Application", Chapter 1, John Wiley & Sons Ltd., pp. 5, 1997, ISBN 0-471-92758-9.

140.   Hecht, J.: "Understanding Fiber Optics", Third Edition, Chapter 5, Prentice-Hall, pp.85, 1999, ISBN 0-13-956145-5.

141.   Starodubov, D.S., Grubsky, V., Feinberg, J., Kobrin, B. and Juma, S.: "Bragg Grating Fabrication in Germanosilicate Fibers by Use of Near-UV Light: A New Pathway for Refractive Index Changes", Optics Letters, Vol. 22, No. 14, pp. 1086-1088, 1997.

142.   De Vries, M., Bhatia, V., D'Alberto, T., Arya, V. and Claus, R.O.: "Photoinduced Grating-Based Optical Fiber Sensors for Structural Analysis and Control", Engineering Structures, Vol 20, No. 3, pp. 206-208, 1998.

143.   Dockney, M.L., James, S.W. and Tatum, R.P.: "Fibre Bragg Gratings Fabricated Using a Wavelength Tunable Laser Source and a Phase Mask Based Interferometer", Meas. Sci. Technol., Vol. 7, pp. 445-448, 1996.

144.   Handerek, V.A., "Optical Fibre Bragg Gratings: a New Sensor Multiplexing Tool", Sensor Review, Vol. 18 No. 1, pp. 41, 1998.

145.   Laming, R.I. and Loh, W.H.: "Fibre Bragg Gratings; Application to Lasers and Amplifiers", ORC Research Review, pp. 2, 1997, http://www.orc.soton.ac.uk/orchelp/pubs.

146.   Hecht, J.: "Understanding Fiber Optics", Third Edition, Chapter 7, Prentice-Hall, pp.131-132, 1999, ISBN 0-13-956145-5.

147.   Senior, J.M.: "Optical Fiber Communications: Principles and Practice", 2nd Edition, Chapter 4, Prentice Hall, pp. 180, 183, 1992, ISBN 0-13635-426-2.

148.   Keiser, G.: "Optical Fiber Communications", 3rd Edition, Chapter 2, McGraw-Hill, pp. 41, 2000, ISBN 0-07-232101-6.

149.   Hecht, J.: "Understanding Fiber Optics", Third Edition, Chapter 4, Prentice-Hall, pp.57, 1999, ISBN 0-13-956145-5.

150.   Giles, C.R.: "Lightwave Applications of Fibre Bragg Gratings", JOLT, Vol. 15, No. 8, pp.1391 1997.

151.   Hecht, J.: "Understanding Fiber Optics", Third Edition, Chapter 7, Prentice-Hall, pp.133-134, 1999, ISBN 0-13-956145-5.

152.   Hill, K.O. and Meltz, G.:"Fiber Bragg Grating Technology Fundamentals and Overview", JOLT, Vol 15, No. 8, pp.1267, 1997.

153.   Kersey, A.D., Davis, M.A., Patrick, H.J., LeBlanc, M., Koo, K.P., Askins, C.G., Putnam, M.A. and Friebele, E.J.: "Fibre Grating Sensors", JOLT, Vol. 15, No. 8, pp.1442, 1997.

154.   Kersey, A.D.: "A Review of Recent Developments in Fiber Optic Sensor Technology", Optical Fiber Technology, Vol. 2, pp.304, 1996.

155.   Keiser, G.: "Optical Fiber Communications", 3rd Edition, Chapter 2, McGraw-Hill, pp. 41,42, 2000, ISBN 0-07-232101-6.

156.   Hecht, J.: "Understanding Fiber Optics", Third Edition, Chapter 7, Prentice-Hall, pp.132, 1999, ISBN 0-13-956145-5.

157.   Mizrahi, V. and Sipe, J.E.: "Optical Properties of Photosensitive Fiber Phase Gratings", JOLT, Vol 11, No. 10, pp.1514, 1993.

158.   Kersey, A.D.:"A Review of Recent Developments in Fiber Optic Sensor Technology", Optical Fiber Technology, Vol 2, pp.304-305, 1996.

159.   Hill, K.O. and Meltz, G.:"Fiber Bragg Grating Technology Fundamentals and Overview", JOLT, Vol 15, No. 8, pp.1273, 1997.

160.   Hill, K.O. and Meltz, G.:"Fiber Bragg Grating Technology Fundamentals and Overview", JOLT, Vol 15, No. 8, pp.1272, 1997.

161.   Kersey, A.D., Davis, M.A., Patrick, H.J., LeBlanc, M., Koo, K.P., Askins, C.G., Putnam, M.A. and Friebele, E.J.: "Fibre Grating Sensors", JOLT, Vol. 15, No. 8, pp.1442-1446, 1997.

162.   Morey, W.W., Dunphy, J.R. and Meltz, G.: "Multiplexing Fiber Bragg Grating Sensors", SPIE, Vol. 1586, pp.216-223, 1991.

163.   Tolpegin, B and Jones, M.: "Long-Period Gratings", Photonics Spectra, pp.104, 1997.

164.   Patrick, H.J., Kersey,A.D. and Bucholtz,F.: "Analysis of the Response of Long Period Fiber Gratings to External Index of Refraction", JOLT, Vol.16, No. 9, pp. 1607, 1998.

165.   Bhatia, V. and Vengsarkar, A.M.: "Optical Fiber Long Period Grating Sensors", Optics Letters, Vol. 21, No.9, pp.693, 1996.

166.   Kueh, R.M., Parnas, R.S. and Advani, S.G.: "A Methodology for Using Long-Period Gratings and Mold-Filling Simulations to Minimizs the Intrusiveness of Flow Sensors in Liquid Composite Molding", Composites Science and Technology, Vol. 62, pp.312, 2002.

167.   Cole, M.J., Aina, S., Durkin, M., Ibsen, M., Vaninetti, L., Gusmeroli, V. and Laming, R.I. : "Design and Application of Long Continously Chirped Fibre Gratings", ORC Research Review, pp.1, 1997, http://www.orc.soton.ac.uk/orchelp/pubs.

168. Asseh, A., Storoy, H., Sahlgren, B.E., Sandgren, S. and Stubbe, R.A.H.: "A Writing Technique for Long Fibre Bragg Gratings with Complex Reflectivity Profiles", JOLT, Vol.15, No. 8, pp. 1419, 1997.

169. Chen, K.P. and Herman, P.R.: "Fabrication of Long-Period Fiber Gratings with 157-nm F_2 Laser Radiation", OSA Tech. Digest, BThC19, 2001.

170. Grubsky, V., Skorucak, A., Starodubov, D.S. and Feinburg, J.: "Fabrication of Long-Period Gratings with No Harmonics", IEE Photonics Technology Letters, Vol. 11, No. 1, 1999.

171. Grubsky, V., Skorucak, A., Starodubov, D.S. and Feinburg, J.: "Fabrication of Spectrally Clean Long-Period Grating Filters", Int. Conf. On Integrated Optics and Optical Fibre Communications OFC/IOOC 99, Technical Digest, Vol. 4, pp. 174-176, 1999.

172. Patrick, H.J., Kersey,A.D. and Bucholtz,F.: "Analysis of the Response of Long Period Fiber Gratings to External Index of Refraction", Journal of Lightwave Technology, Vol.16, No. 9, pp.1608, 1998.

173. Jang, J.N., Kim, H.G., Shin, S.G., Kim, M.S., Lee, S.B. and Kwack, K.H.: "Effects of Hydrogen Molecule Diffusion on LP_{0m} Mode Coupling of Long-Period Gratings", Journal of Non-Crystalline Solids, Vol. 259, pp. 156-164, 1999.

174. Kersey, A.D., Davis, M.A., Patrick, H.J., LeBlanc, M., Koo, K.P., Askins, C.G., Putnam, M.A. and Friebele, E.J.: "Fibre Grating Sensors", JOLT, Vol. 15, No. 8, pp.1455, 1997.

175. Allsop, T, Zhang, L. and Bennion, I.: "Detection of Organic Compounds in Paraffin by a Long-Period Fiber Grating Optical Sensor with Optimized Sensitivity", Optics Communications, Vol. 191, pp.182, 2001.

176. Patrick, H.J., Kersey,A.D. and Bucholtz,F.: "Analysis of the Response of Long Period Fiber Gratings to External Index of Refraction", Journal of Lightwave Technology, Vol.16, No. 9, pp.1606, 1998.

177. Tolpegin, B and Jones, M.: "Long-Period Gratings", Photonics Spectra, pp.106, 1997.

178. Chen, L.R.: "Phase Shifted Long-Period Gratings by Refractive Index-Shifting", Optics Communications, Vol. 200, pp.187, 2001.

179. Jang, J.N., Kim, H.G., Shin, S.G., Kim, M.S., Lee, S.B. and Kwack, K.H.: "Effects of Hydrogen Molecule Diffusion on LP_{0m} Mode Coupling of Long-Period Gratings", Journal of Non-Crystalline Solids, Vol. 259, pp.157, 1999.

180. Bhatia, V. and Vengsarkar, A.M.: "Optical Fiber Long Period Grating Sensors", Optics Letters, Vol. 21, No.9, pp.692, 1996.

181. Allsop, T., Zhang, L. and Bennion, I.: "Detection of Organic Compounds in Paraffin by a Long-Period Fiber Grating Optical Sensor with Optimized Sensitivity", Optics Communications, Vol. 191, pp.181, 2001.

182. Erdogan, T.: "Cladding-Mode Resonances in Short-and-Long-Period Fiber Grating Filters",J.Opt.Soc.Am.A, Vol.14, No.8, pp.1762, 1997.

183. Erdogan, T.: "Cladding-Mode Resonances in Short-and-Long-Period Fiber Grating Filters",J.Opt.Soc.Am.A, Vol.14, No.8, pp.1765, 1997.

184. "Pulse Spreading", pp. 2, http//floti.bell.ac.uk/MathsPhysics/4pulse.htm.

185. Hecht, E.: "Optics", Second Edition, Chapter 10, Addison-Wesley, pp. 399, 1987, ISBN 0-201-11611-1.

186. Wolfbeis, O.S.: "Fiber Optic Chemical Sensors and Biosensors", Vol. 1, Chapter 2, CRC Press Inc., pp. 243, 1991, ISBN 0-8493-5508-7.

187. Grattan, K.T.V. and Meggitt, B.T.: "Optical Fiber Sensor Technology", Chapter 2, Chapman and Hall, pp. 23, 1995, ISBN 0-412-59210-X.

188. Keiser, G.: "Optical Fiber Communications", 3rd Edition, Chapter 2, McGraw-Hill, pp. 44, 2000, ISBN 0-07-232101-6.

189. Goff, D.R.: "Fiber Optic Reference Guide", Chapter 3, Butterworth-Heinemann, pp. 20, 1996, ISBN 0-240-80263-2.

190. Hecht, E.: "Optics", Second Edition, Chapter 4, Addison-Wesley, pp. 99-104, 1987, ISBN 0-201-11611-1.

191. Patrick, H.J., Kersey, A.D., Bucholtz, F. and Ewing, K.J.: "Chemical Sensor Basesd on Long Period Fiber Grating Response to Index of Refraction", in Proc. Conf. Lasers Electro-Opt., Vol.11, pp.420-421, 1997.

192. Patrick, H.J., Kersey, A.D. and Bucholtz, F.: "Analysis of the Response of Long Period Fiber Gratings to External Index of Refraction", Journal of Lightwave Technology, Vol.16, No. 9, pp.1608-1610, 1998.

193. Patrick, H.J., Kersey, A.D. and Bucholtz, F.: "Analysis of the Response of Long Period Fiber Gratings to External Index of Refraction", Journal of Lightwave Technology, Vol.16, No. 9, pp. 1606-1611, 1998.

194. Chen, Y., Palmer, J., Davis, P. and Li, L.: "High Order Harmonic Reflections from Long Pitch Fibre Grating", Electronics Letters, Vol.34, No.1, pp.114-116, 1998.

195. Hecht, E.: "Optics", Second Edition, Chapter 9, Addison-Wesley, pp.373, 1987, ISBN 0-201-11611-1.

196. Pollock, C.R.: "Fundamentals of Optoelectronics", Irwin, pp.357-382, 1995, ISBN 0-256-10104-3.

197.   Selvarajan,A.: "Fiber Optic Sensors and Their Applications", pp.3, 1999, http://www.ntu.edu.sg/mpe/resear...sensors/sensors/fos/fosselva.html.

198.   Horowitz, P. and Hill, W.: "The Art of Electronics", Second Edition, Cambridge University Press, pp.998-1001, 1989, ISBN 0-521-37095-7.

199.   http://www.sciencedirect.com/science...5=a1ae7f41f68437108bbc0f70a2f801 07, 1999.

200.   Ezbiri, A. and Tatam, R.P.: "Interrogation of Low Finesse Optical Fibre Extrinsic Fabry-Perot Interferometers Using a Four Wavelength Technique", Meas. Sci. Technol. Vol 7, IOP Publishing Ltd., pp. 119, 1996.

201.   Seok, H.Y., Richardson, D.J. and Kim, B.Y.: "Interrogation of Fiber Grating Sensor Arrays Using a Wavelength-Swept Fiber Laser", Internal Report Optoelectronics Research Centre, University of Southampton, 1997.

202.   Erdogan, T.: "Fiber Grating Spectra" JOLT, Vol.15, No.8, pp.1277-1293, 1997.

203.   Patrick, H.J., Kersey,A.D. and Bucholtz,F.: "Analysis of the Response of Long Period Fiber Gratings to External Index of Refraction", Journal of Lightwave Technology, Vol.16, No. 9, pp.1609-1611, 1998.

204.   Okushi, T.: "Optical Fibers", Chapter 4, Academic Press, pp.48-65, 1982, ISBN 0-12-525260-9.

205.   Yariv, A.: "Optical Electronics in Modern Communications", Fifth Edition, Chapter 3, Oxford University Press, pp.76-96, 1996, ISBN 0-19-510626-1.

206.   Tsao, C.: "Optical Fibre Waveguide Analysis", Oxford University Press, pp.298-369, 1992, ISBN 0-19-856344-2.

207.   Erdogan, T.: "Cladding-Mode Resonances in Short-and-Long-Period Fiber Grating Filters",J.Opt.Soc.Am.A, Vol.14, No.8, pp.1760-1773, 1997.

208.   Rogers, A.: "Distributed Optical Fibre Sensing", Meas. Sci. Technol. Vol 10, IOP Publishing Ltd., pp. R77-R78, 1999.

209.   Bhatti, S.: "Optical Fibre Waveguide" pp. 2, 1995, http://www.cs.ucl.ac.uk/staff/S.Bhatti/D51-notes/node21.html.

210.   Wilson, J. and Hawkes, J.F.B.: "Optoelectronics: An Introduction", Chapter 9, Prentice-Hall, pp. 392-393, 1983, ISBN 0-13-63895-5.

211.   Fowles, G.R.: "Intorduction to Modern Optics", 2nd Edition, Chapter 2, Constable & Co. Ltd., pp. 46-47, 1989, ISBN 0-486-65957-7.

212.	Senior, J.M.: "Optical Fiber Communications: Principles and Practice", 2nd Edition, Chapter 2, Prentice Hall, pp. 17, 1992, ISBN 0-13635-426-2.

213.	Hecht, J.: "Understanding Fiber Optics", Third Edition, Chapter 2, Prentice-Hall, pp.25, 1999, ISBN 0-13-956145-5.

214.	Hecht, J.: "Understanding Fiber Optics", Third Edition, Chapter 5, Prentice-Hall, pp.89, 1999, ISBN 0-13-956145-5.

215.	Wolfbeis, O.S.: "Fiber Optic Chemical Sensors and Biosensors", Vol. 1, Chapter 6, CRC Press Inc., pp. 242, 1991, ISBN 0-8493-5508-7.

216.	"Total Internal Reflection", http://floti.bell.ac.uk/MathsPhysics/1total.htm.

217.	Keiser, G.: "Optical Fiber Communications", 3rd Edition, Chapter 2, McGraw-Hill, pp. 41, 45, 2000, ISBN 0-07-232101-6.

218.	Senior, J.M.: "Optical Fiber Communications: Principles and Practice", 2nd Edition, Chapter 2, Prentice Hall, pp. 27, 1992, ISBN 0-13635-426-2.

219.	Madsen, C.K. and Zhao, J.H.: "Optical Filter Design and Analysis: A Signal Processing Approach", Chapter 2, John Wiley & Sons, pp. 41, 1999, ISBN 0-471-18373-3.

220.	Senior, J.M.: "Optical Fiber Communications: Principles and Practice", 2nd Edition, Chapter 2, Prentice Hall, pp. 28, 1992, ISBN 0-13635-426-2.

221.	Dakin, J. and Culshaw, B.: "Optical Fiber Sensors", Vol. 1, Chapter 9, Norwood, pp.280, 1988, ISBN 0-89006-317-6.

222.	Wilson, J. and Hawkes, J.F.B.: "Optoelectronics: An Introduction", Chapter 8, Prentice-Hall, pp. 343, 1983, ISBN 0-13-63895-5.

223.	Keiser, G.: "Optical Fiber Communications", 3rd Edition, Chapter 2, McGraw-Hill, pp. 44-45, 2000, ISBN 0-07-232101-6.

224.	Madsen, C.K. and Zhao, J.H.: "Optical Filter Design and Analysis: A Signal Processing Approach", Chapter 2, John Wiley & Sons, pp. 40, 1999, ISBN 0-471-18373-3.

225.	Senior, J.M.: "Optical Fiber Communications: Principles and Practice", 2nd Edition, Chapter 2, Prentice Hall, pp. 27, 28, 1992, ISBN 0-13635-426-2.

226.	Dakin, J. and Culshaw, B.: "Optical Fiber Sensors", Vol. 1, Chapter 3, Norwood, pp.27, 1988, ISBN 0-89006-317-6.

227.	Fowles, G.R.: "Introduction to Modern Optics", 2nd Edition, Chapter 2, Constable & Co. Ltd., pp. 24, 1989, ISBN 0-486-65957-7.

228.	Keiser, G.: "Optical Fiber Communications", 3rd Edition, Chapter 2, McGraw-Hill, pp. 28, 2000, ISBN 0-07-232101-6.

229.   Hecht, J.: "Understanding Fiber Optics", Third Edition, Chapter 4, Prentice-Hall, pp.76, 1999, ISBN 0-13-956145-5.

230.   Dakin, J. and Culshaw, B.: "Optical Fiber Sensors", Vol. 1, Chapter 9, Norwood, pp.279, 1988, ISBN 0-89006-317-6.

231.   Rogers, A.: "Distributed Optical Fibre Sensing", Meas. Sci. Technol. Vol 10, IOP Publishing Ltd., pp. R78, 1999.

232.   Senior, J.M.: "Optical Fiber Communications: Principles and Practice", 2nd Edition, Chapter 2, Prentice Hall, pp. 20, 1992, ISBN 0-13635-426-2.

233.   Senior, J.M.: "Optical Fiber Communications: Principles and Practice", 2nd Edition, Chapter 2, Prentice Hall, pp. 36, 1992, ISBN 0-13635-426-2.

234.   Okushi, T.: "Optical Fibers", Chapter 4, Academic Press, pp.59, 1982, ISBN 0-12-525260-9.

235.   Senior, J.M.: "Optical Fiber Communications: Principles and Practice", 2nd Edition, Chapter 2, Prentice Hall, pp. 36,37, 1992, ISBN 0-13635-426-2.
236.   Yariv, A.: "Optical Electronics in Modern Communications", Fifth Edition, Chapter 3, Oxford University Press, pp.89, 1996, ISBN 0-19-510626-1.

237.   Erdogan, T.: "Cladding-Mode Resonances in Short-and-Long-Period Fiber Grating Filters",J.Opt.Soc.Am.A, Vol.14, No.8, pp.1761, 1997.

238.   Yariv, A.: "Optical Electronics in Modern Communications", Fifth Edition, Chapter 3, Oxford University Press, pp.89-99, 1996, ISBN 0-19-510626-1.
239.   Marcuse, D., "Theory of Dielectric Optical Waveguides", 2nd Edition, Chapter 1, Academic Press Ltd., pp. 8, 1991, ISBN 0-12-470951-6.

240.   Madsen, C.K. and Zhao, J.H.: "Optical Filter Design and Analysis: A Signal Processing Approach", Chapter 2, John Wiley & Sons, pp. 35, 1999, ISBN 0-471-18373-3.

241.   Senior, J.M.: "Optical Fiber Communications: Principles and Practice", 2nd Edition, Chapter 2, Prentice Hall, pp. 37, 1992, ISBN 0-13635-426-2.

242.   Senior, J.M.: "Optical Fiber Communications: Principles and Practice", 2nd Edition, Chapter 2, Prentice Hall, pp. 38, 1992, ISBN 0-13635-426-2.

243.   Keiser, G.: "Optical Fiber Communications", 3rd Edition, Chapter 2, McGraw-Hill, pp. 59, 2000, ISBN 0-07-232101-6.

244.   Okushi, T.: "Optical Fibers", Chapter 4, Academic Press, pp.63, 1982, ISBN 0-12-525260-9.

245.   Keiser, G.: "Optical Fiber Communications", 3rd Edition, Chapter 2, McGraw-Hill, pp. 52, 2000, ISBN 0-07-232101-6.

246.   Yariv, A.: "Optical Electronics in Modern Communications", Fifth Edition, Chapter 3, Oxford University Press, pp.83, 1996, ISBN 0-19-510626-1.

247.   Ungar, S.: "Fibre Optics: Theory and Application", Chapter 3, John Wiley & Sons Ltd., pp. 42, 1997, ISBN 0-471-92758-9.

248.   Yariv, A.: "Optical Electronics in Modern Communications", Fifth Edition, Chapter 3, Oxford University Press, pp.87, 1996, ISBN 0-19-510626-1.

249.   Keiser, G.: "Optical Fiber Communications", 3rd Edition, Chapter 2, McGraw-Hill, pp. 55, 2000, ISBN 0-07-232101-6.

250.   Okushi, T.: "Optical Fibers", Chapter 4, Academic Press, pp.58, 1982, ISBN 0-12-525260-9.

251.   Yariv, A.: "Optical Electronics in Modern Communications", Fifth Edition, Chapter 6, Oxford University Press, pp.189, 1996, ISBN 0-19-510626-1.

252.   Okushi, T.: "Optical Fibers", Chapter 4, Academic Press, pp.57, 1982, ISBN 0-12-525260-9.

253.   Keiser, G.: "Optical Fiber Communications", 3rd Edition, Chapter 2, McGraw-Hill, pp. 57, 2000, ISBN 0-07-232101-6.

254.   Ungar, S.: "Fibre Optics: Theory and Application", Chapter 3, John Wiley & Sons Ltd., pp. 44, 1997, ISBN 0-471-92758-9.

255.   Yariv, A.: "Optical Electronics in Modern Communications", Fifth Edition, Chapter 3, Oxford University Press, pp.83 & 95, 1996, ISBN 0-19-510626-1.

256.   Fontaine, F.: "Optical Fibers as Open-Boundary Waveguides", pp. 5, http://www.cooper.edu/engineering/...way/ee/solidmat/modelc4/node.1.html.

257.   Senior, J.M.: "Optical Fiber Communications: Principles and Practice", 2nd Edition, Chapter 2, Prentice Hall, pp. 61, 1992, ISBN 0-13635-426-2.

258.   Keiser, G.: "Optical Fiber Communications", 3rd Edition, Chapter 3, McGraw-Hill, pp. 125, 2000, ISBN 0-07-232101-6.

259.   Ungar, S.: "Fibre Optics: Theory and Application", Chapter 5, John Wiley & Sons Ltd., pp. 93, 1997, ISBN 0-471-92758-9.

260.   Hecht, J.: "Understanding Fiber Optics", Third Edition, Chapter 4, Prentice-Hall, pp.70-71, 1999, ISBN 0-13-956145-5.

261.   Goff, D.R.: "Fiber Optic Reference Guide", Chapter 5, Butterworth-Heinemann, pp. 42-43, 1996, ISBN 0-240-80263-2.

262. Hecht, J.: "Understanding Fiber Optics", Third Edition, Chapter 4, Prentice-Hall, pp.62, 1999, ISBN 0-13-956145-5.

263. Senior, J.M.: "Optical Fiber Communications: Principles and Practice", 2nd Edition, Chapter 2, Prentice Hall, pp. 43,44, 1992, ISBN 0-13635-426-2.

264. Erdogan, T.: "Cladding-Mode Resonances in Short-and-Long-Period Fiber Grating Filters",J.Opt.Soc.Am.A, Vol.14, No.8, pp.1767, 1997.

265. Okushi, T.: "Optical Fibers", Chapter 4, Academic Press, pp. 99, 1982, ISBN 0-12-525260-9.

266. Marcuse, D.: "Theory of Dielectric Optical Waveguides", 2nd Edition, Chapter 1, Academic Press Ltd., pp. 5, 1991, ISBN 0-12-470951-6.

267. Hecht, E.: "Optics", Second Edition, Appendix 1, Addison-Wesley, pp.621, 1987, ISBN 0-201-11611-1.

268. Wolfbeis, O.S.: "Fiber Optic Chemical Sensors and Biosensors", Vol. 1, Chapter 1, CRC Press Inc., pp.16, 1991, ISBN 0-8493-5508-7.

269. Dakin, J. and Culshaw, B.: "Optical Fiber Sensors", Vol. 1, Chapter 3, Norwood, pp.103, 1988, ISBN 0-89006-317-6.

270. Udd, E.: "Fiber Optic Sensors An Introduction for Engineers and Scientists", Chapter 2, Wiley, pp. 12, 1991, ISBN 0-471-83007-0.

271. Fowles, G.R.: "Introduction to Modern Optics", 2nd Edition, Chapter 2, Constable & Co. Ltd., pp. 23, 1989, ISBN 0-486-65957-7.

272. Jacobsen, C.: "Maxwell's Equations Again", pp.2, 1999, http://xray1.physics.sunysb.edu/~jacobsen/p352s99/refind/node3.html.

273. Lacroix, S.: "Fiber Optics and All-Fiber Components", Section 2.2.1, pp. 1, 1996, http://opt-fibres.phys.polymtl.ca/Fibers_html/node10.html.

274. Wolfbeis, O.S.: "Fiber Optic Chemical Sensors and Biosensors", Vol. 1, Chapter 2, CRC Press Inc., pp. 26,38, 1991, ISBN 0-8493-5508-7.

275. Fowles, G.R.: "Introduction to Modern Optics", 2nd Edition, Chapter 2, Constable & Co. Ltd., pp. 25, 1989, ISBN 0-486-65957-7.

276. Keiser, G.: "Optical Fiber Communications", 3rd Edition, Chapter 2, McGraw-Hill, pp. 37, 48, 2000, ISBN 0-07-232101-6.

277. Madsen, C.K. and Zhao, J.H.: "Optical Filter Design and Analysis: A Signal Processing Approach", Chapter 2, John Wiley & Sons, pp. 28, 1999, ISBN 0-471-18373-3.

278. Senior, J.M.: "Optical Fiber Communications: Principles and Practice", 2nd Edition, Chapter 2, Prentice Hall, pp. 31, 1992, ISBN 0-13635-426-2.

279. Fontaine, F.: "Optical Fibers as Open-Boundary Waveguides", pp. 4, http://www.cooper.edu/engineering/...way/ee/solidmat/modelc4/node.1.html.

280. Yariv, A.: "Optical Electronics in Modern Communications", Fifth Edition, Chapter 3, Oxford University Press, pp.77, 78, 1996, ISBN 0-19-510626-1.

281. Senior, J.M.: "Optical Fiber Communications: Principles and Practice", 2nd Edition, Chapter 2, Prentice Hall, pp. 25, 1992, ISBN 0-13635-426-2.

282. Ungar, S.: "Fibre Optics: Theory and Application", Chapter 3, John Wiley & Sons Ltd., pp. 38, 1997, ISBN 0-471-92758-9.

283. http://www.cooper.edu/engineering/...way/ee/solidmat/modelc4/node.1.html.

284. Dakin, J. and Culshaw, B.: "Optical Fiber Sensors", Vol. 1, Chapter 6, Norwood, pp.201, 1988, ISBN 0-89006-317-6.

285. Dakin, J. and Culshaw, B.: "Optical Fiber Sensors", Vol. 1, Chapter 6, Norwood, pp.200, 1988, ISBN 0-89006-317-6.

286. McCall, M.: "On the Application of Coupled Mode Theory for Modelling Fiber Bragg Gratings", JOLT, Vol. 18, No. 2, pp.236-242, 2000.

287. Giles, C.R.: "Lightwave Applications of Fibre Bragg Gratings", JOLT, Vol. 15, No. 8, pp.1391-1393, 1997.

288. Ghatak, A.K. and Thyagarajan, K.: "Optical Electronics", Appendix G, Cambridge University Press, pp. 609-612, 1989, ISBN 0-521-30643-4.

289. Saleh, B.E.A. and Teich, M.C.: "Fundamentals of Photonics", Chapter 2, John Wiley & Sons Inc., pp. 60-62, 1991, ISBN 0-471-83965-5.

290. Erdogan, T.: "Fiber Grating Spectra" JOLT, Vol.15, No.8, pp.1278, 1997.

291. Hecht, J.: "Understanding Fiber Optics", Third Edition, Chapter 7, Prentice-Hall, pp.131, 1999, ISBN 0-13-956145-5.

292. Madsen, C.K. and Zhao, J.H.: "Optical Filter Design and Analysis: A Signal Processing Approach", Chapter 5, John Wiley & Sons, pp. 285, 1999, ISBN 0-471-18373-3.

293. De Vries, M., Bhatia, V., D'Alberto, T., Arya, V. and Claus, R.O.: "Photoinduced Grating-Based Optical Fiber Sensors for Structural Analysis and Control", Engineering Structures, Vol 20, No. 3, 1998.

294. Morey, W.W., Dunphy, J.R. and Meltz, G.: "Multiplexing Fiber Bragg Grating Sensors", SPIE, Vol. 1586, pp.219, 1991.

295. Guemes, J.A., Diaz-Carrillo, S., Menendez, J.M., Pardo de Vera, C., Vionis, P., Scherer, R., Bercebal, D. and Cuerva, A.: "Strain and Damage Monitoring of

Wind Turbine Blades by Piezoelectrics and Fiber Optic Sensors", pp. 1-5, 1999, http://www.dmpa.upm.es/smart/napoles.htm.

296. Morey, W.W., Dunphy, J.R. and Meltz, G.: "Multiplexing Fiber Bragg Grating Sensors", SPIE, Vol. 1586, pp.217, 1991.

297. Grattan, K.T.V. and Meggitt, B.T.: "Optical Fiber Sensor Technology", Chapter 2, Chapman and Hall, pp. 15, 1995, ISBN 0-412-59210-X.

298. Senior, J.M.: "Optical Fiber Communications: Principles and Practice", 2nd Edition, Chapter 2, Prentice Hall, pp. 63, 1992, ISBN 0-13635-426-2.

299. Ungar, S.: "Fibre Optics: Theory and Application", Chapter 2, John Wiley & Sons Ltd., pp. 12, 1997, ISBN 0-471-92758-9.

300. Madsen, C.K. and Zhao, J.H.: "Optical Filter Design and Analysis: A Signal Processing Approach", Chapter 2, John Wiley & Sons, pp. 68, 1999, ISBN 0-471-18373-3.

301. Madsen, C.K. and Zhao, J.H.: "Optical Filter Design and Analysis: A Signal Processing Approach", Chapter 2, John Wiley & Sons, pp. 42, 1999, ISBN 0-471-18373-3.

302. Yin, S., Chung, K. and Zhu, X.: "A Novel All-Optic Long-Period Grating Using a Unique Double-Cladding Layer", Optics Communications, Vol. 196, pp.185, 2001.

303. Shu, X., Huang, D.: "Highly Sensitive Chemical Sensor Based on the Measurement of the Separation of Dual Resonant Peaks in a 100-μm-Period Fiber Grating", Optics Communications 171, pp.69, 1999.

304. Jang, J.N., Kim, H.G., Shin, S.G., Kim, M.S., Lee, S.B. and Kwack, K.H.: "Effects of Hydrogen Molecule Diffusion on LP_{0m} Mode Coupling of Long-Period Gratings", Journal of Non-Crystalline Solids, Vol. 259, pp.156, 1999.

305. Qin, L., Wei, Z.X., Wang, Q.Y., Li, H.P., Zheng, W., Zhang, Y.S. and Gao, D.S.: "Compact Temperature Compensating Package for Long-Period Fiber Gratings", Optical Materials, Vol. 14, pp. 240, 2000.

306. Chen, L.R.: "Phase Shifted Long-Period Gratings by Refractive Index-Shifting", Optics Communications, Vol. 200, pp.188, 2001.

307. Yin, S., Chung, K. and Zhu, X.: "A Novel All-Optic Long-Period Grating Using a Unique Double-Cladding Layer", Optics Communications, Vol. 196, pp.182, 2001.

308. Shu, X., Zhang, L. and Bennion, I.: "Fabrication and Characterisation of Ultra-Long-Period Fibre Gratings", Optics Communications, Vol. 203, pp.278, 2002.

309. Lee, B.H., Liu, Y, Lee, S.B., Choi, S.S. and Jang, N.J.: "Displacements of the Resonant Peaks of a Long Period Fiber Grating Induced by a Change of Ambient Refractive Index", Optics Letters, Vol.22, No.23, pp.1769, 1997.

310. Ghatak, A.K. and Thyagarajan, K.: "Optical Electronics", Chapter 14, Cambridge University Press, pp. 447-453, 1989, ISBN 0-521-30643-4.

311. Hawkins, G.: "Predictive Bulk Substrate Characterisation", Chapter 2, pp.17, 2000, http://www.gary.hawkins.ukgateway.net/cahpter2.htm.

312. Fowles, G.R.: "Intorduction to Modern Optics", 2nd Edition, Chapter 2, Constable & Co. Ltd., pp. 51, 1989, ISBN 0-486-65957-7.

313. Keiser, G.: "Optical Fiber Communications", 3rd Edition, Chapter 2, McGraw-Hill, pp. 34-35, 2000, ISBN 0-07-232101-6.

314. Bahaa, E.A. and Teich, M.C.: "Fundamentals of Photonics", Chapter 6, John Wiley & Sons Inc., pp207-208.

315. Saleh, B.E.A. and Teich, M.C.: "Fundamentals of Photonics", Chapter 6, John Wiley & Sons Inc., pp. 206, 1991, ISBN 0-471-83965-5.

316. Saleh, B.E.A. and Teich, M.C.: "Fundamentals of Photonics", Chapter 6, John Wiley & Sons Inc., pp. 209, 1991, ISBN 0-471-83965-5.

317. Hawkins, G.: "Predictive Bulk Substrate Characterisation", Chapter 2, pp.3, 2000, http://www.gary.hawkins.ukgateway.net/cahpter2.htm.

318. Udd, E.: "Fiber Optic Sensors An Introduction for Engineers and Scientists", Chapter 2, Wiley, pp. 15, 1991, ISBN 0-471-83007-0.

319. Dakin, J. and Culshaw, B.: "Optical Fiber Sensors", Vol. 1, Chapter 3, Norwood, pp.42, 1988, ISBN 0-89006-317-6.

320. Udd, E.: "Fiber Optic Sensors An Introduction for Engineers and Scientists", Chapter 2, Wiley, pp. 16, 1991, ISBN 0-471-83007-0.

321. Pedrotti, F.L. and Pedrotti, L.S.: "Introduction to Optics", Second Edition, Chapter 20, Prentice-Hall International Inc., pp. 410-412, 1993, ISBN 0-13-016973-0.

322. Fowles, G.R.: "Intorduction to Modern Optics", 2nd Edition, Chapter 2, Constable & Co. Ltd., pp. 44, 1989, ISBN 0-486-65957-7.

323. Hecht, E.: "Optics", Second Edition, Chapter 4, Addison-Wesley, pp.99-104, 1987, ISBN 0-201-11611-1.

324. Kersey, A.D., Davis, M.A., Patrick, H.J., LeBlanc, M., Koo, K.P., Askins, C.G., Putnam, M.A. and Friebele, E.J.: "Fibre Grating Sensors", JOLT, Vol. 15, No. 8, pp. 1455-1457, 1997.

325.   Qin, L., Wei, Z.X., Wang, Q.Y., Li, H.P., Zheng, W., Zhang, Y.S. and Gao, D.S.: "Compact Temperature Compensating Package for Long-Period Fiber Gratings", Optical Materials, Vol. 14, pp. 239-242, 2000.

326.   Harumoto, M., Shigehara, M., Kakui, M., Kanamori, H. and Nishimura, M.: "Compact Long-Period Grating Module with Multi-Attenuation Peaks", Electronics Letters, Vol. 36, No. 6, 2000.

327.   Pedrotti, F.L. and Pedrotti, L.S.: "Introduction to Optics", Second Edition, Chapter 19, Prentice-Hall International Inc., pp. 396, 1993, ISBN 0-13-016973-0.

328.   Erdogan, T.: "Cladding-Mode Resonances in Short-and-Long-Period Fiber Grating Filters",J.Opt.Soc.Am.A, Vol.14, No.8, pp.1762, 1997.

329.   Grattan, K.T.V. and Meggitt, B.T.: "Optical Fiber Sensor Technology", Chapter 2, Chapman and Hall, pp. 18, 1995, ISBN 0-412-59210-X.

330.   Ungar, S.: "Fibre Optics: Theory and Application", Chapter 3, John Wiley & Sons Ltd., pp. 47, 1997, ISBN 0-471-92758-9.

331.   Bhatia, V.: "Properties and Sensing Applications of Long-Period Gratings", Thesis for Doctor of Philosophy in Electrical Engineering, Chapter 3, pp68, 1996.

332.   Yariv, A.: "Optical Electronics in Modern Communications", Fifth Edition, Chapter 3, Oxford University Press, pp.84,91, 1996, ISBN 0-19-510626-1.

333.   Wu, C.I., Hill, G. and Kahn, A.: "Band Alignment at Organic-Inorganic Semiconductor Interfaces: α-NPD and CuPc on InP(110)", Journal of Applied Physics, Volume 85, No. 9, pp. 6590, 1999.

334.   Starodub, V.M. Nabok, A.V., Starodub, N.F. and Torbicz, W.: "Approaches for the Structured Immobilisation of Recognising Elements on the Transducer Surface of Biosensors", pp.11, http://nano.materials.drexel.edu/NATOARW/NATOPapers/Chapter4/Starodub.

335.   Nabok, A.V., Davis, F., Hassan, A.K., Ray, A.K., Majeed, R. and Ghassemlooy, Z.: "Polyelectrolyte Self-Assembled Thin Films Containing Cyclo-tetrachromotropylene for Chemical and Bio-Sensing", Materials Science Engineering, C, Vol. 8-9, pp. 123, 1999.

336.   Cartmell, E. and Fowles, G.W.A.: "Valency and Molecular Structure", 3rd Edition, Chapter 11, Butterworths and Co., pp. 177-178, 1966.

337.   http://www.nature.com/nature/journal/v389/n6650/fig_tab/389469a0_F1.html

338.   Amend, J.R., Mundy, B.P. and Armold, M.T.: "General, Organic, and Biological Chemistry", Chapter 15, Saunders College Publishing, pp. 382, 1990, ISBN 0-03-046988-0.

339. Amend, J.R., Mundy, B.P. and Armold, M.T.: "General, Organic, and Biological Chemistry", Chapter 17, Saunders College Publishing, pp. 461, 1990, ISBN 0-03-046988-0.

340. Amend, J.R., Mundy, B.P. and Armold, M.T.: "General, Organic, and Biological Chemistry", Chapter 17, Saunders College Publishing, pp. 457, 1990, ISBN 0-03-046988-0.

341. Lvov, Y.M., Decher, G. and Mohwald, H.: "Assembly, Structural Characterization, and Thermal Behaviour of Layer by Layer Deposited Ultrathin Films of Poly(vinyl sulphate) and Poly(allylamine)", Langmuir, Vol. 9, pp. 481-486, 1993.

342. Lvov, Y.M. and Decher, G.: "Assembly of Multilayer Ordered Films by Alternating Adsorption of Oppositely Charged Macromolecules", Crystallography Reports, Vol. 39, No. 4, pp. 628-647, 1994.

343. Nabok, A.V., Davis, F., Hassan, A.K., Ray, A.K., Majeed, R. and Ghassemlooy, Z.: "Polyelectrolyte Self-Assembled Thin Films Containing Cyclo-Tetrachromotropylene for Chemical and Bio-Sensing", Materials Science and Engineering, C 8-9, pp. 123-126, 1999.

344. Yamada, M and Shiratori, S.S.: "Smoke Sensor Using Mass Controlled Layer-by-Layer Self Assembly of Polyelectrolytes Films", Sensors and Actuators, B64, pp.124-127, 2000.

345. Nabok, A.V., Ray, A.K., Hassan, A.K., Yates, R. and Majeed, R.: "Composite Polyelectrolyte Self-Assembled Films for Optical Bio-Sensors", Proceedings of SPIE's 6th Annual Intern. Synopsium on Smart Structures and Materials, Vol. 3673, pp. 230-238, 1999.

346. Howard, K.A., Dash, P.R., Read, M.L., Ward, K., Tomkins, L.M. Nazarova, O., Ulbrich, K. and Seymour, L.W.: "Influence of Hydrophilicity of Cationic Polymers on the Biophysical Properties of Polyelectrolyte Complexes Formed by Self-Assembly with DNA", Biochemica et Biophysica Acta, Vol. 1475, pp. 245-255, 2000.

347. Nabok, A.V., Hassan, A.K. and Ray, A.K.: "Optical and electrical characterisation of polyelectrolyte self-assembled thin films", Materials Science and Engineering, C, Vol. 8-9, pp. 505-508, 1999.

348. Lvov, Y.M. and Decher, G.: "Assembly of Multilayer Ordered Films by Alternating Adsorption of Oppositely Charged Macromolecules", Crystallography Reports, Vol. 39, No. 4, pp. 630, 1994.

349. "Refractive Index Sensing with Surface Plasmon Resonance", Spreeta Technology Overview, 2001, http://www.ti.com/sc/docs/products/msp/control/spreeta/refract.htm.

350.   Harris, R.D., Luff, B.J., Wilkinson, J.S., Wilson, R. Schriffrin, D.J., Piehler, J., Brecht, A., Abuknesha, R.A. and Mouvet, C.: "Integrated Optical Surface Plasmon Resonance Biosensor for Pesticide Ananysis", 1995/6 ORC Research Journal, Optical Fibres Group, pp. 1, 1996, http://www.ecs.soton.ac.uk/publications/rj/1995-1996/ofg/rdh/paper.htm.

351.   Dakin, J. and Culshaw, B.: "Optical Fiber Sensors", Vol. 1, Chapter 6, Norwood, pp.203-204, 1988, ISBN 0-89006-317-6.

352.   Nabok, A.V., Hassan, A.K, Ray, A.K., Omar, O. and Kalchenko, V.I.: "Study of Adsorption of Some Organic Molecules in Calix[4]resorcinolarene LB Films by Surface Plasmon Resonance", Sensors and Actuators, B45, pp.115-121, 1997.

353.   Ray. A.K., Hassan, A.K. and Saatchi, M.R.: "Surface Plasmon Resonance Studies on Longmuir-Blodgett Films of Novel Octa-Substituted Metal-Free Pthalocyanine Molecules", Philosophical Magazine, B, Vol. 76, No. 6, pp. 961-971, 1997.

354.   Nabok, A.V., Hassan, A.K. and Ray, A.K.: "Condensation of Organic Vapours within Nanoporous Calixarene Thin Films", Journal of Materials Chemistry, Vol. 10, pp. 189-194, 2000.

355.   Erdogan, T.: "Cladding-Mode Resonances in Short-and-Long-Period Fiber Grating Filters", J.Opt.Soc.Am.A, Vol.14, No.8, pp.1764, 1997.

356.   "High Performance of Erbium-Doped Fiber Amplifiers with Long Period Fiber Grating Filter", 1999, http://phohonics.kist.re.kr/research/EDFA.html.

357.   Vengsarkar, A.M., Lemaire, P.J., Judkins, J.B., Bhatia, V., Erdogan, T. and Sipe, J.E.: "Long-Period Fiber Gratings as Band Rejection Filters", JOLT, Vol. 14, No.1, pp. 58-64, 1996.

358.   Bhatia, V. and Vengsarkar, A.M.: "Optical Fiber Long Period Grating Sensors", Optics Letters, Vol. 21, No.9, 1996.

359.   Dianov, E.M., Vasiliev, S.A., Kurkov, A.S., Medvedkov, O.I. and Protopopov, V.N.: "In Fiber Mach-Zender Interferometer Based on a Pair of Long-Period Gratings", 22nd European Conference on Optical Communication – ECOC'96, Oslo, 1996.

360.   Shu, X., Zhu, X., Jiang, S., Shi, W. and Huang, D.: "High Sensitivity of Dual Resonant Peaks of Long Period Fibre Grating to Surrounding Refractive Index Changes", Electronics Letters, Vol.35, No.18, pp.1580-1581, 1999.

361.   Patrick, H.J., Chang, C.C. and Vohra, S.T.: "Long Period Fibre Gratings for Structural Bend Sensing", Electronics Letters, Vol. 34, No. 18, 1998.

362.   Allsop, T, Zhang, L. and Bennion, I.: "Detection of Organic Compounds in Paraffin by a Long-Period Fiber Grating Optical Sensor with Optimized Sensitivity", Optics Communications, Vol. 191, pp.181-190, 2001.

363. Bhatia, V.: "Applications of Long Period Gratings to Single and Multi-parameter Sensing", Optics Express, Vol 4, No.11, pp.459, 1999.

364. Bhatia, V.: "Applications of Long Period Gratings to Single and Multi-parameter Sensing", Optics Express, Vol 4, No.11, pp. 459,460, 1999.

365. Omar, O., Ray, A.K., Hassan, A.K., Ghassemlooy, Z. and Cook, M.J.: "Optical Characterisation of Amphiphilic Metal-Free Non-Peripheral Phthalocyanine in Langmuir-Blodgett Films", SPIE, Vol. 2852, pp.81 – 88, 1996.

366. Nabok,A.V. et al: "Further Optical Studies on Langmuir-Blodgett Films of Octa-Substituted Metal Free Phthalocyanines", Supramolecular Science, Vol.4, pp.407-411, 1997.

367. Johal, S.S. et al.: "A Technique for Depositing Non-Centrosymmetric Langmuir-Blodgett Films onto Optical Fibres", Meas. Sci. Technol. Vol. 10, pp. N60-N62, 1999.

368. Lee, Y., Tsai, W. and Maa, J.: "Effects of Substrate Temperature on the Film Characteristics and Gas-Sensing Properties of Copper Phthalocyanine Films", Applied Surface Science, Vol. 173, pp. 352-361, 2001.

369. Slota, R., Dyrda, G. and Waclawek, W.: "Investigation of Phthalocyanine Crystals Exposed to NO_2 Ambient Gas", Polyhedron, Vol. 21, pp. 677-681, 2002.

370. Qui, W. et al.: "The Gas Sensitivity of a Substituted Metallophthalocyanine, Tetra-Iso Propoxyphthalocyaninato Copper II", Sensors and Actuators B75, pp. 62-66, 2001.

371. Nabok, A.V., Lavrik, N.V., Kazantseva, Z.I., Nesterenko, B.A., Markovskiy, L.N., Kalchenko, V.I. and Shivaniuk, A.N.: "Complexing Properties of Calix[4]resorcinolarene LB Films", Thin Solid Films, Vol. 259, pp. 244-247, 1995.

372. Shirshov, Y.M., Svechnikov, S.V., Kiyanovskii, A.P., Ushenin, Y.V., Vengar, E.F., Samoylov, A.V. and Merker, R.: "A Sensor Based on the Planar-Polarisation Interferometer", Sensors and Actuators A68, pp. 348-387, 1998.

373. Shirshov, Y.M., Snopok, B.A., Samoylov, A.V., Kiyanovskij, A.P., Venger, E.F., Nabok, A.V. and Ray, A.K.: "Analysis of the Response of Planar-Polarisation Interferometer to Molecular Layer Formation: Fibrinogen Adsorption on Silicon Nitride Surface", Biosensors and Bioelectronics, Vol. 16, pp. 381-390, 2001.

374. El-Nahass, M.M., Bahabri, F.S. and Al-Harbi, S.R.: "Optical Properties of Copper Phthalocyanine (CuPc) Thin Films", Egypt, J. Sol., Vol. 24, No. 1, pp. 11-19, 2001.

Appendix 1

Reflection / Transmission at an Optical Interface

For transverse electric (TE) waves
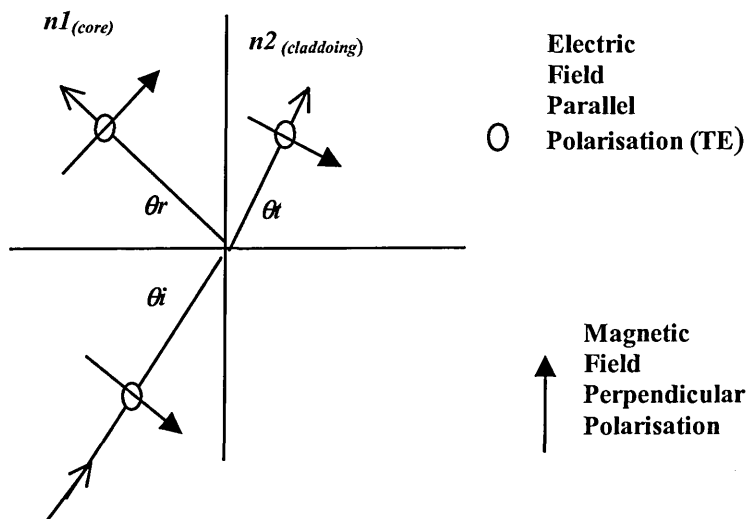
Figure A1.1: Reflection and transmission of a TE wave at a refractive index boundary

If the electric field component of a TE wave incident on the boundary as shown in Figure A1.1 is described by [272-277]:

$$E = E_0 e^{i(k.r-\omega t)} \tag{A1.1}$$

then the electric field components E_R and E_T of the reflected and transmitted waves respectively can be described by

$$E_R = E_{0R} e^{i(k_R.r-\omega_R t)} \tag{A1.2}$$

$$E_T = E_{0T} e^{i(k_T.r-\omega_T t)} \tag{A1.3}$$

For transverse magnetic (TM) waves
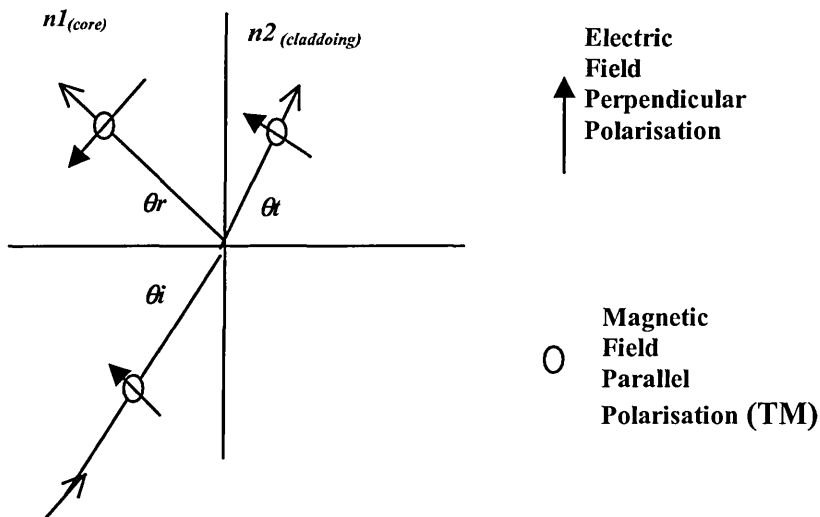
Figure A1.2: Reflection and transmission of a TM wave at a refractive index Boundary

The same assumption can be made for the magnetic field components of a TM wave as shown in Figure A1.2 [272-277]:

$$B = B_0 e^{i(k.r-\omega t)} \tag{A1.4}$$

then the magnetic field components B_R and B_T of the reflected and transmitted waves respectively can be described by

240

$$B_R = B_{0R}e^{i(k_R.r-\omega_R t)} \tag{A1.5}$$

$$B_T = B_{0T}e^{i(k_T.r-\omega_T t)} \tag{A1.6}$$

At the interface of the 2 media where all 3 waves coincide Maxwell's equations give the boundary conditions that the components of the electric and magnetic fields parallel to the interface should be continuous at each side of the boundary.

Thus for TE waves

as E is parallel to the interface

$$E_I + E_R = E_T \tag{A1.7}$$

or
$$E_R = E_T - E_I \tag{A1.7a}$$

as the component of B parallel to the interface is $B\cos\theta$

$$B_I\cos\theta_I + (-B_R\cos\theta_R) = B_T\cos\theta_T$$

As $\theta_I = \theta_R$, and B = nE/c, this can be re-written in terms of the electric field as:

$$n_1 E_I\cos\theta_I - n_1 E_R\cos\theta_I = n_2 E_T\cos\theta_T \tag{A1.8}$$

For TM waves by the same reasoning

as B is parallel to the interface

$$B_I + B_R = B_T$$

$$n_1 E_I + n_1 E_R = n_2 E_T \tag{A1.9}$$

or
$$E_R = \frac{n_2 E_T - n_1 E_I}{n_1} \tag{A1.9a}$$

as the component of E parallel to the interface is $E\cos\theta$

$$-E_I\cos\theta_I + E_R\cos\theta_R = -E_T\cos\theta_T \tag{A1.10}$$

241

To determine an equation for TE waves involving only the incident angle, substituting

(A1.7) into (A1.8) to eliminate E_T

$$n_1 E_I \cos\theta_I - n_1 E_R \cos\theta_I = n_2(E_I + E_R)\cos\theta_T$$

$$n_1 E_I \cos\theta_I - n_1 E_R \cos\theta_I = n_2 E_I \cos\theta_T + n_2 E_R \cos\theta_T$$

$$n_1 E_I \cos\theta_I - n_2 E_I \cos\theta_T = n_1 E_R \cos\theta_I + n_2 E_R \cos\theta_T$$

$$E_I(n_1 \cos\theta_I - n_2 \cos\theta_T) = E_R(n_1 \cos\theta_I + n_2 \cos\theta_T)$$

$$\frac{E_R}{E_I} = \frac{(n_1 \cos\theta_I - n_2 \cos\theta_T)}{(n_1 \cos\theta_I + n_2 \cos\theta_T)} \tag{A1.11}$$

As reflection coefficient $\rho = E_R / E_I$

$$\rho_{TE} = \frac{(\cos\theta_I - \dfrac{n_2}{n_1}\cos\theta_T)}{(\cos\theta_I + \dfrac{n_2}{n_1}\cos\theta_T)}$$

To remove the θ_T term

As $\cos\theta_T = \sqrt{1 - \sin^2\theta_T}$

$$\rho_{TE} = \frac{\cos\theta_I - \dfrac{n_2}{n_1}\sqrt{1 - \sin^2\theta_T}}{\cos\theta_I + \dfrac{n_2}{n_1}\sqrt{1 - \sin^2\theta_T}} \tag{A1.12}$$

As Snell's law states $n_1\sin\theta_I = n_2\sin\theta_T$, and letting $\dfrac{n_2}{n_1} = N$ (relative refractive index)

(A1.12) can be re-written in terms of the incident angle only as:

$$\rho_{TE} = \frac{\cos\theta_I - \sqrt{N^2 - \sin^2\theta_I}}{\cos\theta_I + \sqrt{N^2 - \sin^2\theta_I}} \tag{A1.13}$$

242

To determine an equation for TM waves involving only the incident angle

Substituting (A1.9) into (A1.10) to eliminate E_T gives

$$-E_I \cos\theta_I + E_R \cos\theta_I = -\frac{(n_1 E_I + n_1 E_R)}{n_2}\cos\theta_T$$

$$-n_2 E_I \cos\theta_I + n_2 E_R \cos\theta_I = -n_1 E_I \cos\theta_T - n_1 E_R \cos\theta_T$$

$$n_2 E_I \cos\theta_I - n_1 E_I \cos\theta_T = n_2 E_R \cos\theta_I + n_1 E_R \cos\theta_T$$

$$E_I(n_2 \cos\theta_I - n_1 \cos\theta_T) = E_R(n_2 \cos\theta_I + n_1 \cos\theta_T)$$

$$\frac{E_R}{E_I} = \frac{(n_2 \cos\theta_I - n_1 \cos\theta_T)}{(n_2 \cos\theta_I + n_1 \cos\theta_T)}$$

As reflection coefficient $\rho = E_R / E_I$

$$\rho_{TM} = \frac{\left(\frac{n_2}{n_1}\cos\theta_I - \cos\theta_T\right)}{\left(\frac{n_2}{n_1}\cos\theta_I + \cos\theta_T\right)}$$

To remove the θ_T term

As $\cos\theta_T = \sqrt{1 - \sin^2\theta_T}$

$$\rho_{TM} = \frac{\frac{n_2}{n_1}\cos\theta_I - \sqrt{1 - \sin^2\theta_T}}{\frac{n_2}{n_1}\cos\theta_I + \sqrt{1 - \sin^2\theta_T}}$$

$$\rho_{TM} = \frac{\frac{n_2}{n_1}\cos\theta_I - \sqrt{1 - \sin^2\theta_T}}{\frac{n_2}{n_1}\cos\theta_I + \sqrt{1 - \sin^2\theta_T}}$$

$$\rho_{TM} = \frac{\left(\dfrac{n_2}{n_1}\right)^2 \cos\theta_I - \sqrt{\left(\dfrac{n_2}{n_1}\right)^2 - \left(\dfrac{n_2}{n_1}\right)^2 \sin^2\theta_T}}{\left(\dfrac{n_2}{n_1}\right)^2 \cos\theta_I + \sqrt{\left(\dfrac{n_2}{n_1}\right)^2 - \left(\dfrac{n_2}{n_1}\right)^2 \sin^2\theta_T}} \qquad (A1.14)$$

As Snell's law states $n_1 \sin\theta_I = n_2 \sin\theta_T$, and letting $\dfrac{n_2}{n_1} = N$ (relative refractive index)

(A1.14) can be re-written in terms of the incident angle only as:

$$\rho_{TM} = \frac{N^2 \cos\theta_I - \sqrt{N^2 - \sin^2\theta_I}}{N^2 \cos\theta_I + \sqrt{N^2 - \sin^2\theta_I}} \qquad (A1.15)$$

Thus (A1.13) and (A1.15) predict the reflection coefficients for TE and TM waves [319,320].

The Transmission coefficient can be similarly determined using equations (A1.7) to

(A1.10), but this time eliminating E_R rather than E_T

For TE, substituting (A1.7a) into (A1.8)

$$n_1 E_I \cos\theta_I - n_1 E_T \cos\theta_I + n_1 E_I \cos\theta_I = n_2 E_T \cos\theta_T$$

$$n_1 E_I \cos\theta_I + n_1 E_I \cos\theta_I = n_1 E_T \cos\theta_I + n_2 E_T \cos\theta_T$$

$$E_I \left(n_1 \cos\theta_I + n_1 \cos\theta_I\right) = E_T \left(n_1 \cos\theta_I + n_2 \cos\theta_T\right)$$

$$\frac{E_T}{E_I} = \frac{\left(2n_1 \cos\theta_I\right)}{\left(n_1 \cos\theta_I + n_2 \cos\theta_T\right)}$$

As transmission coefficient $\tau = E_T / E_I$

$$\tau_{TE} = \frac{2\cos\theta_I}{\cos\theta_I + \dfrac{n_2}{n_1}\cos\theta_T}$$

To remove the θ_T term, as $\cos\theta_T = \sqrt{1 - \sin^2\theta_T}$

244

$$\tau_{TE} = \frac{2\cos\theta_I}{\cos\theta_I + \sqrt{\left(\dfrac{n_2}{n_1}\right)^2 - \left(\dfrac{n_2}{n_1}\right)^2 \sin^2\theta_T}}$$

as Snell's law states $n_1\sin\theta_I = n_2\sin\theta_T$

$$\tau_{TE} = \frac{2\cos\theta_I}{\cos\theta_I + \sqrt{\left(\dfrac{n_2}{n_1}\right)^2 - \left(\dfrac{n_1}{n_1}\right)^2 \sin^2\theta_I}}$$

$$\tau_{TE} = \frac{2\cos\theta_I}{\cos\theta_I + \sqrt{N^2 - \sin^2\theta_I}} \qquad\qquad (A1.16)$$

For TM

Substituting (A1.9a) into (A1.10)

$$-E_I\cos\theta_I + \frac{n_2 E_R\cos\theta_I}{n_1} - \frac{n_1 E_I\cos\theta_I}{n_1} = -E_T\cos\theta_T$$

$$E_I\cos\theta_I + \frac{n_1 E_I\cos\theta_I}{n_1} = E_T\cos\theta_T + \frac{n_2 E_R\cos\theta_I}{n_1}$$

$$n_1 E_I\cos\theta_I + n_1 E_I\cos\theta_I = n_1 E_T\cos\theta_T + n_2 E_R\cos\theta_I$$

$$E_I(2n_1\cos\theta_I) = E_T(n_1\cos\theta_T + n_2\cos\theta_I)$$

$$\frac{E_T}{E_I} = \frac{(2n_1\cos\theta_I)}{(n_1\cos\theta_T + n_2\cos\theta_I)}$$

As transmission coefficient $\tau = E_T / E_I$

$$\tau_{TM} = \frac{2\cos\theta_I}{\cos\theta_T + \dfrac{n_2}{n_1}\cos\theta_I}$$

To remove the θ_T term, as $\cos\theta_T = \sqrt{1 - \sin^2\theta_T}$

245

$$\tau_{TM} = \frac{2Cos\theta_I}{\sqrt{1-\sin^2\theta_T} + \frac{n_2}{n_1}\cos\theta_I}$$

as Snell's law states $n_1\sin\theta_I = n_2\sin\theta_T$, so $\sin\theta_T = n_1\sin\theta_I / n_2$

$$\tau_{TM} = \frac{2Cos\theta_I}{\frac{n_2}{n_1}\cos\theta_I + \sqrt{1-\left(\frac{n_1}{n_2}\right)^2\sin^2\theta_I}}$$

$$\tau_{TM} = \frac{\frac{n_2}{n_1}(2Cos\theta_I)}{\left(\frac{n_2}{n_1}\right)^2\cos\theta_I + \sqrt{\left(\frac{n_2}{n_1}\right)^2 - \left(\frac{n_2}{n_1}\right)^2\left(\frac{n_1}{n_2}\right)^2\sin^2\theta_I}}$$

$$\tau_{TM} = \frac{2NCos\theta_I}{N^2\cos\theta_I + \sqrt{N^2 - \sin^2\theta_I}} \qquad (A1.17)$$

Thus (A1.16) and (A1.17) predict the transmission coefficients for TE and TM waves [318,319].

Appendix 2

Brewster Angle
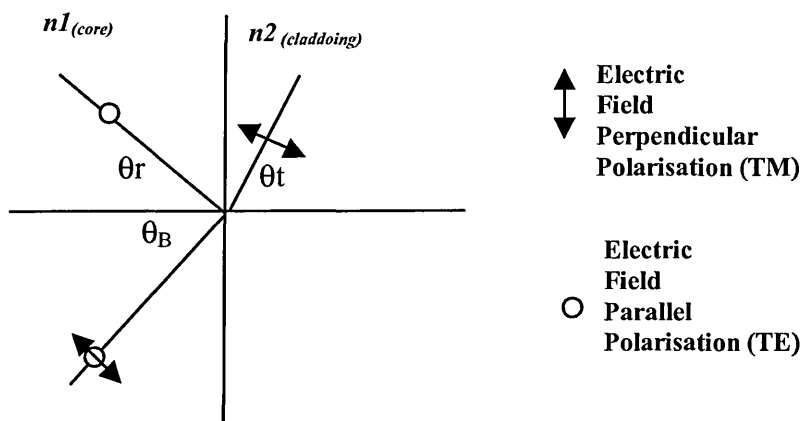
Figure A2.1: Brewster angle of electro-magnetic wave at refractive index boundary

When the light is incident on the core/cladding interface at the Brewster angle as shown in

Figure A2.1, the reflected light has only the parallel (TE) component, while the transmitted

light has only the perpendicular (TM) component. Thus if the incident light is polarised parallel (TE) to the surface of the boundary there will be no transmitted component, only reflection and if the incident light is polarised perpendicular (TM) to the surface of the boundary there will be no reflected component, only transmission. Total transmission or zero reflection occurs therefore only for perpendicular polarisation (TM), thus the Brewster angle is useful for transmitting light across a boundary (in either direction) without reflection losses. The Brewster angle is greater for light travelling from low (cladding) to high (core) RI than for high (core) to low (cladding) RI. When light is incident on a boundary travelling from a higher RI (core) to a lower RI (cladding) a critical angle is reached at which TIR occurs. When light is incident on a boundary travelling from a lower RI (cladding) to a higher RI (core), TIR will not occur. TIR occurs for both polarisations at the same angle.

Appendix 3

Program Code to Determine Propagation Constants, β, and Propagation Angles, θ, in Core and Cladding Using Equation 4.2

```
%DETERMINTAION OF PROPAGATION CONSTANTS (Bcl) FOR CORE &
CLADDING OF SINGLE MODE FIBRE
%for  HEml where m = 1
%Matlab file:  HecladmodesthesisYariv
clear all
format long
Fid =
fopen('d:\PaulDowker\Matlab\PaulD\results.txt','w');
                                        %OPEN FILE
fprintf('\nHecladmodesthesisYariv');
fprintf(Fid,'\nHecladmodesthesisYariv');
fprintf('\nProg to find coupling from HE11 (LP01) core to
HEml Cladding modes (where m = 1)');
fprintf(Fid,'\nProg to find coupling from HE11 (LP01)
core to HEml Cladding modes (where m = 1)');
```

```matlab
L=1500*10^(-9);                          %START
                                           WAVELENGTH

while L<1551*10^(-9);                    %OPEN WAVELENGTH
                                           LOOP


    k=2*pi/L;                            %WAVE NUMBER
    r1=2.625*10^(-6);                    %CORE RADIUS
    r2=62.5*10^(-6);                     %CLADDING RADIUS
    n1=1.458;                            %CORE RI
    n2=1.455;                            %CLADDING RI
    n3=1;                                %AMBIENT RI


    %determination of core modes
        Bc= k*n1:-((k.*n1)-(k.*n2))/10^(6):k*n2;   %β_CORE
                                                     RANGE
                                                      TO TEST

    uc=r1*sqrt((k*k*n1*n1)-(Bc.*Bc));
    wc=r1*sqrt((Bc.*Bc)-(k*k*n2*n2));
    M=0;
    if M==0
        f1 =BESSELJ(M,uc)./(uc.*BESSELJ(M+1,uc));
        f2 =BESSELK(M,wc)./(wc.*BESSELK(M+1,wc));
    else
        f1 =BESSELJ(M,uc)./(uc.*BESSELJ(M-1,uc));
        f2 =-BESSELK(M,wc)./(wc.*BESSELK(M-1,wc));
    end

    f=f1-f2;
    %PLOT GRAPH OF CORE MODES
    figure(1)
    plot(Bc,f,'b')
    Title('Core modes')
    xlabel('Bc')
    ylabel('f')
    grid

    %when f = 0 this is the value of Bcl which is correct
    %for both equations, f1 and f2, and is thus the value
of Bcl for the
    %single mode (HE11 or LP01)in this core.
    a1=0;
    %TEST TO FIND VALUES OF CORE MODES
    index1=1;
    for a2=1:length(Bc)-1
        if ((f(a2)*f(a2+1)<0)&((f(a2)^2)+(f(a2+1)^2)<0.1))

            Bcore(index1)=(Bc(a2)+Bc(a2+1))/2;
```

```matlab
Bang1(index1)=(asin(Bcore(index1)/(k*n1)))*360/(2*pi);
        fval1(index1)=(f(a2)+f(a2+1))/2;
        a1=a1+1;
        index1=index1+1;
    end
  end


  no_of_core_modes=a1

%PRINT INFO TO SCREEN & FILE
  for a3 = 1:length(Bcore)
      fprintf('\nFor L = %.2fnm:    Bcore value %d: %f,
Bcore angle %d: %f, F value %d:
%0.4f\n',((L*10^(9))),a3,Bcore(a3),a3,Bang1(a3),a3,fval1(
a3));
      fprintf(Fid,'\nFor L = %.2fnm:    Bcore value %d:
%f, Bcore angle %d: %f, F value %d:
%0.4f\n',((L*10^(9))),a3,Bcore(a3),a3,Bang1(a3),a3,fval1(
a3));
  end
  Bcl=k.*n2:-(((k.*n2)-(k.*n3)).*10^(-6)):0.98.*k.*n2;
                                        %β_{CLAD} RANGE TO TEST
  u=r2.*sqrt((k*k*n2*n2)-(Bcl.*Bcl));
  w=r2.*sqrt((Bcl.*Bcl)-(k*k*n3*n3));
  m=1;

  JHE=(BESSELJ(m+1,u))./(u.*BESSELJ(m,u));
  K1HE=-(((n2*n2)+(n3*n3)).*(-BESSELK(m-1,w)-
BESSELK(m+1,w)))./((2.*w.*BESSELK(m,w)).*(2*n2*n2));
  K2HE=(((n2*n2)-(n3*n3))/((2*n2*n2)*(2*n2*n2))).*((((-
BESSELK(m-1,w)-
BESSELK(m+1,w)))./(2.*w.*BESSELK(m,w))).*(((-BESSELK(m-
1,w)-BESSELK(m+1,w)))./(2.*w.*BESSELK(m,w))));

K3HE=((m*m.*Bcl.*Bcl)./(n2*n2*k*k)).*(((1./(w.*w))+(1./(u
.*u))).*((1./(w.*w))+(1./(u.*u))));
  KHE=K1HE+(1./(u.*u))-((K2HE+K3HE).^(0.5));

  fHE=JHE-KHE;

%PLOT GRAPH OF CLADDING MODE
  figure(2)
  plot(Bcl,fHE,'r');
  Title('Cladding modes')
  xlabel('Bcl')
  ylabel('fHE')
  grid
```

```matlab
%Bcl values are obtained where f crosses Bcl axis,
(i.e.f=0)

    zerosHE=0;
    index3 = 1;
    for a5=1:length(Bcl)-1
        if
((fHE(a5)*fHE(a5+1)<0)&((fHE(a5)^2)+(fHE(a5+1)^2)<0.01))
            zerosHE=zerosHE+1;

            BcladHE(index3)=(Bcl(a5)+Bcl(a5+1))/2;

BangHE(index3)=(asin(BcladHE(index3)/(k*n2)))*360/(2*pi);
            fvalHE(index3)=(fHE(a5)+fHE(a5+1))/2;
            PHE(index3)=(k.*L./(Bcore-
BcladHE(index3))).*10^(6);

            index3=index3+1;
        end
    end
    no_of_HE_modes=zerosHE

%PRINT INFO TO SCREEN & FILE
    for f = 1:length(BcladHE)
        fprintf('Bclad value HE1%d: %f, Bcl angle HE1%d:
%f, F value HE1%d: %0.4f,Period %d: %f
um\n',f,BcladHE(f),f,BangHE(f),f,fvalHE(f),f,PHE(f));
        fprintf(Fid,'Bclad value HE1%d: %f, Bcl angle
HE1%d: %f, F value HE1%d: %0.4f,Period %d: %f
um\n',f,BcladHE(f),f,BangHE(f),f,fvalHE(f),f,PHE(f));

    end

    L=L+1*10^-(9)                        %INCREMENT WAVELENGTH
End                                      %CLOSE WAVELENGTH LOOP

return
```

Appendix 4

Program Code to Determine Propagation Constants, β, and Propagation Angles, θ, in Core and Cladding Using Equation 4.3

```
%DETERMINAION OF PROPAGATION CONSTANTS (Bcl) FOR CORE &
CLADDING OF SINGLE MODE FIBRE
%for   HEml where m = 1
%Matlab file: HEcladmodesthesisErdogan


clear all, clc;

fid = fopen('d:\PaulDowker2\Matlab\results.doc','w');
                                        %OPEN FILE

fprintf(fid,'\HEcladmodesthesisErdogan');
fprintf('\n HEcladmodesthesisErdogan \n')
fprintf('\n %s \n',date)
fprintf(fid,'\n %s\n',date);
```

```matlab
fprintf('\nProg to find coupling from HE11 (LP01) core to
HEm1 Cladding modes (where m = 1)');
fprintf(fid,'\nProg to find coupling from HE11 (LP01)
core to HEm1 Cladding modes (where m = 1)');


L=1500*10^-9;                           %WAVELENGTH
r1=2.625*10^(-6);                       %CORE RADIUS
r2=62.5*10^(-6);                        %CLADDING
RADIUS
n1=1.458;                               %CORE RI
n2=1.455;                               %CLADDING RI
n3=1;                                   %AMBIENT RI
Zo=377;                                 %CONSTANT
k=2*pi./L;                              %WAVE NUMBER

index3=0;

    while L<1551*10^-9;                 %OPEN
                                        WAVELENGTH LOOP


 %determination of core modes at nth wavelength
    Bc=k.*n1:-((k.*n1)-(k.*n2))/10^(6):k.*n2; %β_CORE RANGE
                                              TO TEST

    neff1=Bc./k;
    u=r1.*sqrt((k.*k.*n1*n1)-(Bc.*Bc));
    w=r1.*sqrt((Bc.*Bc)-(k.*k.*n2*n2));
    M=0;

    f1 =BESSELJ(M,u)./(u.*BESSELJ(M+1,u));
    f2 =BESSELK(M,w)./(w.*BESSELK(M+1,w));

    f=f1-f2;

%PLOT GRAPH OF CORE MODES
    figure(1)
    plot(Bc,f,'b')
    Title('Core modes')
    xlabel('Bc')
    ylabel('f')
    grid
    index1=0;

%TEST TO FIND VALUES OF CORE MODES
    for a1=1:length(Bc)-1
        if
((f(a1).*f(a1+1)<0)&((f(a1)^2)+(f(a1+1)^2)<0.01))
        index1=index1+1;
        Bcore(index1)=(Bc(a1)+Bc(a1+1))./2;
```

```matlab
            Bang1(index1)=(asin(Bcore(index1)./(k.*n1)))*36
            0/(2*pi);
            fval1(index1)=(f(a1)+f(a1+1))./2;
        end
    end
    fprintf('\n\n\nThe following info is for wavelength
%.2fnm',(L*10^(9)))
    fprintf(fid,'\n\n\nThe following info is for
wavelength %.2fnm',(L*10^(9)));

%%PRINT NO OF CORE MODES TO SCREEN & FILE
    fprintf('\nno_of_core_modes = %d',index1)
    fprintf(fid,'\nno_of_core_modes = %d',index1);

    PRINT INFO TO SCREEN & FILE
    for a2 = 1:length(Bcore(index1))
        fprintf('\nBcore value %d: %f, Bcore angle %d: %f,
F value %d: %0.4f\n',a2,Bcore(a2),a2,
Bang1(a2),a2,fval1(a2));
        fprintf(fid,'\nBcore value %d: %f, Bcore angle %d:
%f, F value %d: %0.4f\n',a2,Bcore(a2),a2,
Bang1(a2),a2,fval1(a2));
        %disp(sent);
    end

%CLEAR USED VALUES TO SAVE MEMORY
    clear Bc
    clear neff1
    clear u
    clear w
    clear f1
    clear f2
    clear f


    Bcl=k.*n2:-((k.*n2)-(k.*n3))./10^(6):0.98.*k.*n2; %β_CLAD
                                            RANGE TO TEST

    neff2=Bcl./k;
    u1=sqrt((k.*k.*n1*n1)-(Bcl.*Bcl));
    u2=sqrt((k.*k.*n2*n2)-(Bcl.*Bcl));
    w1=sqrt((Bcl.*Bcl)-(k.*k.*n2*n2));
    w2=sqrt((Bcl.*Bcl)-(k.*k.*n3*n3));


    m=1;
    s1=(j*m.*neff2)./Zo;
    s2=(j*m.*neff2).*Zo;
    u21=(1./(u2.*u2))-(1./(u1.*u1));
    u32=(1./(w2.*w2))+(1./(u2.*u2));
```

```
   J=((BESSELJ(m-1,(u1.*r1)))-
(BESSELJ(m+1,(u1.*r1)))).*(2.*u1.*BESSELJ(m,(u1.*r1)));
   K=((-BESSELK(m-1,(w2.*r2)))-
(BESSELK(m+1,(w2.*r2)))).*(2.*w2.*BESSELK(m,(w2.*r2)));
   p=(BESSELJ(m,(u2.*r2)).*BESSELY(m,(u2.*r1)))-
(BESSELJ(m,(u2.*r1)).*BESSELY(m,(u2.*r2)));
   q=(BESSELJ(m,(u2.*r2)).*((BESSELY(m-1,(u2.*r1)))-
(BESSELY(m+1,(u2.*r1))))/2))-(((BESSELJ(m-1,(u2.*r1)))-
BESSELJ(m+1,(u2.*r1)))./2).*BESSELY(m,(u2.*r2)));
   r=(((BESSELJ(m-1,(u2.*r2)))-
(BESSELJ(m+1,(u2.*r2))))/2).*BESSELY(m,(u2.*r1))-
(BESSELJ(m,(u2.*r1)).*((BESSELY(m-1,(u2.*r2)))-
(BESSELY(m+1,(u2.*r2))))/2));
   s=((((BESSELJ(m-1,(u2.*r2)))-
(BESSELJ(m+1,(u2.*r2))))/2).*((BESSELY(m-1,(u2.*r1)))-
(BESSELY(m+1,(u2.*r1))))/2))-(((BESSELJ(m-1,(u2.*r1)))-
(BESSELJ(m+1,(u2.*r1))))/2).*((BESSELY(m-1,(u2.*r2)))-
(BESSELY(m+1,(u2.*r2))))/2));




top1=(u2.*((J.*K)+((s1.*s2.*u21.*u32)./(n2*n2*r1*r2)))).*p
)-(K.*q)+(J.*r)-(s./u2);
   bot1=((-u2.*(((u32.*J)./(n2*n2*r2))-
((u21.*K)./(n1*n1*r1))).*p)+((u32.*q)./(n1*n1*r2))+((u21.
*r)./(n1*n1*r1)));

   top2=((u2.*((u32.*J./r2)-
((n3*n3*u21.*K)./(n2*n2*r1))).*p)-(u32.*q./r2)-
(u21.*r./r1));

bot2=(u2.*(((n3*n3.*J.*K)./(n2*n2))+((s1.*s2.*u21.*u32)./
(n1*n1*r1*r2))).*p)-((n3*n3.*K.*q)./(n1*n1))+(J.*r)-
((n2*n2.*s)./(n1*n1.*u2)));
   Go=top1./bot1;
   Go2=(m^(2)).*(neff2.^(2)).*(top2./bot2);
   G=Go+Go2;


%PLOT GRAPH
   figure(2)
   plot(Bcl,G,'r');
   Title('Cladding modes')
   xlabel('Bcl')
   ylabel('G')
   grid
```

```matlab
%CLEAR USED VALUES TO SAVE MEMORY
    clear neff2
    clear u1
    clear u2
    clear w1
    clear w2
    clear s1
    clear s2
    clear u21
    clear u32
    clear J
    clear K
    clear p
    clear q
    clear r
    clear s
    clear top1
    clear bot1
    clear top2
    clear bot2
    clear Go
    clear Go2
    index2=0;


%TEST TO FIND VALUES OF CLADDING MODES
    for a3=1:length(Bcl)-1
        if
((G(a3)*G(a3+1)<0)&((abs(G(a3)))<5)&((abs(G(a3+1)))<5))
            index2=index2+1;
            BcladHE(index2)=(Bcl(a3)+Bcl(a3+1))/2;

BcladangHE(index2)=(asin((BcladHE(index2))/(k*n2)))*360/(
2*pi);
            GcladHE(index2)=(G(a3)+G(a3+1))/2;
            P(index2)=L*k./(Bcore-BcladHE(index2));
        end
    end
    clear Bcl

    %PRINT INFO TO SCREEN & FILE
    fprintf('\nno_of_cladding_modes = %d',index2)
    fprintf(fid,'\nno_of_cladding_modes = %d',index2);
    for a4=1:length(BcladHE)
        fprintf('\nB value %d: %f, B angle %d: %f, G value
%d: %0.4f',a4,BcladHE(a4),a4,
BcladangHE(a4),a4,GcladHE(a4));
        fprintf(fid,'\nB value %d: %f, B angle %d: %f, G
value %d: %0.4f',a4,BcladHE(a4),a4,
BcladangHE(a4),a4,GcladHE(a4));
    end
```

```
clear index2
        L=L+1*10^-(9)                          %INCREMENT
                                          WAVELENGTH LOOP
End                                %CLOSE WAVELENGTH LOOP

return
```

Appendix 5

Program Code to Determine Coupling Wavelength Shifts Using Ideal Fibre Parameters

```
clear all, clc;

%THIS PART OF PROGRAM DETERMINES THE GRATING PERIOD
REQUIRED TO COUPLE WAVELENGTH
%OF 1550nm into the 6th CLADDING MODE
%==========================================================
=======================


Fid = fopen('d:\PaulD\Paul.doc','w');    %OPEN FILE
fprintf(Fid,'\nActualprog2');
fprintf('\n Actualprog2 \n')


L=1550*10^-9;                            %WAVELENGTH
k=2*pi./L;                               %WAVE NUMBER
r1=2.625*10^(-6);                        %CORE RADIUS
r2=62.5*10^(-6);                         %CLADDING RADIUS
```

```matlab
n1=1.458;                              %CORE RI
n2=1.45;                               %CLADDING RI
n3=1;                                  %AMBIENT RI
Zo=377;                                %CONSTANT


%determination of core modes
Bc=k*n2:((k.*n1)-(k.*n2))/10^(6):k*n1;  %CORE PROPAGATION
                                            CONSTANT RANGE
neff1=Bc./k;                           %CLADDING EFFECTIVE RI
u=r1*sqrt((k.*k.*n1*n1)-(Bc.*Bc));       %CORE u VALUE
w=r1*sqrt((Bc.*Bc)-(k.*k.*n2*n2));       %CORE w VALUE

M=0;
f1 =BESSELJ(M,u)./(u.*BESSELJ(M+1,u));    %LHS OF EQU
f2 =BESSELK(M,w)./(w.*BESSELK(M+1,w));    %RHS OF EQU


f=f1-f2;          %GIVES BN VALUES WHICH SATISFY BOTH SIDES




index1=0;
for a1=1:length(Bc)-1                  %FIND ZERO CROSSINGS
    if ((f(a1)*f(a1+1)<0)&((f(a1)^2)+(f(a1+1)^2)<0.01))
        index1=index1+1;
        Bcore(index1)=(Bc(a1)+Bc(a1+1))./2; %FIND ZERO
                                        CROSSING B VALUES
        Bang1(index1)=(asin(Bcore(index1)./(k.*n1)))*360/(2
        *pi);                           %FIND MODE ANGLES
        fval1(index1)=(f(a1)+f(a1+1))./2;   %FIND ACCURACCY
                                        OF ZERO CROSSING PT

    end
end


%PRINT INFO TO SCREEN & FILE
fprintf('\nThe following info is for wavelength of
%.2fnm',L*10^(9))
fprintf('\nno_of_core_modes = %d',index1)
fprintf(Fid,'\nno_of_core_modes = %d',index1);


for a2 = 1:length(Bcore)
   neff1c=Bcore./k;
   fprintf('\nBcore value %d: %f, Bcore angle %d: %f, F
value %d:
%0.4f\n',a2,Bcore(a2),a2,Bang1(a2),a2,fval1(a2));
   fprintf(Fid,'\nBcore value %d: %f, Bcore angle %d: %f,
F value %d:
%0.4f\n',a2,Bcore(a2),a2,Bang1(a2),a2,fval1(a2));
```

```matlab
    %disp(sent1);
end



%determination of cladding modes
B=k*n2:-((k.*n2)-(k.*n3))/10^(6):0.998*k.*n2;    %CLADDING
                                 PROPAGATION CONSTANT RANGE

neff2=B./k;                         %CLADDING EFFECTIVE RI
u1=sqrt((k.*k.*n1*n1)-(B.*B));         %CORE u VALUE
u2=sqrt((k.*k.*n2*n2)-(B.*B));         %CLADDING u VALUE
w1=sqrt((B.*B)-(k.*k.*n2*n2));         %CORE w VALUE
w2=sqrt((B.*B)-(k.*k.*n3*n3));         %CLADDING w VALUE



m=1;
s1=(j*m.*neff2)./Zo;
s2=(j*m.*neff2).*Zo;
u21=(1./(u2.*u2))-(1./(u1.*u1));
u32=(1./(w2.*w2))+(1./(u2.*u2));



J=((BESSELJ(m-1,(u1.*r1)))-
(BESSELJ(m+1,(u1.*r1))))./(2.*u1.*BESSELJ(m,(u1.*r1)));
K=((-BESSELK(m-1,(w2.*r2)))-
(BESSELK(m+1,(w2.*r2))))./(2.*w2.*BESSELK(m,(w2.*r2)));
p=(BESSELJ(m,(u2.*r2)).*BESSELY(m,(u2.*r1)))-
(BESSELJ(m,(u2.*r1)).*BESSELY(m,(u2.*r2)));
q=(BESSELJ(m,(u2.*r2)).*((BESSELY(m-1,(u2.*r1)))-
(BESSELY(m+1,(u2.*r1))))/2))-(((BESSELJ(m-1,(u2.*r1)))-
BESSELJ(m+1,(u2.*r1)))./2).*BESSELY(m,(u2.*r2)));
r=(((BESSELJ(m-1,(u2.*r2)))-
(BESSELJ(m+1,(u2.*r2))))/2).*BESSELY(m,(u2.*r1))-
(BESSELJ(m,(u2.*r1)).*((BESSELY(m-1,(u2.*r2)))-
(BESSELY(m+1,(u2.*r2))))/2));
s=((((BESSELJ(m-1,(u2.*r2)))-
(BESSELJ(m+1,(u2.*r2))))/2).*((BESSELY(m-1,(u2.*r1)))-
(BESSELY(m+1,(u2.*r1))))/2))-(((BESSELJ(m-1,(u2.*r1)))-
(BESSELJ(m+1,(u2.*r1))))/2).*((BESSELY(m-1,(u2.*r2)))-
(BESSELY(m+1,(u2.*r2))))/2));



top1=(u2.*((J.*K)+((s1.*s2.*u21.*u32)./(n2*n2*r1*r2))).*p
)-(K.*q)+(J.*r)-(s./u2);
bot1=((-u2.*(((u32.*J)./(n2*n2*r2))-
((u21.*K)./(n1*n1*r1))).*p)+((u32.*q)./(n1*n1*r2))+((u21.
*r)./(n1*n1*r1)));
```

```matlab
top2=((u2.*((u32.*J./r2)-
((n3*n3*u21.*K)./(n2*n2*r1))).*p)-(u32.*q./r2)-
(u21.*r./r1));
bot2=(u2.*(((n3*n3.*J.*K)./(n2*n2))+((s1.*s2.*u21.*u32)./
(n1*n1*r1*r2))).*p)-((n3*n3.*K.*q)./(n1*n1))+(J.*r)-
((n2*n2.*s)./(n1*n1.*u2)));
Go=top1./bot1;

Go2=(m^(2)).*(neff2.^(2)).*(top2./bot2);



G=Go+Go2;

;

index2= 0;

for a3=1:length(B)-1   %FIND ZERO CROSSINGS FOR CLADDING

    if
((G(a3)*G(a3+1)<0)&((abs(G(a3)))<5)&((abs(G(a3+1)))<5))
        index2=index2+1;
        Bval(index2)=(B(a3)+B(a3+1))/2; %FIND ZERO CROSSING
                                                B VALUES

Bang(index2)=(asin(Bval(index2)/(k*n2)))*360/(2*pi);%FIND
                                            MODE ANGLES
        Gval(index2)=(G(a3)+G(a3+1))/2;   %FIND ACCURACCY OF
                                        ZERO CROSSING PT
        P(index2)=L*k./(Bcore-Bval(index2)); %FIND MATCHING
                                        PERIOD FOR EACH MODE
    end

end


%PRINT INFO TO SCREEN & FILE
fprintf('\nno_of_cladding_modes = %d',index2)
fprintf(Fid,'\nno_of_cladding_modes = %d',index2);

for a4 = 1:length(Bval)
    fprintf('\nB value %d: %f, B angle %d: %f, G value %d:
%0.4f, Period %d:
%fum',a4,Bval(a4),a4,Bang(a4),a4,Gval(a4),a4,(P(a4)*10^6)
);
    fprintf(Fid,'\nB value %d: %f, B angle %d: %f, G value
%d: %0.4f, Period %d:
%fum',a4,Bval(a4),a4,Bang(a4),a4,Gval(a4),a4,(P(a4)*10^6)
);
    %disp(sent2);
```

```matlab
end
fprintf('\n\nPeriod required to couple 1550nm t0 6th
clading mode = %f',P(6))
fprintf(Fid,'\n\nPeriod required to couple 1550nm t0 6th
clading mode = %f',P(6))



%using period which will couple 1550nm to 6th clad mode,
check that 1550nm couples to 6th clad mode
%=========================================================
=========================================

%CALC WAVELENGTH WHICH WILL COUPLE USING LPG EQU

Pg=P(6)

for a5=1:length(Bval)
    L1(a5)=((Bcore)-(Bval(a5))).*Pg./k;
    x(a5)=round(L1(a5).*10^(9));
    y(a5)=round(L.*10^(9));
    X(a5)=x(a5)-y(a5);
    fprintf('\nX value %d: %.2fnm,',a5,X(a5));%PRINT TO
                                        SCREEN & FILE
    fprintf(Fid,'\nX value %d: %.2fnm,',a5,X(a5));
        %disp(sent);
end

for a6=1:length(X)

    if (X(a6)==0)   %IF WAVELENGTHS MATCH ENTERED L WILL
                            COUPLE TO THIS MODE
        fprintf('\nwavelength: %.2fnm, Coupling mode :
  %d',L*10^(9),a6);
        fprintf (Fid,'\nwavelength: %.2fnm, Coupling mode
  : %d',L*10^(9),a6);
      %disp(sent1);
    end
end

clear Bval

%FIND WHICH WAVELENGTHS WILL COUPLE TO OTHER 5 LOWER
CLADDING MODES
%=========================================================
===================
%Start loop to find which core wavelengths will couple to
cladding modes 1-5
%=========================================================
===================
```

```matlab
period=Pg
index6=1;
index7=0;

L=1425*10^-9;

while L<1560*10^-9;
    k=2*pi./L;
    r1=2.625*10^(-6);
    r2=62.5*10^(-6);
    n1=1.458;
    n2=1.45;
    n3=1;
    Zo=377;
    B=k*n2:-((k.*n2)-(k.*n3))/10^(6):0.999*k.*n2;
    neff2=B./k;
    u1=sqrt((k.*k.*n1*n1)-(B.*B));
    u2=sqrt((k.*k.*n2*n2)-(B.*B));
    w1=sqrt((B.*B)-(k.*k.*n2*n2));
    w2=sqrt((B.*B)-(k.*k.*n3*n3));


    %determination of core modes at nth wavelength

    Bc=k*n1:-((k.*n1)-(k.*n2))/10^(6):0.995*k*n1;
    neff1=Bc./k;
    u=r1*sqrt((k.*k.*n1*n1)-(Bc.*Bc));
    w=r1*sqrt((Bc.*Bc)-(k.*k.*n2*n2));
    M=0;
    f1 =BESSELJ(M,u)./(u.*BESSELJ(M+1,u));
    f2 =BESSELK(M,w)./(w.*BESSELK(M+1,w));

    f=f1-f2;
    index3=0;
    for a7=1:length(Bc)-1
        if ((f(a7)*f(a7+1)<0)&((f(a7)^2)+(f(a7+1)^2)<0.01))
            index3=index3+1;
            Bcore(index3)=(Bc(a7)+Bc(a7+1))./2;

Bang1(index3)=(asin(Bcore(index3)./(k.*n1)))*360/(2*pi);

Dang(index3)=(asin(((n1*sin(Bang1(index3)*2*pi/360))-
(L/(period)))/n1))*360/(2*pi);
            Critang(index3)=asin(n2/n1)*360/(2*pi);
            fval1(index3)=(f(a7)+f(a7+1))./2;
        end
    end
    fprintf('\n\n\nThe following info is for wavelength
%.2fnm',(L*10^(9)))
    fprintf(Fid,'\n\n\nThe following info is for
wavelength %.2fnm',(L*10^(9)));
```

```
        sprintf('\nno_of_core_modes = %d',index3)
        fprintf(Fid,'\nno_of_core_modes = %d',index3);
        for a8 = 1:length(Bcore(index3))
            neff1c=Bcore(index3)./k;
            fprintf('\nBcore value %d: %f, Bcore angle %d: %f,
Diff Angle %d: %f,  Crit Angle: %fF value %d:
%0.4f\n',a8,Bcore(a8),a8,Bang1(a8),a8,Dang(a8),Critang(a8
),a8,fval1(a8));
            fprintf(Fid,'\nBcore value %d: %f, Bcore angle %d:
%f, Diff Angle %d: %f,  Crit Angle: %fF value %d:
%0.4f\n',a8,Bcore(a8),a8,Bang1(a8),a8,Dang(a8),Critang(a8
),a8,fval1(a8));          %disp(sent);
        end


    %determination of cladding modes at nth wavelength

    m=1;
    s1=(j*m.*neff2)./Zo;
    s2=(j*m.*neff2).*Zo;
    u21=(1./(u2.*u2))-(1./(u1.*u1));
    u32=(1./(w2.*w2))+(1./(u2.*u2));


    J=((BESSELJ(m-1,(u1.*r1)))-
(BESSELJ(m+1,(u1.*r1))))./(2.*u1.*BESSELJ(m,(u1.*r1)));
    K=((-BESSELK(m-1,(w2.*r2)))-
(BESSELK(m+1,(w2.*r2))))./(2.*w2.*BESSELK(m,(w2.*r2)));
    p=(BESSELJ(m,(u2.*r2)).*BESSELY(m,(u2.*r1)))-
(BESSELJ(m,(u2.*r1)).*BESSELY(m,(u2.*r2)));
    q=(BESSELJ(m,(u2.*r2)).*((BESSELY(m-1,(u2.*r1))-
(BESSELY(m+1,(u2.*r1))))/2))-(((BESSELJ(m-1,(u2.*r1))-
BESSELJ(m+1,(u2.*r1)))./2).*BESSELY(m,(u2.*r2)));
    r=(((BESSELJ(m-1,(u2.*r2)))-
(BESSELJ(m+1,(u2.*r2))))/2).*BESSELY(m,(u2.*r1))-
(BESSELJ(m,(u2.*r1)).*((BESSELY(m-1,(u2.*r2))-
(BESSELY(m+1,(u2.*r2))))/2));
    s=((((BESSELJ(m-1,(u2.*r2)))-
(BESSELJ(m+1,(u2.*r2))))/2).*((BESSELY(m-1,(u2.*r1))-
(BESSELY(m+1,(u2.*r1))))/2))-(((BESSELJ(m-1,(u2.*r1))-
(BESSELJ(m+1,(u2.*r1))))/2).*((BESSELY(m-1,(u2.*r2))-
(BESSELY(m+1,(u2.*r2))))/2));


top1=(u2.*((J.*K)+((s1.*s2.*u21.*u32)./(n2*n2*r1*r2))).*p
)-(K.*q)+(J.*r)-(s./u2);
    bot1=((-u2.*(((u32.*J)./(n2*n2*r2))-
((u21.*K)./(n1*n1*r1))).*p)+((u32.*q)./(n1*n1*r2))+((u21.
*r)./(n1*n1*r1)));
```

```matlab
    top2=((u2.*((u32.*J./r2)-
((n3*n3*u21.*K)./(n2*n2*r1))).*p)-(u32.*q./r2)-
(u21.*r./r1));

bot2=(u2.*(((n3*n3.*J.*K)./(n2*n2))+((s1.*s2.*u21.*u32)./
(n1*n1*r1*r2))).*p)-((n3*n3.*K.*q)./(n1*n1))+(J.*r)-
((n2*n2.*s)./(n1*n1.*u2));
    Go=top1./bot1;
    Go2=(m^(2)).*(neff2.^(2)).*(top2./bot2);
    G=Go+Go2;
    index4=0;

  for a9=1:length(B)-1

      if
((G(a9)*G(a9+1)<0)&((abs(G(a9)))<5)&((abs(G(a9+1)))<5))
          index4=index4+1;
          Bval(index4)=(B(a9)+B(a9+1))/2;

Bang(index4)=(asin((Bval(index4))/(k*n2)))*360/(2*pi);
          Gval(index4)=(G(a9)+G(a9+1))/2;
      end
    end
    fprintf('\nno_of_cladding_modes = %d',index4)
    fprintf(Fid,'\nno_of_cladding_modes = %d',index4);

    for a10=1:length(Bval)

        fprintf('\nB value %d: %f, B angle %d: %f, G value
%d: %0.4f',a10,Bval(a10),a10,Bang(a10),a10,Gval(a10));
        fprintf(Fid,'\nB value %d: %f, B angle %d: %f, G
value %d:
%0.4f',a10,Bval(a10),a10,Bang(a10),a10,Gval(a10));
        %disp(sent);
    end

 %find if this wavelength will couple into any of the
cladding modes available

 %for this wavelength (ie. if L(calc)=L(entered))

    for a11=1:length(Bval)
      L1(a11)=((Bcore-(Bval(a11)))).*Pg./k;
      x(a11)=round(L1(a11).*10^(9));
      y(a11)=round(L.*10^(9));
      X(a11)=x(a11)-y(a11);
      fprintf('\nX value %d: %.2fnm,',a11,X(a11));%PRINT
                                    TO SCREEN & FILE
      fprintf(Fid,'\nX value %d: %.2fnm,',a11,X(a11));
```

```matlab
        end


    a12=0;
    index5=0;

  for a13=1:length(X)

    if ((X(a13)>=-1)&(X(a13)<=1))  %IF WAVELENGTHS MATCH
                          ENTERED L WILL COUPLE TO THIS MODE
        index5=index5+1;
        index7=index7+1;
        fprintf('\nwavelength: %.2fnm, Coupling mode :
%d',L*10^(9),a13);
        fprintf (Fid,'\nwavelength: %.2fnm, Coupling
mode : %d',L*10^(9),a13);
        Lcup(index5)=L;
        Bcup(index5)=Bval(a13);
        mode(index5)=a13;
        Bcorecup(index5)=Bcore;
        store_Lcup(index7)=Lcup(index5);
        store_Bcup(index7)=Bcup(index5);
        store_mode(index7)=mode(index5);
        store_Bcorecup(index7)=Bcorecup(index5);

store(index7,:)=[store_Lcup(index7),store_Bcup(index7),

store_Bcorecup(index7)];

index6=index6+1;


     else
         a12=a12+1;
     end
   end



    if a12==a13    %IF WAVELENGTHS NOT MATCH ENTERED L
                              PRINT 'NO COUPLING'
     fprintf('\nno mode coupling at wavelength
%.2fnm',L*10^(9));
     fprintf (Fid,'\nno mode coupling at wavelength
%.2fnm',L*10^(9));
   else
     fprintf('\n\n\n
L%d=%f,Lcup%d=%f,Bcup%d=%f,mode%d=%d,Bcorecup%d=%f
\n',(index7),L*10^(9),(index7),Lcup(index5)*10^(9),(index
7),Bcup(index5)*10^(6),(index7),mode(index5),(index7),Bco
recup(index5)*10^(6));
```

```matlab
        fprintf (Fid,'\n\n\n
L%d=%f,Lcup%d=%f,Bcup%d=%f,mode%d=%d,Bcorecup%d=%f
\n',(index7),L*10^(9),(index7),Lcup(index5)*10^(9),(index
7),Bcup(index5)*10^(6),(index7),mode(index5),(index7),Bco
recup(index5)*10^(6));
    end

    index6=index6+1;


    increase=1*10^(-9);
    L=L+increase;      %END OF WAVELENGTH LOOP
end

store
```

Appendix 6

Program Code to Determine Coupling Wavelength Shifts Using Actual Fibre Parameters for Ambient Indices Less than Cladding

```matlab
%Erdogan3Layer
clear all, clc;
fid =
fopen('d:\PaulDowker\Matlab\PaulD\results.doc','w');
                                              %OPEN FILE
fprintf(fid,'\nErdogan3Layer);
fprintf('\n Erdogan3Layer \n')
fprintf('\n %s \n',date)
fprintf(fid,'\n %s\n',date);
fprintf('\nProg to find coupling from HE11 (LP01) core to
HEml Cladding modes (where m = 1)');
fprintf(fid,'\nProg to find coupling from HE11 (LP01)
core to HEml Cladding modes (where m = 1)');
```

```matlab
L=995*10^-9;

r1=4.1*10^(-6);
r2=62.5*10^(-6);
n1=1.4535;
n2=1.4483;
n3=1;
Zo=377;
period=280*10^(-6);

index3=0;

while L<1700*10^-9;
    %determination of core modes at nth wavelength
    k=2*pi./L;
    Bc=k*n1:-((k.*n1)-(k.*n2))/10^(6):k*n2;
    neff1=Bc./k;
    u=r1*sqrt((k.*k.*n1*n1)-(Bc.*Bc));
    w=r1*sqrt((Bc.*Bc)-(k.*k.*n2*n2));
    M=0;
    f1 =BESSELJ(M,u)./(u.*BESSELJ(M+1,u));
    f2 =BESSELK(M,w)./(w.*BESSELK(M+1,w));

    f=f1-f2;
    index1=0;
    for a1=1:length(Bc)-1
        if ((f(a1)*f(a1+1)<0)&((f(a1)^2)+(f(a1+1)^2)<0.01))
            index1=index1+1;
            Bcore(index1)=(Bc(a1)+Bc(a1+1))./2;

Bang1(index1)=(asin(Bcore(index1)./(k.*n1)))*360/(2*pi);
            fval1(index1)=(f(a1)+f(a1+1))./2;
        end
    end
    fprintf('\n\n\nThe following info is for wavelength
%.2fnm',(L*10^(9)))
    fprintf(fid,'\n\n\nThe following info is for
wavelength %.2fnm',(L*10^(9)));

    fprintf('\nno_of_core_modes = %d',index1)
    fprintf(fid,'\nno_of_core_modes = %d',index1);

    for a2 = 1:length(Bcore(index1))
        neff1c=Bcore(index1)./k;
        fprintf('\nBcore value %d: %f, Bcore angle %d: %f,
F value %d: %0.4f\n',a2,Bcore(a2),a2,
Bang1(a2),a2,fval1(a2));
        fprintf(fid,'\nBcore value %d: %f, Bcore angle %d:
%f, F value %d: %0.4f\n',a2,Bcore(a2),a2,
Bang1(a2),a2,fval1(a2));
        %disp(sent);
```

```matlab
    end


    %determination of cladding modes at nth wavelength
    Bcl=k*n2:-((k.*n2)-(k.*n3))/10^(6):0.998*k.*n2;
    neff2=Bcl./k;
    u1=sqrt((k.*k.*n1*n1)-(Bcl.*Bcl));
    u2=sqrt((k.*k.*n2*n2)-(Bcl.*Bcl));
    w1=sqrt((Bcl.*Bcl)-(k.*k.*n2*n2));
    w2=sqrt((Bcl.*Bcl)-(k.*k.*n3*n3));


    m=1;
    s1=(j*m.*neff2)./Zo;
    s2=(j*m.*neff2).*Zo;
    u21=(1./(u2.*u2))-(1./(u1.*u1));
    u32=(1./(w2.*w2))+(1./(u2.*u2));


    J=((BESSELJ(m-1,(u1.*r1)))-
(BESSELJ(m+1,(u1.*r1))))./(2.*u1.*BESSELJ(m,(u1.*r1)));
    K=((-BESSELK(m-1,(w2.*r2)))-
(BESSELK(m+1,(w2.*r2))))./(2.*w2.*BESSELK(m,(w2.*r2)));
    p=(BESSELJ(m,(u2.*r2)).*BESSELY(m,(u2.*r1)))-
(BESSELJ(m,(u2.*r1)).*BESSELY(m,(u2.*r2)));
    q=(BESSELJ(m,(u2.*r2)).*((BESSELY(m-1,(u2.*r1))-
(BESSELY(m+1,(u2.*r1))))/2))-(((BESSELJ(m-1,(u2.*r1))-
BESSELJ(m+1,(u2.*r1)))./2).*BESSELY(m,(u2.*r2)));
    r=(((BESSELJ(m-1,(u2.*r2)))-
(BESSELJ(m+1,(u2.*r2))))/2).*BESSELY(m,(u2.*r1))-
(BESSELJ(m,(u2.*r1)).*((BESSELY(m-1,(u2.*r2))-
(BESSELY(m+1,(u2.*r2))))/2));
    s=((((BESSELJ(m-1,(u2.*r2)))-
(BESSELJ(m+1,(u2.*r2))))/2).*((BESSELY(m-1,(u2.*r1))-
(BESSELY(m+1,(u2.*r1))))/2))-(((BESSELJ(m-1,(u2.*r1))-
(BESSELJ(m+1,(u2.*r1))))/2).*((BESSELY(m-1,(u2.*r2))-
(BESSELY(m+1,(u2.*r2))))/2));




top1=(u2.*((J.*K)+((s1.*s2.*u21.*u32)./(n2*n2*r1*r2))).*p
)-(K.*q)+(J.*r)-(s./u2);
    bot1=((-u2.*(((u32.*J)./(n2*n2*r2))-
((u21.*K)./(n1*n1*r1))).*p)+((u32.*q)./(n1*n1*r2))+((u21.
*r)./(n1*n1*r1)));

    top2=((u2.*((u32.*J./r2)-
((n3*n3*u21.*K)./(n2*n2*r1))).*p)-(u32.*q./r2)-
(u21.*r./r1));

bot2=(u2.*(((n3*n3.*J.*K)./(n2*n2))+((s1.*s2.*u21.*u32)./
```

```matlab
(n1*n1*r1*r2))).*p)-((n3*n3.*K.*q)./(n1*n1))+(J.*r)-
((n2*n2.*s)./(n1*n1.*u2));
    Go=top1./bot1;
    Go2=(m^(2)).*(neff2.^(2)).*(top2./bot2);
    G=Go+Go2;
    %plot(B,G,'r'),grid;
    index2=0;
    for a3=1:length(Bcl)-1
        if
((G(a3)*G(a3+1)<0)&((abs(G(a3)))<5)&((abs(G(a3+1)))<5))
            index2=index2+1;
            BcladHE(index2)=(Bcl(a3)+Bcl(a3+1))/2;

BcladangHE(index2)=(asin((BcladHE(index2))/(k*n2)))*360/(
2*pi);
            GcladHE(index2)=(G(a3)+G(a3+1))/2;
            P(index2)=L*k./(Bcore-BcladHE(index2));
        end
    end

    %PRINT INFO TO SCREEN & FILE
    fprintf('\nno_of_cladding_modes = %d',index2)
    fprintf(fid,'\nno_of_cladding_modes = %d',index2);
    for a4=1:length(BcladHE)
        fprintf('\nB value %d: %f, B angle %d: %f, G value
%d: %0.4f',a4,BcladHE(a4),a4,
BcladangHE(a4),a4,GcladHE(a4));
        fprintf(fid,'\nB value %d: %f, B angle %d: %f, G
value %d: %0.4f',a4,BcladHE(a4),a4,
BcladangHE(a4),a4,GcladHE(a4));
    end

%find if this wavelength will couple into any of the
cladding modes available

    %for this wavelength (ie. if L(calc)=L(entered))

    for a5=1:length(BcladHE)
        L1(a5)=((Bcore-(BcladHE(a5)))).*period./k;
        x(a5)=round(L1(a5).*10^(9));
        y(a5)=round(L.*10^(9));
        X(a5)=x(a5)-y(a5);
        fprintf('\nX value %d: %.2fnm,',a5,X(a5));%PRINT TO
                                    SCREEN & FILE
        fprintf(fid,'\nX value %d: %.2fnm,',a5,X(a5));

    end
```

```matlab
a6=0;

for a7=1:length(X)
        if ((X(a7)>=-1)&(X(a7)<=1))   %IF WAVELENGTHS MATCH
                                 ENTERED L WILL COUPLE TO THIS MODE
            index3=index3+1;
            fprintf('\nwavelength: %.2fnm, Coupling mode
:HE1,%d',L*10^(9),a7);
            fprintf (fid,'\nwavelength: %.2fnm, Coupling
mode :HE1,%d',L*10^(9),a7);
            Lcup(a7)=L;
            Bcladcup(a7)=BcladHE(a7);
            mode(a7)=a7;
            Bcorecup(a7)=Bcore;
            fprintf('\n\n\n coupling mode=HE1,%d,
LcupHE1,%d=%f, BcladcupHE1,%d=%f, BcorecupHE1,%d=%f
\n',mode(a7),a7,Lcup(a7)*10^(9),a7,Bcladcup(a7),a7,Bcorec
up(a7));
            fprintf (fid,'\n\n\n coupling mode=HE1,%d,
LcupHE1,%d=%f, BcladcupHE1,%d=%f, BcorecupHE1,%d=%f
\n',mode(a7),a7,Lcup(a7)*10^(9),a7,Bcladcup(a7),a7,Bcorec
up(a7));

            store_mode(index3)=mode(a7);
            store_Lcup(index3)=Lcup(a7);
            store_Bcladcup(index3)=Bcladcup(a7);
            store_Bcorecup(index3)=Bcorecup(a7);

store(index3,:)=[store_mode(index3),store_Lcup(index3),st
ore_Bcladcup(index3),store_Bcorecup(index3)];

        else
            a6=a6+1;
        end
    end


    if a6==a7     %IF WAVELENGTHS NOT MATCH ENTERED L PRINT
                                        'NO COUPLING'
      fprintf('\nno mode coupling at wavelength
%.2fnm',L*10^(9));
      fprintf (fid,'\nno mode coupling at wavelength
%.2fnm',L*10^(9));
    end


    L=L+1*10^(-9);     %END OF WAVELENGTH LOOP
end
```

```matlab
for a8=1:size(store)
    fprintf('\n\ncoupling mode=HE1,%d, LcupHE1,%d = %4fnm,
BcladcupHE1,%d = %f, BcorecupHE1,%d =
%f',store(a8,1),store(a8,1),store(a8,2)*10^(9),store(a8,1
),store(a8,3),store(a8,1),store(a8,4));
    fprintf(fid,'\n\ncoupling mode=HE1,%d, Lcup %d =
%4fnm, Bcladcup %d = %f, Bcorecup %d =
%f',store(a8,1),store(a8,1),store(a8,2)*10^(9),store(a8,1
),store(a8,3),store(a8,1),store(a8,4));
end

fclose(fid);

return
```

Appendix 7

Program Code to Determine Coupling Wavelength Shifts Using Actual Fibre Parameters For Ambient Indices Greater Than Cladding

```
%Yarivbign3multithesis
clear all,clc;
format long
Fid =
fopen('d:\PaulDowker\Matlab\PaulD\results.txt','w');
                                            %OPEN FILE
fprintf('\nYarivbign3multithesis');
fprintf(Fid,'\nYarivbign3multithesis');
fprintf('\n %s \n',date)
fprintf(Fid,'\n %s\n',date);
fprintf('\nProg to find coupling from HE11 (LP01) core to
HEml Cladding modes (where m = 1)');
fprintf(Fid,'\nProg to find coupling from HE11 (LP01)
core to HEml Cladding modes (where m = 1)');
```

```matlab
%start wavelength loop
%=========================================================

index4=0;

L=990*10^-9;                                    %WAVELENGTH

while L<1600*10^-9;

    k=2*pi./L;                                  %WAVE NUMBER
    r1=4.1*10^(-6);                             %CORE RADIUS
    r2=62.5*10^(-6);                            %CLADDING RADIUS
    n1=1.4535;                                  %CORE RI
    n2=1.4483;                                  %CLADDING RI
    n3=1                                        %AMBIENT RI
    period=280*10^(-6);

    %determination of core modes

    Bc=k*n1:-((k.*n1)-(k.*n2))/10^(4):k*n2;
                        %CORE PROPAGATION CONSTANT RANGE
    neff1=Bc./k;                        %CORE EFFECTIVE RI
    u1=r1*sqrt((k.*k.*n1*n1)-(Bc.*Bc));     %CORE u VALUE
    w1=r1*sqrt((Bc.*Bc)-(k.*k.*n2*n2));     %CORE w VALUE

    M=0;
    f1 =BESSELJ(M,u1)./(u1.*BESSELJ(M+1,u1)); %LHS OF EQU
    f2 =BESSELK(M,w1)./(w1.*BESSELK(M+1,w1)); %RHS OF EQU

    f=f1-f2;        %GIVES BN VALUES WHICH SATISFY BOTH SIDES


    index1=0;
    for a1=1:length(Bc)-1
    %FIND ZERO CROSSINGS
        if ((f(a1)*f(a1+1)<0)&((f(a1)^2)+(f(a1+1)^2)<0.01))
            index1=index1+1;
            Bcore(index1)=(Bc(a1)+Bc(a1+1))./2; %FIND ZERO
                                        CROSSING B VALUES
Bang1(index1)=(asin(Bcore(index1)./(k.*n1)))*360/(2*pi);
                                        %FIND MODE ANGLES
            fval1(index1)=(f(a1)+f(a1+1))./2; %FIND
                            ACCURACCY OF ZERO CROSSING PT

        end
    end



%PRINT INFO TO SCREEN & FILE
```

```matlab
    fprintf('\nThe following info is for wavelength of
%.2fnm',L*10^(9))
    fprintf('\nno_of_core_modes = %d',index1)
    fprintf(Fid,'\nno_of_core_modes = %d',index1);

    for a2 = 1:length(Bcore)
        neff1c=Bcore./k;
        fprintf('\nBcore value %d: %f, Bcore angle %d: %f,
F value %d:
%0.4f\n',a2,Bcore(a2),a2,Bang1(a2),a2,fval1(a2));
        fprintf(Fid,'\nBcore value %d: %f, Bcore angle %d:
%f, F value %d:
%0.4f\n',a2,Bcore(a2),a2,Bang1(a2),a2,fval1(a2));
        %disp(sent1);
    end



    %determination of cladding modes

    Bclmax=n2*k;
    Bclmin=0.997.*k.*n2;
    Bclstep=(Bclmax-Bclmin)*10^(-4);
        Bcl=Bclmax:-Bclstep:Bclmin;     %CLADDING PROPAGATION
                                        CONSTANT RANGE
    neff2=Bcl./k;                       %CLADDING EFFECTIVE RI
    u2=r2.*sqrt((k.*k.*n2*n2)-(Bcl.*Bcl));  %CLADDING u
                                            VALUE
    w2=r2.*sqrt((Bcl.*Bcl)-(k.*k.*n3*n3));  %CLADDING w
                                            VALUE


    m=1;

    JHE=(BESSELJ(m-1,u2))./(u2.*BESSELJ(m,u2));
    K1HE=-((((n2*n2)+(n3*n3))/(2*n2*n2)).*((-BESSELK(m-
1,w2)-((m./w2).*BESSELK(m,w2)))./(w2.*BESSELK(m,w2))));

    K2HE=((((n2*n2)-(n3*n3))/(2*n2*n2))*(((n2*n2)-
(n3*n3))/(2*n2*n2))).*(((-BESSELK(m-1,w2)-
((m./w2).*BESSELK(m,w2)))./(w2.*BESSELK(m,w2))).*   ((-
BESSELK(m-1,w2)-
((m./w2).*BESSELK(m,w2)))./(w2.*BESSELK(m,w2))));

K3HE=((m*m.*Bcl.*Bcl)./(n2*n2*k*k)).*(((1./(w2.*w2))+(1./
(u2.*u2))).*((1./(w2.*w2))+(1./(u2.*u2))));
    KHE=K1HE+(m./(u2.*u2))-((K2HE+K3HE).^(0.5));
        GHE=JHE-KHE;


    %Bcl values are obtained where GHE crosses Bcl axis,
(i.e.GHE=0)
```

```matlab
index2=0;
for a3=1:length(Bcl)-1

    if
((real(GHE(a3))*real(GHE(a3+1))<0)&(((real(GHE(a3)))^2)+(
(real(GHE(a3+1)))^2)<0.001))%FIND ZERO CROSSINGS FOR
                                    CLADDING

        index2=index2+1;
        BcladHE(index2)=(Bcl(a3)+Bcl(a3+1))/2;    %FIND
                            ZERO CROSSING Bclad VALUES

BcladangHE(index2)=(asin(BcladHE(index2)/(k*n2)))*360/(2*
pi);                                %FIND MODE ANGLES
        GcladHE(index2)=(GHE(a3)+GHE(a3+1))/2;    %FIND
                            ACCURACCY OF ZERO CROSSING
PT
        P(index2)=L*k./(Bcore-BcladHE(index2));  %FIND
                        MATCHING PERIOD FOR EACH MODE

    end
end

%PRINT INFO TO SCREEN & FILE
fprintf('\nno_of_cladding_modes = %d',index2)
fprintf(Fid,'\nno_of_cladding_modes = %d',index2);

for a4=1:length(BcladHE)
    fprintf('\nB value HE1%d: %f, Bcl angle HE1%d: %f,
G value HE1%d: %0.4f, Period HE1%d:
%fum',a4,BcladHE(a4),a4,BcladangHE(a4),a4,GcladHE(a4),a4,
(P(a4)*10^(6)));
    fprintf(Fid,'\nB value HE1%d: %f, Bcl angle HE1%d:
%G, F value HE1%d: %0.4f, Period HE1%d:
%fum',a4,BcladHE(a4),a4,BcladangHE(a4),a4,GcladHE(a4),a4,
(P(a4)*10^(6)));
end


for a5=1:length(BcladHE)

%find which Bclad modes match conditions for coupling
from core mode

    L1(a5)=((Bcore-
(BcladHE(a5)))).*period./k;%CALCULATE VALUE OF COUPLING
                        EQU FOR EACH CLAD MODE
    x(a5)=round(L1(a5).*10^(10));%ROUND THIS VALUE TO
                            1dp
```

```matlab
            y(a5)=round(L.*10^(10));        %ROUND ACTUAL
                            WAVELEENGTH VALUE TO 1 dp
            X(a5)=(x(a5)-y(a5))/10;      %FIND DIFFERENCE BETWEEN
                        CALCULATED & ACTUAL WAVELENGTH VALUE
        fprintf('\nX value %d = %.2fnm,',a5,X(a5));%PRINT
                                    TO SCREEN & FILE
        fprintf(Fid,'\nX value %d: %.2fnm,',a5,X(a5));
    end


    %COUNTS NO OF COUPLING CLADDING MODES

    a6=0;
    index3=0;

    for a7=1:length(X)

        if ((X(a7)>=-1)&(X(a7)<=1))    %IF WAVELENGTHS MATCH
                    ENTERED L COUPLING TO THIS MODE WILL OCCUR
            index3=index3+1;
            index4=index4+1;
            fprintf('\nwavelength: %.2fnm, Coupling mode
:HE1,%d',L*10^(9),a7);
            fprintf (Fid,'\nwavelength: %.2fnm, Coupling
mode :HE1,%d',L*10^(9),a7);
            Lcup(index3)=L*10^9;
            Bcladcup(index3)=BcladHE(a7);
            mode(index3)=a7;
            Bcorecup(index3)=Bcore;
            store_Lcup(index4)=Lcup(index3);
            store_Bcladcup(index4)=Bcladcup(index3);
            store_mode(index4)=mode(index3);
            store_Bcorecup(index4)=Bcorecup(index3);

        else
            a6=a6+1;
        end

    end

    if a6==a7
        fprintf('\nNo Coupling at wavelenght %d',L);
        fprintf(Fid,'\nNo Coupling at this wavelenght
%d',L);
    else
        fprintf('\n wavelength %dnm, cladding mode HE 1%d
',Lcup(index3)*10^9,mode(index3));
        fprintf(Fid,'\n wavelength %d, cladding mode HE 1%d
',Lcup(index3)*10^9,mode(index3));
```

```
store(index4,:)=[store_Lcup(index4),store_Bcladcup(index4
),store_Bcorecup(index4)];

    end

    L=L+1*10^(-9);

end
store
fclose(Fid);
```

Appendix 8

Transmission Profiles of LPGs in Air at Constant Room Temperature
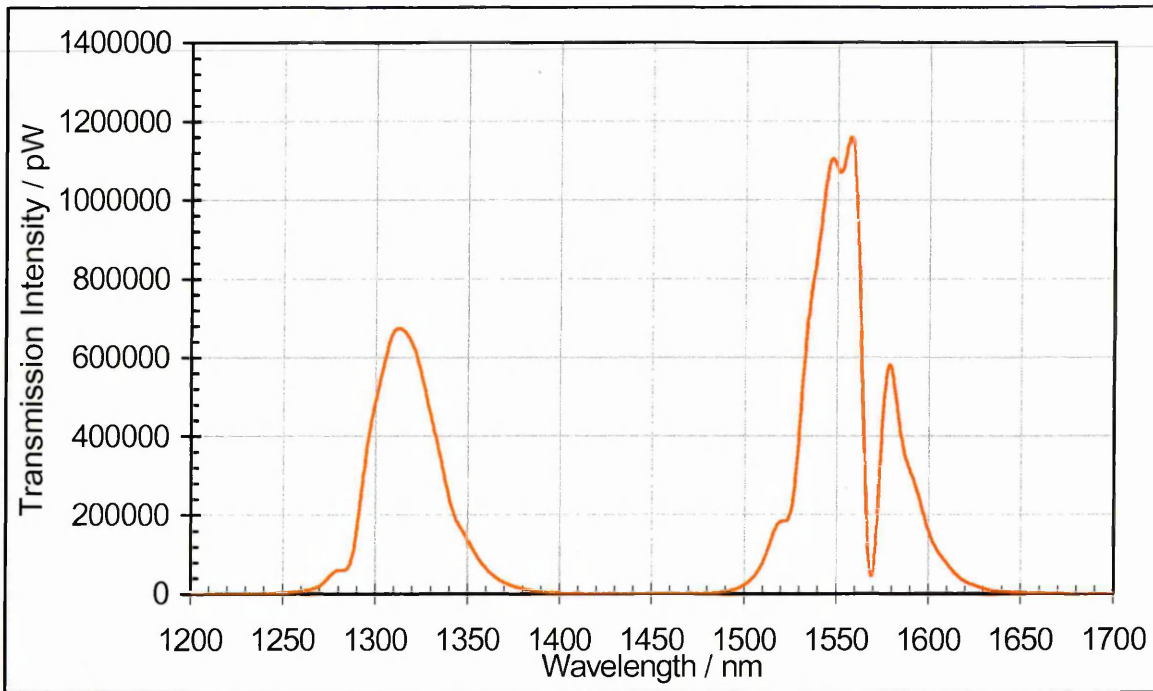
Figure A8.1: Transmission profile of LPG S3 in air at room temperature
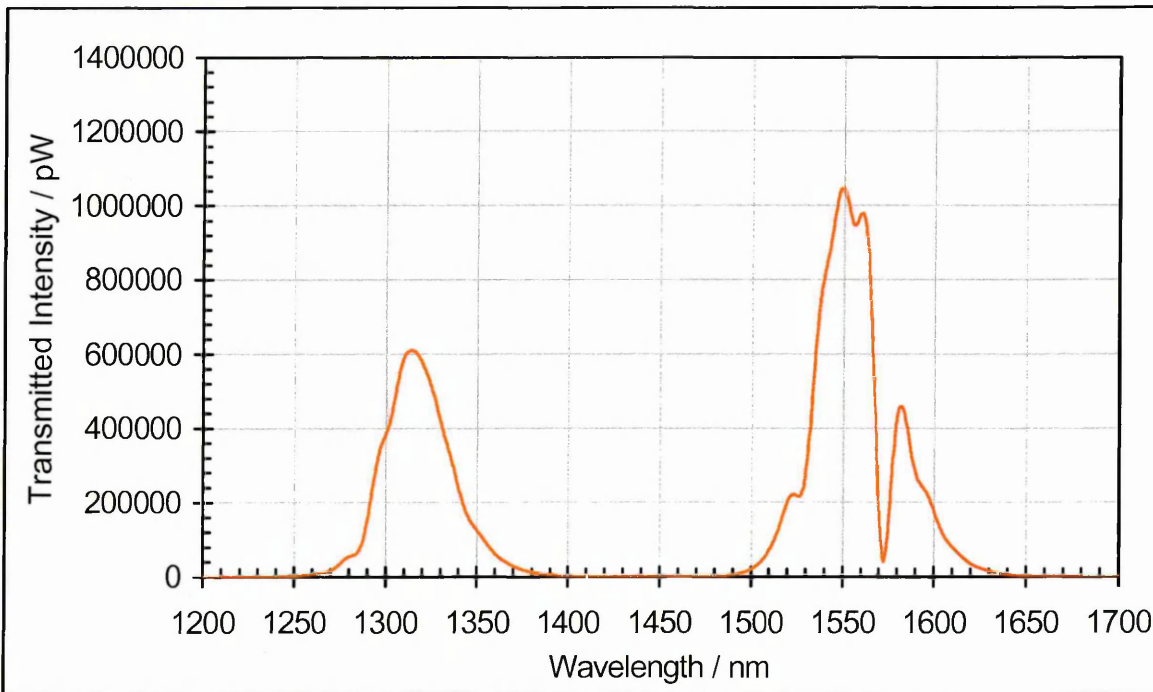
Figure A8.2: Transmission profile of LPG S4 in air at room temperature
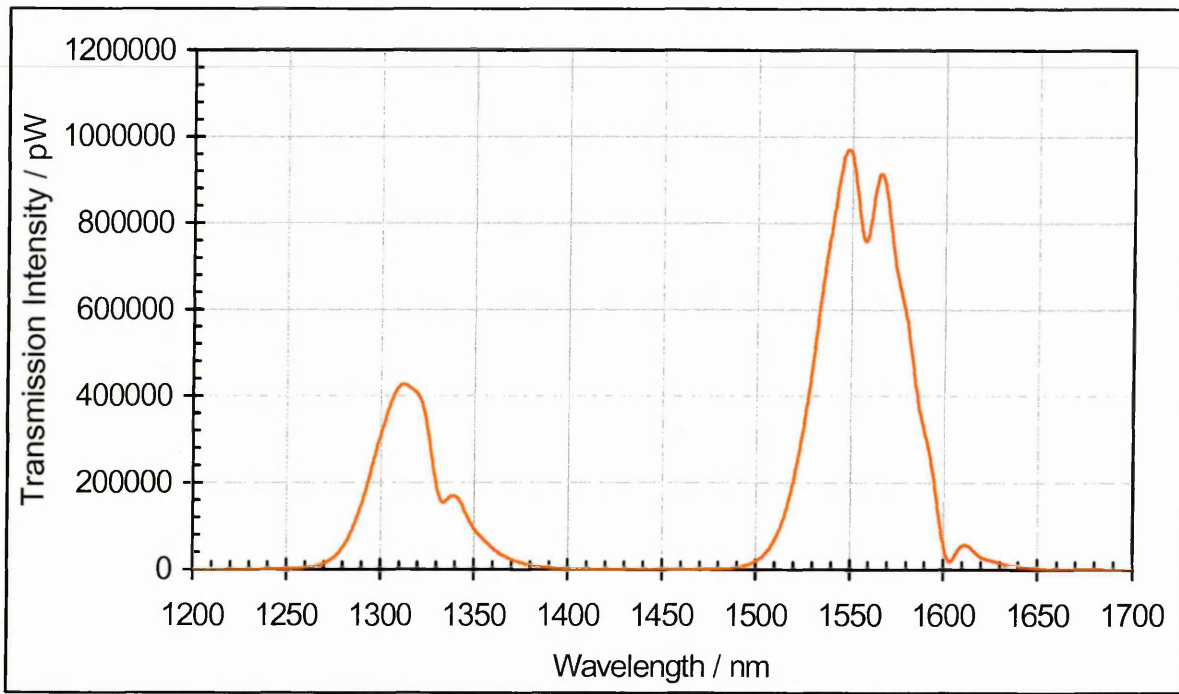
Figure A8.3: Transmission profile of LPG S5 in air at room temperature
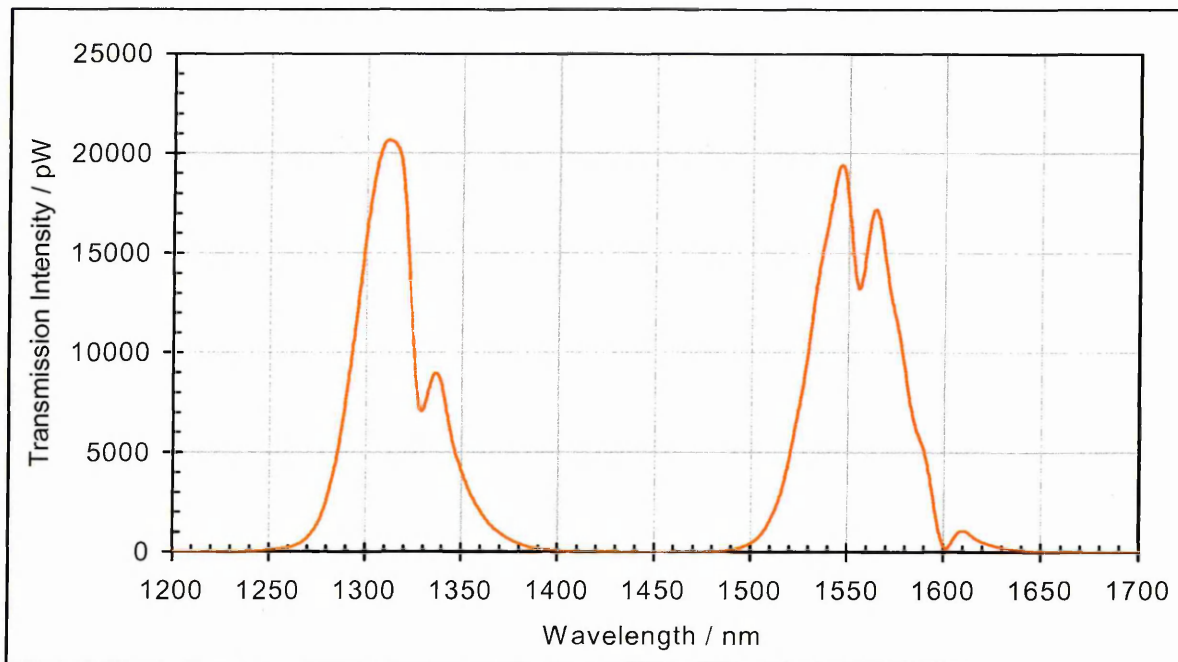
Figure A8.4: Transmission profile of LPG S6 in air at room temperature
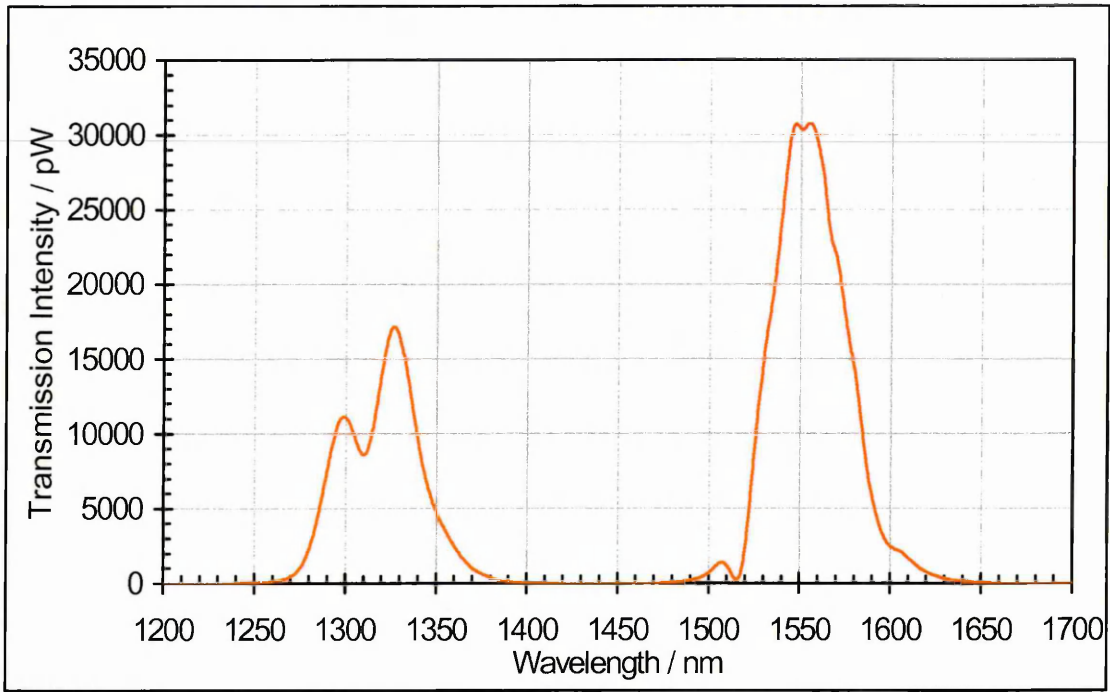
Figure A8.5: Transmission profile of LPG S7 in air at room temperature
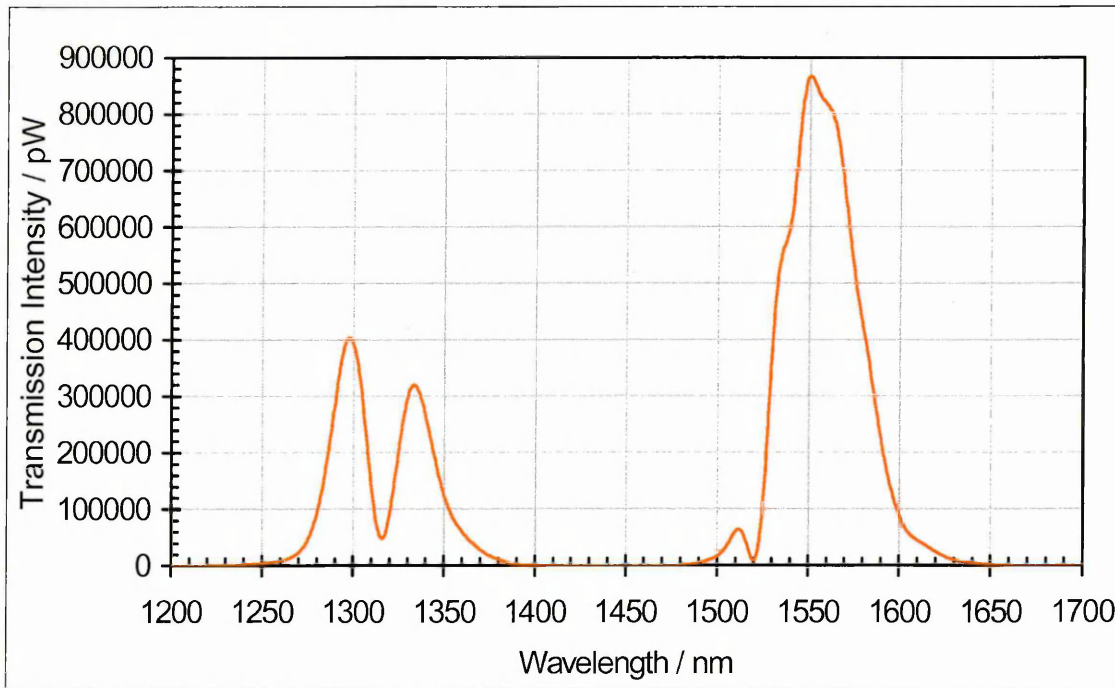
Figure A8.6: Transmission profile of LPG S8 in air at room temperature
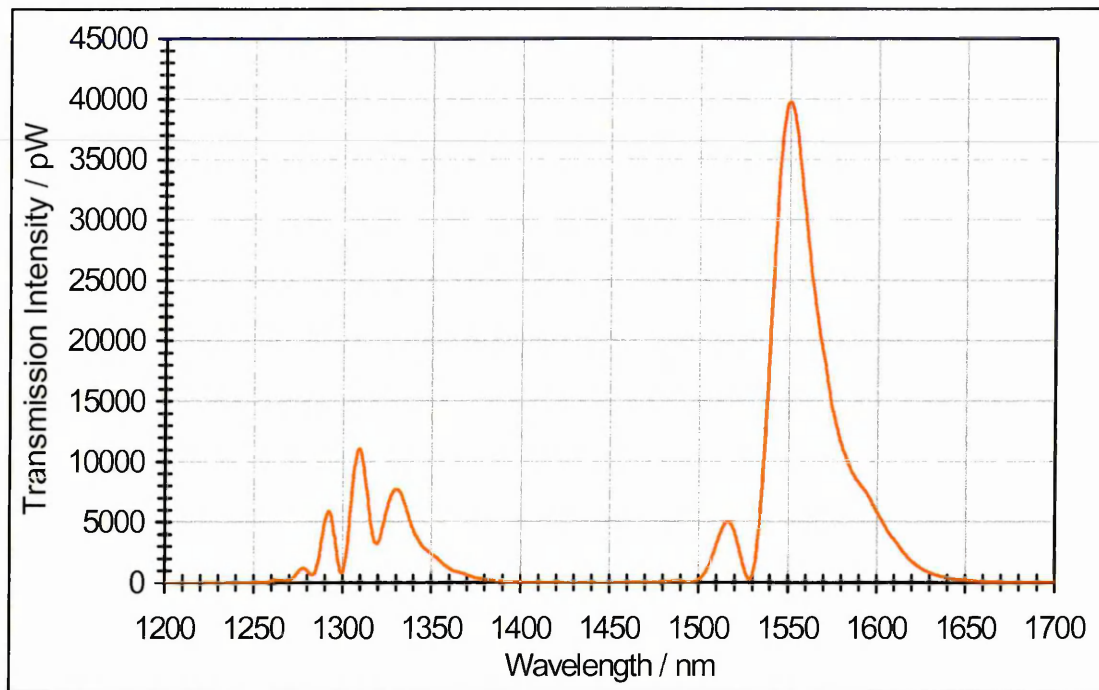
Figure A8.7: Transmission profile of LPG C1 in air at room temperature
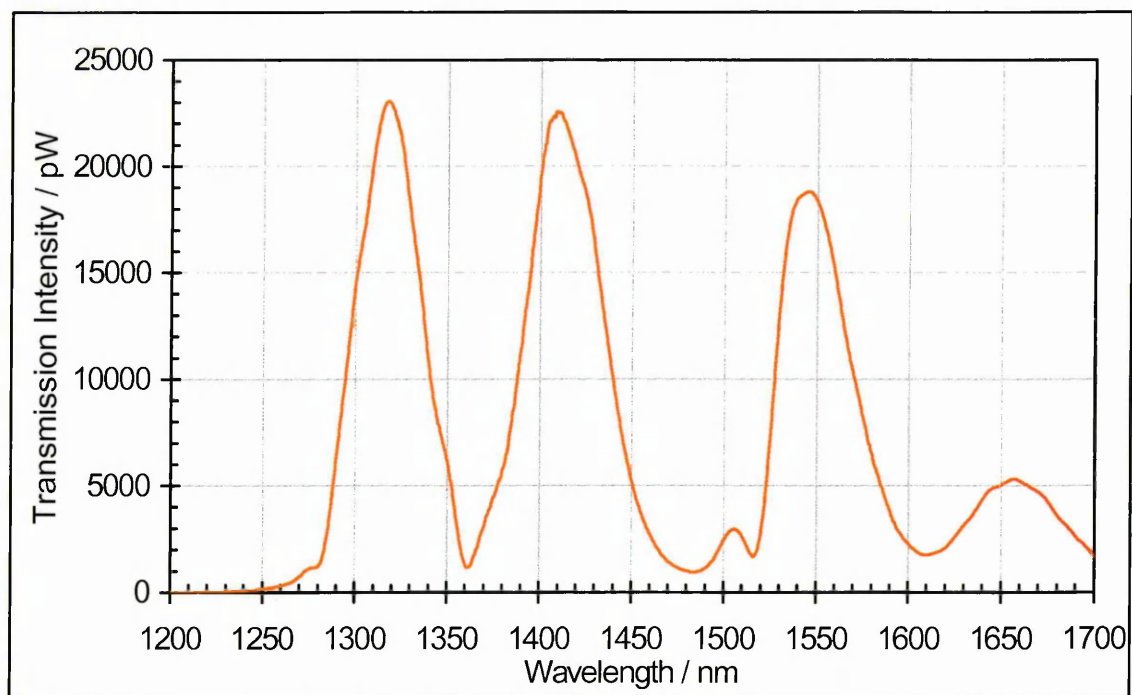
Figure A8.8: Transmission profile of LPG A400 in air at room temperature
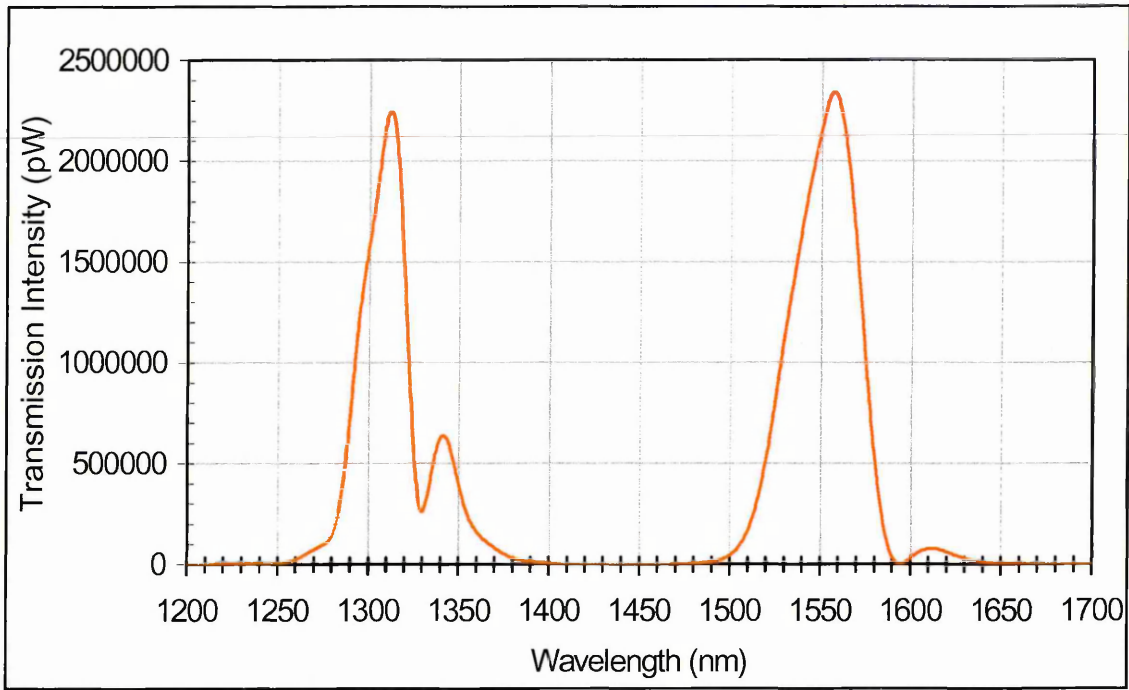
Figure A8.9: Transmission profile of LPG A403 in air at room temperature
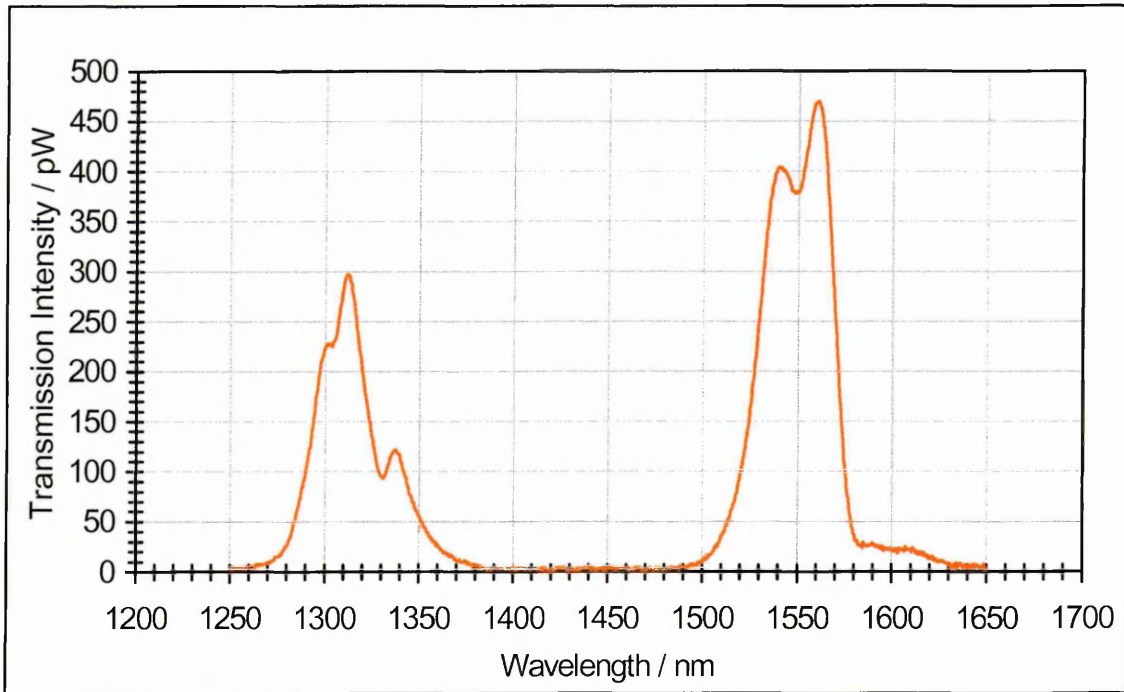
Figure A8.10: Transmission profile of LPG A407 in air at room temperature
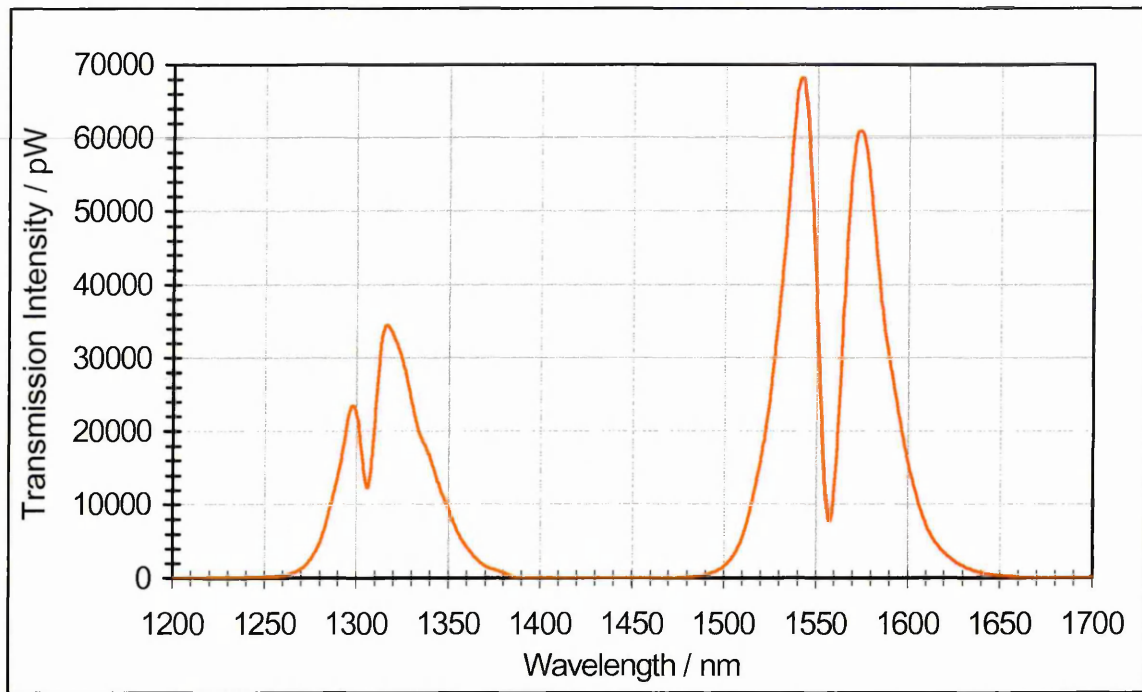
Figure A8.11: Transmission profile of LPG A410 in air at room temperature
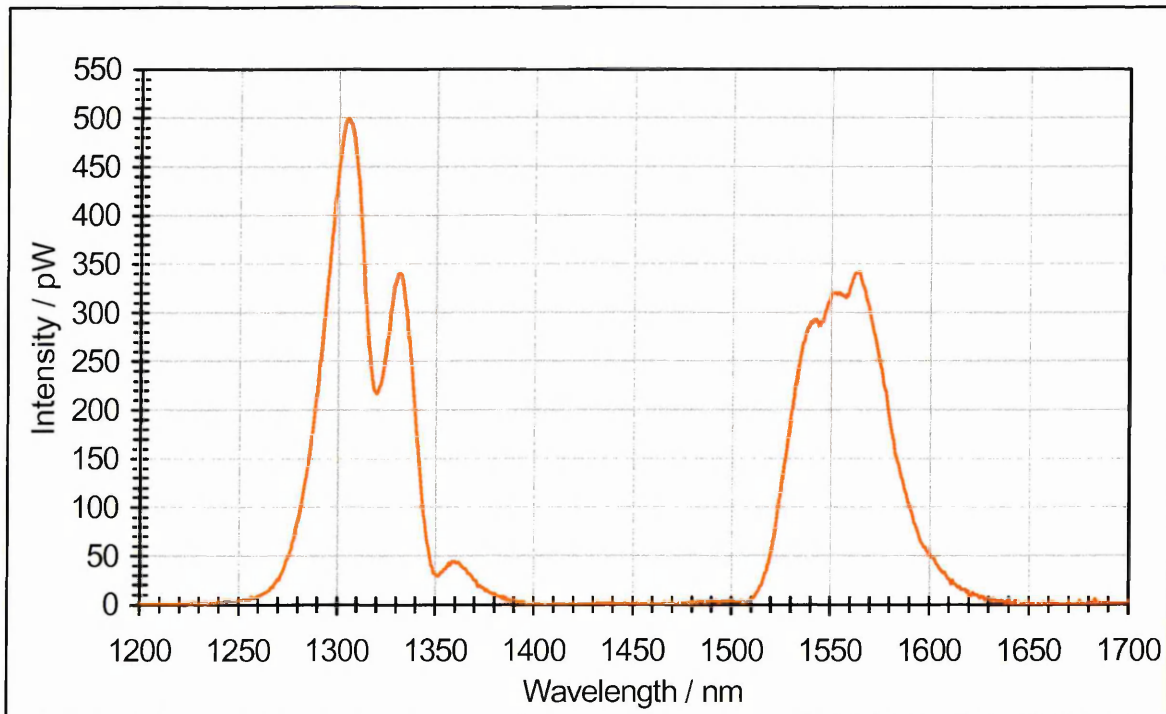
Figure A8.12: Transmission profile of LPG A416 in air at room temperature

287

Appendix 9

Ambient Refractive Index Profiles of All LPGs
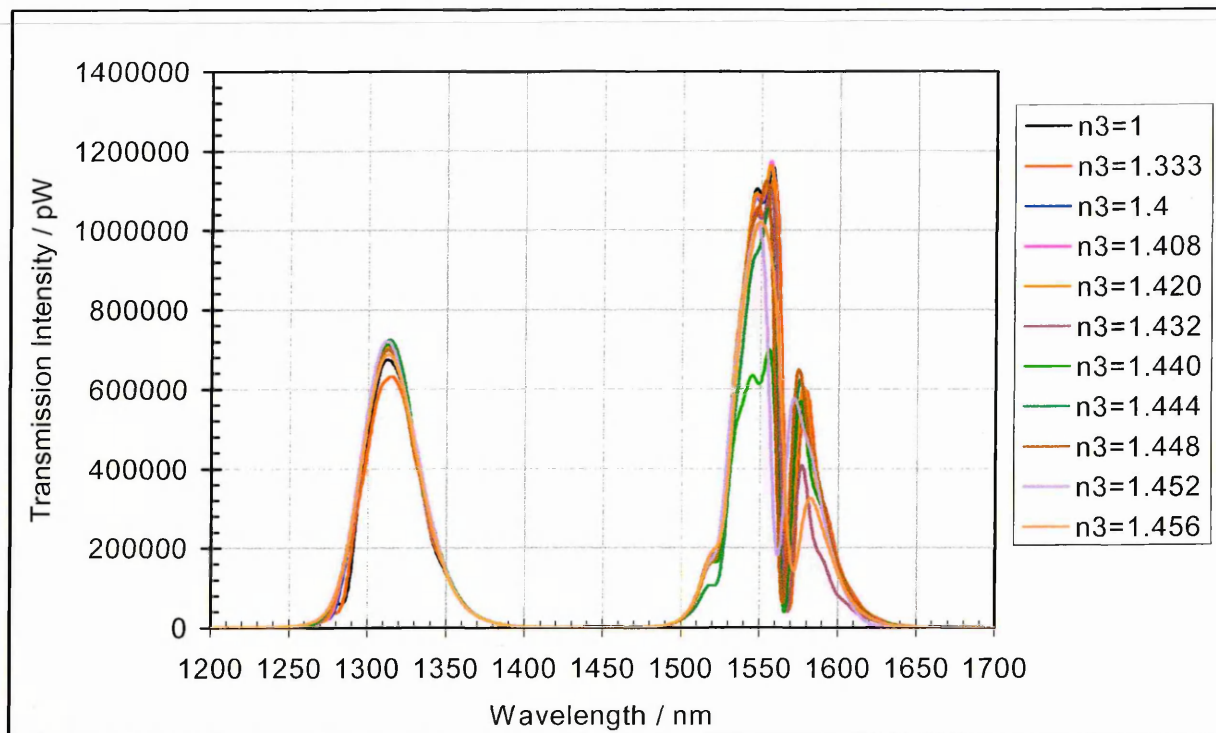
**Figure A9.1: Ambient refractive index profile of LPG S3**
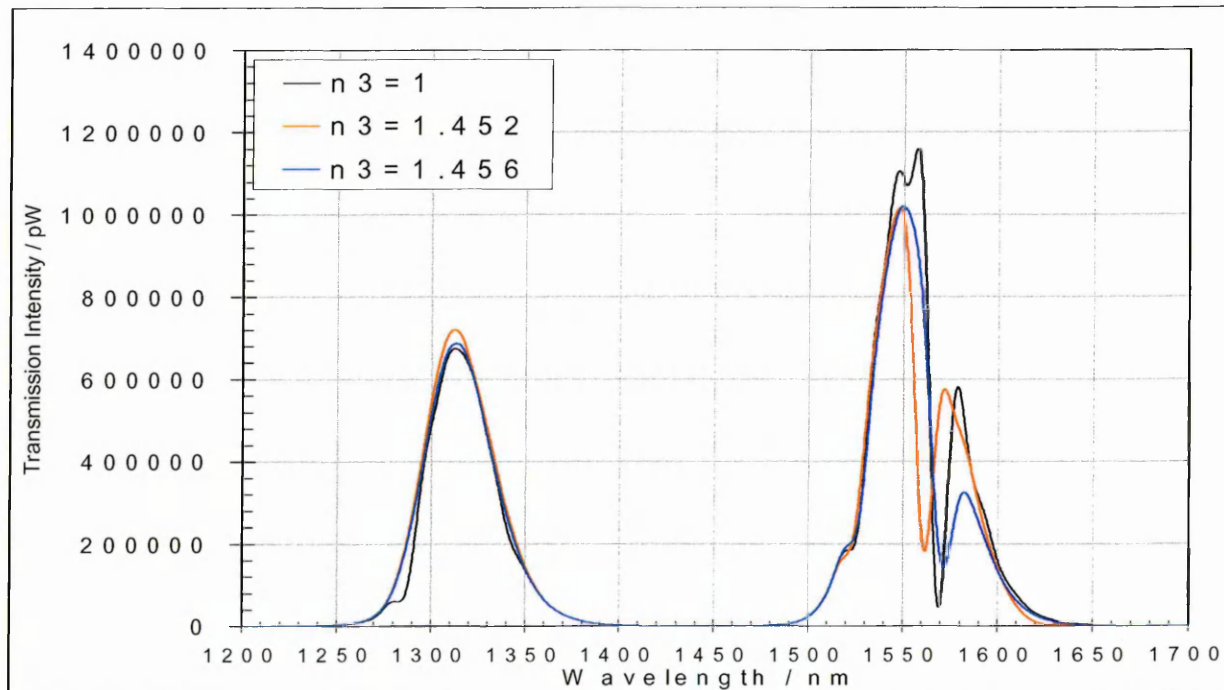
Figure A9.2: Ambient refractive index profile of LPG S3 at selected values to allow clearer observation of shifts
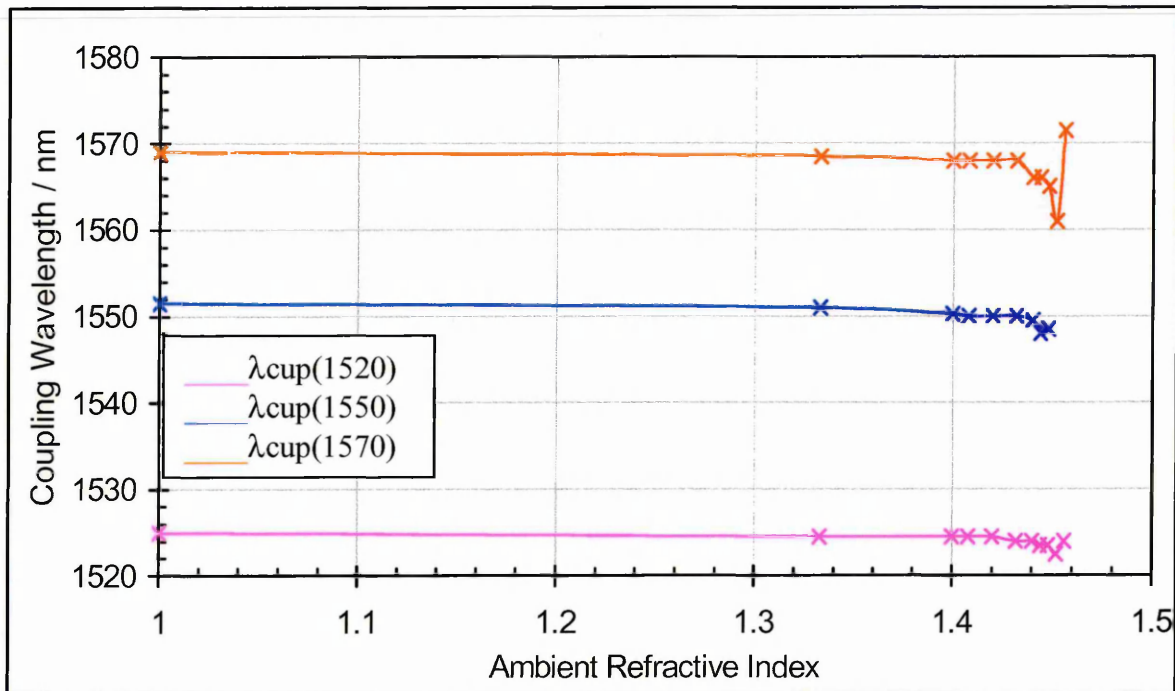
Figure A9.3: Change in coupling wavelength with ambient refractive index for LPG S3


Figure A9.4: Relative change in coupling wavelength with ambient refractive index for LPG S3
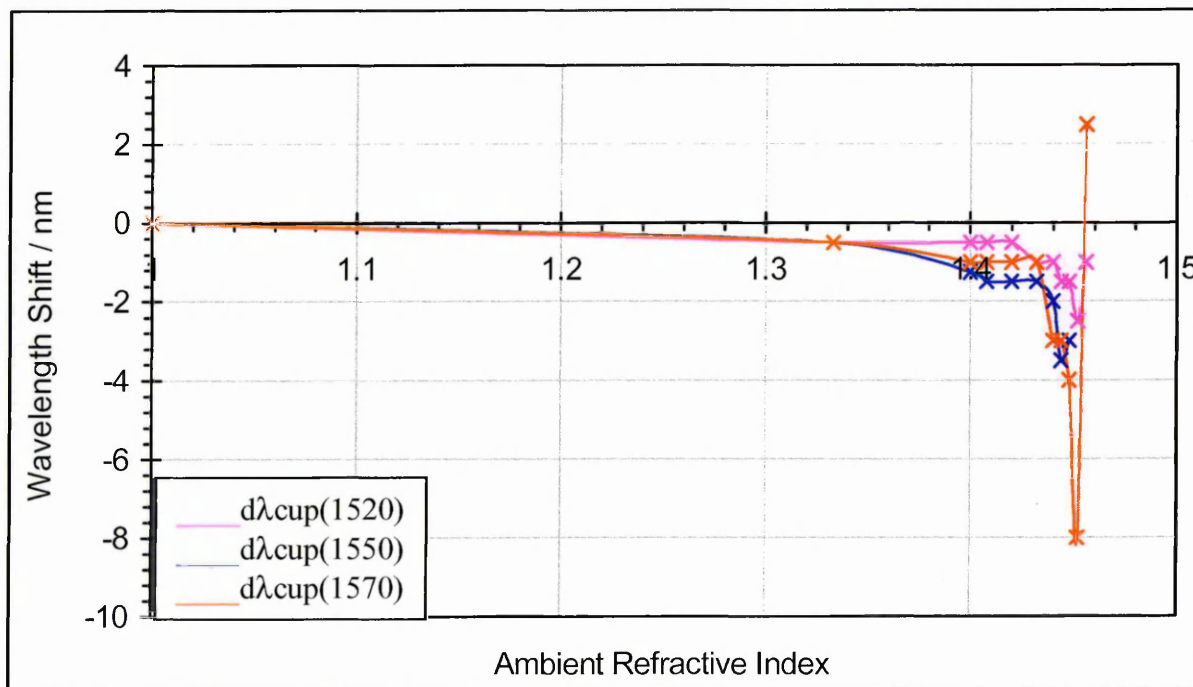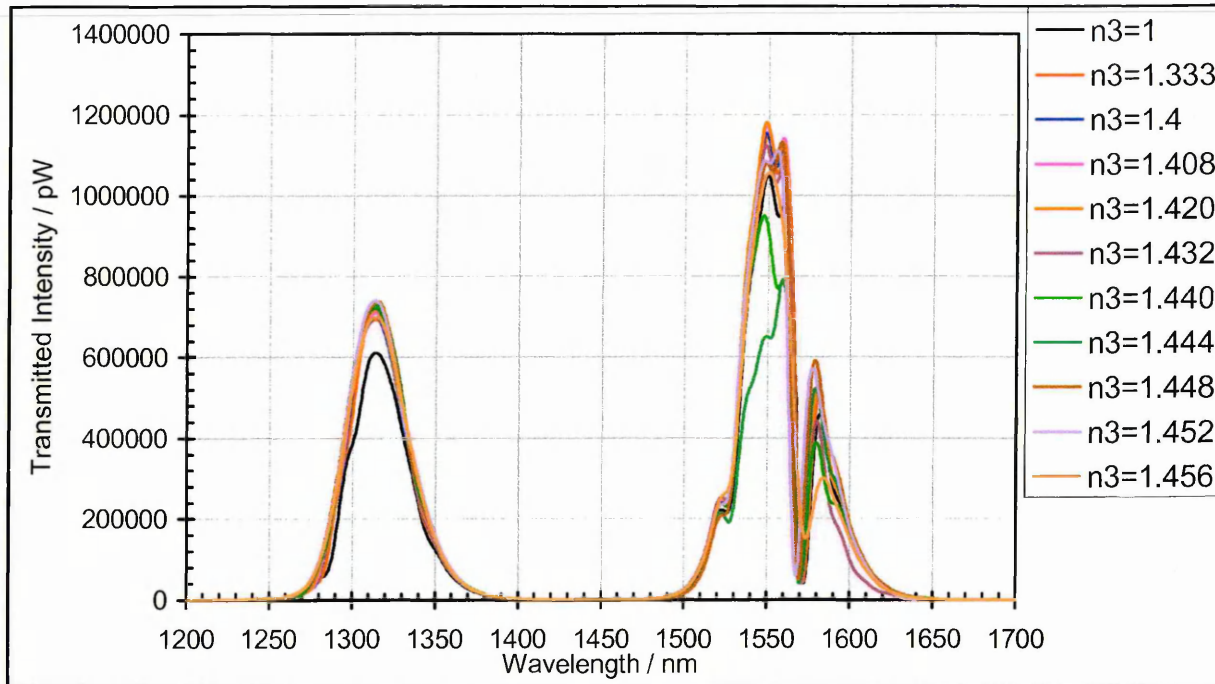
Figure A9.5: Ambient refractive index profile of LPG S4
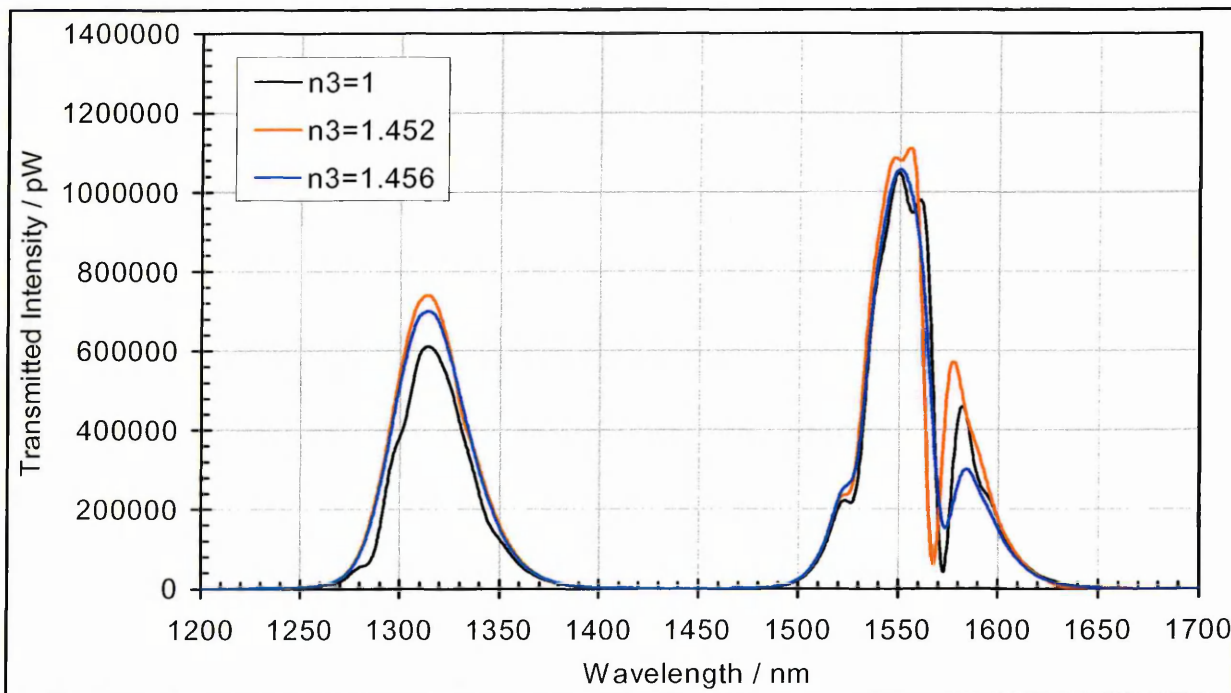
Figure A9.6: Ambient refractive index profile of LPG S4 at selected values to allow clearer observation of shifts
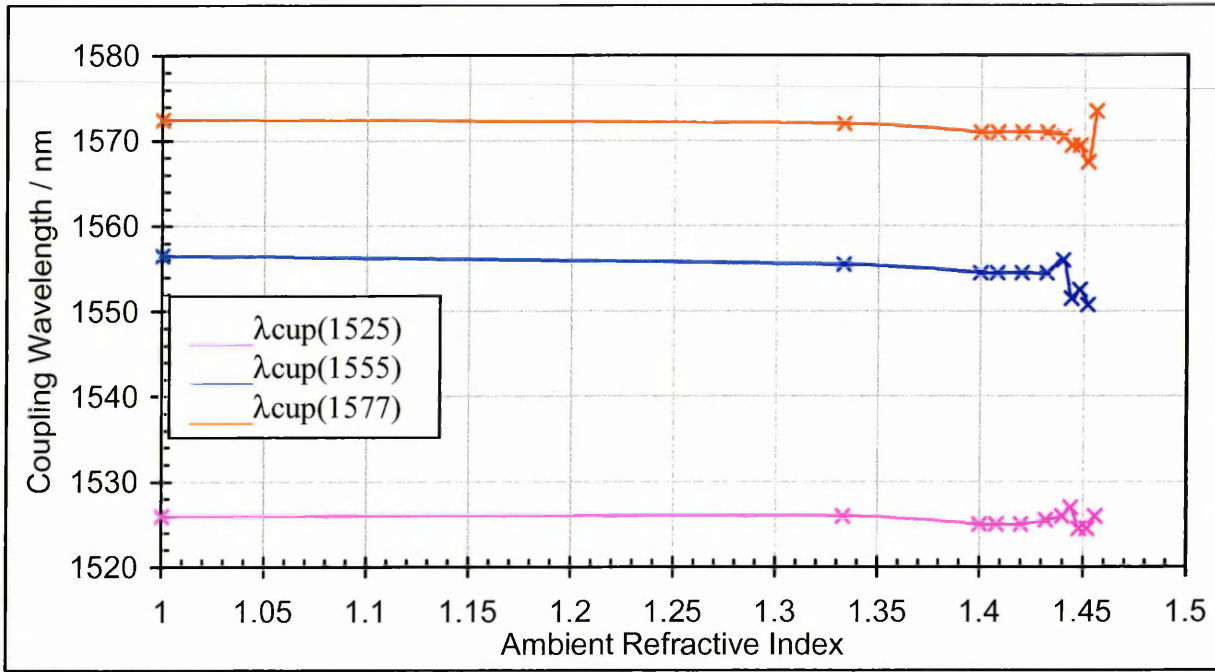
Figure A9.7: Change in coupling wavelength with ambient refractive index for LPG S4
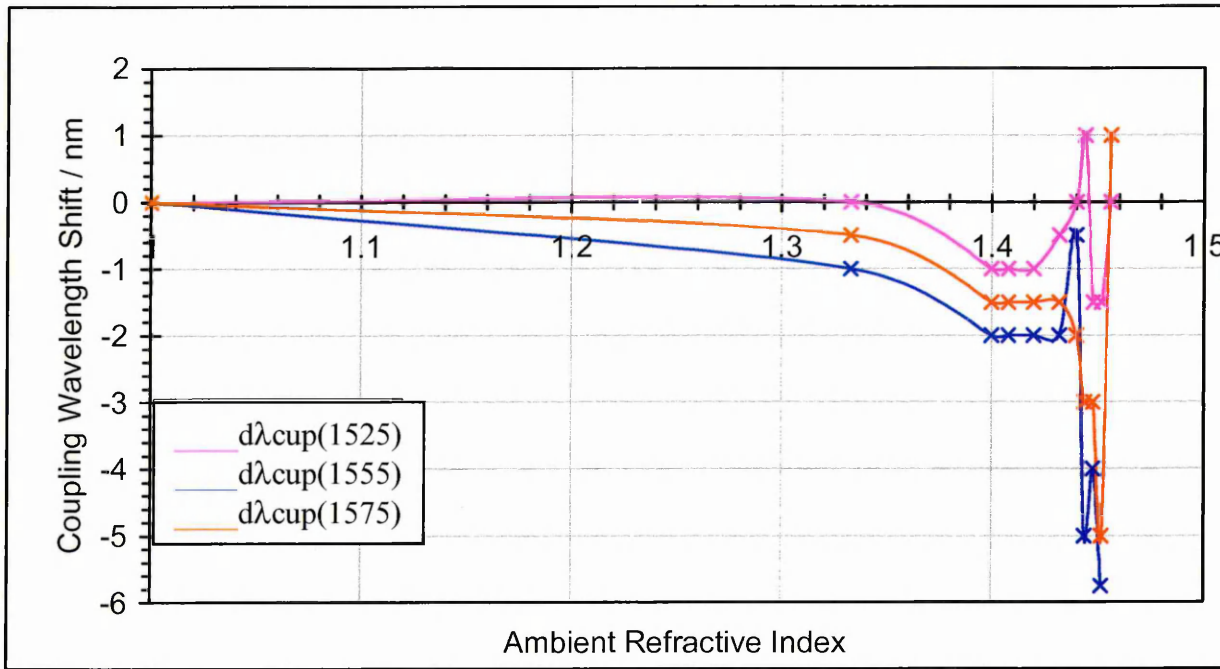
**Figure A9.8: Relative change in coupling wavelength with ambient refractive index for LPG S4**
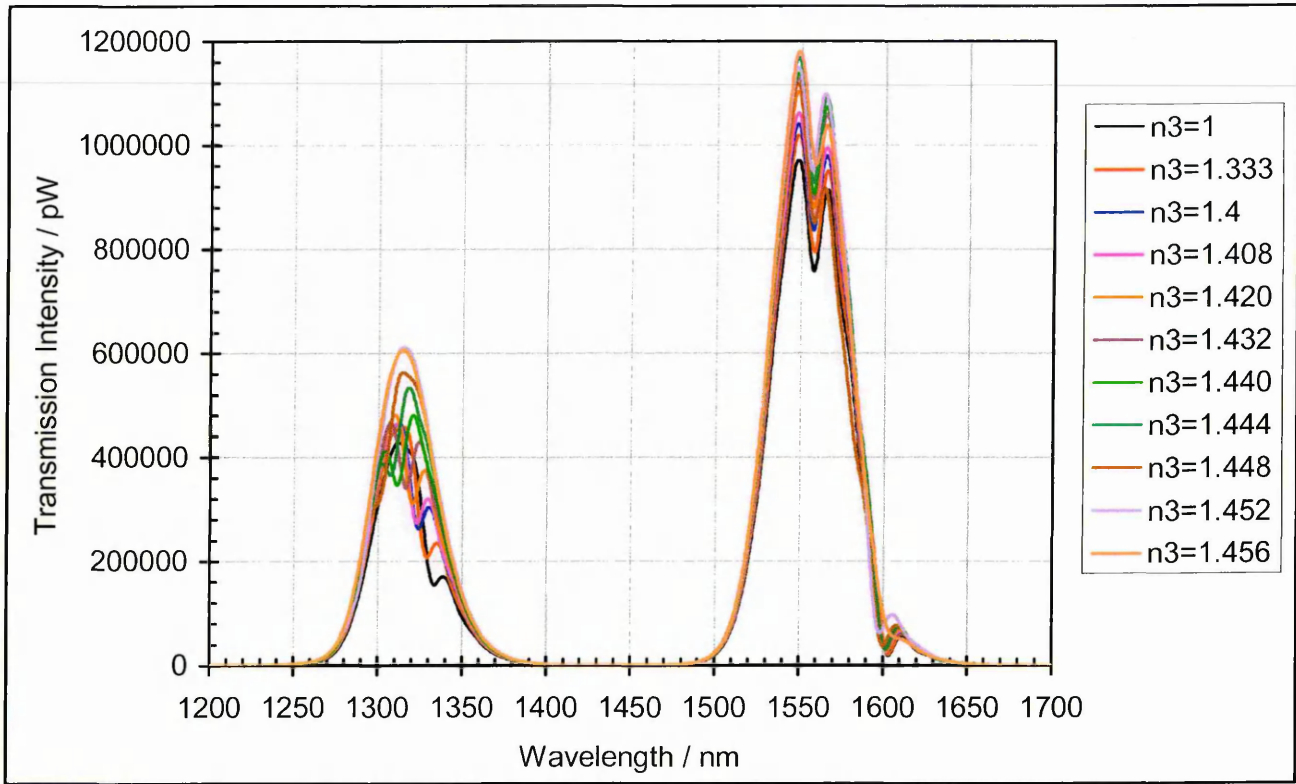
Figure A9.9: Ambient refractive index profile of LPG S5
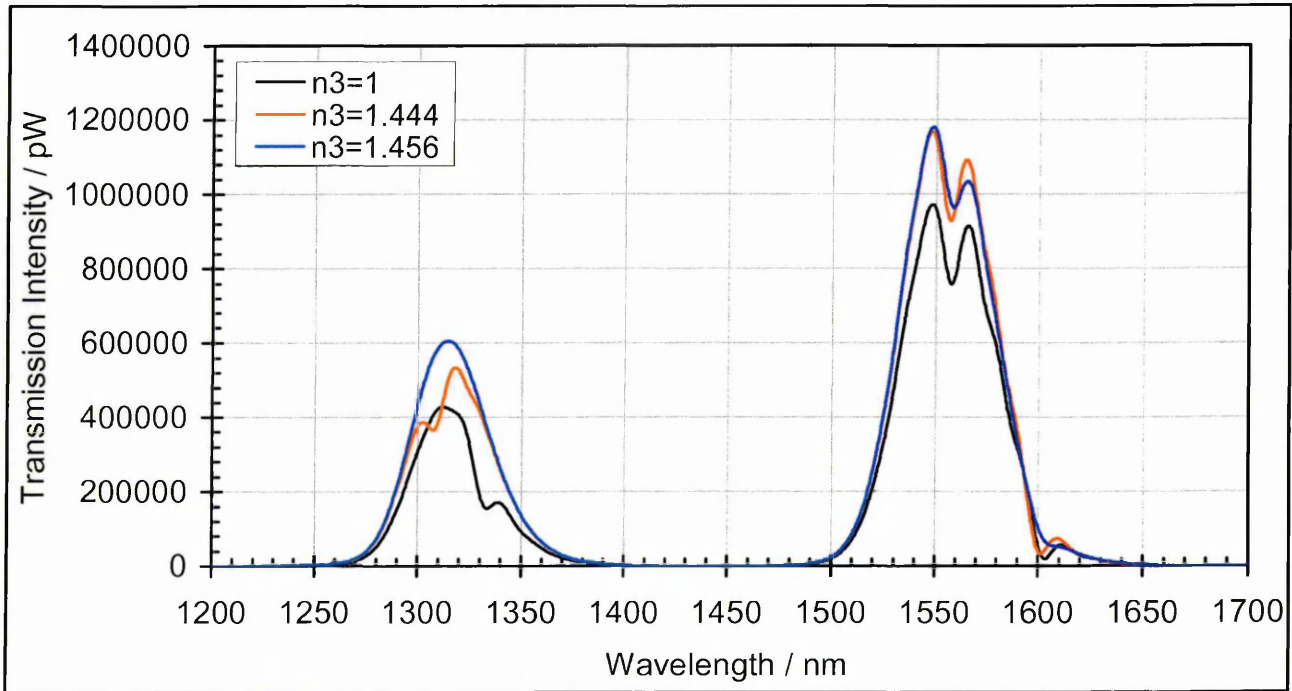
Figure A9.10: Ambient refractive index profile of LPG S5 at selected values to allow clearer observation of shifts
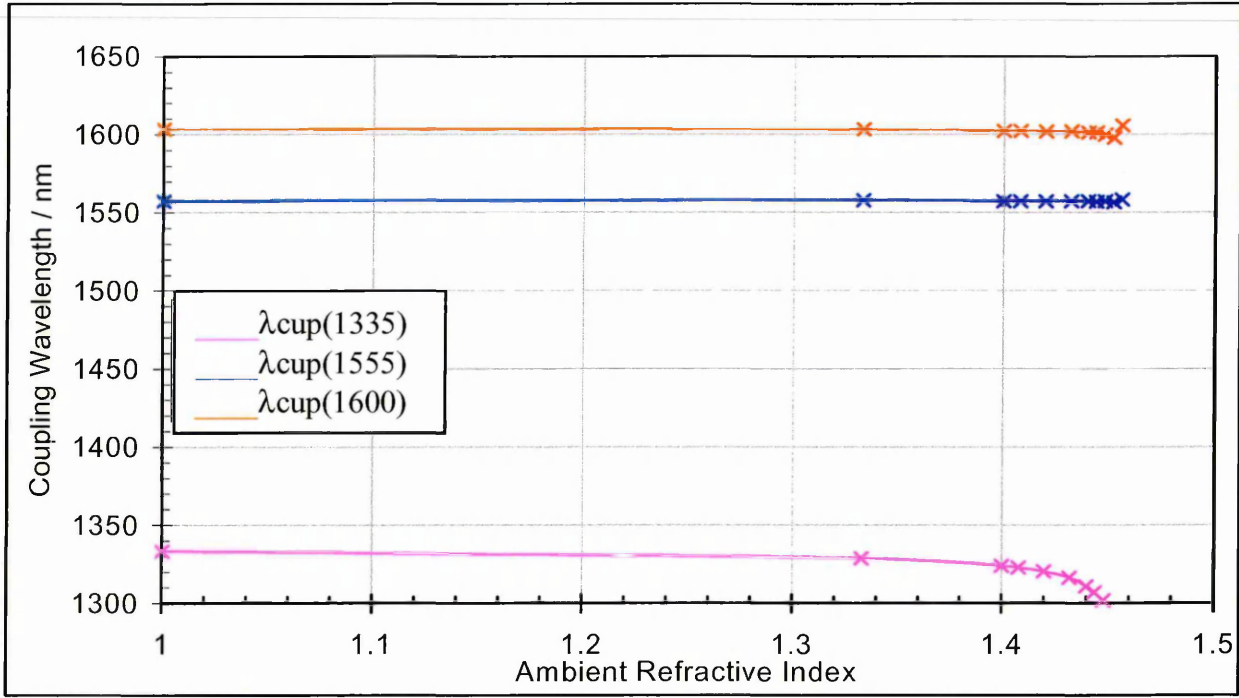
**Figure A9.11: Change in coupling wavelength with ambient refractive index
for LPG S5**
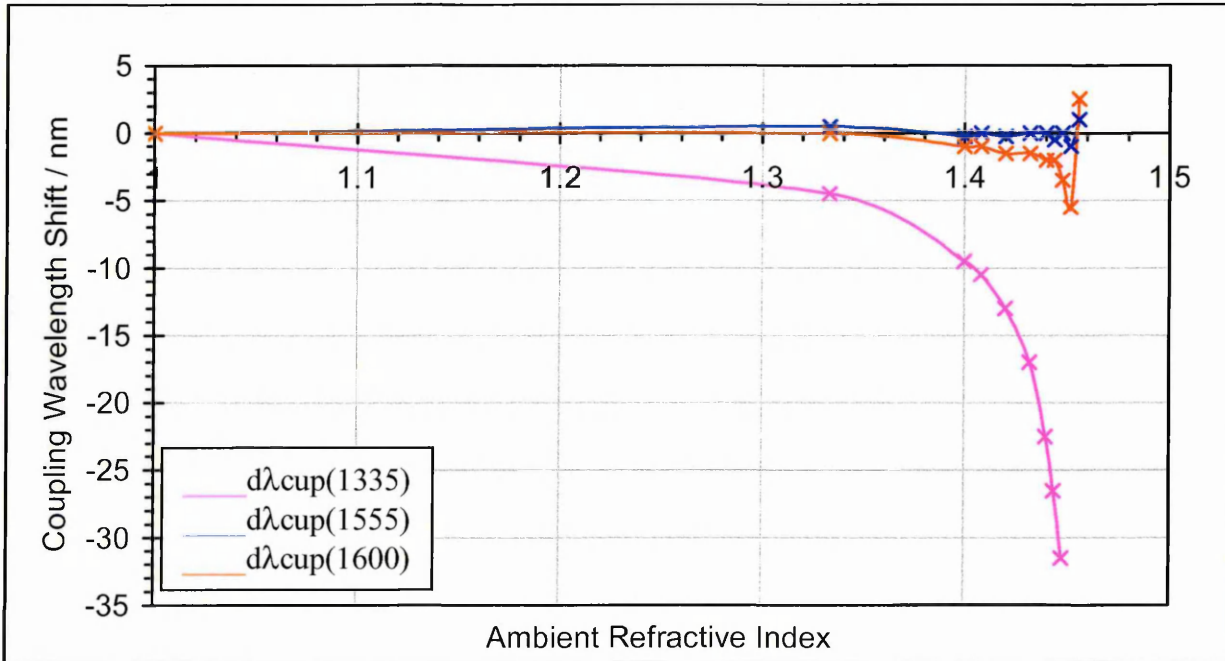
**Figure A9.12: Relative change in coupling wavelength with ambient refractive
index for LPG S5**

294
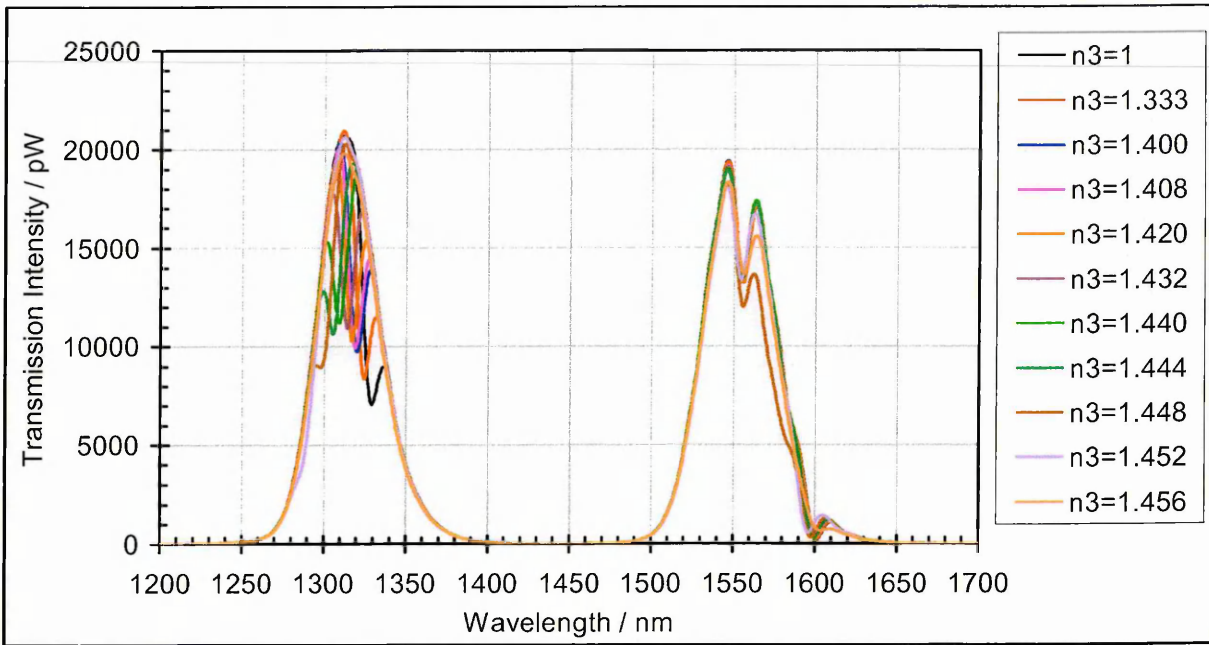
Figure A9.13: Ambient refractive index profile of LPG S6
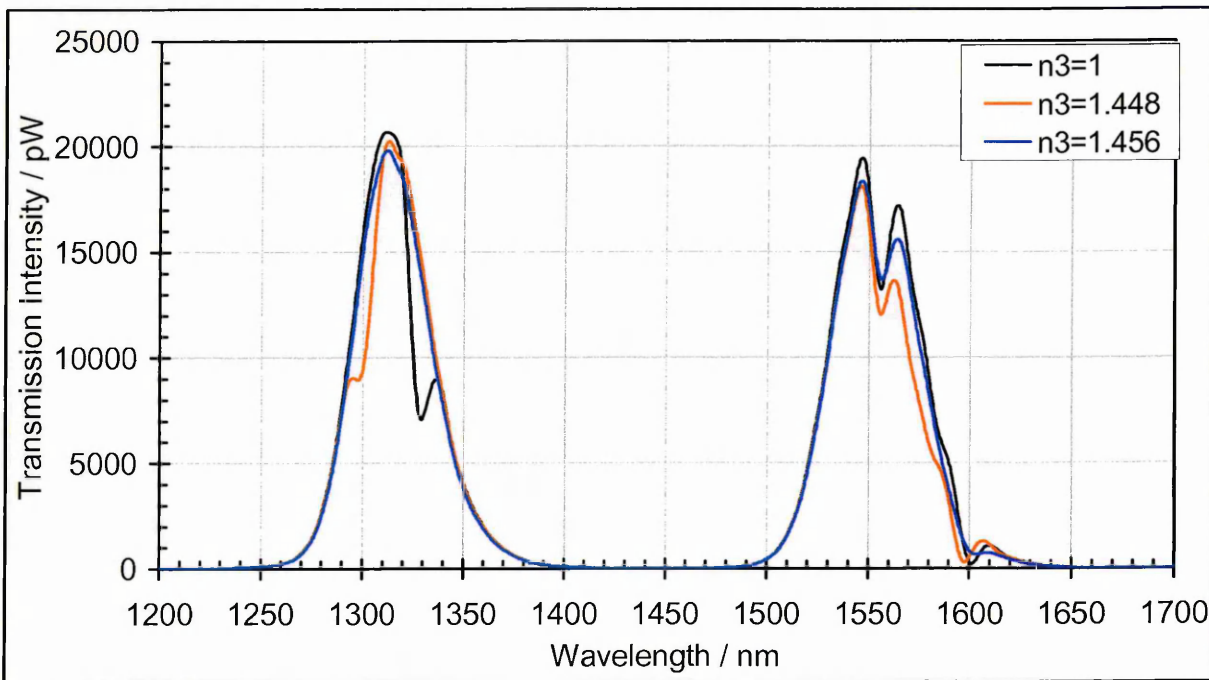
Figure A9.14: Ambient refractive index profile of LPG S6 at selected values to allow clearer observation of shifts
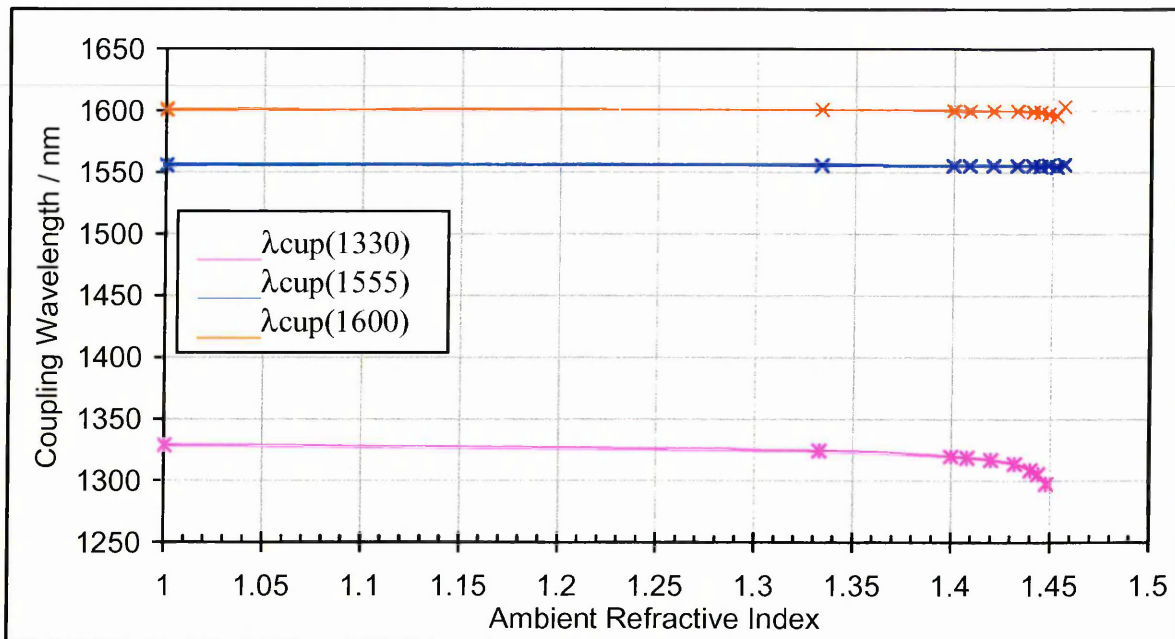
**Figure A9.15: Change in coupling wavelength with ambient refractive index for LPG S6**
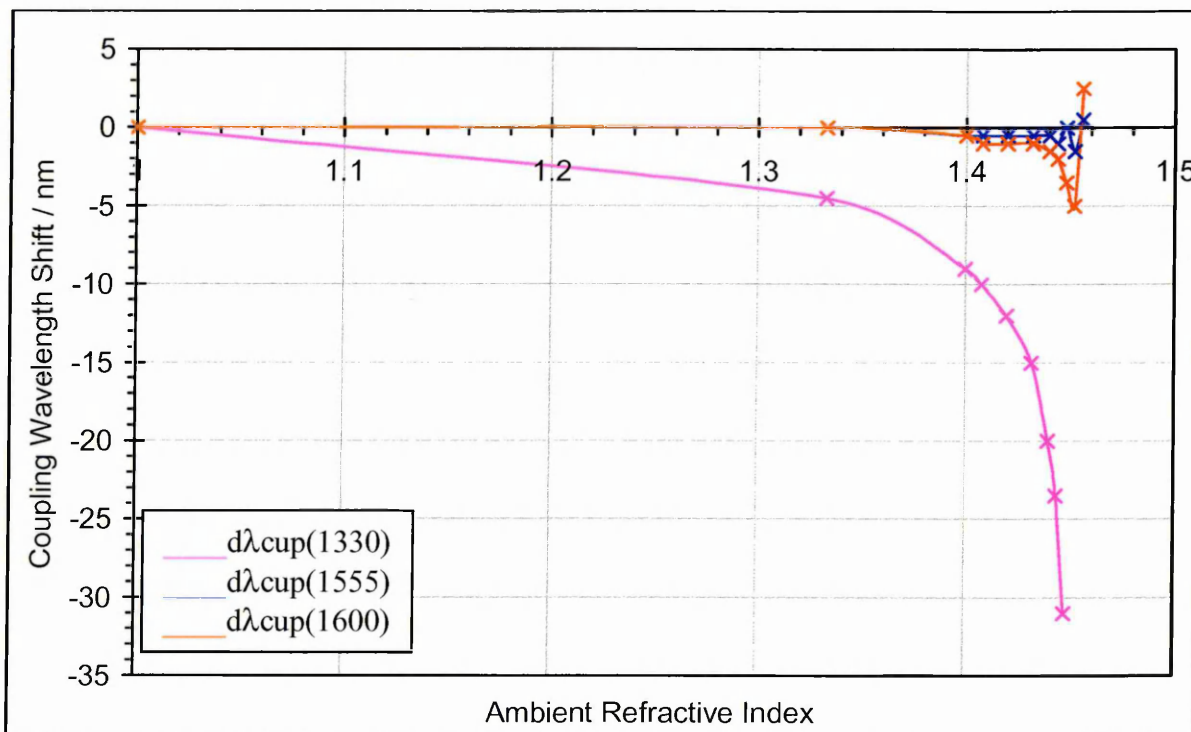
Figure A9.16: Relative change in coupling wavelength with ambient refractive index for LPG S6
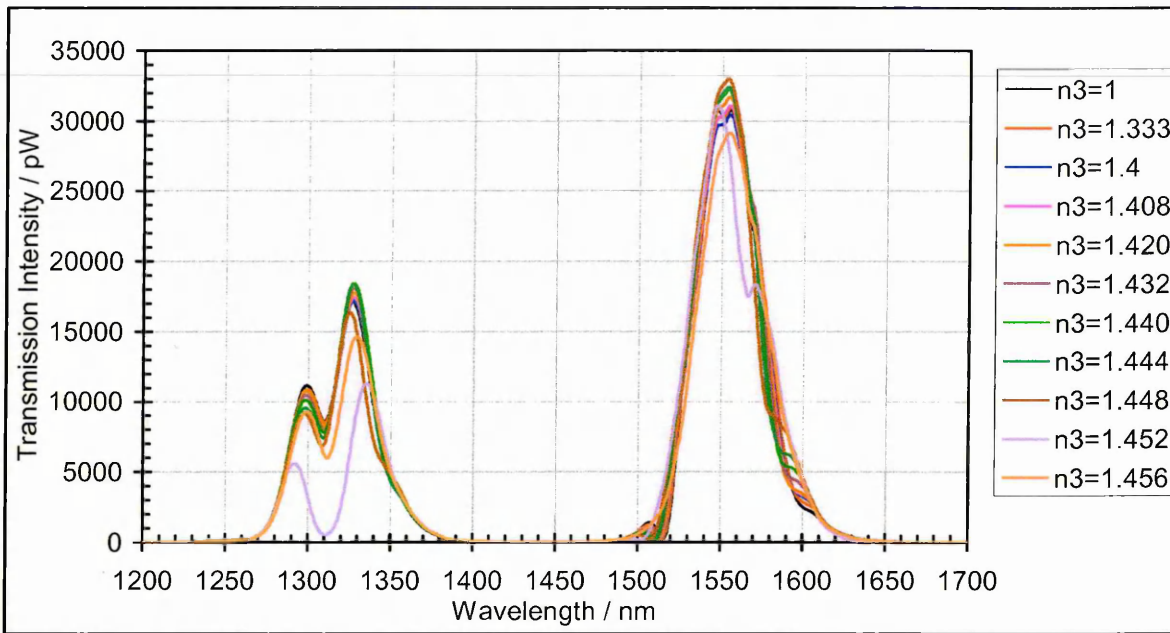
**Figure A9.17: Ambient refractive index profile of LPG S7**
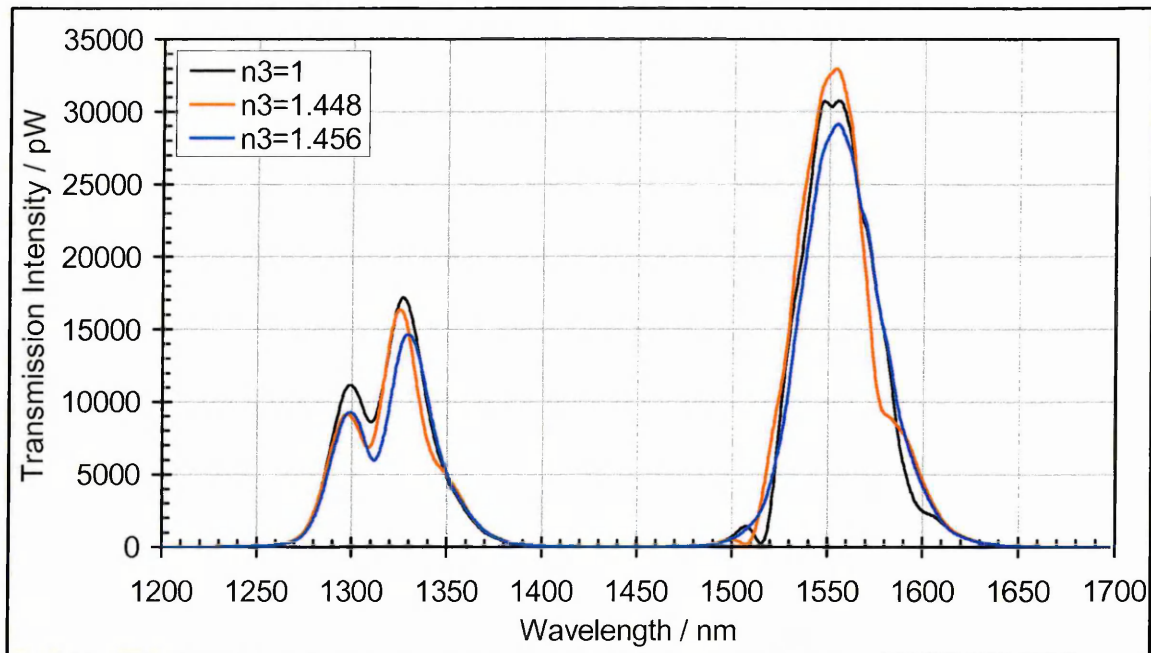
Figure A9.18: Ambient refractive index profile of LPG S7 at selected values to allow clearer observation of shifts
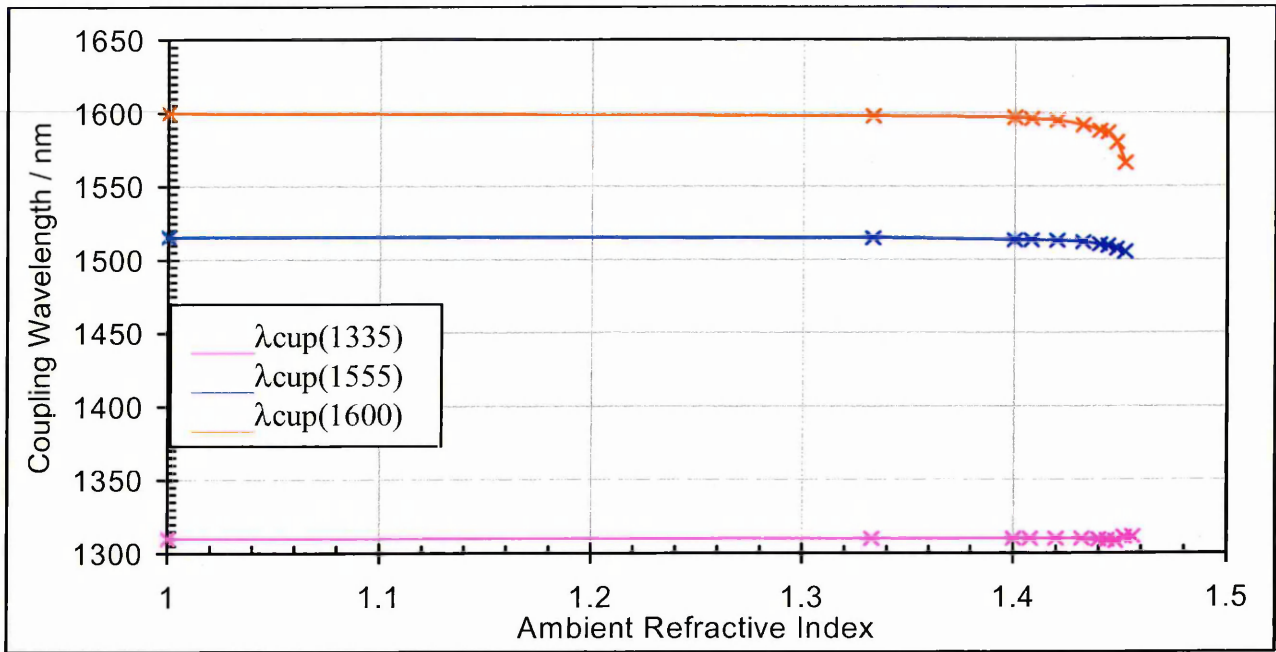
Figure A9.19: Change in coupling wavelength with ambient refractive index for LPG S7
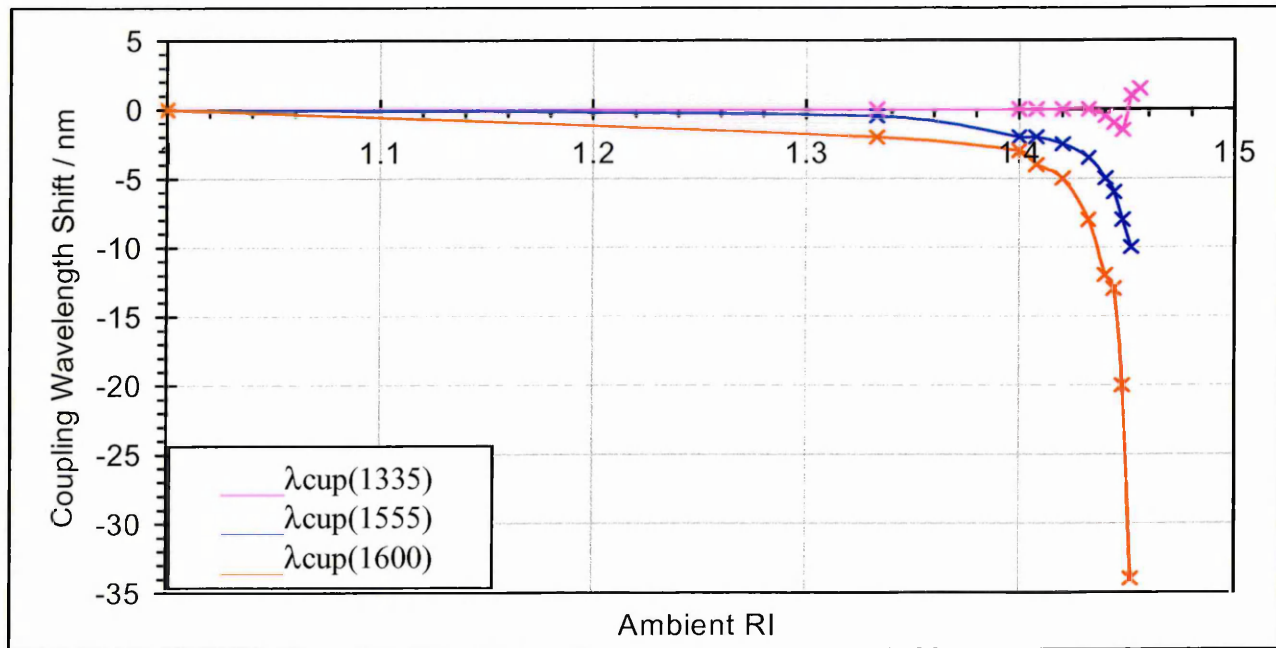
Figure A9.20: Relative change in coupling wavelength with ambient refractive index for LPG S7
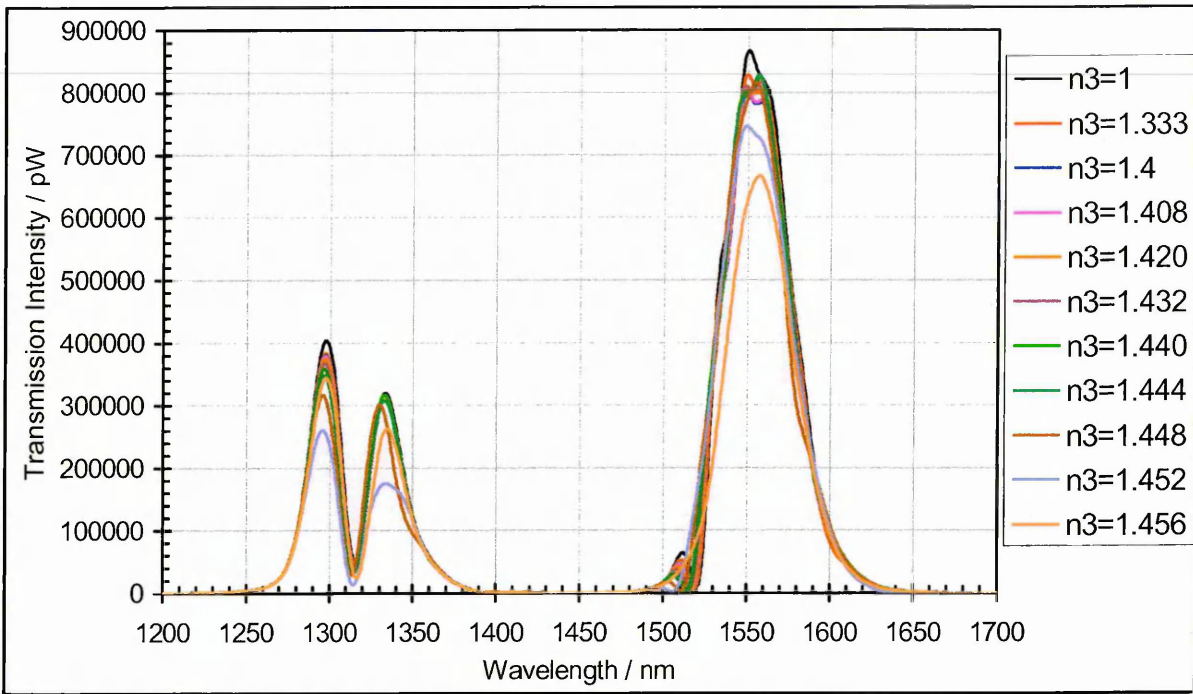
Figure A9.21: Ambient refractive index profile of LPG S8
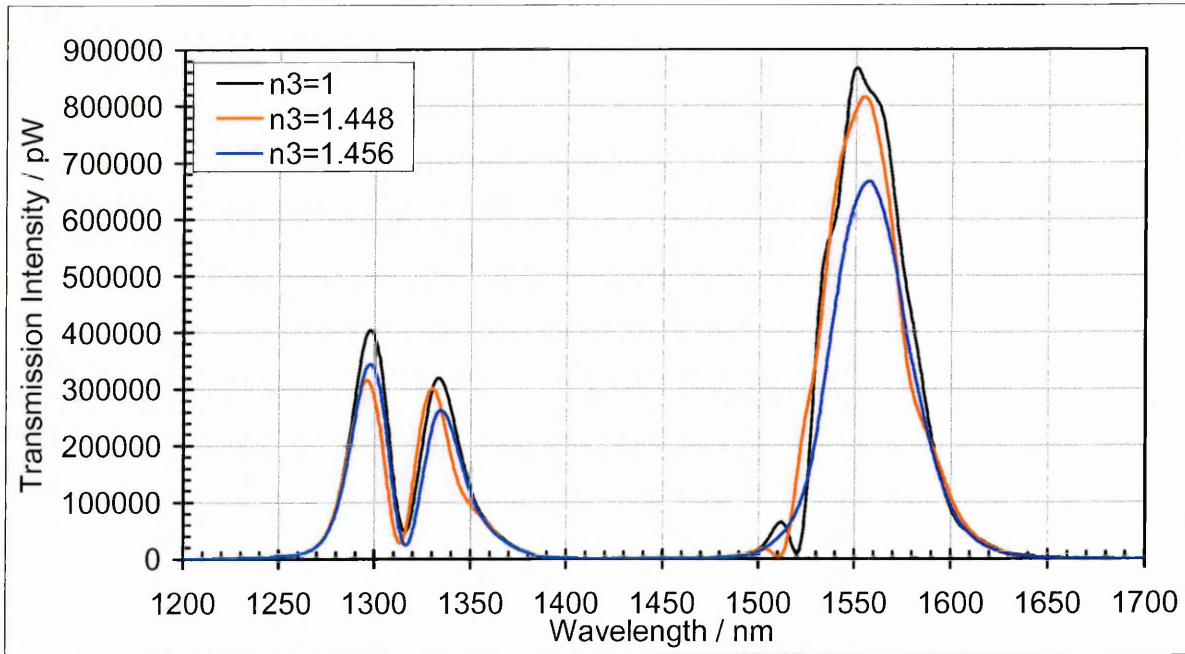
Figure A9.22: Ambient refractive index profile of LPG S8 at selected values to allow clearer observation of shifts
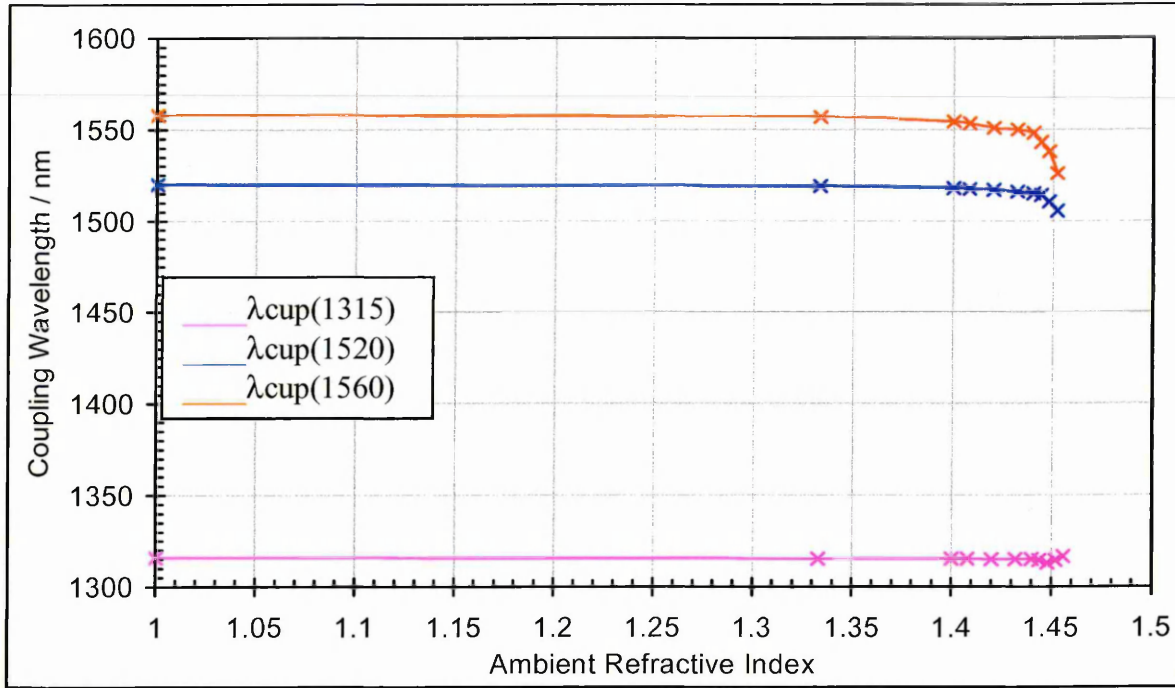
Figure A9.23: Change in coupling wavelength with ambient refractive index for LPG S8
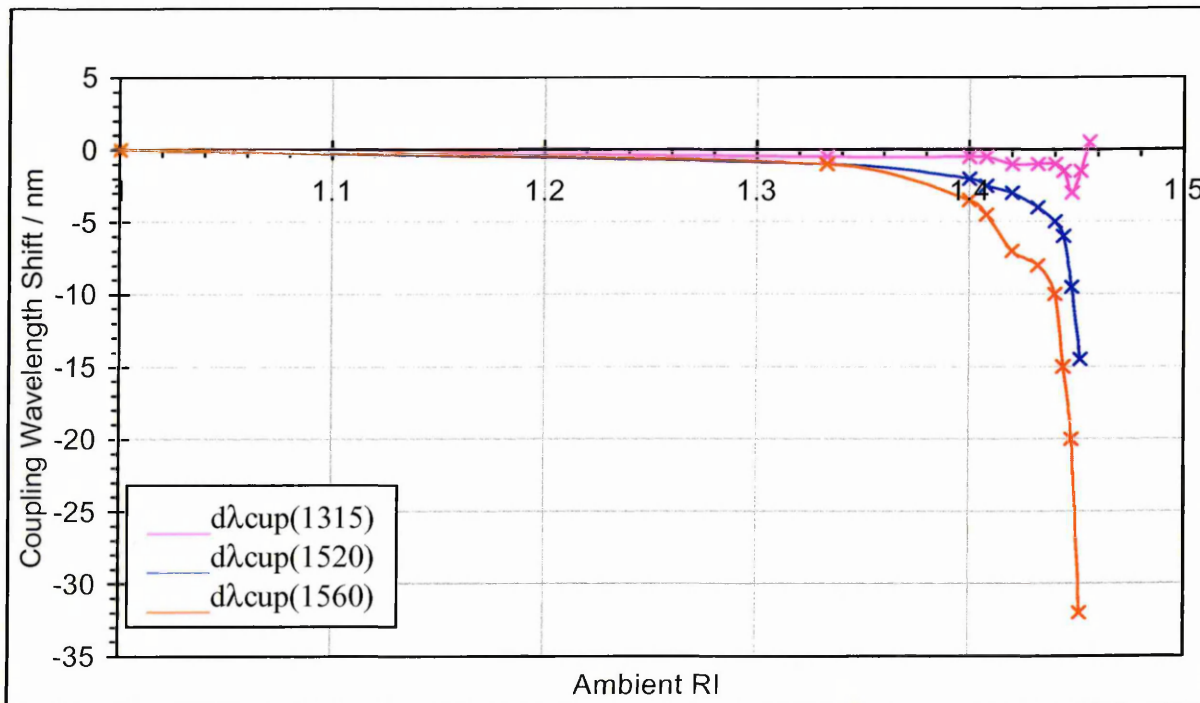

Figure A9.24: Relative change in coupling wavelength with ambient refractive index for LRP S8
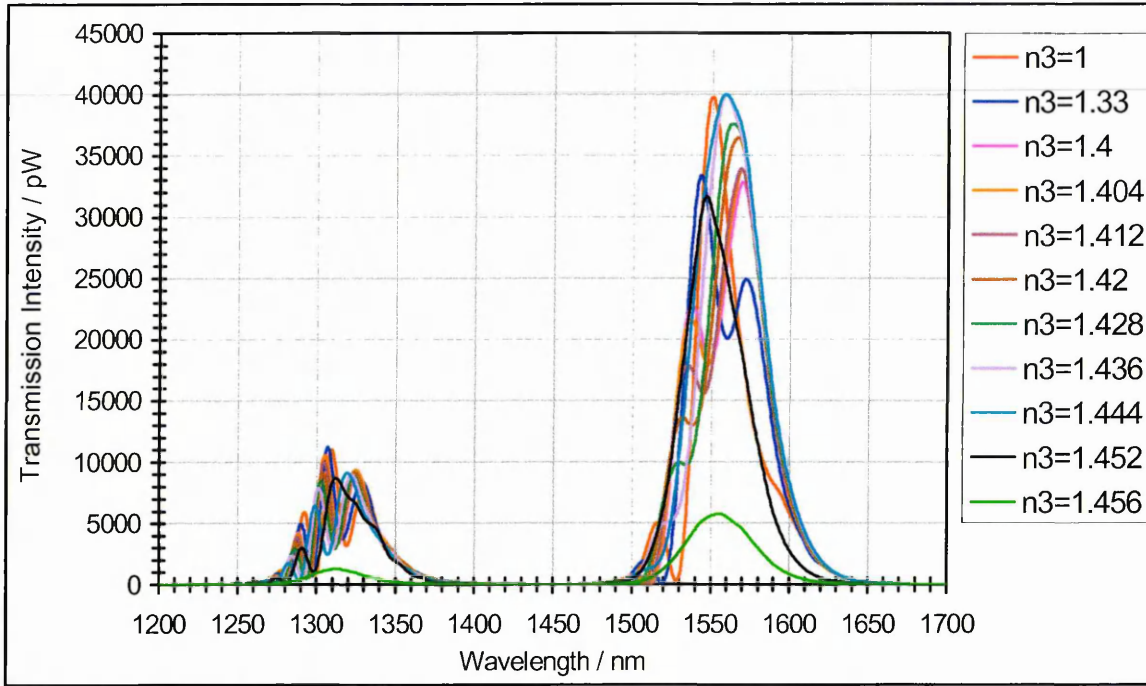
Figure A9.25: Ambient refractive index profile of LPG C1
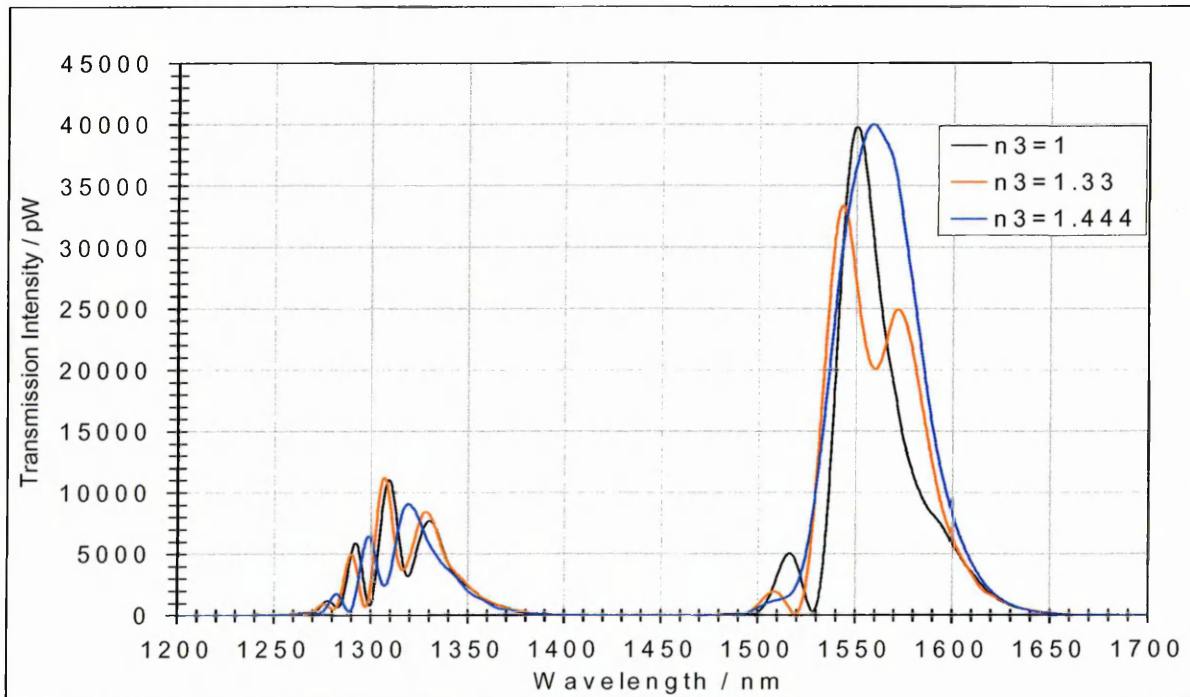
Figure A9.26: Ambient refractive index profile of LPG C1 at selected values to allow clearer observation of shifts
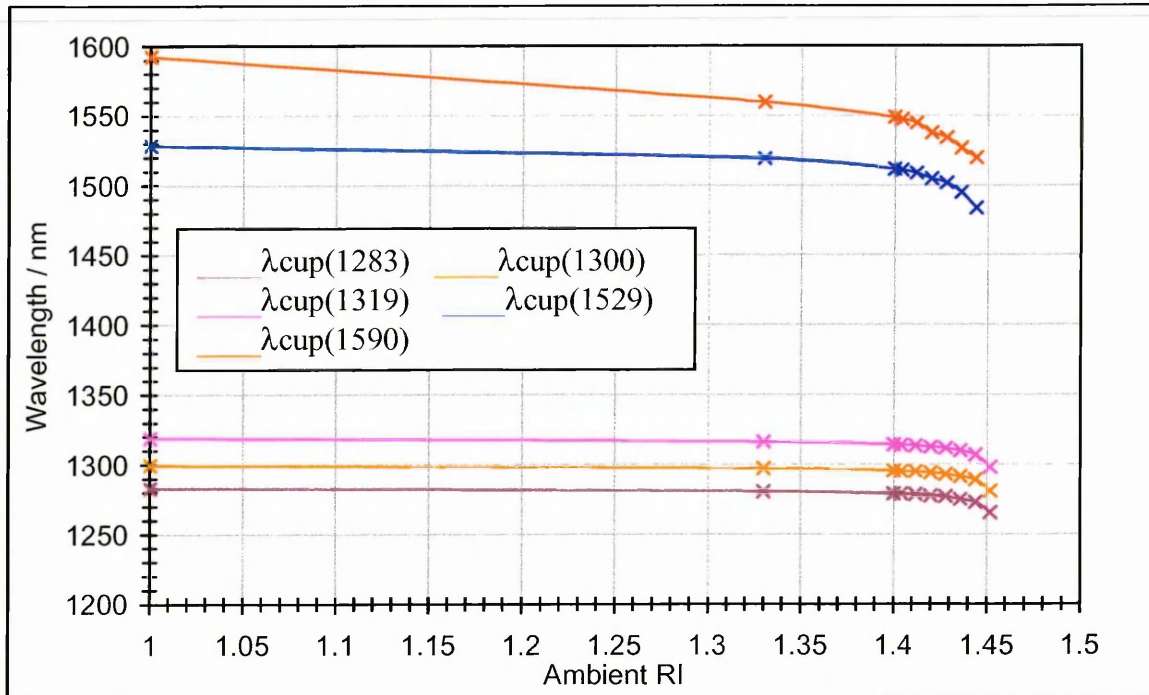
Figure A9.27: Change in coupling wavelength with ambient refractive index for LPG C1
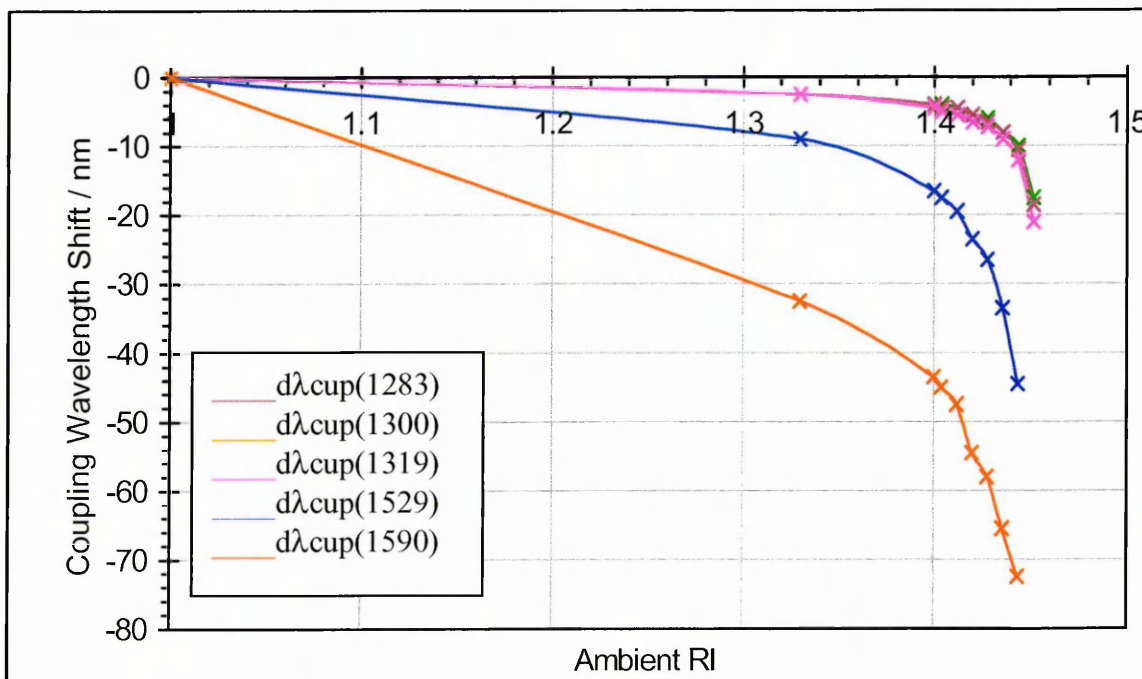
Figure A9.28: Relative change in coupling wavelength with ambient refractive index for LPG C1
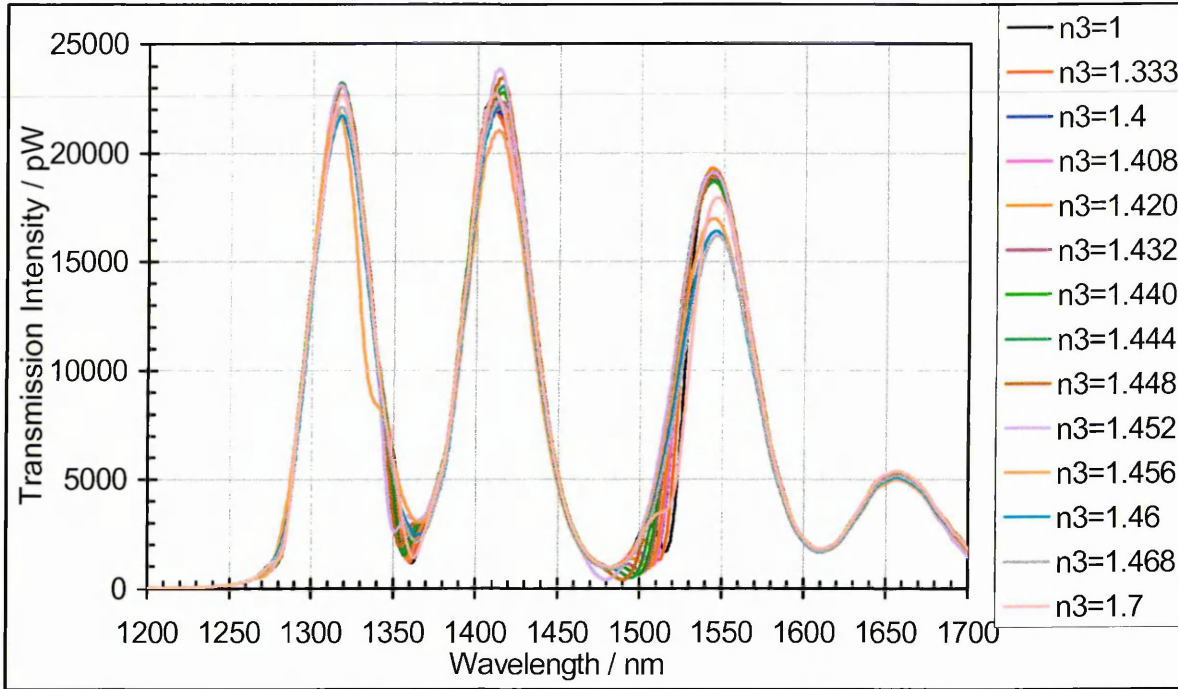
Figure A9.29: Ambient refractive index profile of LPG A400
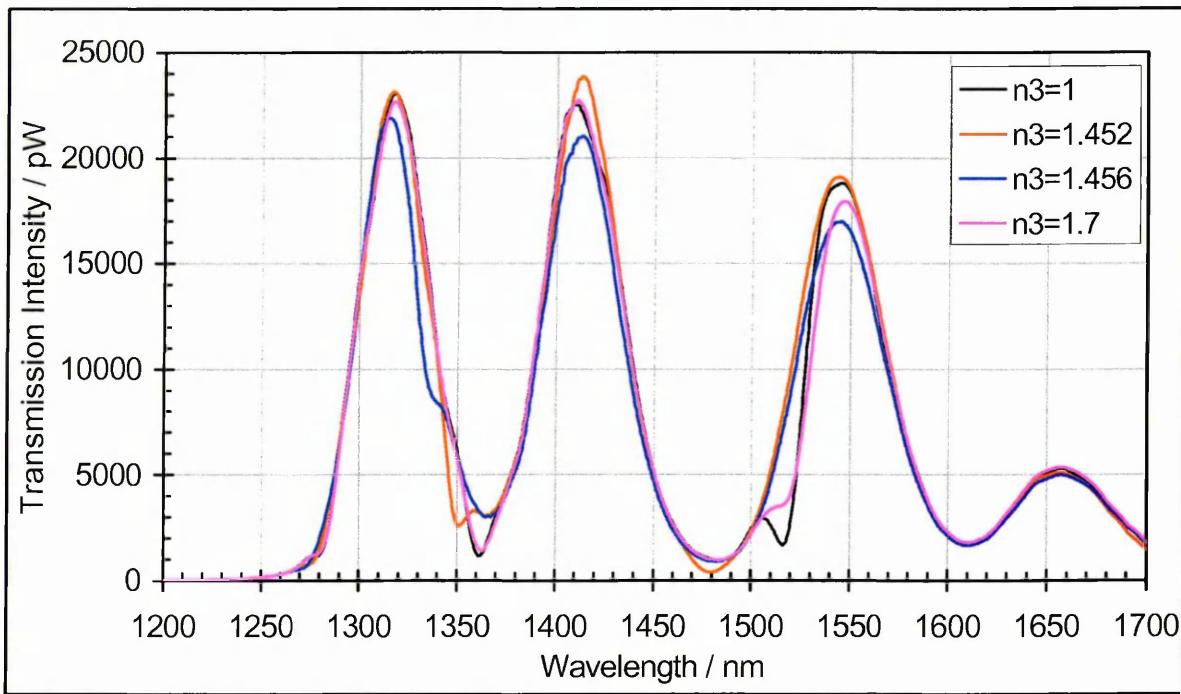
Figure A9.30: Ambient refractive index profile of LPG A400 at selected values to allow clearer observation of shifts
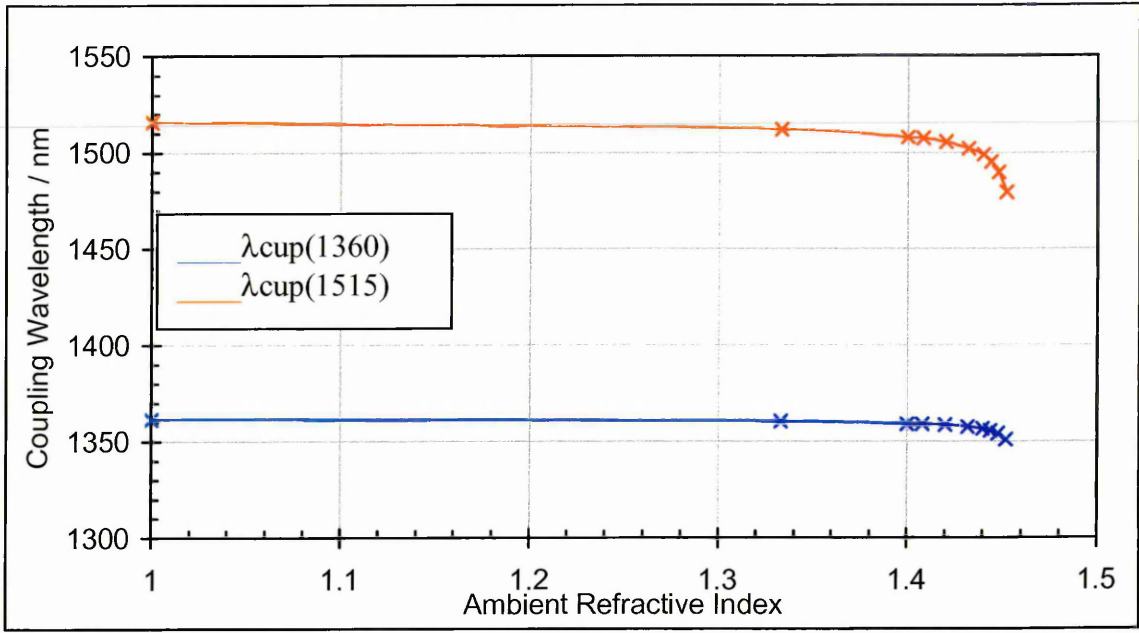
Figure A9.31: Change in coupling wavelength with ambient refractive index for LPG A400
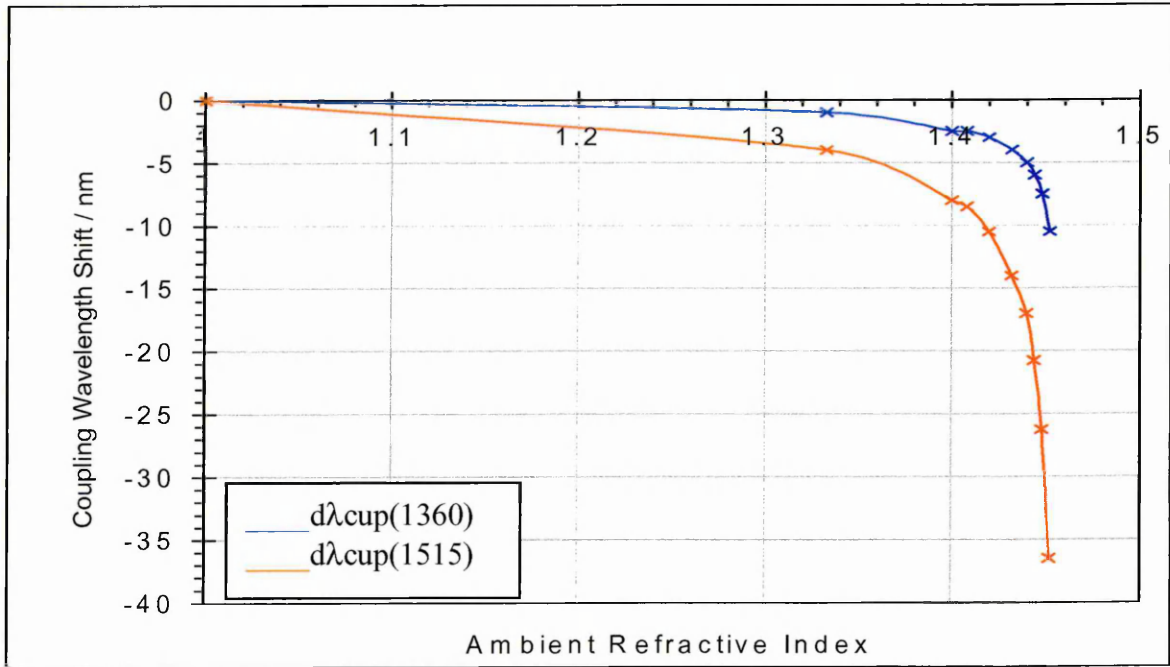

Figure A9.32: Relative change in coupling wavelength with ambient refractive index for LPG A400
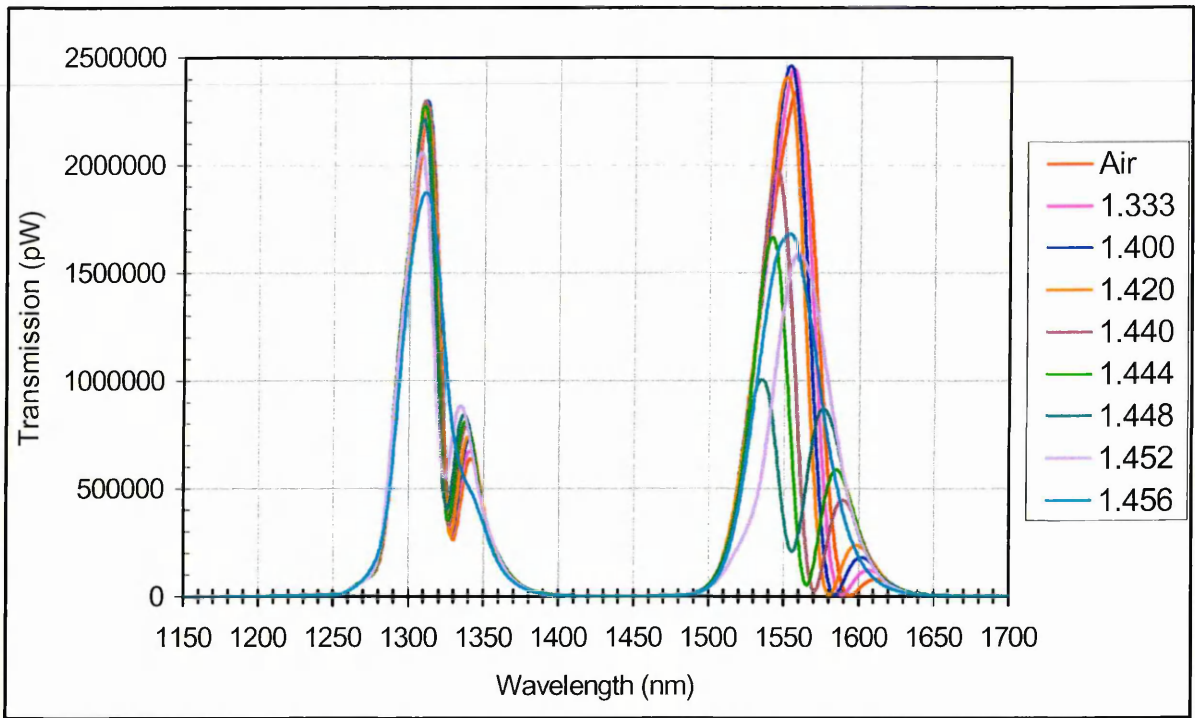
Figure A9.33: Ambient refractive index profile of LPG A403
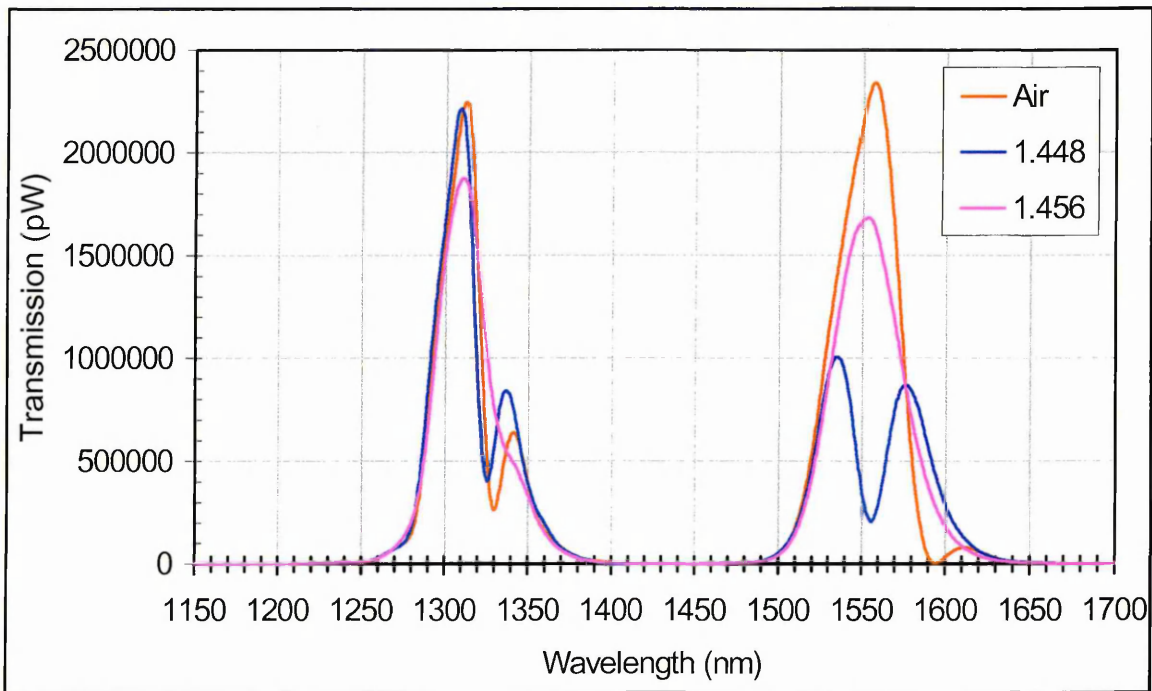
Figure A9.34: Ambient refractive index profile of LPG A403 at selected values to allow clearer observation of shifts
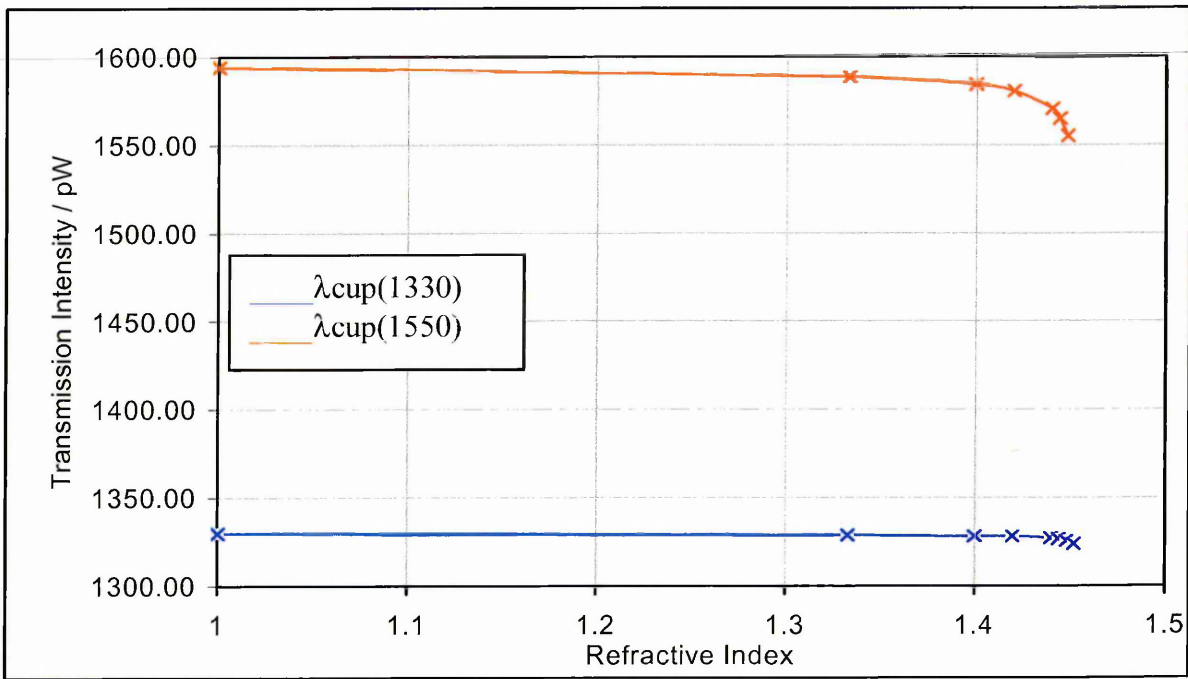
Figure A9.35: Change in coupling wavelength with ambient refractive index for LPG A403
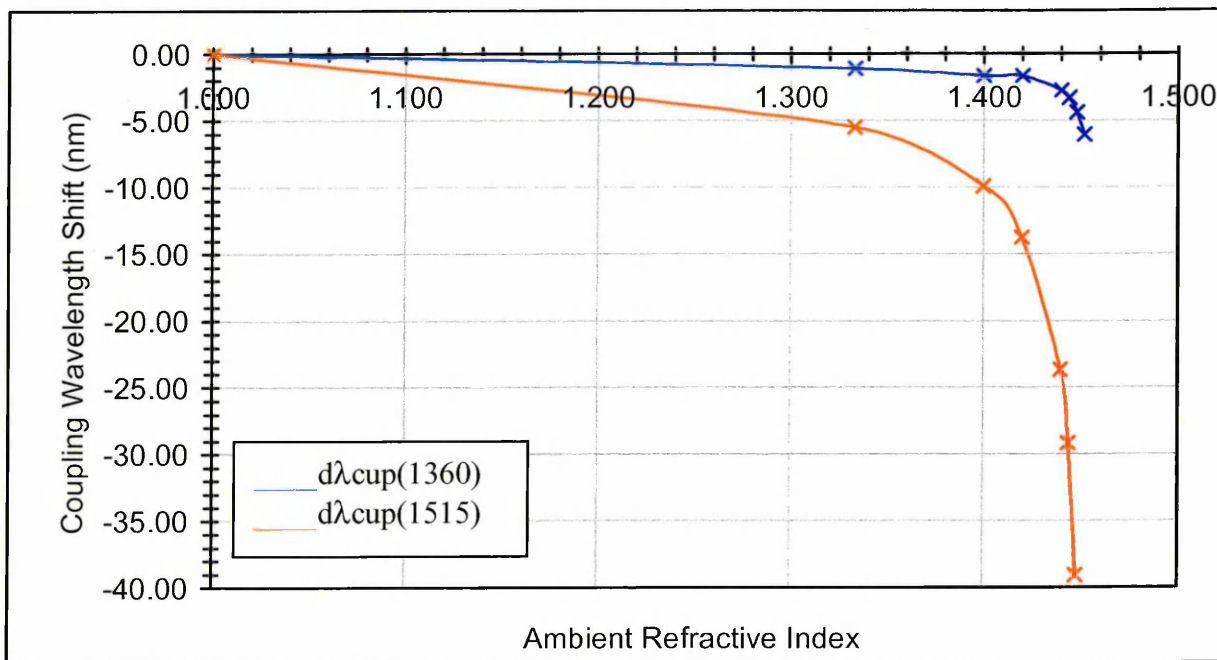
Figure A9.36: Relative change in coupling wavelength with ambient refractive index for LPG A403
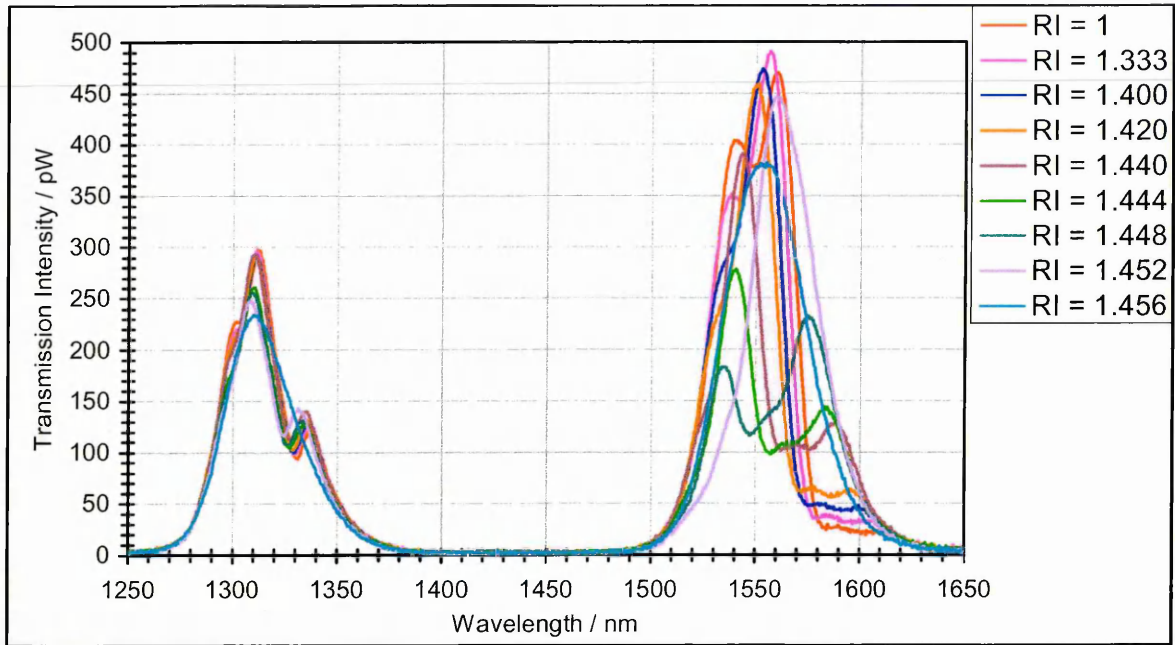
Figure A9.37: Ambient refractive index profile of LPG A407
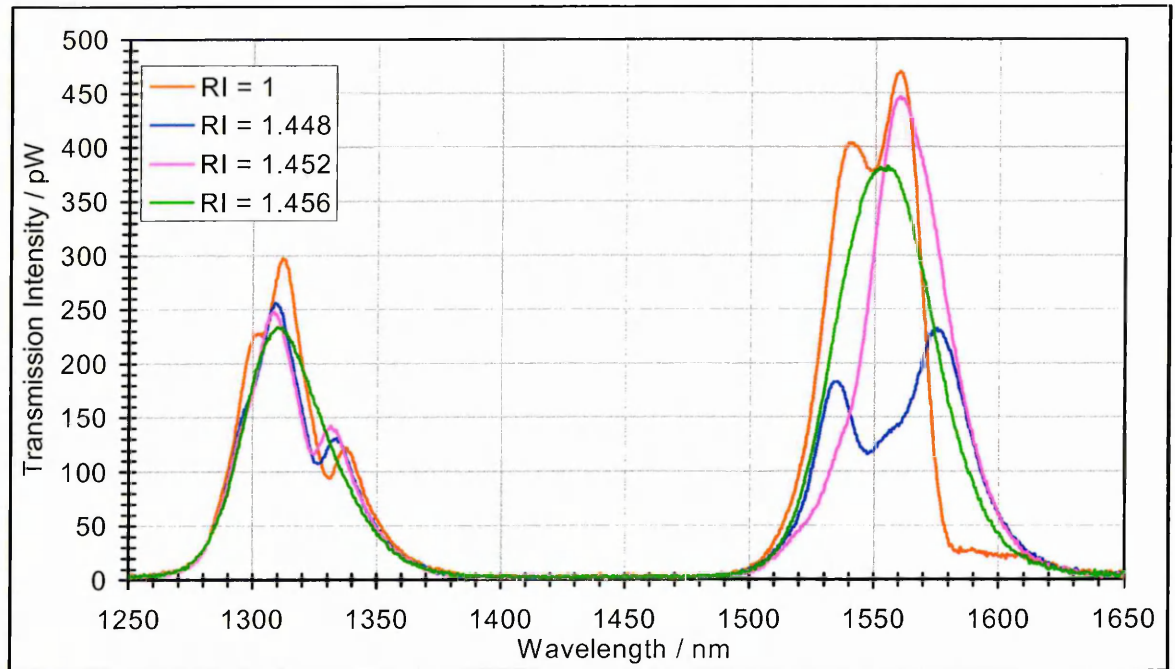
Figure A9.38: Ambient refractive index profile of LPG A407 at selected values to allow clearer observation of shifts
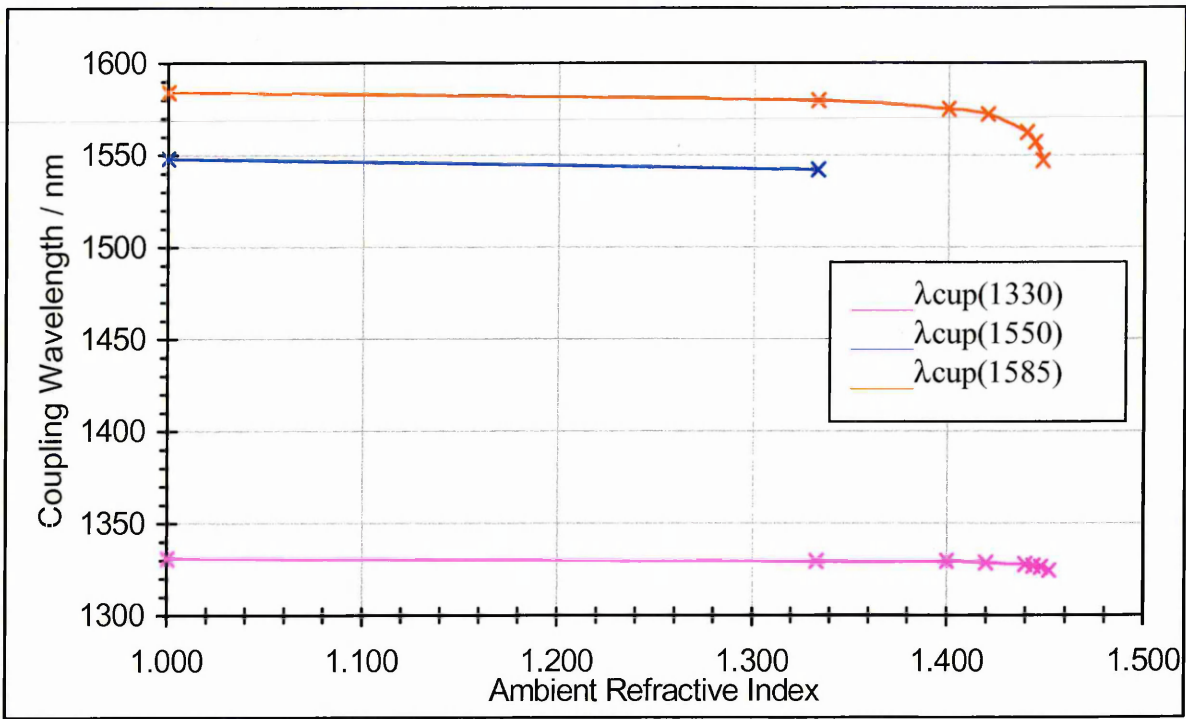
Figure A9.39: Change in coupling wavelength with ambient refractive index for LPG A407
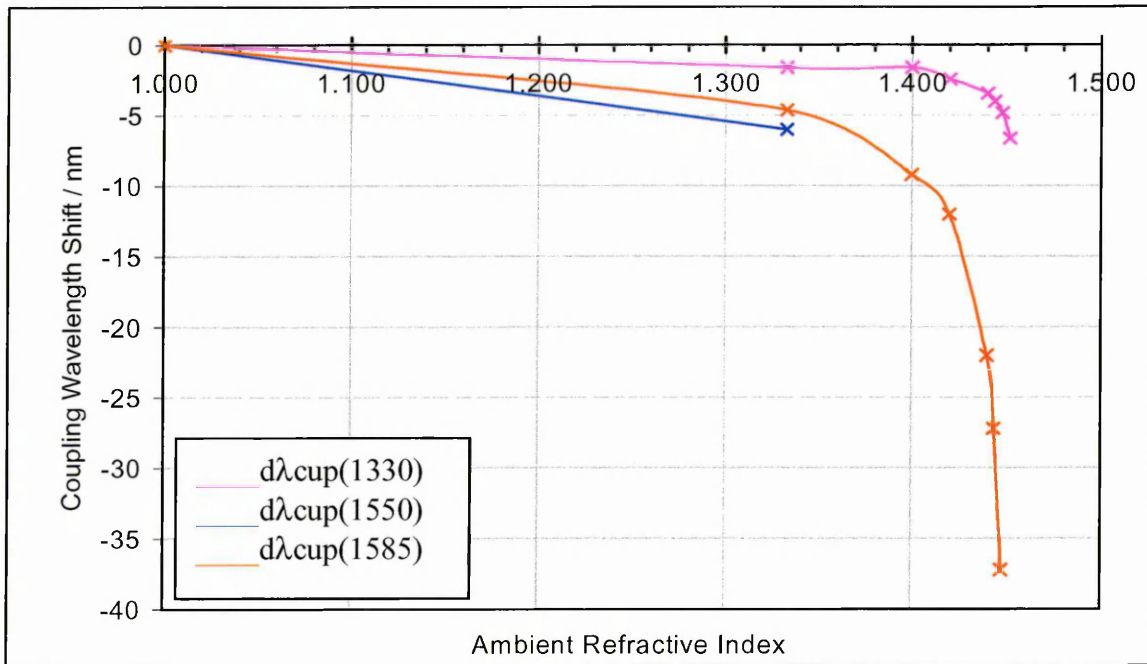
Figure A9.40: Relative change in coupling wavelength with ambient refractive index for LPG A407
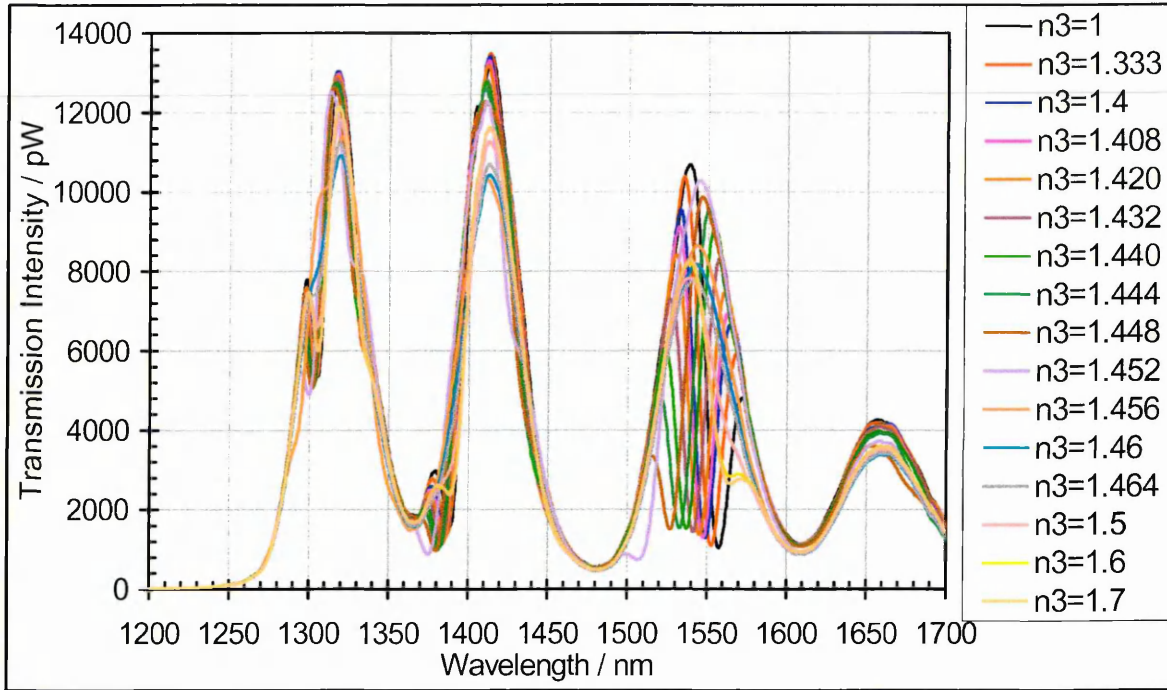
Figure A9.41: Ambient refractive index profile of LPG A410
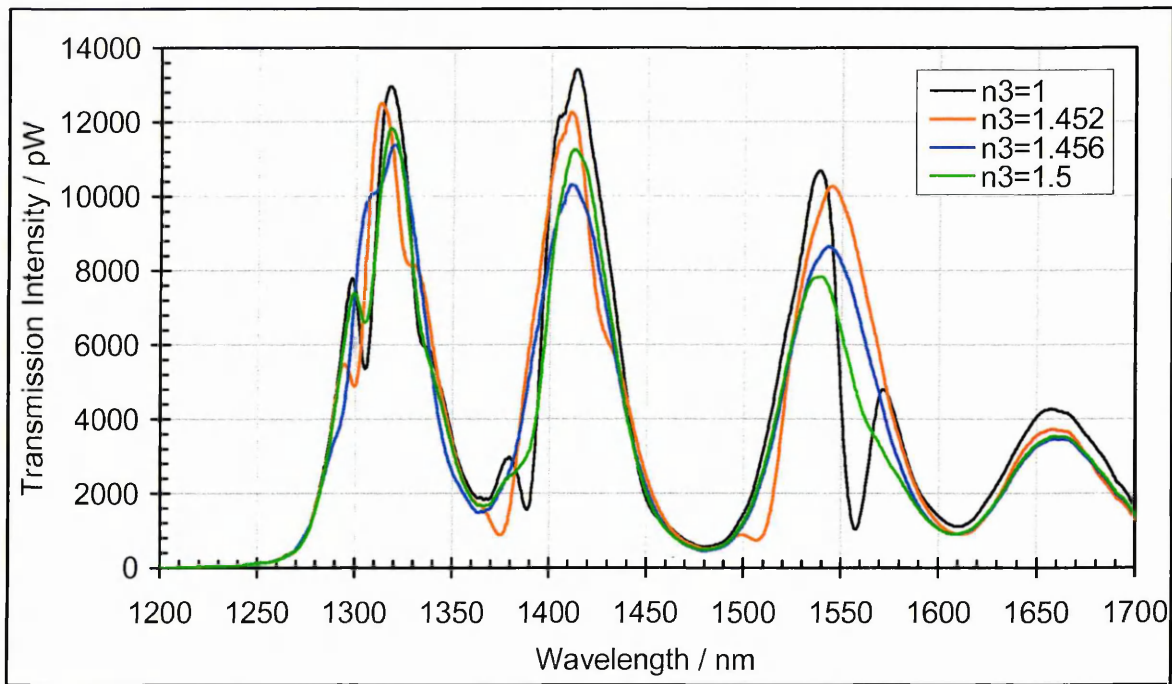
**Figure A9.42: Ambient refractive index profile of LPG A410 at selected values
to allow clearer observation of shifts**
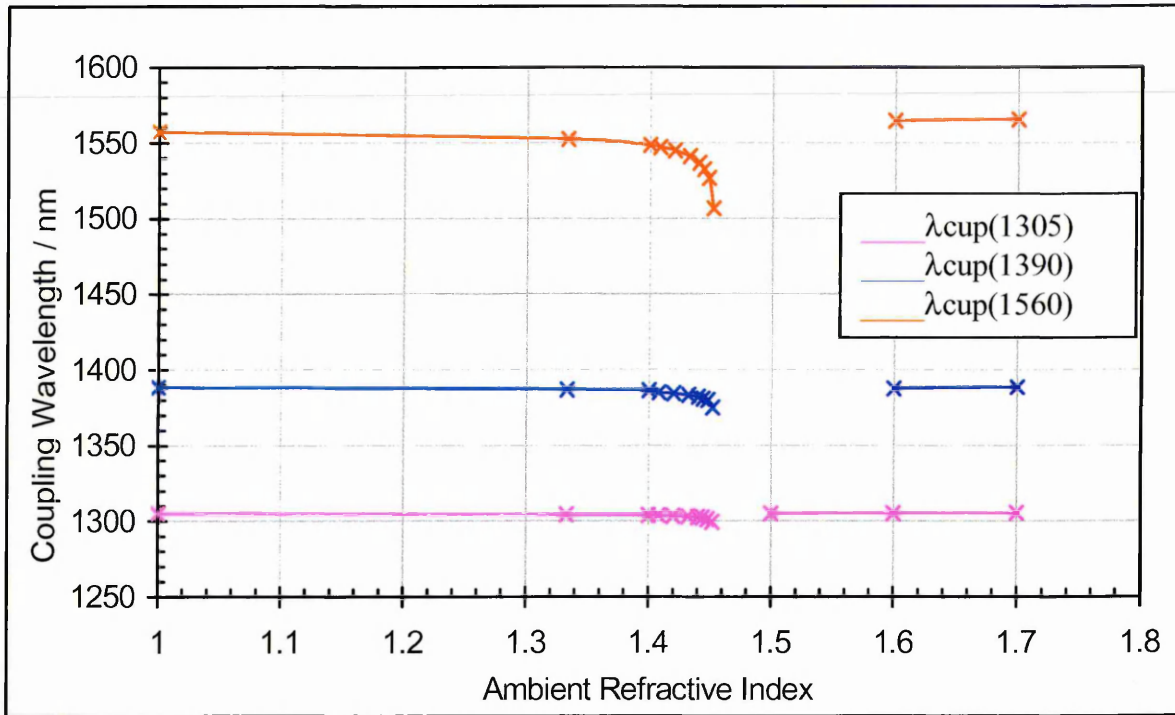
**Figure A9.43: Change in coupling wavelength with ambient refractive index for LPG A410**
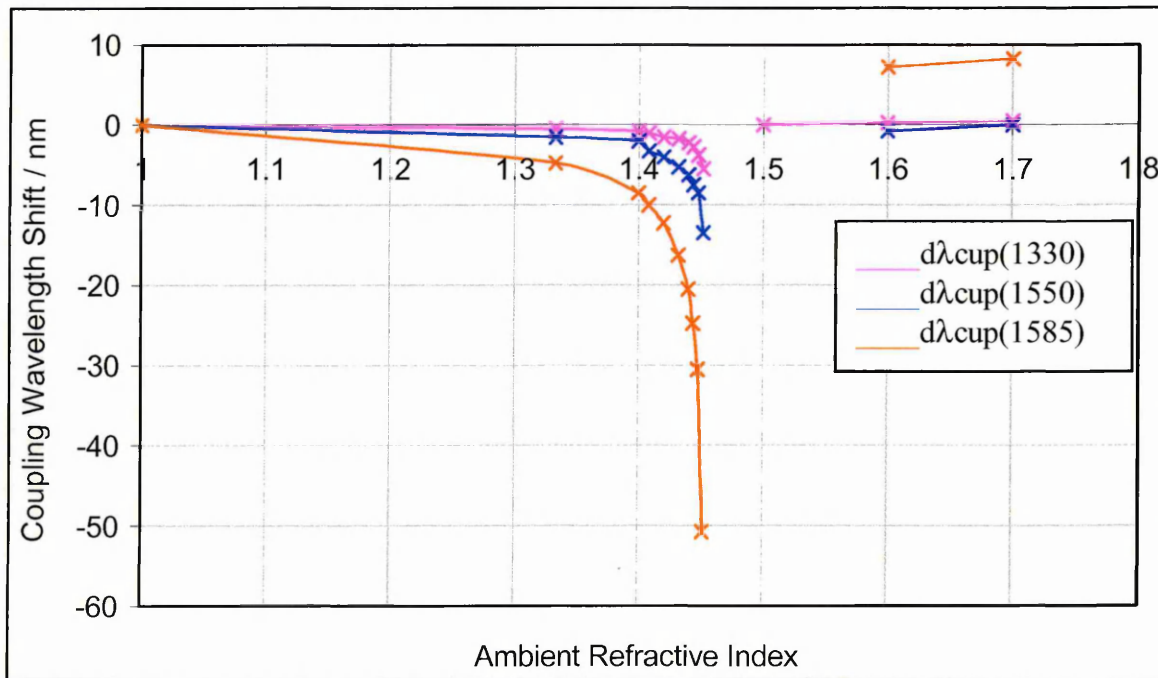
Figure A9.44: Relative change in coupling wavelength with ambient refractive index for LPG A410

310
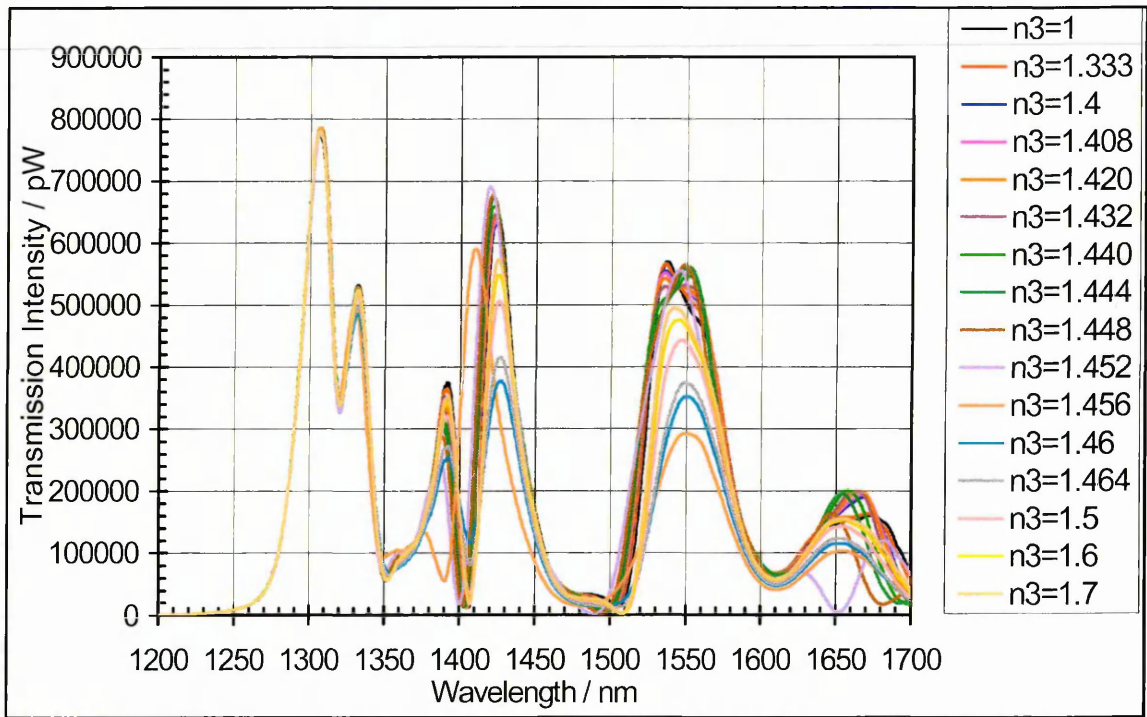
Figure A9.45: Ambient refractive index profile of LPG A416
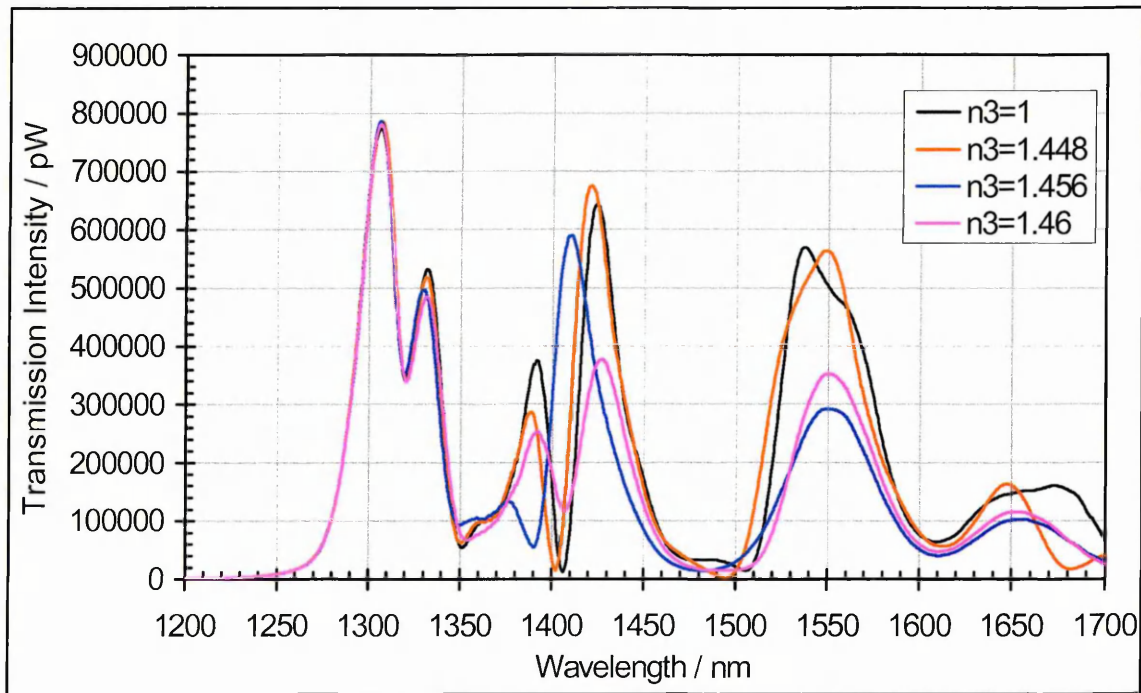
Figure A9.46: Ambient refractive index profile of LPG A416 at selected values to allow clearer observation of shifts
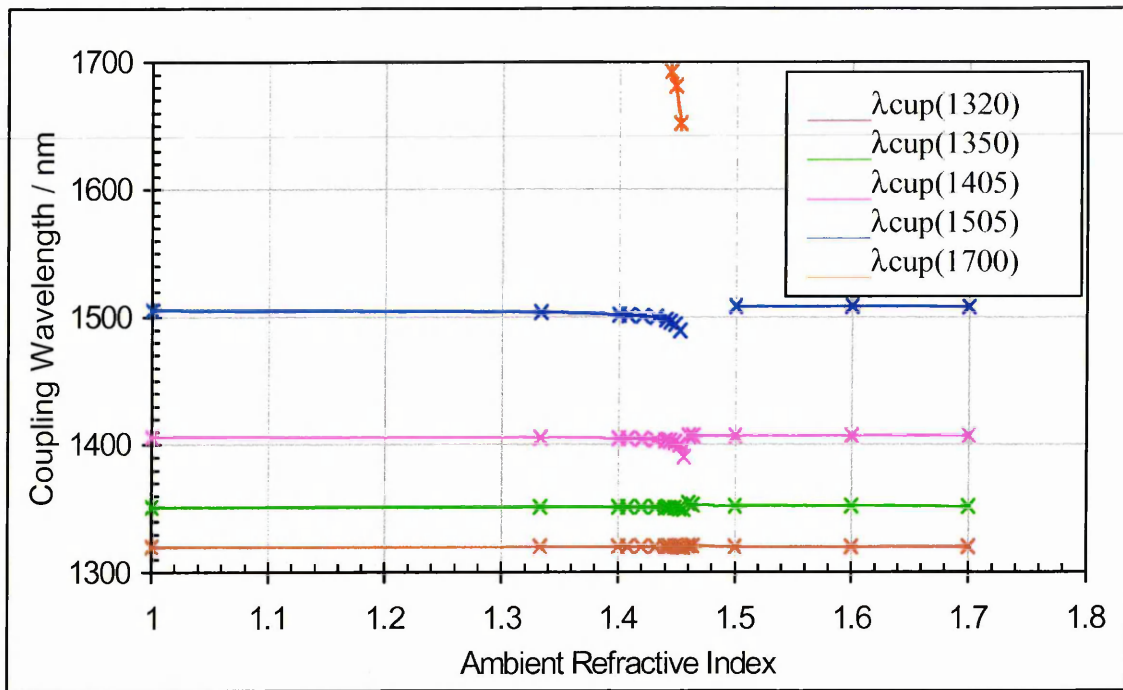
Figure A9.47: Change in coupling wavelength with ambient refractive index for LPG A416
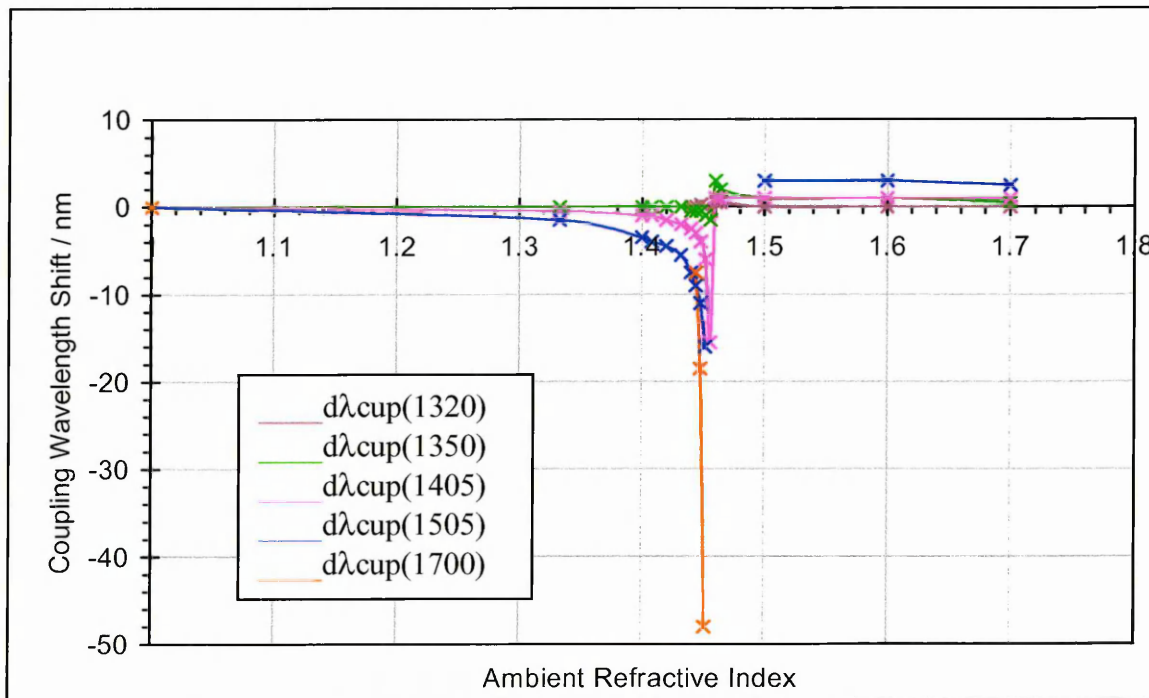
Figure A9.48: Relative change in coupling wavelength with ambient refractive index for LPG A416

Appendix 10

Ambient Temperature Profiles of All LPGs
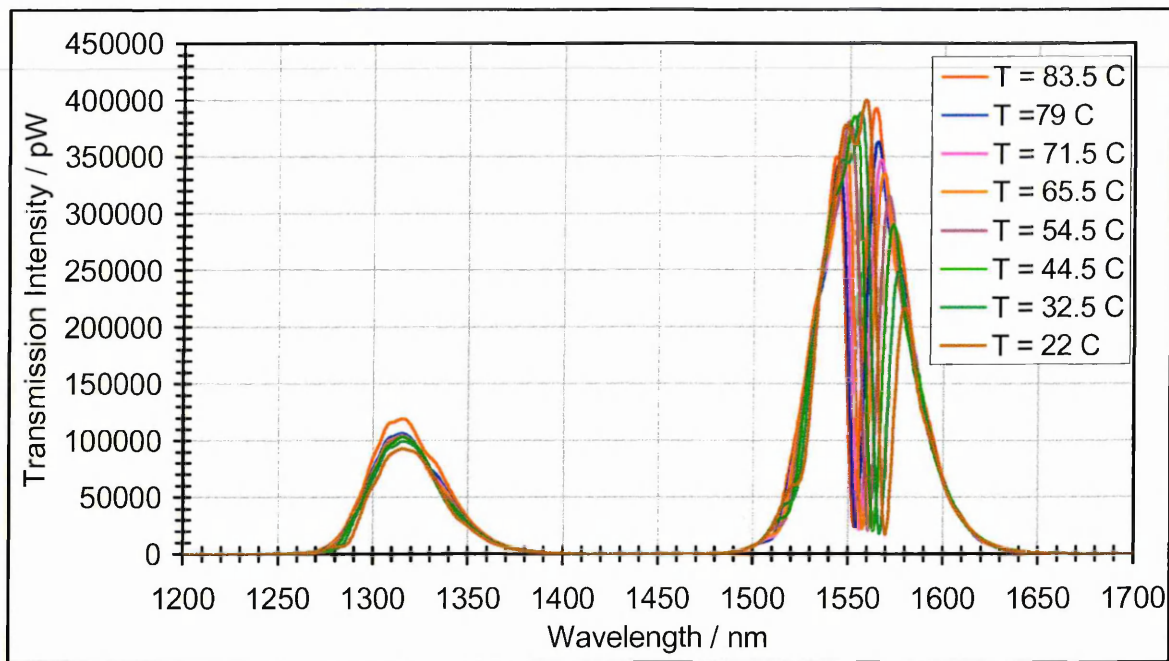
Figure A10.1: Ambient temperature profile of LPG S3
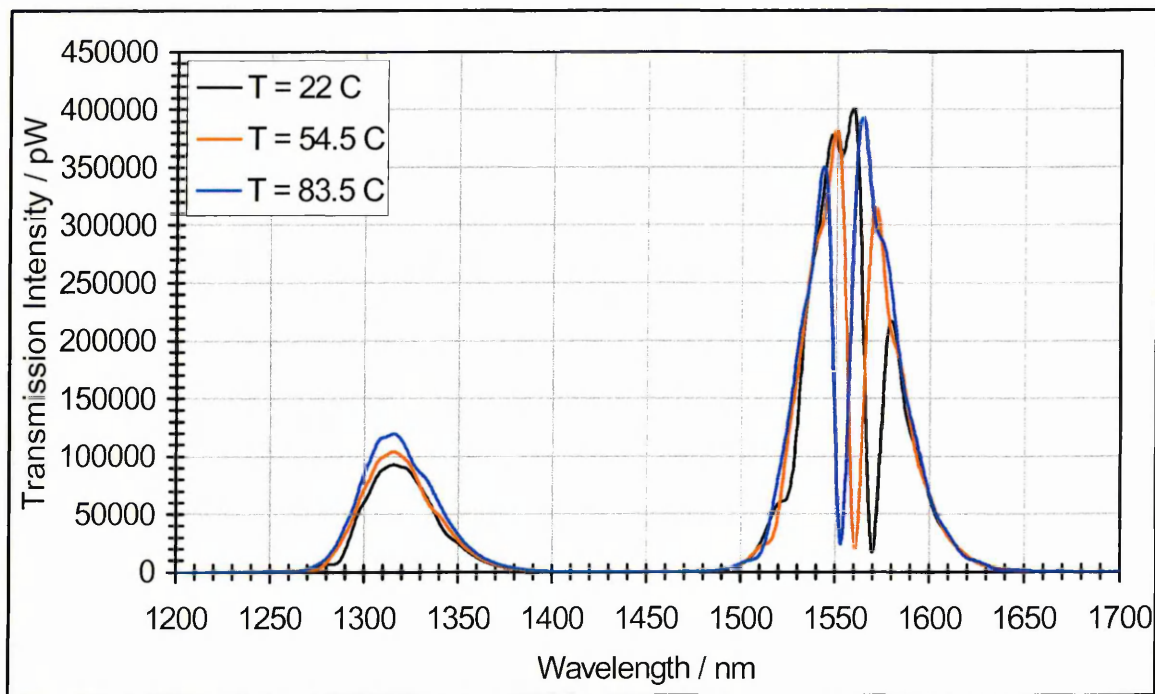
Figure A10.2: Ambient temperature profile of LPG S3 at selected values to allow clearer observation of shifts
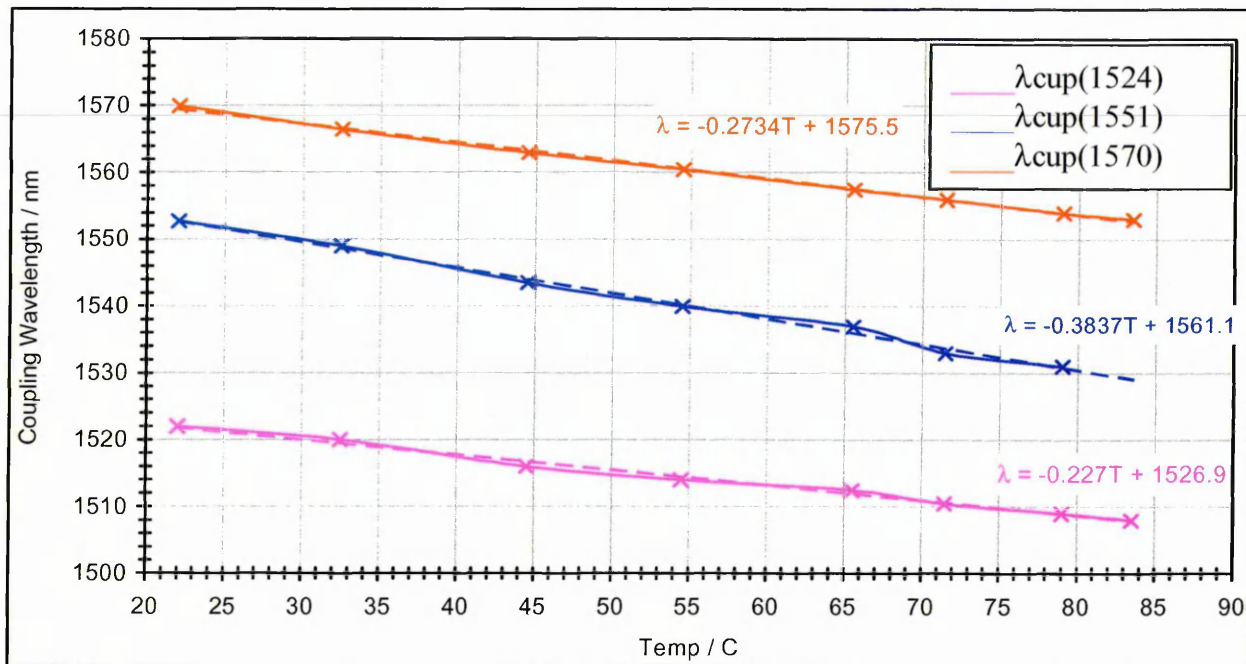
Figure A10.3: Change in coupling wavelength with ambient temperature for LPG S3

Legend:
- λcup(1524)
- λcup(1551)
- λcup(1570)

$\lambda = -0.2734T + 1575.5$

$\lambda = -0.3837T + 1561.1$

$\lambda = -0.227T + 1526.9$
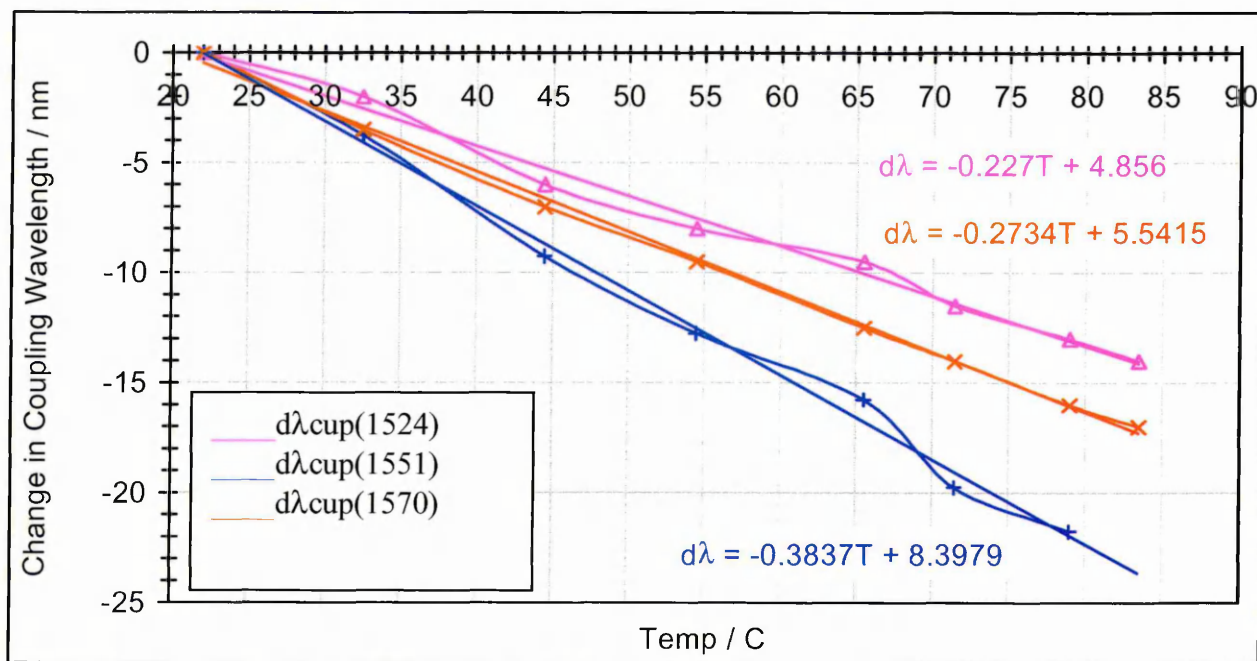
Figure A10.4: Relative change in coupling wavelength with ambient temperature for LPG S3

Legend:
- dλcup(1524)
- dλcup(1551)
- dλcup(1570)

$d\lambda = -0.227T + 4.856$

$d\lambda = -0.2734T + 5.5415$

$d\lambda = -0.3837T + 8.3979$

315
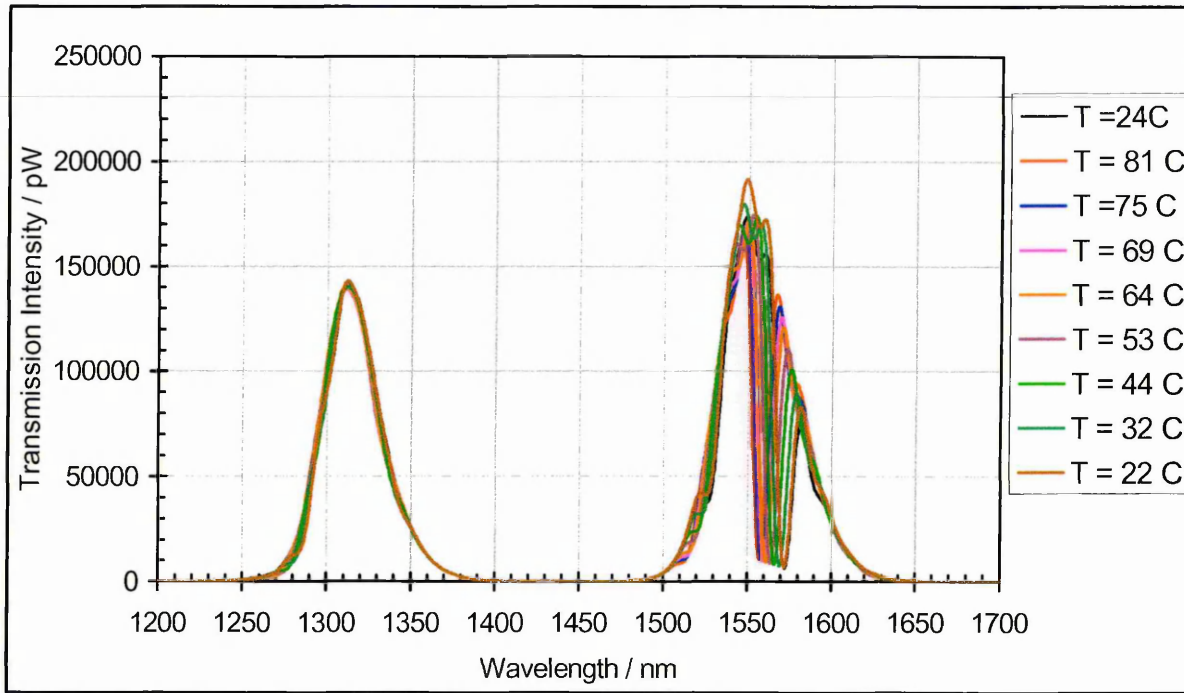
Figure A10.5: Ambient temperature profile of LPG S4
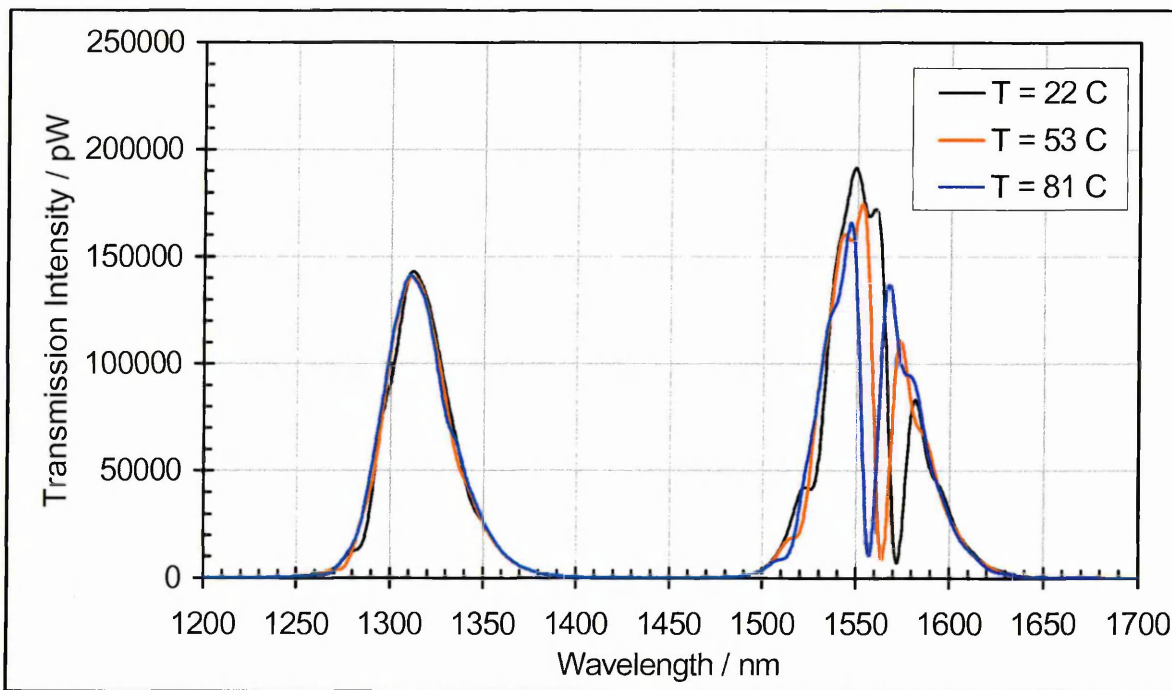

Figure A10.6: Ambient temperature profile of LPG S4 at selected values to allow clearer observation of shifts
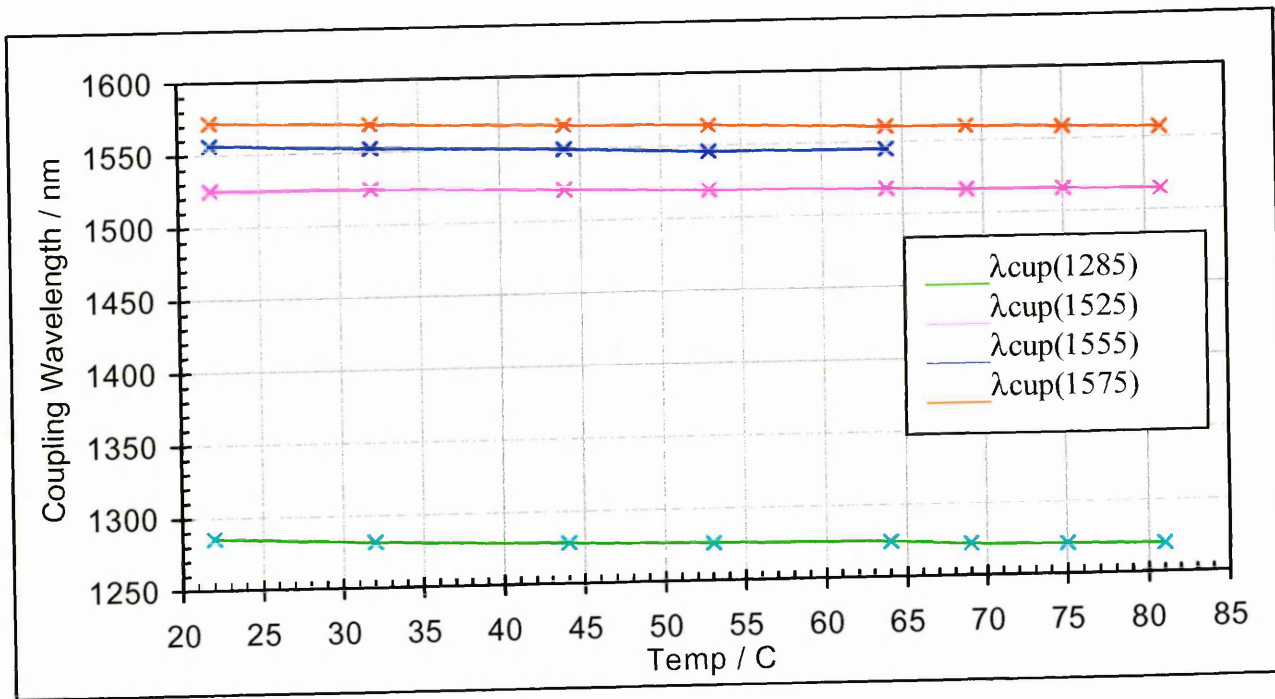
**Figure A10.7: Change in coupling wavelength with ambient temperature for LPG S4**

$d\lambda = -0.1907T + 4.4901$

$d\lambda = -0.2544T + 5.4898$

$d\lambda = -0.2544T + 4.5523$

$d\lambda = -0.2853T + 5.769$
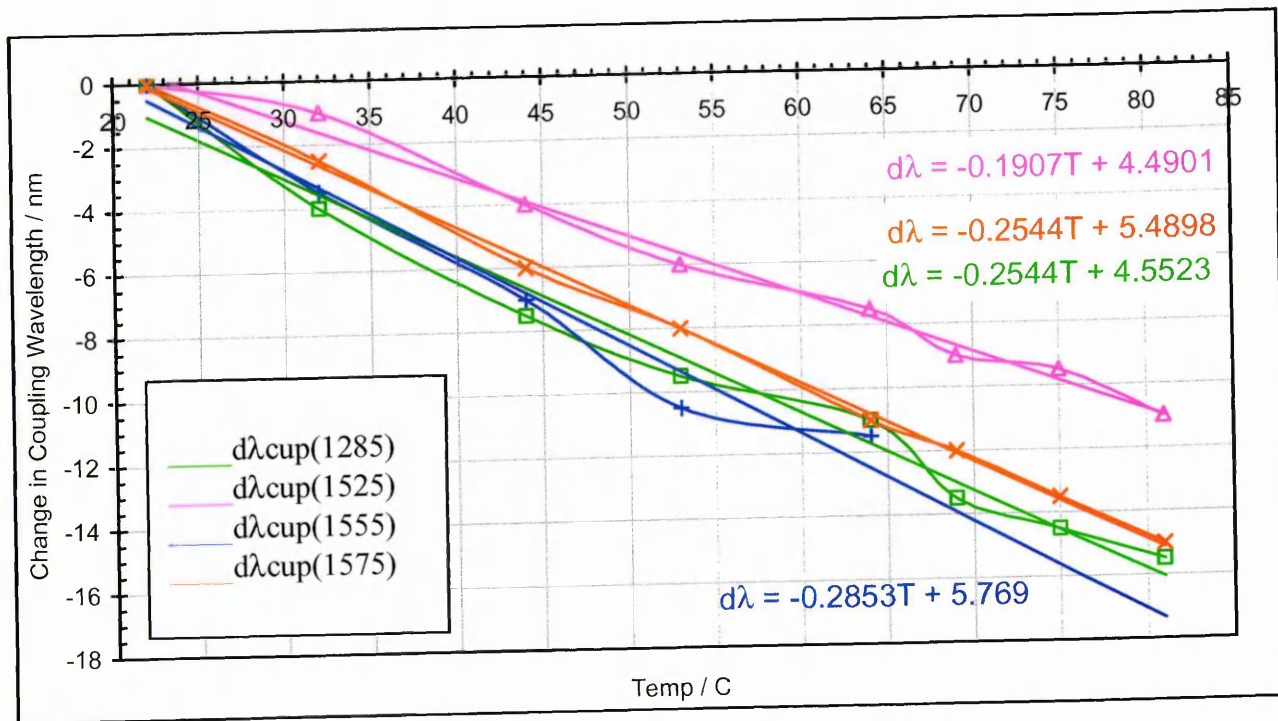
Figure A10.8: Relative change in coupling wavelength with ambient temperature for LPG S4
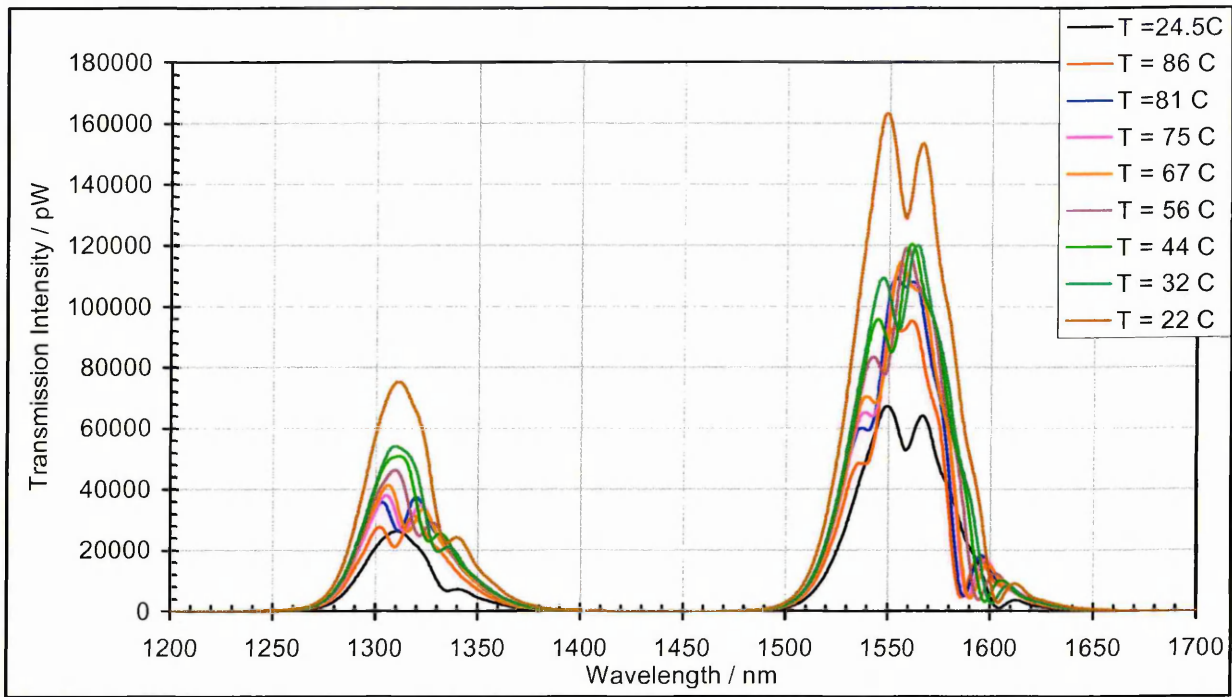
Figure A10.9: Ambient temperature profile of LPG S5
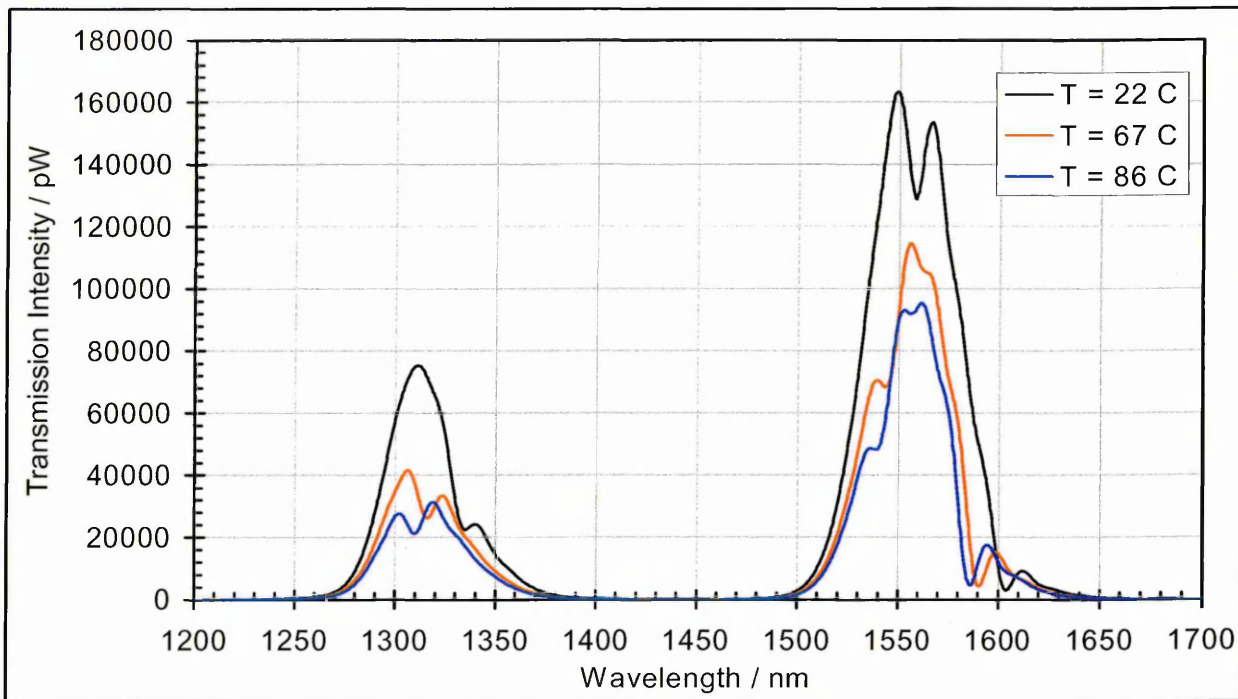
Figure A10.10: Ambient temperature profile of LPG S5 at selected values to allow clearer observation of shifts
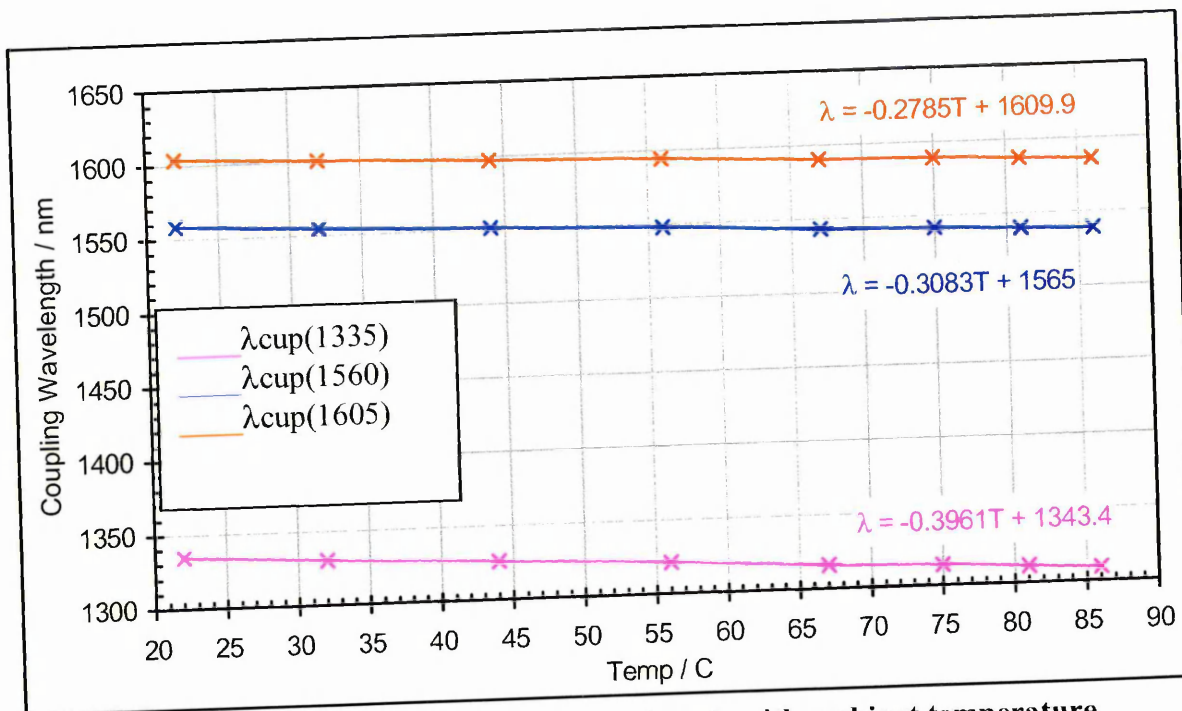
Figure A10.11: Change in coupling wavelength with ambient temperature for LPG S5
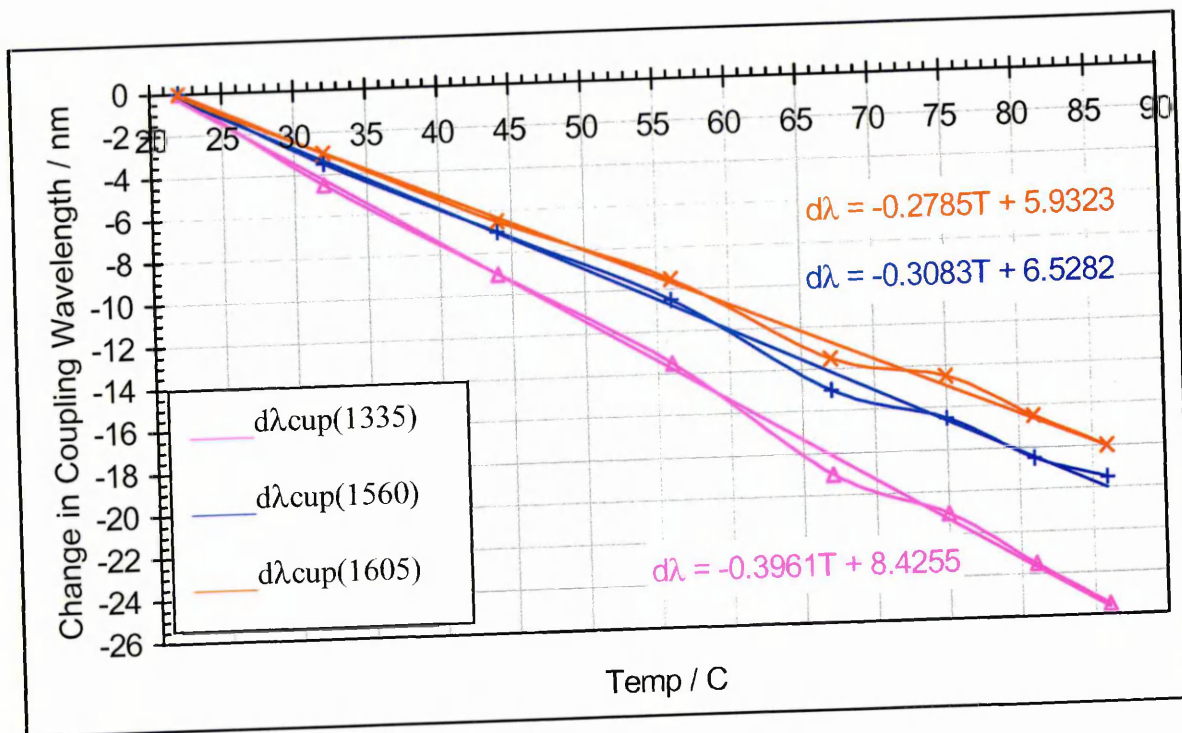
Figure A10.12: Relative change in coupling wavelength with ambient temperature for LPG S5
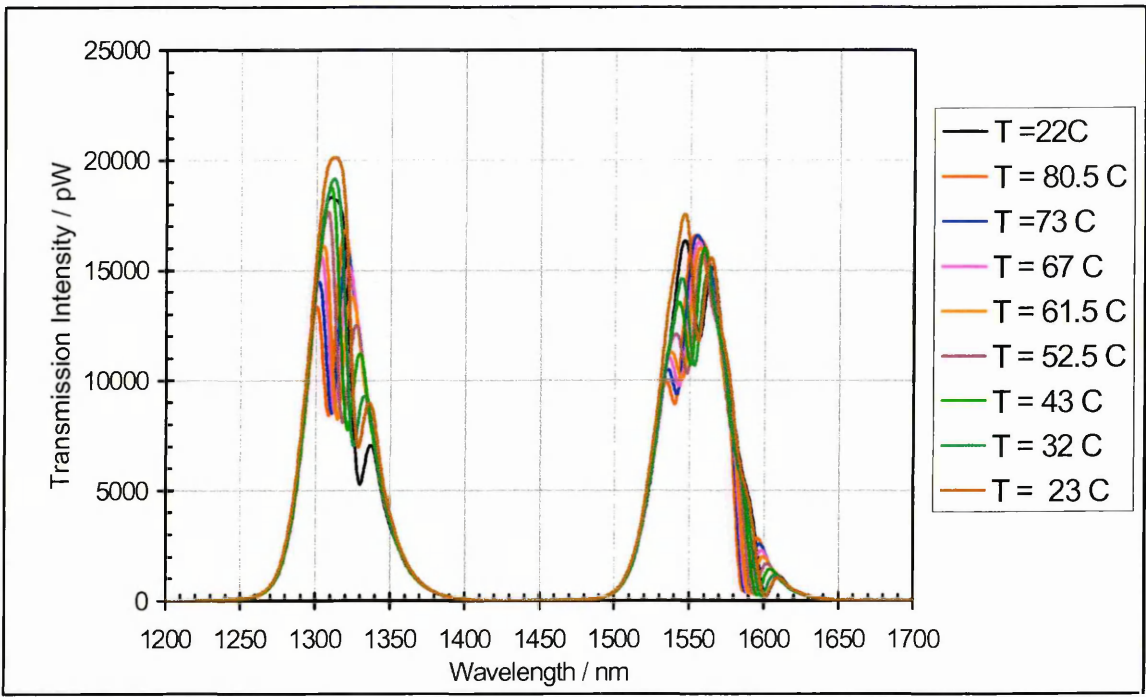
Figure A10.13: Ambient temperature profile of LPG S6
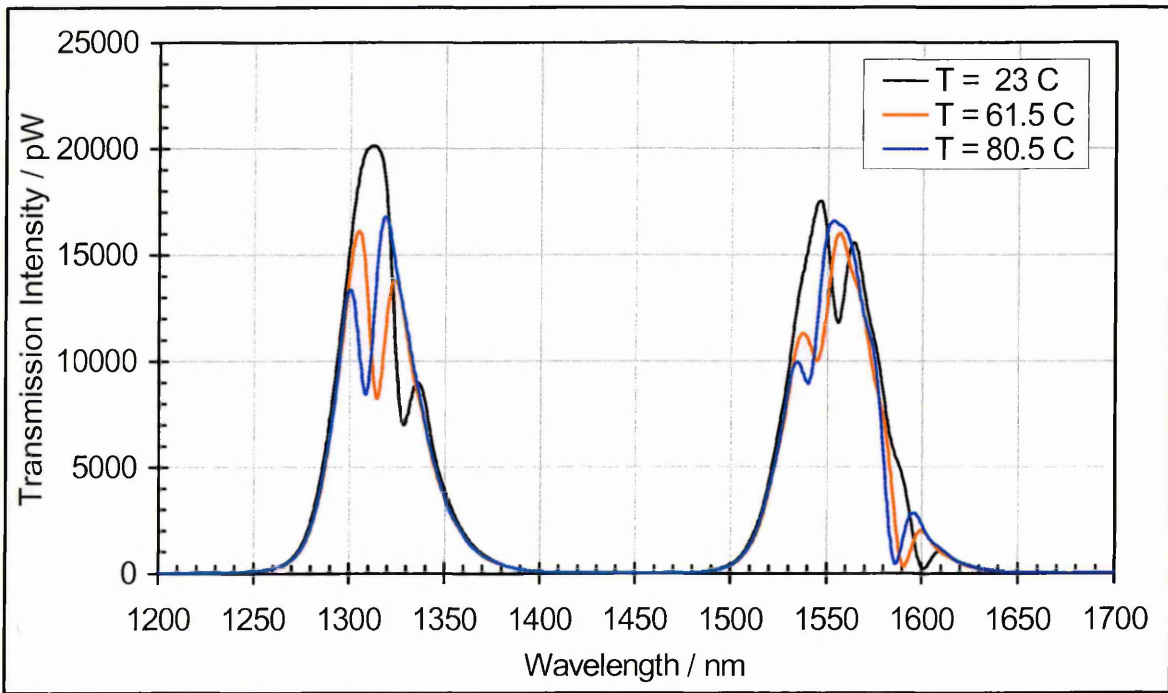
Figure A10.14: Ambient temperature profile of LPG S6 at selected values to allow clearer observation of shifts
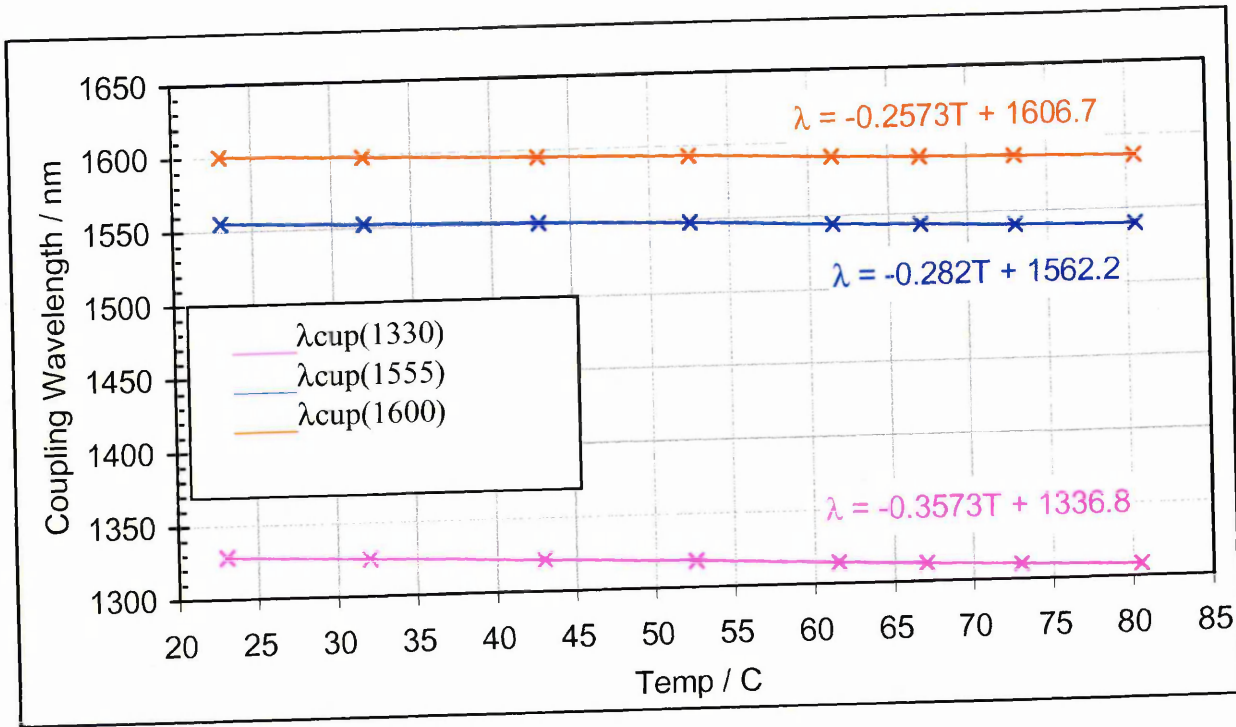
**Figure A10.15: Change in coupling wavelength with ambient temperature for LPG S6**
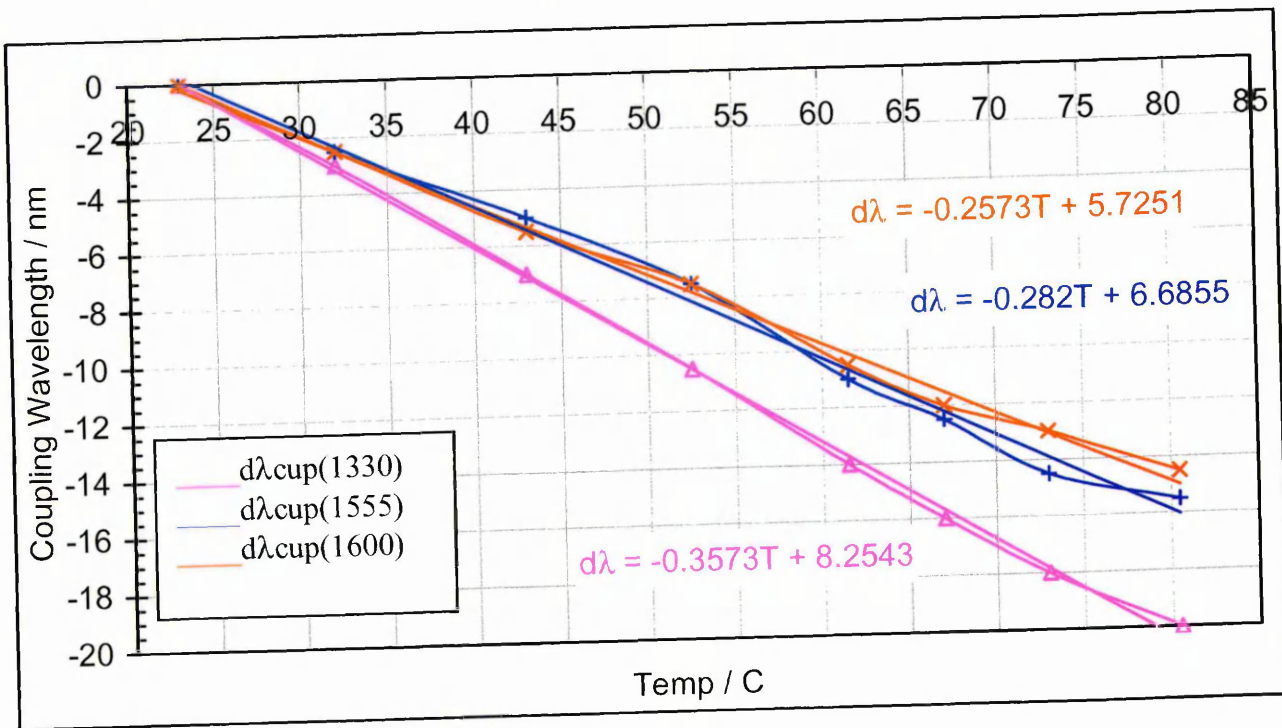
Figure A10.16: Relative change in coupling wavelength with ambient temperature for LPG S6
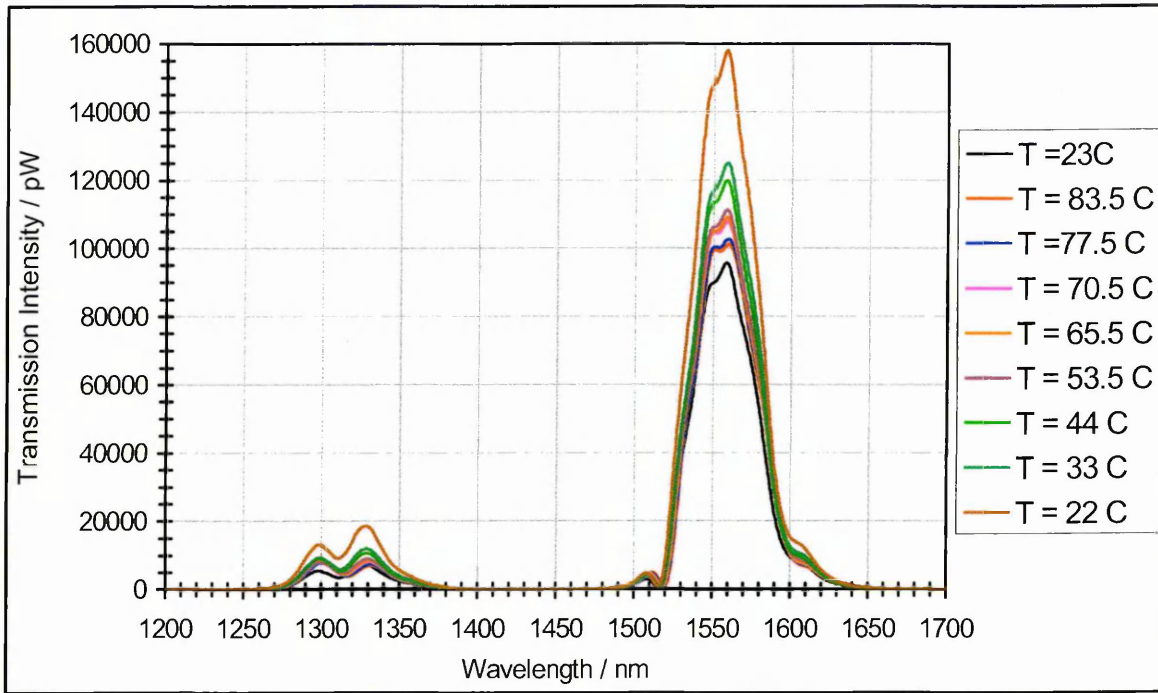
Figure A10.17: Ambient temperature profile of LPG S7
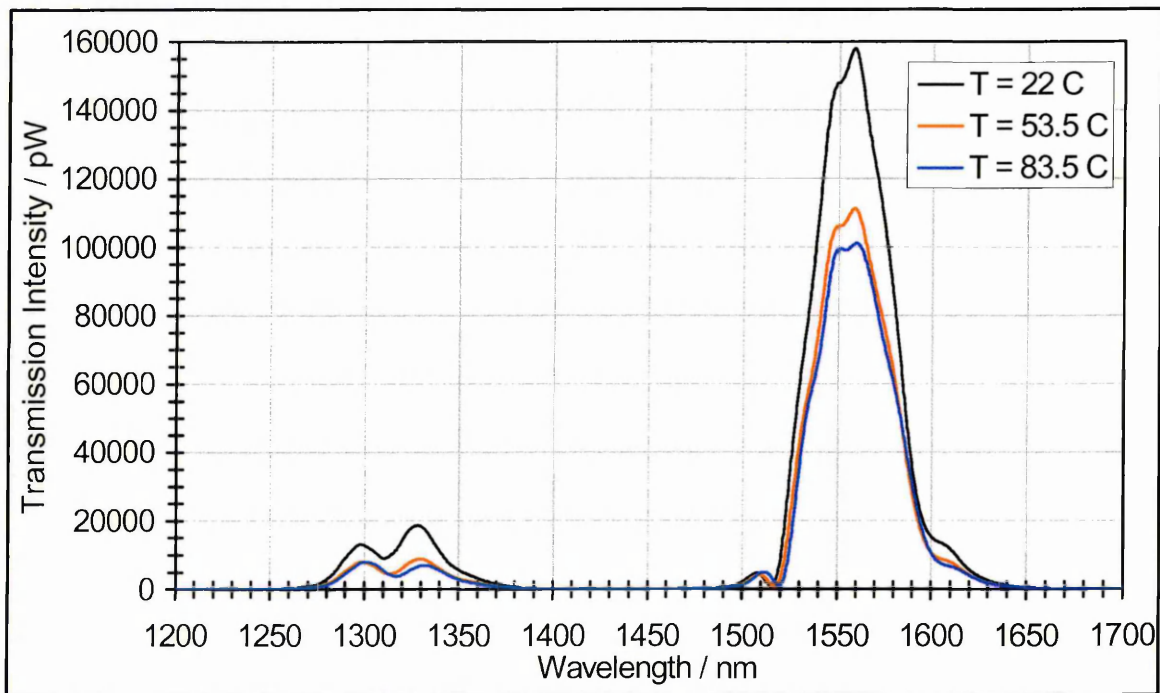
Figure A10.18: Ambient temperature profile of LPG S7 at selected values to allow clearer observation of shifts
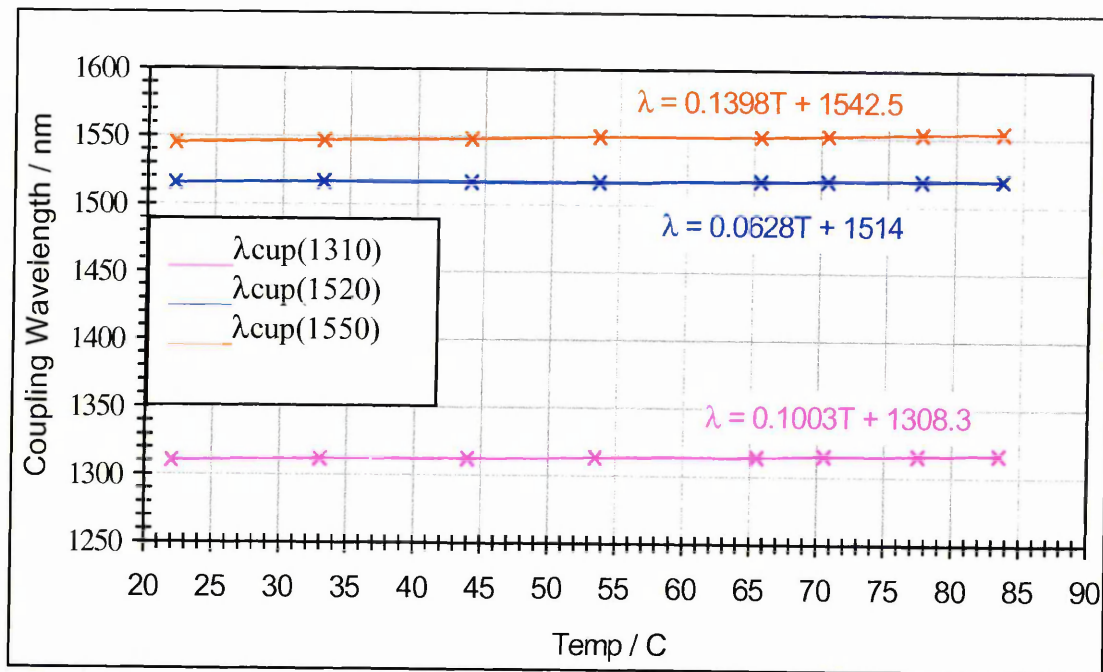
Figure A10.19: Change in coupling wavelength with ambient temperature for LPG S7
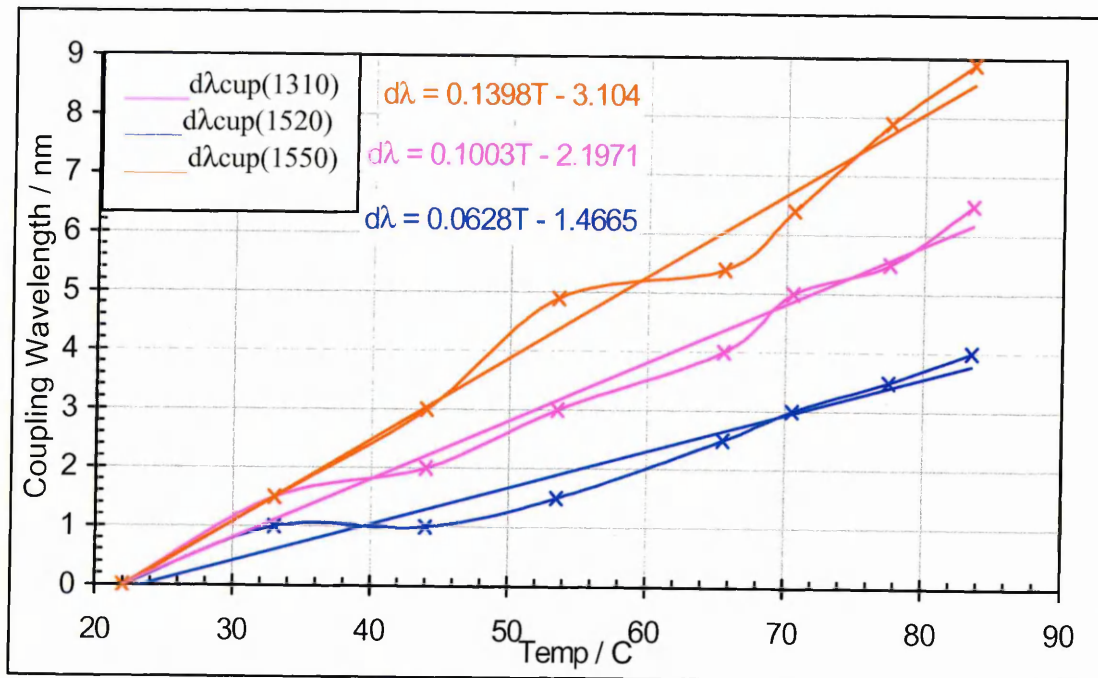
**Figure A10.20: Relative change in coupling wavelength with ambient temperature for LPG S7**
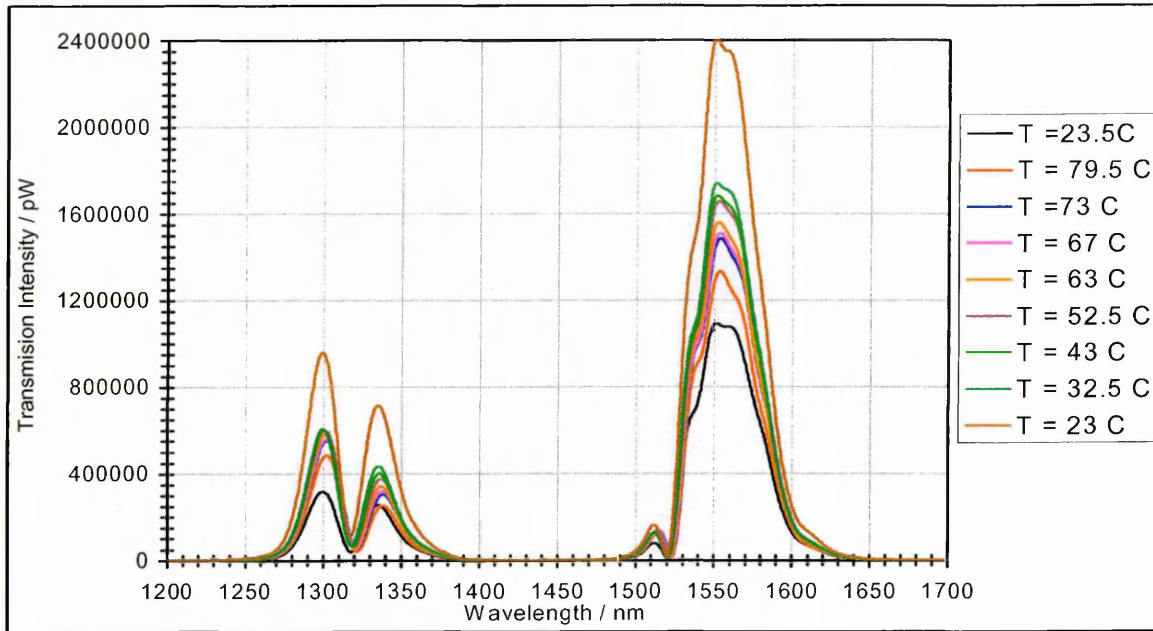
**Figure A10.21: Ambient temperature profile of LPG S8**
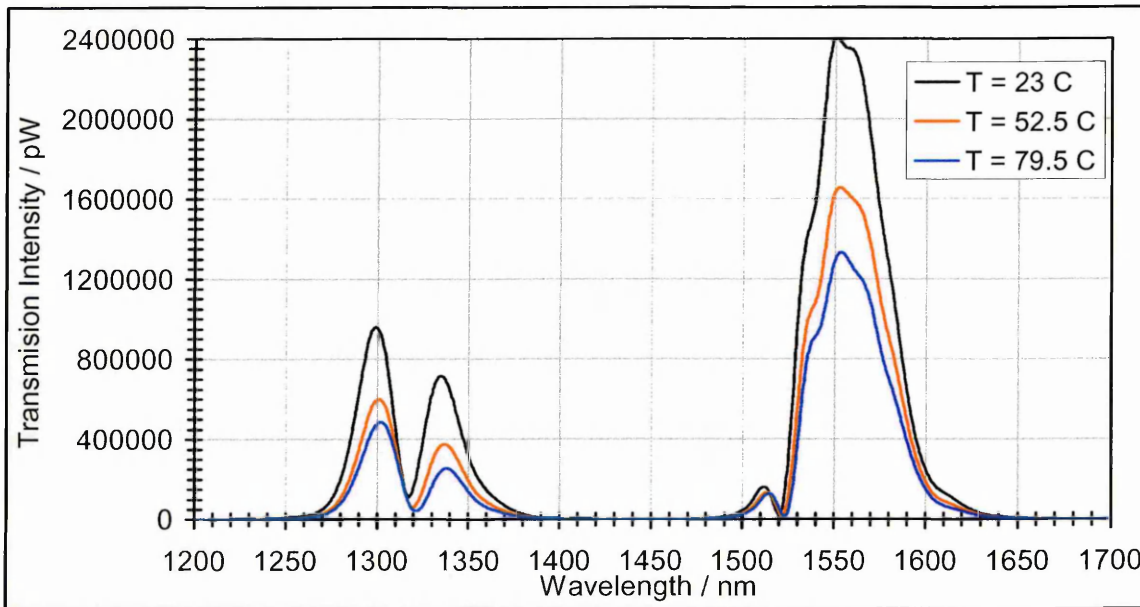
Figure A10.22: Ambient temperature profile of LPG S8 at selected values to allow clearer observation of shifts
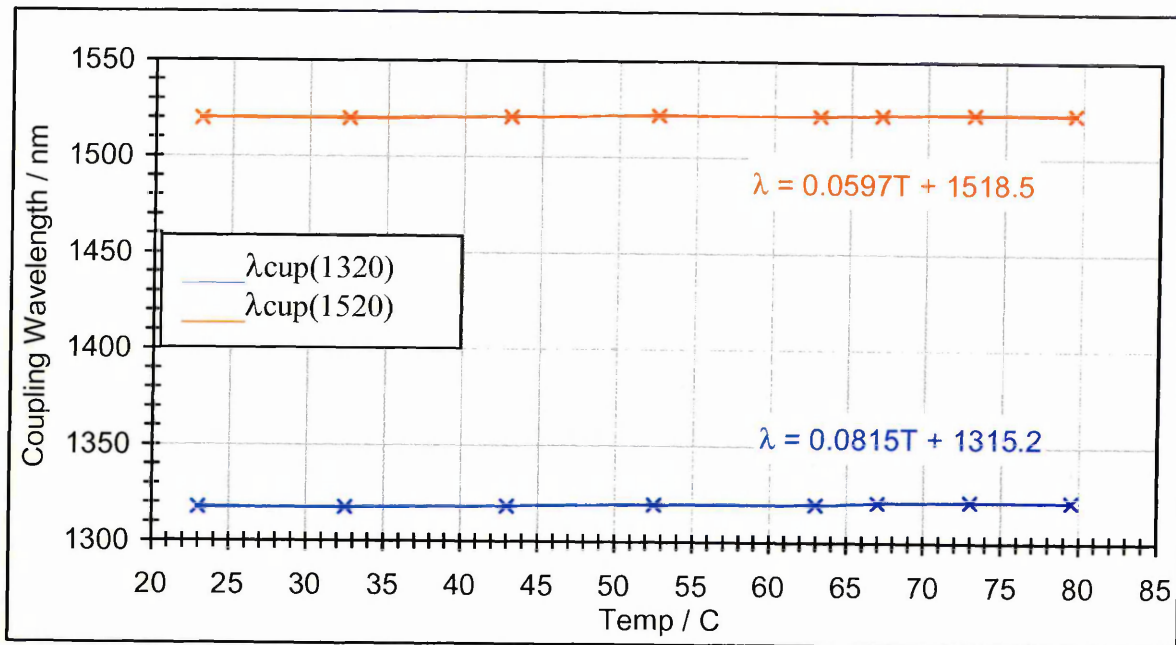
Figure A10.23: Change in coupling wavelength with ambient temperature for LPG S8
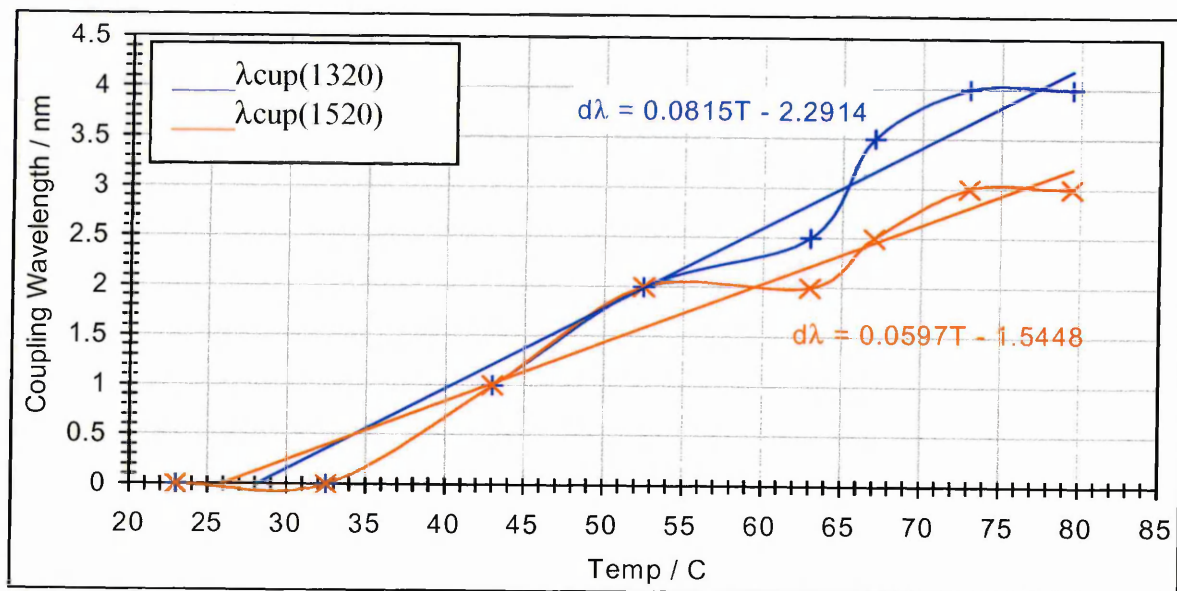
Figure A10.24: Relative change in coupling wavelength with ambient temperature for LPG S8
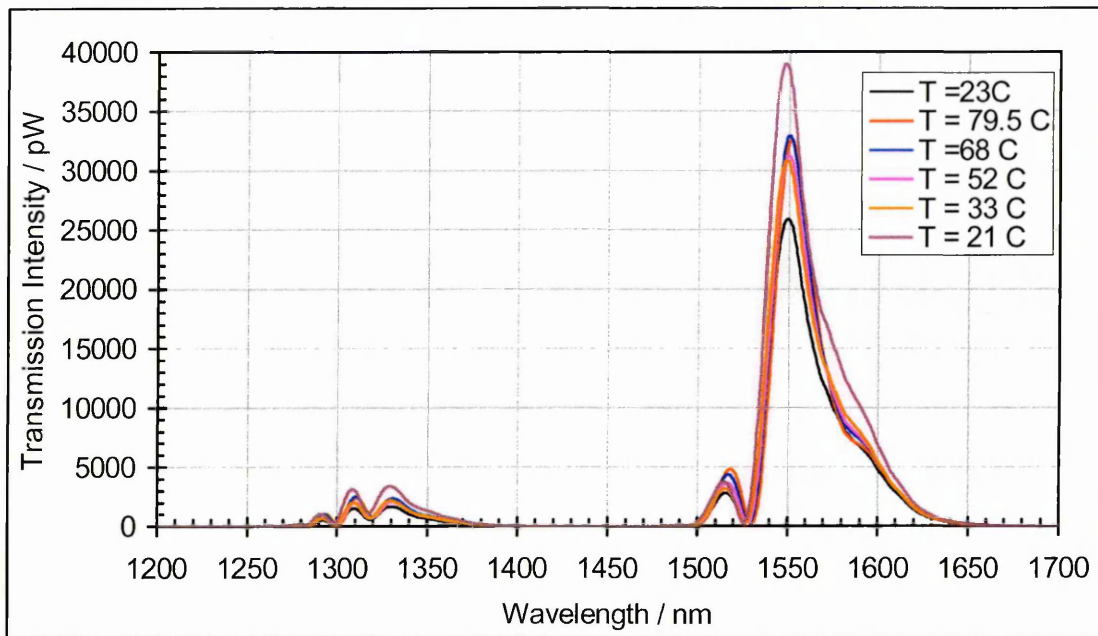
Figure A10.25: Ambient temperature profile of LPG C1
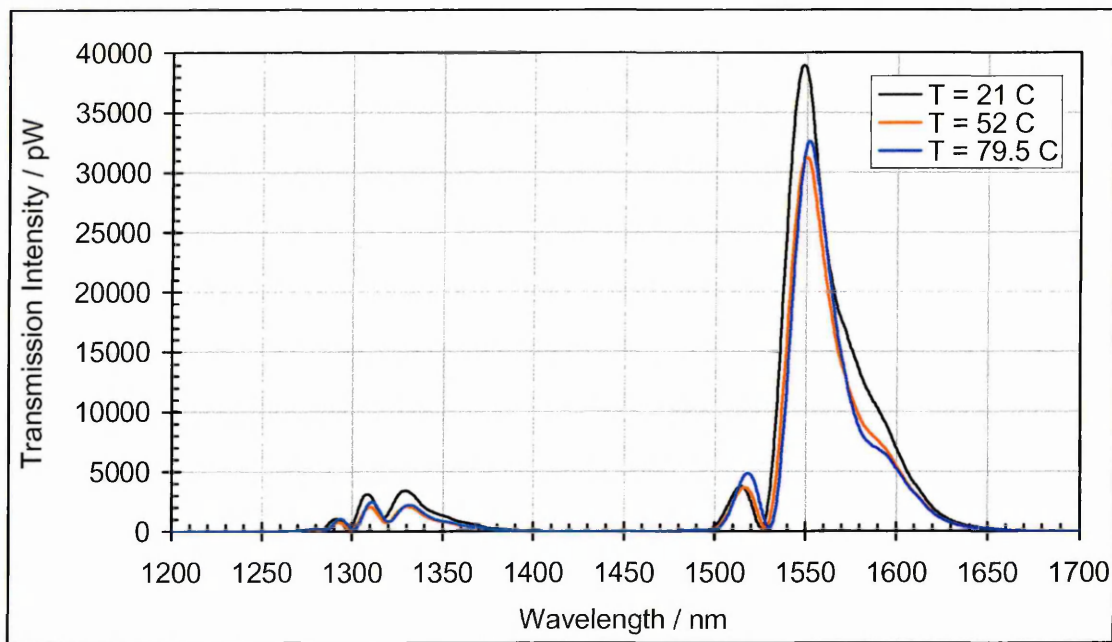
Figure A10.26: Ambient temperature profile of LPG C1 at selected values to allow clearer observation of shifts
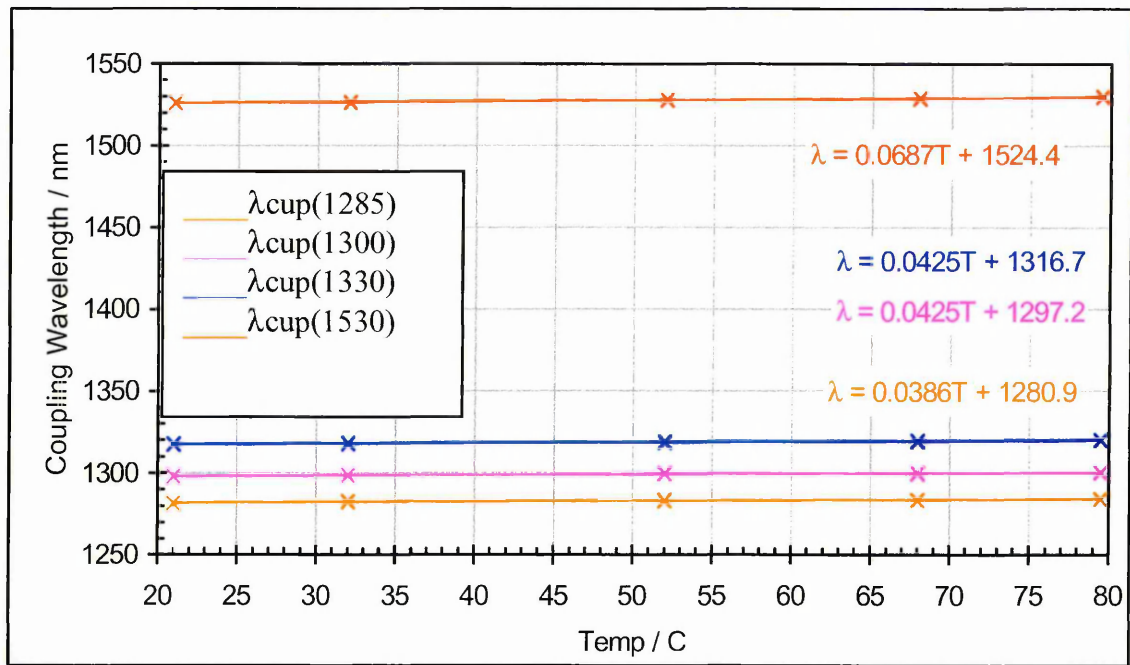
**Figure A10.27: Change in coupling wavelength with ambient temperature for LPG C1**
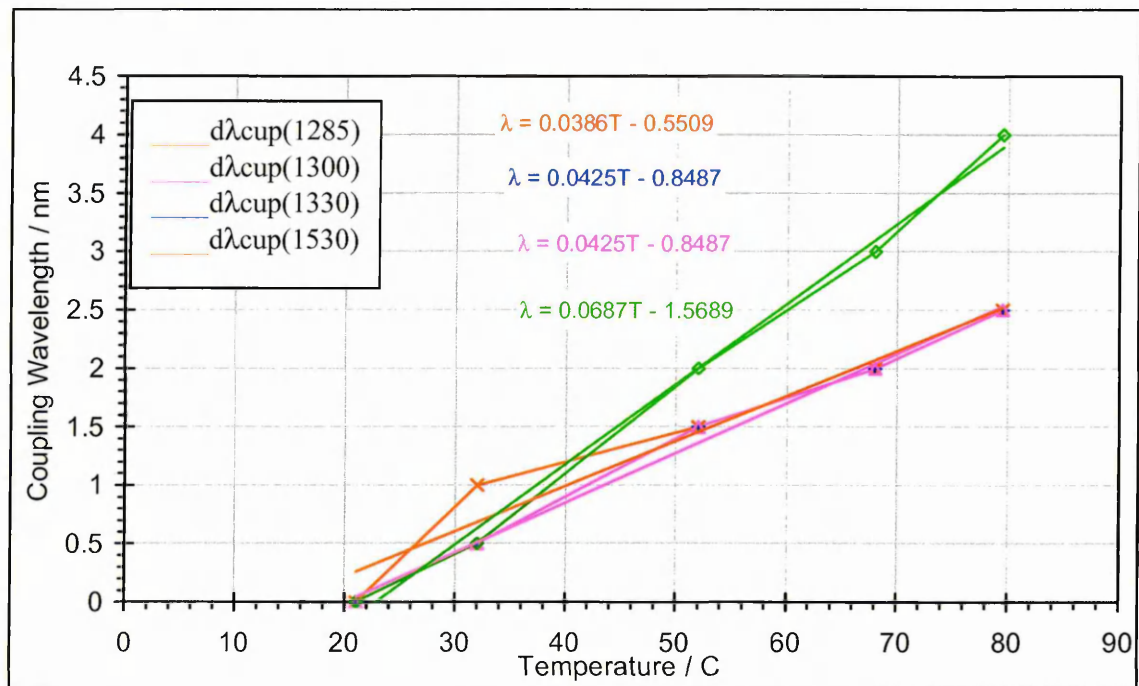
Figure A10.28: Relative change in coupling wavelength with ambient temperature for LPG C1
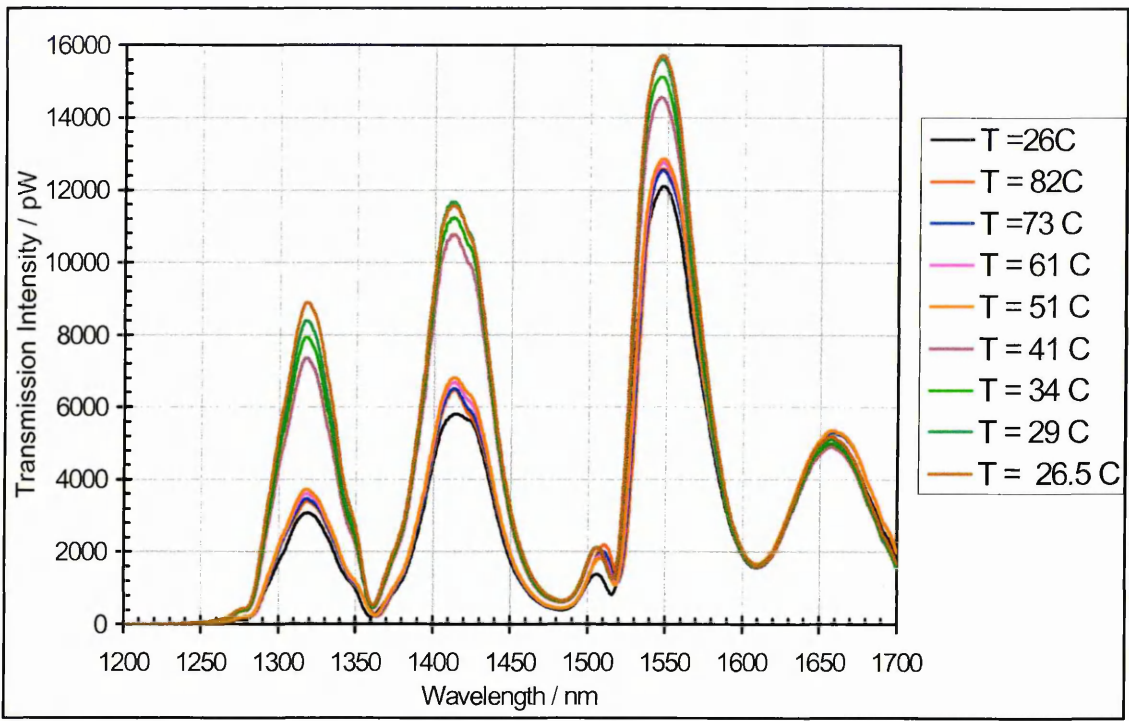
**Figure A10.29: Ambient temperature profile of LPG A400**
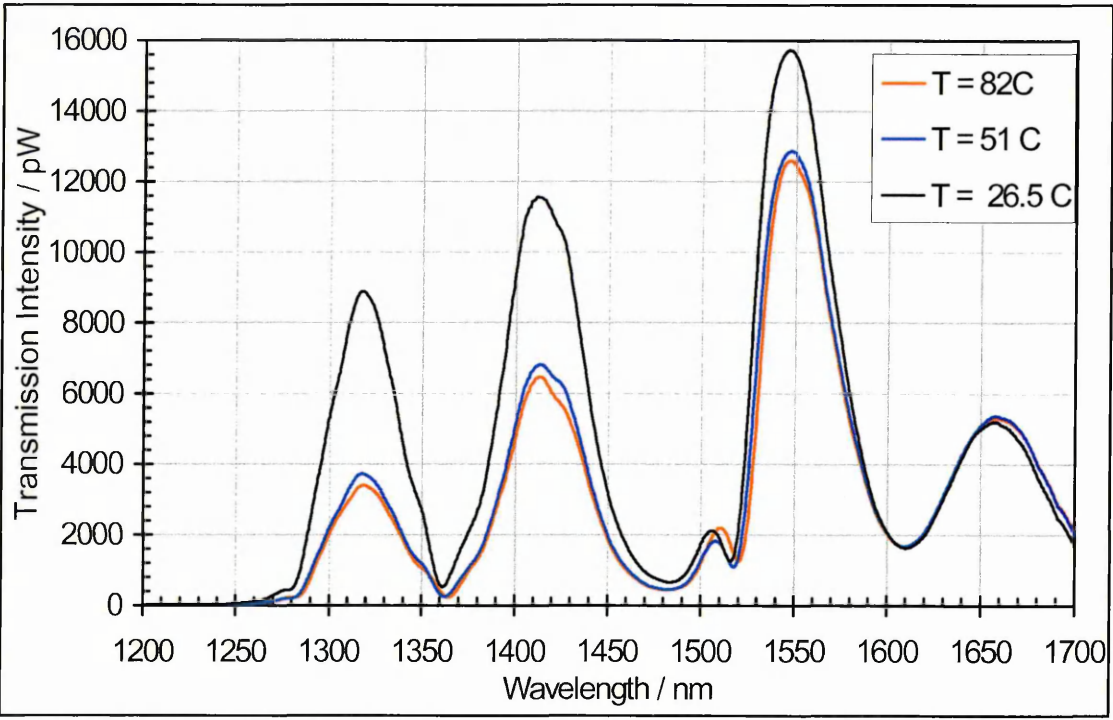
Figure A10.30: Ambient temperature profile of LPG A400 at selected values to allow clearer observation of shifts
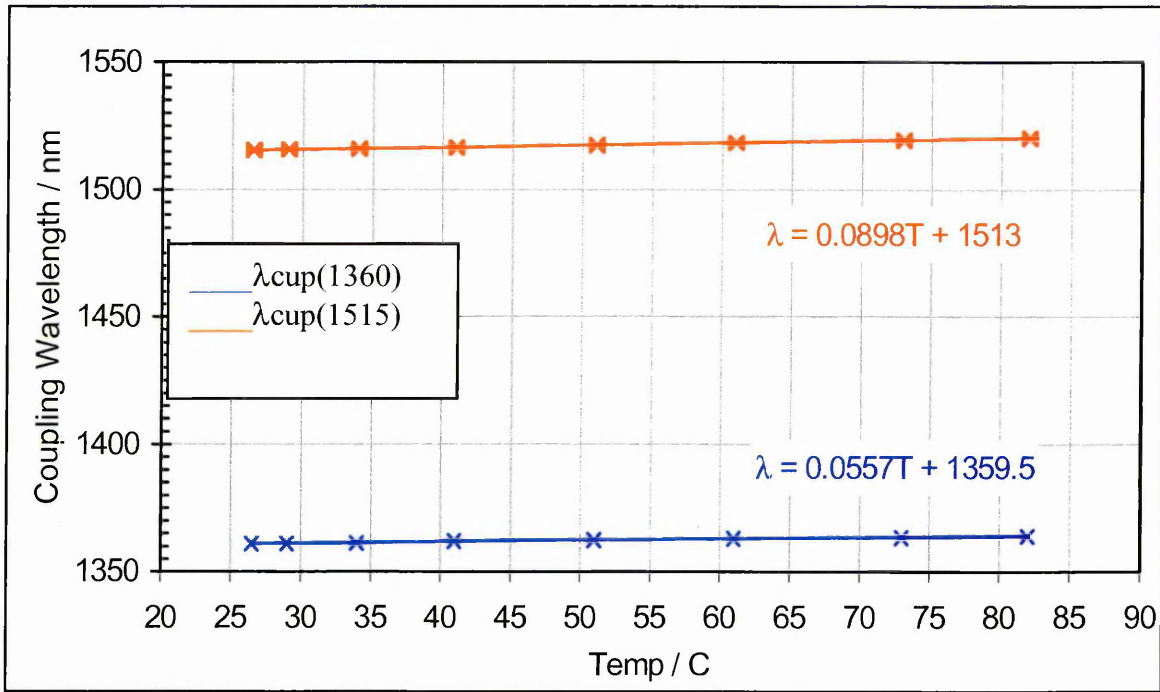
Figure A10.31: Change in coupling wavelength with ambient temperature for LPG A400
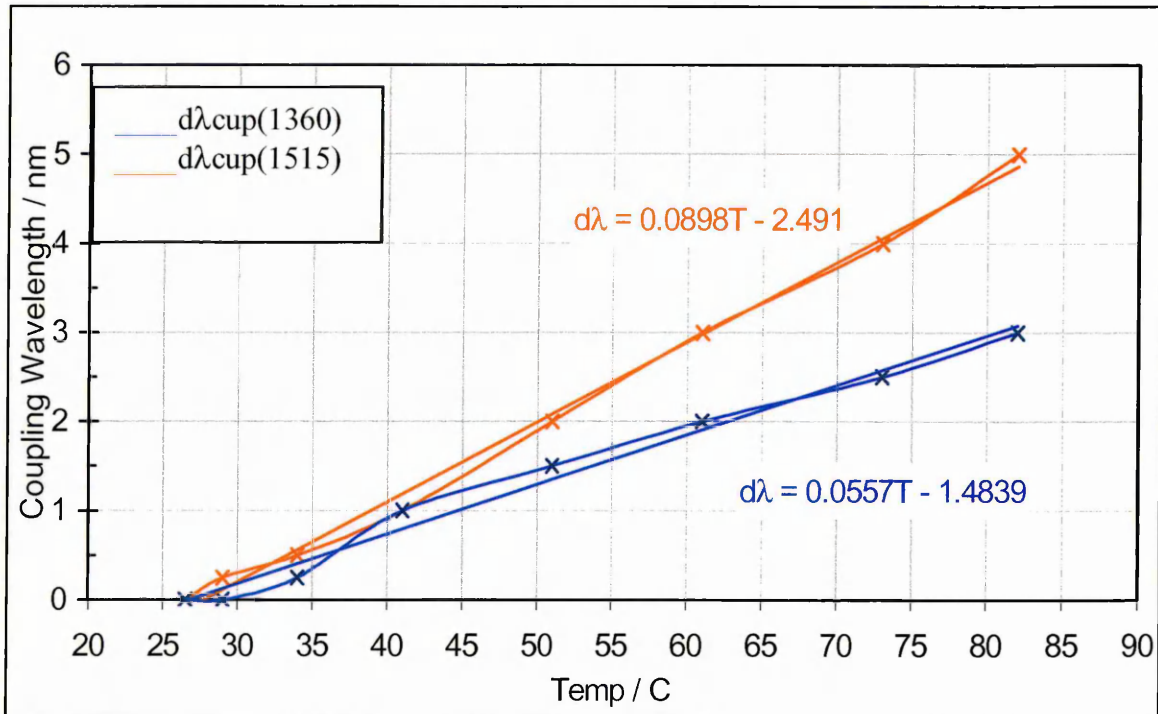
Figure A10.32:   Relative change in coupling wavelength with ambient temperature for LPG A400
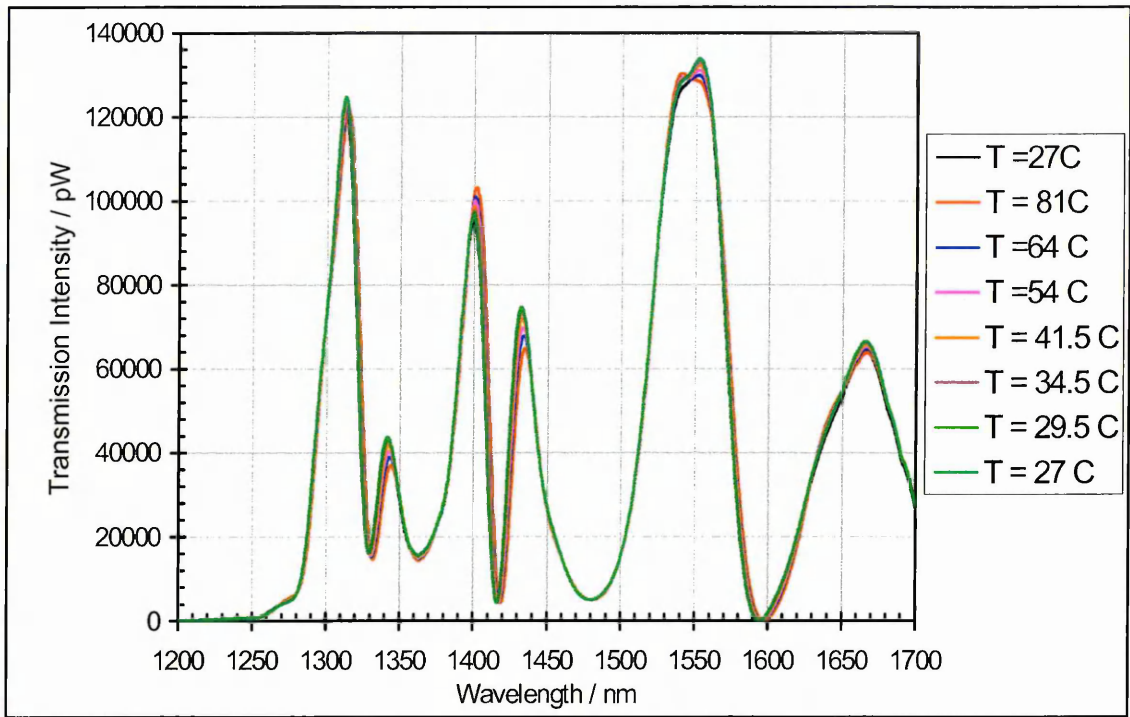
Figure A10.33: Ambient temperature profile of LPG A403
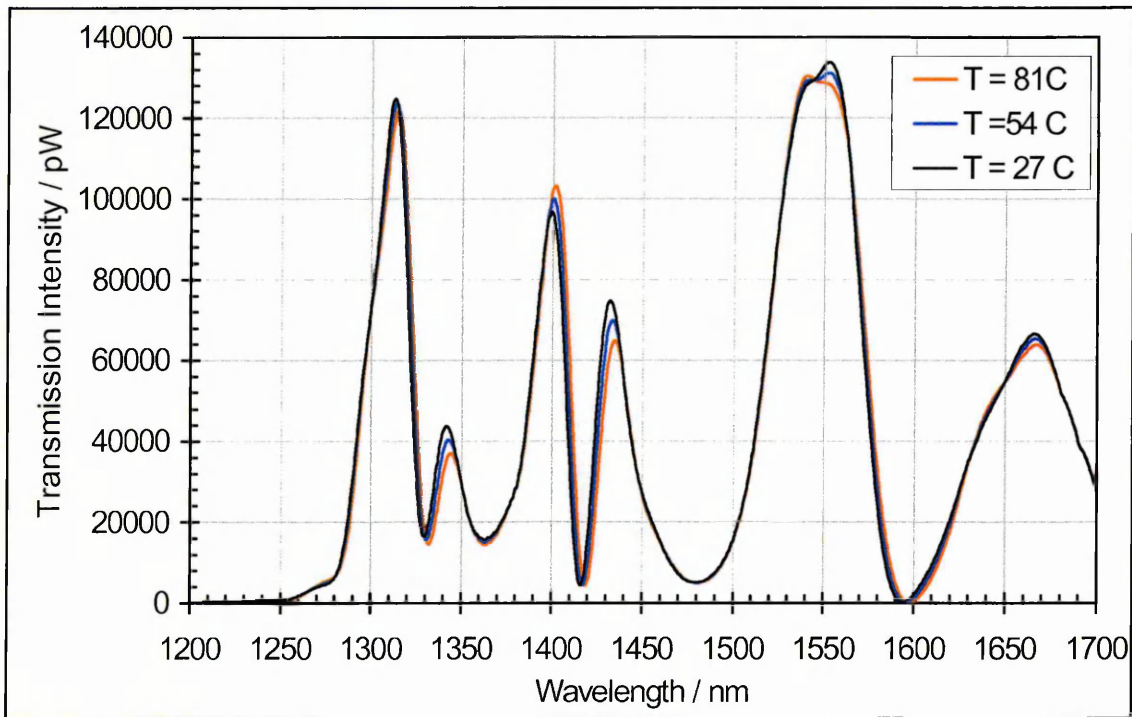
Figure A10.34: Ambient temperature profile of LPG A403 at selected values to allow clearer observation of shifts
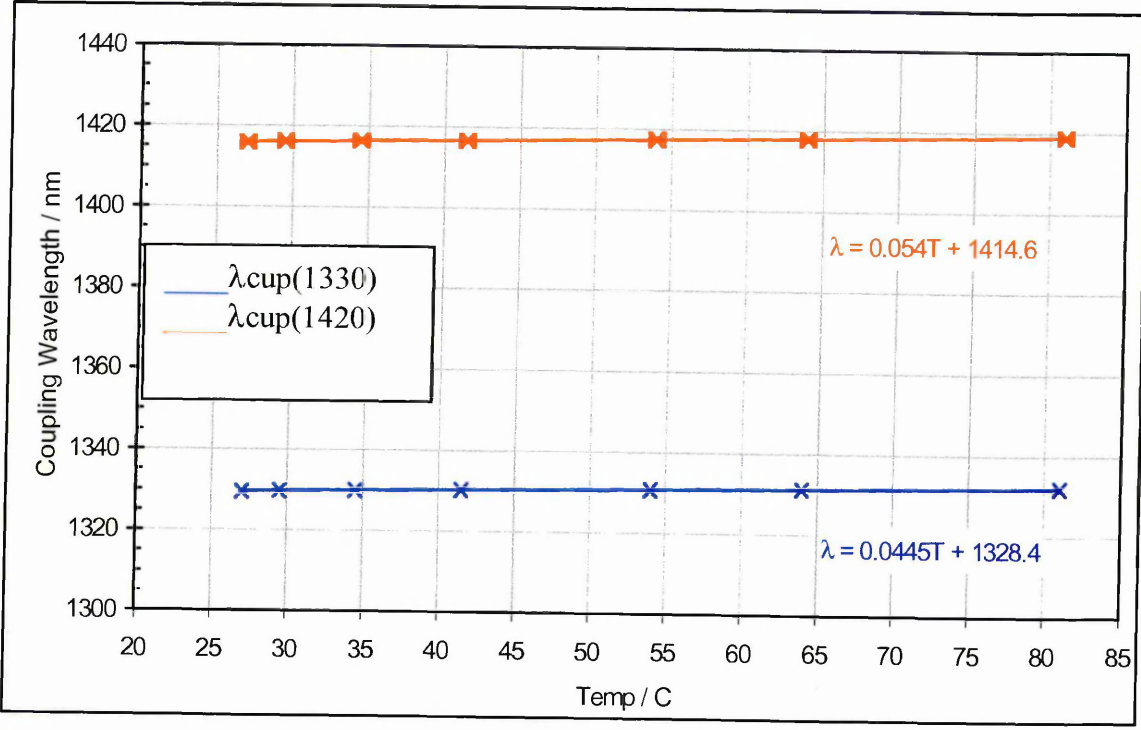
Figure A10.35: Change in coupling wavelength with ambient temperature for LPG A403

In figure A10.35 the upper (orange) dataset is labelled $\lambda\text{cup}(1420)$ with fit $\lambda = 0.054T + 1414.6$, and the lower (blue) dataset is labelled $\lambda\text{cup}(1330)$ with fit $\lambda = 0.0445T + 1328.4$.
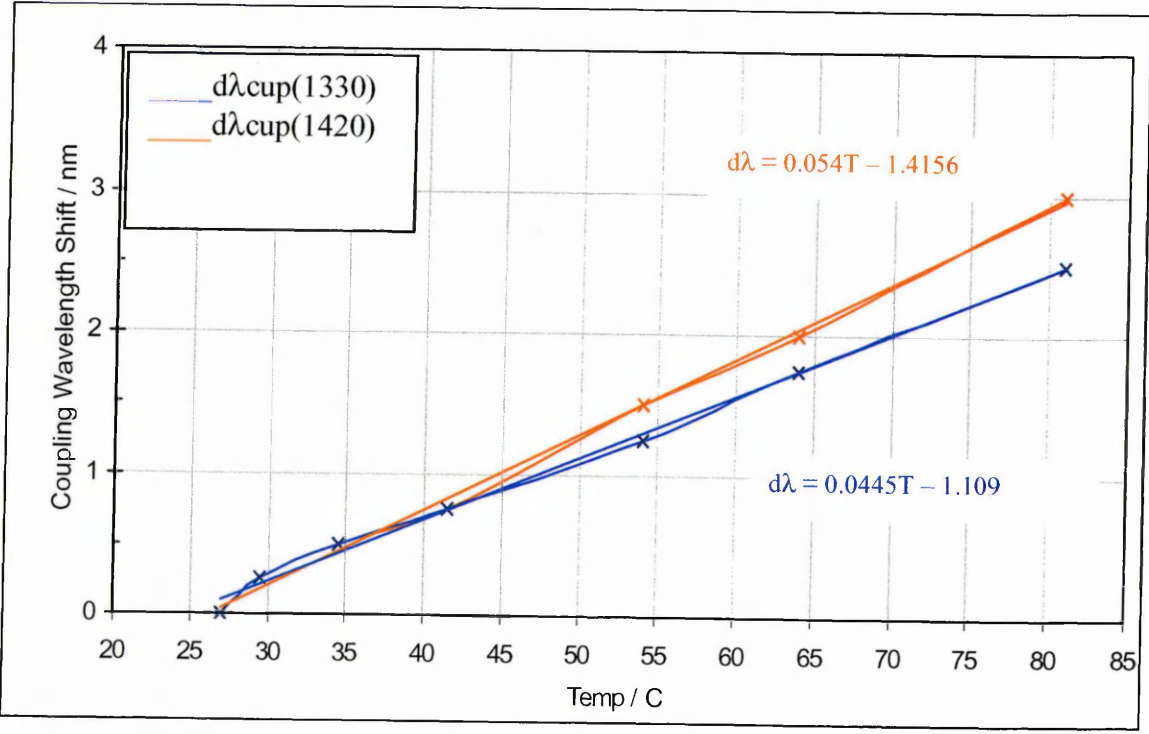
Figure A10.36: Relative change in coupling wavelength with ambient temperature for LPG A403

In figure A10.36 the datasets are labelled $d\lambda\text{cup}(1330)$ and $d\lambda\text{cup}(1420)$, with fits $d\lambda = 0.054T - 1.4156$ and $d\lambda = 0.0445T - 1.109$.
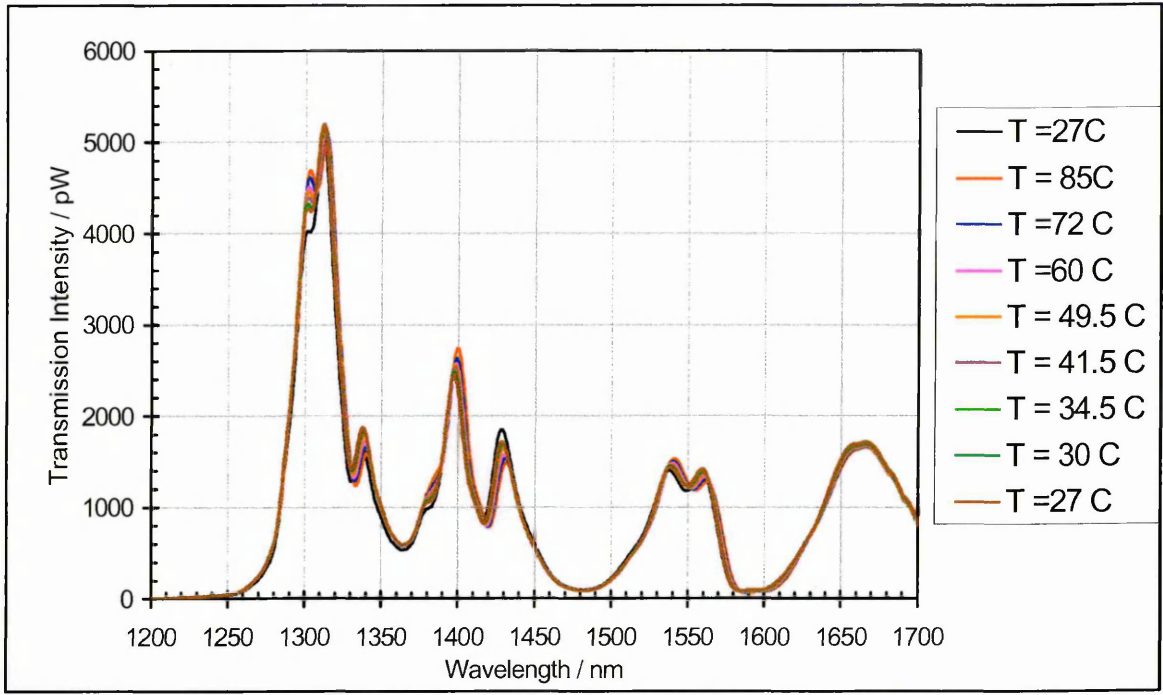
Figure A10.37: Ambient temperature profile of LPG A407
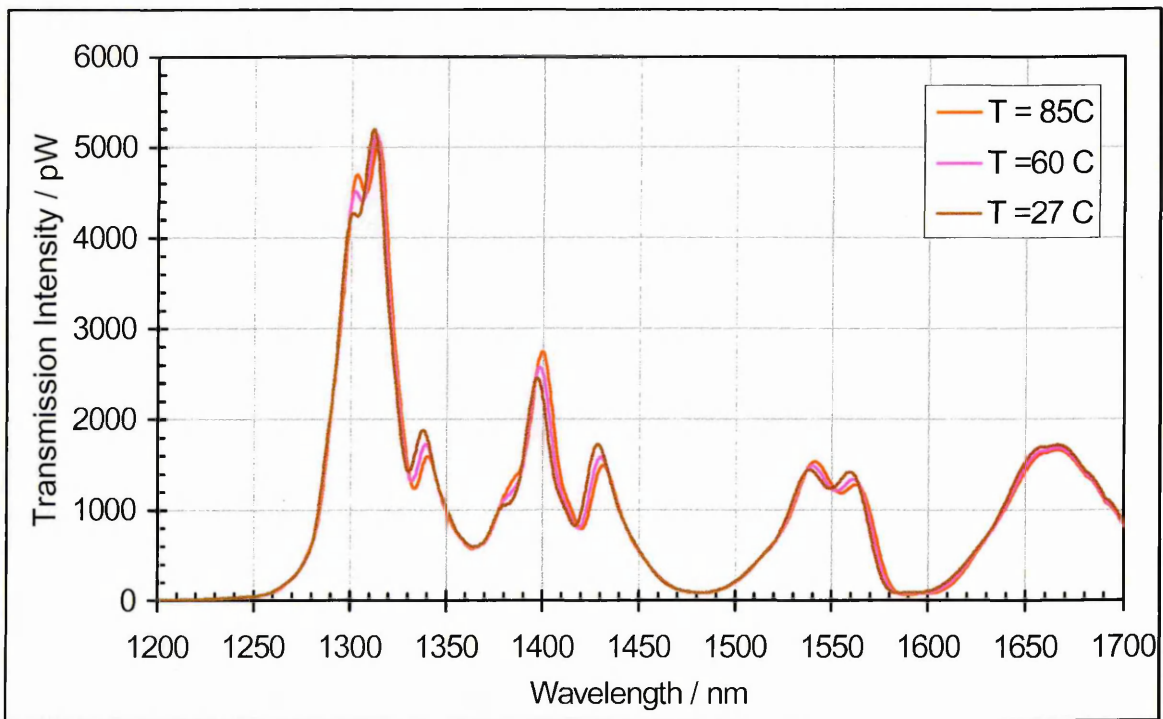
Figure A10.38: Ambient temperature profile of LPG A407 at selected values to allow clearer observation of shifts
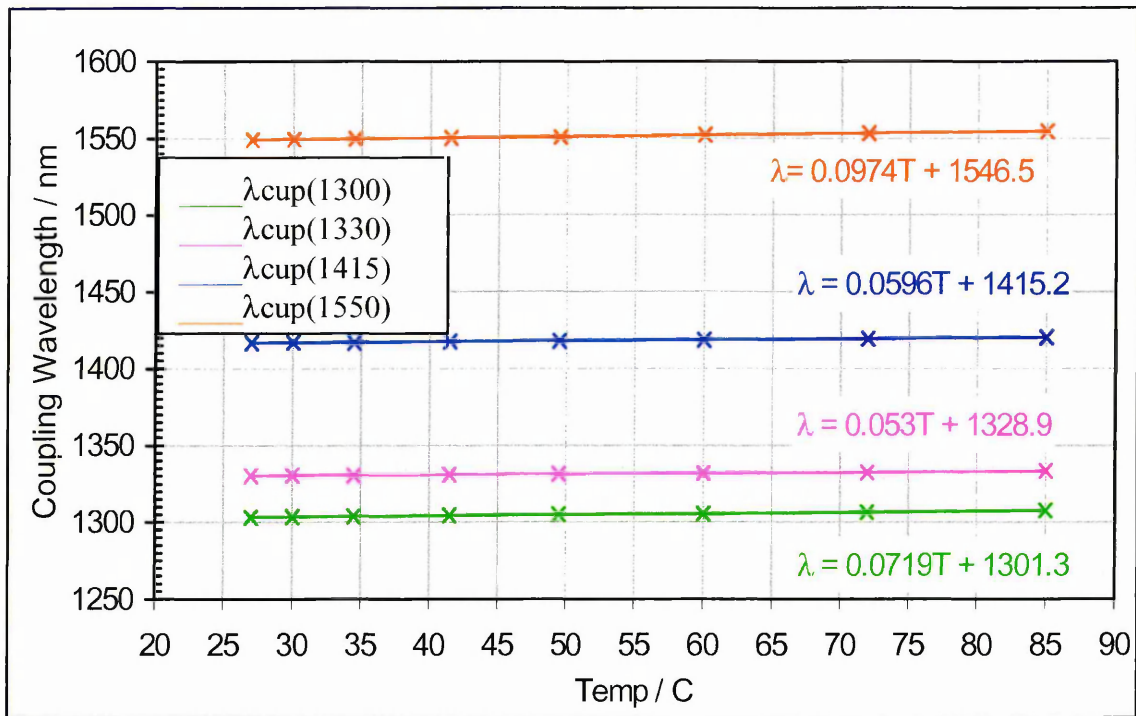
Figure A10.39: Change in coupling wavelength with ambient temperature for LPG A407
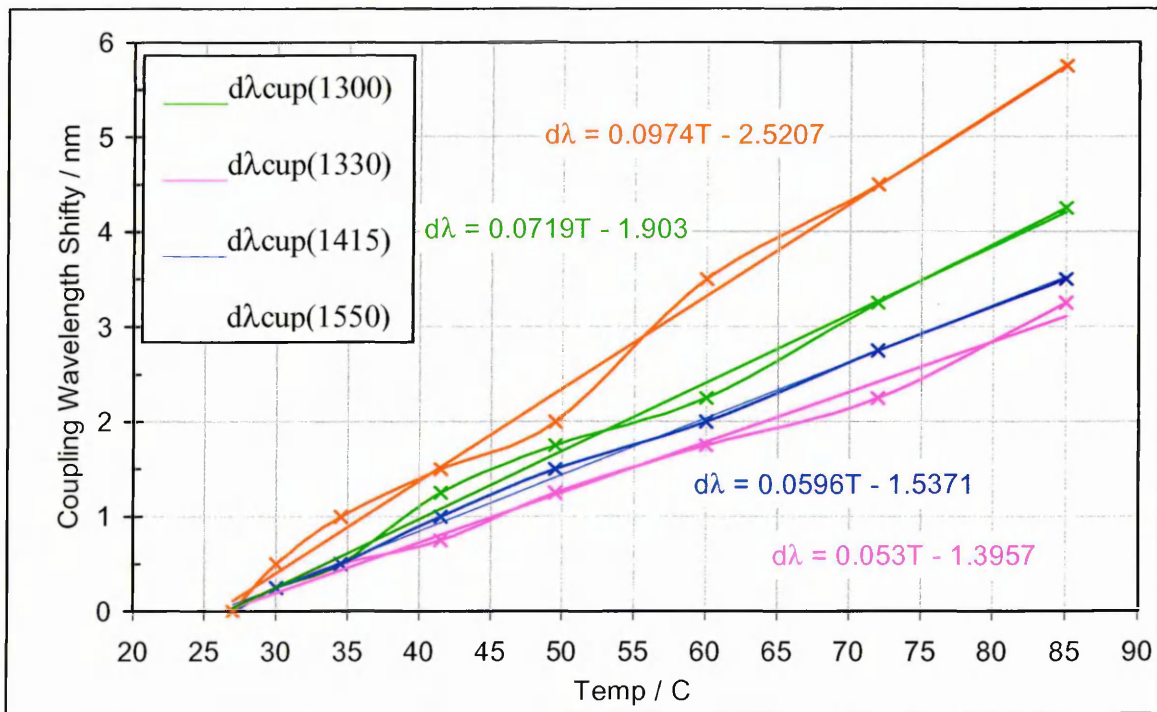
**Figure A10.40: Relative change in coupling wavelength with ambient temperature for LPG A407**
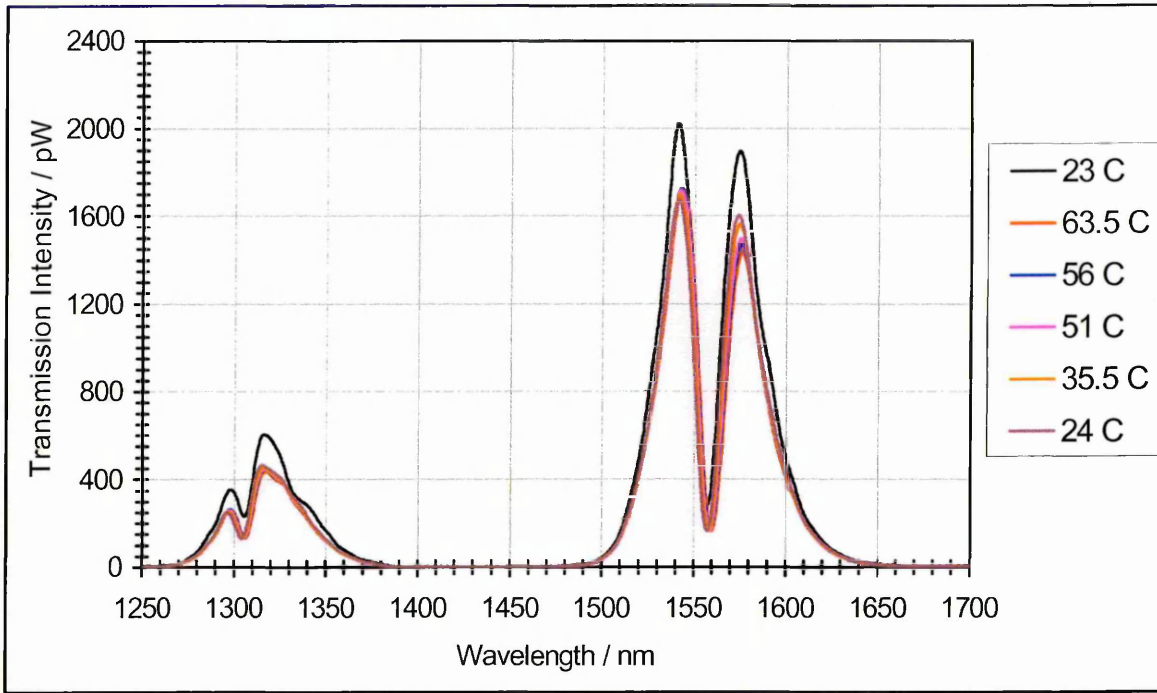
**Figure A10.41: Ambient temperature profile of LPG A410**
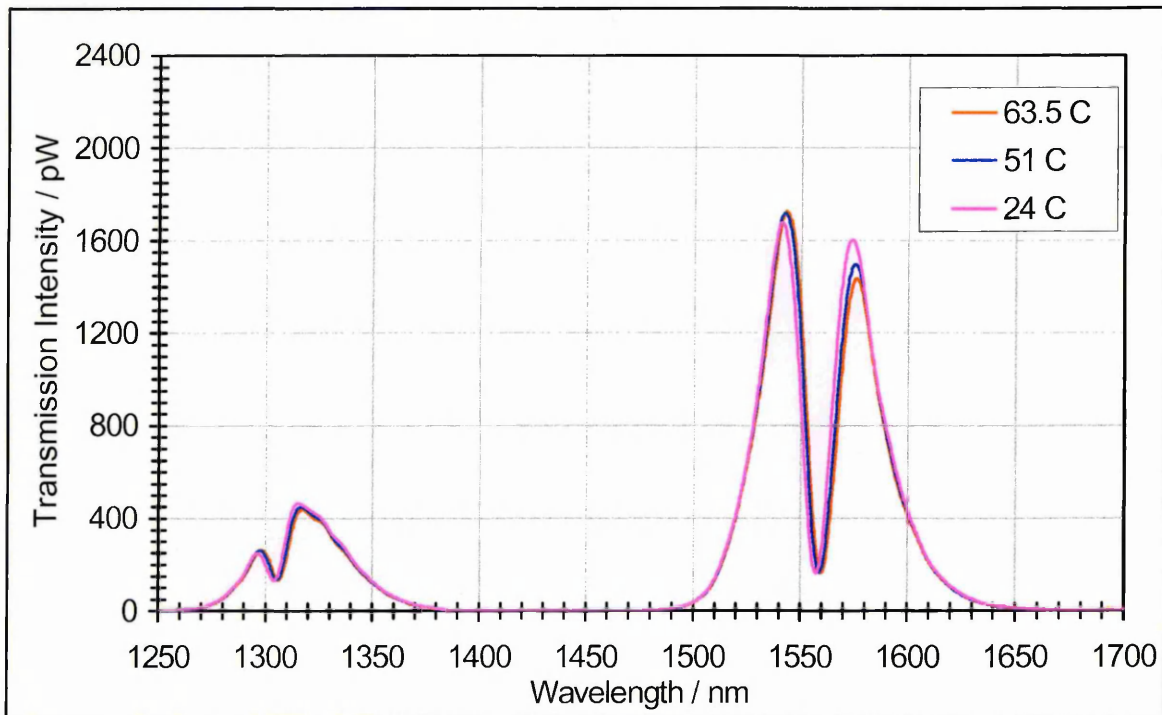
Figure A10.42: Ambient temperature profile of LPG A410 at selected values to allow clearer observation of shifts

334
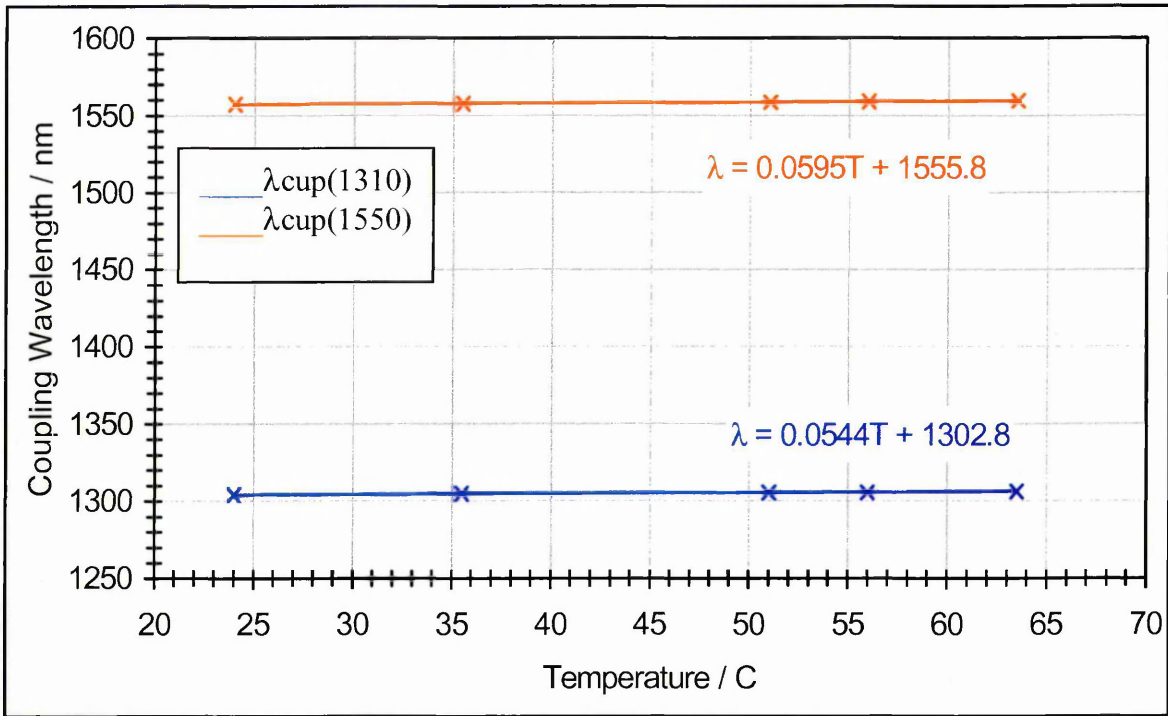
Figure A10.43: Change in coupling wavelength with ambient temperature for LPG A410
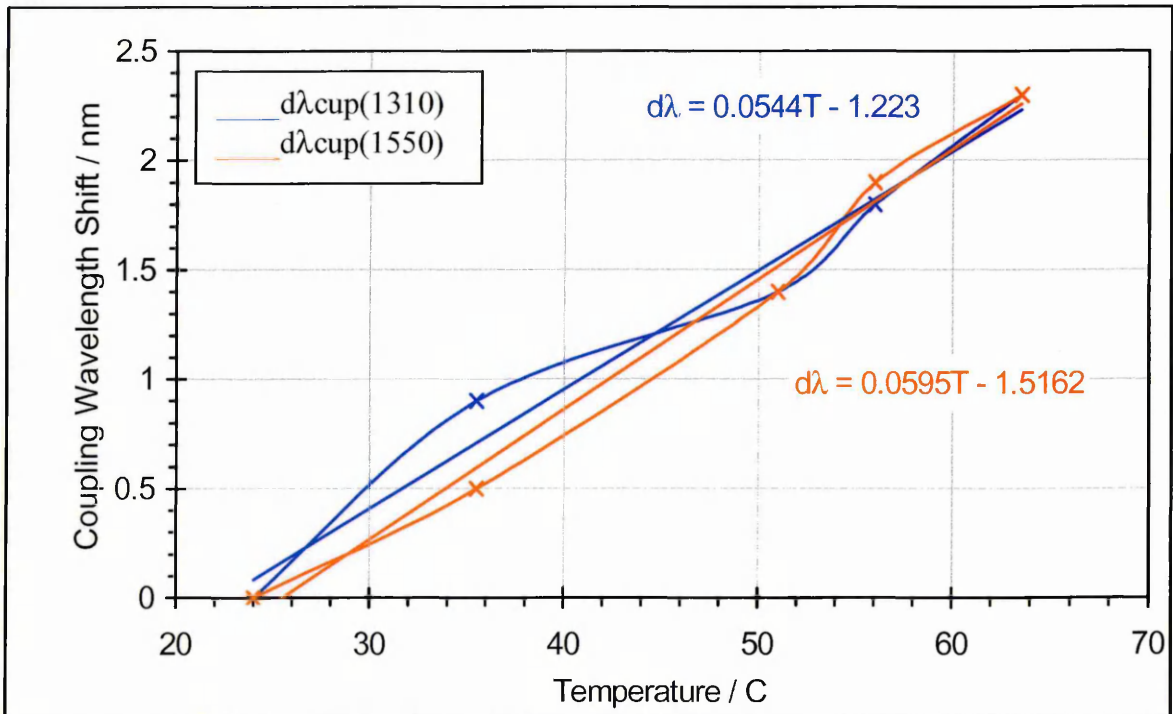
**Figure A10.44: Relative change in coupling wavelength with ambient temperature for LPG A410**

335
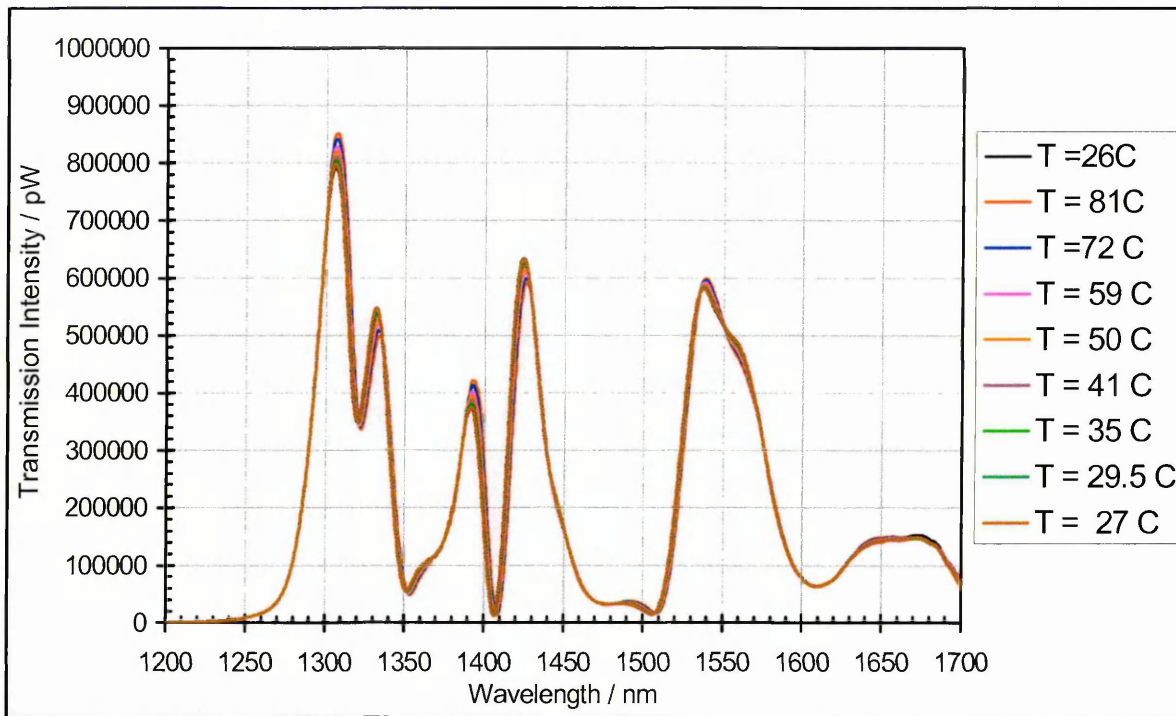
**Figure A10.45: Ambient temperature profile of LPG A416**
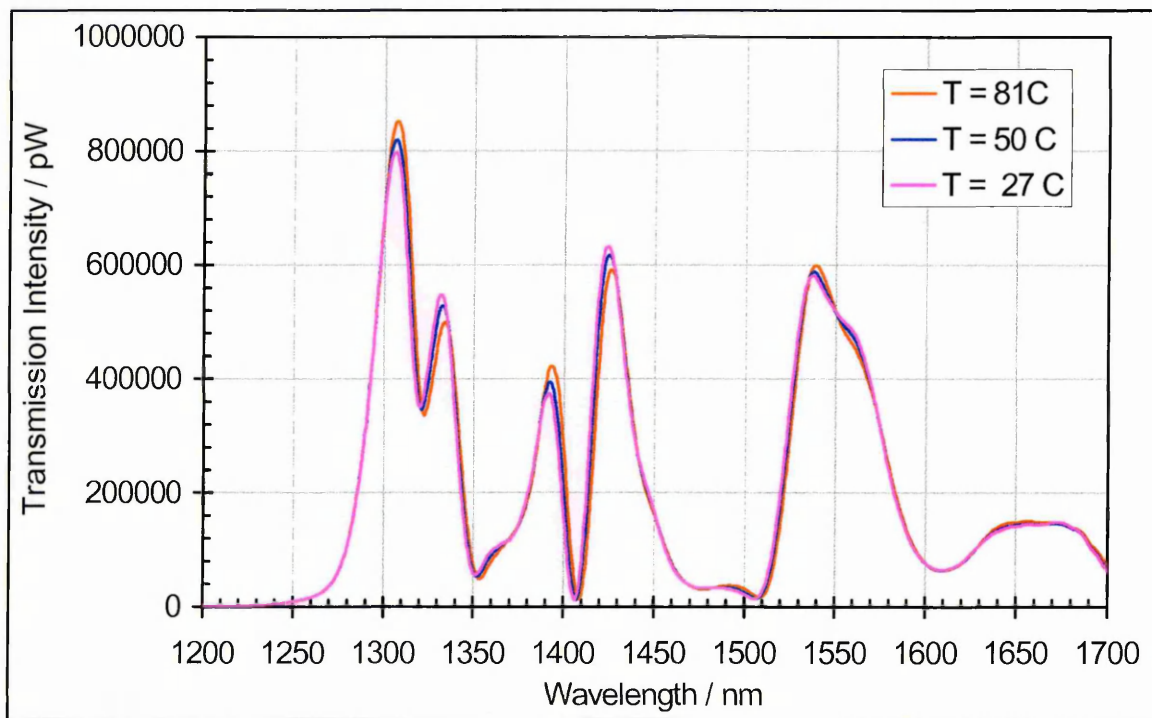
Figure A10.46: Ambient temperature profile of LPG A416 at selected values to allow clearer observation of shifts
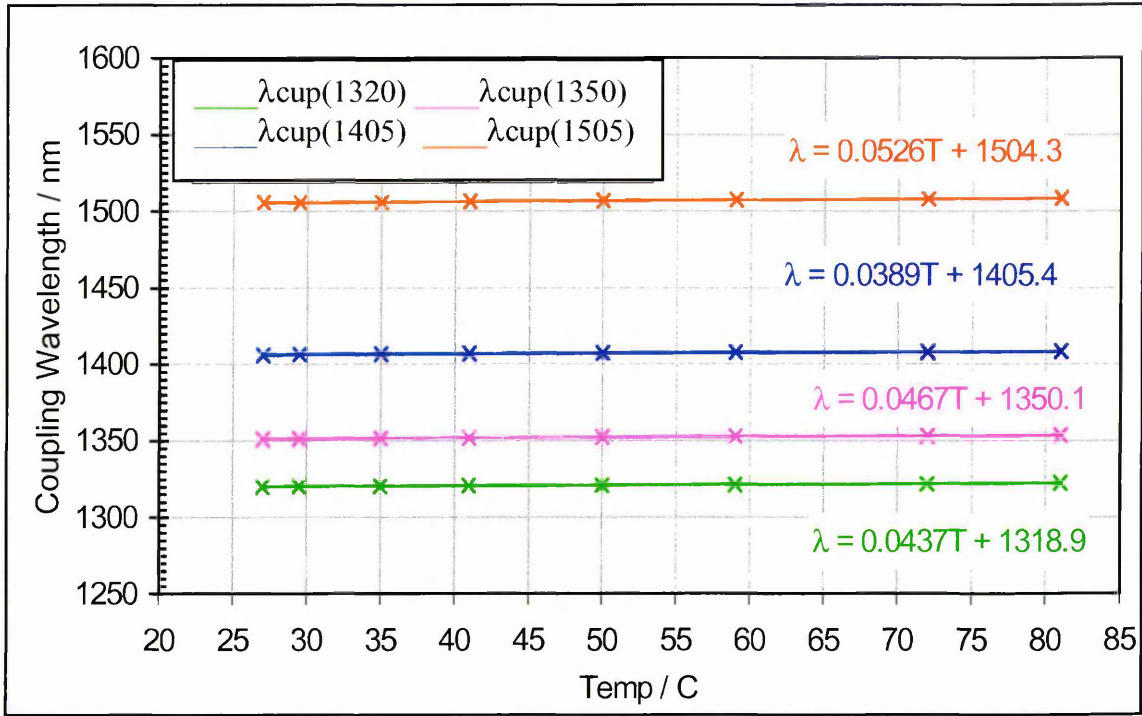
**Figure A10.47: Change in coupling wavelength with ambient temperature for LPG A416**
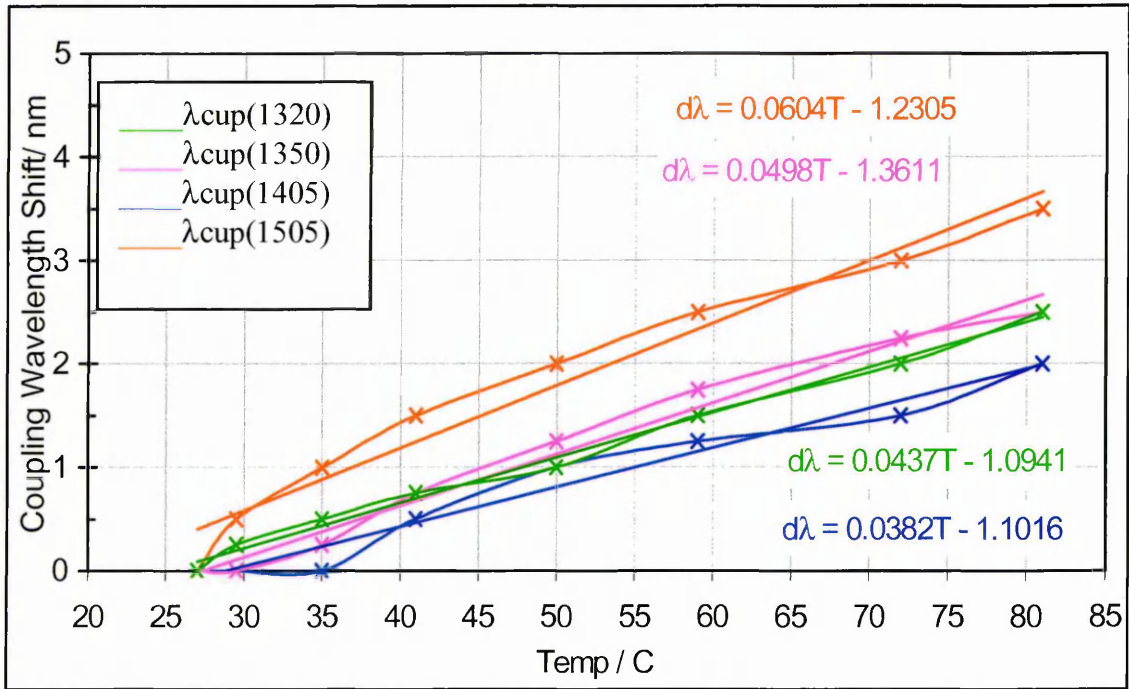
Figure A10.82: Relative change in coupling wavelength with ambient temperature for LPG A416

Appendix 11

Number of Modes in Fibre

A11.1 For Light Rays Incident on Refractive Index Boundary at Angles Less than 45°
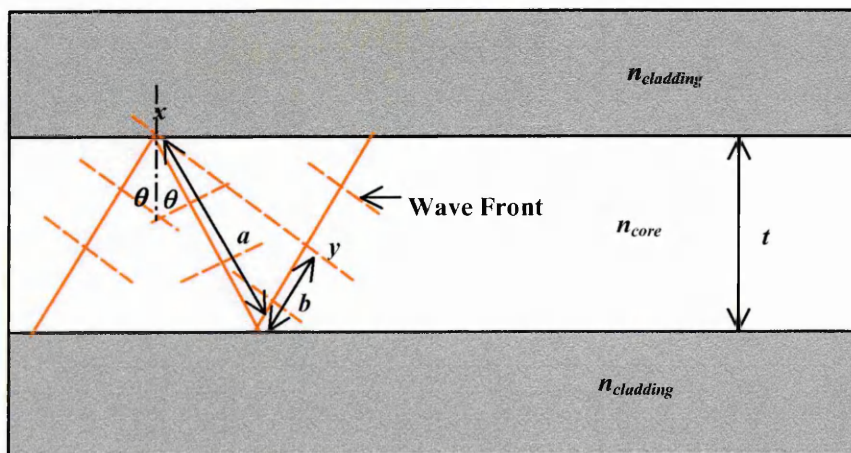

Figure A11.1: Conditions for interference in fibre for incident angle, θ, less than 45°

For constructive interference optical path length $(a+b+2\phi)$ between 2 wave fronts as shown in Figure A11.1 must be a whole number of wavelengths, therefore:

$$m\lambda_{n_1} = a + b + 2\phi \qquad\qquad (A11.1)$$

where $\qquad \lambda_{n_1} = \dfrac{\lambda_{AIR}}{n_1}, \qquad a = \dfrac{t}{\cos\theta} \qquad$ and $\qquad b = \dfrac{t\cos 2\theta}{\cos\theta}$

so (A11.1) becomes: $\qquad \dfrac{m\lambda_{AIR}}{n_1} = \dfrac{t}{\cos\theta}(1 + \cos 2\theta) + 2\phi$

as $\qquad \cos 2\theta = 2\cos^2\theta - 1$

$$m\lambda_{AIR} = n_1\left(\frac{t}{\cos\theta}(1 + 2\cos^2\theta - 1) + 2\phi\right)$$

thus: $\qquad\qquad m = \dfrac{n_1}{\lambda_{AIR}}(2t\cos\theta + 2\phi) \qquad\qquad (A11.2)$

## A11.2 For Light Rays Incident on Refractive Index Boundary at Angles Greater than 45°
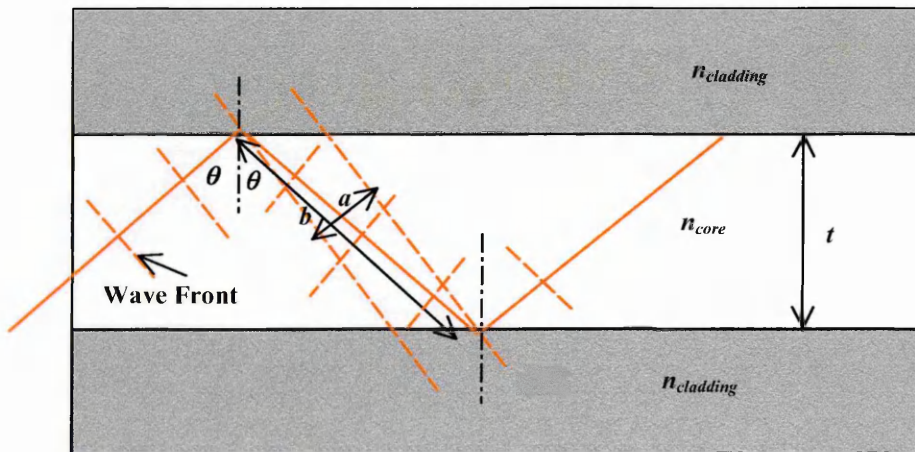
Figure A11.2: Conditions for interference in fibre for incident angle, θ, greater than 45°

For constructive interference optical path difference (*b-a+2ϕ*) between 2 wave fronts as shown in Figure A11.2 must be a whole number of wavelengths, therefore:

$$m\lambda_{n_1} = b - a + 2\phi \qquad\qquad (A11.3)$$

where $\lambda_{n_1} = \dfrac{\lambda_{AIR}}{n_1}, \qquad a = \dfrac{t}{\cos\theta}\cos[2(90-\theta)] \qquad$ and $\qquad b = \dfrac{t}{\cos\theta}$

so (A11.3) becomes: $\qquad \dfrac{m\lambda_{AIR}}{n_1} = \dfrac{t}{\cos\theta}[1 - \cos\{2(90-\theta)\}] + 2\phi$

as $\qquad \cos 2\theta = \cos^2\theta - \sin^2\theta$

$$\dfrac{m\lambda_{AIR}}{n_1} = \dfrac{t}{\cos\theta}[1 - \cos^2(90-\theta) + \sin^2(\theta-90)] + 2\phi$$

as $1 - \cos^2\theta = \sin^2\theta$

$$\dfrac{m\lambda_{AIR}}{n_1} = \dfrac{t}{\cos\theta}2\sin^2(\theta-90) + 2\phi$$

$\sin(90-\theta) = \cos\theta$

thus: $\qquad m = \dfrac{n_1}{\lambda_{AIR}}(2t\cos\theta + 2\phi) \qquad\qquad (A11.4)$

Appendix 12

Author's Publications

K. P. Dowker, Z. Ghassemlooy, A. K. Hassan A. V. Nabok and A. K. Ray: "Polyelectrolyte-coated LPG fibre for gas sensing applications", EPSRC PREP 2002, 17-19 April 2002, University of Nottingham, Oral Presentation, pp-88-89, 2002.

K.P. Dowker, Z. Ghassemlooy, A. K. Ray, F. J. O'Flaherty, and P. S. Mangat: "Period dependent temperature and ambient index effect on long period fibre gratings ", Sensor and Their Applications XII, 2-4 Sep. 2003, Ireland.

R. Hou, Z. Ghassemlooy, A. Hassan, C. Lu, and K. P. Dowker: "Modelling of long-period fibre gratings response to refractive index higher than that of cladding", Measurement Science and Technology, Vol. 12, 2001, pp. 1709-1713.

R. Hou, Z.Ghassemlooy, A. Hassan, A. Nabok, K. P. Dowker, 'Modelling of Optical Fibre Long Period Grating Sensors' , Applied Optics and Opto-electronics Conference, University of Loughborough, UK, September 2000.

A.V. Nabok, A.K. Ray, N.F. Starodub, K P. Dowker, "Enzyme/indicator optrodes for detection of heavy metal ions and pesticides, Proceedings of SPIE, Biochemical and Biomolecular sensing, Environmental and Industrial Sensing, Photonics East, Boston, MA, 5-8 November, 2000, 4200-07

K.P. Dowker, F.J. O'Flaherty, et al, "Temperature Characterisation of LPG Sensors for Monitoring Deterioration in Reinforced Concrete", Second International Symposium, ILCDES 2003, Integrated Lifetime Engineering of Buildings and Civil Infrastructures, December 1-3, 2003, Kuopio, Finland.